INVESTIGATION OF SPACE PACKAGE ALIGHTMENT DYNAMIC LOAD DESIGN CRITERIA

K. C. YORK
C. R. INGELS
J. G. MALONEY

FOREWORD

The report was prepared by General Dynamics Pomona Division, Pomona, California, under USAF Contract Number AF33(615)-1832. The contract was initiated under Project Number 1370, "Dynamic Problems in Flight Vehicles", Task Number 137008, "Prediction and Prevention of Dynamic Load Problems". The work was administered under the direction of the Air Force Flight Dynamics Laboratory, Research and Technology Division, Wright-Patterson Air Force Base, Ohio. Mr. R. G. Aschenbrenner was project engineer for the Laboratory.

This report covers work conducted from July 1964 to March 1966.

The manuscript was released by the authors K. C. York, C. R. Ingels and J. G. Maloney in May 1966 for publication as an RTD Technical Report.

The work was performed within the Structural Dynamics Group of General Dynamics Pomona Division, Mr. David A. Underhill, Section Head. Mr. N. D. Rickard is due special acknowledgement for his work in developing the digital simulations and Miss C. A. Lewis for her help in verifying the mathematical expressions.

The authors wish to acknowledge the assistance of the Bendix Corporation, South Bend, Indiana; NASA-Langley; NASA-Marshall; and Grumman Aviation Corporation, Bethpage, Long Island during the conduct of the state-of-the-art review preparatory to initiating the analytical work.

This technical report has been reviewed and is approved.

Walter J. Mykytow

WALTER J. MYKYTOW
Asst. for Research & Technology
Vehicle Dynamics Division

ABSTRACT

This report presents the results of a limited parametric study of ten space package alightment systems. A state-of-the-art review in alightment dynamics was conducted prior to beginning the parametric study. Two three-dimensional digital simulations were developed for use in the parametric study. Each of these simulates a basic design concept of an alightment system. Two types of alightment systems were examined. One for a 300 pound capsule with electronic cargo and one for a 3000 pound capsule with human cargo. An experimental program was performed to permit a comparison of predicted and measured acceleration time histories during alightment. Generally, excellent correlation was shown. Energy absorbing material or techniques are shown to be a secondary consideration in determining the efficiency of an alightment system. A three-dimensional digital simulation of alightment dynamics is concluded to be mandatory in the development of an alightment system. The feasibility of an alightment system, weighing 6 percent of the total capsule weight, to alight successfully on a 35 degree slope with a 12 degree capsule inclination is shown. Such a system is capable of handling a vertical velocity of 35 feet per second and a horizontal velocity of 15 feet per second.

CONTENTS

CONTENTS (Continued)

CONTENTS (Continued)

LIST OF TABLES

LIST OF FIGURES

LIST OF FIGURES (Continued)

LIST OF FIGURES (Continued)

LIST OF FIGURES (Continued)

LIST OF FIGURES (Continued)

LIST OF SYMBOLS (TEXT)

χ = Body fixed geometric axes of the space package

η = Principal axes of inertia of the space package

$\rho^{(i)}$ = Coordinate system of the i^{th} alightment system

$\mathcal{A}$ = Body centered axes of the space package

ϵ = Local terrain inertial coordinate system

$\vec{r}$ = Position of the center of gravity of the space package in the ϵ coordinate system

$\dot{\vec{r}}$ = Velocity of the center of gravity of the space package in the ϵ coordinate system

$\ddot{\vec{r}}$ = Acceleration of the center of gravity of the space package in the ϵ coordinate system

$\vec{V}$ = Initial translational velocity of the space package referenced in the $\mathcal{A}$ body centered axes system

$\ddot{\vec{x}}$ = Translational acceleration of the center of gravity of the space package referenced in the instantaneous direction of the χ geometric body fixed axes.

R = Roll angle

Y = Yaw angle

P = Pitch angle

$\dot{R}$ = Rate of change of the roll angle with respect to time

$\dot{Y}$ = Rate of change of the yaw angle with respect to time

$\dot{P}$ = Rate of change of the pitch angle with respect to time

$\vec{\Omega}$ = Angular velocity of the space package referenced to the χ axes

$\dot{\vec{\Omega}}$ = Angular acceleration of the space package referenced to the χ axes

$\vec{\omega}$ = Angular velocity of the space package referenced in the η principal axes system

$\dot{\vec{\omega}}$ = Angular acceleration of the space package referenced in the η principal axes system

χ = Euler precession angle

θ = Euler nutation angle

φ = Euler spin angle

ψ = Rate of change of the Euler precession angle with respect to time

$\dot{\theta}$ = Rate of change of the Euler nutation angle with respect to time

$\dot{\phi}$ = Rate of change of the Euler spin angle with respect to time

$\dot{\Theta}_i$ = Rotational rate of the space package about the minimum lever arm between the i^{th} pair of legs

t = Time after the instant of impact

Δt = Integration increment of the independent variable t

γ = Terrain slope

m = Mass of the space package

g = Acceleration of gravity

A = Mass moment of inertia about the η_1 principal axis

B = Mass moment of inertia about the η_2 principal axis

C = Mass moment of inertia about the η_3 principal axis

$\vec{f}$ = Force acting on the space package referenced in the ϵ inertial coordinate system

$\vec{M}$ = Moment acting on the space package referenced in the η principal axes system

$\vec{F}^{(i)}$ = Dynamic load forces at the i^{th} alightment system referenced in the i^{th} alightment coordinate system

$\vec{m}^{(i)}$ = Dynamic load moments at the i^{th} alightment system referenced in the i^{th} alightment coordinate system

$\vec{\sigma F}^{(i)}$ = Dynamic load forces at the i^{th} alightment system referenced in the $\varkappa$ geometric body fixed axes

$\vec{ff}$ = The total force acting on the space package referenced in the $\varkappa$ geometric body fixed axes system

$\vec{\mathcal{L}}$ = The moment due to the dynamic load forces referenced in the $\varkappa$ geometric body fixed axes

$\vec{YM}^{(i)}$ = Dynamic load moments at the i^{th} alightment system referenced in the $\varkappa$ geometric body fixed axes

$\vec{FE}^{(i)}$ = Reaction force at the i^{th} foot pad referenced in the ϵ local terrain coordinate system

$FE_{12}^{(i)}$ = Inplane reaction force at the i^{th} foot pad

$FE_{3}^{(i)}$ = Normal reaction force at the i^{th} foot pad

$FF^{(i)}$ = Potential frictional force

$AF_{j}^{(i)}$ = Reaction force of the j^{th} absorber of the i^{th} leg

$M\alpha^{(i)}$ = Reaction moment of the i^{th} telescoping leg resolved about the axis of rotation of the angular deflection $\alpha^{(i)}$

$M\beta^{(i)}$ = Reaction moment of the i^{th} telescoping leg resolved about an axis perpendicular to the $M\alpha^{(i)}$ axis

$F\alpha^{(i)}$ = Reaction force at the i^{th} foot pad producing the moment $M\alpha^{(i)}$

$F\beta^{(i)}$ = Reaction force at the i^{th} foot pad producing the moment $M\beta^{(i)}$

$\psi^{(i)}$ = Angular position of the parallelogram of the i^{th} alightment system relative to the $\rho_1^{(i)} - \rho_2^{(i)}$ plane

$\alpha^{(i)}$ = Rotational deflection of the leg of the i^{th} alightment system

$\beta^{(i)}$ = Direction of the deflection $\alpha^{(i)}$ relative to the $\rho_1^{(i)}$ direction

$al^{(i)}$ = Axial length of the i^{th} telescoping leg

$Ual^{(i)}$ = Unloaded axial length of the i^{th} telescoping leg

$U\alpha^{(i)}$ = Unloaded value of $\alpha^{(i)}$

$U\beta^{(i)}$ = Unloaded value of $\beta^{(i)}$

ρ = Initial axial length of the telescoping legs and the initial undeflected length of the articulating leg parallelogram absorber

$\Delta Z^{(i)}$ = Permanent deflection of the i^{th} axial absorber

$\Delta_j^{(i)}$ = The deflection of the j^{th} absorber of the i^{th} alightment system

$\dot{\Delta}_j$ = Velocity across the j^{th} absorber of the i^{th} alightment system

γ_j = The angular location of the j - 1 rotational absorber

ae = Lever arm which strokes the rotational absorbers of the telescoping leg configuration or the peg leg absorbers of the articulated leg configuration

au = Length of the $\rho_1^{(i)} - \rho_3^{(i)}$ plane projection of the upper and lower parallelogram members

ao = Horizontal offset of the peg leg axis from the pivot point of the lower parallelogram member

al = Height of the peg leg

ae = Height of the lower parallelogram pivot point above the top of the peg leg

aa = Horizontal offset of the inboard pivot points of the parallelogram energy absorber and lower members

ab = Vertical offset of the inboard pivot points of the parallelogram energy absorber and lower members

ah = Horizontal offset of the outboard pivot points of the parallelogram energy absorber and upper members

ag = Vertical offset of the outboard pivot points of the parallelogram energy absorber and upper members

ad = Distance between the upper and lower pivot points of the parallelogram members

ap = Height of the upper pivot point of the peg leg absorber above the top of the peg leg

aq = Height of the lower pivot point of the peg leg absorber below the top of the peg leg

ϕ' = Angular offset of the inboard attach points of the parallelogram of the articulated leg configurations

$\overrightarrow{b}^{(i)}$ = Position of the attach point of the i^{th} alightment system referenced in the x axes

$\overrightarrow{\rho}^{(i)}$ = Loaded position of the foot pad of the i^{th} alightment system referenced to the $\rho^{(i)}$ alightment coordinate system

$\overrightarrow{\rho}^{(i)}$ = Position of the attach point of the i^{th} alightment system referenced in the $\in$ local terrain inertial coordinate system

$\overrightarrow{\rho}^{(i)}$ = Position of the foot pad of the i^{th} alightment system referenced in the $\in$ local terrain inertial coordinate system

$\overrightarrow{s\rho}^{(i)}$ = The terrain plane position of the i^{th} foot pad

$\overrightarrow{\rho}^{(i)}$ = Unloaded position of the foot pad of the i^{th} alightment system referenced to the $\rho^{(i)}$ alightment coordinate system

$\overrightarrow{F}^{(i)}$ = Position vector of the foot pad of the i^{th} alightment system relative to the center of gravity of the space package in the x geometric body fixed axes

$\overrightarrow{\rho x}^{(i)}$ = Vector position of the outboard end of the parallelogram relative to the inboard end referenced in the directions of the $\rho^{(i)}$ coordinate system

$\overrightarrow{\rho_p}^{(i)}$ = Vector position of the lower pivot point of the peg leg absorber relative to the upper pivot point referenced in the directions of the $\rho^{(i)}$ coordinate system

μ_D = Dynamic or sliding coefficient of friction

μ_S = Static coefficient of friction

LIST OF SYMBOLS (Continued)

$G(\sin \alpha^{(i)})$ = Quartic trancendental function in sin $\alpha^{(i)}$

$G'(\sin \alpha^{(i)})$ = First derivative of G(sin $\alpha^{(i)}$) with respect to sin $\alpha^{(i)}$

$\vec{H}$ = Angular momentum vector of the space package

$\eta^{(i)}$ = Direction of the longitudinal axis of the i^{th} parallelogram absorber relative to the $\rho_1^{(i)} - \rho_2^{(i)}$ plane.

h_i = Minimum lever arm of capsule rotation between the i^{th} pair of legs

δ_i = Angle between the line h_i and the vertical inertial direction

$\varphi_1^{(i)}$ = $\rho_1^{(i)} - \rho_3^{(i)}$ plane component of the load in the lower parallelogram members of the i^{th} alightment system

$\varphi_2^{(i)}$ = $\rho_1^{(i)} - \rho_3^{(i)}$ plane component of the load in the upper parallelogram members of the i^{th} alightment system

$R_{ij}^{(i)}$ = Reaction component in the j^{th} $\rho^{(i)}$ direction between the top of the i^{th} peg leg and its seat

XDD(I) = $\ddot{x}_i$

OMD(I) = $\dot{\Omega}_i$

LIST OF SYMBOLS (APPENDICES)

ρ	= Angular inclination of the outer members of the lower parallelogram assembly
θ	= Angular inclination of the members of the upper parallelogram assembly
γ	= Angular inclination of the cross members of the lower parallelogram assembly
$L_3 = L_1$	= Length of the outer members of the lower parallelogram assembly
$L_2 = L_6$	= Length of the cross members of the lower parallelogram assembly
$U_1 = U_2$	= Length of the members of the upper parallelogram assembly
V_3	= Distance between the inboard ends of the members of the upper parallelogram assembly
R_{1213}	= Magnitude of the $\rho_1^{(i)} - \rho_2^{(i)}$ plane component of the reaction between the top of the peg leg and its seat
R_{123}	= Magnitude of the reaction between the top of the peg leg and its seat
$RA^{(i)}$	= $\rho_2^{(i)}$ direction component of the load in the upper parallelogram members
$RB^{(i)}$	= $\rho_2^{(i)}$ direction component of the load in the lower parallelogram members
$PU_j^{(i)}$	= Axial load in the j^{th} upper parallelogram member of the i^{th} alightment system
$PL_j^{(i)}$	= Axial load in the j^{th} lower parallelogram member of the i^{th} alightment system
A	= Cross sectional area
I	= Area moment of inertia of a cross section

C	= Distance from the neutral axis to the outermost fiber of a cross section
M	= Moment acting on a cross section
d	= Diameter of cross section
t	= Thickness of cross section
b	= Width of rectangular cross section
h	= Height of rectangular cross section
σ_B	= Stress due to bending
σ_C	= Stress due to compression
P_{CB}	= Critical column buckling load
σ_{LB}	= Critical local buckling stress
σ_{BR}	= Average bearing stress
σ_{max}	= Principal normal stress
f	= Design or safety factor based on working stress and yield stress
τ_{max}	= Principal shear stress
σ_t	= Normal stress in tangential direction
σ_r	= Normal stress in radial direction
K	= Estimate of the weight of an item to its assembly weight
ρ_{TM}	= Material density of the test model member material
A_{TM}	= Area of the test model member cross section
ℓ_{TM}	= Length or thickness of the test model member
W_{TM}	= Weight of the test model member

SECTION I

INTRODUCTION

This report presents the results of a limited parametric study for earth alightment of both human and electronic cargos. Two basic types of alightment systems were conceived, designed, and analyzed for their alightment capabilities. A telescoping leg is used for alightment of electronic cargo and an articulated leg is used principally for human alightment. Three-dimensional digital simulations were developed for each of the alightment systems and used in the limited parametric study. Capsule motion time histories and dynamic loads were computed with the simulations. A scale model of the articulated leg was fabricated and used in a test program aimed at examining the adequacy of the digital simulation. A detailed load, stress, and weight analysis was performed for each alightment system configuration examined.

The main body of the report contains a discussion of the basic criteria and concepts, a summary of the parametric study, and the approach used in the analysis with a section showing the adequacy of the approach. General conclusions are contained in Section VII. Eight appendixes are used to present supplementary information, detailed results, or descriptions of the various efforts comprising the total study program.

A. CONTRACT SCOPE

A parametric study of ten alightment system configurations for twenty combinations of initial conditions was to be performed. Each configuration was to be primarily defined by its energy absorption technique. Space capsule motion time histories (three-dimensional) and capsule dynamic loads were to be computed for each configuration. The relative merits of each configuration was then to be assessed based on alightment capability, dynamic loads, and alightment system weight.

The adequacy of the digital simulations was to be determined by comparing the results of a test program to the predicted results of the digital simulation.

B. PRINCIPAL CONCLUSIONS

The program has shown that a three-dimensional digital simulation of a space package alightment system can accurately predict capsule response during landing. A simulation of this type provides a valuable design tool permitting low cost and accurate definition of all the various alightment parameters. Also, mechanical design parameters such as system loading can be obtained from the analysis. This approach permits design optimization without the expense of actual hardware fabrication followed by modifications during test.

The following paragraphs present the principal conclusions for each phase of the program.

1. Literature Search

The literature search showed that previous digital simulations have been limited to two-dimensional solutions. The second significant point was that energy absorbing material or techniques will produce an efficiency greater than 10,000 foot-pounds of energy per pound of material. This means for the 35 feet per second vertical velocity combined with the 15 feet per second horizontal velocity, the weight of energy absorbing material required is less than 0.5 percent of the capsule weight. The landing system weight is composed primarily of leg struts or other structure necessary for capsule stability and the long stroking required for low g landing. Therefore, emphasis has to be placed on optimizing the alightment system geometry and mechanical design with the type of energy absorbing material being of secondary importance.

2. Analytical Phase

The program has indicated that an adequate simulation must be a three-dimensional solution. For example, the gyroscopic effects of a 3 radian per second roll rate can make the difference between a stable and non-stable solution. Alightment gear/surface interaction can also be critical in terms of stability as shown by the parametric study. The complexity of the alightment problem with its many parameters dictates a digital simulation for an economical design tool. It is estimated that at least 400 computer runs would be necessary to optimize, then finalize, a single system design. This program with 294 runs for 10 configurations merely provides a cursory definition of the problem.

3. Experimental Phase

The use of telemetering to obtain experimental data was highly successful. Data acquisition was 100 percent successful for all eleven drops. This system permits great test flexibility with the drop site capable of being remote from the receiving station. The use of digital data reduction techniques greatly enhanced the ease with which the comparison phase was conducted. Test data and digital simulation output were in the same format and mechanical plotting was used for data presentation.

4. Comparison Phase

The vertical acceleration provided excellent correlation between test and digital simulation. This proves the validity of the simulation. However, the lateral acceleration and angular rates provided poor correlation for several drops. This was due to asymmetry of the leg forces and slippage at the pegleg/alightment surface interface. A 5 percent variation in force from energy cell

to energy cell will have little effect on vertical acceleration but will produce large errors in capsule pitching. Hence, for future correlation studies, the cell forces should be monitored during the test and the digital program modified to accept different forces for each energy cell. Also, it is to be noted that non-uniform leg forces can have a significant effect on capsule stability and should be included as a parameter in any design study.

C. FUTURE STUDIES

It is recommended that the digital simulation developed for the articulated leg be used for the detailed design of an alightment system. This design development could be broken into the following three phases:

(1) Complete the parametric study of alightment using the existing program. A minimum of 400 digital runs is recommended.

(2) Perform a design analysis to accomplish a specific mission or missions. This phase would result in a modified digital simulation representing the final alightment system mechanical design as well as a complete set of design parameters from which a full-scale or scaled alightment system could be developed.

(3) This phase would consist of detailed design to the requirements developed in phase (2) and the fabrication of an alightment system. A test program would be performed on the alightment system under various impact conditions to verify the performance predicted in phase (2).

The end result of the three-phase program summarized above is a proven alightment system capable of meeting a particular set of objectives.

SECTION II

SPACE CAPSULE DESIGN CRITERIA

The basic design criterion was to obtain successful alightment for as many of the impact conditions as possible without exceeding acceleration limits. Weight was a secondary consideration. The limited time and computer runs did not permit design optimization from a weight standpoint.

The basic criteria are discussed in the following paragraphs.

A. CRITERIA BASED ON PAYLOAD LOADINGS

Two capsule configurations were studied; a 3000 pound capsule for human alightment and a 300 pound capsule for instrument alightment.

1. Human

Human tolerances to g loadings are based on the loadings the test subjects think are their limits. A human is subjected to increasing loadings until he states that his endurance limit has been reached. Therefore, there is a large variance in tolerance limit depending on test techniques, physical condition of subjects and their willingness to undergo discomfort. No previous limits were found in the literature search. Therefore, values were selected based on the lower limits quoted in Reference 1. The design criteria is based on an adequate couch with the subject facing upwards. The following are the limits assumed for the study:

Vertical Upwards:	20 g applied at a rate not exceeding 10,000 g/second
Other Directions:	10 g applied at a rate not exceeding 1000 g/second

These values are considered conservative with higher accelerations required for major injury assuming an adequate couch with the human in the proper position.

2. Scientific or Electronic

No specific fragility limits for electronic or scientific equipment could be found. Most shock resistant electronic equipment will withstand 100 g or more. However, equipment for scientific experiments may be quite delicate. Alightment parameters for delicate equipment can be derived from the 20 g human alightment system assuming 20 g is an acceptable deceleration limit for scientific experiments. Therefore, a 50 g limit was chosen for the 300 pound

equipment capsule. This will be adequate for most electronic equipment and the majority of the scientific equipment.

It is to be noted that capsules which can withstand accelerations of 100 g or more generally will have a different type of landing system. The high deceleration greatly inhibits turning the capsule during landing because the set-down time is so short. Therefore, this type of system can best be designed using simple cushioning without legs, etc., for stability. This was a factor in selecting the 50 g limit for the instrument capsule. Both systems studied are of the "soft landing" type.

B. CAPSULE STABILITY

The criteria for capsule stability were:

(1) No bottoming of any cushioning member.

(2) No tumbling of capsule.

The digital runs were terminated when an energy cell bottomed or when the capsule inclination exceeded the critical angle for tumbling considering the geometry of the situation. Another factor terminated some of the runs. This was excessive time. The capsule, on a 35 degree slope, with an articulated leg system would "walk" down the slope picking up velocity. This type of condition was handled by placing a time limit on the run. These runs were considered successful because the alightment system successfully landed the capsule. However, in an actual alightment, the walking action would continue until the bottom of the slope is reached or until a tree, rock, etc., is impacted. This is a separate problem and was not considered in this program.

C. ENERGY ABSORBERS

The original intent of the program was to include the type of energy absorber as a design parameter. The literature search showed that metal honeycomb, frictional, or frictional combined with metal deformation energy absorbers will have cushioning efficiencies above 10,000 foot-pounds per pound of material. Also, these types of absorbers can be designed to produce any desired force deflection curve. This efficiency of 10,000 foot-pounds per pound means that the absorbing material will be less than 0.5 percent of the capsule weight for a vertical impact velocity of 35 feet per second and a horizontal velocity of 15 feet per second. The actual energy to be absorbed is:

$$E = 1/2\ W/G\ (35^2 + 15^2) = 22.54\ W$$

where

W = Weight of Capsule

The amount of cushioning required for a 100 percent efficient system is:

$$\frac{E}{10,000} = \frac{22.54\ W}{10,000} = 2.254 \times 10^{-3}\ W \text{ lbs}$$

This is 0.225 percent of the capsule weight for 100 percent design efficiency. If a design efficiency of slightly less than 50 percent is assumed, the cushioning material will be 0.5 percent of the capsule weight. Since the design goal is 6 percent of capsule weight for the complete system, the type of energy cell used is not a significant parameter provided a highly efficient absorber is used. Therefore, the program was based on the use of metal honeycomb energy cells. The honeycomb type cells are totally proven and used in the majority of alightment systems.

D. ALIGHTMENT SYSTEM WEIGHT

The design goal for alightment system weight was 6 percent of the capsule weight.

The telescoping legs could be fabricated to weigh 11 pounds for a 300 pound capsule; i.e., 3.7 percent of the capsule weight. This does not include the weight of the "outrigger" leg support structure. Hence, this weight is representative of a system for a flat pancake type re-entry vehicle with a capsule body radius at least equal to the leg attachment radius. The Mercury shaped capsule has a small body radius and would require additional leg supporting structure with a resultant increase in the 3.7 percent weight. A detailed discussion of the geometric relationship between a Mercury shaped capsule and the telescoping leg is contained in Section III, A. Telescoping Leg.

The articulated legs with the mechanical design used in the test program would have a weight of 450 pounds for a 3000 pound capsule; i.e., 15 percent. This is excessive and is not representative of a final design. The study shows several design changes which would improve the system efficiency with a total weight of 180 pounds (6 percent) being feasible. This will be discussed in Section III, B. Articulated Leg.

E. ALIGHTMENT SYSTEM COMPLIANCE

The compliance of the alightment system is a second-order effect considering the large system displacements required for soft landing. Consider the articulated legs for the 3000 pound capsule. Elastic deflections near one inch would occur assuming all the members are stressed to their elastic limits. This would occur under a 20 g loading condition with a total stored energy of 2500 foot-pounds for all four legs or 625 foot-pounds for a single leg. The maximum kinetic energy of the capsule at impact is 68,000 foot-pounds.

Therefore, the energy stored in leg compliance is always less than 3.7 percent of the total impact energy for a flat drop with all four legs under maximum loading. The energy stored in a single leg under an inclined drop is less than 1 percent of the total energy. This energy was assigned to the unloading curve of the energy cell in the simulation.

A second point to consider about the effect of compliance is the energy absorbed during yielding of the structure. The landing is unsuccessful once an energy cell bottoms in the simulation. However, in an actual alightment system, yielding of the structure will absorb additional energy after bottoming. Also, when bottoming does occur, only a single leg is usually affected. Therefore, if the system is not overdesigned, the yielding will not cause excessive acceleration. If an actual system is designed using the simulation, the yielding of the structure should be added to the simulation. This can be accomplished very simply by adding a second force plateau following the bottoming deflection point of the energy cell. Structural yielding in the articulated leg would provide an additional 5 to 10 percent energy absorption. This additional absorption would mean that the failures due to bottoming would be eliminated in the majority of the cases simulated. Also, the initial parallelogram position could be adjusted slightly to eliminate some of the tumbling cases. This refinement would greatly ease the design task with resulting weight savings.

SECTION III

SPACE CAPSULE ALIGHTMENT SYSTEM DESIGN

This section discusses the design concepts and physical characteristics of each of two alightment systems. Two types of cargo were assumed, electronic for a 300 pound capsule and human for a 3000 pound capsule.

A. TELESCOPING LEG

The telescoping leg limits the deceleration of a 300 pound capsule to 50 g's in a single coordinate. Two sets of energy cells are employed, one designed primarily for vertical energy and one primarily for horizontal energy. The concept does not lend itself well to a Mercury type capsule.

1. Geometry

The telescoping leg is a tube within a tube with two sets of aluminum honeycomb for absorbing both horizontal and vertical capsule energy. Figure 1 shows the basic geometry of the telescoping leg. The aluminum honeycomb located radially around the leg is primarily for absorption of capsule horizontal energy. A maximum constant force angular deflection of 15 degrees is permitted. Located within the leg is the aluminum honeycomb for absorbing vertical energy. A maximum constant force linear deflection of .683 feet is permitted.

The horizontal placement of the telescoping leg was varied to arrive at three configurations for the parametric study. The relationship of telescoping legs located on a radius of 2.0 feet to a Mercury type capsule is shown in Figure 2. Vertical positioning of the legs relative to the capsule center of gravity was fixed for all configurations. The legs were located as high as possible consistent with adequate clearance at the bottom of the capsule. In fixing the vertical placement, consideration was given to both inclined and flat alightments. For flat alightments, all four legs are in contact and minimum stroking of the individual axial absorbers occurs since each leg absorbs about a fourth of the total energy. Consequently there is no need to provide enough ground clearance to permit stroking all four legs the full amount. For inclined and/or slope impacts, maximum stroking is required for the leading leg or legs and is available since either capsule inclination or terrain slope provides greater ground clearance. This results from the fact that the trailing legs have little or no axial deflection.

By varying only horizontal distance from the center of gravity, the effect of increasing the righting moments on capsule stability may be deduced from the parametric study.

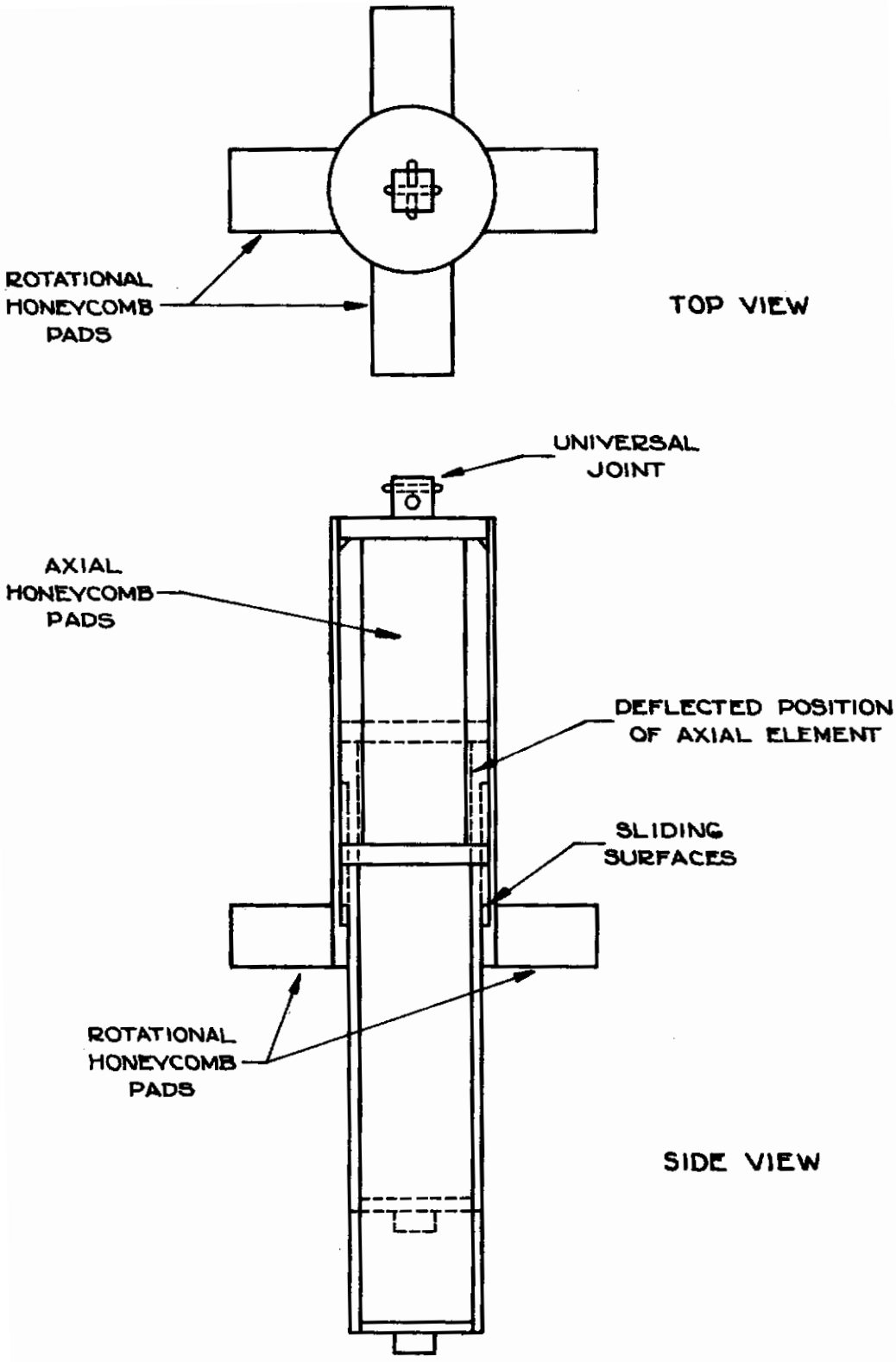

Figure 1, Telescoping Leg Conceptual Sketch

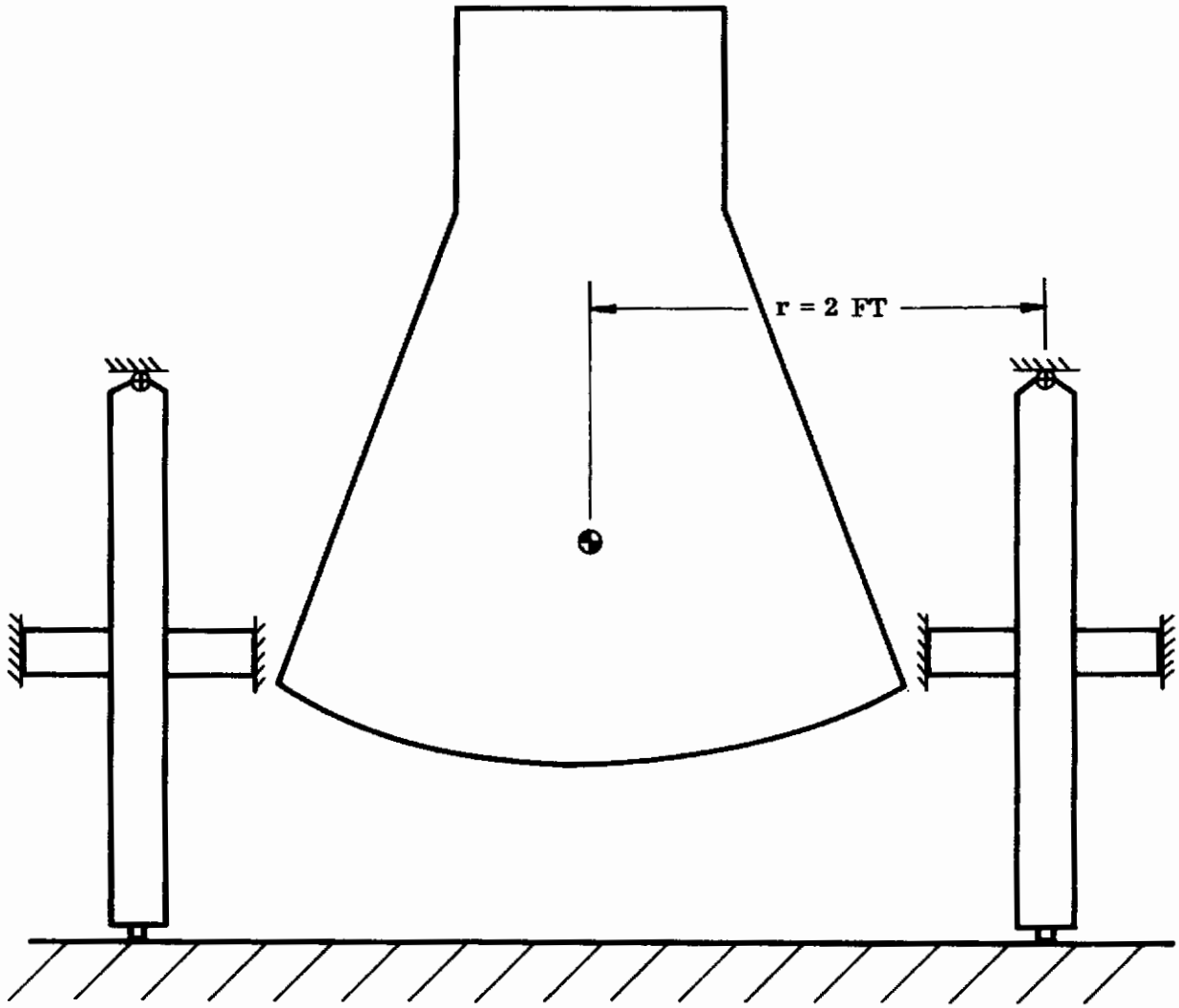

Figure 2, Capsule And Telescoping Leg

2. Leg Action

Both axial and angular deflection may occur simultaneously in the telescoping leg. Coupling between the vertical and rotational energy cells is a function of the angular position of the leg. As the rotational pads are crushed, the force normal to the terrain surface contributes to the force causing crushing of the rotational pads. This is illustrated in the following sketch.

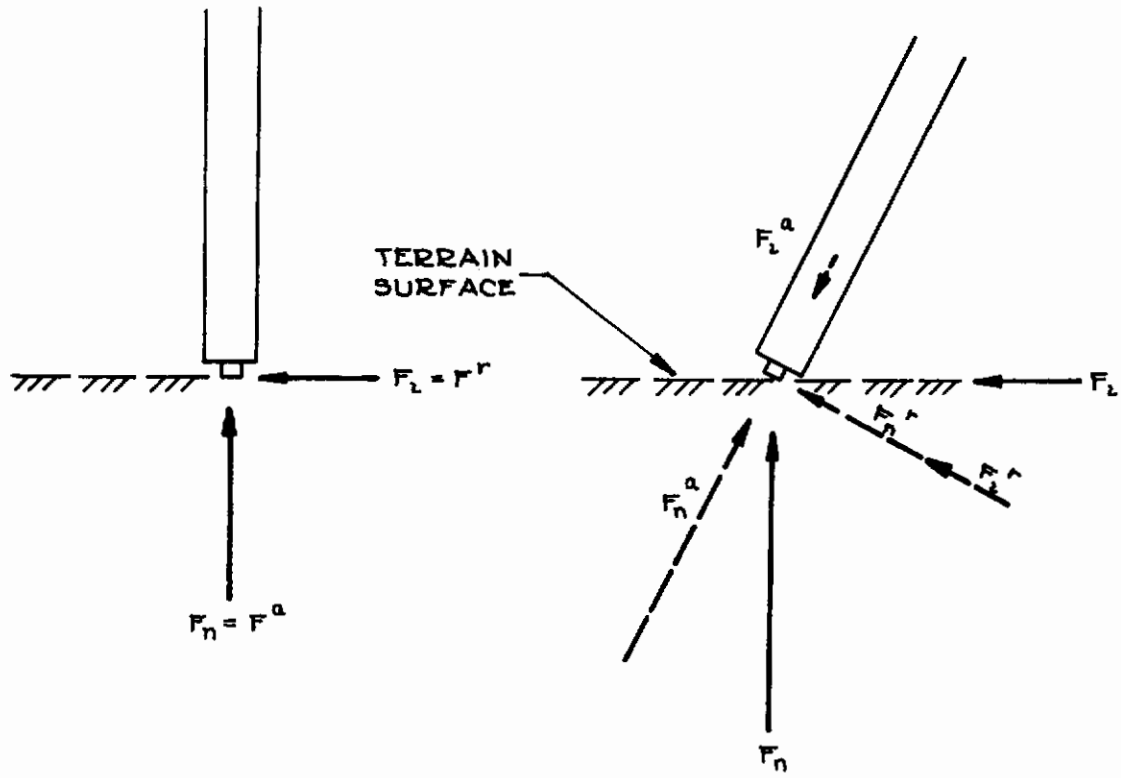

As shown, the components of the normal and in-plane forces tending to crush the rotational pads add, whereas the components tending to crush the axial energy cell subtract. Initially the leg is perpendicular to the terrain surface and no coupling occurs. As the leg rotates due to the horizontal velocity, the coupling increases as the angular deflection increases. Figure 3 illustrates this effect for combinations of capsule inclination and terrain slope. It may be seen that both capsule inclination and terrain slope aggravate the problem of rotational pad bottoming.

Two possible solutions to the bottoming problem are: firstly, increase the energy absorption capability of the rotational pads or secondly, adjust the moments applied to the capsule so that the capsule develops angular rates tending

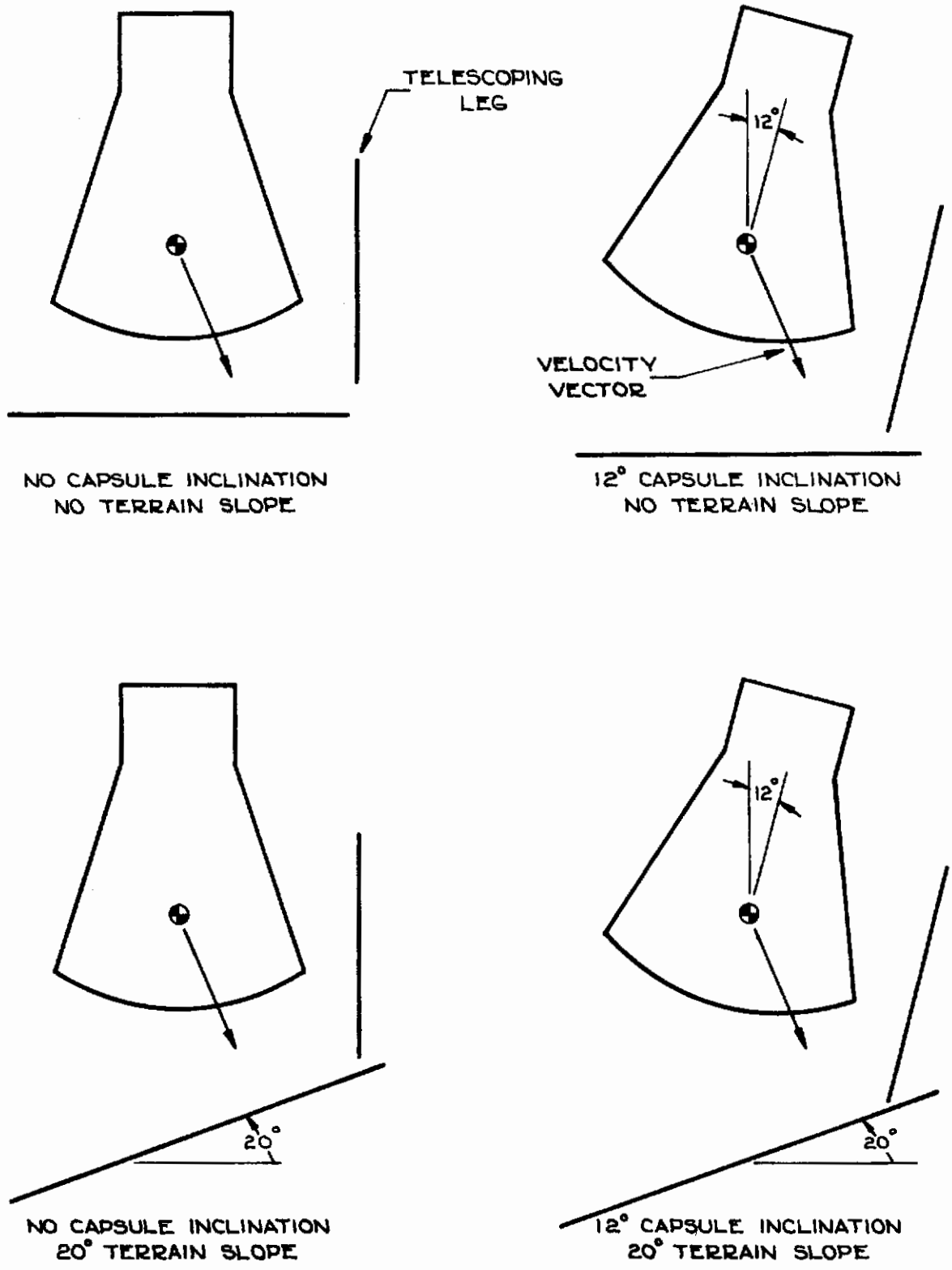

Figure 3, Effect of Inclination and Slope On Energy Absorber Coupling

to unload the leading legs. The latter method requires a finite time to develop adequate rates and, due to the short alightment time for 50 g deceleration, is not usable for the telescoping leg. The first approach of increasing energy absorption capability was used for the telescoping leg.

3. Force Deflection Characteristics

The force deflection characteristics within the telescoping leg are determined by the crushing force of the aluminum honeycomb energy cells. Forces and moments applied to the capsule are a function of the number of legs in contact, how much deflection has occurred in the energy cells and whether or not slipping at the terrain surface is taking place.

Figure 4 illustrates the force and geometric relationships that exist prior to leg deflection for a single leg with no slippage. For the rotational pads to crush

$$F_2 = \frac{F_1 \ell_1}{\ell_2}$$

However, ℓ_2 will decrease as a result of the axial deflection due to F_3 and F_2 will therefore increase proportional to the decrease in ℓ_2. The forces applied to the capsule will therefore depend upon both axial and angular deflection of the telescoping leg. Referring to the same Figure, the net moment applied to the capsule is the difference between $F_2\ell_3$ and $F_3\ell_4$, once again a function of the same variables.

Figure 5 shows a telescoping leg with maximum deflection for both energy cells. Figures 4 and 5 are drawn to the same scale and a visual comparison of moment arms may be made. It may be seen that ℓ_3 decreases more rapidly than ℓ_2 and consequently the moment $F_2\ell_3$ decreases more than $F_3\ell_4$ decreases. The net result is a righting moment large enough, for some terrain slope cases, to cause the capsule to tumble down the hill. In others, the capsule may bottom the rotational pads or tumble into the terrain slope.

Maintaining an adequate balance between these moments for a stable alightment requires careful analysis for an efficient alightment system to be developed. Expanding the simplified example to a three dimensional case requires the use of a digital simulation if an economical parametric study is to be made. In the course of debugging the telescoping leg digital simulation, numerous test cases were tried and it was found that force deflection characteristics suitable for alightment on, for example, 20 degree slopes were not always adequate for flat alightments.

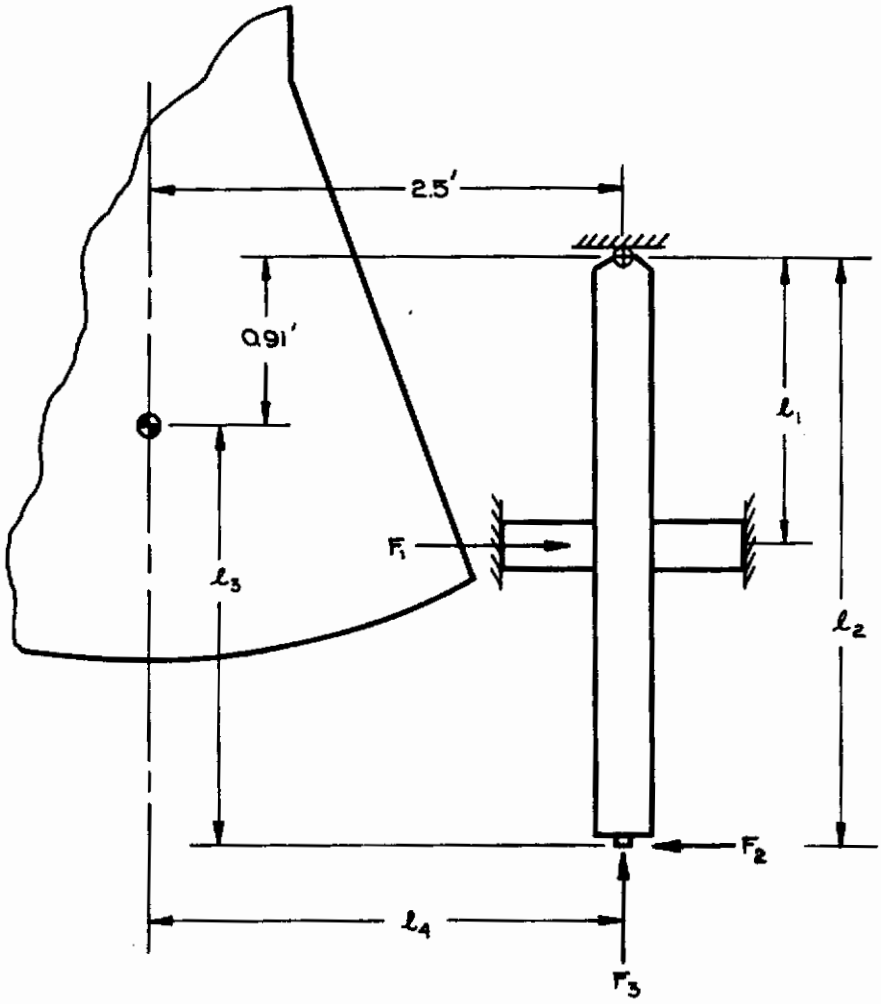

Figure 4, Telescoping Leg, Undeflected

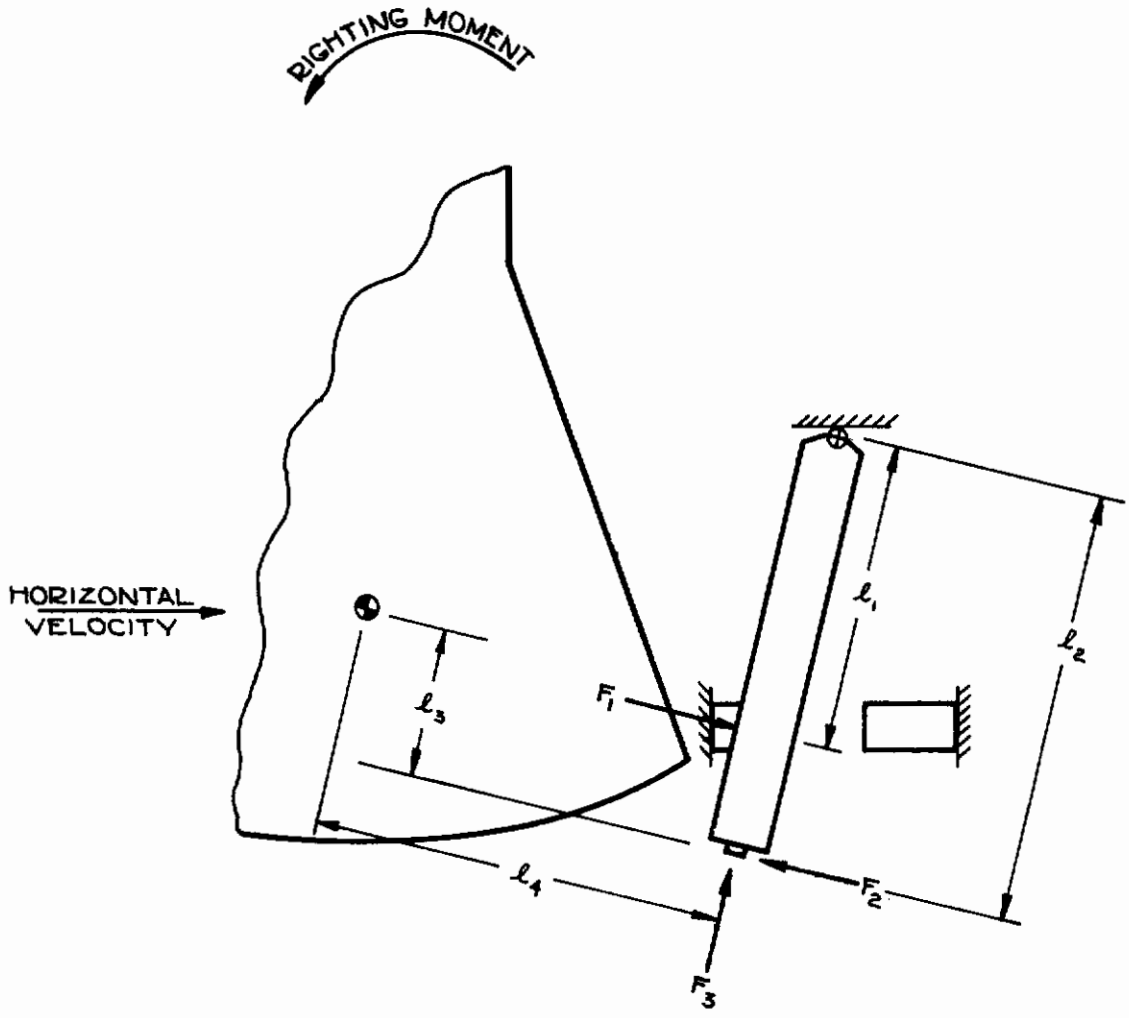

Figure 5, Telescoping Leg, Fully Deflected

It was not possible under this program to optimize the force deflection characteristics of the energy cells. It is possible that relatively minor changes such as an increase in rotational absorber crushing force after 5 or 10 degrees of stroking could materially increase the alightment capabilities of the telescoping leg systems.

B. ARTICULATED LEG

Figures 6, 7, and 8 are pictures of the display model showing the articulated leg in various deflected positions. The legs have two energy absorbing systems. A parallelogram with a diagonal energy cell absorbs vertical energy. A conical peg leg, seated in a fulcrum ring, strokes an energy cell when deflected in any lateral direction. This absorbs lateral energy.

1. Geometry

Figure 9 presents the leg geometry. The parallelogram has a major length of 44 inches and a minor length of 24 inches. The 24 inch minor length is necessary to reduce peg leg reaction forces to a reasonable level. The peg leg seats in a fulcrum ring which is attached to the outer minor member of the parallelogram. The peg leg is 25 inches long with a 16 inch diameter base.

The original intent was to stroke the parallelogram through a total angle of 60 degrees (from -30 degrees depression to 30 degrees elevation). This produces a linear stroke of 44 inches with an initial 35.5 inch clearance between the bottom of the capsule and the ground. Unfortunately, initial computer runs showed that this configuration causes bottoming of the peg leg under one leg impact with horizontal velocity and inclination of a capsule. Therefore, it was necessary to increase the angular acceleration of the capsule at initial impact. This was accomplished by having the initial position of the parallelogram at -15 degrees instead of -30 degrees. This solved the peg leg bottoming problem for the test configuration at the expense of reducing the linear stroke of the parallelogram from 44 inches to 33.5 inches. This provides only 25 inches clearance between the bottom of the capsule and the ground for a flat drop. Since 35 feet per second impact velocity is obtained by one g acting through 19 feet, the 25 inches (2.08 feet) clearance means the minimum deceleration cannot be less than 9.2 g for a perfect system. An actual system will have overshoot due to compliance. Also an allowance must be made for non-uniformity in energy cells and for deceleration on-set rates. Therefore, an actual system with 25 inches clearance must be designed for 15 g instead of the 9.2 g theoretically possible. This is five g higher than the original design goal of 10 g. However, it is still below the 20 g limit assumed for a human.

The peg leg of the configuration analyzed is 25 inches long and has a 16 inch diameter fulcrum ring. Sliding between the peg leg and impact surface was eliminated in the test program by using a pointed tip on the peg leg. This was necessary to eliminate undefined slipping during test drops so that correlation

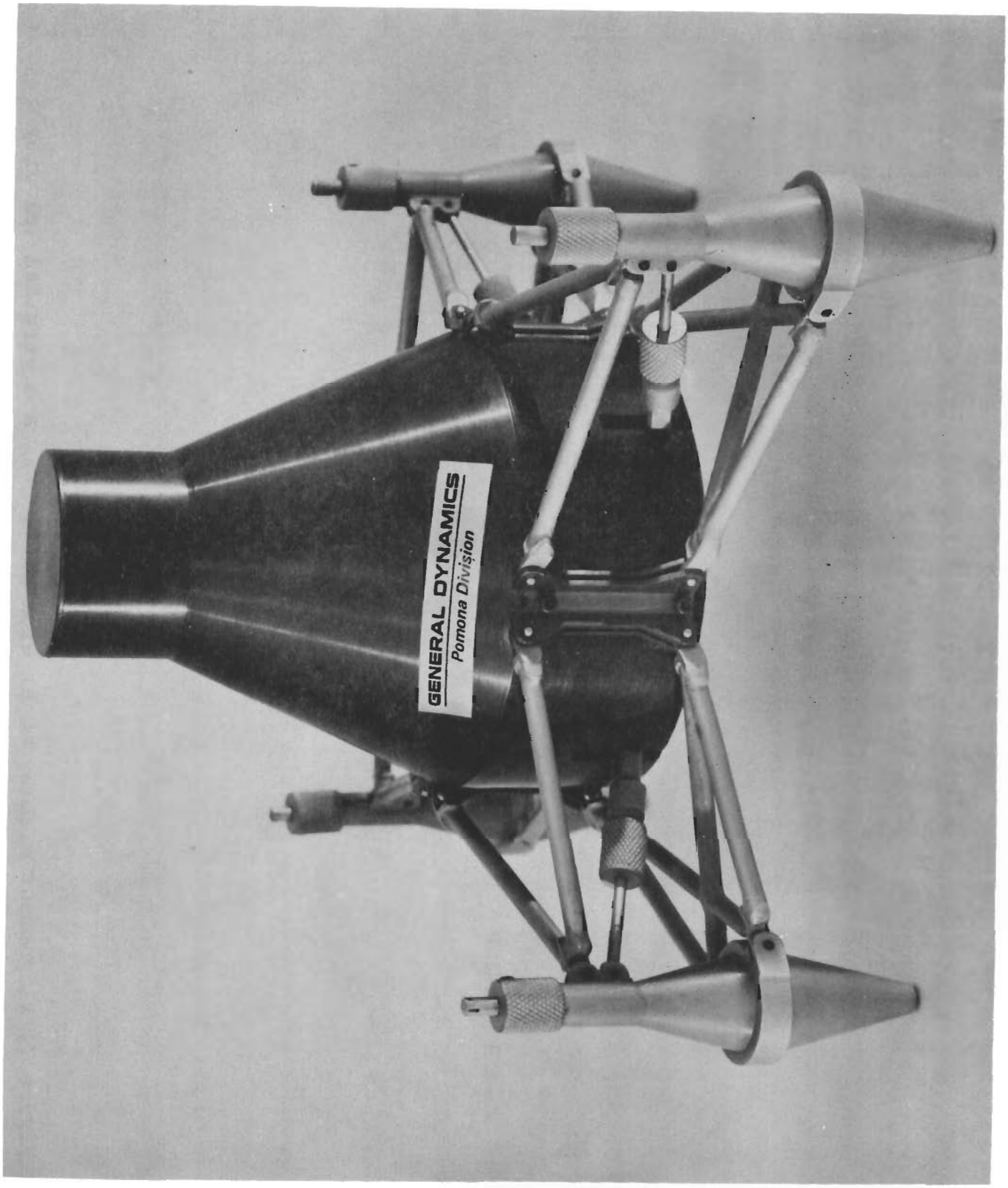

Figure 6, Alightment Display Model

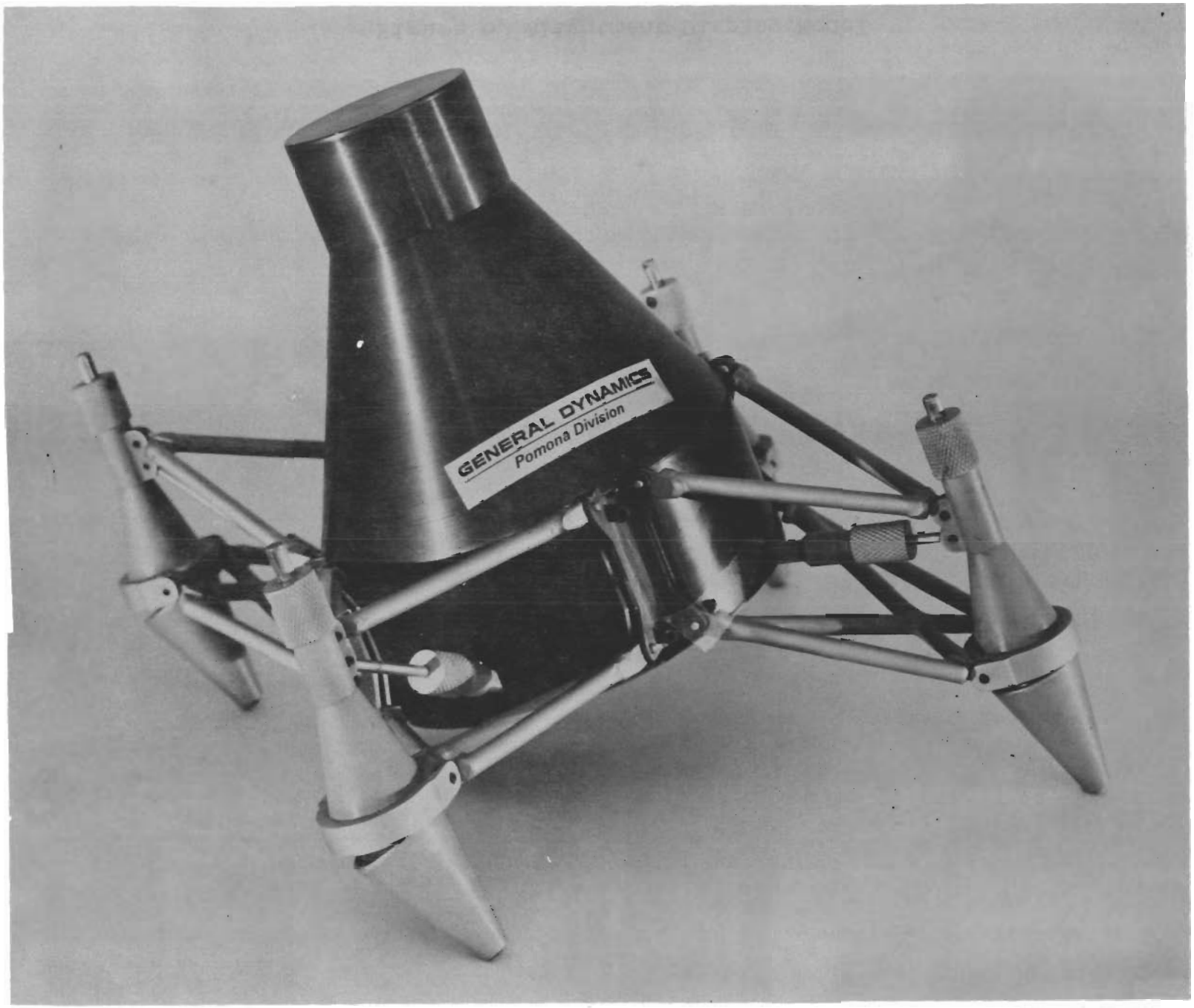

Figure 7. Alightment Display Model with Horizontal and Vertical Velocity

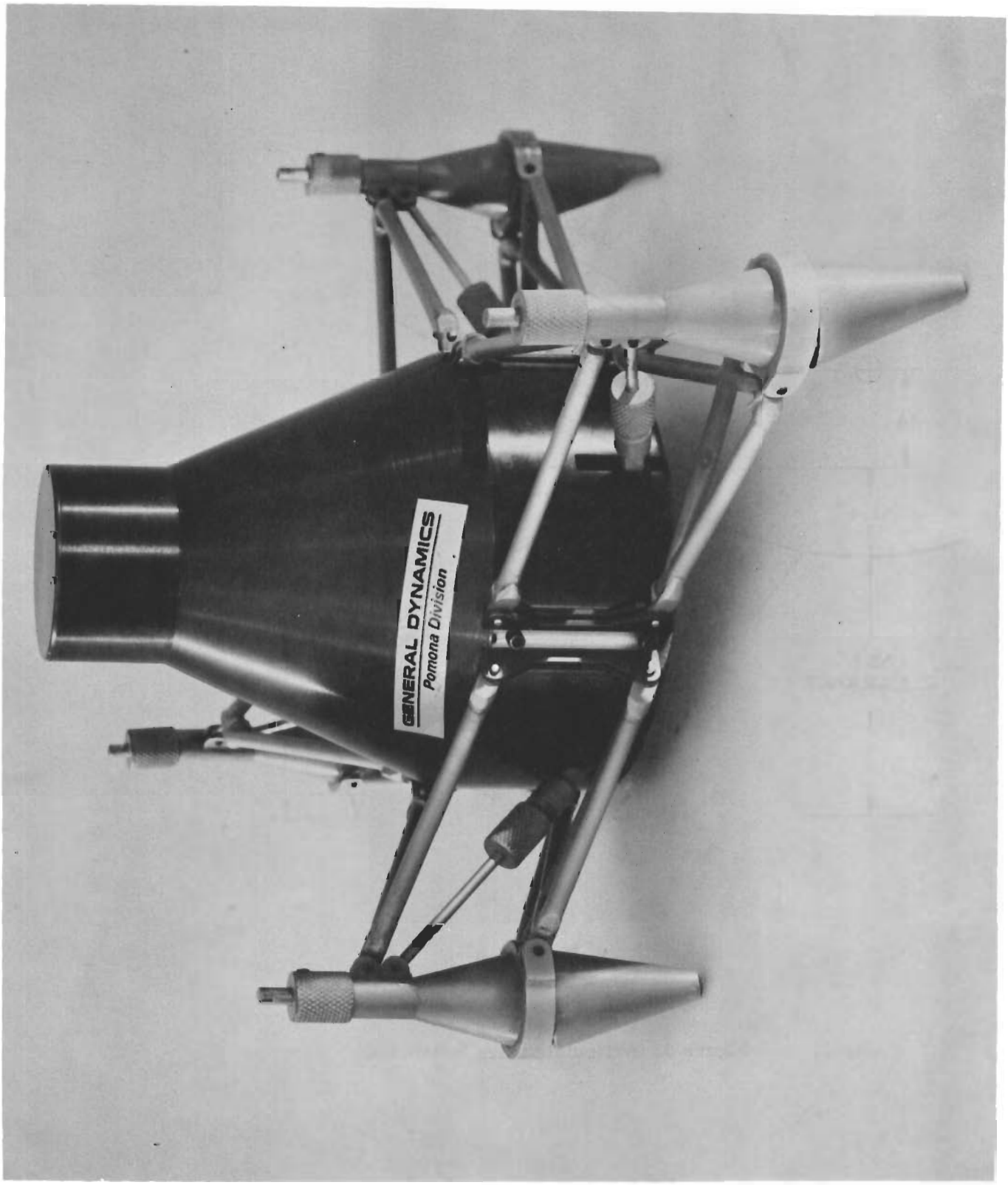

Figure 8, Alightment Display Model Landing on Slope

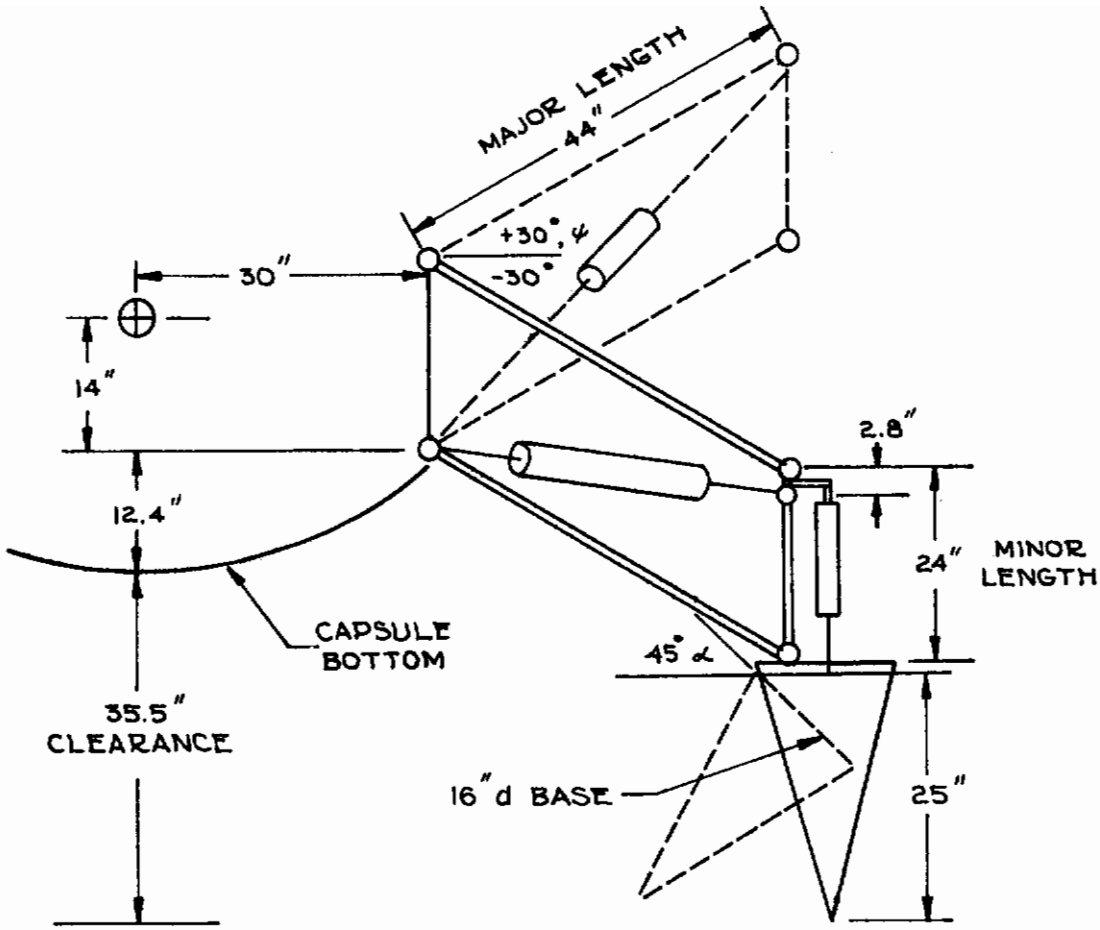

Figure 9. Articulated Leg Schematic

with the digital simulation could be obtained. The large diameter of the fulcrum ring was necessary to obtain sufficient peg leg rigidity to assure deflection of the parallelogram. The following figure illustrates this.

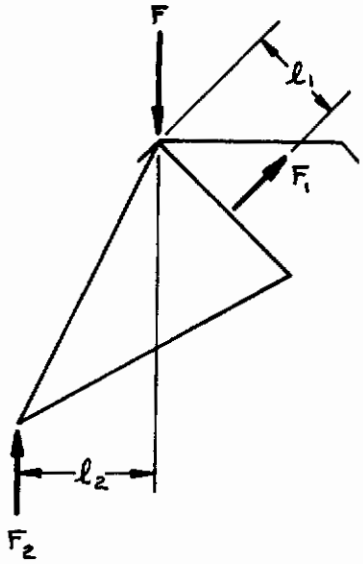

If $F_2 \ell_2$ exceeds $F_1 \ell_1$, the peg leg will deflect instead of the parallelogram. This happened in several of the computer runs causing peg leg bottomings. The force of the upper energy cells was increased to prevent bottoming of the parallelogram. This caused the peg leg to absorb vertical energy resulting in the peg leg bottoming. This was noted after the majority of the computer runs were made. Additional runs were made with the parallelogram force reduced by 10 percent and with the peg leg force increased at the end of the stroke. This configuration works for slopes up to 35 degrees with a 15 foot per second horizontal velocity and 12 degrees of capsule inclination.

This problem illustrates the complexity of a system of this type. Minor changes can greatly improve the system performance.

2. Force Deflection Characteristics

The force deflection characteristics can be controlled by the shape of the honeycomb energy cells. For example, tapering the honeycomb will provide increasing force with displacement. This parameter was changed in the various runs. In addition, the geometry of the system can be changed to produce a softening spring action with deflection. Therefore, almost any desired force versus deflection curves can be generated.

Figure 10 presents the basic force versus deflection for the geometry used in the analysis. The curves are normalized presenting stroking force divided by energy cell force. The upper figure is for the parallelogram. This system produces a mechanical advantage slightly over two with the force ratio starting at 0.55 at an initial parallelogram angle of -30 degrees. The ratio decreases to 0.40 at +30 degrees. The total deflection is 44 inches for the full range of -30 degrees to +30 degrees. Most of the computer runs were made at an initial angle of -15 degrees. For this configuration, the initial position is at a deflection of 10.5 inches.

The lower figure presents the force ratio for the peg leg. The curve starts at 0.35, decreases to slightly under 0.30, then approaches 0.35 again as the stroke is completed. The peg leg maximum angular deflection is 45 degrees. This produces a stroke of 19.5 inches at the tip.

The parallelogram and peg leg are severely cross coupled. The first coupling can be defined fixing the end of the peg leg and stroking the parallelogram. As the parallelogram swings up, it also moves out, thereby deflecting the peg leg. The upper curve of Figure 11 presents this coupling. Note at 22 inches deflection the leg coupling is reversed. Since the peg leg has stiffness for initial stroking only, the coupling no longer exists insofar as force is concerned.

The lower curve of Figure 11 presents the coupling for stroking of the peg leg. The parallelogram applies a force to the fulcrum ring of the peg leg. This force adds to the energy cells' force as long as the tip of the peg leg is inside a projected cylinder normal to and equal in size to the fulcrum ring. Once the tip passes through this cylinder, the coupling is negative with the parallelogram force working against the energy cell. This coupling rate at zero deflection is 0.33, decreasing to -0.48 at maximum deflection. Note, this negative coupling was the reason it was necessary to use a 16 inch diameter fulcrum ring. If the peg leg horizontal force is less than 48 percent of the parallelogram force, the peg leg will tend to buckle without stroking the parallelogram. (This happened in some of the computer runs causing peg leg bottoming.) If the diameter of the fulcrum ring was decreased to eight inches, this coupling factor would increase by 35 percent for a maximum negative coupling of 65 percent. This could not be tolerated, hence, the 16 inch diameter was necessary for the fulcrum ring. These force curves are applicable to configurations three to eight. They also are applicable to configuration nine, a 300 pound instrument capsule, by scaling the deflection to 45 percent of the presented values.

3. Design Improvements

Configuration five, with special forces, was quite successful from the alightment standpoint. It successfully landed on a 35 degree slope with a 12

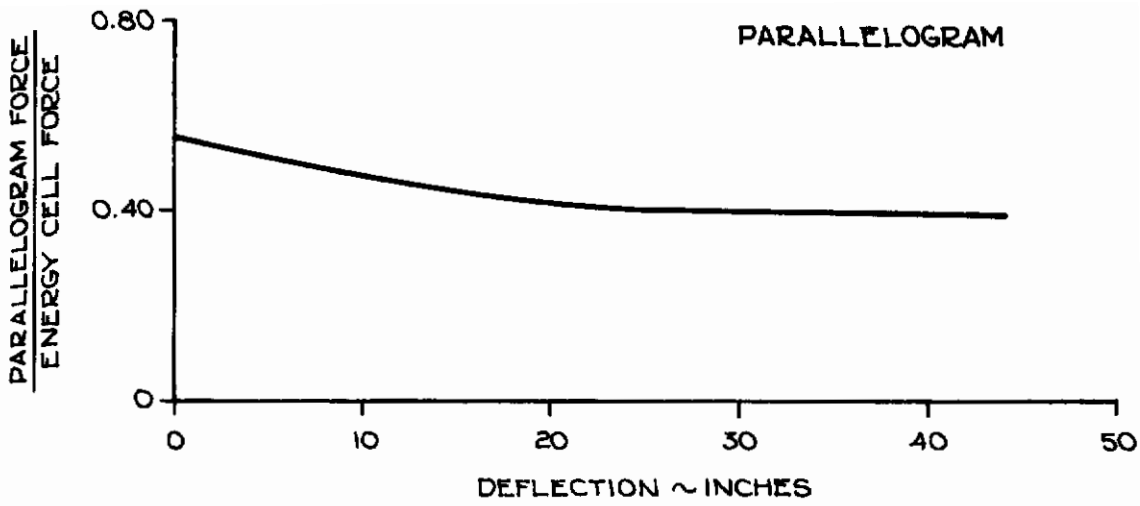

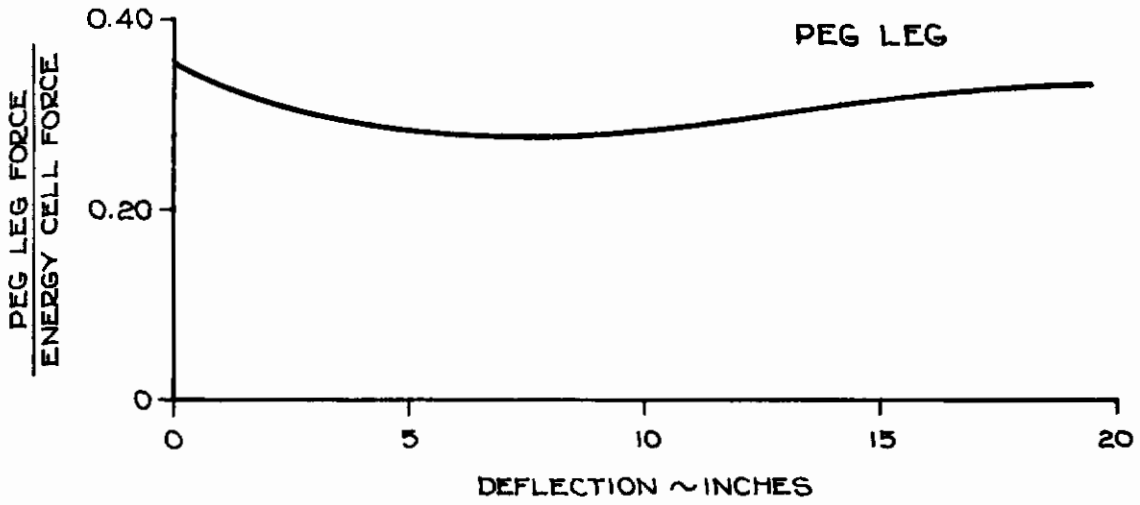

Figure 10, Articulated Leg Base Force vs Deflection

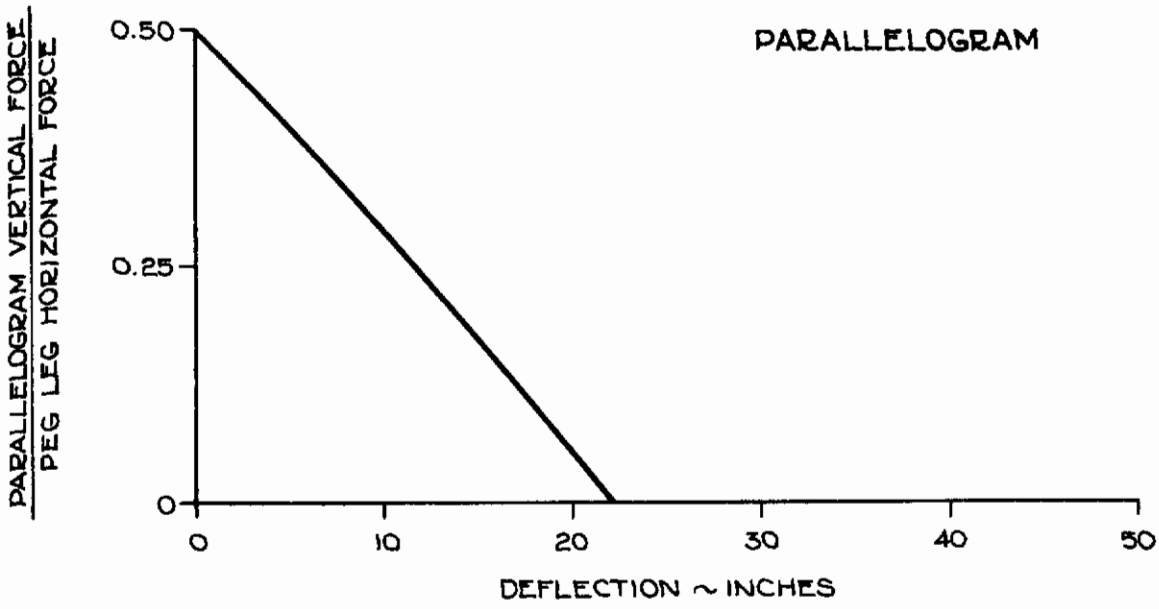

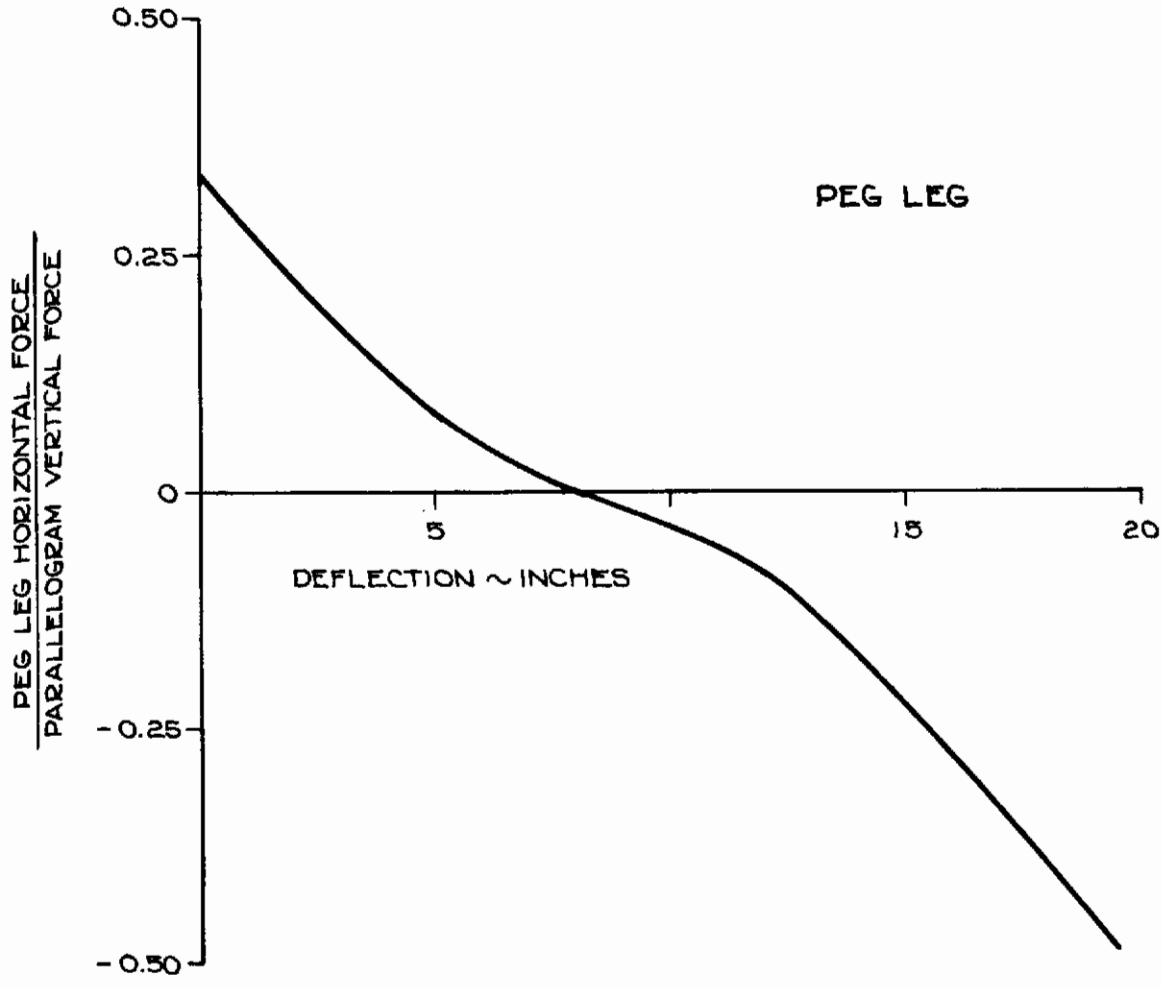

Figure 11, Peg Leg/Parallelogram Cross Coupling

degree capsule inclination and 15 feet per second horizontal velocity towards the slope. Also, it landed on a 10 degree slope with a horizontal velocity down the slope. At higher slopes, with a down slope velocity, it tipped. This basic configuration with some improvements would probably handle the full range of impact conditions.

The weight of this configuration was excessive. The four parallelogram and energy cells weigh approximately 90 pounds which is two percent of the capsule weight. This is adequate with the design being highly efficient. The peg leg assembly weighs approximately 300 pounds or 10 percent of the capsule weight. This is excessive. However, the analysis has indicated several improvements which would greatly improve the weight and system efficiency.

The digital simulation treatment of bottoming causes a weight penalty. Many runs were terminated unsuccessfully due to peg leg bottoming at 45 degrees deflection. In an actual alightment, the deflected peg leg would act as a skid. Therefore, the bottoming would not produce excessive acceleration nor cause system failure. Adding this to the computer runs would greatly relax peg leg requirements and result in weight savings.

The second point is the non-slip test model required for the comparison phase. It was necessary to use pointed legs to allow correlation. This severely penalizes the design. A large diameter flat pressure pad on the bottom of the peg leg greatly reduces the leg requirement. As the leg is stroked, the contact will be on the outer edge. Therefore, negative coupling with the parallelogram will not occur until the edge of the pad passes under the fulcrum ring. This means that an eight inch diameter cylindrical leg is equivalent to the peg leg with a point and a 16 inch diameter ring. Figure 12 presents a leg design based on this concept. The estimated weight for the complete assembly is less than 30 pounds which is to be compared to 75 pounds for the configuration analyzed. The bottom consists of a 12 inch diameter sandwich construction pressure pad. The 12 inch diameter allows 10 inch deflection before negative coupling with the parallelogram occurs. The pressure pads bolt to an eight inch O. D. cylindrical high-strength aluminum forging. This is the peg leg. The forging at the top has a conical inner-section which supports the energy cell. The fulcrum ring is another high-strength forging with a conical center section. The energy cell is attached to this center section using an eyebolt arrangement. The top assembly is another high-strength forging which has attachment holes for the parallelogram. This top bolts to the fulcrum ring. This design should weigh less than 30 pounds per leg or four percent of the capsule weight for four legs. The parallelogram weighs two percent of the capsule weight which means a total weight of six percent should be possible.

Additional studies could result in more weight savings. For example, the configuration has an energy absorbing capability equal to almost four times the impact energy. Each leg can absorb almost the complete impact energy. Considering this, a three leg instead of four leg design should be more efficient. This

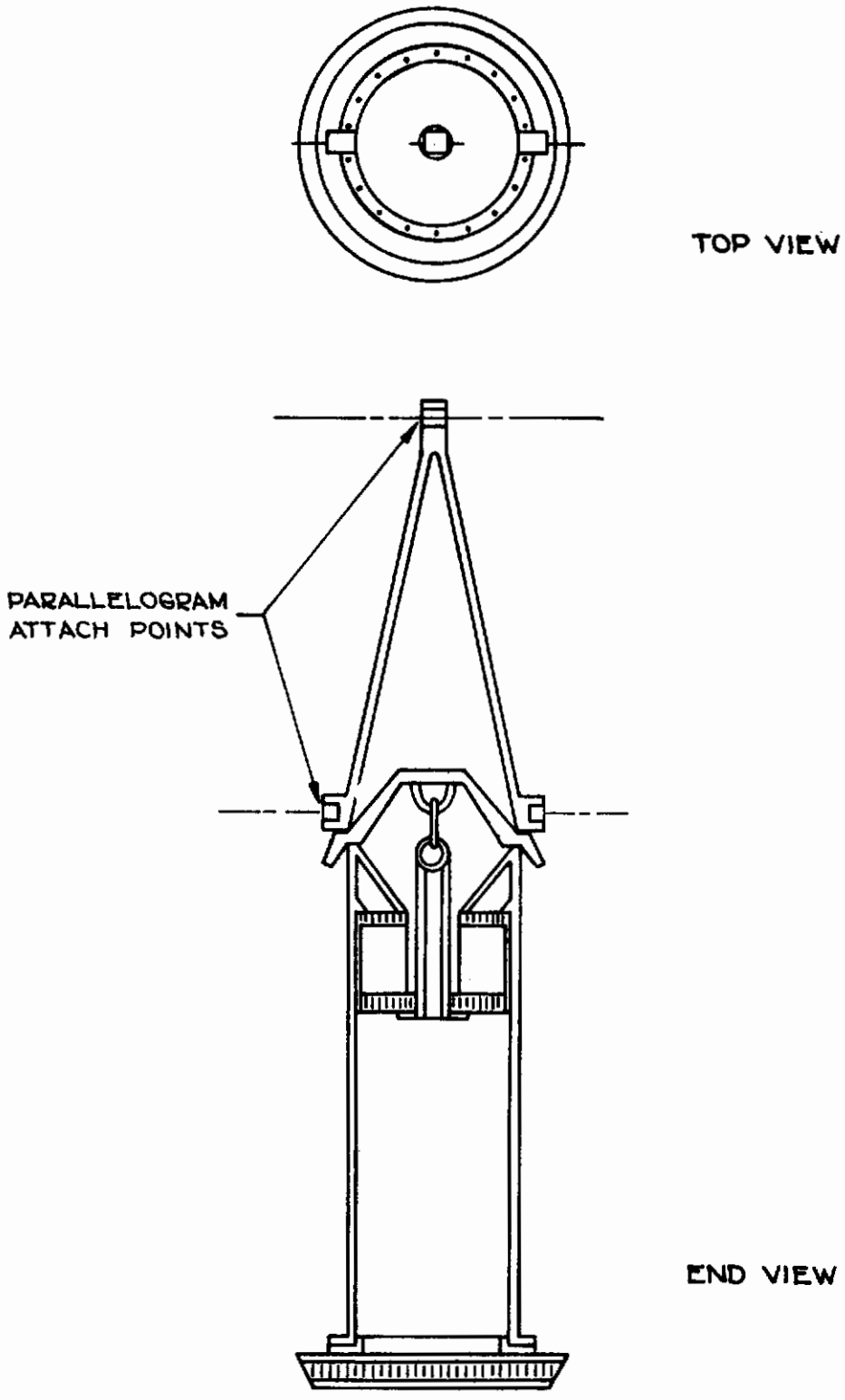

Figure 12, Cylindrical Peg Leg With Pressure Pad

system would be far superior for impacts with horizontal velocity into the slope. However, stability may be a problem for velocities down the slope. This three leg configuration should be investigated with emphasis placed on landings with velocity down the slope. It is probable that configuration five with three legs would be satisfactory. This would mean a 25 percent weight savings.

Another design improvement may be to stiffen the peg leg and let the energy be absorbed through sliding or plowing the surface of the earth. (This requires a more complex simulation of the dynamics of earth impact.) Peg leg deflection would occur only under alightment into the slope or due to hitting a rock, etc., on the ground. The existing design has very "soft" peg leg action to obtain rapid turning of the capsule under impact with horizontal velocity and inclination in the direction of the velocity, i.e., leading leg down conditions. A design utilizing sliding would have much stiffer peg leg action probably obtained through the use of a shorter leg. Also, the parallelogram would be longer. This type of design should provide maximum stability for velocity down the slope.

Another design improvement would be to use a single energy cell for all the legs. The legs would be attached to the cell using cables. This means that if alightment were to occur on a single leg, it would be capable of absorbing all the energy. If all the legs contact simultaneously, the action is softer for each leg, thereby producing the same average acceleration as for a single leg contact. The system would have a spring action which retracts dormant legs as active legs are being exercised. This greatly improves system performance.

There are many additional design factors which can be varied to obtain improvement. One would be to control the coupling between the peg leg and parallelogram by having the arms of different lengths. This would mean that the peg leg fulcrum ring would rotate as the parallelogram is deflected. This effect could be used to reduce peg leg requirements for critical landing conditions. Another possibility is to use a non-symmetrical peg leg. The studies to date indicate that the leg should have maximum energy absorption for deflection towards the capsule. Stability should be greatly increased if the force in lateral and outward directions were considerably less than for inward motion. This can be accomplished by using an oval peg leg with the energy cell off center. Finally just optimizing the basic geometry by varying dimensions, mechanical advantages, etc., could improve the system.

The articulated leg can have many different mechanical designs yet produce the same alightment dynamics. The peg leg concept used in the analysis would be difficult to store due to the large diameter. Also some of the structural members are not necessary. For example, the bottom half of the parallelogram and some of the structure of the top half of the peg leg are necessary to react the force of the peg leg energy cell. A weight saving would result if the cells were connected directly to the capsule. Figure 13 presents a design which accomplishes this. Functionally it has the same general characteristics as the articulated leg except for two features. Firstly, the peg leg forces in the lateral

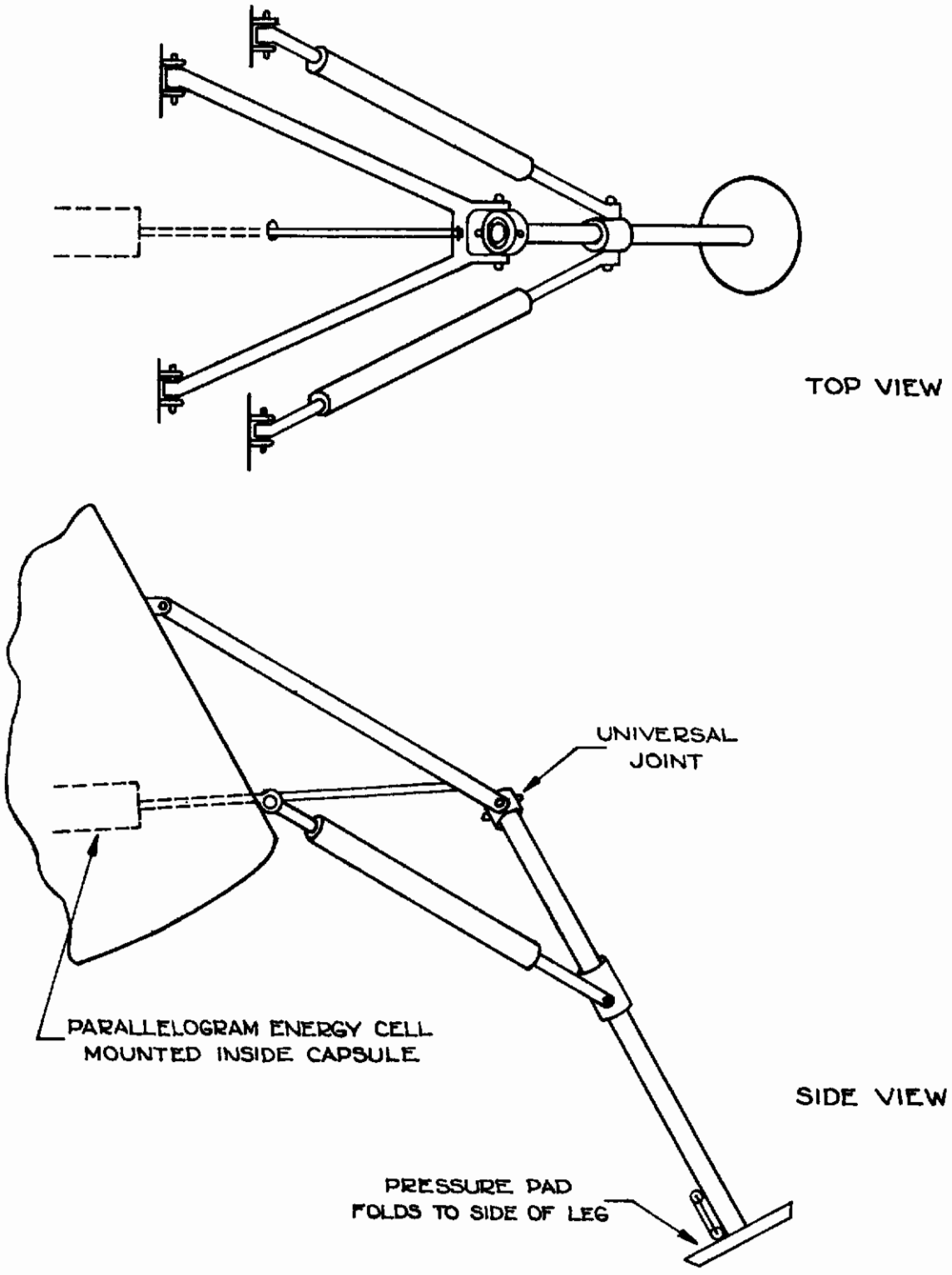

Figure 13, Improved Articulated Leg

direction would be approximately 50 percent of the force in the inward and outward directions. Secondly, the leg is at a 30 degree angle instead of being vertical and a pressure pad has been added at the bottom. These changes should greatly improve capsule stability.

This design is far more efficient than the original version of the peg leg design. The top of the parallelogram and cable/energy cell arrangement absorb vertical impact energy. The energy cell is shown inside the capsule with a cable attachment to the top of the parallelogram. This is necessary for minimum cubage in the stowed position. The bottom of the parallelogram is replaced with tension/compression energy cells which absorb horizontal energy. The peg leg assembly is replaced with a simple tube attached at the top with a universal joint. The attachment to the energy cell at the center is made using rod end bearings to allow for the necessary motion. This design should meet the programs' alightment conditions with a weight near four percent of the capsule weight. However, the existing digital programs will not handle this configuration so specific design parameters cannot be generated without modifying the program. The concept is presented as being representative of a final design which could evolve from additional articulated leg studies.

SECTION IV

PARAMETRIC STUDY

This section summarizes the digital simulation runs and discusses each of the parameters in terms of its significance for each of the configurations. Approximate upper bounds on impact conditions were obtained for each of the ten configurations. A configuration was derived, capable of a stable alightment on a 35 degree slope with the capsule inclined into the slope at 12 degrees.

A. SUMMARY OF DIGITAL RUNS

A total of 294 digital runs were made for the parametric study. Ten configurations were examined with the digital simulations. Two basic simulations were developed in the course of the contract. One covers the telescoping leg system intended only for the alightment and recovery of electronic equipment. The other simulation is for the articulated leg system and is suitable for both human and electronic cargoes depending upon geometric size and energy cell force deflection characteristics.

The configurations are categorized in the following manner:

Telescoping Leg. Three configurations using a 300 pound capsule were examined for this basic concept. Leg location relative to the capsule is the parameter distinguishing each configuration. The legs were located in 90 degree quadrants at 1.7, 2.0, and 2.5 foot radii from the capsule vertical axis for configurations 0, 1 and 2, respectively, with appropriate adjustments in the mass moments of inertia. Vertical placement, relative to the capsule center of gravity, was constant. Maximum permissible single coordinate deceleration was limited to 50 g's.

The force deflection characteristics used for each of the energy cells are:

AXIAL		ROTATIONAL	
Force (lb)	Deflection (ft)	Force (lb)	Deflection (ft)
0000.	0.000	0000.	0.000
3750.	0.020	1500.	0.003
3750.	0.683	1500.	0.333
11250.	0.690	6950.	0.344

Approximate upper bounds for these three configurations are given in Table 1. All of the results of the telescoping leg digital runs are summarized in Table 2.

TABLE 1

APPROXIMATE UPPER BOUNDS ON ALIGHTMENT CONDITIONS

CONFIGURATION	PARAMETERS: TERRAIN SLOPE	HORIZONTAL VELOCITY	PITCH ANGLE	ROLL RATE	TERRAIN SURFACE	RUN NO.
0	-10	7.5	4	3	NS	01012
1	0	15	4	0	S	10211
	0	10	8	0	S	10121
	-20	10	0	3	NS	12102
2	-10	15	0	0	NS	21200
	-20	10	0	3	NS	22102
	0	15	4	0	S	20211
3	-20	15	0	0	NS	32200X
	10	15	12	3	NS	31232
4	-20	15	0	0	NS	42200X
	10	15	12	3	NS	41232
5	-35	15	12	0	NS	53230*
	10	15	12	3	NS	51232
6	-20	15	0	0	NS	62200X
	20	15	12	3	S	62233
7	-10	15	0	3	NS	71202X
	20	15	0	0	NS	72200
8	-35	15	0	3	S	83203X
	20	15	12	3	S	82233
9	-20	15	0	0	S	92200X
	10	15	12	3	S	91233

* SPECIAL FORCE 5

NS DENOTES NO SLIPPING BETWEEN FOOTPAD/TERRAIN

S DENOTES SLIPPING MAY OCCUR BETWEEN FOOTPAD/TERRAIN

TABLE 2

TELESCOPING LEG DIGITAL RUNS
(ALIGHTMENT INTO SLOPE)

	RUN NO. 6	PARAMETERS: TERRAIN SLOPE	HORIZONTAL VELOCITY	PITCH ANGLE	ROLL RATE	TERRAIN SURFACE	CONFIGURATION: 0	1	2
PRODUCTION RUNS	A0000	0	7.5	0	0	NS	X		
	A0001	0	7.5	0	0	S	X		
	A0010	0	7.5	4	0	NS	X		
	A0011	0	7.5	4	0	S	X		
	A0002	0	7.5	0	3	NS	X		
	A0003	0	7.5	0	3	S	X		
	A0012	0	7.5	4	3	NS	X		
	A0013	0	7.5	4	3	S	X		
	A1000	-10	7.5	0	0	NS	X		
	A1001	-10	7.5	0	0	S	X		
	A1002	-10	7.5	0	3	NS	X		
	A1003	-10	7.5	0	3	S	X		
	A0021	0	7.5	8	0	S	◆		
	A2001	-20	7.5	0	0	S	◆		
	A0101	0	10	0	0	S	◆	X	X
	A1012	-10	7.5	4	3	NS	X		
	A0100	0	10	0	0	NS		X	X
	A0120	0	10	8	0	NS		◆	X
	A0121	0	10	8	0	S		X	X
	A0102	0	10	0	3	NS		X	X
	A0103	0	10	0	3	S		X	X
	A0122	0	10	8	3	NS		◆	X
	A0123	0	10	8	3	S		◆	X
	A2100	-20	10	0	0	NS		X	X
	A2101	-20	10	0	0	S		X	X
	A2102	-20	10	0	3	NS		X	X
	A2103	-20	10	0	3	S		X	X
	A0131	0	10	12	0	S		●	●
	A3101	-35	10	0	0	S		●	
	A0201	0	15	0	0	S		X	X
	A2120	-20	10	8	0	NS		●	●
ADDITIONAL RUNS	A3100	-35	10	0	0	NS			◆
	A0211	0	15	4	0	S		X	X
	A0200	0	15	0	0	NS		◆	
	A1011	-10	7.5	4	0	S	X		
	A0210	0	15	4	0	NS		●	●
	A1200	-10	15	0	0	NS			X
	A1201	-10	15	0	0	S			X

X STABLE
● BOTTOMED ROTATIONAL PAD
◆ TIPPED

6 Substitute configuration number for A to obtain complete run number (applies to Tables 3 and 4 also).

Articulating Leg. Seven configurations were examined for this concept. Of the seven configurations, six were for a 3000 pound capsule and one for a 300 pound capsule.

The distinguishing parameters for each of the 3000 pound capsule configurations are the force deflection characteristics of the energy cells and the initial position of the parallelogram. Unless noted, this initial angle is -15 degrees. Snubbing of both the parallelogram and peg leg energy cell was examined as was the effect of changing the parallelogram initial angle. The effect on alightment system capability when controlling acceleration onset rates or jerk was also examined. The geometry of the articulating leg was held constant for all six configurations. The maximum single coordinate deceleration was limited to 20 g.

For the 300 pound capsule, the articulating leg for the 3000 pound capsule was scaled and the energy cell forces chosen to provide a maximum deceleration of 50 g. The following force deflection characteristics were used for the indicated configuration. All forces are in pounds and all deflections are in feet.

Configuration 3
(Jerk Control on Both Cells)

UPPER[1]		LOWER[2]	
Force	Deflection	Force	Deflection
00000.	0.00	00000.	0.00
36000.	0.16	30000.	0.02
36000.	0.97	30000.	0.40
72000.	1.00	60000.	0.50

[1] The term "upper" refers to the parallelogram energy cell and is synonymous with ψ in the tables.

[2] The term "lower" refers to the peg leg energy cell and is synonymous with α in the tables.

Configuration 4
(Jerk Control on Lower Cell)

UPPER		LOWER	
Force	Deflection	Force	Deflection
00000.	0.00	00000.	0.00
36000.	0.04	30000.	0.02
36000.	0.97	30000.	0.40
72000.	1.00	60000.	0.50

Configuration 5
(No Jerk Control)

UPPER		LOWER	
Force	Deflection	Force	Deflection
00000.	0.00	00000.	0.000
36000.	0.04	30000.	0.005
36000.	0.97	30000.	0.400
72000.	1.00	60000.	0.500

Configuration 5
(Special Force 1, ψ + 50%[3], α -10%[4])

UPPER		LOWER	
Force	Deflection	Force	Deflection
00000.	0.00	00000.	0.000
54000.	0.06	27000.	0.005
54000.	0.97	27000.	0.400
108000.	1.00	54000.	0.500

---

[3] Denotes an increase (or decrease) in the upper cell force by the indicated percent.

[4] Denotes a decrease (or increase) in the lower cell force by the indicated percent.

Configuration 5
(Special Force 2, ψ -10%)

UPPER		LOWER	
Force	Deflection	Force	Deflection
00000.	0.00	00000.	0.000
32400.	0.04	30000.	0.005
32400.	0.97	30000.	0.400
64800.	1.00	60000.	0.500

Configuration 5
(Special Force 3, ψ -20%)

UPPER		LOWER	
Force	Deflection	Force	Deflection
00000.	0.000	00000.	0.000
28800.	0.128	30000.	0.005
28800.	0.970	30000.	0.400
57600.	1.000	60000.	0.500

Configuration 5
(Special Force 4, ψ -10%, Snub[5] α 50K)

UPPER		LOWER	
Force	Deflection	Force	Deflection
00000.	0.00	00000.	0.000
32400.	0.04	30000.	0.005
32400.	0.97	30000.	0.100
64800.	1.00	50000.	0.104
		50000.	0.400
		100000.	0.500

[5] A second, higher force plateau of the indicated values is included in the energy cell.

Configuration 5
(Special Force 5, ψ -10%, Snub α 60K)

UPPER		LOWER	
Force	Deflection	Force	Deflection
00000.	0.00	00000.	0.000
32400.	0.04	30000.	0.005
32400.	0.97	30000.	0.100
64800.	1.00	60000.	0.104
		60000.	0.400
		120000.	0.500

Configuration 5
(Special Force 6, ψ -20%, Snub α 60K)

UPPER		LOWER	
Force	Deflection	Force	Deflection
00000.	0.00	00000.	0.000
28800.	0.04	30000.	0.005
28800.	0.97	30000.	0.100
57600.	1.00	60000.	0.104
		60000.	0.400
		120000.	0.500

Configuration 6
(Jerk Control, Snub ψ)

UPPER		LOWER	
Force	Deflection	Force	Deflection
00000.	0.00	00000.	0.00
36000.	0.16	30000.	0.02
36000.	0.47	30000.	0.40
72000.	0.51	60000.	0.50
72000.	0.97		
144000.	1.00		

Configuration 7
(Parallelogram Initially at -20^{o})

UPPER		LOWER	
Force	Deflection	Force	Deflection
00000.	0.00	00000.	0.00
36000.	0.04	30000.	0.02
36000.	1.10	30000.	0.40
72000.	1.13	60000.	0.50

Configuration 8
(Parallelogram Initially at -10^{o}, Snub ψ)

UPPER		LOWER	
Force	Deflection	Force	Deflection
00000.	0.00	00000.	0.00
36000.	0.04	30000.	0.02
36000.	0.35	30000.	0.40
72000.	0.39	60000.	0.50
72000.	0.85		
144000.	0.88		

Configuration 9
(300 lb Capsule)

UPPER		LOWER	
Force	Deflection	Force	Deflection
0000.	0.000	0000.	0.00000
6688.	0.018	5852.	0.00228
6688.	0.443	5852.	0.18250
13376.	0.456	11700.	0.22800

Approximate upper bounds on impact conditions for each of the articulating leg configurations are given in Table 1. All of the results from the articulating leg digital runs are summarized in Tables 3 and 4. It should be noted that both alightment into the slope and away from slope was examined for the articulating leg. Only alightments into the slope were examined for the telescoping leg.

TABLE 3

ARTICULATED LEG DIGITAL RUNS
(ALIGHTMENT INTO SLOPE)

	RUN[7] NO.	PARAMETERS: TERRAIN SLOPE	HORIZONTAL VELOCITY	PITCH ANGLE	ROLL RATE	TERRAIN SURFACE	SPECIAL * FORCES	CONFIGURATION: 3	4	5	6	7	8	9
PRODUCTION RUNS	A0200X	0	15	0	0	NS		X	X	X	X	X	X	+
	A0201X	0	15	0	0	S		X	X	X	X	X	X	X
	A0230X	0	15	12	0	NS		⬢	⬢	⬢	⬢	⬢	⬢	X
	A0231X	0	15	12	0	S		⬢	⬢	⬢	⬢	⬢	⬢	X
	A1202X	-10	15	0	3	NS		X	X	X	X	X	+	X
	A1203X	-10	15	0	3	S		X	X	X	X	X	+	X
	A1232X	-10	15	12	3	NS		⬢	⬢	⬢	⬢	⬢	⬢	⬢
	A1233X	-10	15	12	3	S		⬢	⬢	⬢	⬢	⬢	⬢	⬢
	A2200X	-20	15	0	0	NS		+	+	+	+	⬢	◆	+
	A2201X	-20	15	0	0	S		+	+	+	+	⬢	+	+
	A2232X	-20	15	12	3	NS		⬢	⬢	⬢	⬢	⬢	⬢	⬢
	A2233X	-20	15	12	3	S		⬢	⬢	⬢	⬢	⬢	⬢	⬢
	A3202X	-35	15	0	3	NS		⬢	⬢	⬢	⬢	⬢	⬢	⬢
	A3203X	-35	15	0	3	S		⬢	⬢	⬢	⬢	⬢	+	⬢
	A3230X	-35	15	12	0	NS		⬢	⬢	⬢	⬢	⬢	⬢	⬢
	A3231X	-35	15	12	0	S		⬢	⬢	⬢	⬢	⬢	⬢	⬢
ADDITIONAL RUNS	A0130	0	10	12	0	NS				X				
	A1132	-10	10	12	3	NS				⬢				
	A2100	-20	10	0	0	NS				+				
	A2132	-20	10	12	3	NS				⬢				
	A3130	-35	10	12	0	NS				⬢				
	A3102	-35	10	0	3	NS				+				
	A0230	0	15	12	0	NS	1			⬢				
	A0230	0	15	12	0	NS	2			X				
	A0230	0	15	12	0	NS	3			X				
	A1232	-10	15	12	3	NS	2			⬢				
	A1232	-10	15	12	3	NS	3			⬢				
	A1232	-10	15	12	3	NS	4			⬢				
	A2232	-20	15	12	3	NS	4			⬢				
	A2232	-20	15	12	3	NS	5			X				
	A2232	-20	15	12	3	NS	6			■				
	A3202	-35	15	0	3	NS	5			+				
	A3230	-35	15	12	0	NS	5			+				
	A3230	-35	15	12	0	NS	6			■				

* SPECIAL FORCES

1 ψ + 50%, α - 10%
2 ψ - 10%
3 ψ - 20%
4 ψ - 10%, SNUB α 50K
5 ψ - 10%, SNUB α 60K
6 ψ - 20%, SNUB α 60K

X STABLE
⬢ BOTTOMED α
■ BOTTOMED ψ
\+ FLIGHT TIME OUT, CAPSULE "WALKING"
◆ TIPPED

7 A run number with a succeeding X denotes alightment into the slope and is used to differentiate between runs shown in Tables 3 and 4.

TABLE 4

ARTICULATED DIGITAL RUNS
(ALIGHTMENT OUT OF SLOPE)

RUN NO.	PARAMETERS					CONFIGURATION						
	TERRAIN SLOPE	HORIZONTAL VELOCITY	PITCH ANGLE	ROLL RATE	TERRAIN SURFACE	3	4	5	6	7	8	9
A0200	0	15	0	0	NS	■	X	X	X	X	X	X
A0201	0	15	0	0	S	+	X	+	X	+	X	■
A0230	0	15	12	0	NS	●	●	●	●	●	●	X
A0231	0	15	12	0	S	ND	●	●	●	●	●	X
A1202	10	15	0	3	NS	■	X	X	+	◆	X	■
A1203	10	15	0	3	S	■	+	X	+	+	+	■
A1232	10	15	12	3	NS	X	X	X	+	+	+	◆
A1233	10	15	12	3	S	X	X	+	+	+	+	X
A2200	20	15	0	0	NS	◆	◆	◆	+	X	●	◆
A2201	20	15	0	0	S	◆	◆	◆	+	◆	+	ND
A2232	20	15	12	3	NS	■	■	◆	●	◆	◆	■
A2233	20	15	12	3	S	■	■	■	+	◆	+	■
A3202	35	15	0	3	NS	◆	◆	◆	●	●	●	◆
A3203	35	15	0	3	S	◆	◆	ND	◆	●	ND	◆
A3230	35	15	12	0	NS	■	◆	●	●	◆	●	◆
A3231	35	15	12	0	S	◆	◆	◆	◆	◆	◆	◆

X STABLE
● BOTTOMED α
■ BOTTOMED ψ
+ FLIGHT TIME OUT, CAPSULE "WALKING"
◆ TIPPED
ND NO DATA, RUN TERMINATED DUE TO NON-CONVERGENCE IN SUP ROUTINE

B. ALIGHTMENT CONDITIONS

Sixteen combinations of initial conditions were used for each of the configurations. Some, such as pitch angle or horizontal velocity, have more influence on alightment gear design than, for example, roll rate. Each, however, can be the critical parameter for a certain combination of the other parameters.

1. Terrain Slope

Values of 0, 10, 20 and 35 degrees for terrain slope were used in an attempt to define upper limits for each of the configurations. For alightments into the slope (a negative slope in the tables), the leading leg bears the brunt of the initial contact and must either be capable of absorbing a large percentage of the system energy or be capable of turning the capsule to engage the other legs.

For the telescoping legs, upper limits on terrain slopes are dependent primarily on energy absorption capability. Referring to Table 1, configuration 1 shows improvement in slope handling capability when compared to configuration 0. Configuration 2, however, shows minimal improvement when compared to configuration 1. The latter illustrates the inability to achieve adequate turning of the capsule during alightment even though a 25 percent increase in righting moment was achieved by increasing the footprint diameter of the alightment system. A terrain slope is less severe than having the capsule inclined from the vertical. This is shown by comparing runs 01003 and 00021 in Table 2. Configuration 0 can handle a 10 degree slope but tumbles for an 8 degree inclination with no slope.

The articulated leg was thought to have the potential of handling slopes up to 35 degrees due to its large footprint diameter.

Sufficient energy absorption capability, however, was not available in the peg leg and for the bulk of the articulated configurations, the peg leg bottomed at slopes of 20 degrees or less. Detailed examination of the digital runs also indicated that an increase of about 20 percent in the footprint diameter should prove beneficial. Alightment into a slope was generally easier than alightment out of the slope. Comparing the results of Tables 3 and 4, it may be seen that into the slope alightments, up to 20 degrees, can be handled, whereas out of the slope alightments are generally limited to 10 degrees. Additional runs were made for configuration 5 and the forces in both the parallelogram and peg leg modified. To handle a 35 degree slope with a 12 degree capsule inclination it was necessary to decrease the parallelogram forces 10 percent and increase the peg leg forces by 50 percent. Neither energy cell bottoming nor capsule tumbling occurred for this set of forces. The results of twelve additional runs with special forces are shown at the bottom of Table 3.

For many of the alightments into the slopes, the articulated leg ended up "walking" down the slope. The capsule was in a stable position as far

as tumbling was concerned but due to rocking from one leg to another, "walked" down the slope. These simulation runs were terminated after 5 seconds of flight time with the capsule having moved down the slope as much as 200 feet along with an increase in down slope velocity.

2. Horizontal Velocity

Horizontal velocity is one of the more difficult parameters to handle unless skidding is used as the dissipative force. For this program, skidding was not a permissible means of absorbing horizontal energy. Of the total kinetic energy, a horizontal velocity of 15 feet per second contributes only 15.5 percent, yet the presence of a horizontal velocity greatly aggravates the leading leg energy absorption problem. During alightment, the capsule tends to pitch forward increasing the load on the leading leg. Values of 7.5, 10, and 15 feet per second were used in the parametric study. The relationship of the horizontal velocity vector and the capsule is shown in Figure 14.

In Table 2, configuration 0 can handle 7.5 feet per second for a flat alightment yet tumbles for a velocity of 10 feet per second (runs 00001 and 00101, respectively). Configurations 1 and 2 can both handle 10 feet per second and 15 feet per second (runs 10101, 20101, 10201, and 20201, respectively) for flat alightments yet horizontal velocity decreases the capability for handling capsule inclination from 8 degrees to 4 degrees for both configurations 1 and 2. (Runs 10121, 10211, 20121, and 20211, respectively.)

For the articulated leg configurations, a decrease in terrain slope handling capability occurs. Run numbers 53202X and 53102 in Table 3 show a capability for alighting on a 35 degree slope with a 10 foot per second horizontal velocity yet for 15 feet per second the peg leg bottoms. Similarly, for a capsule inclination of 12 degrees the peg leg bottoms at 15 feet per second and a stable alightment occurs at 10 feet per second. These are run numbers 50230X and 50130 in Table 3.

Horizontal velocity is one of the most critical parameters to be examined for stable alightment. As noted previously, it contributes only 15.5 percent of the total kinetic energy, yet can decrease the system alightment capability by 100 percent for other parameters. The magnitude of the horizontal velocity used for this study is relatively low, assuming it results from wind velocity. Fifteen feet per second corresponds to a wind velocity of about 10 miles per hour and should be considered a minimum value.

3. Pitch Angle

Pitch angle or capsule inclination is the angular position of the capsule vertical relative to the inertial vertical. Values of 0, 4, 8 and 12 degrees were used depending on the configuration being examined. The capsule was pitched in the direction of the horizontal velocity vector as shown in Figure 14.

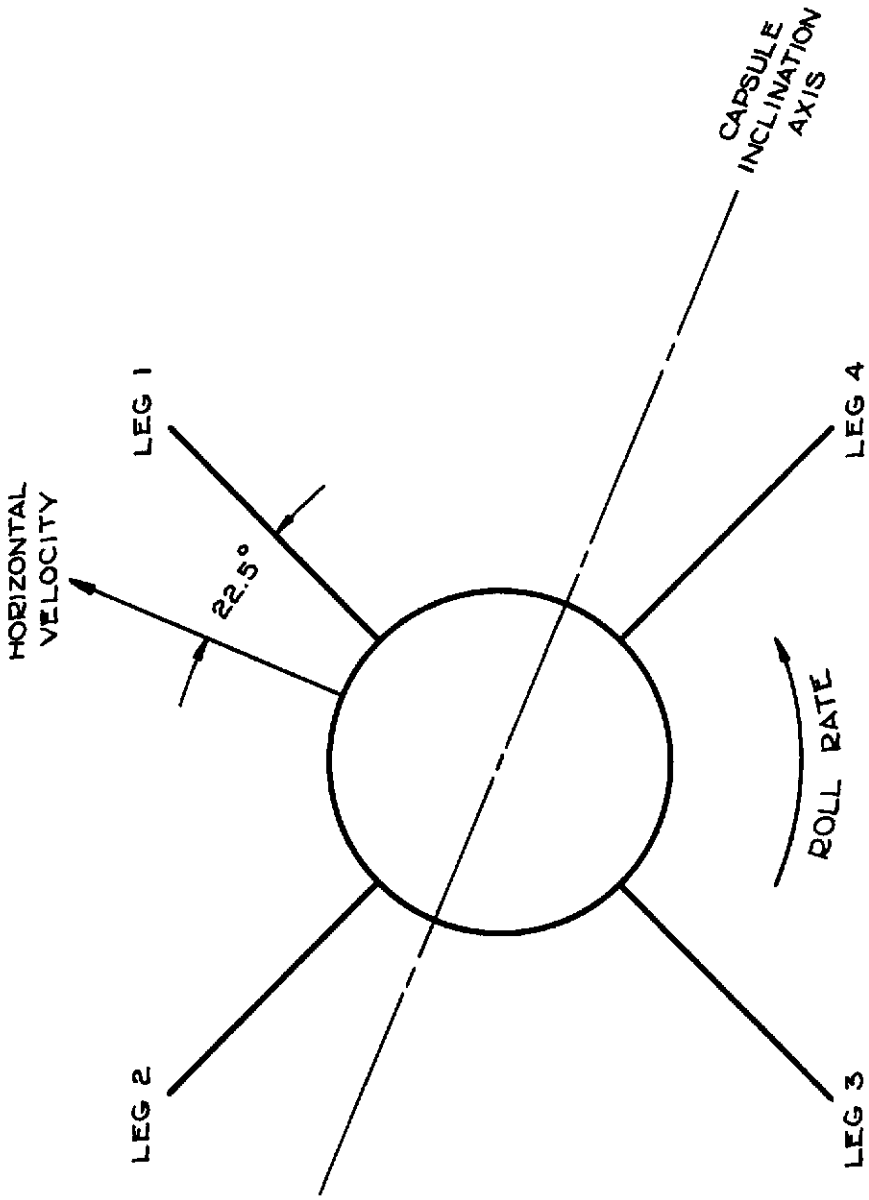

Figure 14 Capsule Orientation

The telescoping leg configurations used all four values with no stable alightments occurring for a 12 degree pitch angle. A pitch angle of 8 degrees was handled satisfactorily by configurations 1 and 2 for no terrain slope and a horizontal velocity of 10 feet per second, runs 10121 and 20121, for example, in Table 2. Configuration 0 was able to alight satisfactorily with a pitch angle of 4 degrees on a -10 degree slope (runs 01012 and 01011). For a given configuration, pitch angle is more difficult to handle than a terrain slope. Configuration 0, for example, handled a 10 degree slope with no pitch (run 01002) yet tipped for an 8 degree pitch with no slope (run 00021). Similarly, configurations 1 and 2 could handle an 8 degree pitch but not 12 degrees, yet could alight on a -20 degree slope (run numbers 10121, 20121, 12101, 22101, 10131 and 20131 in Table 2).

Configurations 3 through 8, the 3000 pound articulated system, were unable to handle a 12 degree pitch angle for any of the production run alightments in Table 3. For out of the slope alightments, configuration 6 performed the best, as shown in Table 4. Only configuration 9 was able to alight satisfactorily for no terrain slope and a pitch angle of 12 degrees.

The difficulties in handling a pitch angle as opposed to a terrain slope results from the change in angular position of the peg leg relative to the resultant velocity vector. When a pitch angle is introduced, the component of the resultant velocity vector that is normal to the peg leg is increased over that resulting from a zero pitch angle. Figure 3 in Section III illustrates this effect. In the same figure, it may be seen that a terrain slope is identical to a flat alightment as far as the relationship between peg leg and the resultant velocity vector.

4. Roll Rate

Capsule roll rates of 0 and 3 radians per second (rps) were used in the parametric study. Little effect is noted on alightment criteria unless a marginal alightment without a roll rate occurs.

The telescoping leg had no runs terminate due to the introduction of a roll rate. For some articulated leg runs, the 3 rps roll rate caused bottoming of the peg leg. The sense of the roll rate was chosen so that it added to the peg leg stroke resulting from horizontal velocity (Figure 14). Run number 51232, special force 4, in Table 3 results in bottoming of the peg leg. If the roll rate is 0, a stable alightment occurs. The stable alightment, however, results in a peg leg deflection that is almost bottomed (43 degrees versus 45 degrees). The introduction of the roll rate is then sufficient to cause bottoming. This illustrates the small increase in energy absorption capability required to adequately handle a roll rate of 3 rps. Sufficient runs were not made to determine the effect of a roll rate on capsule tumbling.

5. Roll Attitude

Roll attitude was fixed at 67.5 degrees for all of the runs summarized in Tables 2 and 3. This angle makes leg 1 the leading leg which is skewed 22.5 degrees from the horizontal velocity vector. This is illustrated in Figure 14. For all of the runs in Table 4 without capsule inclination, an impact with leg 2 leading was used. The horizontal velocity was directed outward along leg 2. For capsule inclination, the capsule's attitude was the same as for Tables 2 and 3.

C. PARALLELOGRAM/CAPSULE BODY INITIAL POSITION

Three initial positions of the parallelogram were used for the articulated leg. These are ψ's of -10, -15 and -20 degrees. As discussed in Section III.B, this initial position can strongly influence the tendency to bottom energy cells or tip the capsule.

Generally, a ψ of -10 degrees produces greater turning rates, tending to unload the leading leg, than a ψ of -15 or -20 degrees. This reduces the tendency to bottom the peg leg but increases potential bottoming of the parallelogram due to the decrease in stroking capability.

Tables 3 and 4 do not show a clear advantage or disadvantage for a particular ψ. Configurations 6 and 8 may be compared for the effect of decreasing ψ from -15 degrees to -10 degrees. A slight improvement in alightment capability is seen for -10 degrees. Configurations 5 and 7 may be compared for the effect of increasing ψ from -15 degrees to -20 degrees. Alightment capability is slightly decreased for an initial position of -20 degrees.

D. JERK[8] CONTROL

The effect of controlling jerk was examined in configurations 3, 4, and 5. Configuration 3 has decreased loading slopes on both types of energy cells and limited vertical jerk to 1000 jolts[9] for a flat alightment. Configuration 4 has a decreased loading slope on the peg leg cell to limit jerk to 1000 jolts. Configuration 5 has no jerk control and values of 10,000 to 15,000 jolts were obtained.

No effect on alightment capability is indicated in Table 3 for alightment into the slope. For alightments out of the slope (Table 4), the parallelogram

---

[8] Jerk is defined as the third time derivative of displacement.

[9] 1 g per second = 1 jolt.

energy cell bottoms in configuration 3 and does not for configurations 4 and 5 (runs 30200, 31202, 31203, 40200, 41202, 41203, 50200, 51202, and 51203).

Jerk control decreases the energy absorption capability of a given energy cell due to the force deflection curve deviating further from the ideal rectangular shape. The loss in energy absorption capability due to jerk control can be regained by increasing the stroking capability or by increasing the energy cell force toward the end of its stroke. Depending on the alightment system design, the introduction of jerk control may or may not result in a weight penalty. Jerk control in the articulated design is easily compensated for by increasing the energy cell forces toward the end of stroking. This could be accomplished by tapering or stepping the honeycomb. Due to the nonlinear force deflection characteristics, this increased loading produces small changes in the leg structural loadings.

E. SNUBBING ACTION

Snubbing of both parallelogram and peg leg energy cells was examined. Force deflection characteristics for the energy cells were modified so that after some initial stroking a second plateau was reached for the force. Appendix IV discusses the effect of snubbing action on structural loads for the articulated leg. Parallelogram snubbing was used for configuration 6. Comparing configurations 5 and 6 in Table 3 shows no improvement for alightments into a slope. Table 4 shows a marked improvement of configuration 6 over configuration 5. Configuration 6 was able to alight successfully on a 20 degree slope with a 12 degree capsule inclination while configuration 5 was limited to a 10 degree slope with a 12 degree capsule inclination.

A combination of peg leg snubbing and decreasing the parallelogram force was necessary to alight successfully on a 35 degree slope. The additional runs, shown in Table 3 for configuration 5, summarize the energy cell force characteristics used in obtaining successful alightments. Section III.B discusses design changes that could be made to the peg leg that would result in the same improvement in alightment capability without the need for increasing the peg leg energy cell force by 100 percent.

F. FOOT PAD/TERRAIN SLIPPAGE

A frictional model of the foot pad/terrain was used for the parametric study. A dynamic and static coefficient of friction was used and is discussed in detail in Section V.E.5. For the cases where slipping was permitted, the static coefficient was 1.5 and the dynamic coefficient was 1.0. For non-slip cases, values of 1.5×10^6 and 1.0×10^6 were used. The 35 degree slope dictated that a value of at least 0.7 be used for the dynamic coefficient of friction or the capsule would accelerate down the slope.

The occurrence of slippage at the foot pad/terrain interface is generally beneficial. As discussed earlier, horizontal energy is best dissipated through

sliding on a prepared surface yet was not permissible for this program. Local slippage was permissible and many times in the parametric study permitted a stable alightment when the non-slip case did not. The following run numbers illustrate the effect of slippage versus non-slippage.

In Table 2

10120, 10121

10210, 10211

10200, 10201

20210, 20211

In Table 3

82200X, 82201X

83202X, 83203X

In Table 4

30200, 30201

90200, 90201

71202, 71203

91232, 91233

82200, 82201

62232, 62233

82232, 82233

Slippage is especially beneficial for the peg leg and many energy cell bottomings may have been eliminated with a slightly different mathematical model in the digital simulation. This effect was discussed in Section III.B.3.

SECTION V

DIGITAL SIMULATIONS

A. GENERAL APPROACH

The alightment dynamics for this program were simulated in three dimensions on a large (32,768 words of memory) floating point digital computer. The space package is modeled as a six-degree-of-freedom rigid body with the alightment system (telescoping or articulated legs) generating the dynamic loads on the rigid body. The kinematics of the alightment system are used to generate the energy absorber stroke-time histories. The known load-stroke characteristics of the energy absorbers are then used to generate the alightment system force reactions (dynamic loads). The slippage of the alightment system foot pads with respect to the terrain is also simulated. This is based on a coefficient of friction mathematical model.

Numerical integration of the six rigid body accelerations yields the time-motion history of the space package. The numerical integration is performed under the control of a Runge-Kutta-Merson Differential Equation Monitor digital computer program. The digital simulation yields the acceleration, velocity, displacement, and load-time histories of the rigid body plus the displacement time history of the alightment system.

There exist two different simulations. Since both the articulated and telescoping leg configuration simulations were programmed and debugged intermittently, there is little interchangeability between potentially compatible portions of the simulations. The generation of the forcing functions is the one area in which the simulations are necessarily different.

B. COORDINATE SYSTEMS

The three-dimensional simulation of the space package alightment dynamics requires the establishment of several reference frames. These coordinate systems were also selected to facilitate the input of the initial conditions and the interpretation of the space package time-motion histories.

Three types of coordinate systems are used in the simulation. These are body fixed axes, body centered axes, and space fixed axes. A body fixed axes system is one which is fixed to some point on a rigid body and both translates and rotates with the point. A body centered axes system is one which translates with some point on a rigid body, but does not rotate about the point. A space fixed axes system is defined here to be a reference frame fixed relative to the earth. The coordinate systems used are illustrated in Figure 15.

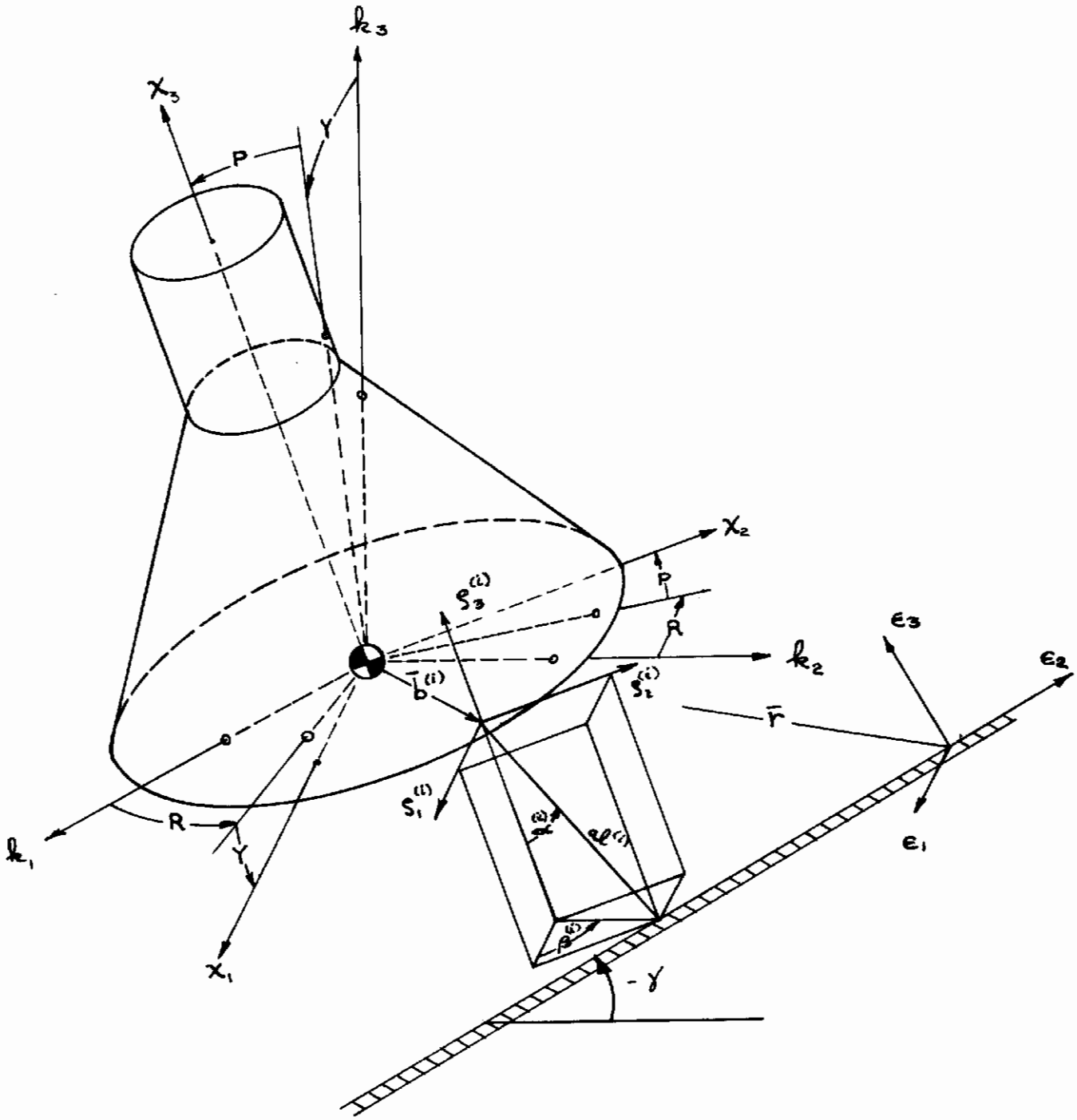

Figure 15: Coordinate Systems

A body fixed axes system is established at the center of gravity of the space package and aligned parallel to (or coincident with) the geometric axes of the space package. This coordinate system is referred to as the χ coordinate system. The χ coordinate system is used to reference the instantaneous angular accelerations ($\dot{\vec{\Omega}}$) and velocities ($\vec{\Omega}$), to reference the angular displacements (Φ , Ψ and Θ) and to describe the geometric locations of the alightment system on the space package ($\vec{b}^{(i)}$).

A body fixed coordinate system is established at the center of gravity of the space package and oriented in a manner so as to constitute the principal axes of inertia of the space package. These body fixed axes are referred to as the η coordinate system. The η coordinate system is used for the basic equations of rotational motion (Euler's dynamical equations for principal axes).

A body fixed coordinate system is established at each attachment location of the alightment system. These coordinate systems are referred to as the $\xi^{(i)}$ coordinate systems. The $\xi^{(i)}$ coordinate systems are used to describe the kinematics of the alightment system.

A set of body centered axes are located at the space package center of gravity with the 3 axis aligned parallel to the gravitational vector, the 2 axis in the horizontal direction, and the 1 axis out of the plane of the page. These are referred to as the ℓ coordinate system. The ℓ coordinate system is used to reference the angular displacements. The angular displacements are described by a set of roll, yaw and pitch angles which follow a 3-2-1 axes rotation from the χ body centered system to the ℓ body fixed coordinate system (Figure 15).

An inertial coordinate system is established with its origin in the plane of the terrain, its 3 axis normal to the plane of the terrain, and its 2 axis in the downhill direction for positive terrain slopes. The inertial coordinate system is referred to as the ϵ coordinate system. The ϵ coordinate system is used to describe the translational velocities and displacements of the space package center of gravity ($\dot{\vec{r}}$ and $\vec{r}$), and to generate contact criteria for the alightment system.

C. COORDINATE TRANSFORMATIONS

Transformations between the various coordinates are required for solution of the basic equations, computation of the forcing functions, and physical interpretation of the space package motions. The transformations given here relate the position of a point in the coordinate systems relative to the origins of the coordinate systems. The translation of the origins is accounted for by the displacement vector in one system which describes the position of the origin of the

other coordinate system. Four basic transformation matrices are required to permit total freedom of transformation among the coordinate systems.

All transformation matrices used here are orthogonal and, therefore, the inverse of any transformation matrix is merely equal to the transpose of the matrix (Reference 2). The following conventions are used throughout the report to denote transformation matrices.

$$\{\alpha\} = [\ell^{\alpha\beta}]\{\beta\}$$

The transformation from the k body centered to the ϵ local terrain inertial coordinate system is a single axis rotation about the negative ϵ_1 axis which is a function of the terrain slope (γ).

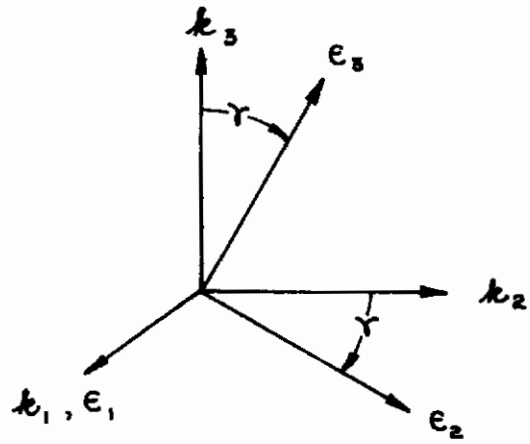

It can be seen that

$$[\ell^{\epsilon k}] = \begin{bmatrix} 1 & 0 & 0 \\ 0 & \cos\gamma & -\sin\gamma \\ 0 & \sin\gamma & \cos\gamma \end{bmatrix} \qquad (1)$$

The transformation between the η body fixed principal axes and the x geometric body fixed axes is determined by the solution of the eigenvalue problem formed by the moments and products of inertia about the x geometric axes. The three eigenvalues are the moments of inertia about the principal axes. The three eigenvectors form the transformation matrix $[\ell^{\eta x}]$.

The rigid body characteristics of a space package of a Mercury shaped capsule approximate a body of revolution with negligible cross products of inertia. Therefore, the principal axes of inertia are considered to be coincident with the geometric $\mathcal{X}$ body fixed axes. The transformation matrix is then a unit matrix for this special case.

The transformation from the $\mathcal{X}$ geometric body fixed axes to the $\mathcal{L}$ body centered axes is a function of the roll, yaw, and pitch angles as found in Reference 3, page 102. The roll, yaw, and pitch angles are the three successive rotations about the $\mathcal{X}_3$, $\mathcal{X}_2$, and $\mathcal{X}_1$ axes required to rotate the space package from the $\mathcal{L}$ body centered axes position to any arbitrary angular position.

$$\left[\ell^{\mathcal{L}\mathcal{X}}\right] = \begin{bmatrix} \cos R \cos Y & \cos R \sin Y \sin P - \sin R \cos P & \cos R \sin Y \cos P + \sin R \sin P \\ \sin R \cos Y & \sin R \sin Y \sin P + \cos R \cos P & \sin R \sin Y \cos P - \cos R \sin P \\ -\sin Y & \cos Y \sin P & \cos Y \cos P \end{bmatrix} \quad (2)$$

The dynamic loads are calculated in a set of local body fixed axes referred to as the $\mathcal{S}^{(i)}$ alightment system attachment coordinate system. The orientation of the i^{th} body fixed alightment system coordinate system with respect to the geometric body fixed axes is described by an input transformation matrix denoted as the i^{th} $\left[\ell^{\mathcal{X}\mathcal{S}^{(i)}}\right]$ matrix. Thus, it is to be noted that the orientation of each of the alightment system attachment coordinate systems is an externally controllable parameter.

The remainder of the transformation matrices which allow a transformation between any two coordinate systems are generated by the proper combination of the following four basic transformation matrices or their transposes:

$$\left[\ell^{\epsilon k}\right], \quad \left[\ell^{nx}\right], \quad \left[\ell^{kx}\right], \text{ and } \quad \left[\ell^{x s^{(i)}}\right]$$

For example, the transformation matrix from the directions of the local terrain inertial coordinate system ϵ to the i^{th} alightment system coordinate system $s^{(i)}$ is formed in this manner:

$$\left[\ell^{s^{(i)}\epsilon}\right] = \left[\ell^{\epsilon s^{(i)}}\right]^{T}$$

where

$$\left[\ell^{\epsilon s^{(i)}}\right] = \left[\ell^{\epsilon k}\right]\left[\ell^{kx}\right]\left[\ell^{x s^{(i)}}\right]$$

D. EQUATIONS OF RIGID BODY MOTION

The equations of rigid body motion are separable into the equations of translational motion and rotational motion.

1. Translational Equations of Motion

Newton's second law applied to the center of gravity of the rigid body and referenced to the inertial coordinate system (ϵ) is used to describe the translational accelerations. The acceleration due to gravity is directly accounted for in the translational acceleration equations.

$$\ddot{r}_1 = f_1/m \tag{3}$$

$$\ddot{r}_2 = g \sin\gamma + f_2/m \tag{4}$$

$$\ddot{r}_3 = -g \cos\gamma + f_3/m \tag{5}$$

where: $\ddot{r}_i$ = acceleration vector in the i^{th} direction of the ϵ inertial coordinate system

f_i = sum of the forces acting on the space package in the i^{th} direction of the ϵ inertial coordinate system

m = mass of the space package

g = acceleration of gravity

γ = terrain slope

2. Rotational Equations of Motion

Euler's dynamical equations for principal axes are used to describe the rotational accelerations about the η body fixed principal axes (Reference 4, page 113).

$$\dot{\omega}_1 = \left[M_1 - \omega_3 \omega_2 (C - B) \right] / A \tag{6}$$

$$\dot{\omega}_2 = \left[M_2 - \omega_1 \omega_3 (A - C) \right] / B \tag{7}$$

$$\dot{\omega}_3 = \left[M_3 - \omega_2 \omega_1 (B - A) \right] / C \tag{8}$$

where: $\dot{\omega}_i$ = angular acceleration about the i^{th} principal axis

ω_i = angular rate about the i^{th} η principal axis

M_i = sum of the moments about the i^{th} principal axis

A = mass moment of inertia about the η_1 principal axis

B = mass moment of inertia about the η_2 principal axis

C = mass moment of inertia about the η_3 principal axis

3. Numerical Integration of the Equations of Motion

The equations of motion are solved by numerical integration. The numerical integration technique used is a fourth order Runge-Kutta-Merson method which is based on a truncated Taylor series involving the first five terms. Thus, the error is of the fifth order of the integration increment of the independent variable time.

The Runge-Kutta-Merson numerical integration technique involves four evaluations (passes) of the dependent variables over each integration interval (Δt). The first and second passes evaluate the variables at a time of $t + \Delta t/3$, the third pass at $t + \Delta t/2$, and the fourth pass at $t + \Delta t$. The fourth pass yields the final values of the variables while the first, second, and third pass values of the variables are only approximations generated for use in the truncated series. The fourth pass values of the variables are then used as conditions from which to integrate to the next increment in time ($t + 2\Delta t$).

The translational equations of motion are integrated twice with respect to time to yield the translational displacement time history.

$$\int \ddot{r}_i \, dt = \dot{r}_i$$

$$\int \dot{r}_i \, dt = r_i$$

Euler's dynamical equations are integrated with respect to time to yield the instantaneous angular rates about the η principal axes of the rigid body.

$$\int \dot{\omega}_i \, dt = \omega_i$$

The angular rates $\vec{\omega}$ about the principal axes of the space package are then transformed to the χ geometric body fixed axes.

$$\{\Omega\} = [\ell^{\chi\eta}]\{\omega\}$$

The angular rates $\vec{\Omega}$ about the χ geometric body fixed axes are then transformed to the instantaneous roll, yaw, and pitch rates, $\dot{R}$, $\dot{Y}$ and $\dot{P}$, (Reference 3, page 103).

$$\dot{R} = \frac{1}{\cos Y}\left[\Omega_2 \sin P + \Omega_3 \cos P\right] \quad (9)$$

$$\dot{Y} = \Omega_2 \cos P - \Omega_3 \sin P \quad (10)$$

$$\dot{P} = \Omega_1 + \tan Y\left[\Omega_2 \sin P + \Omega_3 \cos P\right] \quad (11)$$

These equations are then integrated with respect to time to yield the roll, yaw, and pitch angles or rotational displacements of the space package.

$$\int \dot{R}\, dt = R$$

$$\int \dot{Y}\, dt = Y$$

$$\int \dot{P}\, dt = P$$

The above scheme generates the translational and rotational accelerations, velocities, and displacements of the space package as functions of the initial conditions and forcing functions.

4. Initial Conditions

The initial conditions at impact are read into the program in the most convenient physical reference systems. Certain of these initial conditions require transformation into other coordinate systems to generate the initial conditions for the equations of motion. The initial conditions consist of the translational and rotational displacements and velocities at the instant of contact of one or more foot pads of the alightment system with the terrain. The initial conditions are in the following forms.

The initial translational displacements are described by the three components of the translational displacement vector $\vec{r}$ in the local terrain inertial coordinate system e. The third component r_3 is adjusted by the digital program so that the instant of initial contact with the terrain occurs at time zero. This is done to insure the accuracy of the initial conditions.

The initial translational velocities $\vec{v}$ are described by the vertical v_3, (+ upward), the horizontal v_2, (+ downhill for positive terrain slopes), and the cross plane v_1, (+ out of the plane of the page) inertial components of the velocity vector. These three directions correspond to the directions of the body centered b coordinate system. The program will accept only a negative third component of the velocity.

The initial translational velocities must be expressed in the directions of the ϵ local terrain inertial coordinate system.

$$\{\dot{r}\} = [\ell^{\epsilon k}]\{V\}$$

The angular orientation of the space package at impact is described by the initial values of the roll, yaw, and pitch angles (R , Y and P) in degrees.

The initial rotational velocities $\vec{\Omega}$ are the angular rates about χ body fixed axes at the instant of impact. These are transformed in the simulation to generate the rates about the principal axes.

$$\{\omega\} = [\ell^{n\chi}]\{\Omega\}$$

5. Forcing Function Transformations

The forcing functions are generated by the FORCE subroutine structure in the $S^{(i)}$ alightment system coordinate systems. The dynamic loads are the forces $\vec{F}^{(i)}$ and the moments $\vec{m}^{(i)}$ acting at the body fixed location $\vec{b}^{(i)}$ with respect to the center of gravity of the space package. The dynamic loads must be transformed from their $S^{(i)}$ coordinate systems into the proper coordinate systems for use as the forcing functions ($\vec{f}$ and $\vec{M}$) in the equations of motion.

The three components of the force vector ($F_1^{(i)}$, $F_2^{(i)}$ and $F_3^{(i)}$) in each alightment system coordinate system($S^{(i)}$) must be transformed into the local terrain inertial coordinate system (ϵ). This is performed by first transforming $\vec{F}^{(i)}$ into the geometric body fixed axes (χ). These forces expressed in the χ geometric body fixed axes are denoted as $\vec{\sigma_\chi}^{(i)}$

$$\{\vec{\sigma_\chi}^{(i)}\} = [\ell^{\chi S^{(i)}}]\{\vec{F}^{(i)}\}$$

The forces ($\vec{\mathcal{F}}^{(i)}$) in the χ geometric body fixed axes at each alightment system attachment are then summed in each of the χ directions.

$$\vec{ff} = \sum_{i=1}^{n} \vec{\mathcal{F}}^{(i)}$$

The three force components ($\vec{ff}$) in the χ geometric body fixed axes are then transformed into the ϵ local terrain inertial coordinate system for use in the basic equations of translational motion (equations 3 through 5).

$$\{f\} = [\ell^{\epsilon\chi}]\{ff\}$$

The moments acting upon the space package must be resolved about the principal axes (η) for use in Euler's dynamical equations. There are two sources of moments which act about the η axes.

The dynamic load forces ($\vec{F}^{(i)}$) at each alightment system attachment point act through the attachment point lever arms to generate moments about the center of gravity of the space package. The attachment point lever arms $\vec{b}^{(i)}$ are in the geometric body fixed axes. Therefore, the transformed dynamic load forces in the χ system ($\vec{\mathcal{F}}^{(i)}$) can be directly used. These moments about the χ geometric body fixed axes when summed are denoted as $\vec{\mathcal{L}}$.

$$\vec{\mathcal{L}} = \sum_{i=1}^{n} \vec{b} \times \vec{\mathcal{F}}^{(i)}$$

or

$$\mathcal{L}_1 = \sum_{i=1}^{n} \left(b_2^{(i)} \mathcal{F}_3^{(i)} - b_3^{(i)} \mathcal{F}_2^{(i)} \right)$$

$$\mathcal{L}_2 = \sum_{i=1}^{n} \left(b_3^{(i)} \mathcal{F}_1^{(i)} - b_1^{(i)} \mathcal{F}_3^{(i)} \right)$$

$$\mathcal{L}_3 = \sum_{i=1}^{n} \left(b_1^{(i)} \mathcal{F}_2^{(i)} - b_2^{(i)} \mathcal{F}_1^{(i)} \right)$$

The dynamic load moments at the alightment system attachment points in the $S^{(z)}$ alightment system attachment coordinate systems are generated in the FORCE subroutine structure and denoted as $\vec{m}^{(z)}$. These moments are transformed into the x geometric body fixed axes by the $\left[\ell^{xs^{(z)}} \right]$ transformation matrices.

$$\left\{ YM^{(z)} \right\} = \left[\ell^{xp^{(z)}} \right] \left\{ m^{(z)} \right\}$$

The moments from the two sources ($\vec{L}$ and $\vec{YM}^{(z)}$) must be summed and transformed from the x geometric body fixed axes to the principal axes for use in the basic equations of rotational motion (equations 6 through 8).

$$\left\{ M \right\} = \left[\ell^{nx} \right] \left\{ L + \sum_{z=1}^{n} YM^{(z)} \right\}$$

6. Output Transformations

The output generated by the basic equations of motion are the translational accelerations, velocities, and displacements ($\ddot{\vec{r}}$, $\dot{\vec{r}}$, $\vec{r}$) in the local terrain inertial coordinate system (ϵ), the rotational accelerations and velocities ($\dot{\vec{\omega}}$ and $\vec{\omega}$) in the body fixed principal axes (η), and the rotational displacements (R , Y , and P) between the geometric body fixed axes (x) and the body centered axes (ℓ). It is desired to have the output data in the most convenient form for physical interpretation and comparison with experimental measurements. Any instrumentation which is attached to the space package will sense motion referenced in the directions of a moving body fixed axes system. The sensing axes of the instrumentation would generally be aligned in the geometric body fixed axes (x). Therefore, the translational accelerations, and the rotational velocities and accelerations would preferably be expressed in or about the geometric body fixed axes (x).

The instantaneous translational accelerations in the geometric body fixed axes (x) may be found by transforming the translational accelerations ($\ddot{\vec{r}}$) in the local terrain inertial coordinate system (ϵ) by the $\left[\ell^{x\epsilon} \right]$ transformation matrix.

$$\left\{ \ddot{\chi} \right\} = \left[\ell^{\chi e} \right] \left\{ \ddot{\vec{r}} \right\} = \left[\ell^{ex} \right]^T \left\{ \ddot{\vec{r}} \right\}$$

The angular velocities and accelerations in the geometric body fixed axes (χ) may be found by transforming the rotational velocities ($\vec{\omega}$) and accelerations ($\dot{\vec{\omega}}$) in the body fixed principal axes (η) by the transpose of the $\left[\ell^{\eta\chi} \right]$ transformation matrix.

$$\left\{ \Omega \right\} = \left[\ell^{\chi\eta} \right] \left\{ \omega \right\} = \left[\ell^{\eta\chi} \right]^T \left\{ \omega \right\}$$

$$\left\{ \dot{\Omega} \right\} = \left[\ell^{\chi\eta} \right] \left\{ \dot{\omega} \right\} = \left[\ell^{\eta\chi} \right]^T \left\{ \dot{\omega} \right\}$$

E. TELESCOPING LEG FORCING FUNCTIONS

The telescoping leg configuration and the articulated leg configuration forcing functions are derived in the same basic manner. However, since the geometries are quite different, the forcing function equations are quite different in their final form. The difference in the equations necessitated programming two nearly independent simulations. This difference also requires that the description of the forcing functions be separated into two sections. The telescoping leg forcing function description contains an entire description of the generation of the forcing functions for a specific geometric configuration. The description of the generation of the articulated leg forcing functions contains only the aspects which are not common to both configurations. This is done to avoid redundant descriptions.

1. Alightment System Position

The pertinent space package coordinate systems are shown in Figure 15. A spherical coordinate system is now introduced at each leg to describe the position of each foot pad with respect to the attachment location of each telescoping leg. The three spherical coordinates are the axial length of the simple leg $a\ell^{(i)}$, the rotational deflection angle $\alpha^{(i)}$ between the negative $S_3^{(i)}$ axis and the deflected longitudinal axis of the simple leg, and the angle $\beta^{(i)}$ which describes the direction of the rotational deflection measured parallel to the $S_1^{(i)} - S_2^{(i)}$ plane from the positive $S_1^{(i)}$ axis. These coordinates are illustrated in Figures 15 and 16.

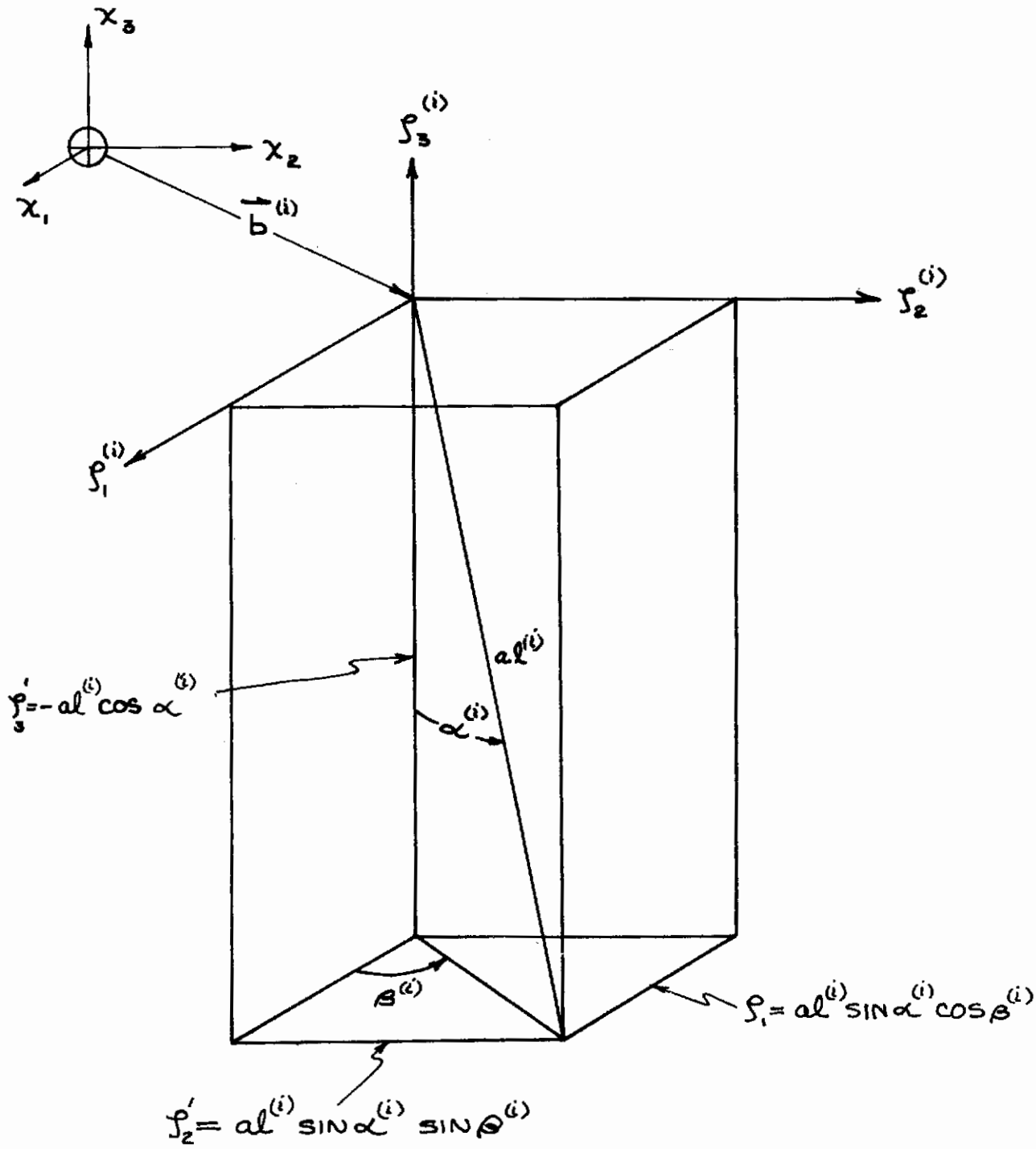

Figure 16: Alightment System Position Coordinates

For the simple leg configurations, it is convenient to select the orientation of all four $S^{(z)}$ alightment system attachment coordinate systems parallel to the geometric body fixed coordinate system χ. In other words, the transformation matrices from the $S^{(z)}$ alightment system attachment coordinate systems to the χ geometric body fixed axes $\left[\ell^{\chi S^{(z)}} \right]$ are all unity matrices.

The vector describing the unloaded position of the foot pad of the simple leg with respect to the attachment point is defined as $\vec{S}^{(z)}$. From Figure 16, it can be seen that this vector expressed in the $S^{(z)}$ absorber coordinate system is:

$$\left\{ S^{(z)} \right\} = \begin{Bmatrix} U\,al^{(z)} \sin U\alpha^{(z)} \cos U\beta^{(z)} \\ U\,al^{(z)} \sin U\alpha^{(z)} \sin U\beta^{(z)} \\ -U\,al^{(z)} \cos U\alpha^{(z)} \end{Bmatrix} \qquad (12)$$

where: $U\,al^{(z)}$ = unloaded axial length of the leg

$U\alpha^{(z)}$ = unloaded rotational deflection of the leg

$U\beta^{(z)}$ = unloaded rotational direction of the leg

Prior to initial contact of each leg with the ground, the unloaded axial length of the leg is defined as ρ. There is no rotational deflection $\alpha^{(z)}$ at this time and thus $\beta^{(z)}$ is undefined. The initial position vectors of all of the legs become:

$$\left\{ \rho''''^{(z)} \right\} = \begin{Bmatrix} 0 \\ 0 \\ -\rho \end{Bmatrix}$$

After contact with the ground has been made, the axial absorbers and certain of the rotational absorbers experience crushing or permanent deformation. Assuming that the frictional forces are of sufficient magnitude to allow

the leg to maintain its unloaded position without the presence of free play, the unloaded axial length is equal to the original length minus the permanent deformation of the axial absorber. The values of $U\alpha^{(i)}$ and $U\beta^{(i)}$ are approximated by the values of these variables immediately prior to loss of contact of the foot pad with the terrain. Thus, the unloaded position vector of the i^{th} leg becomes:

$$\vec{\vec{\vec{\vec{S}}}}^{(i)} = \begin{Bmatrix} (\rho - \Delta Z^{(i)}) \sin U\alpha^{(i)} \cos U\beta^{(i)} \\ (\rho - \Delta Z^{(i)}) \sin U\alpha^{(i)} \sin U\beta^{(i)} \\ -(\rho - \Delta Z^{(i)}) \cos U\alpha^{(i)} \end{Bmatrix} \qquad (13)$$

where:

$\Delta Z^{(i)}$ = permanent deflection of the i^{th} axial absorber

The position of the attachment point of the i^{th} alightment system referenced to the ϵ local terrain inertial coordinate system is defined as $\vec{\vec{S}}^{(i)}$ From Figure 17, it can be seen that this vector is obtained by vector addition of the $\vec{r}$ and $\vec{b}^{(i)}$ vectors after $\vec{b}^{(i)}$ is transformed from the directions of the X geometric body fixed axes to directions of the ϵ local terrain inertial coordinate system.

$$\left\{ \vec{\vec{S}}^{(i)} \right\} = \left\{ r \right\} + \left[\ell^{\epsilon X} \right] \left\{ b^{(i)} \right\} \qquad (14)$$

The position of the i^{th} foot pad expressed in the ϵ inertial coordinate system is defined as $\vec{\vec{\vec{S}}}^{(i)}$. When the i^{th} leg is not in contact with the ground, the unloaded position of the i^{th} foot pad as illustrated in Figure 17 is:

$$\left\{ \vec{\vec{\vec{S}}}^{(i)} \right\} = \left\{ \vec{\vec{S}}^{(i)} \right\} + \left\{ \vec{\vec{\vec{S}}}^{(i)} \right\} \qquad (15)$$

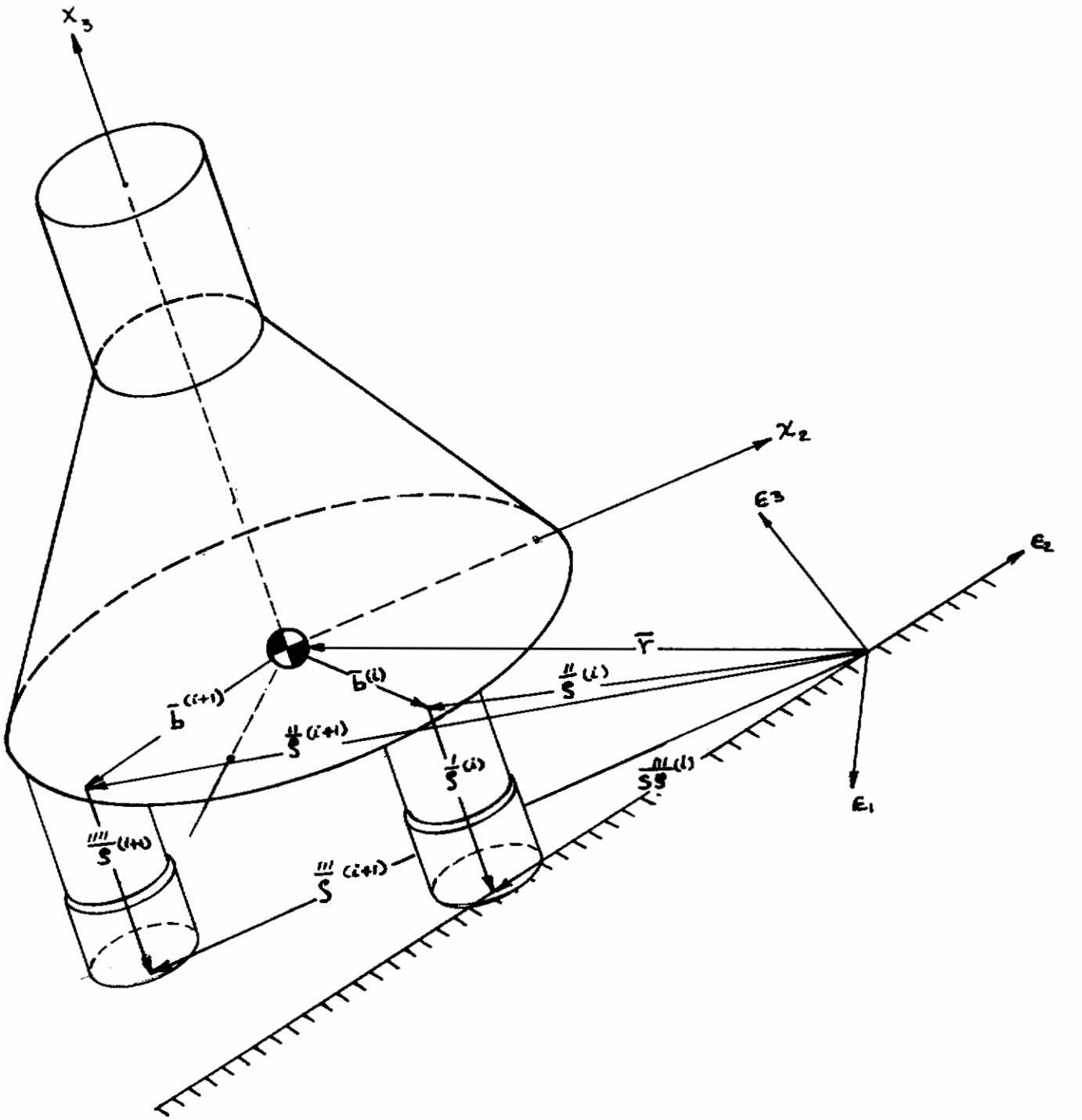

Figure 17: Position of the i^{th} Alightment System

The contact position of the i^{th} footpad is denoted as $\overrightarrow{SS}^{(i)}$. Contact with the terrain is detected when the third component of $\overrightarrow{S}^{(i)}$ (equation 15) changes from positive to negative on successive integration passes. The position of the footpad at this time is stored as the non-slip contact position. Loss of contact with the terrain occurs when the third component of $\overrightarrow{S}^{(i)}$ again becomes positive.

The deflection vector of the i^{th} leg is defined as $\overrightarrow{s}^{(i)}$. From Figure 17, it is seen that this quantity is obtained by vector subtraction of the position of the attachment point of the leg $\overrightarrow{S}^{(i)}$ from the contact position of the footpad $\overrightarrow{SS}^{(i)}$. It is convenient to transform the deflection vector into the absorber attachment coordinate system as illustrated in Figure 15.

$$\left\{ \vec{s}^{(i)} \right\} = \left[\ell^{s^{(i)}\epsilon} \right] \left\{ \overrightarrow{SS}^{(i)} - \vec{S}^{(i)} \right\} \tag{16}$$

From Figure 16, it can be seen that the spherical coordinates $\alpha^{(i)}$, $\beta^{(i)}$, and $al^{(i)}$ are the following functions of the $\vec{s}^{(i)}$ deflection vector of the i^{th} leg.

$$al^{(i)} = + \sqrt{\left(s_1'^{(i)}\right)^2 + \left(s_2'^{(i)}\right)^2 + \left(s_3'^{(i)}\right)^2} \tag{17}$$

$$\alpha^{(i)} = \cos^{-1}\left[\frac{-s_3'^{(i)}}{al^{(i)}}\right] \tag{18}$$

$$\beta^{(i)} = \tan^{-1}\left[\frac{s_2'^{(i)}}{s_1'^{(i)}}\right] \tag{19}$$

It should be noted that these equations imply the presence of certain characteristics. $\alpha^{(i)}$ is always positive and restricted to less than +90 degrees. $\beta^{(i)}$ is undefined when $\alpha^{(i)} = 0$. For the telescoping leg configurations, $\beta^{(i)}$ is set equal to zero when $\alpha^{(i)} = 0$. When $\alpha^{(i)}$ is not equal to zero, the quadrature of $\beta^{(i)}$ is preserved by use of the arctangent with the numerator and denominator separated.

2. Absorber Deflections and Velocities

The deflection of the i^{th} axial absorber is defined as $\Delta_1^{(i)}$. The subscript one denotes the axial absorber of the leg. The axial deflection is:

$$\Delta_1^{(i)} = \rho - a\ell^{(i)} \tag{20}$$

The deflection of the j^{th} rotational pad at the i^{th} leg is defined as $\Delta_j^{(i)}$ ($2 \leq j \leq 1$ + number of pads). Assuming that $\alpha^{(i)}$ is no greater than approximately 15 degrees, small angle approximations may be used (1.2 percent difference between $\alpha^{(i)}$ and $\sin \alpha^{(i)}$ at $\alpha^{(i)}$ = 15 degrees) in the rotational deflection equations. Figure 18 describes the geometry pertinent to the rotational absorber deflections. The rotation of the i^{th} leg through an angle $\alpha^{(i)}$ results in a deflection $\Delta_j^{(i)}$ at the j^{th} rotational pad located at the angular position γ_j.

$$\Delta_j^{(i)} = \left[a_6 \cos \left(\gamma_j - \beta^{(i)} \right) \right] \alpha^{(i)} \tag{21}$$

The velocity across the j^{th} absorber of the i^{th} leg is denoted as $\dot{\Delta}_j^{(i)}$. The velocities across the absorbers are not directly obtainable as functions of the rigid body velocities due to the slippage of the foot pads. The velocities are used only to compute dissipative forces. Therefore, sufficient accuracy in the computation of the velocities across the absorbers may be obtained by numerical differentiation of the deflections across the absorbers.

Since the values of the deflections on integration passes other than the fourth are only approximate, the following averaging method is used. Denote the deflection at any fourth integration pass as Δ, the deflection at the previous fourth integration pass as $P\Delta$, and the deflection at the fourth integration pass prior to that as $PP\Delta$. The average velocity during the previous integration interval was $(P\Delta - PP\Delta) / \Delta t$. The average velocity based on the present deflection and the deflection at the last fourth integration pass is $(\Delta - P\Delta) / (\Delta t / C)$, where $C = 3$ on the first and second integration passes, $C = 2$ on the third integration pass, and $C = 1$ on the fourth integration pass.

The velocity across the absorbers of the i^{th} leg is obtained by using a weighted average of the two velocities

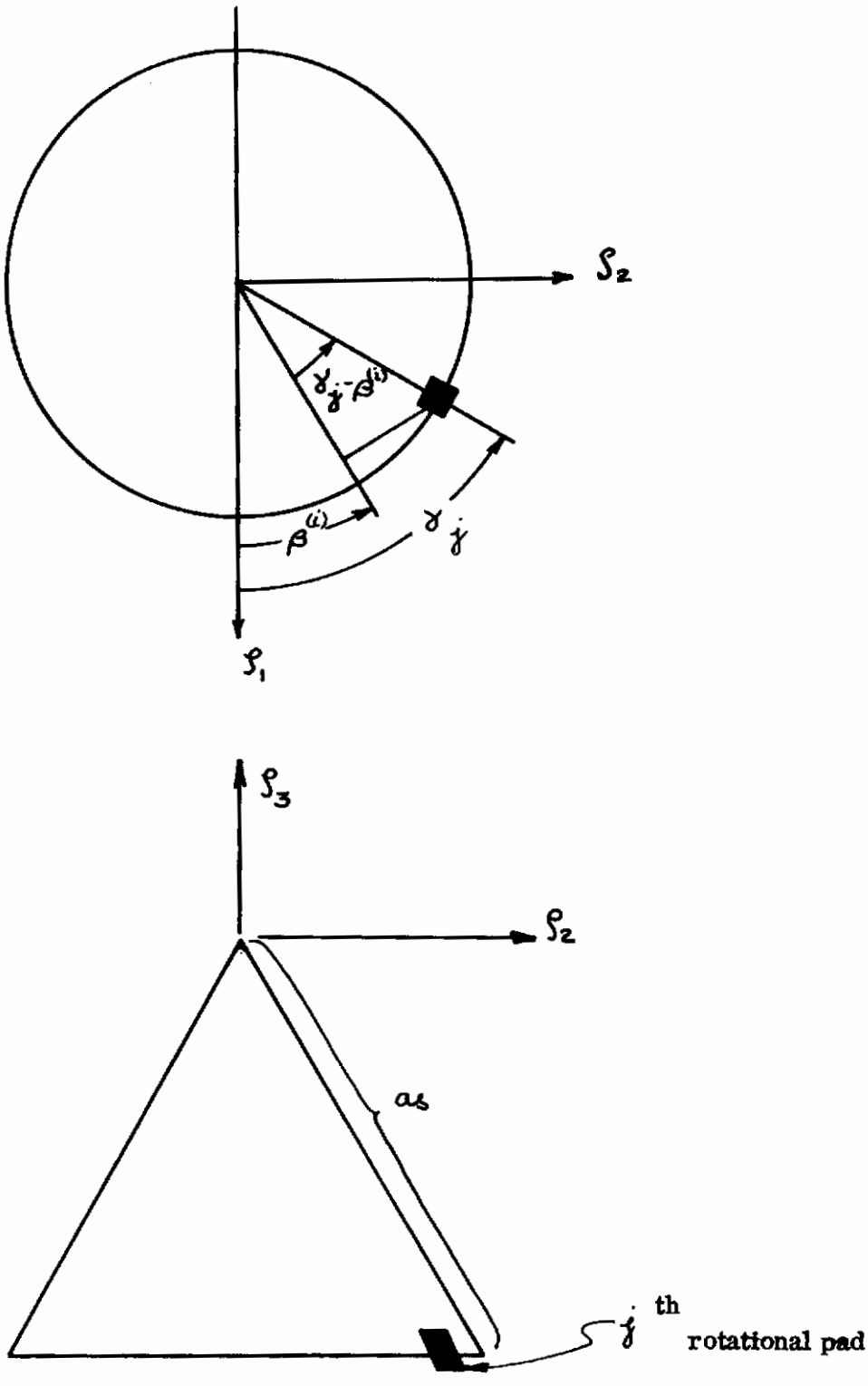

Figure 18: Rotational Absorber Geometry

$$\dot{\Delta}_j^{(2)} = \frac{\dfrac{C_{10}\left(\Delta_j^{(2)} - P\Delta_j^{(2)}\right)}{\Delta t / C} + \dfrac{C_{11}\left(P\Delta_j^{(2)} - PP\Delta_j^{(2)}\right)}{\Delta t}}{C_{10} + C_{11}} \qquad (22)$$

The weighting factors C_{10} and C_{11} are a function of the integration pass. The following weighting factors were selected. The two velocities are weighted equally ($C_{10} = C_{11} = 1$) on the first and second integration passes. The weighting factors are $C_{10}=2$ and $C_{11} = 1$ on the third integration pass. On the fourth integration pass only the velocity based on the present deflection and previous fourth integration pass is used ($C_{10} = 1$ and $C_{11} = 0$).

3. Energy Absorber Reaction Forces

The compressive reaction force across the i^{th} absorber of the j^{th} leg is defined as $AF_j^{(2)}$. The absorbers are crushable cells with reaction force characteristics which are a function of the deflection and velocity across the absorber, and the deflection history of the absorber. The characteristics of the cells fall into two distinct portions. The reaction force characteristics during the initial loading of the cell are referred to as the dynamic force deflection characteristics. The reaction force characteristics during unloading and reloading of the cell (short of the previous maximum deflection) are modeled with a parallel spring and damper. The dynamic force-deflection characteristics are described by a maximum of ten force-deflection points. The unloading-reloading model is described by a spring rate and a viscous damping coefficient. All of the axial absorbers have one set of characteristics and all of the rotational absorbers a second set of characteristics. Figure 19 illustrates a typical absorber force-deflection characteristic during a cycle of loading-unloading-reloading. The damper used in the unloading-reloading model produces a hysteresis loop about the spring characteristic. The damping force of the axial absorber is restricted to always be less in magnitude than the spring force to avoid discontinuities in the reaction forces.

The rotational absorber reaction force $AF_j^{(2)}$ is assumed to remain normal to the conical surface of the moving portion of the leg. The summation of the forces $AF_j^{(2)}$ produces a reaction moment with two components $M\alpha^{(2)}$ and $M\beta^{(2)}$ as illustrated in Figure 20.

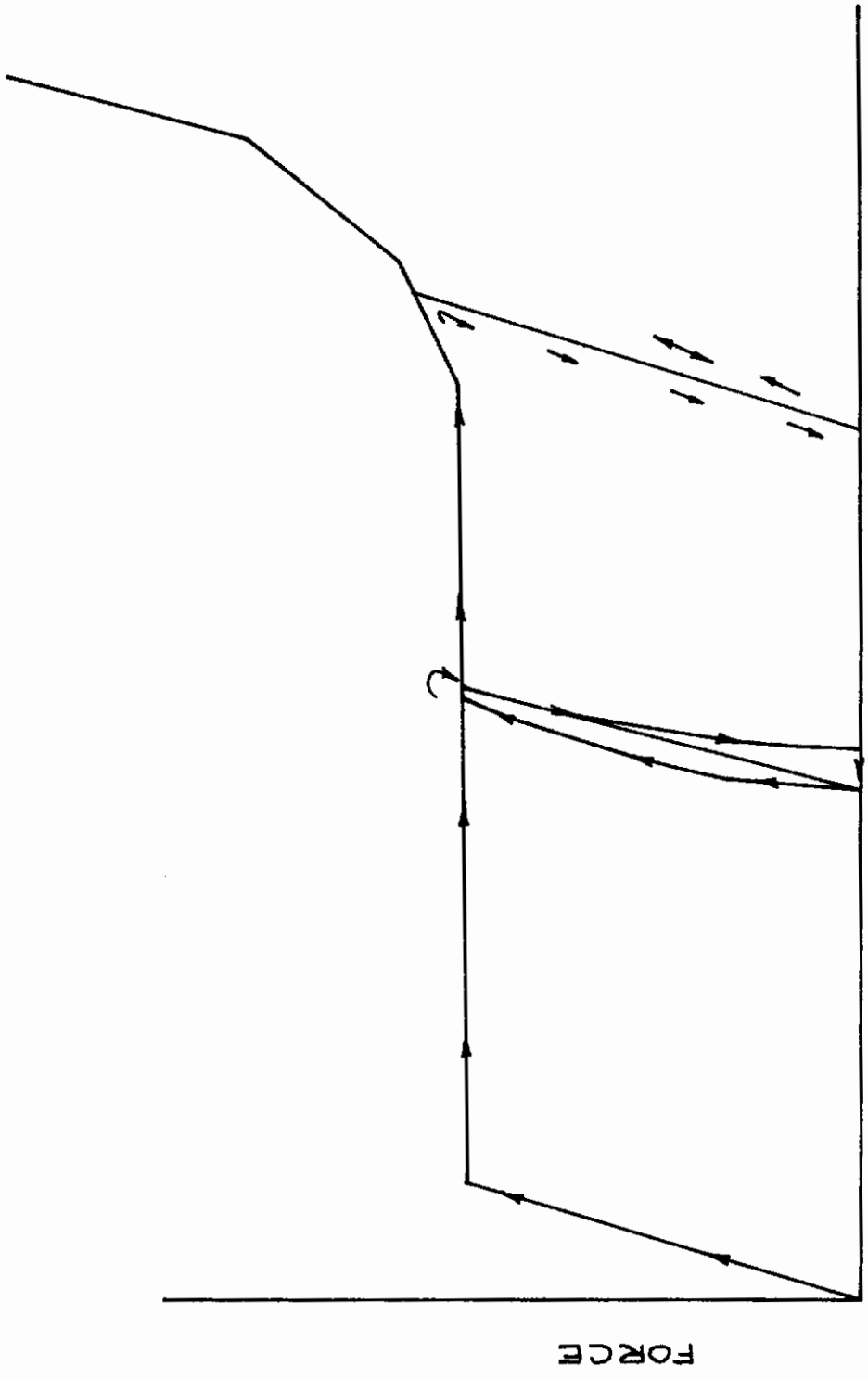

Figure 19: Typical Absorber Force-Deflection Curve

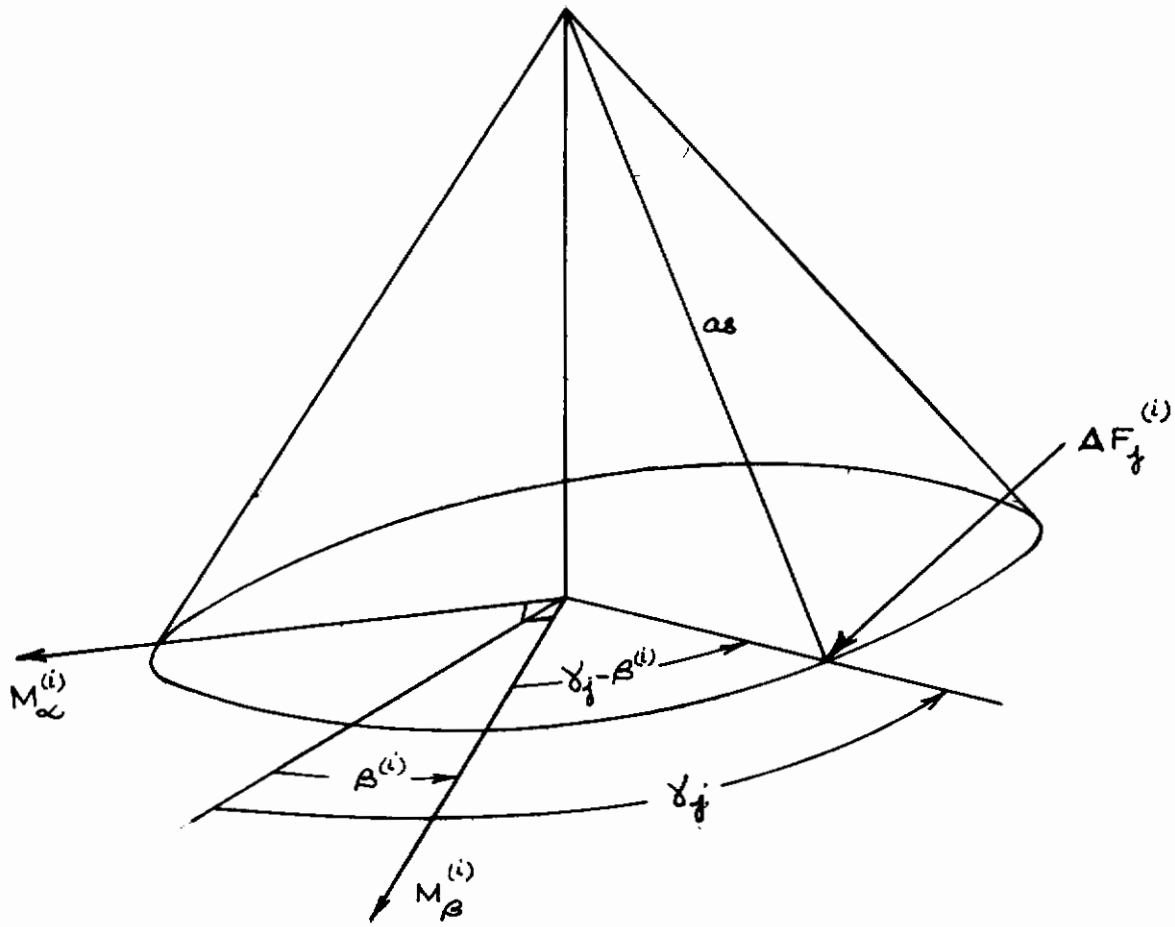

Figure 20: Rotational Absorber Reaction Moments

$$M\alpha^{(2)} = \sum_{J=2}^{1 + NO.PADS} \left[AF_J^{(2)} \, as \cos\left(\gamma_J - \beta^{(2)}\right) \right] \tag{23}$$

$$M\beta^{(2)} = \sum_{J=2}^{1 + NO.PADS} \left[AF_J^{(2)} \, as \sin\left(\gamma_J - \beta^{(2)}\right) \right] \tag{24}$$

4. Dynamic Loads

The absorber reaction forces when expressed in the body fixed absorber attachment coordinate system are denoted as the dynamic load forces $\vec{\mathcal{F}}^{(2)}$ and moments $\vec{\mathcal{M}}^{(2)}$. The absorber reactions $AF_1^{(2)}$, $M\alpha^{(2)}$, and $M\beta^{(2)}$ are expressible in the directions of the $S^{(2)}$ coordinate systems as illustrated in Figure 21. Let $F\alpha^{(2)}$ equal the force at the bottom of the leg producing the moment $M\alpha^{(2)}$ and $F\beta^{(2)}$ equal the force at the bottom of the leg producing the moment $M\beta^{(2)}$.

$$F\alpha^{(2)} = M\alpha^{(2)} / al^{(2)}$$

$$F\beta^{(2)} = M\beta^{(2)} / al^{(2)}$$

The forces $AF_1^{(2)}$, $F\alpha^{(2)}$, and $F\beta^{(2)}$ are expressible as the dynamic loads $\vec{\mathcal{F}}^{(2)}$ and $\vec{\mathcal{M}}^{(2)}$ in the $S^{(2)}$ coordinate system.

$$\mathcal{F}_1^{(2)} = -AF_1^{(2)} \sin\alpha^{(2)} \cos\beta^{(2)} + F\alpha^{(2)} \cos\alpha^{(2)} \cos\beta^{(2)} - F\beta^{(2)} \sin\beta^{(2)} \tag{25}$$

$$\mathcal{F}_2^{(2)} = -AF_1^{(2)} \sin\alpha^{(2)} \sin\beta^{(2)} + F\alpha^{(2)} \cos\alpha^{(2)} \sin\beta^{(2)} + F\beta^{(2)} \cos\beta^{(2)} \tag{26}$$

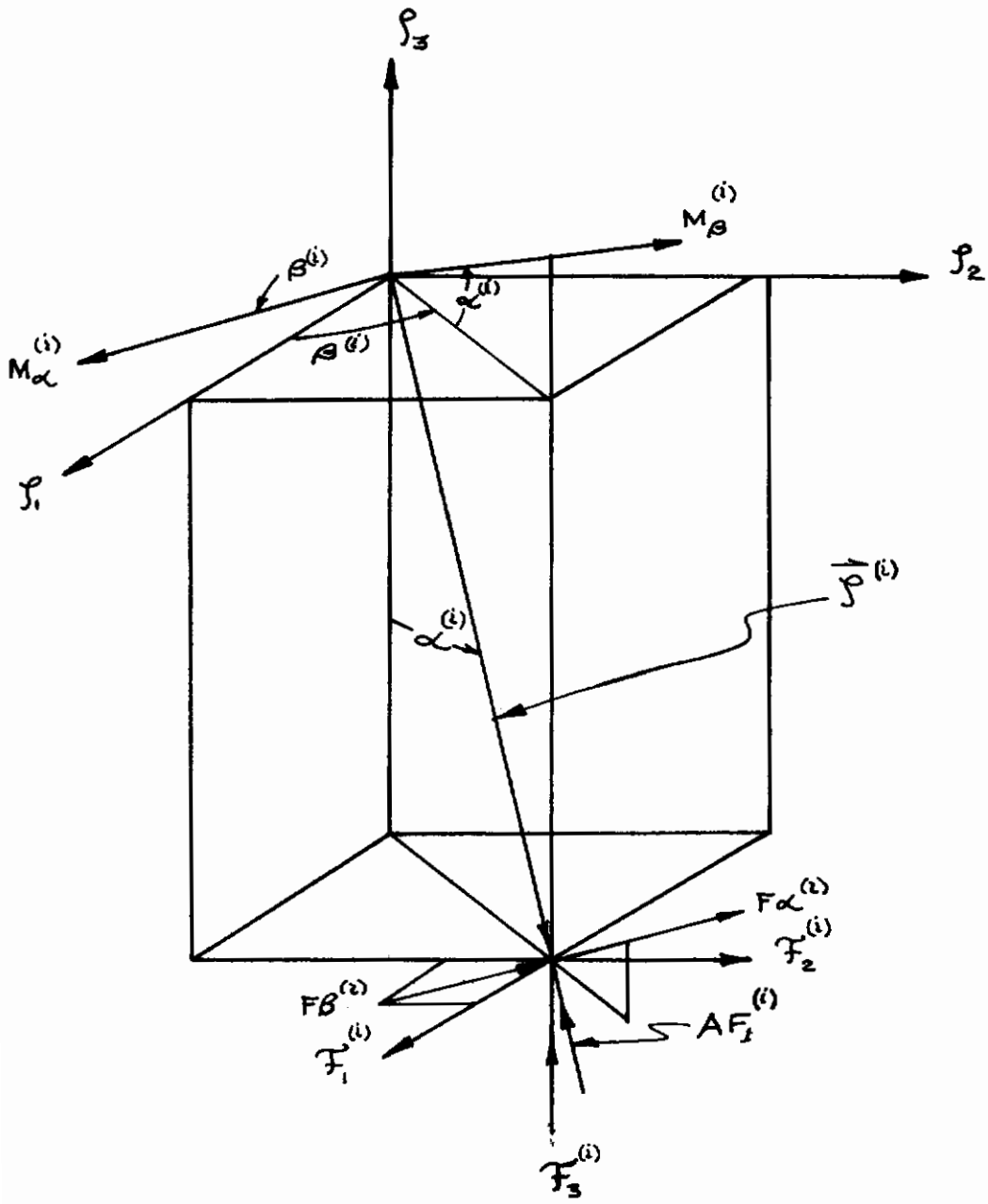

Figure 21: Absorber Reactions in the $\mathcal{S}^{(i)}$ Coordinate Systems

$$\mathcal{F}_3^{(2)} = AF_1^{(2)} \cos\alpha^{(2)} + F\alpha^{(2)} \sin\alpha^{(2)} \tag{27}$$

$$m_1^{(2)} = \mathcal{F}_3^{(2)} S_2'^{(2)} - \mathcal{F}_2^{(2)} S_3'^{(2)} \tag{28}$$

$$m_2^{(2)} = \mathcal{F}_1^{(2)} S_3'^{(2)} - \mathcal{F}_3^{(2)} S_1'^{(2)} \tag{29}$$

$$m_3^{(2)} = \mathcal{F}_2^{(2)} S_1'^{(2)} - \mathcal{F}_1^{(2)} S_2'^{(2)} \tag{30}$$

5. Sliding Forcing Functions

The digital simulation of the alightment dynamics includes the modeling of the sliding of the alightment system foot pads across the terrain. A coefficient of friction mathematical model is used. The forcing functions previously described require a knowledge of the position of the foot pad. The knowledge of the position of a foot pad is lost when sliding commences. The coefficient of friction model introduces force constraints which permit the determination of the sliding foot pad position and the accompanying dynamic loads. The foot pad position is adjusted until the ratio of the inplane ground reaction force to the normal force is equal to the coefficient of friction.

Since the foot pad will not slide if the inplane ground reaction is less than the product of the coefficient of friction and the normal ground reaction component, these quantities are first computed based on a non-slip foot pad position from the previous integration increment. The dynamic load forces $\mathcal{F}^{(2)}$ are expressed in the $S^{(2)}$ body fixed axes. Transforming these forces into the directions of the ϵ local terrain inertial system yields the normal and inplane ground reaction forces which are denoted as $\overrightarrow{F\epsilon}^{(2)}$.

$$\left\{\overrightarrow{F\epsilon}^{(2)}\right\} = \left[\ell^{\epsilon S^{(2)}}\right] \left\{\mathcal{F}^{(2)}\right\} \tag{31}$$

The third component of $\overrightarrow{F\epsilon}^{(2)}$ is the normal reaction force $F\epsilon_3^{(2)}$ exerted on the i^{th} leg by the terrain. The one and two components are the inplane reaction forces exerted on the leg by the terrain in the one and two directions of the ϵ local terrain system. The inplane force is denoted as $F\epsilon_{12}$.

$$FE_{12} = \sqrt{(FE_1^{(2)})^2 + (FE_2^{(2)})^2} \tag{32}$$

A distinction is made for most combinations of materials between the static and the dynamic coefficient of friction. A dynamic coefficient of friction is applicable when the leg is sliding (including recontact with the ground) and is denoted as μ_D. The static coefficient of friction is applicable when the leg is not sliding and is denoted as μ_S. Sliding will occur when the inplane force exceeds the potential frictional force $FF^{(2)}$.

$$FF^{(2)} = \mu_D \, FE_3^{(2)} \qquad \text{while sliding} \tag{33}$$

$$FF^{(2)} = \mu_S \, FE_3^{(2)} \qquad \text{while not sliding} \tag{34}$$

If the inplane force $FE_{12}^{(2)}$ is less than the applicable potential friction force $FF^{(2)}$, sliding is not occurring and the non-slip dynamic loads and foot pad positions computed at this point are applicable. If the inplane force $FE_{12}^{(2)}$ is greater than the applicable potential frictional force $FF^{(2)}$, slippage is occurring and dynamic loads and foot pad positions must be iterated upon.

The iteration is continued until the inplane force $FE_{12}^{(2)}$ converges on the potential frictional force $FF^{(2)}$. A convergence tolerance of 0.001 on the forces is maintained for 20 iterations. In general, convergence will occur within two to four iterations. In certain instances, such as when the leg is about to lift off the ground, the convergence is slow but definite. An additional ten iterations are then made at a temporarily reduced tolerance of 0.1. If convergence does not occur within the 30 iterations, the run is terminated unless the forces are small.

The sliding foot pad position is determined by varying the coordinate $\alpha^{(2)}$ until the force constraints are satisfied. The axial length $a\ell^{(2)}$ will also vary since the foot pad must remain in the plane of the terrain. This geometry coupling produces force coupling which necessitates the use of an iterative procedure. The coordinate $\alpha^{(2)}$ is varied until a set of bounds on the cross over point are located. The boundaries provide points from which to interpolate to determine the cross over point. The forces at the interpolated cross over point are then evaluated. This provides an improved boundary for the next iteration until the convergence criteria is satisfied. A plot of a typical situation appears as follows.

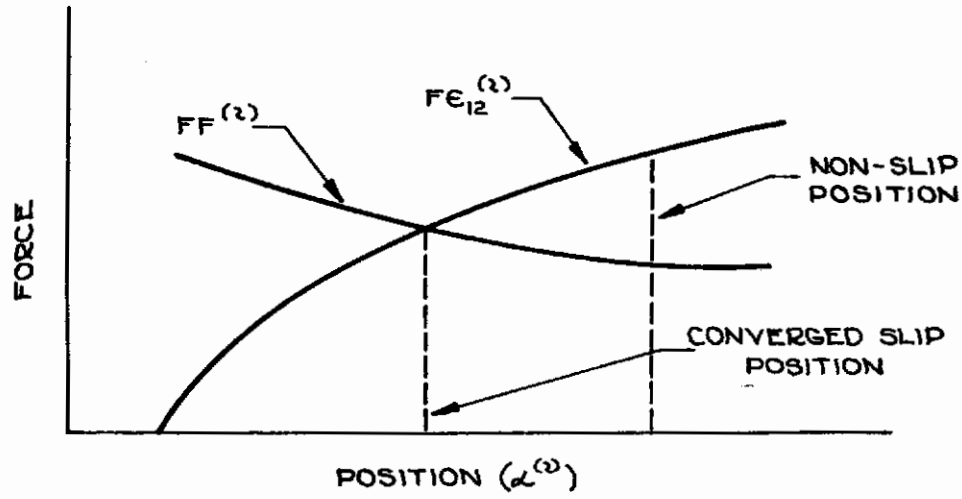

The axial length $\alpha l^{(2)}$ and the foot pad position in the plane of the terrain, $S''S_1^{(2)}$ and $S'''S_2^{(2)}$, for each $\alpha^{(2)}$ are needed in the iteration and are determined in the following manner.

The deflection vector equation (equation 16) relates the deflection vector and the foot pad position vector.

$$\left\{ S'^{(2)} \right\} = \left[l^{S^{(2)}E} \right] \left\{ SS'''^{(2)} - S''^{(2)} \right\} \tag{16}$$

New estimates of the first and second components of the deflection vector $\overrightarrow{S}^{(2)}$ and the third component of the foot pad position vector $S'''S_3^{(2)}$ are available for the above equations. Equation 16 may be rearranged to solve for the three remaining unknowns $S_3'^{(2)}$, $SS_1'''^{(2)}$, and $SS_2'''^{(2)}$. Let

$$\left\{ AR^{(2)} \right\} = - \begin{Bmatrix} S_1'^{(2)} \\ S_2'^{(2)} \\ 0 \end{Bmatrix} - \left[l^{S^{(2)}E} \right] \left\{ S''^{(2)} \right\}$$

and

$$\delta^{(2)} = l_{11}^{S^{(2)}E} \; l_{22}^{S^{(2)}E} - l_{12}^{S^{(2)}E} \; l_{21}^{S^{(2)}E}$$

The remaining three unknowns are:

$$SS_1^{'''(i)} = \frac{1}{\delta^{(i)}}\left(AR_2^{(i)}\, \ell_{12}^{s^{(i)}e} - AR_1^{(i)}\, \ell_{22}^{s^{(i)}e}\right) \tag{35}$$

$$SS_2^{'''(i)} = \frac{1}{\delta^{(i)}}\left(AR_1^{(i)}\, \ell_{21}^{s^{(i)}e} - AR_2^{(i)}\, \ell_{11}^{s^{(i)}e}\right) \tag{36}$$

$$S_3^{'(i)} = AR_3^{(i)} + \frac{AR_1^{(i)}}{\delta^{(i)}}\left(\ell_{21}^{s^{(i)}e}\, \ell_{32}^{s^{(i)}e} - \ell_{31}^{s^{(i)}e}\, \ell_{22}^{s^{(i)}e}\right)$$

$$- \frac{AR_2^{(i)}}{\delta^{(i)}}\left(\ell_{11}^{s^{(i)}e}\, \ell_{32}^{s^{(i)}e} - \ell_{31}^{s^{(i)}e}\, \ell_{21}^{s^{(i)}e}\right) \tag{37}$$

F. ARTICULATED LEG FORCING FUNCTIONS

The articulated leg configuration forcing functions are derived in the same basic manner as the telescoping leg forcing functions. The geometry of the articulated leg configuration involves three degrees of freedom as does the telescoping leg configuration geometry. However, the geometry is much different and no general approach was found which could eliminate the need for different forcing function equations.

1. Alightment System Position Vector

The geometry of the articulated leg alightment system is illustrated in Figure 22. The $S^{(i)}$ coordinate system is established with the origin at the midpoint of the axis of the lower attach point of each leg to reference the alightment system position and the absorber deflection. The three direction ($S_3^{(i)}$) is parallel to the longitudinal axis of the space package, the two direction ($S_2^{(i)}$) is the axis of rotation of the lower parallelogram member, and the positive one direction ($S_1^{(i)}$) is outward from the center of gravity of the space package.

The vector from the lower attach point to the foot pad of the i^{th} leg in the deflected position is denoted as $\overrightarrow{S}^{'(i)}$. The $\overrightarrow{S}^{'(i)}$ vector is described by the three independent quantities $\psi^{(i)}$, $\alpha^{(i)}$, and $\beta^{(i)}$ as illustrated

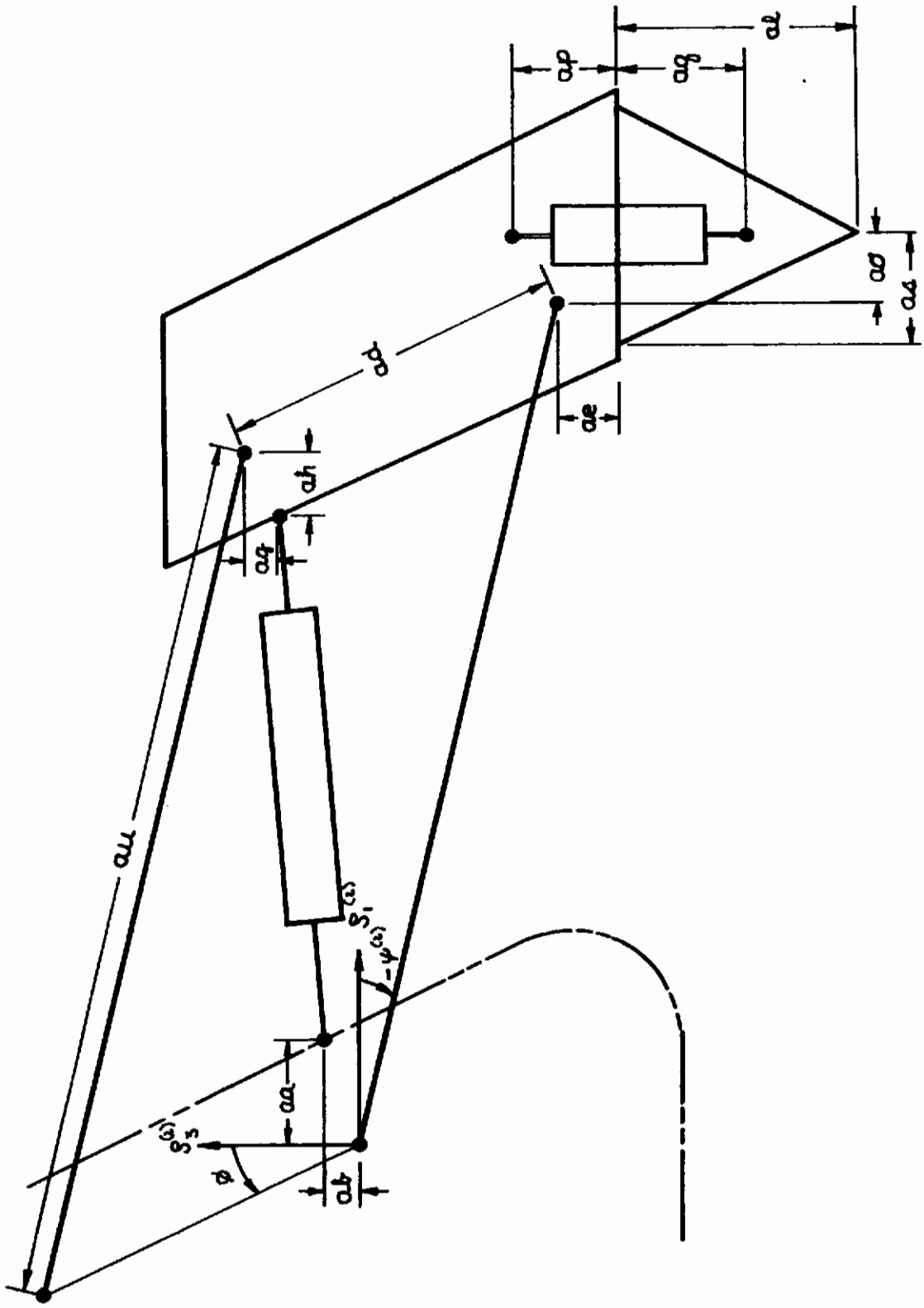

Figure 22: Articulated Leg Geometry

in Figures 22 and 23. $\psi^{(2)}$ is the angular position of the lower parallelogram member measured from the $S_1^{(2)}$ direction. $\alpha^{(2)}$ is the angular deflection of the lower leg relative to the negative $S_3^{(2)}$ direction and $\beta^{(2)}$ is the direction of this deflection relative to the $S_1^{(2)}$ direction as illustrated in Figure 23.

The deflected position vector of the i^{th} articulated leg, as a function of the geometric dimensions and the quantities $\alpha^{(2)}$, $\beta^{(2)}$, and $\psi^{(2)}$, is seen to be as follows:

$$S_1'^{(2)} = au\cos\psi^{(2)} + a\sigma + \left(as - as\cos\alpha^{(2)} + al\sin\alpha^{(2)}\right)\cos\beta^{(2)} \quad (38)$$

$$S_2'^{(2)} = \left(as - as\sin\alpha^{(2)} + al\cos\alpha^{(2)}\right)\sin\beta^{(2)} \quad (39)$$

$$S_3'^{(2)} = au\sin\psi^{(2)} - ae - as\sin\alpha - al\cos\alpha^{(2)} \quad (40)$$

To determine the absorber deflections, it is necessary to determine $\alpha^{(2)}$, $\beta^{(2)}$, and $\psi^{(2)}$ as a function of the geometric dimensions and the deflected position vector $\overrightarrow{S}^{(2)}$. Placing all the unknowns on the left side of the equation yields three simultaneous transcendental equations.

$$au\cos\psi^{(2)} + \left(as - as\cos\alpha^{(2)} + al\sin\alpha^{(2)}\right)\cos\beta^{(2)} = S_1'^{(2)} - a\sigma \quad (38)$$

$$\left(as - as\cos\alpha^{(2)} + al\sin\alpha^{(2)}\right)\sin\beta^{(2)} = S_2'^{(2)} \quad (39)$$

$$au\sin\psi^{(2)} - as\sin\alpha^{(2)} - al\cos\alpha^{(2)} = S_3'^{(2)} + ae \quad (40)$$

Solving for $\sin\beta^{(2)}$ in equation 39 yields:

$$\sin\beta^{(2)} = \frac{S_2'^{(2)}}{as - as\cos\alpha^{(2)} + al\sin\alpha^{(2)}}$$

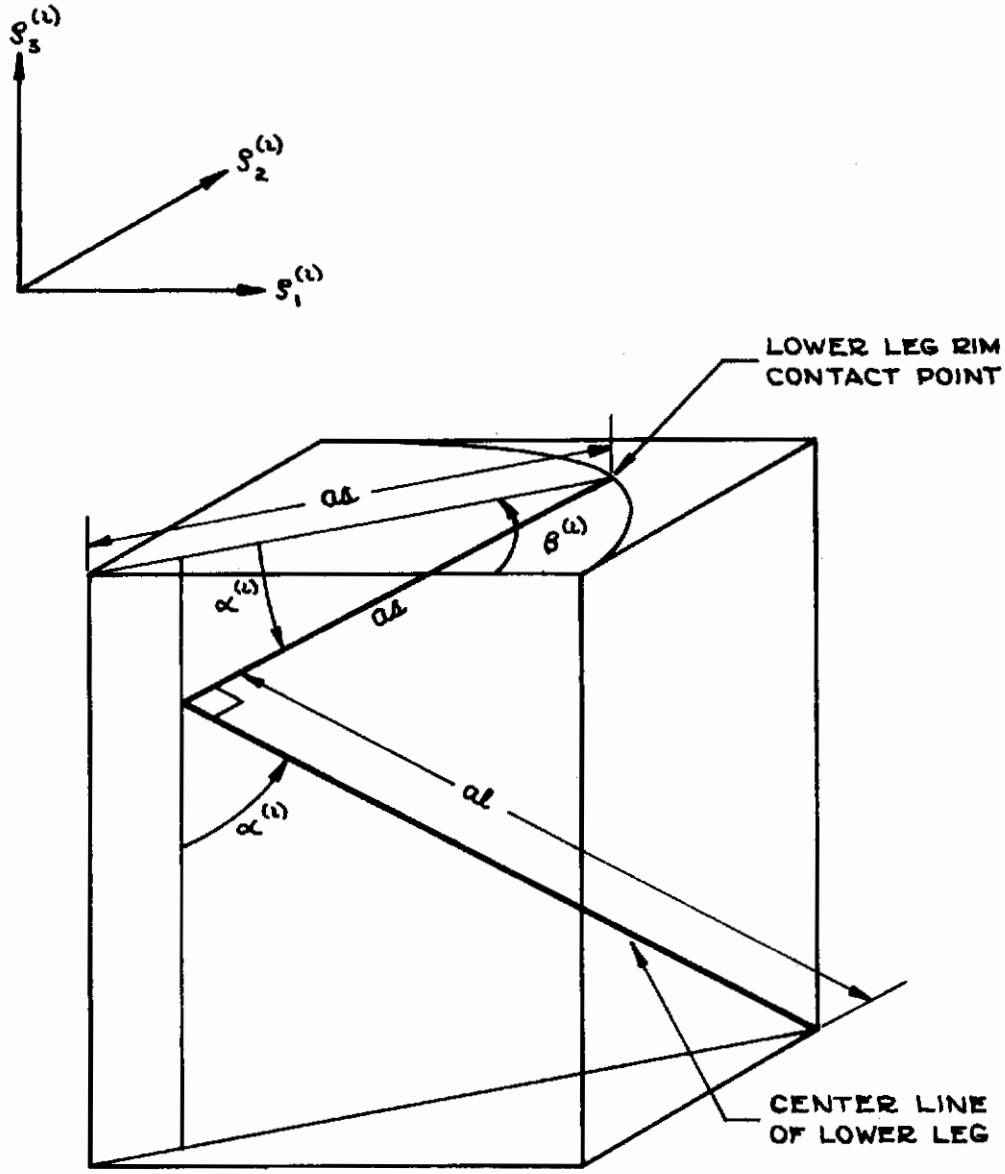

Figure 23: Lower Leg Geometry

Since:

$$\cos\beta^{(2)} = \pm\sqrt{1 - \sin^2\beta^{(2)}}$$

$$\cos\beta^{(2)} = \pm\sqrt{1 - \frac{\left(s_2'^{(2)}\right)^2}{\left(as - as\cos\alpha^{(2)} + al\sin\alpha^{(2)}\right)^2}}$$

$$\cos\beta^{(2)} = \pm\frac{\sqrt{\left(as - as\cos\alpha^{(2)} + al\sin\alpha^{(2)}\right)^2 - \left(s_2'^{(2)}\right)^2}}{as - as\cos\alpha^{(2)} + al\sin\alpha^{(2)}}$$

Solving for $\cos\beta'^{(2)}$ in equation 38 yields:

$$\cos\beta^{(2)} = \frac{s_1'^{(2)} - a\sigma - au\cos\psi^{(2)}}{as - as\cos\alpha^{(2)} + al\sin\alpha^{(2)}}$$

Equating these two identities for $\cos\beta^{(2)}$ and solving for $au\cos\psi^{(2)}$ yields:

$$au\cos\psi^{(2)} = a\sigma - s_1'^{(2)} \pm \sqrt{\left(as - as\cos\alpha^{(2)} + al\sin\alpha^{(2)}\right)^2 - \left(s_2'^{(2)}\right)^2}$$

Solving for $au\sin\psi^{(2)}$ in equation 40, squaring this equation and the above equation, and adding yields:

$$(a\sigma - s_1'^{(2)})^2 \pm 2(a\sigma - s_1'^{(2)})\sqrt{(as - as\cos\alpha^{(2)} + al\sin\alpha^{(2)})^2 - (s_2'^{(2)})^2}$$

$$+ (as - as\cos\alpha^{(2)} + al\sin\alpha^{(2)})^2 - (s_2'^{(2)})^2$$

$$+ (s_3'^{(2)} + ae + as\sin\alpha^{(2)} + al\cos\alpha^{(2)})^2 = au^2$$

Performing the multiplications indicated yields:

$$\pm 2(a\sigma - s_1'^{(2)})\sqrt{(as - as\cos\alpha^{(2)} + al\sin\alpha^{(2)})^2 - (s_2'^{(2)})^2}$$

$$+ as^2 + as^2\cos^2\alpha^{(2)} + al^2\sin^2\alpha^{(2)} - 2as^2\cos\alpha^{(2)} + 2as\,al\sin\alpha^{(2)}$$

$$- 2as\,al\sin\alpha^{(2)}\cos\alpha^{(2)} - (s_2'^{(2)})^2 + (s_3'^{(2)} + ae)^2 + as^2\sin^2\alpha^{(2)}$$

$$+ al^2\cos^2\alpha^{(2)} + 2(s_3'^{(2)} + ae)as\sin\alpha^{(2)} + 2(s_3'^{(2)} + ae)al\cos\alpha^{(2)}$$

$$+ 2as\,al\sin\alpha^{(2)}\cos\alpha^{(2)} + (a\sigma - s_1'^{(2)})^2 = au^2$$

Placing the radical on the right side of the equation yields:

$$\left[-2as^2 + 2(s_3'^{(2)} + ae)al\right]\cos\alpha^{(2)} + \left[2as\,al + 2(s_3'^{(2)} + ae)as\right]\sin\alpha^{(2)}$$

$$+ 2as^2 + al^2 - au^2 - (s_2'^{(2)})^2 + (s_3'^{(2)} + ae)^2 + (a\sigma - s_1'^{(2)})^2$$

$$= \mp 2(a\sigma - s_1'^{(2)})\sqrt{(as - as\cos\alpha^{(2)} + al\sin\alpha^{(2)})^2 - (s_2'^{(2)})^2}$$

Let the following substitutions be made to simplify the manipulations.

$$C_{16} = 2as\left(al + S_3^{\prime(2)} + ae\right)$$

$$C_{17} = 2\left[-as^2 + al\left(S_3^{\prime(2)} + ae\right)\right]$$

$$C_{18} = 2as^2 + al^2 - au^2 - \left(S_2^{\prime(2)}\right)^2 + \left(S_3^{\prime(2)} + ae\right)^2 + \left(ao - S_1^{\prime(2)}\right)^2$$

Squaring both sides of the equation yields:

$$C_{17}^2 \cos^2\alpha^{(2)} + C_{16}^2 \sin^2\alpha^{(2)} + C_{18}^2 + 2C_{16}C_{17}\sin\alpha^{(2)}\cos\alpha^{(2)}$$

$$+ 2C_{17}C_{18}\cos\alpha^{(2)} + 2C_{16}C_{18}\sin\alpha^{(2)}$$

$$= 4\left(ao - S_1^{\prime(2)}\right)^2\left[as^2 + as^2\cos^2\alpha^{(2)} + al^2\sin^2\alpha^{(2)} - \left(S_2^{\prime(2)}\right)^2\right.$$

$$- 2as^2\cos\alpha^{(2)} + 2as\,al\sin\alpha^{(2)}$$

$$\left. - 2as\,al\sin\alpha^{(2)}\cos\alpha^{(2)}\right]$$

Grouping like terms yields:

$$\left[C_{17}^2 - 4(a\sigma - S_1^{(2)})^2 as^2\right]\cos^2\alpha^{(2)} + \left[C_{16}^2 - 4(a\sigma - S_1'^{(2)})^2 al^2\right]\sin^2\alpha^{(2)}$$

$$+ \left[2C_{16}C_{17} + 8(a\sigma - S_1'^{(2)})^2 as\, al\right]\sin\alpha^{(2)}\cos\alpha^{(2)}$$

$$+ \left[2C_{17}C_{18} + 8(a\sigma - S_1'^{(2)})^2 as^2\right]\cos\alpha^{(2)}$$

$$+ \left[2C_{16}C_{18} - 8(a\sigma - S_1'^{(2)})^2 as\, al\right]\sin\alpha^{(2)}$$

$$= -C_{18}^2 + 4(a\sigma - S_1'^{(2)})^2\left[as^2 - (S_2'^{(2)})^2\right]$$

Let the following substitutions be made.

$$C_{19} = C_{17}^2 - 4(a\sigma - S_1'^{(2)})^2 as^2$$

$$C_{20} = C_{16}^2 - 4(a\sigma - S_1'^{(2)})^2 al^2$$

$$C_{21} = 2C_{16}C_{17} + 8(a\sigma - S_1'^{(2)})^2 as\, al$$

$$C_{22} = 2C_{16}C_{18} - 8(a\sigma - S_1'^{(2)})^2 as\, al$$

$$C_{23} = 2C_{17}C_{18} + 8(a\sigma - S_1'^{(2)})^2 as^2$$

$$C_{24} = -C_{18}^2 + 4(a\sigma - S_1'^{(2)})^2\left[as^2 - (S_2'^{(2)})^2\right]$$

Make the substitution $\cos\alpha^{(2)} = \pm\sqrt{1 - \sin^2\alpha^{(2)}}$

$$C_{19}\left(1 - \sin^2\alpha^{(1)}\right) + C_{20}\sin^2\alpha^{(1)} \pm C_{21}\sin\alpha^{(2)}\sqrt{1 - \sin^2\alpha^{(2)}}$$

$$+ C_{22}\sin\alpha^{(2)} \pm C_{23}\sqrt{1 - \sin^2\alpha^{(2)}} = C_{24}$$

Placing the radical products on the right side of the equation yields:

$$\left(C_{20} - C_{19}\right)\sin^2\alpha^{(2)} + C_{22}\sin\alpha^{(2)} + C_{19} - C_{24}$$

$$= \mp\left(C_{21}\sin\alpha^{(2)} + C_{23}\right)\sqrt{1 - \sin^2\alpha^{(2)}}$$

Squaring both sides of this equation yields a quartic in $\sin\alpha^{(2)}$.

$$\left[\left(C_{20} - C_{19}\right)^2 + C_{21}^2\right]\sin^4\alpha^{(2)} + \left[2\left(C_{20} - C_{19}\right)C_{22} + 2C_{21}C_{23}\right]\sin^3\alpha^{(2)}$$

$$+ \left[C_{22}^2 - C_{21}^2 + C_{23}^2 + 2\left(C_{20} - C_{19}\right)\left(C_{19} - C_{24}\right)\right]\sin^2\alpha^{(2)}$$

$$+ \left[2C_{22}\left(C_{19} - C_{24}\right) - 2C_{21}C_{23}\right]\sin\alpha^{(2)} + \left[\left(C_{19} - C_{24}\right)^2 - C_{23}^2\right]$$

$$= 0 = G\left(\sin\alpha^{(2)}\right) \qquad (41)$$

The quartic (equation 41) is most conveniently solved by Newton's method. The value of $\sin\alpha^{(2)}$ during the previous integration is an excellent first estimate of the present value of $\sin\alpha^{(2)}$. Let the previous root be $\sin\alpha_o^{(2)}$, the value of the polynomial evaluated for this root be $G\left(\sin\alpha_o^{(2)}\right)$, and the derivative of the polynomial evaluated for the previous

root be $G' \sin \alpha_o^{(2)}$. The estimate of the present root of the quartic is therefore:

$$\alpha^{(2)} = \sin^{-1}\left[\sin\alpha_o^{(2)} - \frac{G(\sin\alpha_o^{(2)})}{G'(\sin\alpha_o^{(2)})}\right], \quad 0 \leq \alpha^{(2)} \leq \frac{\pi}{2} \qquad (42)$$

The use of Newton's method avoids the necessity for the solution of the three remaining roots of the quartic and selection of the proper root.

The value of $\psi^{(2)}$ is found from equation 40.

$$\psi^{(2)} = \sin^{-1}\left[\frac{S_3'^{(2)} + ae + a_6 \sin\alpha^{(2)} + a_1 \cos\alpha^{(2)}}{a_4}\right], -\frac{\pi}{2} \leq \psi^{(2)} \leq \frac{\pi}{2} \qquad (43)$$

The value of $\beta^{(2)}$ is found by solving for $\sin\beta^{(2)}$ and $\cos\beta^{(2)}$ in equations 39 and 38 respectively, and dividing equation 39 by the equation 38.

$$\beta^{(2)} = \tan^{-1}\left[\frac{S_2'^{(2)}}{S_1'^{(2)} - a_0 - a_4 \cos\psi^{(2)}}\right], \quad 0 \leq \beta^{(2)} \leq 2\pi \qquad (44)$$

Occasionally, the roots of the quartic in $\sin\alpha^{(2)}$ will cross. In this instance, it is possible to follow the wrong root out of the crossing. The use of the wrong root is detected eventually when the equation for $\psi^{(2)}$ becomes undefined. The presence of this condition can be detected rapidly after the cross over by reforming the original vector $S'^{(2)}$ which is, of course, a function of $\alpha^{(2)}$, $\beta^{(2)}$, and $\psi^{(2)}$. A tolerance of 10^{-7} is used to compare the reformed vector to the original vector. If the tolerance is exceeded, the erroneous root is suppressed from the equations by synthetic division of the quartic. The proper root is then determined by Newton's method applied to the resulting cubic equation in $\sin\alpha^{(i)}$.

2. Energy Absorber Deflections and Velocities

The deflection across the upper absorber of the i^{th} leg is denoted as $\Delta_1^{(2)}$. The geometry pertinent to the upper absorber is illustrated in Figure 24.

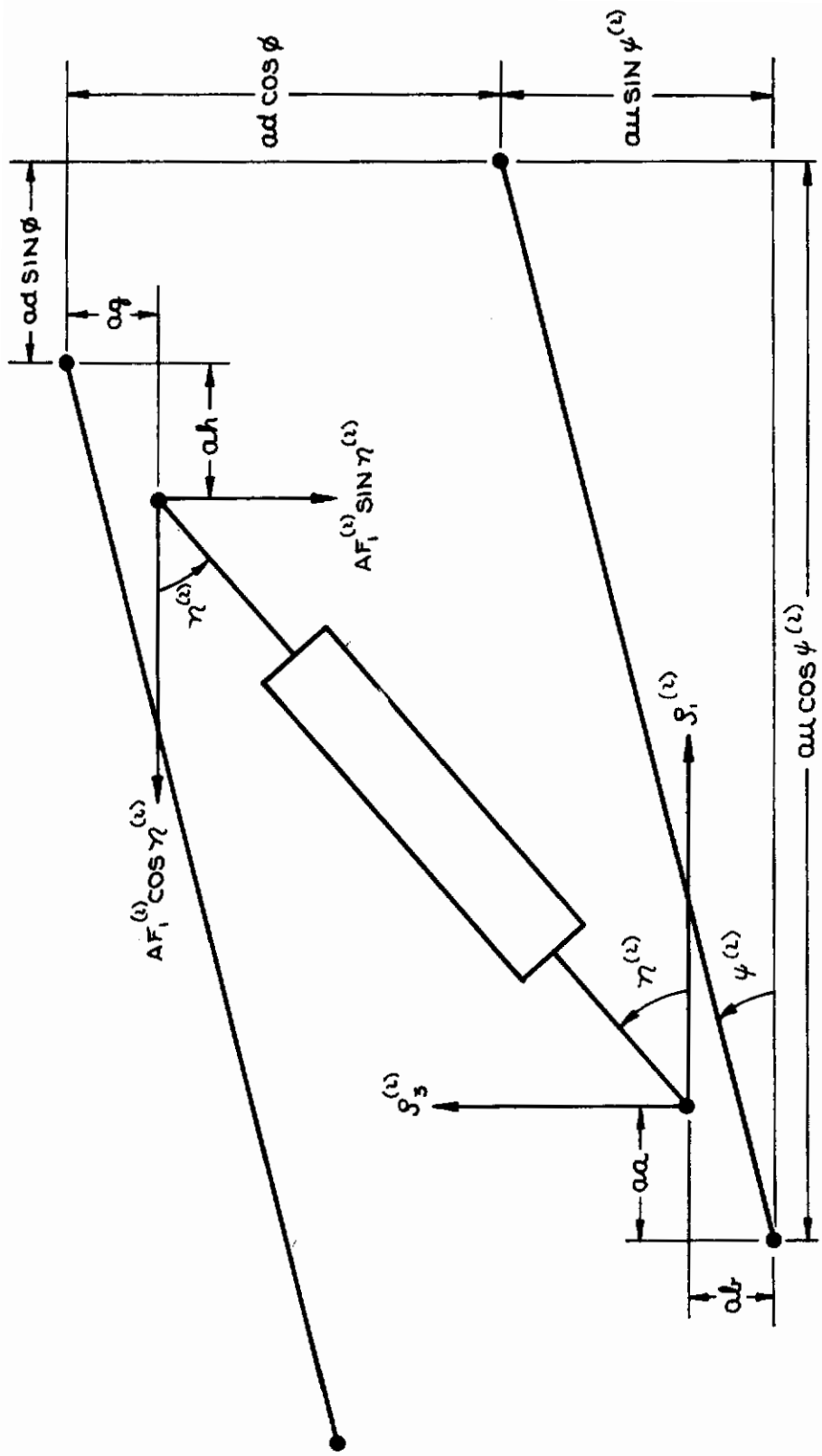

Figure 24: Upper Absorber Geometry

The length across the upper absorber $\vec{St}^{(2)}$ is described by the two components in the $S_1^{(2)}$ and $S_2^{(2)}$ directions.

$$\left\{St^{(2)}\right\} = \begin{Bmatrix} au\cos\psi^{(2)} - ad\sin\phi - aa - ah \\ 0 \\ au\sin\psi^{(2)} + ad\cos\phi - ab - ag \end{Bmatrix} \tag{45}$$

The length across the upper absorber is therefore:

$$\left|St^{(2)}\right| = \left[\left(au\cos\psi^{(2)} - ad\sin\phi - aa - ah\right)^2 + \left(au\sin\psi^{(2)} + ad\cos\phi - ab - ag\right)^2\right]^{1/2}$$

Let $\rho^{(2)}$ be the original undeflected length across the upper absorber. The deflection across the upper absorber is therefore:

$$\Delta_1^{(2)} = \left|St^{(2)}\right| - \rho^{(2)} \tag{46}$$

The deflection across the lower absorber of the i^{th} leg is denoted as $\Delta_2^{(2)}$. The geometry pertinent to the lower absorber is illustrated in Figure 25. The position of the lower end of the lower absorber $\vec{S_2}^{(2)}$ relative to the upper end is seen to be:

$$\left\{S_2^{(2)}\right\} = \begin{Bmatrix} (as - as\cos\alpha^{(2)} + ag\sin\alpha^{(2)})\cos\beta^{(2)} \\ (as - as\cos\alpha^{(2)} + ag\sin\alpha^{(2)})\sin\beta^{(2)} \\ -ap - as\sin\alpha^{(2)} - ag\cos\alpha^{(2)} \end{Bmatrix} \tag{47}$$

The length across the lower absorber is therefore:

$$\left|S_2^{(2)}\right| = \left[\left(as - as\cos\alpha^{(2)} + ag\sin\alpha^{(2)}\right)^2 + \left(-ap - as\sin\alpha^{(2)} - ag\cos\alpha^{(2)}\right)^2\right]^{1/2}$$

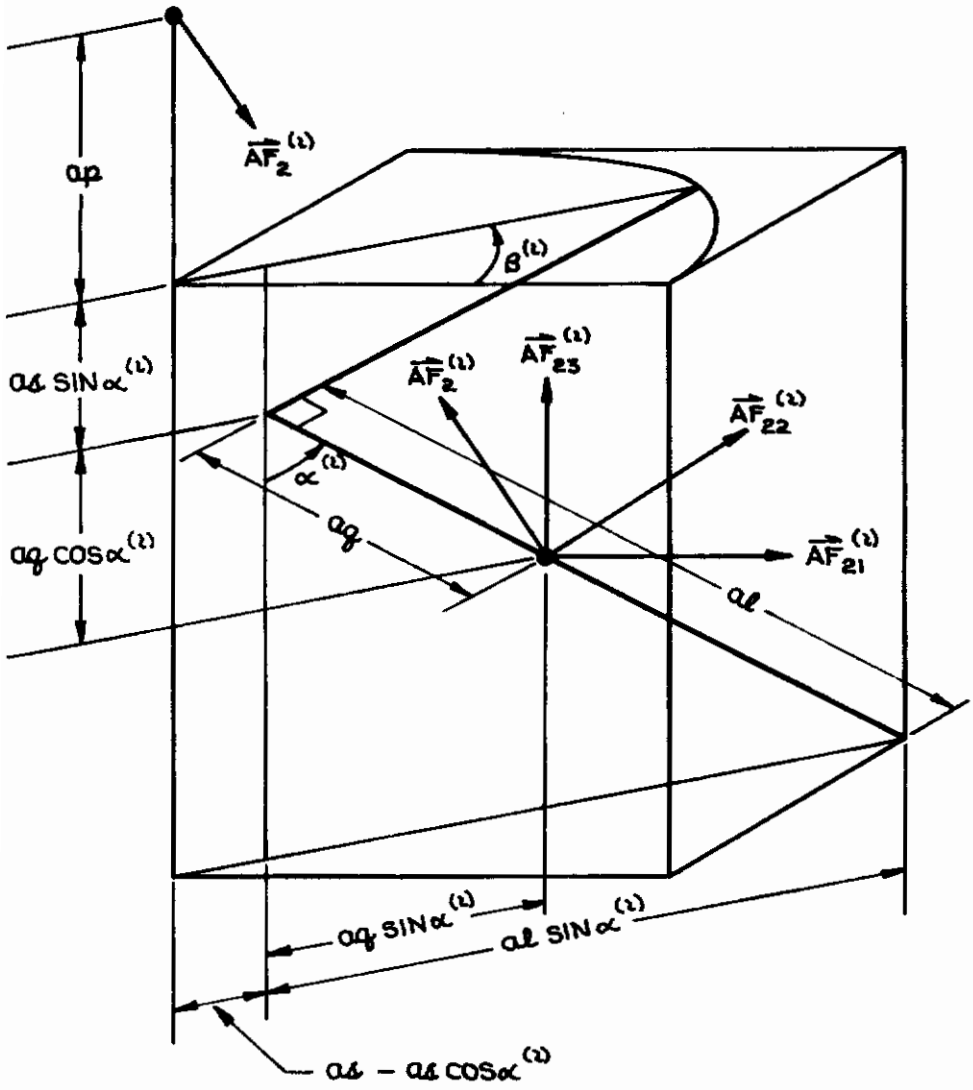

Figure 25: Lower Absorber Geometry

The undeflected length across the absorber is $ap + aq$. The deflection across the lower absorber is seen to be:

$$\Delta_2^{(i)} = \left| S_p^{(i)} \right| - (ap + aq) \tag{48}$$

3. Dynamic Loads

The upper and lower energy absorber reaction forces of the i^{th} leg are denoted as $AF_1^{(i)}$ and $AF_2^{(i)}$, respectively. Figures 24 and 25 illustrate the points of application of the absorber reaction forces.

The angle $\eta^{(i)}$ of the upper absorber with respect to the $S_1^{(i)}$ direction is illustrated in Figure 24. The angle $\eta^{(i)}$ is a function of $\psi^{(i)}$ and the geometry dimensions are seen to be

$$\eta^{(i)} = \tan^{-1}\left[\frac{au \sin\psi^{(i)} + ad\cos\phi - af - aq}{au\cos\psi^{(i)} - ad\sin\phi - aa - ah}\right] \tag{49}$$

The upper absorber reaction may be resolved into its components in the $-S_1^{(i)}$ and $-S_3^{(i)}$ directions as $AF_1^{(i)}\cos\eta^{(i)}$ and $AF_1^{(i)}\sin\eta^{(i)}$, respectively.

The lower absorber reaction forces applied to the lower leg may be resolved into components in the $S^{(i)}$ directions as illustrated in Figure 25.

$$AF_{21}^{(i)} = \frac{-(as - as\cos\alpha^{(i)} + aq\sin\alpha^{(i)})\cos\beta^{(i)} AF_2^{(i)}}{\left| S_p^{(i)} \right|} \tag{50}$$

$$AF_{22}^{(i)} = \frac{-(as - as\cos\alpha^{(i)} + aq\sin\alpha^{(i)})\sin\beta^{(i)} AF_2^{(i)}}{\left| S_p^{(i)} \right|} \tag{51}$$

$$AF_{23}^{(i)} = \frac{(ap + as\sin\alpha^{(i)} + aq\cos\alpha^{(i)})\, AF_2^{(i)}}{\left| S_p^{(i)} \right|} \tag{52}$$

The dynamic load forces and moments resolved at the origin of the $S^{(2)}$ coordinate system are denoted as $\vec{\mathcal{F}}^{(2)}$ and $\vec{m}^{(2)}$, respectively. Figure 26 illustrates a free body diagram of the lower leg of the i^{th} alightment system. The lower end of the lower leg is assumed to be moment free. The ground reaction forces are the dynamic loads $\vec{\mathcal{F}}^{(2)}$. The cross product $\vec{S}^{(2)}$ x $\vec{\mathcal{F}}^{(2)}$ are the dynamic moments $\vec{m}^{(2)}$ about the origin of the coordinate system.

$$m_1^{(2)} = \mathcal{F}_3^{(2)} S_2^{\prime(2)} - \mathcal{F}_2^{(2)} S_3^{\prime(2)}$$

$$m_2^{(2)} = \mathcal{F}_1^{(2)} S_3^{\prime(2)} - \mathcal{F}_3^{(2)} S_1^{\prime(2)}$$

$$m_3^{(2)} = \mathcal{F}_2^{(2)} S_1^{\prime(2)} - \mathcal{F}_1^{(2)} S_2^{\prime(2)}$$

The ground reaction forces $\vec{\mathcal{F}}^{(2)}$ are determined from the equilibrium equations of the lower leg (Figure 26) and the intermediate member (Figure 27).

$$\mathcal{F}_1^{(2)} + R_{12}^{(2)} = -AF_{21}^{(2)} \tag{53}$$

$$\mathcal{F}_3^{(2)} - R_{11}^{(2)} = -AF_{23}^{(2)} \tag{54}$$

$$\begin{aligned}
&(as \sin\alpha^{(2)} + al \cos\alpha^{(2)}) \mathcal{F}_1^{(2)} \\
&\quad + (-as \cos\alpha^{(2)} + al \sin\alpha^{(2)}) \cos\beta^{(2)} \mathcal{F}_3^{(2)} \\
&= -(as \sin\alpha^{(2)} + aq \cos\alpha^{(2)}) AF_{21}^{(2)} \\
&\quad - (-as \cos\alpha^{(2)} + aq \sin\alpha^{(2)}) \cos\beta^{(2)} AF_{23}^{(2)}
\end{aligned} \tag{55}$$

$$Q_2^{(2)} \sin\psi^{(2)} + Q_1^{(2)} \sin\psi^{(2)} + R_{11}^{(2)} = AF_1^{(2)} \sin\eta^{(2)} + AF_{23}^{(2)} \tag{56}$$

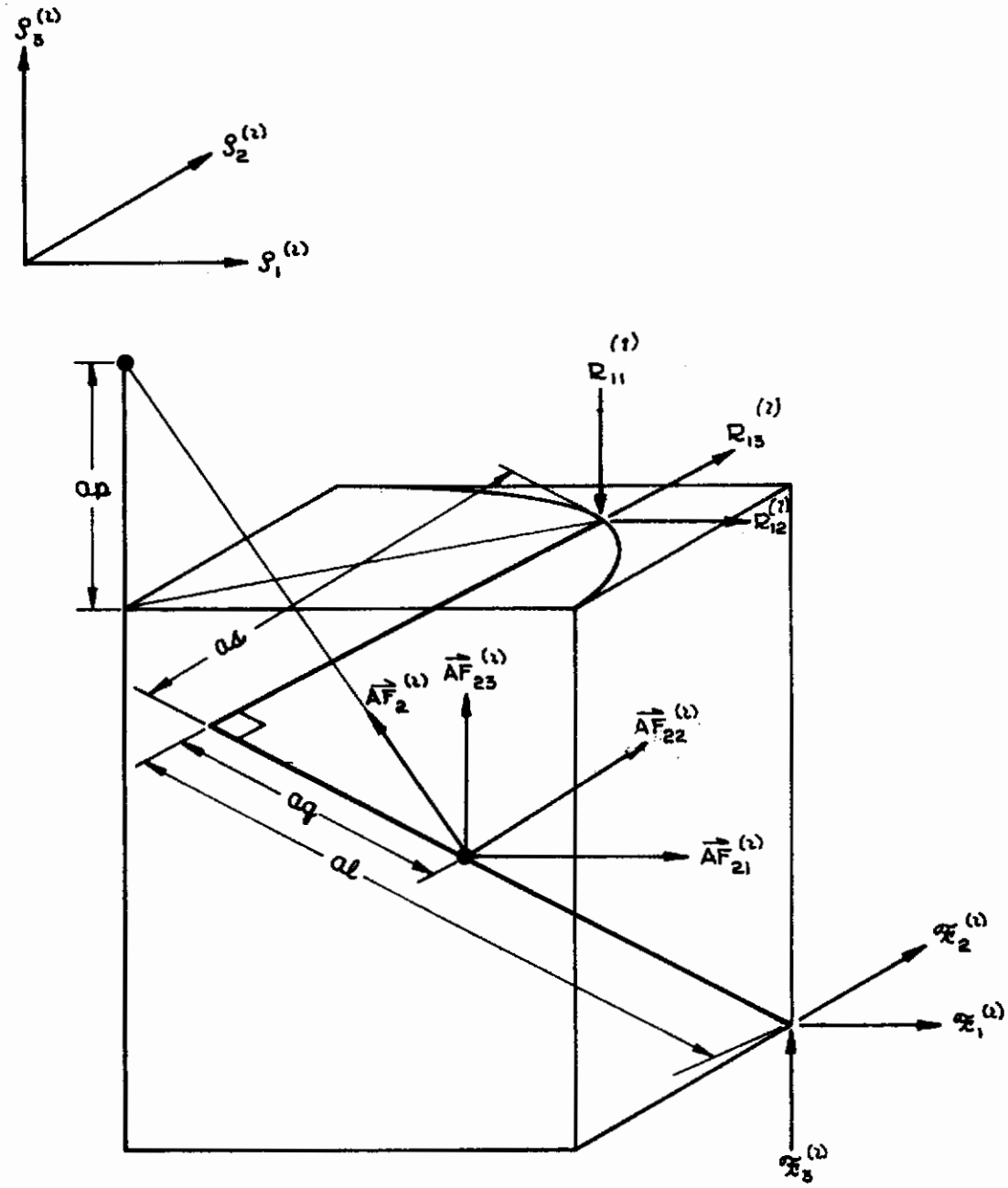

Figure 26: Free Body Diagram of Lower Leg

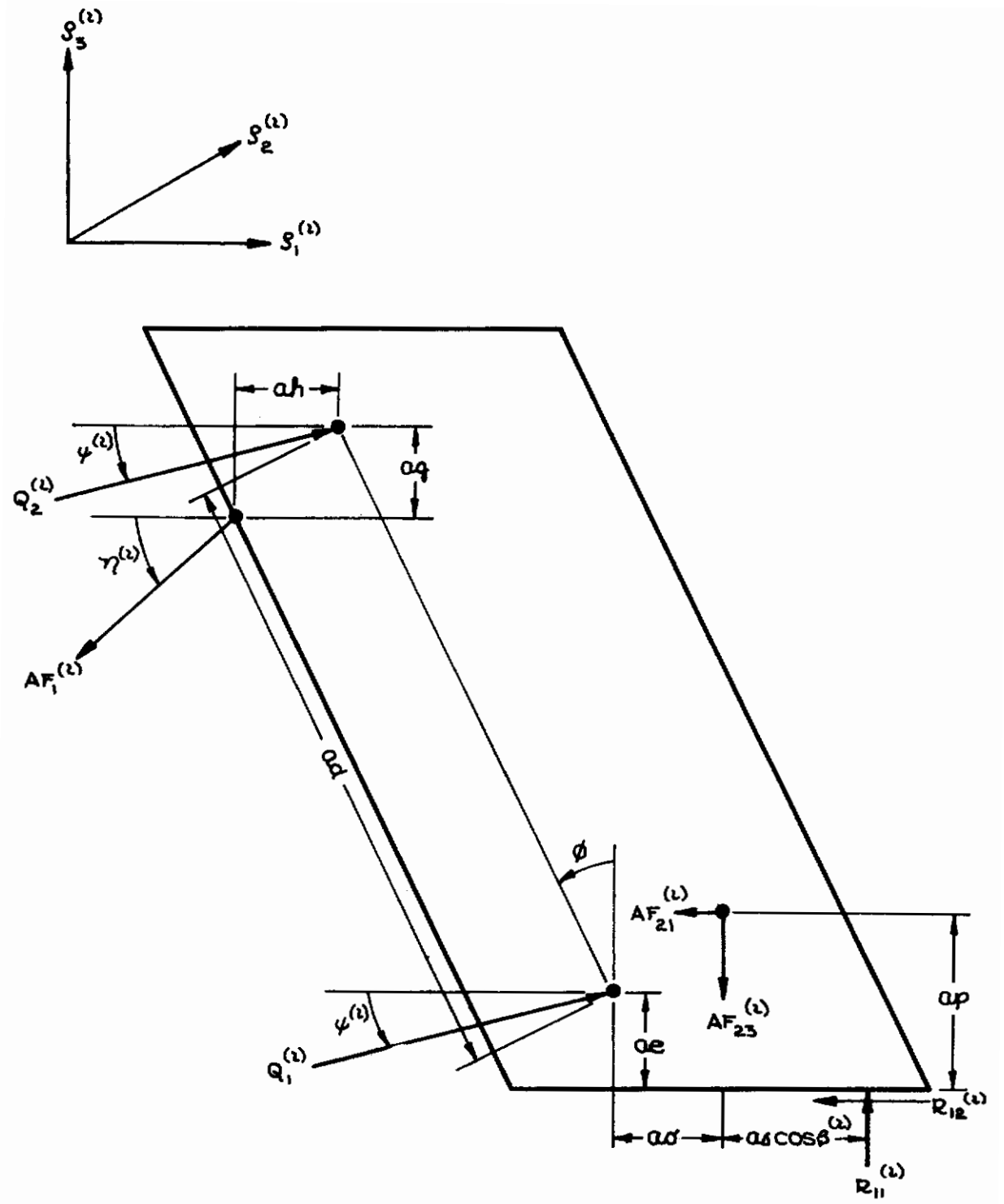

Figure 27: Free Body Diagram of Intermediate Member

$$Q_2^{(2)}\cos\psi^{(2)} + Q_1^{(2)}\cos\psi^{(2)} - R_{12}^{(2)} = AF_1^{(2)}\cos\eta^{(2)} + AF_{21}^{(2)} \tag{57}$$

$$\begin{aligned} &Q_2^{(2)}\left(-\cos\psi^{(2)}\,ad\cos\phi - \sin\psi^{(2)}\,ad\sin\phi\right) - ae\,R_{12}^{(2)} \\ &+ R_{11}^{(2)}\left(as\cos\beta^{(2)} + ao'\right) = (ae - ap)AF_{21}^{(2)} + ao'AF_{23}^{(2)} \\ &- \left[\cos\eta^{(2)}(ad\cos\phi - aq) + \sin\eta^{(2)}(ad\sin\phi + ah)\right]AF_1^{(2)} \end{aligned} \tag{58}$$

The known forces are $AF_1^{(2)}$ and $AF_2^{(2)}$ and all the angles and dimensions are also known. The six unknowns are $\mathcal{X}_1^{(2)}$, $\mathcal{X}_3^{(2)}$, $Q_1^{(2)}$, $Q_2^{(2)}$, $R_{11}^{(2)}$ and $R_{12}^{(2)}$. The two unknowns of interest are $\mathcal{X}_1^{(2)}$ and $\mathcal{X}_3^{(2)}$. These may be obtained by expansion of the 6 by 6 determinant formed by the six equilibrium equations (equations 53 through 58).

$$\begin{aligned} \mathcal{X}_1^{(2)} = &\Big[\cos\psi^{(2)}\left(-as\sin\alpha^{(2)} + aq\cos\alpha^{(2)}\right)AF_{21}^{(2)} \\ &+ \cos\psi^{(2)}\cos\beta^{(2)}\left(as\cos\alpha^{(2)} - aq\sin\alpha^{(2)}\right)AF_{23}^{(2)} \\ &+ \cos\beta^{(2)}\left(\sin\psi^{(2)}\cos\eta^{(2)} - \cos\psi^{(2)}\sin\eta^{(2)}\right)\left(al\sin\alpha^{(2)} - as\cos\alpha^{(2)}\right)AF_1^{(2)}\Big] \\ &\Big/\Big[\sin\psi^{(2)}\cos\beta^{(2)}\left(al\sin\alpha^{(2)} - as\cos\alpha^{(2)}\right) \\ &+ \cos\psi^{(2)}\left(as\sin\alpha^{(2)} + al\cos\alpha^{(2)}\right)\Big] \end{aligned} \tag{59}$$

$$\mathcal{F}_3^{(2)} = \Big[\sin\psi^{(2)}\left(-a_s\sin\alpha^{(2)} - a_q\cos\alpha^{(2)}\right)AF_{21}^{(2)}$$

$$+ \sin\psi^{(2)}\cos\beta^{(2)}\left(a_s\cos\alpha^{(2)} - a_q\sin\alpha^{(2)}\right)AF_{23}^{(2)}$$

$$+ \left(\cos\psi^{(2)}\sin\eta^{(2)} - \sin\psi^{(2)}\cos\eta^{(2)}\right)\left(a_s\sin\alpha^{(2)} + a_l\cos\alpha^{(2)}\right)AF_1^{(2)}\Big]$$

$$\Big/\Big[\sin\psi^{(2)}\cos\beta^{(2)}\left(a_l\sin\alpha_1^{(2)} - a_s\cos\alpha^{(2)}\right)$$

$$+ \cos\psi^{(2)}\left(a_s\sin\alpha^{(2)} + a_l\cos\alpha^{(2)}\right)\Big] \qquad (60)$$

The ground reaction force in the $\mathcal{S}_2^{(2)}$ direction is found by summing the moments about the upper end of the lower leg (Figure 26).

$$\mathcal{F}_2^{(2)} = \Big[\sin\beta^{(2)}\left(a_s\cos\alpha^{(2)} - a_q\sin\alpha^{(2)}\right)AF_{23}^{(2)}$$

$$+ \sin\beta^{(2)}\left(a_s\cos\alpha^{(2)} - a_l\sin\alpha^{(2)}\right)\mathcal{F}_3^{(2)}$$

$$- \left(a_s\sin\alpha^{(2)} + a_q\cos\alpha^{(2)}\right)AF_{22}^{(2)}\Big]$$

$$\Big/\left(a_s\sin\alpha^{(2)} + a_l\cos\alpha^{(2)}\right) \qquad (61)$$

The sliding dynamic loads for the articulated leg configurations are found in a manner similar to that described in Section V.E.5 for the telescoping leg configurations. The non-sliding dynamic loads at each integration increment, as described previously, are used to determine if sliding is occurring. If sliding is occurring, the coordinate $\alpha^{(2)}$ is varied in the iterative procedure to find the alightment system position consistent with the force constraints. The variation in $\alpha^{(2)}$ produces a change in $\psi^{(2)}$. This geometric coupling results in force coupling between the inplane and normal ground reactions. The iteration procedure is basically the same as that for the telescoping leg configurations.

G. FREE FLIGHT EQUATIONS OF MOTION

The motion of the space package is characterized by periods of free flight during which the only forcing function applied to the space package is its weight acting through its center of gravity. These periods of free flight occur after the initial impact and may be described as bounces. The bouncing is not entirely due to stored elastic energy in the absorbers. Bouncing is also due to the rigid body dynamics involved. The impulsive moments which act on the body are capable of lifting a leg off the ground and placing the space package in free flight. The solution to the equations of motion of a rotating rigid body in free flight are of closed form. Thus, it is not necessary to use relatively time consuming numerical integration during free flight. A substantial cost savings in digital computer time has been realized by taking control from the Differential Equation Monitor's numerical integration scheme when the space package bounces off of the ground. Control is transferred to a subroutine structure referred to as BOUNCE. The BOUNCE subroutine structure determines the time of recontact of the space package with the terrain. Control is returned to the Differential Equation Monitor at the time which corresponds to two integration increments prior to the time of recontact. The translational and rotational displacements, velocities, and accelerations of the space package at this time are computed from the free flight equations for use by the Differential Equation Monitor for printing and for initial conditions to restart the numerical integration. Control is returned to the Differential Equation Monitor at this time and recontact with the terrain occurs two integration increments later. The two integration increments of free flight under control of the Differential Equation Monitor are made to insure that all logical switches within the numerical integration structure are set to simulate the free flight conditions prior to recontact.

The Mercury shaped capsule is very nearly symmetric about its longitudinal axis. Thus, the principal inertias (A and B) are nearly equal. The data obtained for use in this program has them equal. It is convenient to take advantage of this symmetry in the equations of free flight motion. The solution to the equations of motion for a freely rotating rigid body with 3 unequal mass moments of inertia about the center of gravity include an elliptic integral and are somewhat involved. The solution to the equations of motion of a freely rotating rigid body with an axis of symmetry is simple enough to insure a savings of machine time over numerical integration. It is further assumed that the principal axes ($\gamma\eta$) are coincident with the χ geometric body fixed axes.

The equations of free flight motion are separable into those of translation and rotation. The situation is illustrated in Figure 28. The weight of the space package acting through its center of gravity is the only forcing function acting on the translational motion of the space package. There are no applied moments acting on the space package; however, angular accelerations about two of the body fixed axes occur due to gyroscopic effects.

The equations of translational motion are a function only of the terrain slope γ , the acceleration of gravity g , and time t . The acceleration

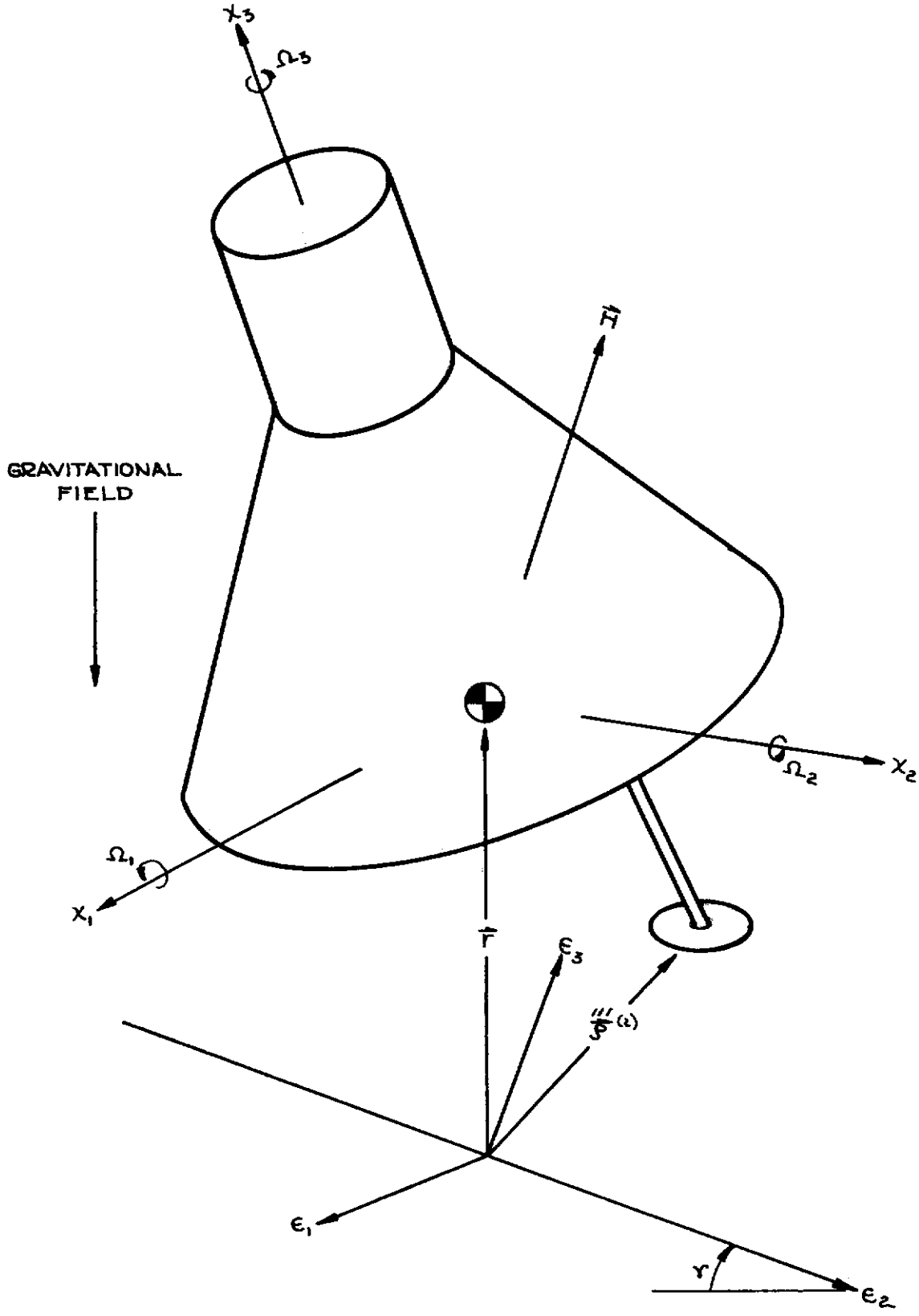

Figure 28: Space Package in Free Flight

equations are:

$$\ddot{r}_1 = 0 \tag{62}$$

$$\ddot{r}_2 = g \sin\gamma \tag{63}$$

$$\ddot{r}_3 = -g \cos\gamma \tag{64}$$

The velocity equations are:

$$\dot{r}_1 = \dot{r}_1\Big|_{t=0} \tag{65}$$

$$\dot{r}_2 = \dot{r}_2\Big|_{t=0} + g(\sin\gamma)t \tag{66}$$

$$\dot{r}_3 = \dot{r}_3\Big|_{t=0} - g(\cos\gamma)t \tag{67}$$

The displacement equations are:

$$r_1 = r_1\Big|_{t=0} + \dot{r}_1\Big|_{t=0} t \tag{68}$$

$$r_2 = r_2\Big|_{t=0} + \dot{r}_2\Big|_{t=0} t + \frac{1}{2} g(\sin\gamma)t^2 \tag{69}$$

$$r_3 = r_3\Big|_{t=0} + \dot{r}_3\Big|_{t=0} t - \frac{1}{2} g(\cos\gamma)t^2 \tag{70}$$

The equations of rotational motion are a function of the angular position, the angular rates and time. Since there are no external applied torques during free flight, the angular momentum $\vec{H}$ remains constant in magnitude and, most importantly, constant in direction. The constant direction of the angular momentum (moment of momentum) vector provides an inertial direction reference during free flight. A set of Euler angles ψ , θ and ϕ are established between the angular momentum vector $\vec{H}$ and the body fixed axes χ as illustrated in Figure 29. The Euler angles are those described in section 3.4 of Reference 4. The following relationships between the rates of change of the Euler angles and the body rates are found in section 5.9 of Reference 4.

$$\Omega_1 = \dot{\psi} \sin\theta \sin\phi \tag{71}$$

$$\Omega_2 = \dot{\psi} \sin\theta \cos\phi \tag{72}$$

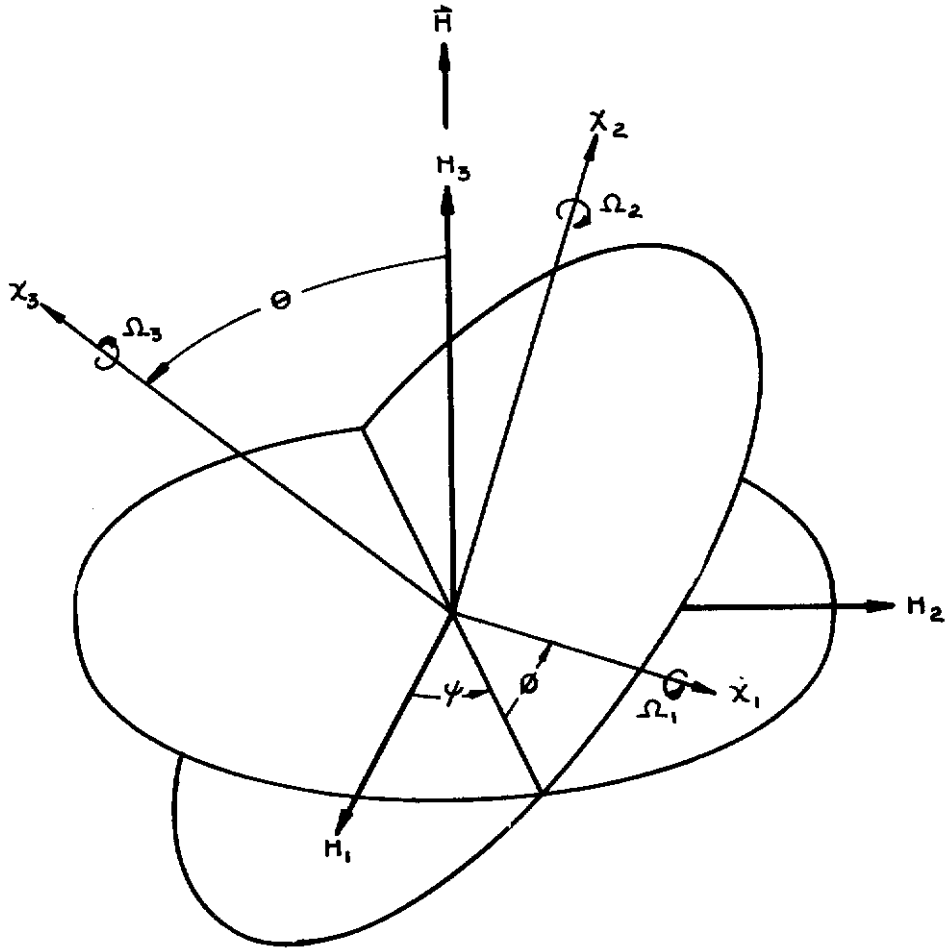

Figure 29: Euler Angles

$$\Omega_3 = \dot{\phi} + \dot{\psi}\cos\theta \tag{73}$$

Solving the first two above equations for $\dot{\psi}\sin\theta$ and equating them, it is found that:

$$\phi = \tan^{-1}\left(\Omega_1/\Omega_2\right) \tag{74}$$

Let Ω_{12} be the magnitude of the rotational rate of the body resolved in the $x_1 - x_2$ plane.

$$\Omega_{12} = \sqrt{(\Omega_1)^2 + (\Omega_2)^2}$$

The magnitude of θ is given by equation 5.8-14 of Reference 4.

$$\theta = \tan^{-1}\left(A\Omega_{12}/C\Omega_3\right) \tag{75}$$

The initial magnitude of the angle ψ is arbitrary since the direction of only H_3 is fixed. Therefore, the initial value of ψ is selected as zero.

$$\psi\big|_{t=0} = 0$$

The angular rate $\dot{\psi}$ is given by equation 5.9-4 of Reference 4.

$$\dot{\psi} = \frac{C\dot{\phi}}{(A-C)\cos\theta} \tag{76}$$

Substituting this equation into equation 73 yields the following relationship for $\dot{\phi}$.

$$\dot{\phi} = \frac{A-C}{A}\,\Omega_3 \tag{77}$$

It is also known that the angle θ and the angular rates $\dot{\phi}$ and $\dot{\psi}$ remain constant. Thus the Euler angles as a function of time are:

$$\phi = \dot{\phi} t + \phi\Big|_{t=0} \tag{78}$$

$$\psi = \dot{\psi} t + \psi\Big|_{t=0} \tag{79}$$

$$\theta = \theta\Big|_{t=0} \tag{80}$$

Thus, it can be seen that the space package angular position as a function of time is known. The position of each of the foot pads as a function of time is now needed. Recontact of a foot pad with the ground occurs when the third component of its position vector $\vec{S}^{(i)}$ in the ϵ inertial coordinate system becomes negative. An iterative procedure to find the time of recontact is used.

The transformation matrix from the body fixed axes χ to the moment of momentum reference frame H is equation 3.4-7 of Reference 4.

$$\left[\ell^{H\chi}\right] = \begin{bmatrix} \cos\phi\cos\psi - \sin\phi\cos\theta\sin\psi & -\sin\phi\cos\psi - \sin\psi\cos\theta\cos\phi & \sin\theta\sin\psi \\ \cos\phi\sin\psi + \sin\phi\cos\theta\cos\psi & -\sin\phi\sin\psi + \cos\psi\cos\theta\cos\phi & -\sin\theta\cos\psi \\ \sin\theta\sin\phi & \sin\theta\cos\phi & \cos\theta \end{bmatrix}$$

The transformation matrices from the angular momentum reference frame H to the body centered k coordinate system and the ϵ local terrain reference frame remain constant and are formed by the following matrix multiplications at time $t = 0$, that is when free flight begins.

$$\left[\ell^{kH}\right] = \left[\ell^{k\chi}\right]\left[\ell^{\chi H}\right]$$

$$\left[\ell^{\epsilon H}\right] = \left[\ell^{\epsilon\chi}\right]\left[\ell^{\chi H}\right]$$

The position vector of the i^{th} foot pad $\vec{\xi}^{(i)}$ relative to the center of gravity of the space package is found as follows:

$$\left\{ \xi^{(i)} \right\} = \left\{ b^{(i)} \right\} + \left[\ell^{\chi s^{(i)}} \right] \left\{ s'^{(i)} \right\} \tag{81}$$

This quantity is then transformed into the ϵ local terrain coordinate system and denoted as $\vec{\rho}^{(i)}$.

$$\left\{ s'''^{(i)} \right\} = \left[\ell^{\epsilon H} \right] \left[\ell^{H \chi} \right] \left\{ \xi^{(i)} \right\} \tag{82}$$

The third component of this vector may then be compared to the third component r_3 of the position vector of the center of gravity of the space package at various times. The time of recontact occurs when the third component of $\vec{\xi}^{(i)}$ becomes equal to r_3. This time is then decreased by two integration increments and denoted as t.

The initial conditions to reinitiate the numerical integration are now needed. The translational displacement, velocity and acceleration are found as functions of the adjusted recontact time t. The present body rates Ω_1, and Ω_2 are found for the new value of the Euler angle ϕ.

$$\Omega_1 = \dot{\psi} \sin\theta \sin\phi \tag{71}$$

$$\Omega_2 = \dot{\psi} \sin\theta \cos\phi \tag{72}$$

The body rate about the χ_3 axis remains constant during the free flight.

The angular accelerations about the body fixed axes are found by differentiating the angular rates (equations 71 through 73) with respect to time and recalling that θ is constant.

$$\dot{\Omega}_1 = \dot{\psi}\dot{\phi} \sin\theta \cos\phi \tag{83}$$

$$\dot{\Omega}_2 = -\dot{\psi}\dot{\phi} \sin\theta \sin\phi \tag{84}$$

$$\dot{\Omega}_3 = 0 \tag{85}$$

The angular velocities and accelerations of the space package must be resolved about principal axes η.

$$\{\omega\} = [\ell^{\eta x}]\{\Omega\}$$

$$\{\dot{\omega}\} = [\ell^{\eta x}]\{\dot{\Omega}\}$$

The translational acceleration must be resolved into the X body fixed axes for printing.

$$\{\ddot{X}\} = [\ell^{xH}][\ell^{H\epsilon}]\{\ddot{r}\}$$

The angular orientation of the space package at the adjusted recontact time t is determined by examining the elements of the transformation matrix from the body fixed X axes to the body centered k axes. This transformation matrix is formed by multiplying the kH transformation matrix which is constant during any one free flight by the HX transformation matrix which is a function of the free flight angular orientation.

$$[\ell^{kx}] = [\ell^{kH}][\ell^{Hx}]$$

The following elements of the kX transformation matrix are of interest.

$$\ell_{32}^{kx} = \cos Y \sin P$$

$$\ell_{33}^{kx} = \cos Y \cos P$$

$$\ell_{11}^{kx} = \cos R \cos Y$$
$$\ell_{21}^{kx} = \sin R \cos Y$$
$$\ell_{31}^{kx} = -\sin Y$$

The expression for the pitch angle is obtained by dividing the 3-2 element by the 3-3 element of the ℓ^{kx} transformation matrix.

$$P = \tan^{-1}\left(\ell_{32}^{kx} / \ell_{33}^{kx}\right) \tag{86}$$

The expression for the roll angle is obtained by dividing the 2-1 element by the 1-1 element.

$$R = \tan^{-1}\left(\ell_{21}^{kx} / \ell_{11}^{kx}\right) \tag{87}$$

The expression for the yaw angle is obtained by dividing the 3-1 element times $-\cos P$ by the 3-3 element.

$$Y = \tan^{-1}\left(-\ell_{31}^{kx} \cos P / \ell_{33}^{kx}\right) \tag{88}$$

The rates of change of the roll, yaw and pitch angles are also needed to restart the numerical integration. These expressions are given in Section V.D.2.

This completes the computation of the variables needed for printing and to restart the numerical integration scheme prior to recontact with the terrain. Control is then returned to the Differential Equation Monitor and the numerical integration and forcing function schemes are resumed.

H. STABILITY CRITERIA

The alightment dynamics of a space package are often characterized by relatively gentle bouncing of the vehicle on the system compliances after the initial impact. The peak dynamic loads and energy absorber strokings have already been experienced. The space package is in a stable position and the motion will damp out. Thus, it can be seen that the pertinent information has already been obtained and the run may be terminated at this point.

A stability criteria has been developed which permits a prediction of the stability of the space package to be made during the run. When the criteria is

met, the run is terminated, thus resulting in substantial savings of digital computer time for this type of run.

The stability criteria is based on energy considerations. The energy at the present time is compared with the energy required to bring the space package to the edge of toppling with zero velocity at this point. If the energy at the present time is insufficient to topple the space package, it is in a stable position and the run is terminated. The stability criteria is applied every fifty integration increments and each time that the free flight equations return the space package to the ground. If the space package is potentially unstable, the simulation is continued. If the space package is stable, the present angular rates and the critical angular rates are printed and the run is terminated.

The approach employed in establishing the stability criteria is an extension of the derivations described in Reference 5. Figure 30 illustrates the geometry involved in the first portion of the derivation. The angle Θ is the instantaneous angle between the capsule roll axis χ_3 and the vertical inertial direction. The distance h_i is the normal from the center of gravity of the space package to a line joining the foot pads of two adjacent legs. The angle τ_i is measured from the horizontal plane of the space package ($\chi_1 - \chi_2$ plane) to the line h_i which is solely a function of the alightment system deflection position. The angle δ_i is the instantaneous angle between the line h_i and the vertical inertial direction. The quantity $\dot{\gamma}_i$ is the angular rate of the space package about the line joining the foot pads of the i^{th} and the $i^{th}+1$ legs.

A conservative approach to the problem from the standpoint of stability is employed. The rotational rate $\dot{\gamma}_i$ of the space package about the minimum level arm h_i is no less than that which occurs if the total translational velocity is in the plane of the page of Figure 30 and the axis of the total rotational velocity about the center of gravity is parallel to the line between the foot pads of the i^{th} and $i^{th}+1$ legs.

$$\dot{\gamma}_i = \frac{\left(\dot{r}_1^2 + \dot{r}_2^2 + \dot{r}_3^2\right)^{1/2}}{h_i} + \left(\omega_1^2 + \omega_2^2 + \omega_3^2\right)^{1/2} \qquad (89)$$

The current rotation rate $\dot{\gamma}_i$ must now be compared to the critical rotational rate which could bring the space package from its present position to the point of tipping over ($\delta_i = 0$) with zero kinetic energy. The system energy at the present time t_1 is the summation of the translational and rotational kinetic energies, the gravitational potential energy, the the elastic potential energy of the energy absorbers.

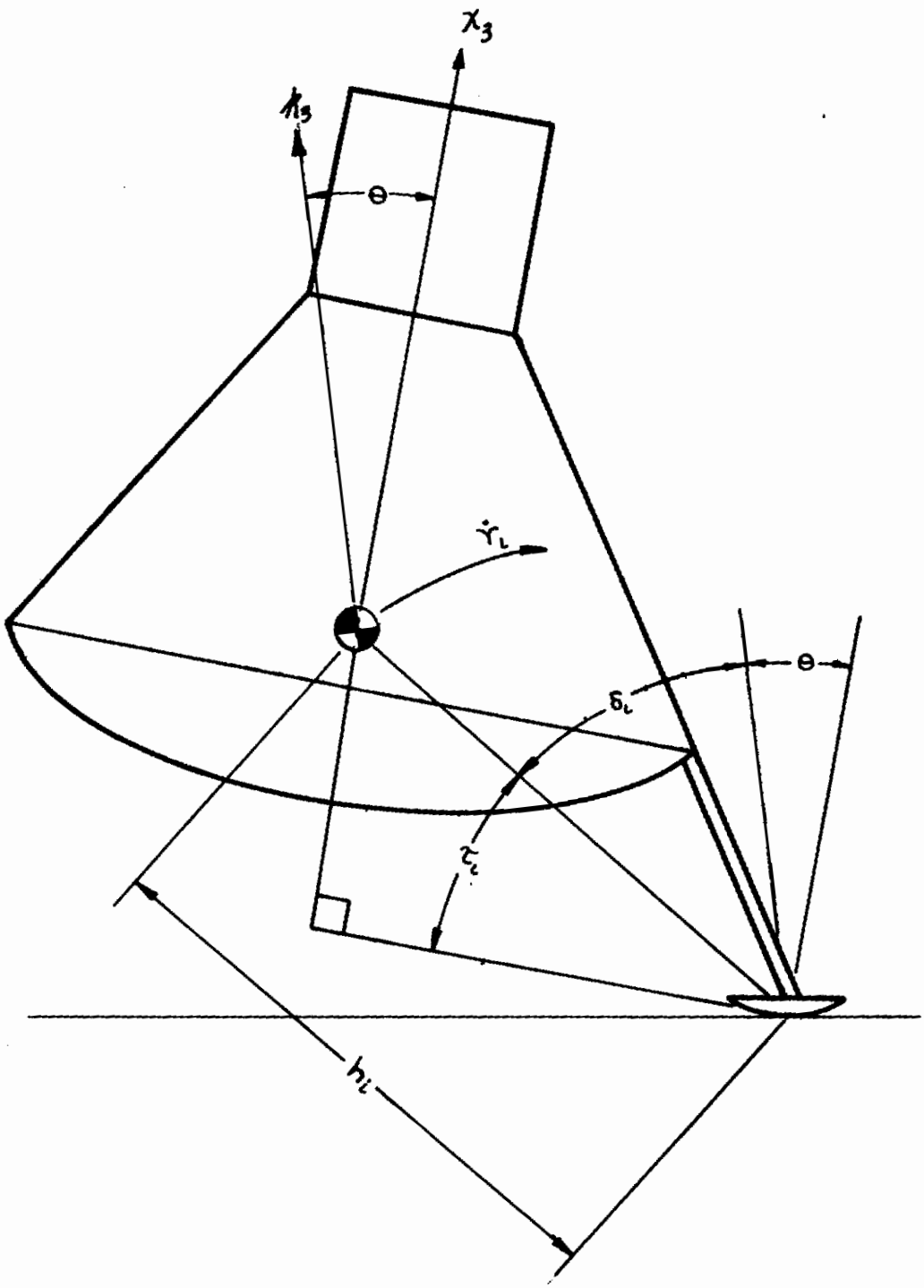

Figure 30: Stability Criteria Geometry

$$E_i = \frac{1}{2}\left(m h_i^2 + A\right)\dot{\gamma}_i^2 + m g h_i \cos\delta_i + \frac{1}{2}\sum_j k_j \Delta_j^2(t_1) \qquad (90)$$

The system energy at the time t_2 and position ($\delta_i = 0$) of tipping over is the summation of the two potential energies.

$$E_i = m g h_i + \frac{1}{2}\sum_j k_j \Delta_j^2(t_2) \qquad (91)$$

The energy between the two times t_1 and t_2 will differ by the energy dissipated by crushing of the absorber material and viscous damping of the system. It is not intended that this criteria be applied until after the majority of the absorber material crushing has occurred. The energy dissipated by viscous damping and possibly some crushing of the absorber material merely adds to the conservative assumptions of the stability criteria. The critical rotational rate at time t_1 is determined by equating the energies at t_1 and t_2.

$$\frac{1}{2}\left(m h_i^2 + A\right)\dot{\gamma}_i^2 + m g h_i \cos\delta_i + \frac{1}{2}\sum_j k_j \Delta_j^2(t_1) = m g h_i + \frac{1}{2}\sum_j k_j \Delta_j^2(t_2) \qquad (92)$$

Solving for the critical rotational rate $\dot{\gamma}_i$ yields:

$$\dot{\gamma}_i^2 = \frac{2 m g h_i (1 - \cos\delta_i) + \sum_j k_j \left[\Delta_j^2(t_2) - \Delta_j^2(t_1)\right]}{m h_i^2 + A}$$

An examination of the order of magnitude of the numerator terms indicates that the elastic potential terms tend to cancel. For a low compliance system such as this, the elastic potential terms are negligible. Therefore, these terms will be dropped.

The angle δ_i may be eliminated from the equation by using the more convenient quantities τ_i and Θ. Since $\tau_i + \delta_i + \Theta = \pi/2$, the substitution $\cos\delta_i = \sin(\tau_i + \Theta)$ may be made. The critical rotational rate $\dot{\gamma}_i$ becomes:

$$\dot{\gamma}_i = \left\{ \frac{2mgh_i\left[1 - \sin(\tau_i + \theta)\right]}{mh_i^2 + A} \right\}^{1/2} \tag{93}$$

The quantities h_i and τ_i are functions of the deflected alightment system position. Figure 31 illustrates the geometry involved in determining the quantities h_i and τ_i.

The vector from the center of gravity of the space package to the foot pad of the i^{th} leg (equation 81) is denoted as $\xi^{(i)}$.

$$\left\{ \xi^{(i)} \right\} = \left\{ b^{(i)} \right\} + \left[\ell^{xs^{(i)}} \right] \left\{ s'^{(i)} \right\} \tag{81}$$

By examining the triangular surfaces in Figure 31, it can readily be shown that

$$h_i = \left\{ \left(\xi^{(i)}\right)^2 + \frac{\left[\left(\xi^{(i)}\right)^2 + \left(\left|\vec{\xi}^{(i+1)} - \vec{\xi}^{(i)}\right|\right)^2 - \left(\xi^{(i+1)}\right)^2\right]^2}{-4\left(\xi_{i+1}\right)^2} \right\}^{1/2} \tag{94}$$

and that

$$\tau_i = \sin^{-1}\left(-\eta_i / h_i\right) \tag{95}$$

where

$$\eta_i = \xi_3^{(i)} + \frac{\left[\left(\xi^{(i)}\right)^2 - (h_i)^2\right]^{1/2}\left(\xi_3^{(i+1)} - \xi_3^{(i)}\right)}{\left|\vec{\xi}^{(i+1)} - \vec{\xi}^{(i)}\right|}$$

The vector $\vec{s}^{(i)}$ is dependent upon the basic configuration type (telescoping or articulated leg) and the permanent deflection of the energy absorbers. The maximum deflection values experienced during the run to the time t_1 are saved for computing a worst position of each pair of adjacent alightment systems with respect to stability. The equations for the computation of the alightment system positions are contained in Sections V.E.1 and V.F.1 for the two basic configuration types. The criteria is applied to each pair of adjacent legs in successive order around the space package.

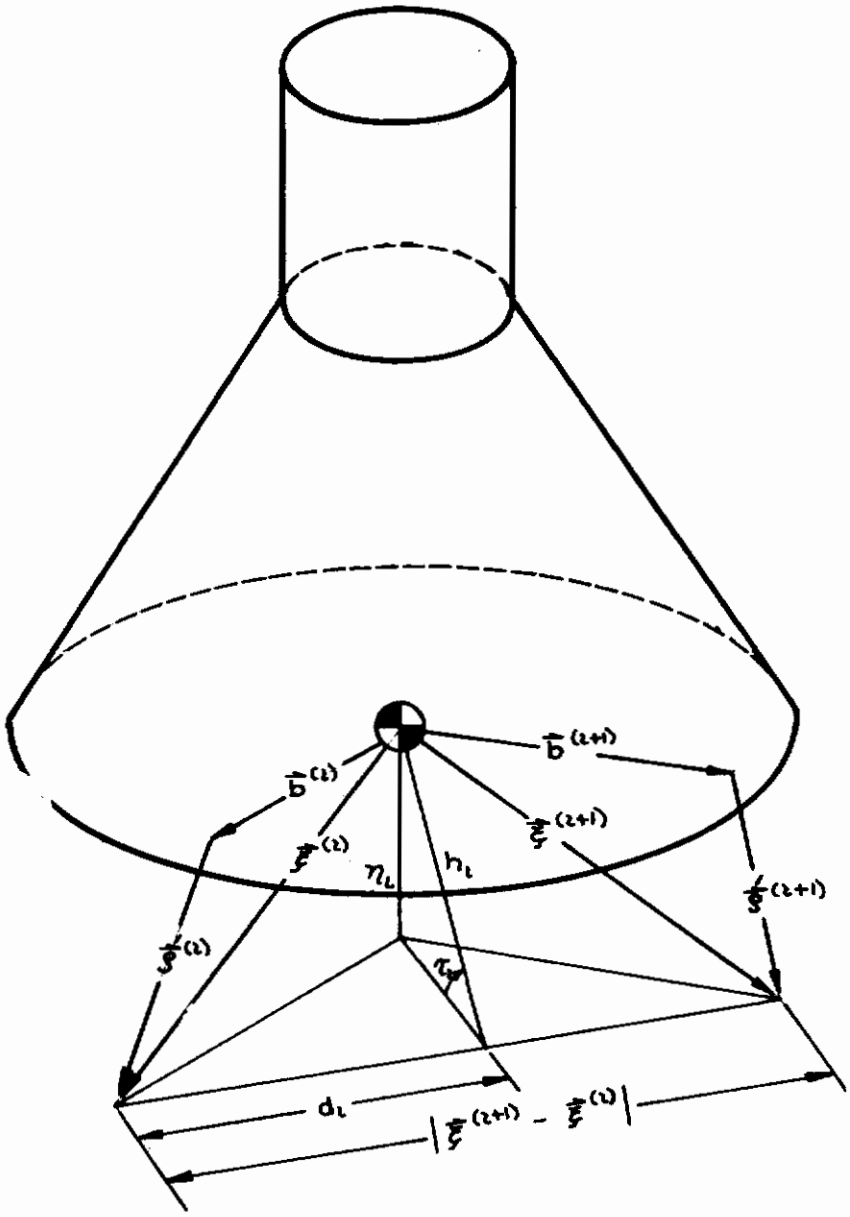

Figure 31: Deflected Alightment System Geometry

SECTION VI

COMPARISON OF ANALYTICAL AND EXPERIMENTAL RESULTS

A. GENERAL RESULTS

The comparison phase of this program provides a means of assessing the adequacy of the digital simulation by comparing measured center of gravity acceleration time histories to the predicted time histories generated by the simulations. Acceleration time histories were chosen as the comparison quantity on the basis of their sensitivity to subtle simulation errors.

The articulated leg has strong coupling between parallelogram and peg leg energy cells. Errors in representing the leg articulation and the resulting force time histories would be averaged out for a velocity (of the center of gravity) comparison and hidden altogether if center of gravity displacements were compared.

The measured acceleration time histories were obtained from the experimental phase, Appendix VI. The test model, fabricated for use in the experimental phase, was mathematically modeled and used in the digital simulation. Initial conditions for each of the ten drops used in the Comparison Phase were obtained from analysis of the high speed motion pictures taken for each drop. These initial conditions were then used in the digital simulation of each drop.

The general results of the Comparison Phase show excellent correlation for capsule vertical acceleration - XDD(3), and poor to excellent correlation for horizontal and angular accelerations. The initial conditions for each drop are listed in the following Table 5.

TABLE 5

INITIAL CONDITIONS FOR ALIGHTMENT TESTS

DROP NO.	ROLL ANGLE	YAW ANGLE	PITCH ANGLE	VERTICAL INCLINATION	TERRAIN SLOPE	TRANSLATIONAL VELOCITIES		
	R	Y	P	Θ	γ	V1	V2	V3
1	0.	0.	0.	0.	0.	0.	0.	-17.5
2	0.	11.5	-6.	13.			0.	-17.5
3	-90.	-3.	0.	3.			7.5	-17.5
4	90.	11.	-4.	11.7			7.5	-17.5
5	0.	6.	2.	6.3			0.	-24.
6	0.	0.	0.	0.			0.	-25.3
8	0.	-12.	-4.	12.6			0.	-25.3
9	40.	0.	-2.	2.0			8.65	-25.3
10	90.	8.	-4.	8.9			7.35	-25.3
11	45.	-6.	6.03	8.5	22.		-4.5	-27.2

Force deflection characteristics of the energy cells for the digital simulation were obtained from pre-test static measurements. Since the simulation requires each type of energy cell to have identical characteristics with the other three, the largest crushing force was used for non-inclined alightments and the characteristics of the leading leg for inclined alightments. The comparison between measured and predicted vertical accelerations for every drop test indicates that the true force across the energy absorbers was higher during the tests than that measured statically prior to the test. On the average, this difference was 23 percent. Two potential causes of this increase in force exist. One involves the aluminum honeycomb and the other results from the parallelogram and energy cell design.

For the former, the Literature Search (Appendix I) and Company Visitations (Appendix II) indicated that no effect on crushing load should be expected due to strain rate hardening or dynamic buckling at the loading rates developed during the drop tests. An increase in apparent crushing force of about five percent could occur due to the air cushion developed during the loading, however.

The remainder of the apparent increase in crushing load is thought to be due to binding of the energy cell loading pads and friction in the parallelogram. This is discussed in detail in Section VI.D and Appendix VI.

The accelerometers used to measure the six capsule rigid body accelerations should be augmented with strain gages on the energy cells for future testing.

The strain gages would be capable of measuring the force-time history of each energy cell during the alightment tests and provide better insight into leg action during alightment.

To insure meaningful test data for comparison purposes, adequate control had to be exercised over the peg leg/surface interaction. The technique used to provide this control had consisted of "digging" the peg leg into the asphalt surface on alightment. Figure 32 shows a peg leg and its penetration after a drop test. The intent was to provide a non-slipping surface for the test that could be represented in the simulation by very large coefficients of friction ($\mu > 1,000,000$).

The technique was generally successful, although the poor correlation shown for the two horizontal accelerations on some drops is indicative of inadequate penetration.

Angular accelerations, especially roll-OMD(3), are also sensitive to the peg leg/surface interaction. If slippage occurs during the test, a lower angular acceleration results than would be predicted by the simulation. A more pronounced effect on the angular accelerations measured during the tests is due to small (5 percent) variations in crushing force between energy cells. Angular accelerations as high as 150 radians per second^2 could be produced by a 5 percent variation in energy cell forces and either add to or subtract from the expected accelerations.

B. COMPARISON OF ACCELERATION TIME HISTORIES

Drops 1 through 5 were performed as a test of an alighting space craft with human cargo. The upper acceleration limit was 20 g's. Drops 6 through 11 were performed as a test of an alighting space craft with electronic cargo. The upper acceleration limit was 50 g's. Drop 7 was deleted from the Comparison Phase due to binding of the parallelogram load pads. Drop 8 is a repeat of Drop 7 after a design change to the loading pads.

Drop 1

The initial conditions for this drop consisted of a downward velocity with no capsule inclination. These conditions produced single coordinate motion in the digital simulation as shown in Figures 33 and 38. The measured accelerations in the out-of-plane coordinates show large deviations from the zero values obtained from the simulation. Close examination of the XDD(1), XDD(2), OMD(1), OMD(2), and OMD(3) time histories (Figures 33, 34, 36, 37 and 38, respectively), indicates that integration of these accelerations would yield small if not zero velocity changes, indicating an oscillatory motion of the capsule. It may be concluded then that only very small errors in capsule center of gravity motion result from the apparent large errors in acceleration time histories.

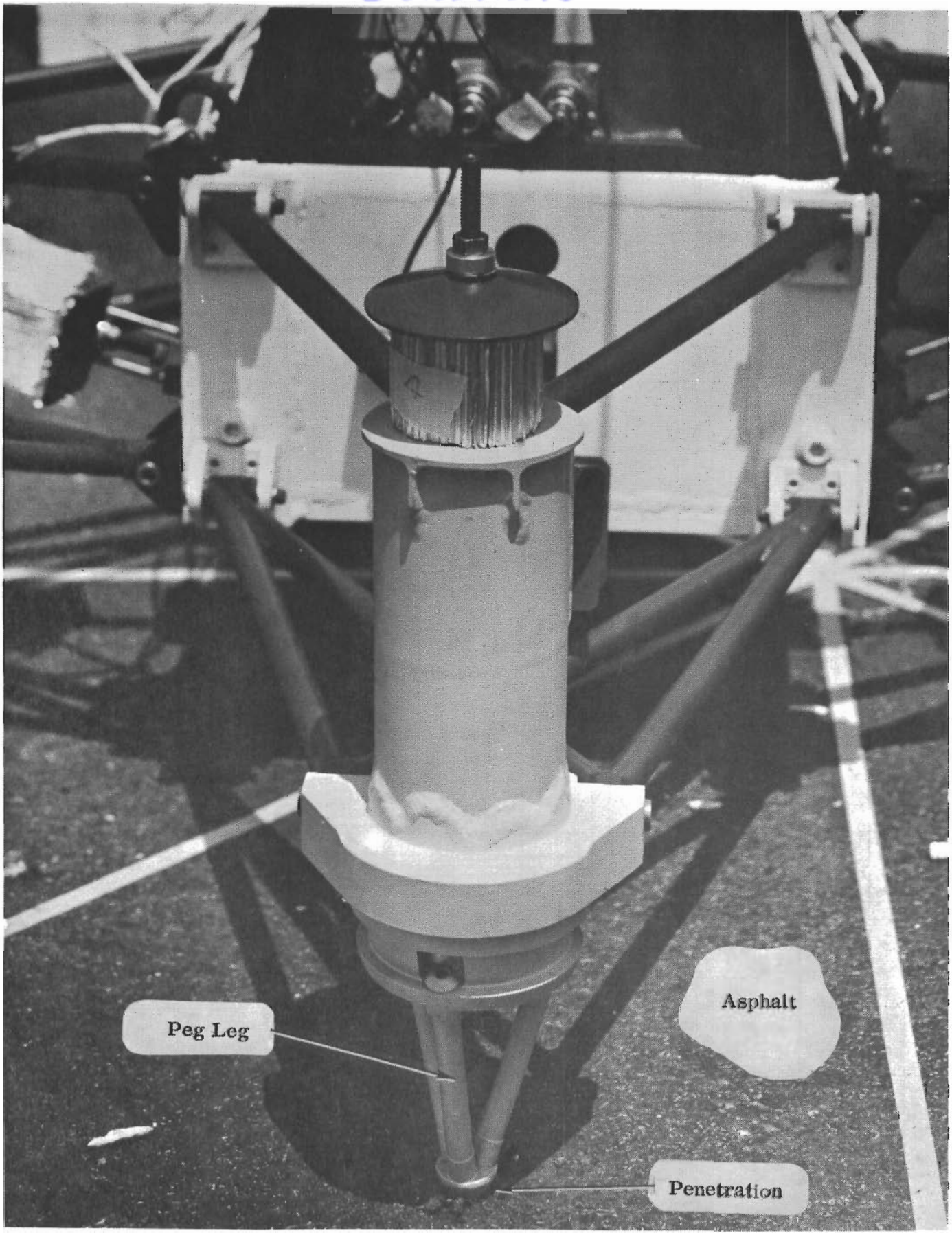

Figure 32, Test Model Leg Penetration

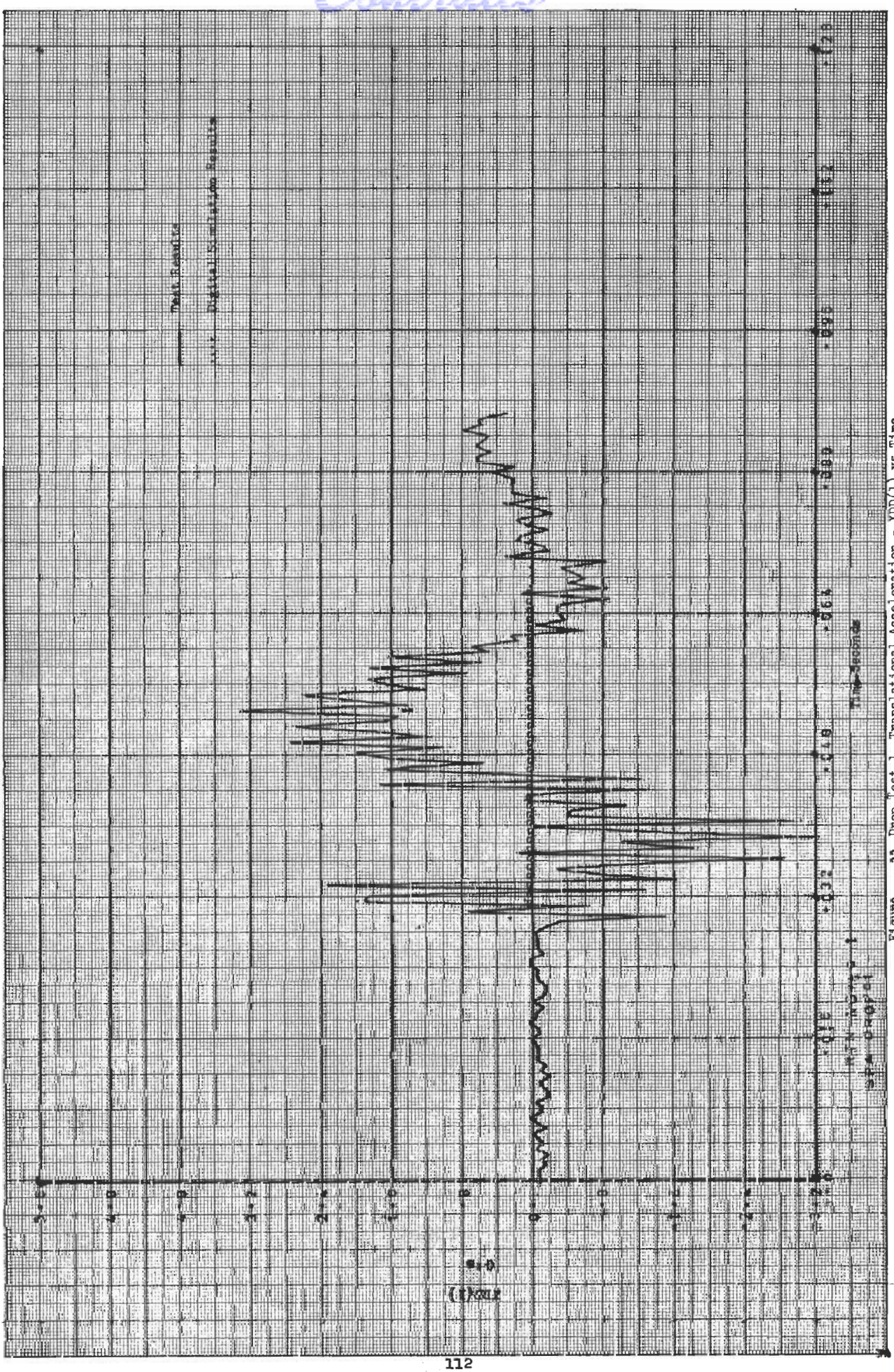

Figure 33 Drop Test 1, Translational Acceleration - $\ddot{X}_{DD}(1)$ vs Time

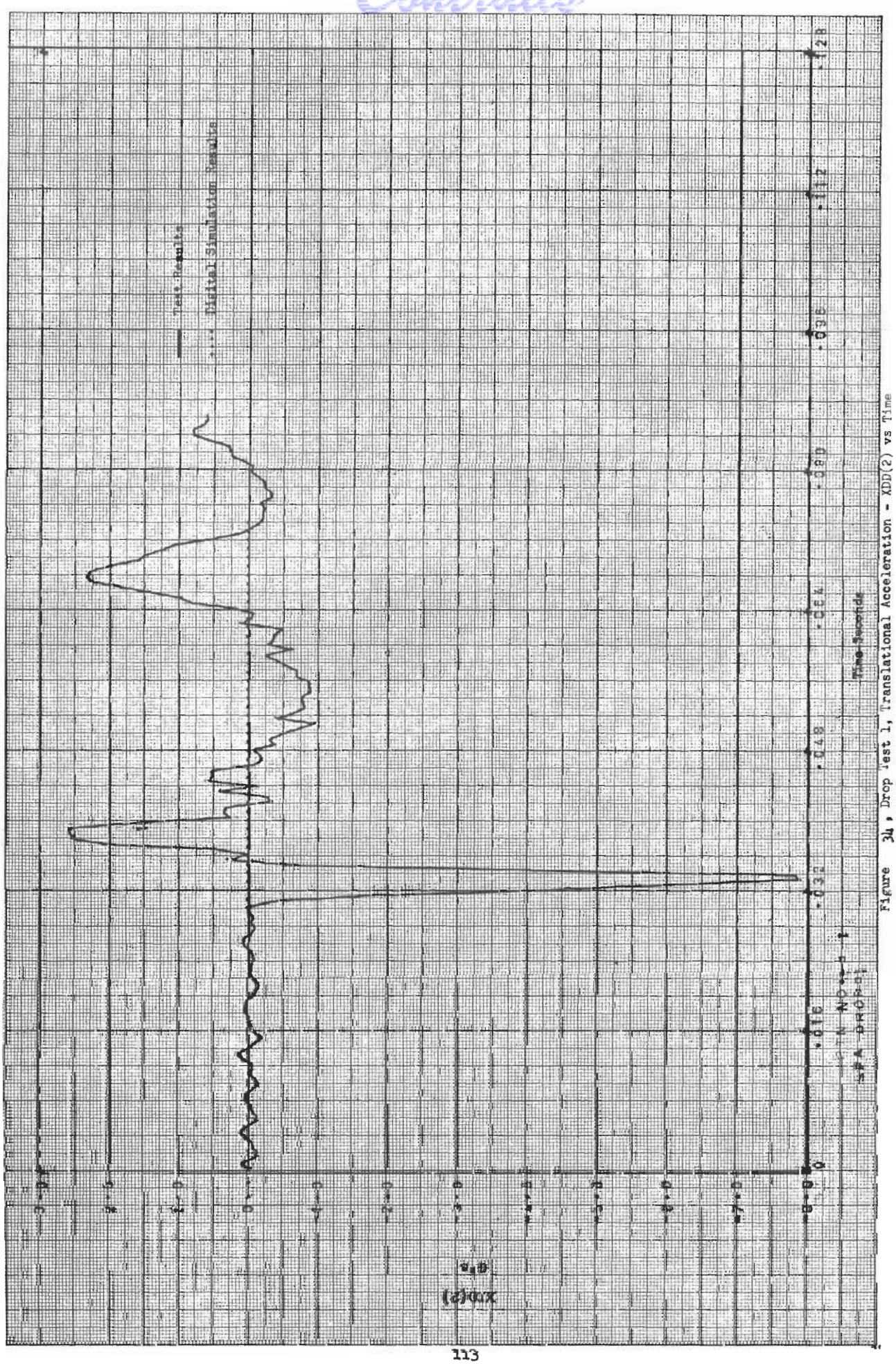

Figure 34, Drop Test 1, Translational Acceleration - $\ddot{X}_{D(2)}$ vs Time

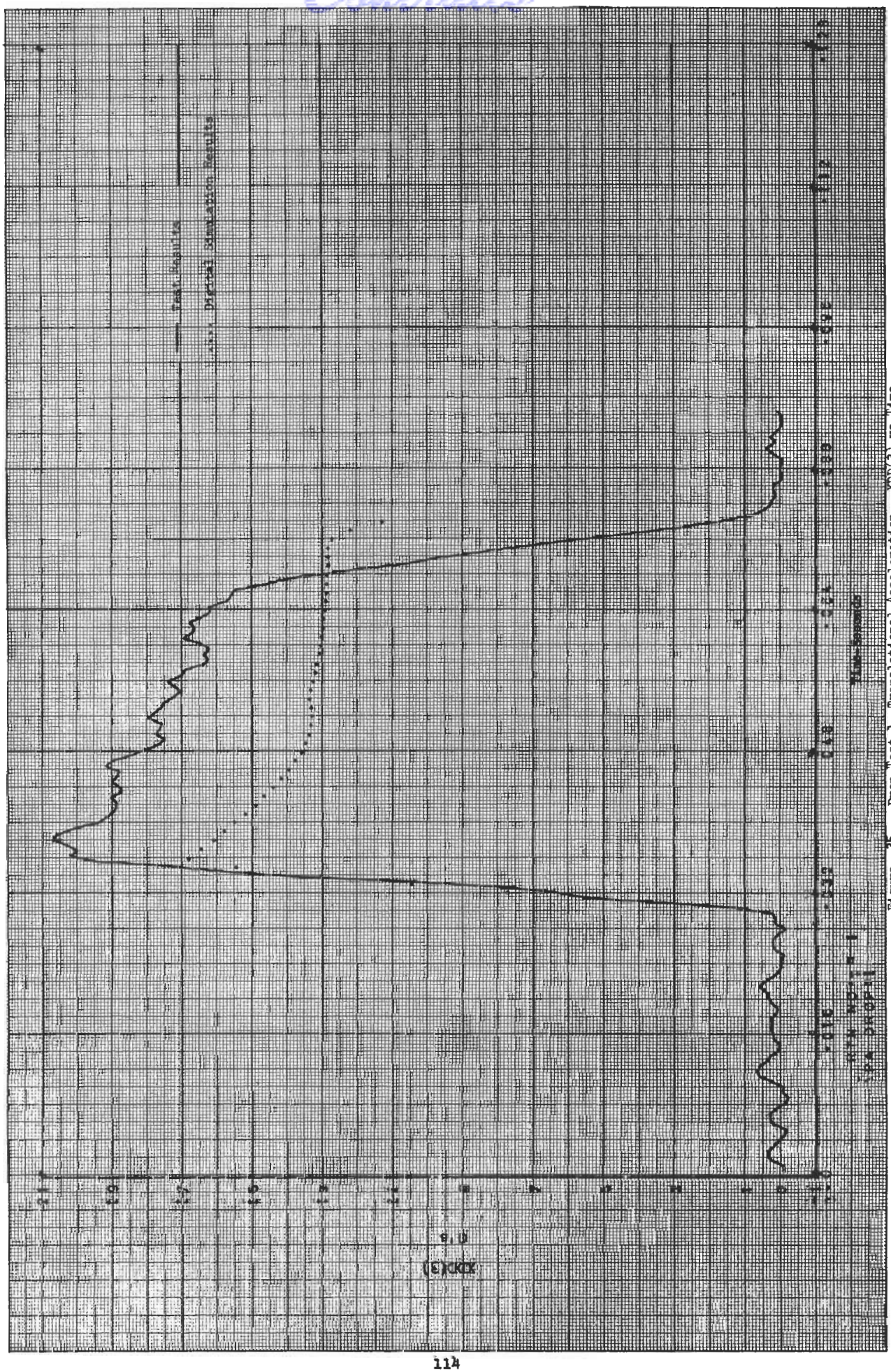

Figure 35 , Drop Test 1, Translational Acceleration - $\ddot{X}_{DD}(3)$ vs Time

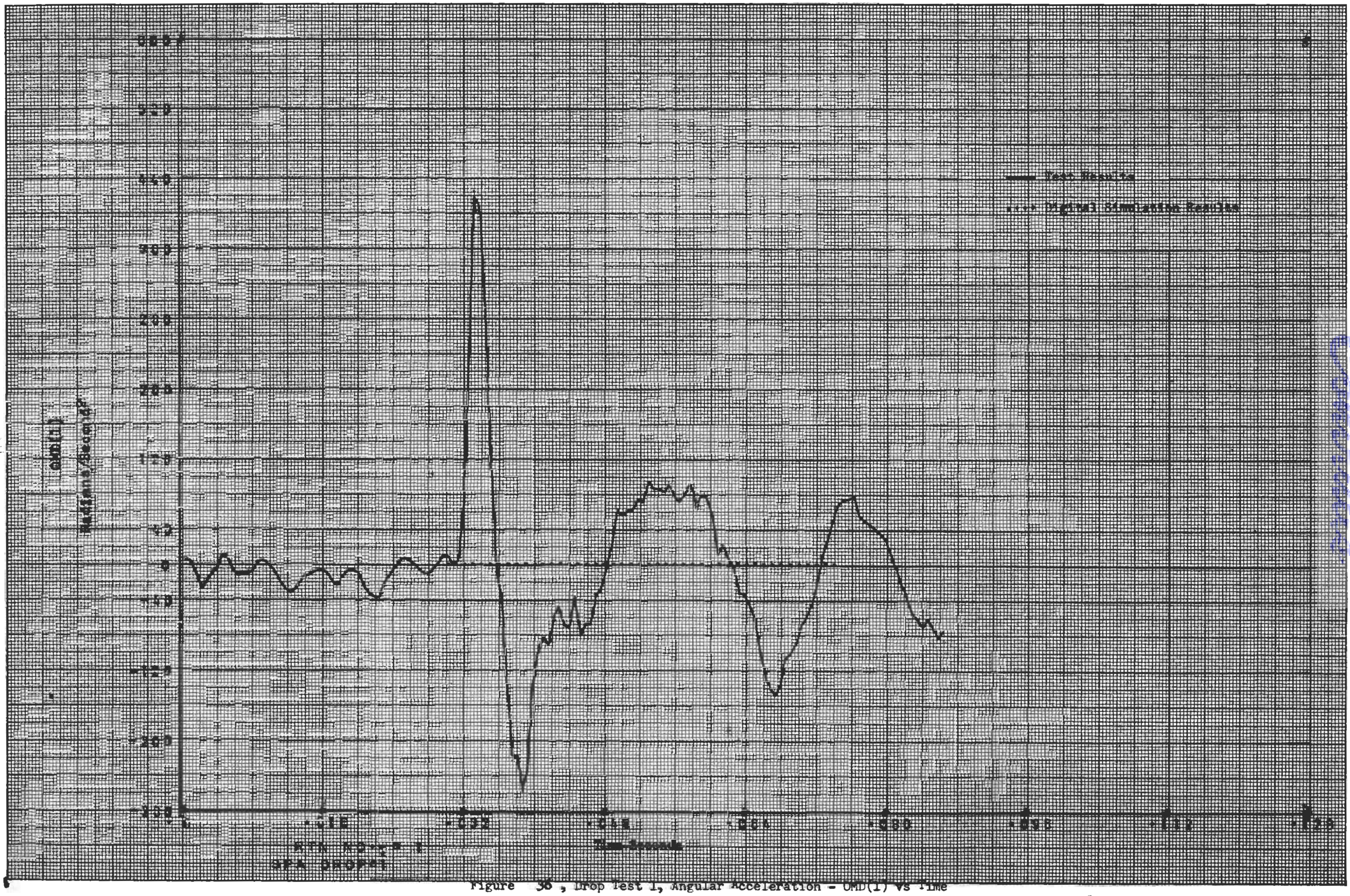

Figure 36 , Drop Test 1, Angular Acceleration - OMD(1) vs Time

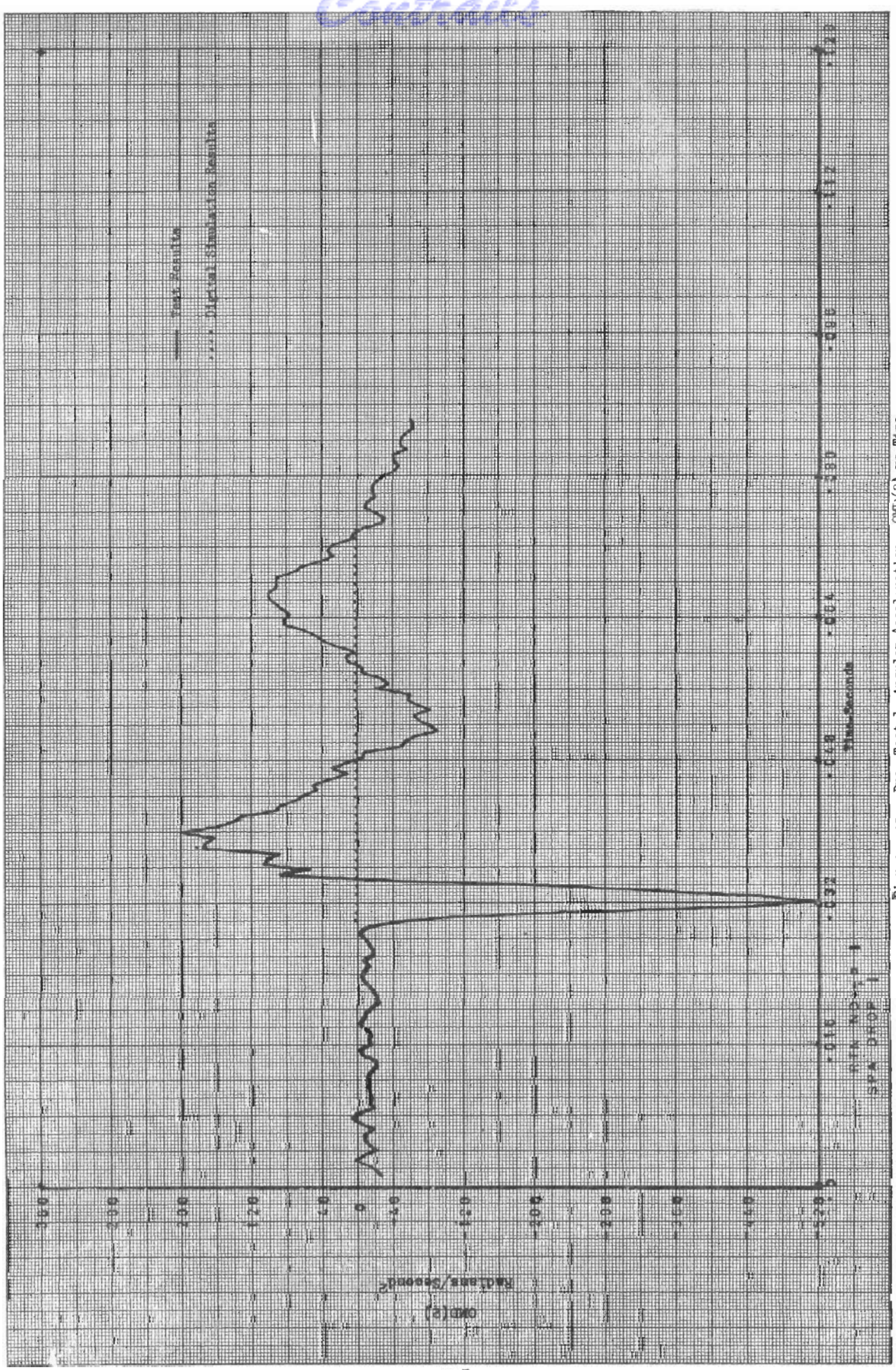

Figure 37 , Drop Test 1, Angular Acceleration - OMD(2) vs Time

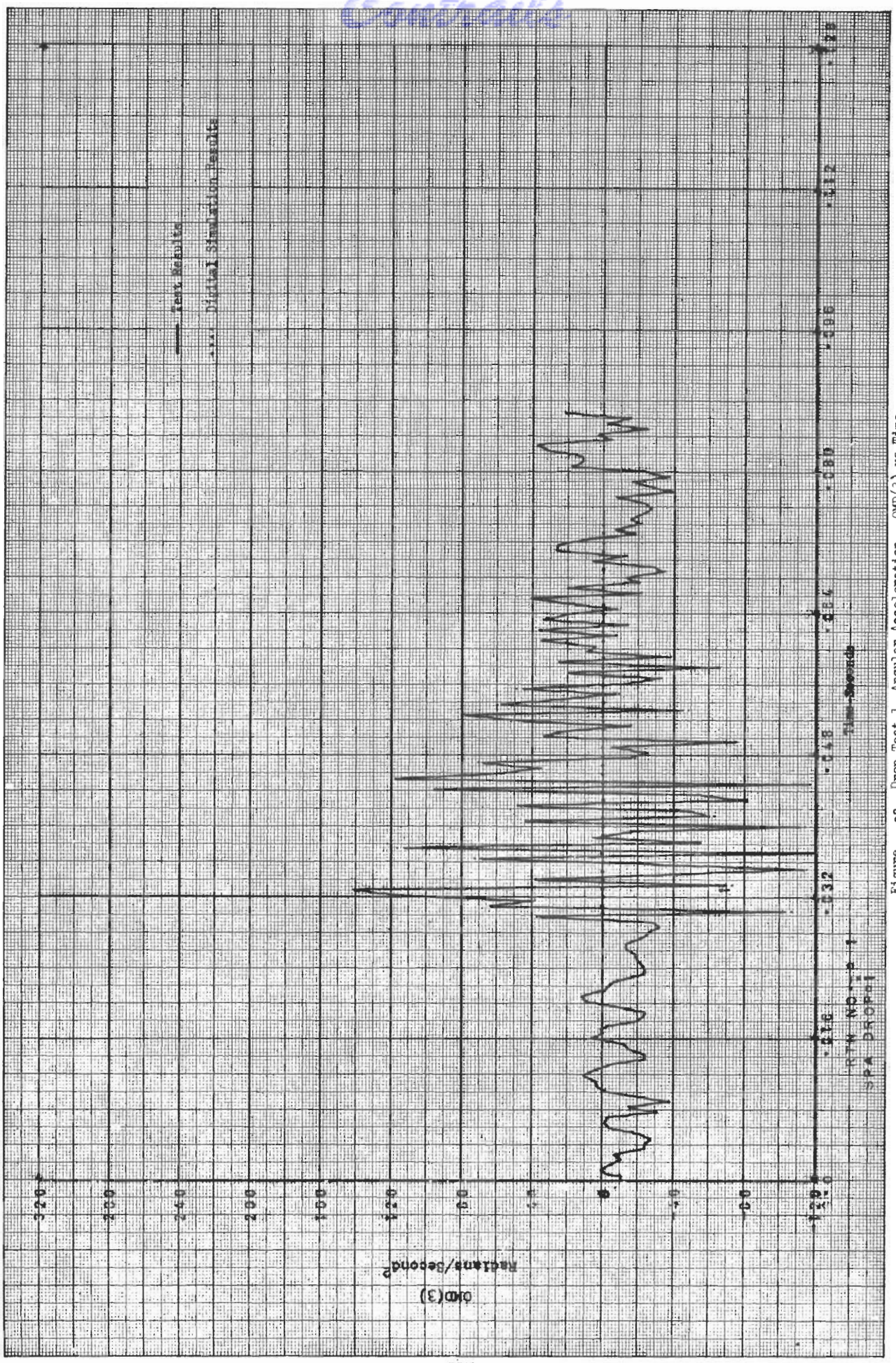

Figure 38, Drop Test 1, Angular Acceleration - OMD(3) vs Time

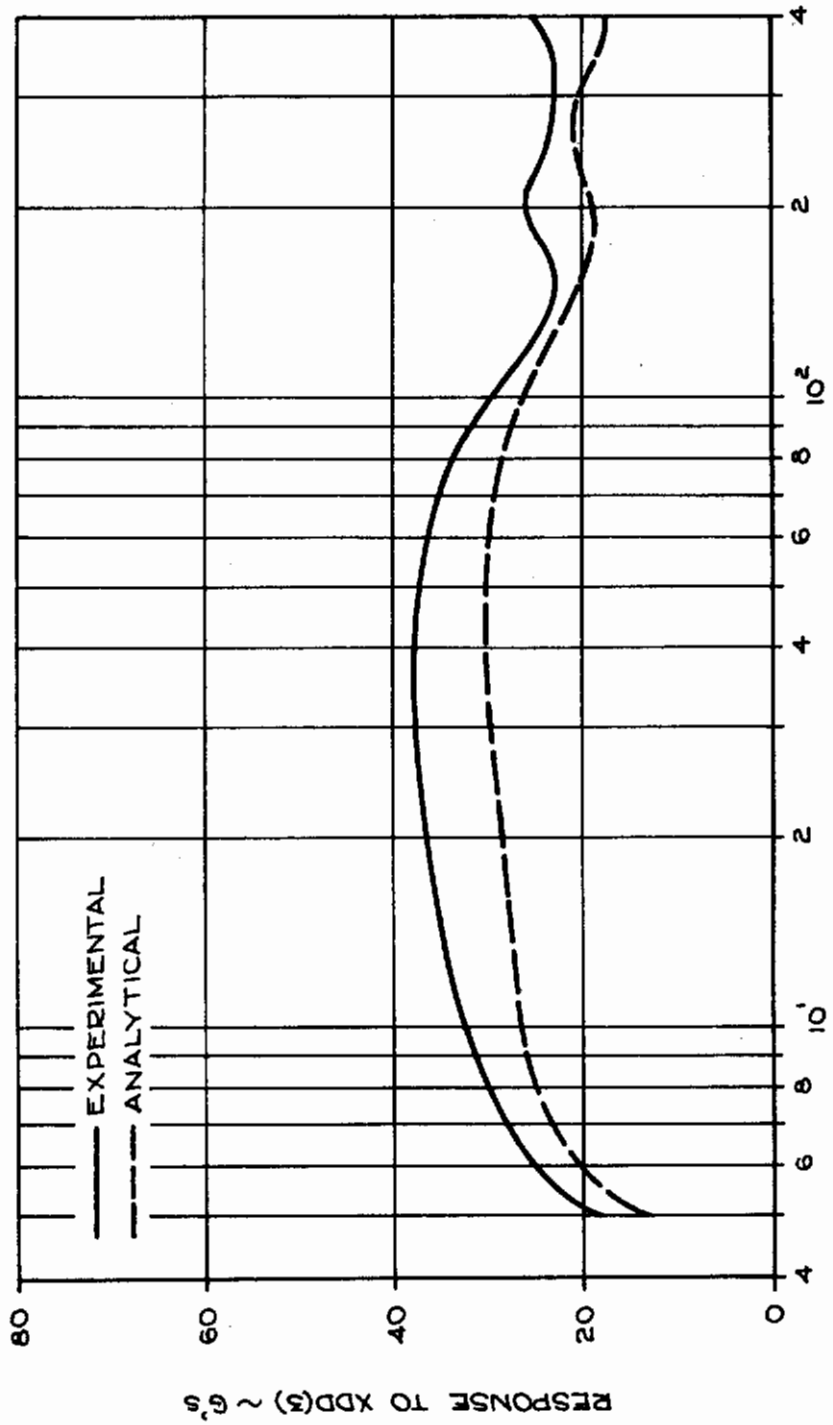

Figure 39, Drop Test 1, Shock Spectra Comparison

Figure 35 exhibits a typical variation in acceleration level for the XDD(3) coordinate resulting from crushing force errors discussed previously. Figure 39 is a comparison between test and simulation shock spectra.

Drop 2

The initial conditions for this drop were a vertical velocity with the capsule pitched, relative to the vertical velocity, 13 degrees down. Leg contact order was 1, 2, 4, 3. The leg numbering sequence has been shown previously in Figure 14, Section IV. Figure 42 shows the effect of sequential leg touchdown on the acceleration time history. In this same figure, the negative acceleration slopes, after reaching a maximum, are typical of the "softening" of the articulated leg as it is stroked. The difference in acceleration level is the result of the aforementioned difference between static and dynamic forces at the energy cells.

The excellent correlation shown in Figures 40, 43, 44 and 45 are indicative of essentially equal energy cell forces and good "digging in" of the peg legs. Figure 41, however, shows only good correlation. Figure 46 presents a comparison of shock spectra.

Drop 3

This drop had both a horizontal and vertical velocity with a slight capsule pitch angle. The vertical acceleration shown in Figure 49 shows that for the test drop, the capsule inclination was slightly greater than indicated from the movie film analysis. To obtain the small step shown on the initial slope would require about a 2 degree error for the pitch angle shown in Table 5 and is within the accuracy limits of the film for this shot due to poor photographic resolution.

Figures 49 and 51 show good correlation while Figures 47, 48, 50 and 52 show poor correlation. A comparison of shock spectra is presented in Figure 53.

Drop 4

A large capsule pitch angle was used in this drop along with both horizontal and vertical velocities. Good correlation is shown in Figures 54, 56, 57 and 58. Poor correlation is shown in Figures 55 and 59 (XDD(2) and OMD(3)). Figure 60 is a comparison of experimental and analytical shock spectra.

Drop 5

This drop was intended to fully stroke the parallelogram energy absorbers by increasing the vertical velocity from 17.5 to 24.0 feet per second. Capsule inclination was 6.3 degrees with no horizontal velocity. The capsule bottom impacted the asphalt surface as shown by the XDD(3) curve in Figure 63. The downward velocity at impact was 8 feet per second and is equivalent to a 1 foot

Figure 40 , Drop Test 2, Translational Acceleration - XDD(1) vs Time

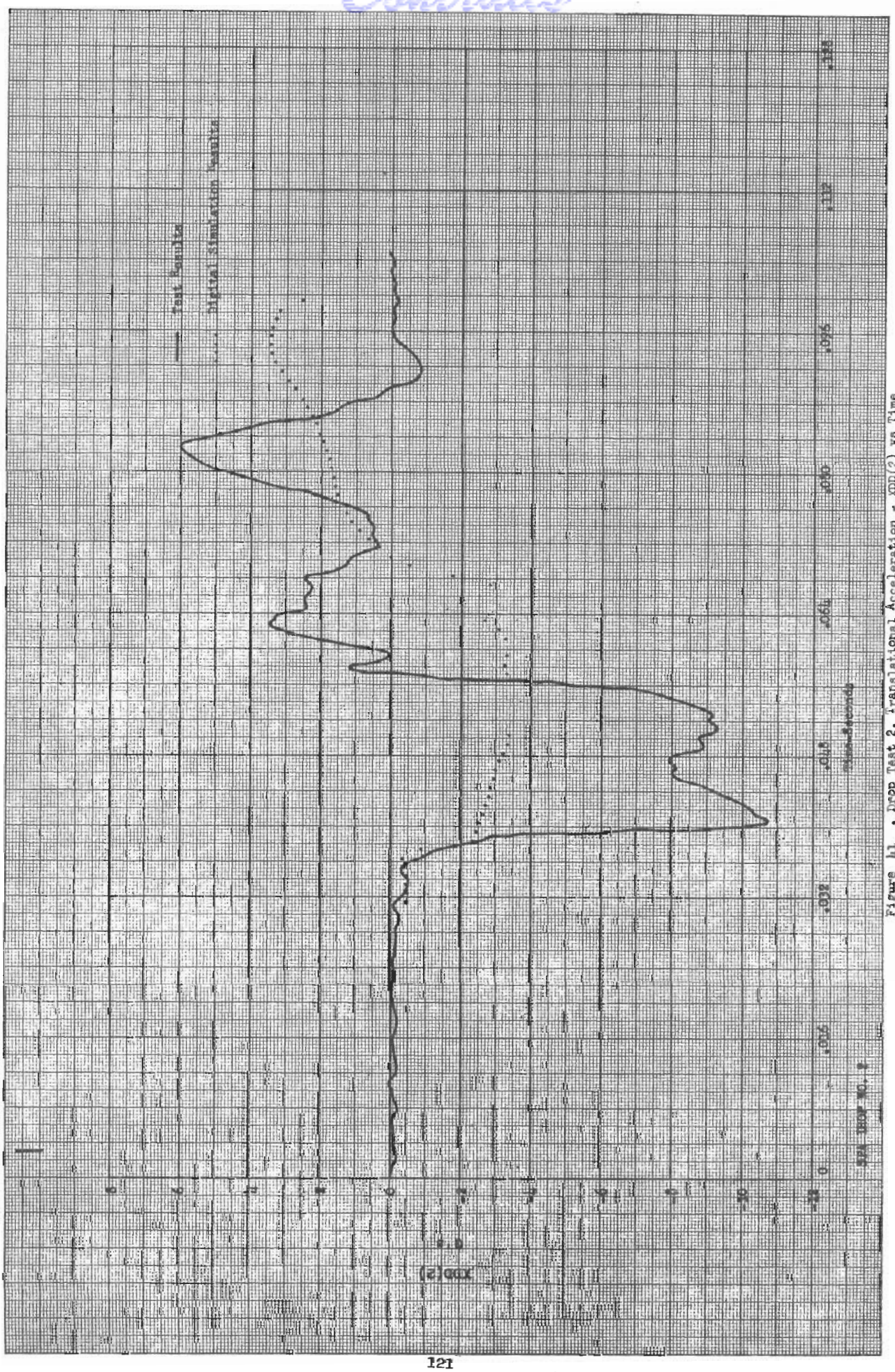

Figure 41 , Drop Test 2, Translational Acceleration - XDD(2) vs Time

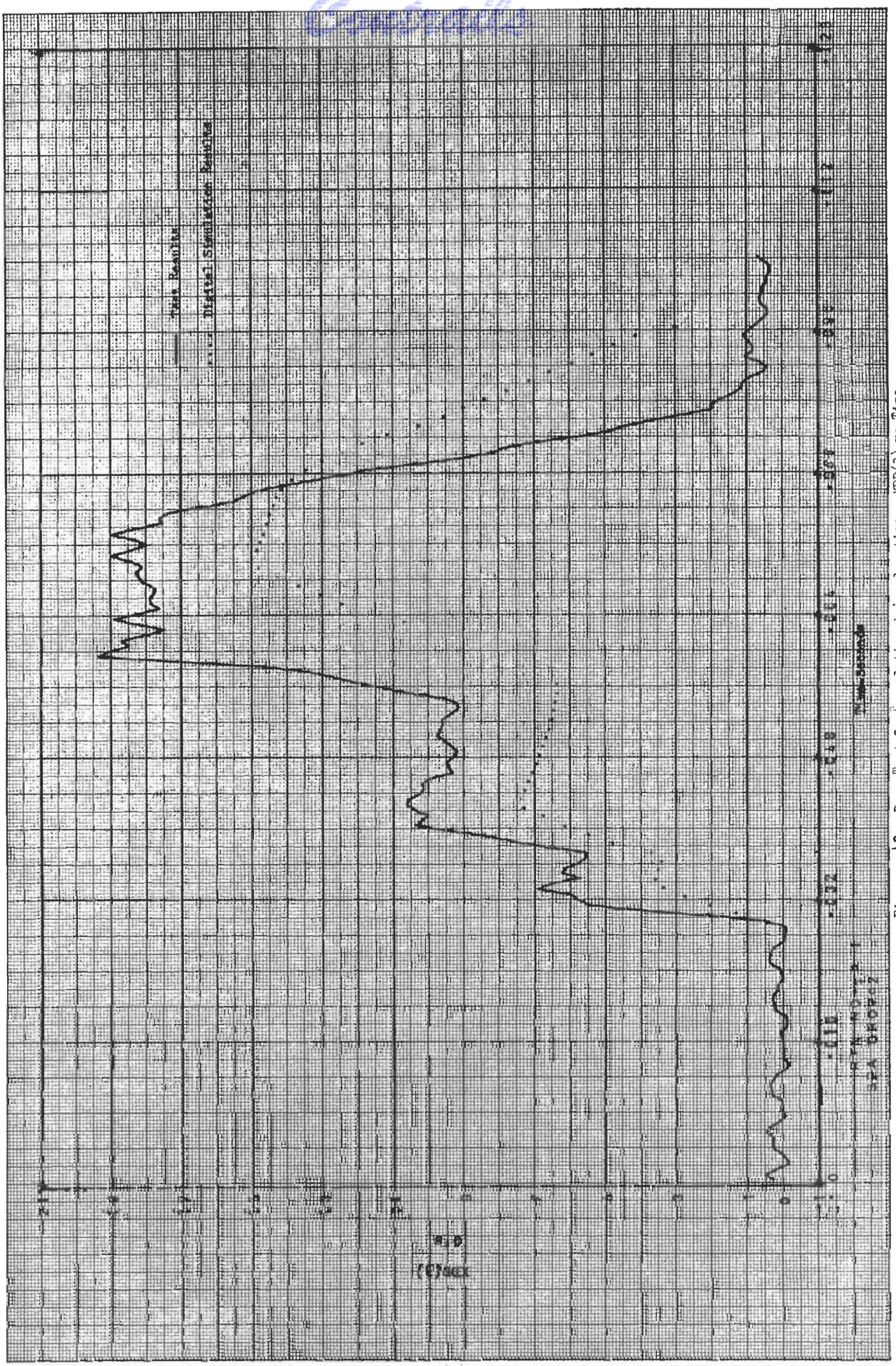

Figure 42 , Drop Test 2, Translational Acceleration - XDD(3) vs Time

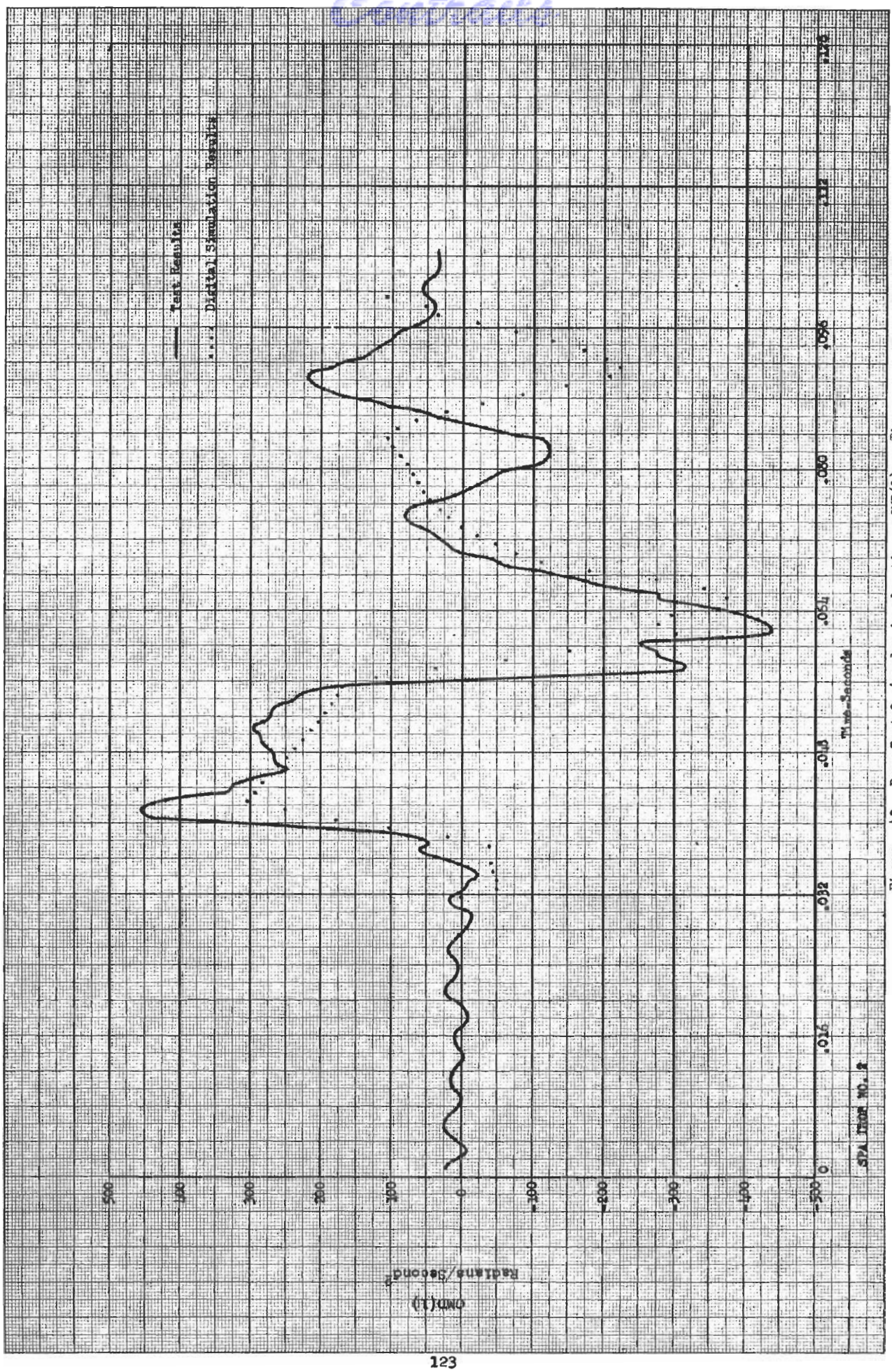

Figure 43 , Drop Test 2, Angular Acceleration - OMD(1) vs Time

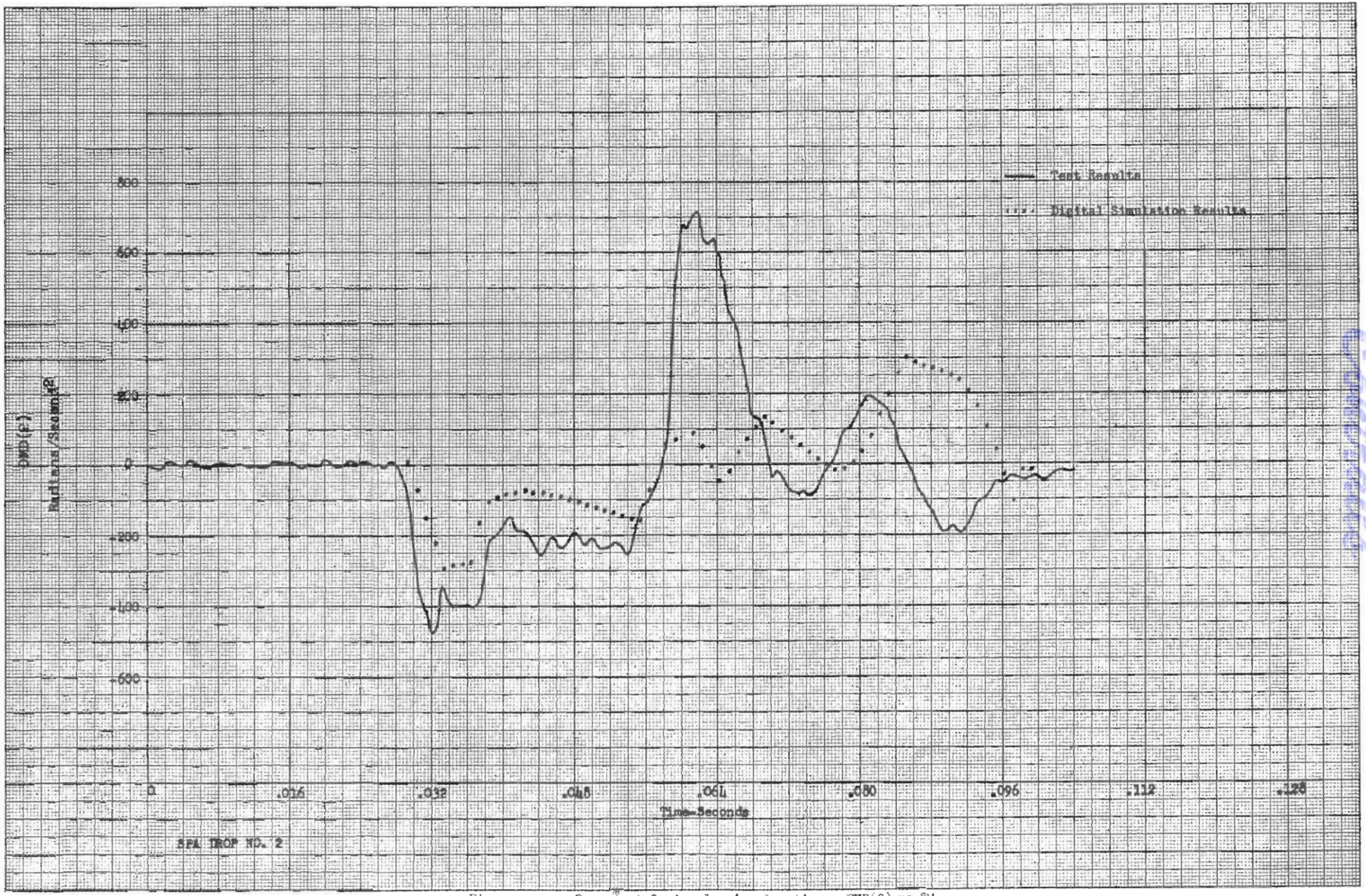

Figure 44 , Drop Test 2, Angular Acceleration - ΩMD(2) vs Time

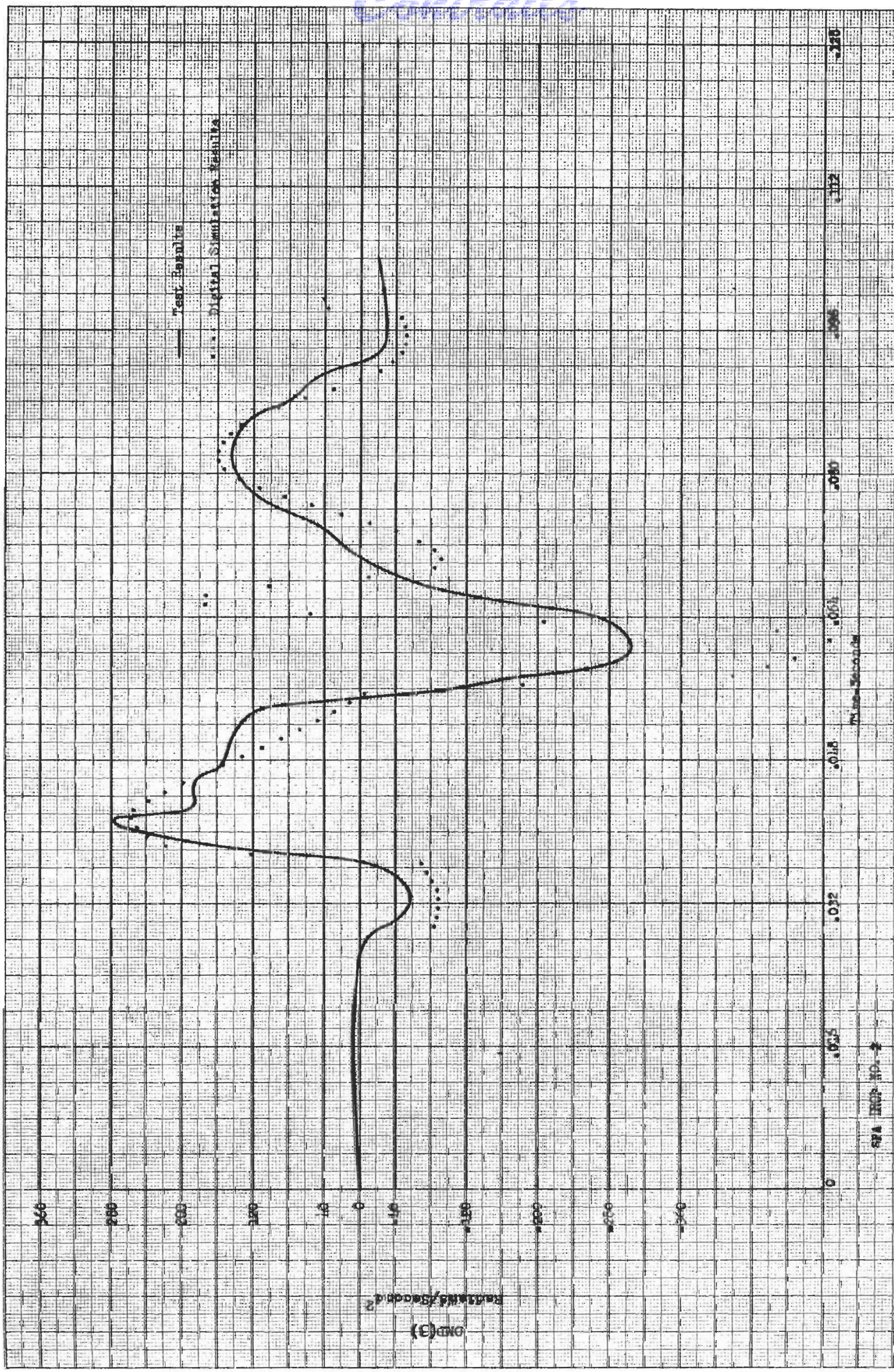

Figure 45 , Drop Test 2, Angular Acceleration - OMD(3) vs Time

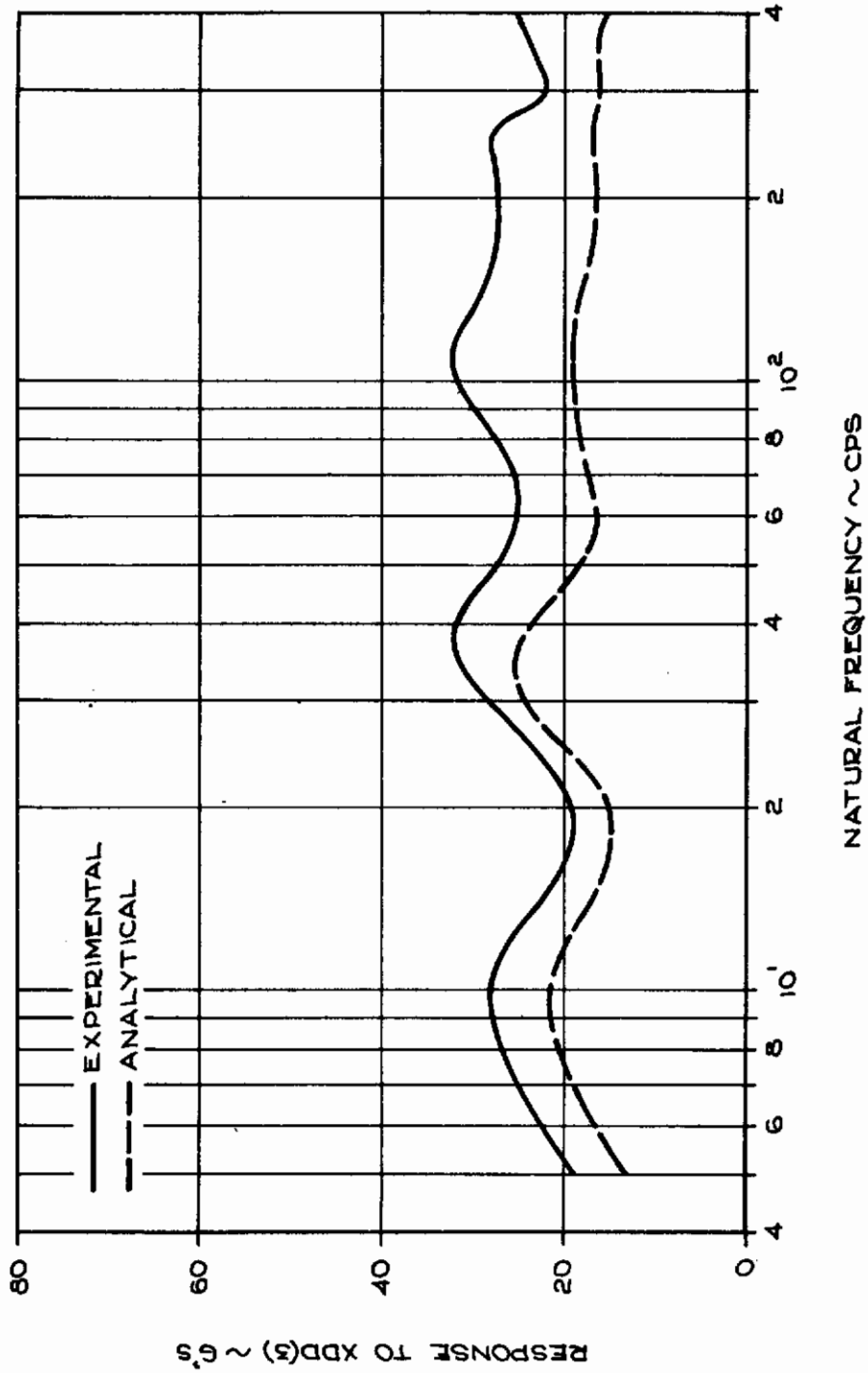

Figure 46, Drop Test 2, Shock Spectra Comparison

Figure 47 , Drop Test 3, Translational Acceleration - XDD(1) vs Time

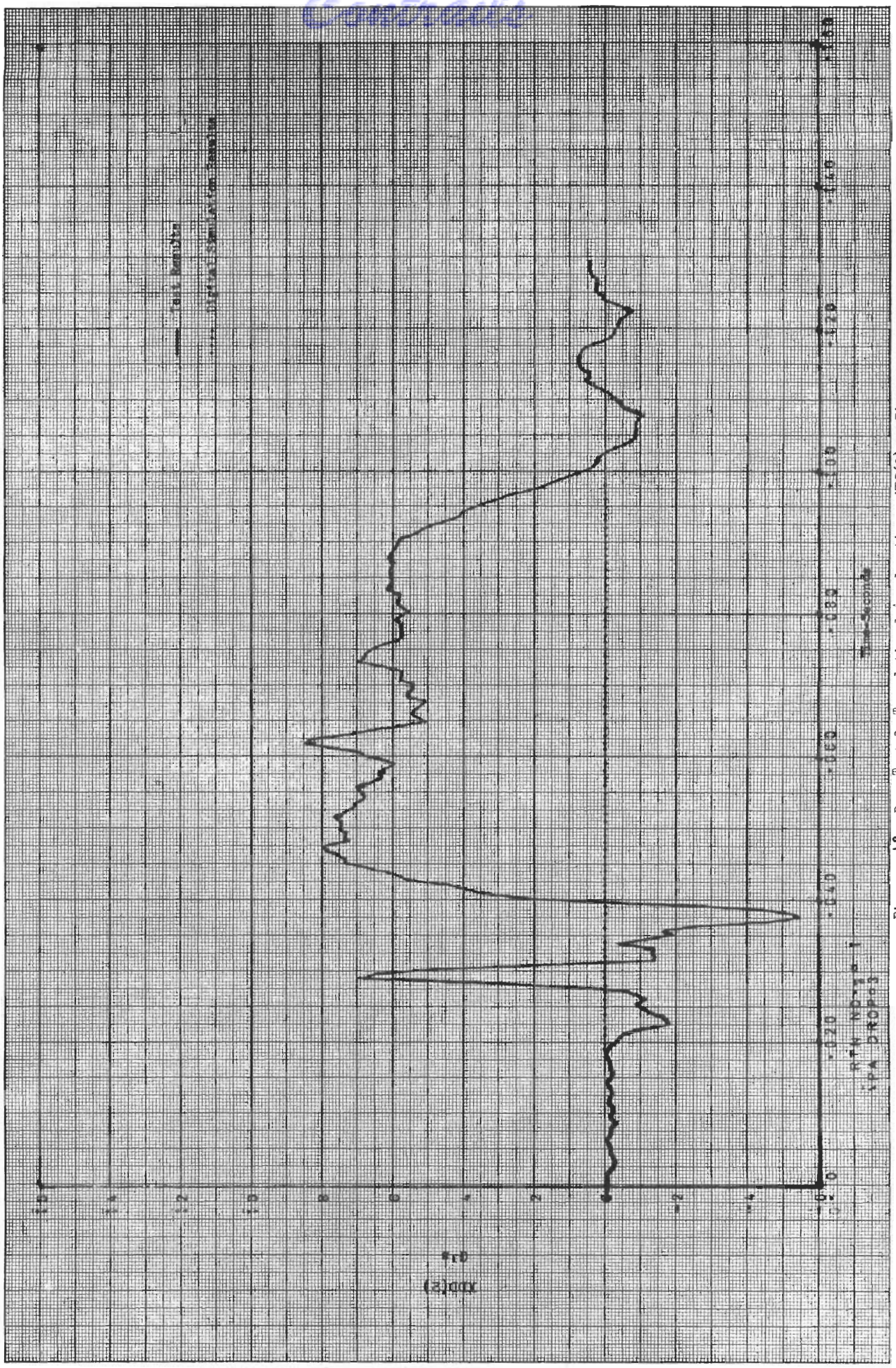

Figure 48, Drop Test 3, Translational Acceleration - XDD(2) vs Time

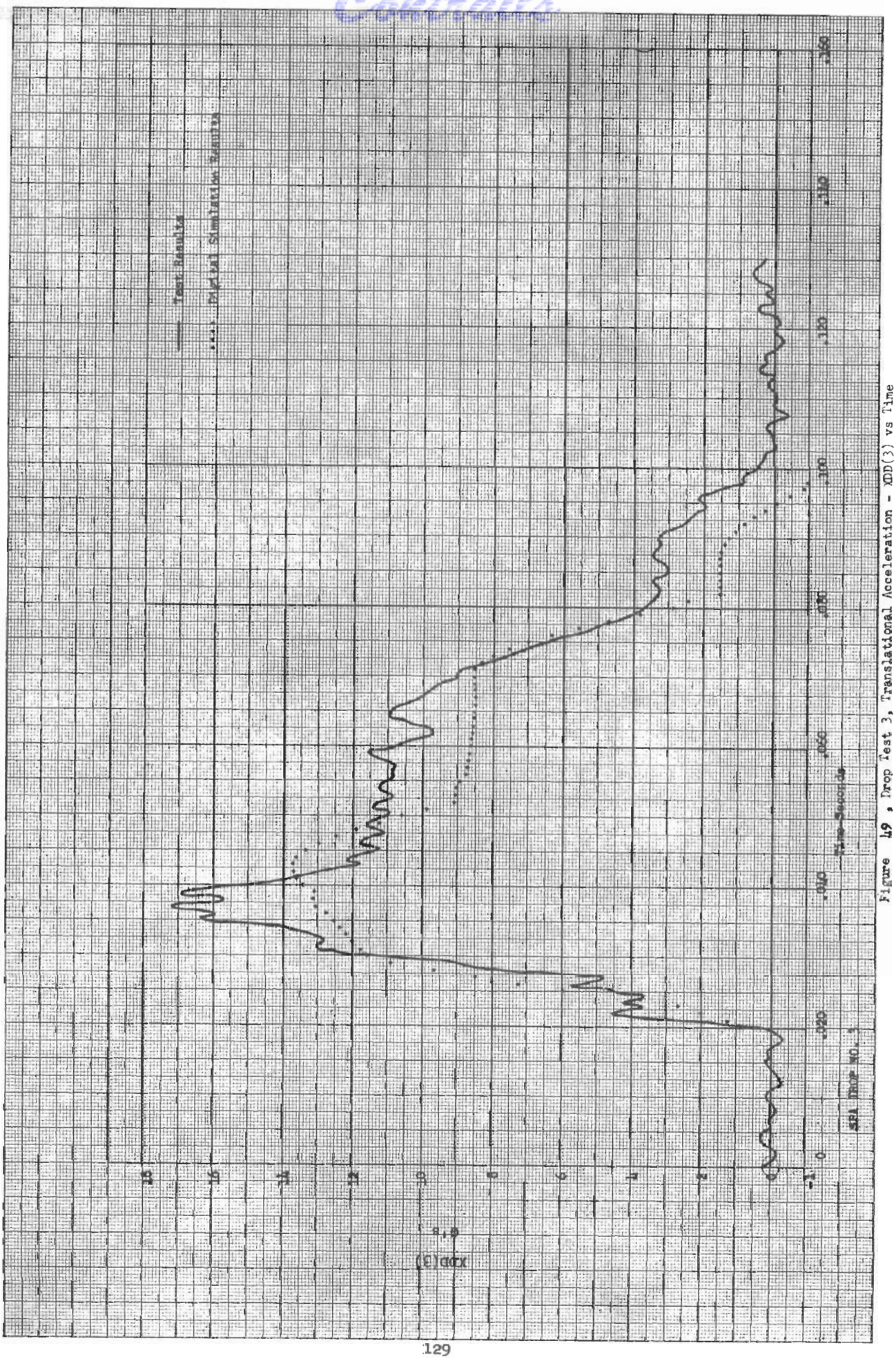

Figure 49 , Drop Test 3, Translational Acceleration - $\ddot{x}_{CG}(3)$ vs Time

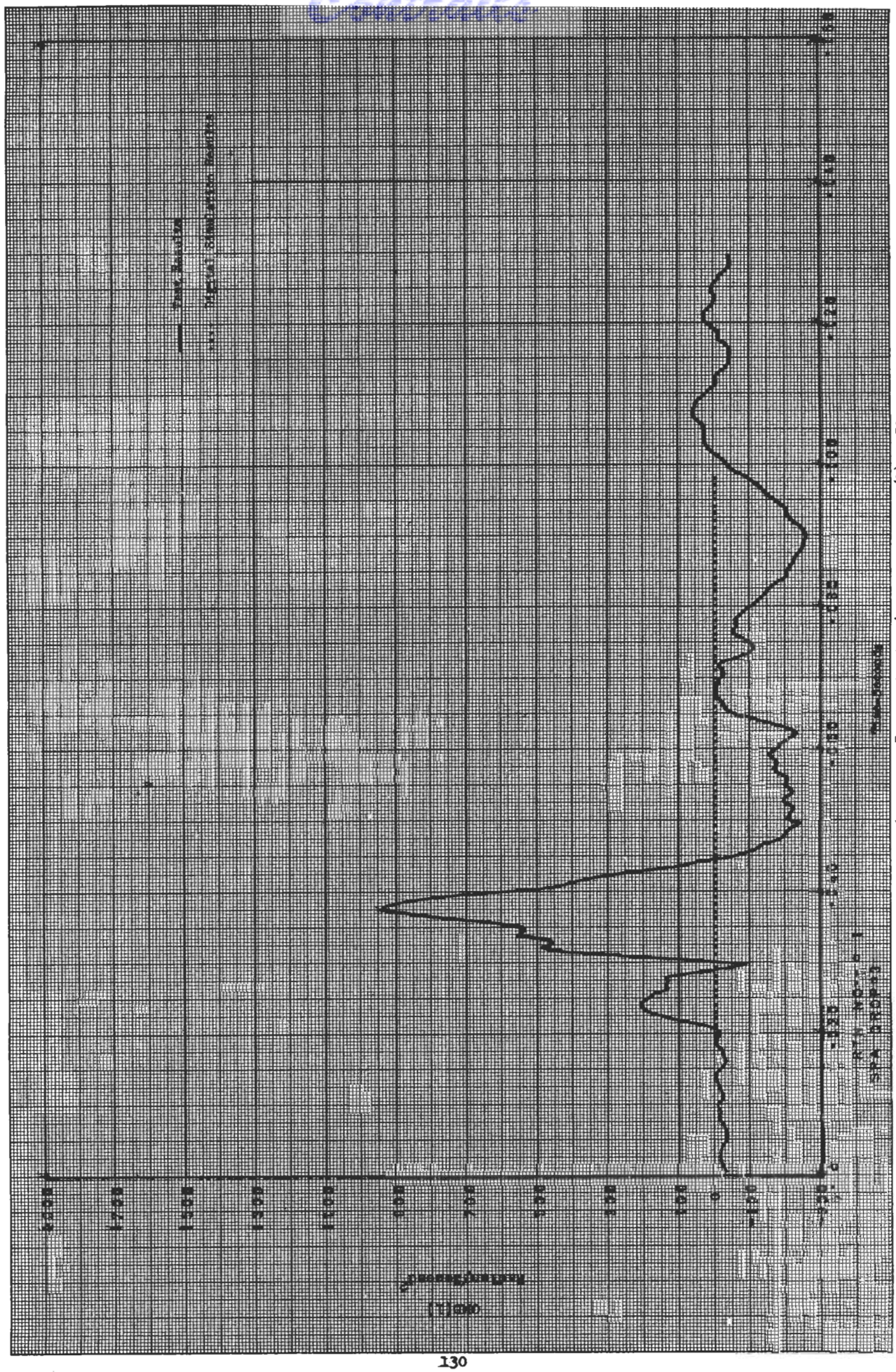

Figure 50 , Drop Test 3, Angular Acceleration - OMD(1) vs Time

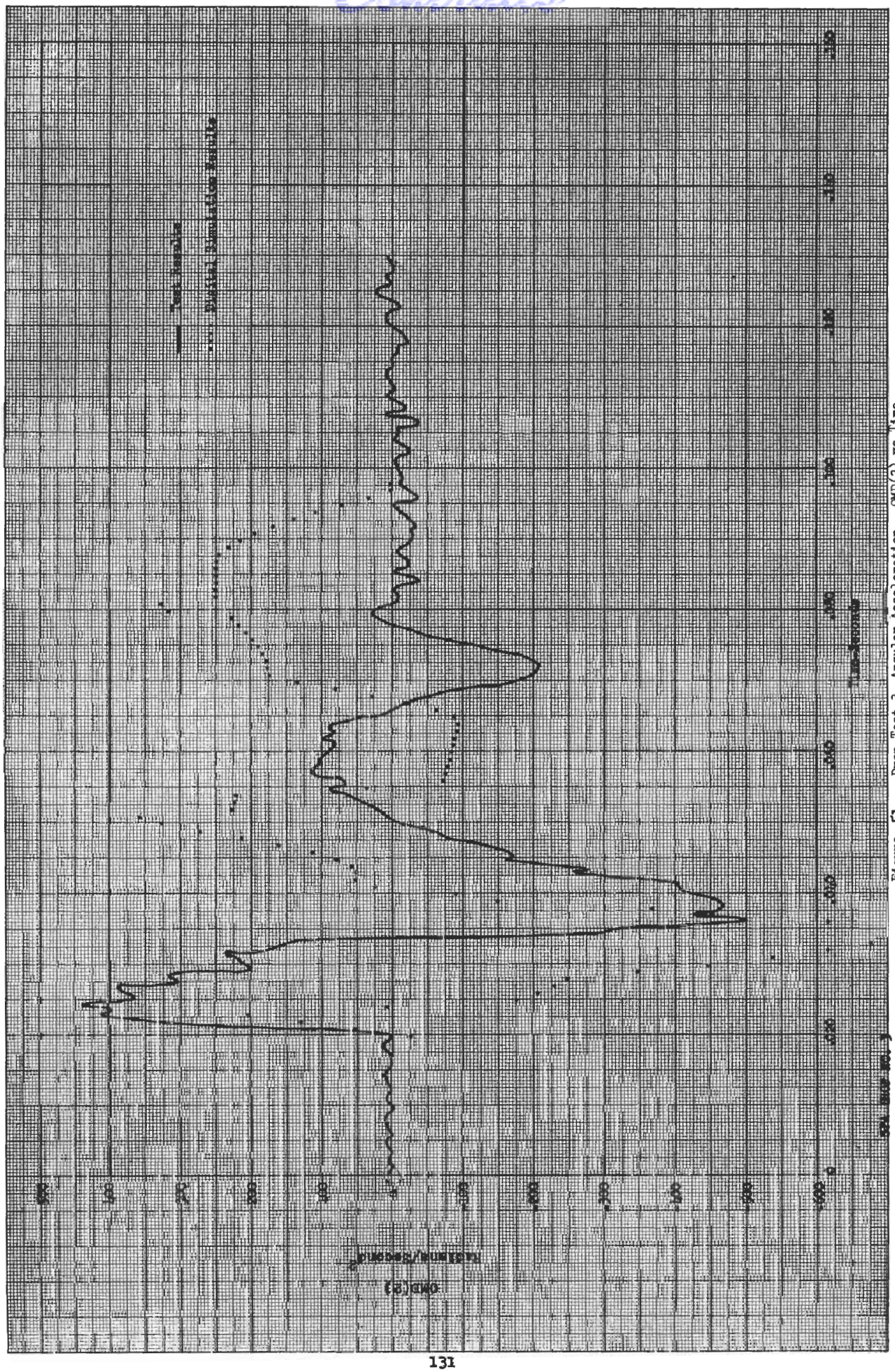

Figure 51 , Drop Test 3, Angular Acceleration - OMD(2) vs Time

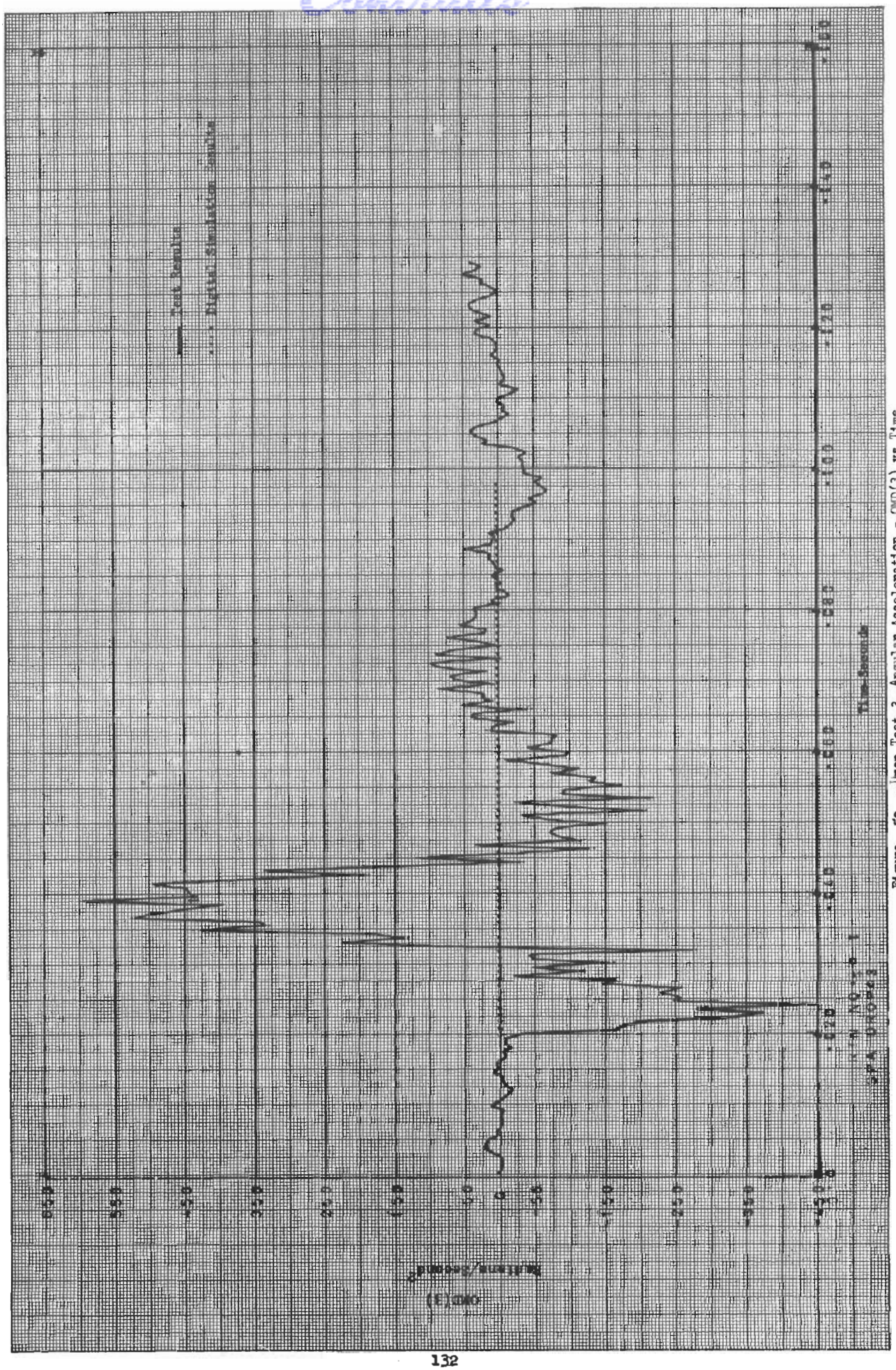

Figure 52 , Drop Test 3, Angular Acceleration - OMD(3) vs Time

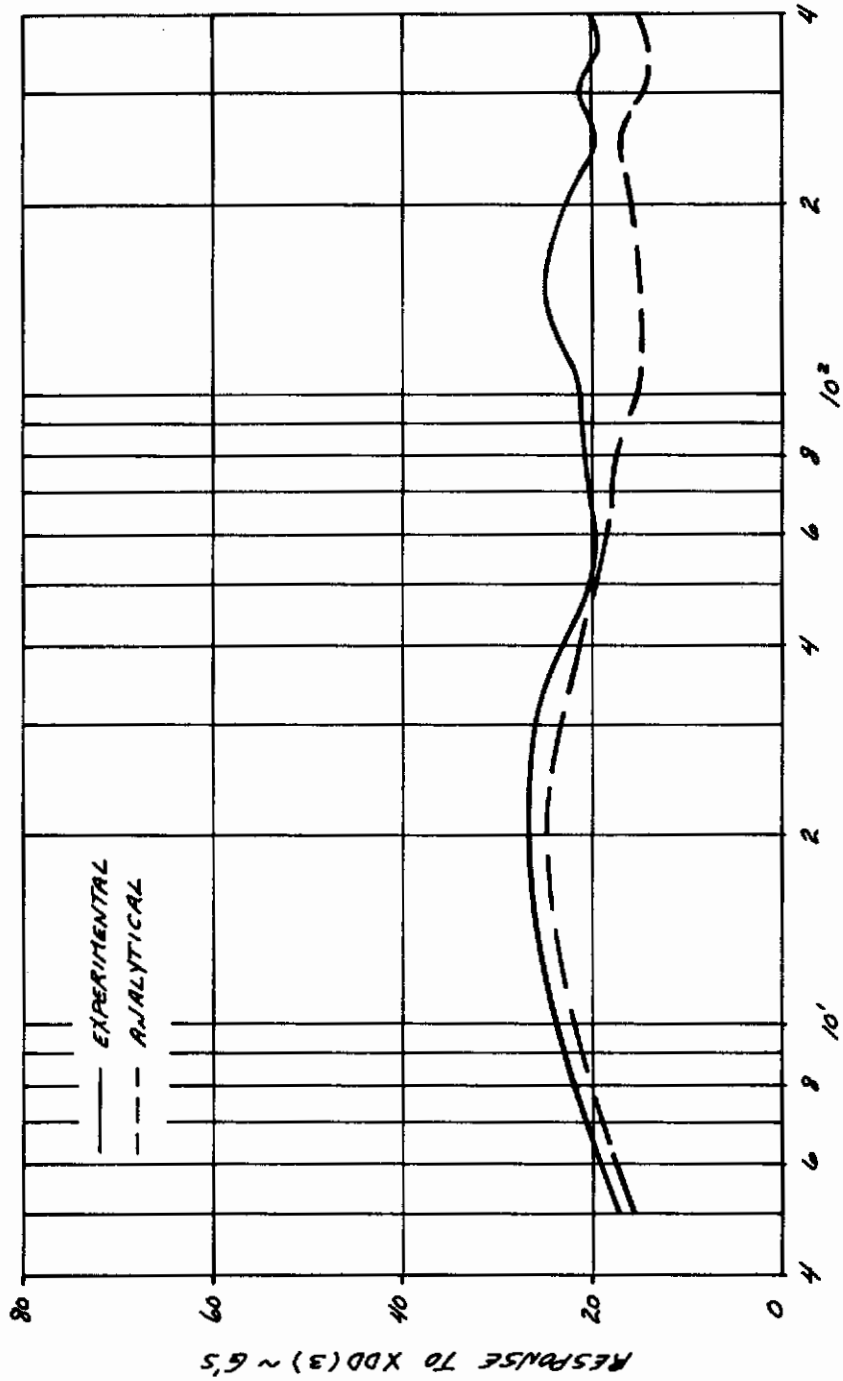

Figure 53, Drop Test 3, Shock Spectra Comparison

Figure 54 , Drop Test 4, Translational Acceleration - XDD(1) vs Time

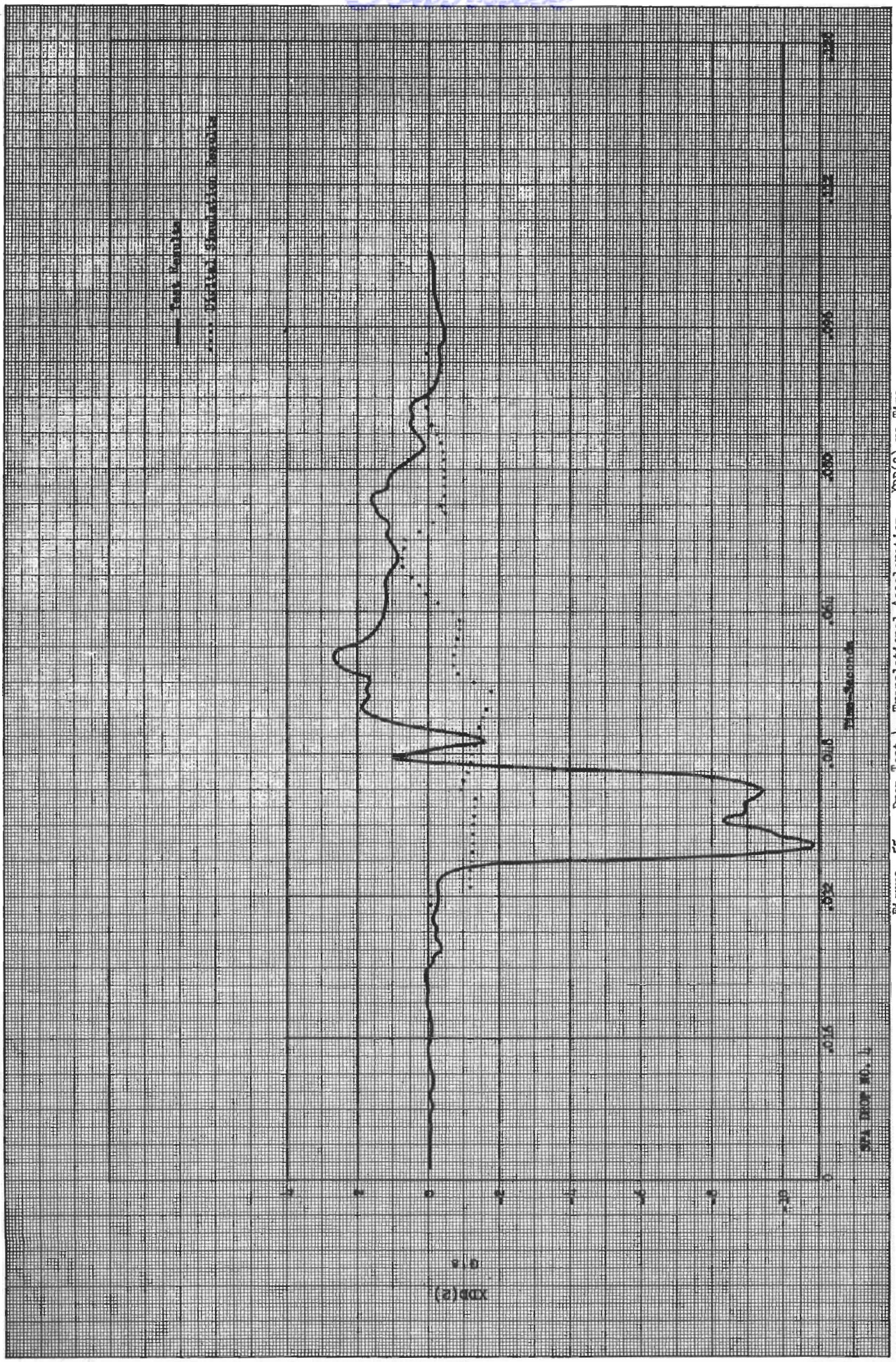

Figure 55 , Drop Test 4, Translational Acceleration - XDD(2) vs Time

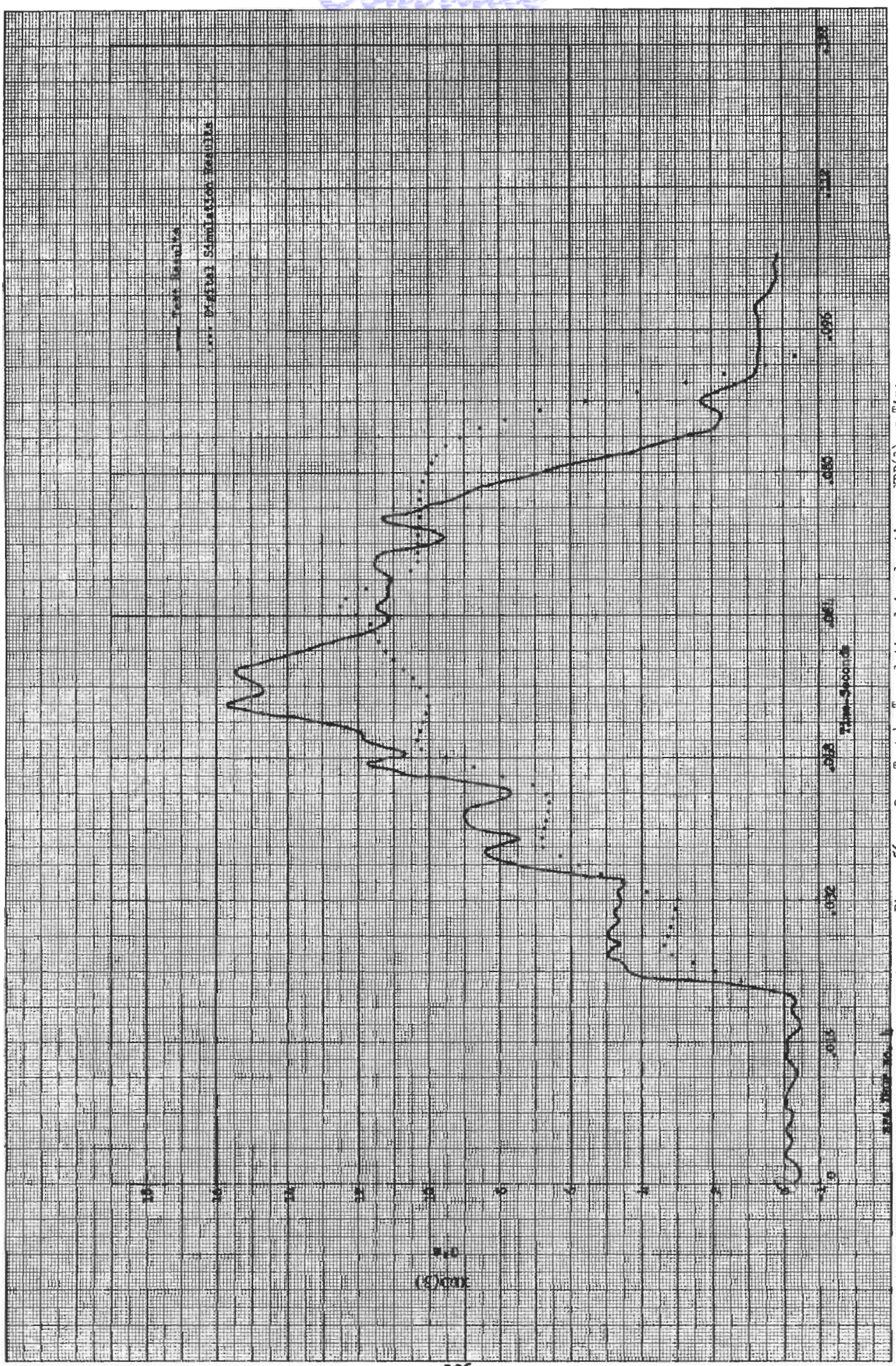

Figure 56 , Drop Test 4, Translational Acceleration - XDD(3) vs Time

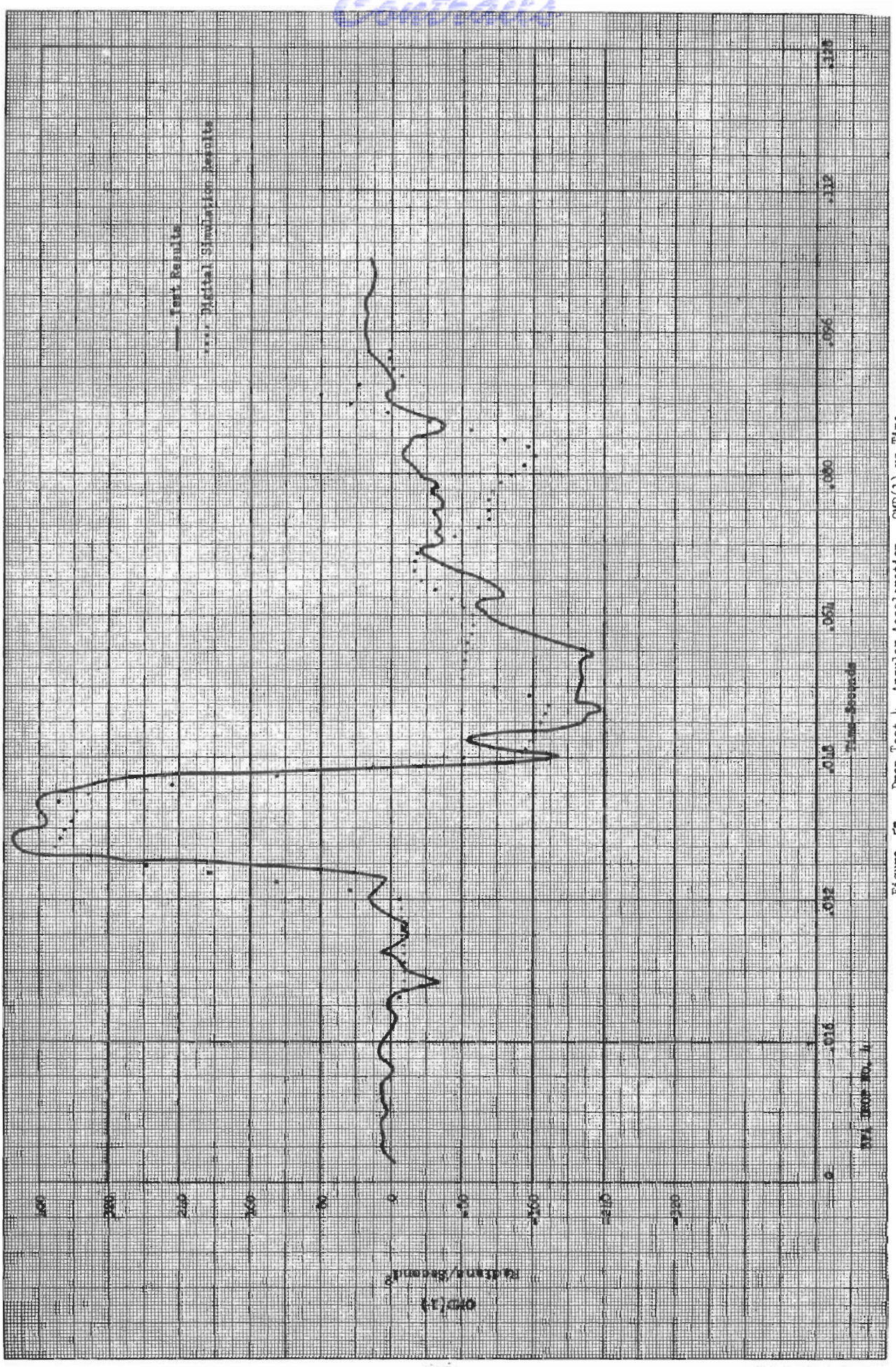

Figure 57 , Drop Test 4, Angular Acceleration - CMD(1) vs Time

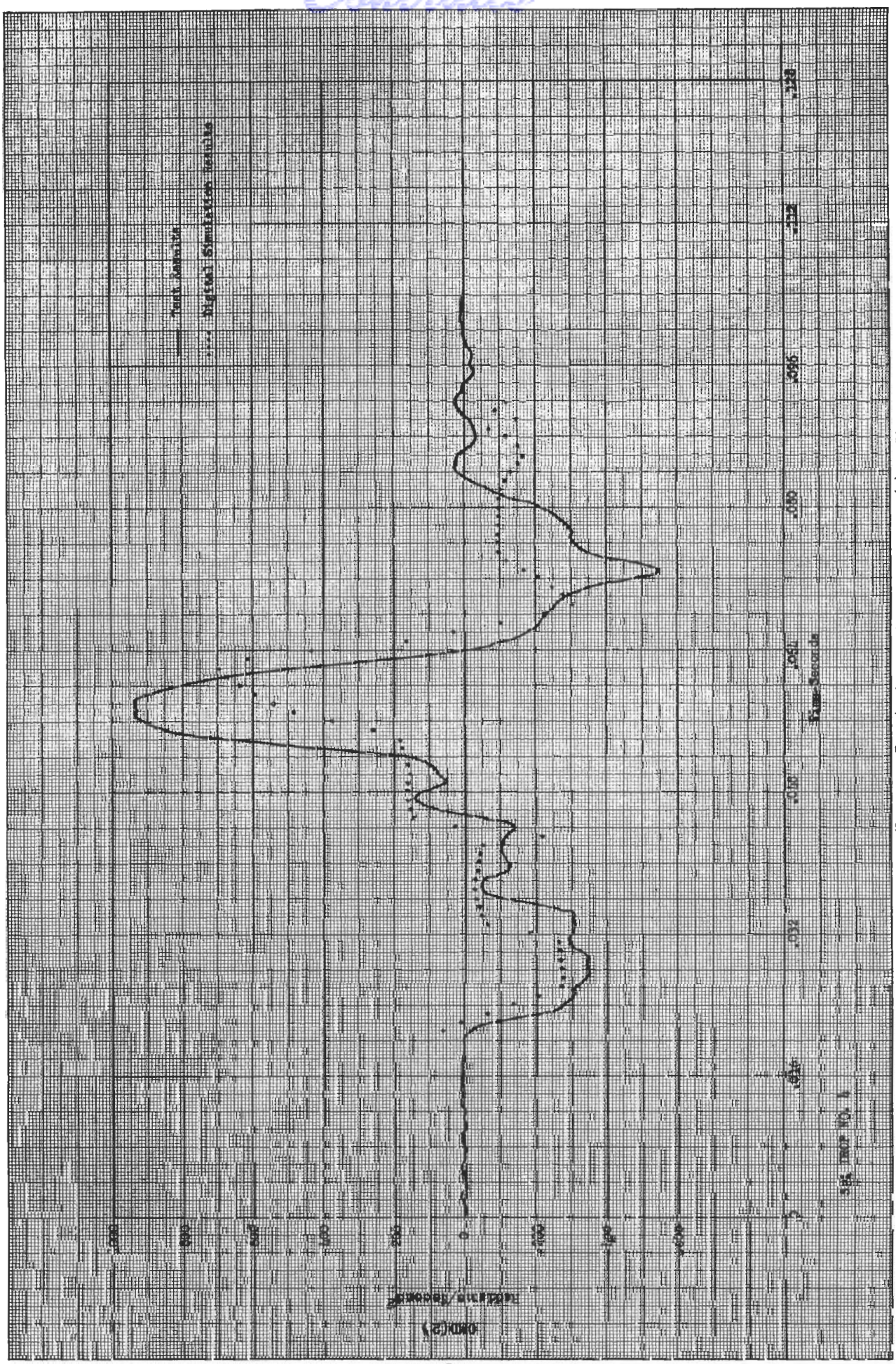

Figure 58 , Drop Test 4, Angular Acceleration - OMD(2) vs Time

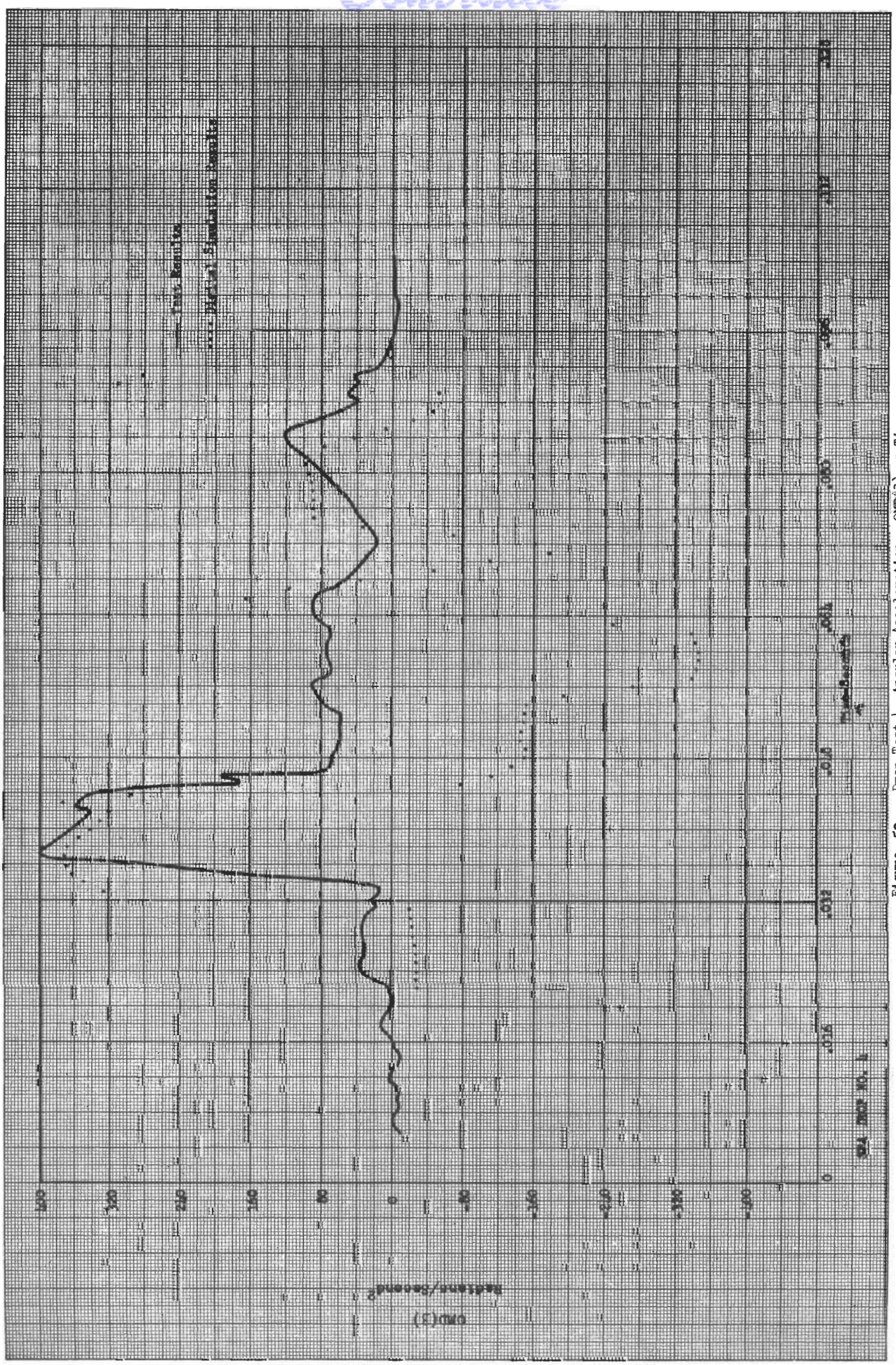

Figure 59 , Drop Test 4, Angular Acceleration - $\dot{\omega}_{(3)}$ vs Time

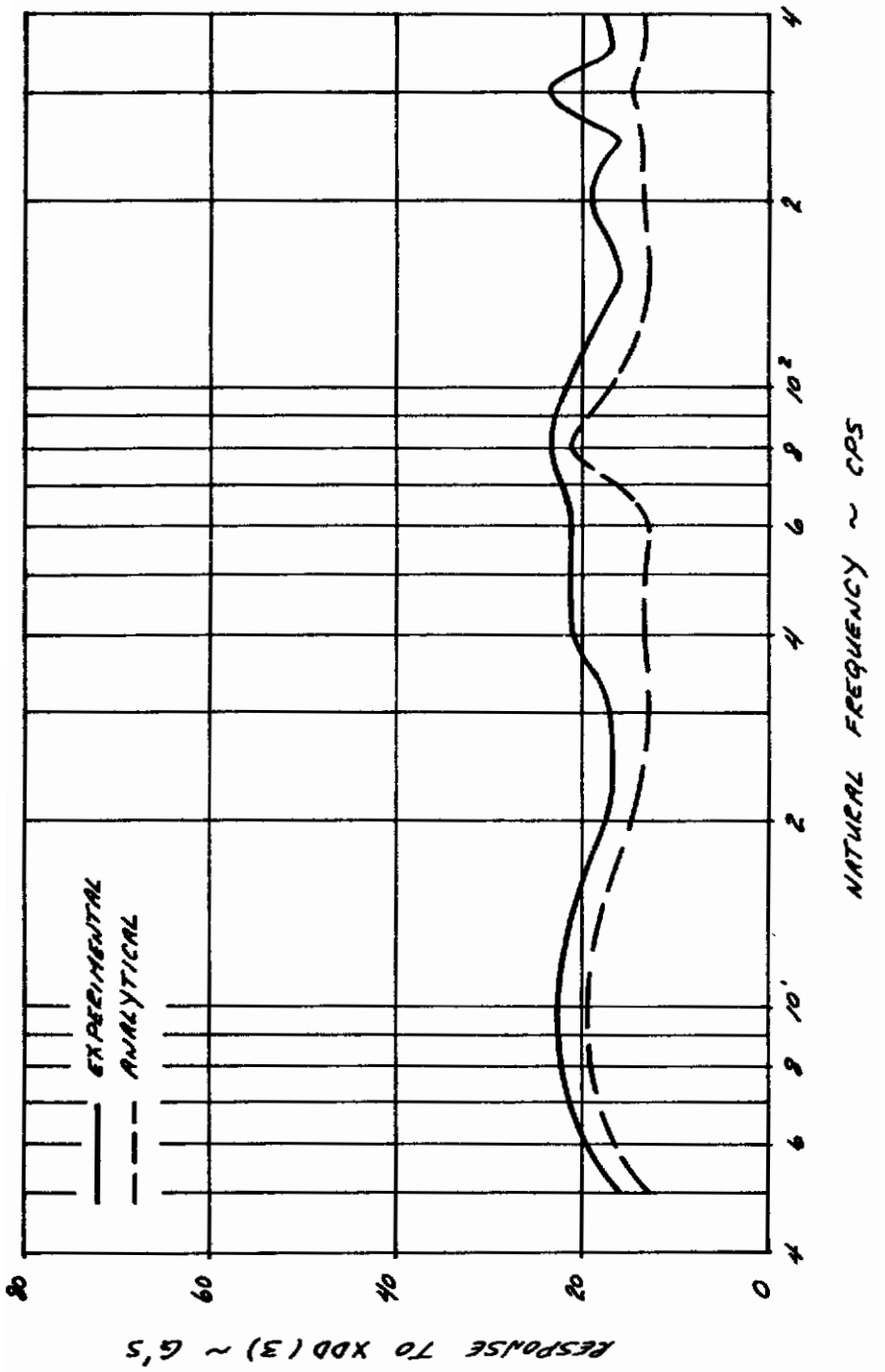

Figure 60, Drop Test 4, Shock Spectra Comparison

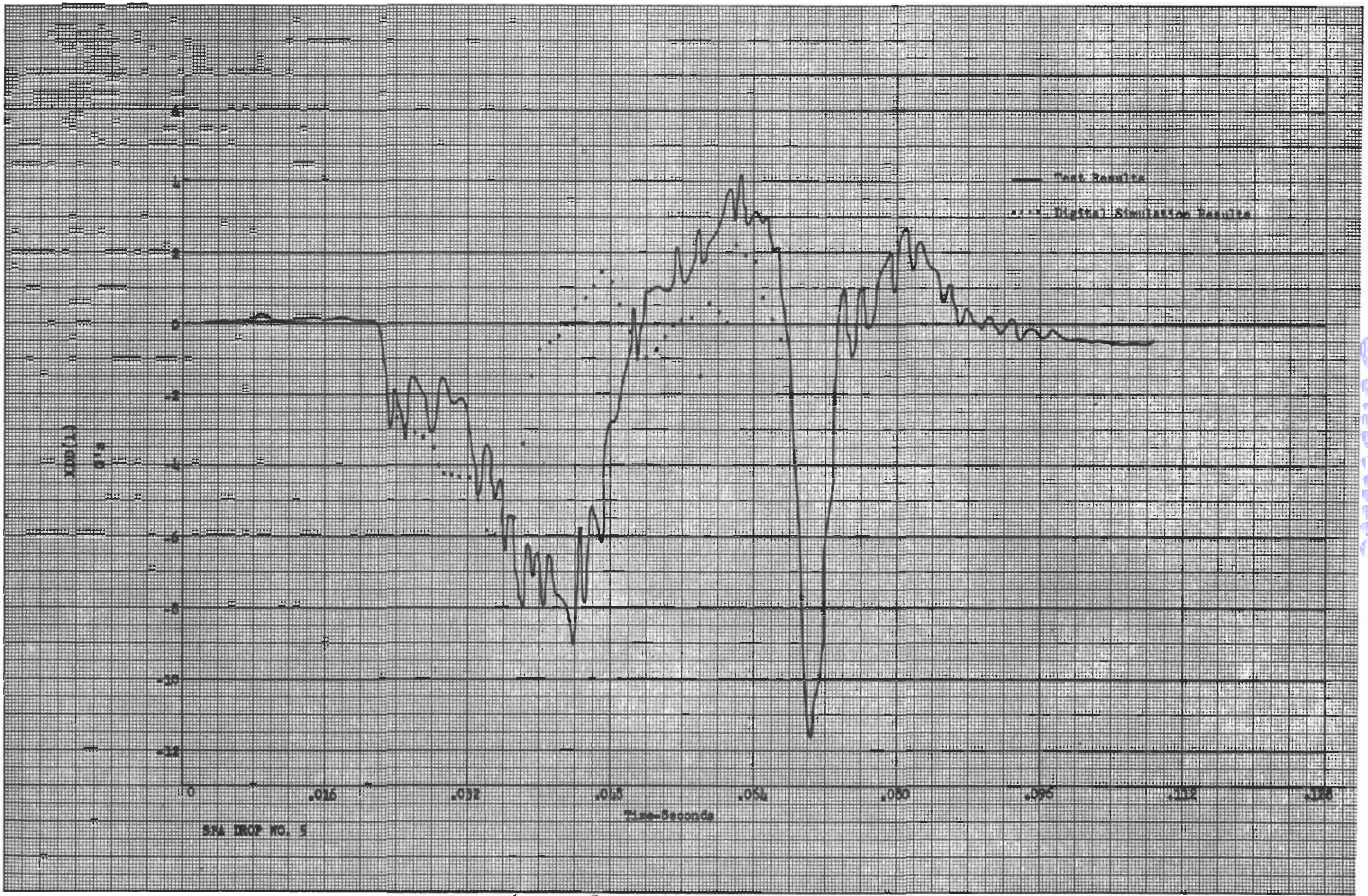

Figure 61 , Drop Test 5, Translational Acceleration - XDD(1) vs Time

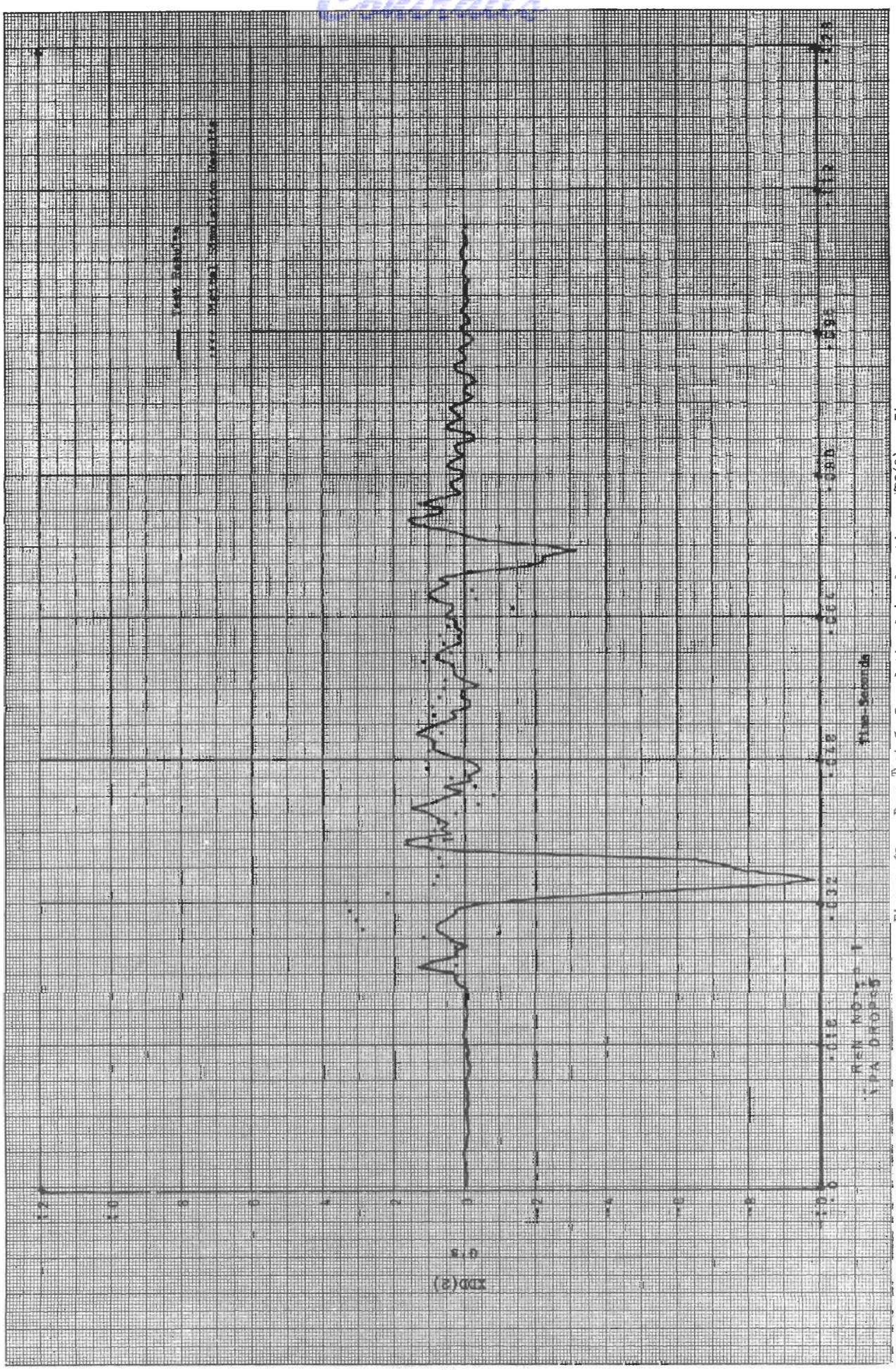

Figure 62 . Drop Test 5, Translational Acceleration - $\ddot{X}D\Gamma(2)$ vs Time

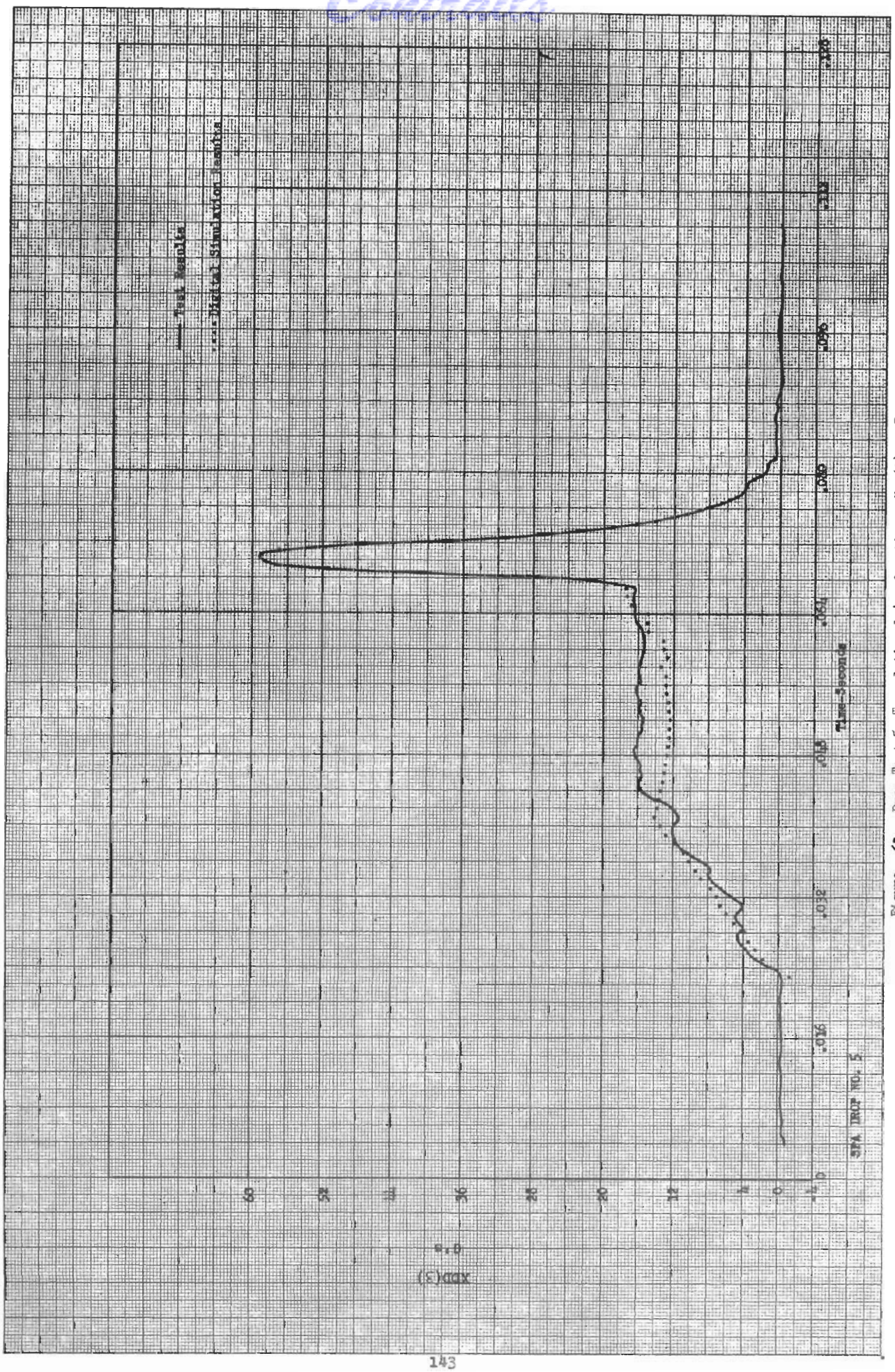

Figure 63 , Drop Test 5, Translational Acceleration - XDD(3) vs Time

Figure 64 , Drop Test 5, Angular Acceleration - OMD(1) vs Time

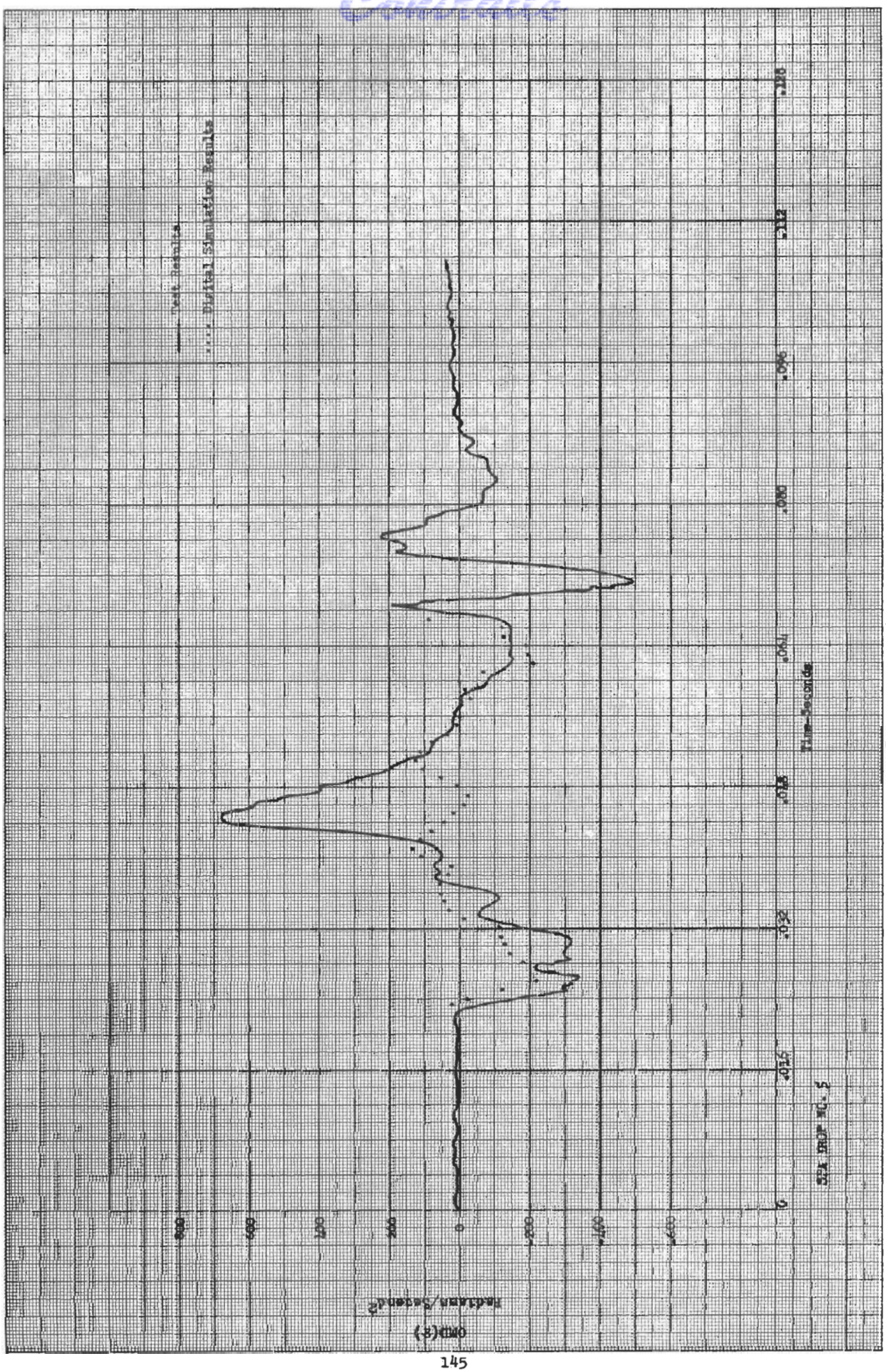

Figure 65 , Drop Test 5, Angular Acceleration - OMD(2) vs Time

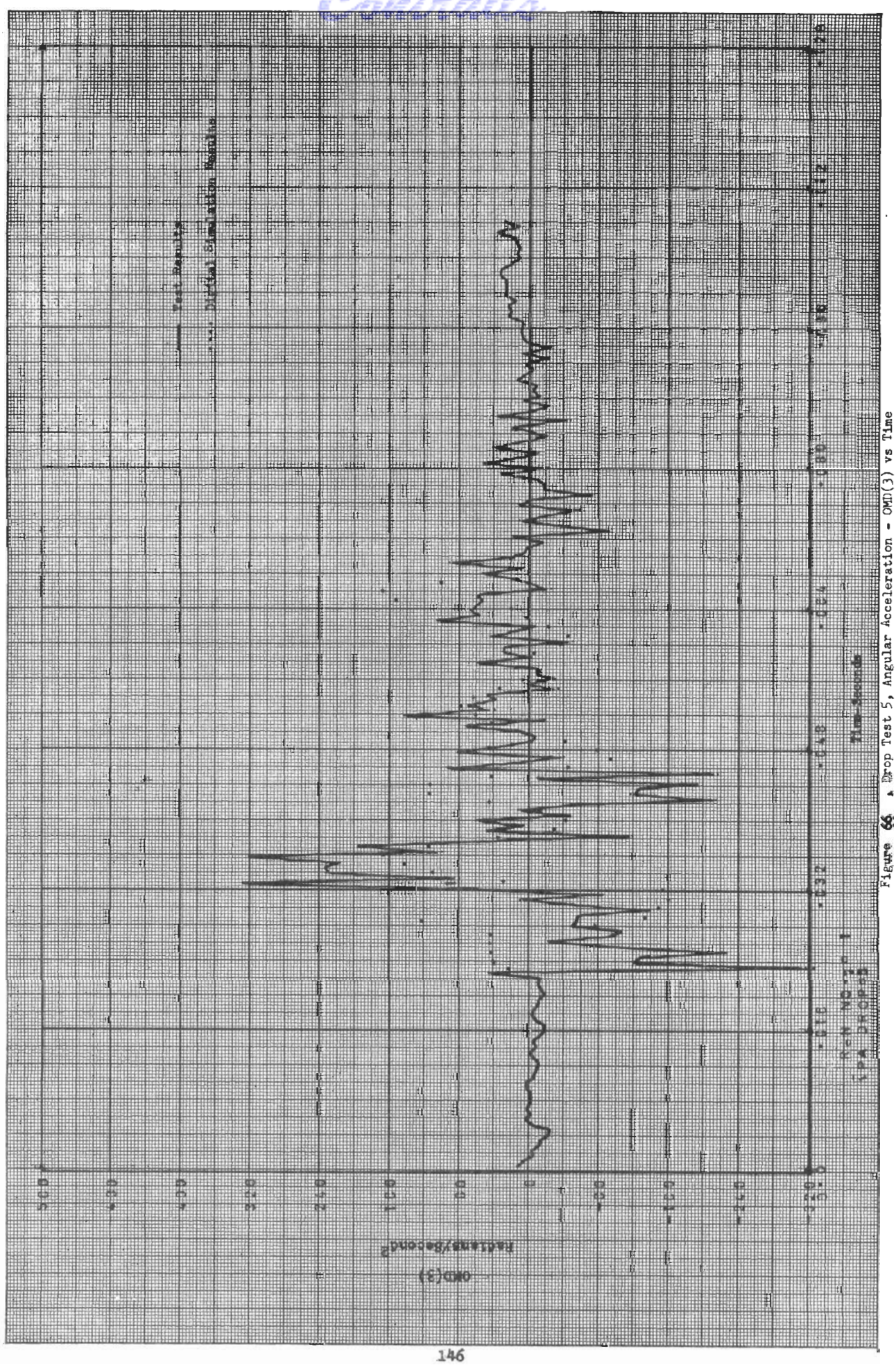

Figure 66 - Drop Test 5, Angular Acceleration - OMD(3) vs Time

free fall drop. Eighty-nine percent of the kinetic energy had been absorbed when the capsule bottom contacted the asphalt. Excellent correlation is shown for XDD(3) in Figure 63 up to the instant of impact. Fair correlation is shown in Figures 61, 62, 64, 65 and 66.

Drop 6

This drop had only a vertical velocity. All four legs contacted simultaneously as indicated in the vertical acceleration, Figure 69. Excellent correlation is shown with the same discrepancy in peak acceleration level as noted previously. Oscillatory capsule motion occurs similar to that observed in Drop 5 as shown in Figures 67, 68, 70, 71 and 72. Experimental and analytical shock spectra are compared in Figure 73.

Drop 7

As noted previously, Drop 7 was deleted from the Comparison Phase due to binding of the energy cells.

Drop 8

The initial conditions for this drop consisted of a vertical velocity and capsule inclination of about 12 degrees from the vertical. Leg touchdown sequence was 3, 4, 2, 1, with 4 and 2 touching down almost simultaneously. Figure 76 shows the best correlation obtained for vertical acceleration. Good correlation is shown in Figures 77 and 78 and poor correlation in Figures 74, 75 and 79.

A comparison of shock spectra for XDD(3) is shown in Figure 80.

Drop 9

This drop had the largest horizontal velocity of the test series. A velocity of 8.65 feet per second was used as opposed to the normal 7.5 feet per second. This represents a 33 percent increase in horizontal kinetic energy. A flat drop was intended; however, the XDD(3) curve in Figure 83 shows that all four legs did not touch the asphalt simultaneously. Film analysis indicated a 2 degree inclination of the capsule; however, this was not a large enough angle to produce the two steps shown in Figure 83. A small increase in inclination (about 2 degrees) would produce the desired acceleration steps in the simulation.

Good correlation is shown in Figures 81, 82, 83, 84 and 85. Figure 86 shows fair correlation. Figure 87 is a comparison of shock spectra.

Drop 10

Horizontal and vertical velocity were combined with a 9 degree capsule inclination for this drop. Five out of 6 acceleration time histories show

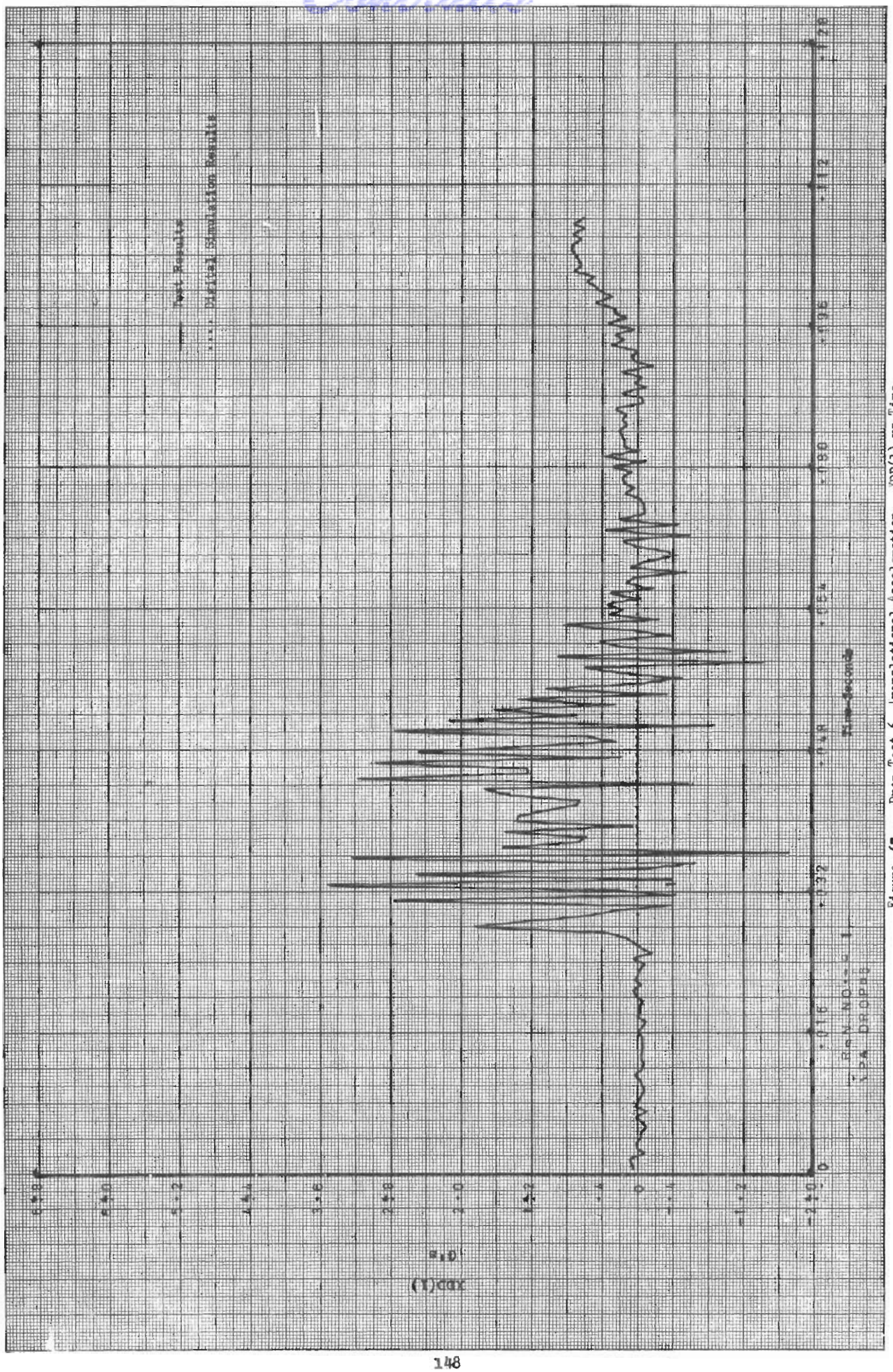

Figure 67 , Drop Test 6, Translational Acceleration - XDD(1) vs Time

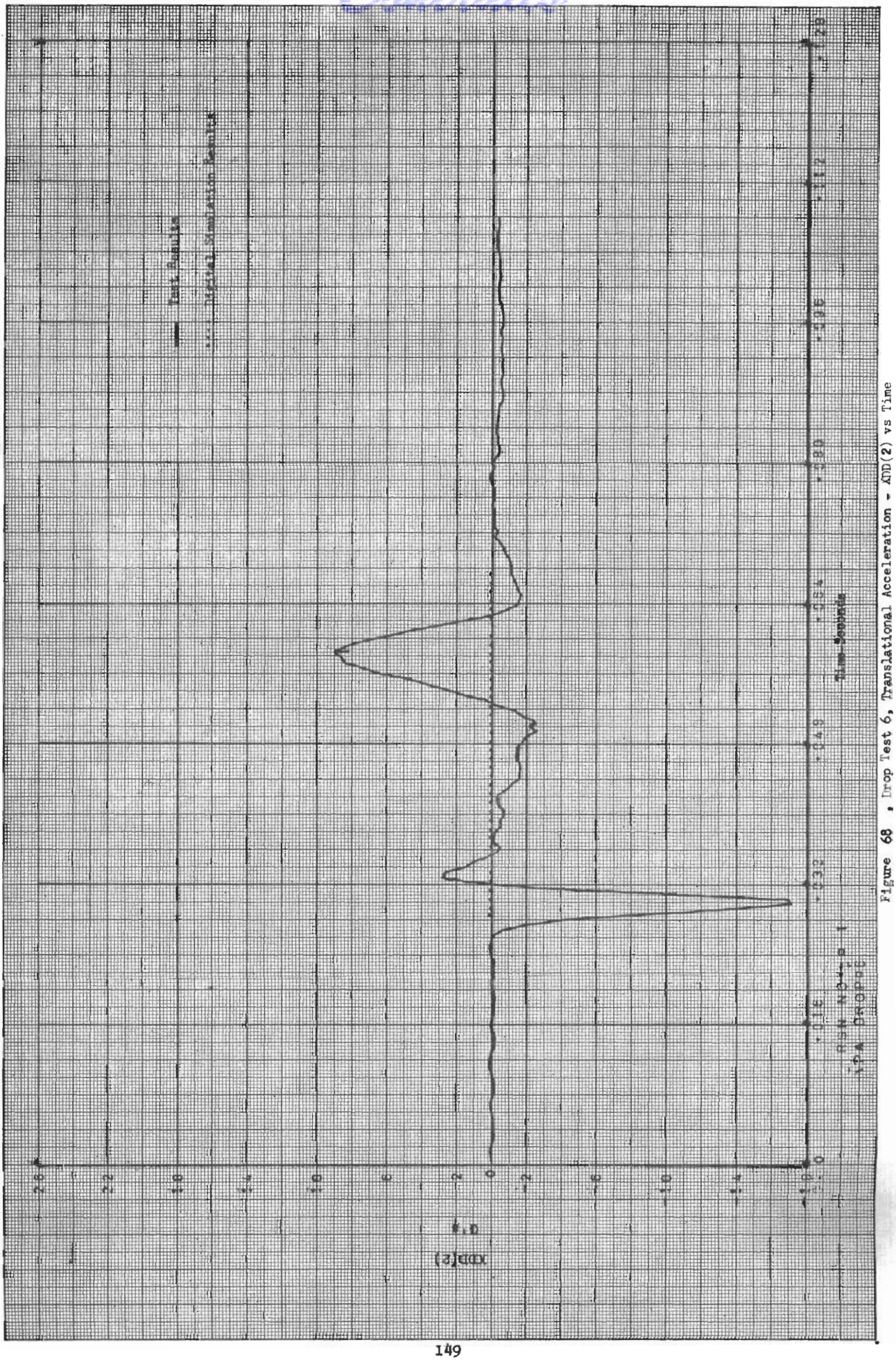

Figure 68 . Drop Test 6, Translational Acceleration - XDD(2) vs Time

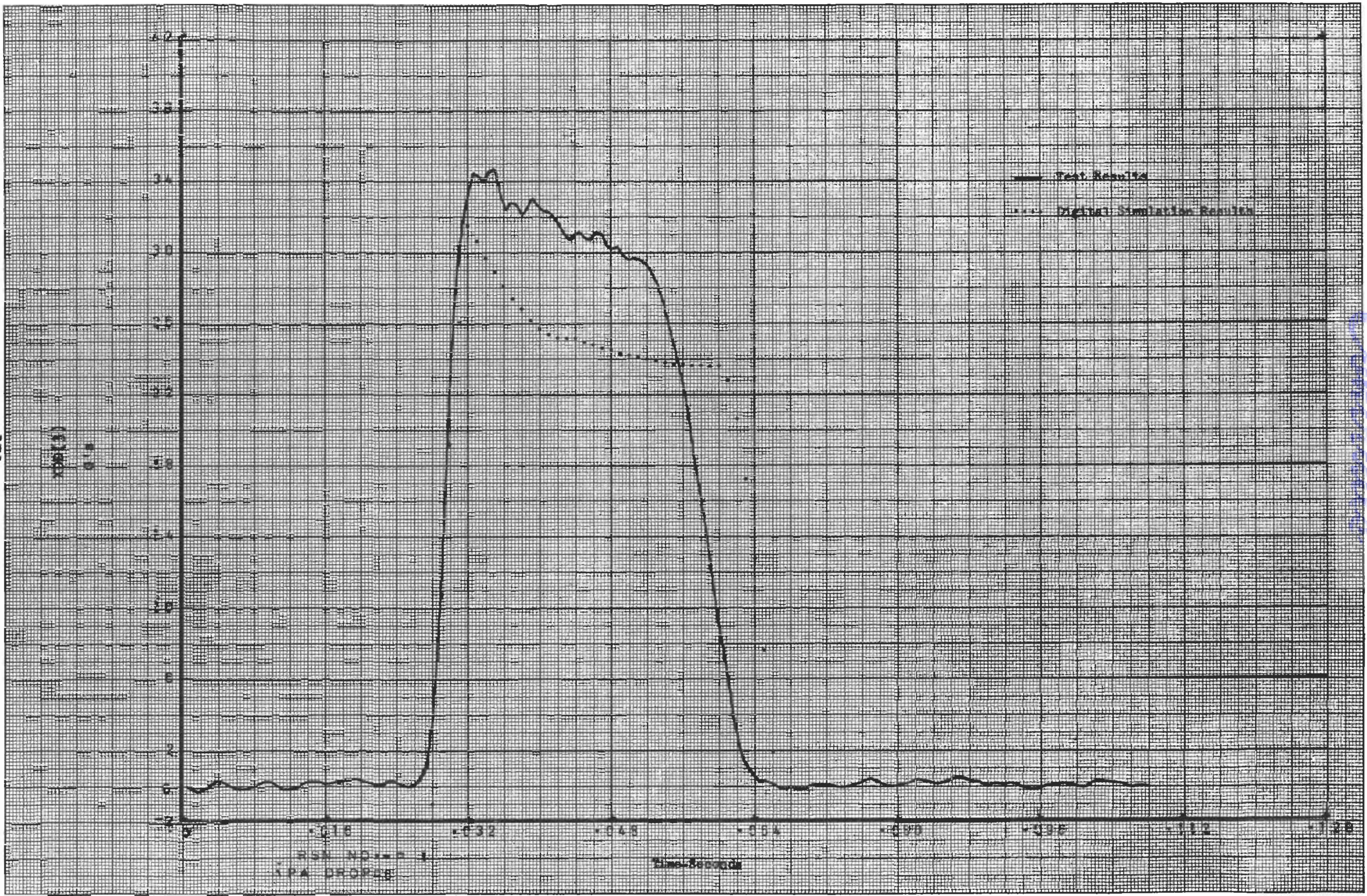

Figure 69 , Drop Test 6, Translational Acceleration - XDD(3) vs Time

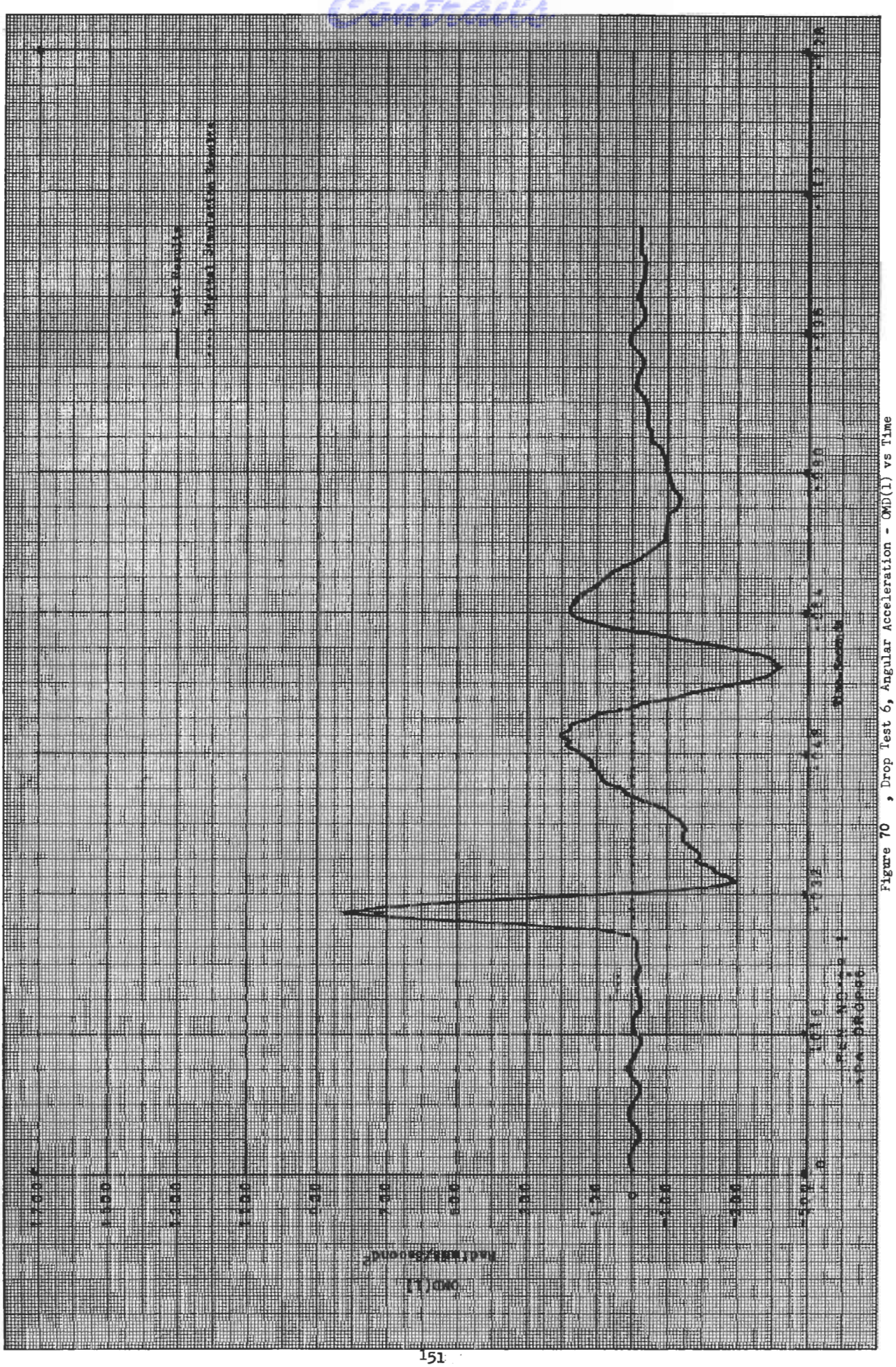

Figure 70 , Drop Test 6, Angular Acceleration - OMD(1) vs Time

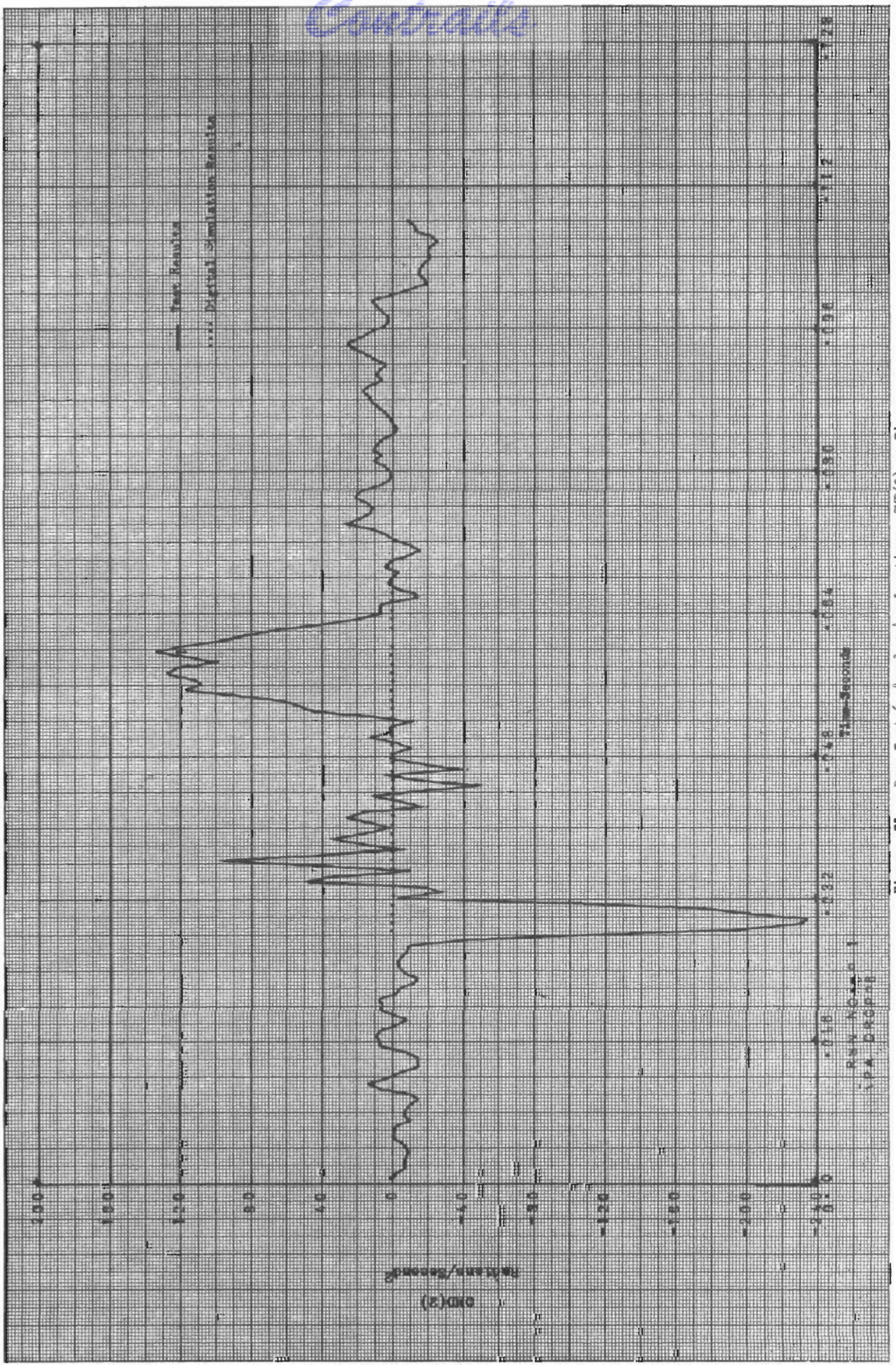

Figure 71 , Drop Test 6, Angular Acceleration - OMD(2) vs Time

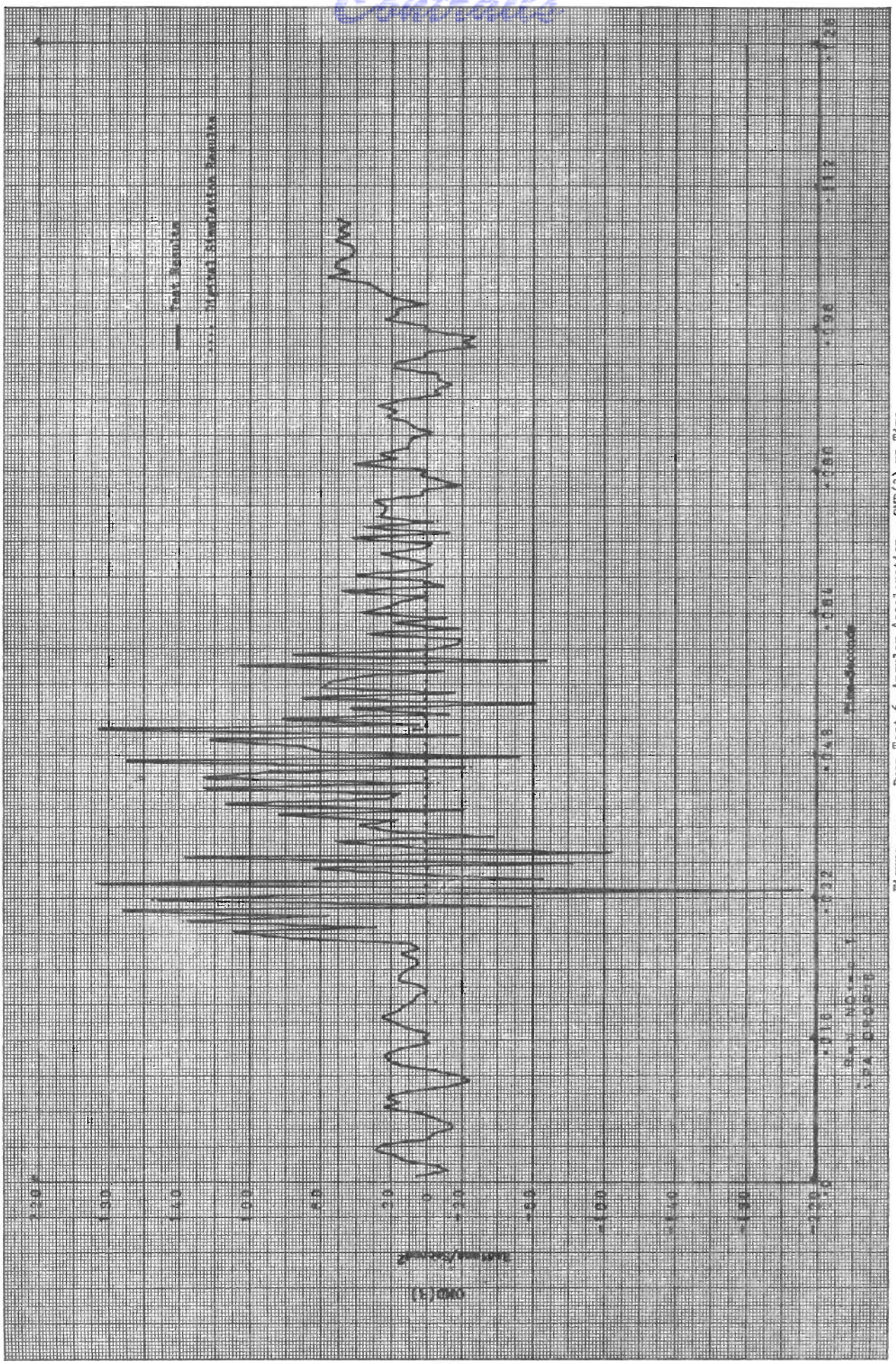

Figure 72 , Drop Test 6, Angular Acceleration - CMD(3) vs Time

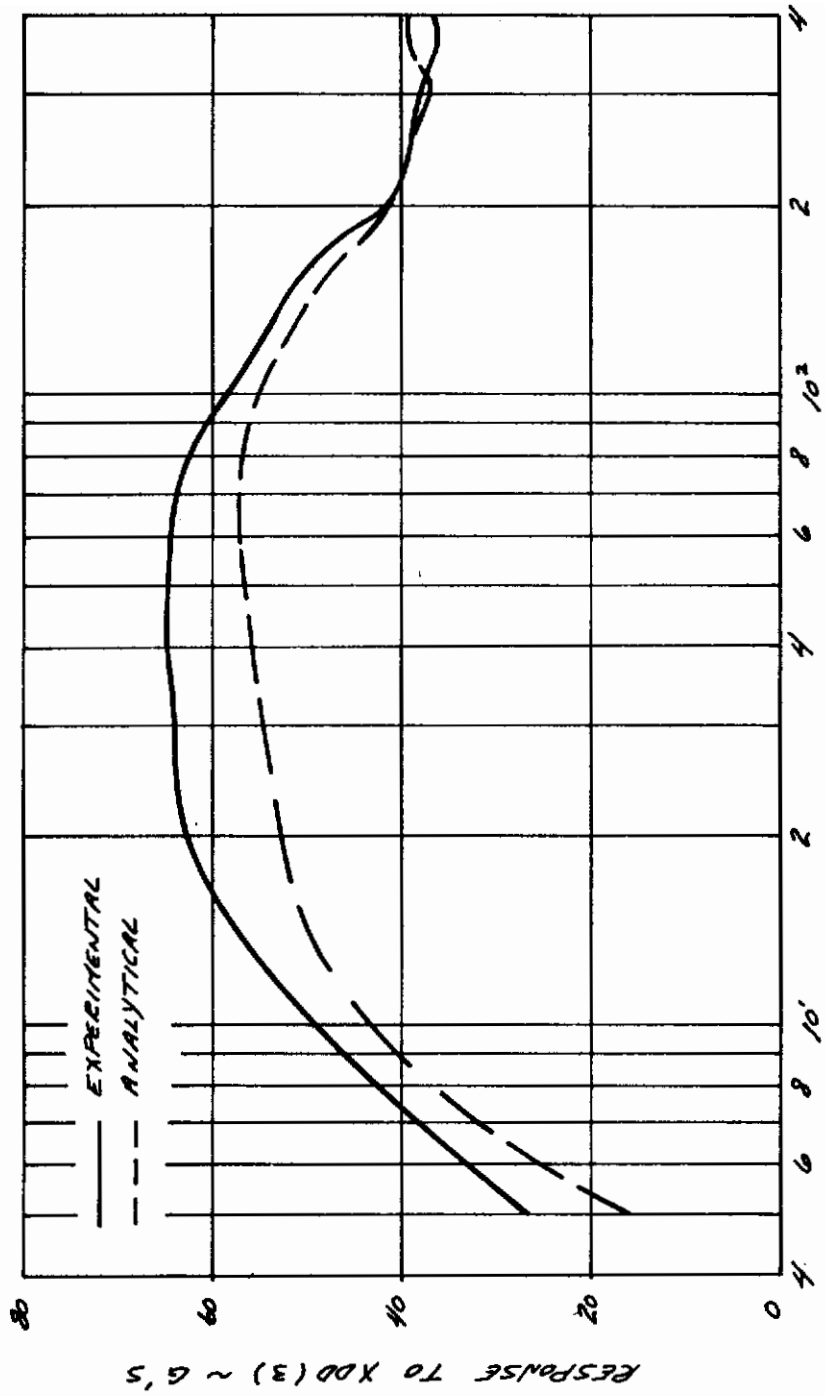

Figure 73, Drop Test 6, Shock Spectra Comparison

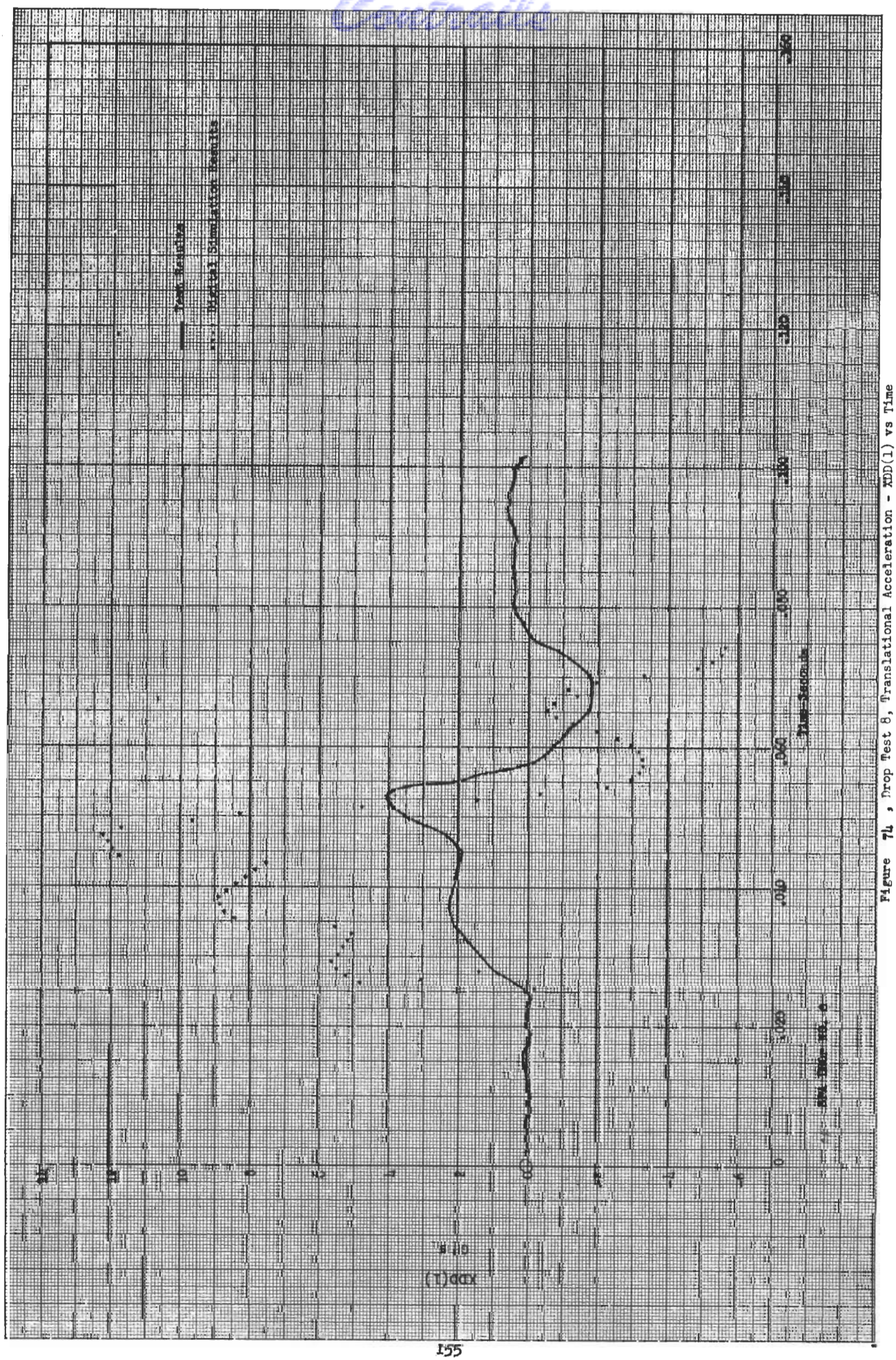

Figure 74 , Drop Test 8, Translational Acceleration - XDD(1) vs Time

Figure 75 , Drop Test 8, Translational Acceleration - XDD(2) vs Time

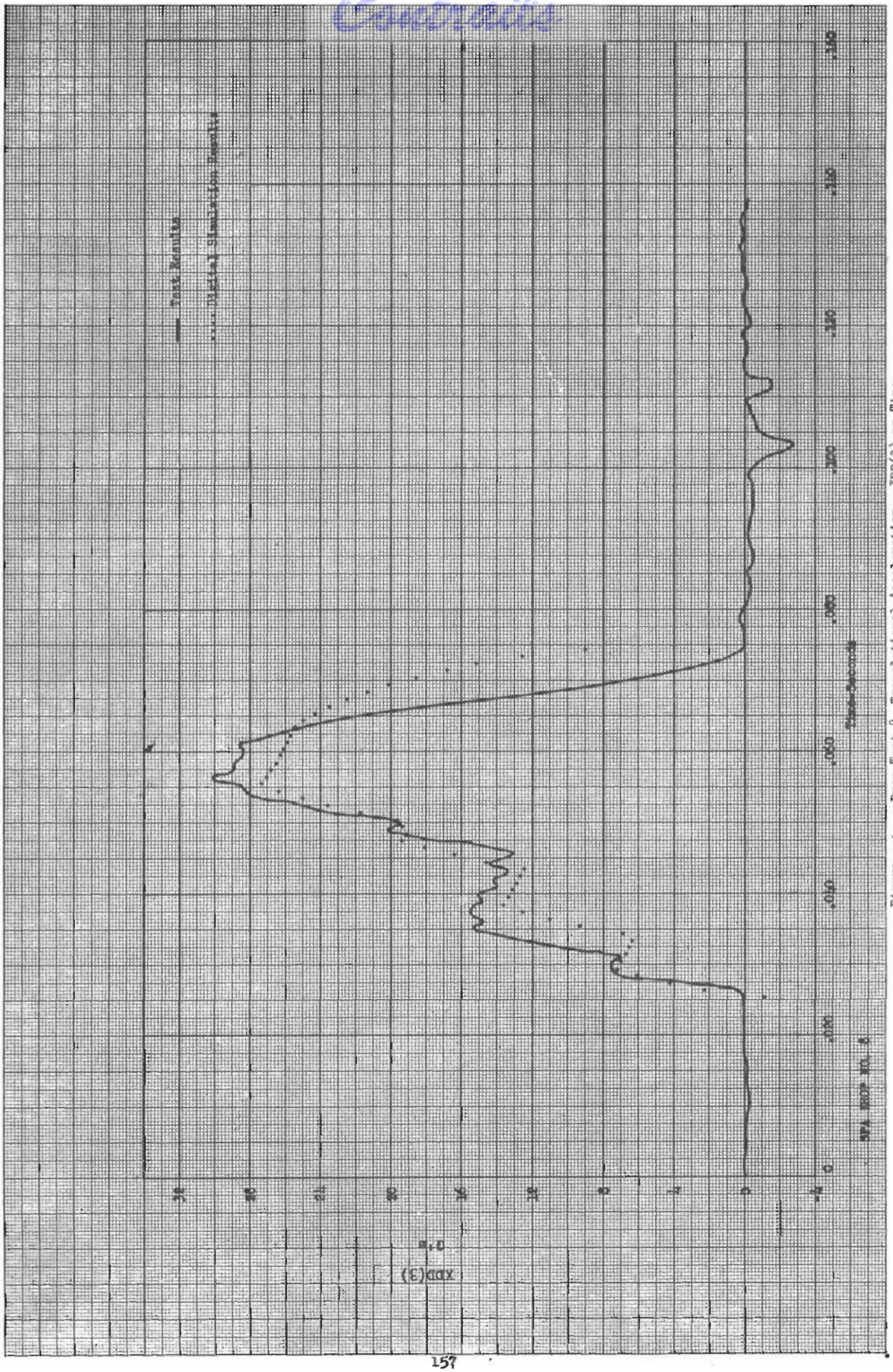

Figure 76 , Drop Test 8, Translational Acceleration - XDD(3) vs Time

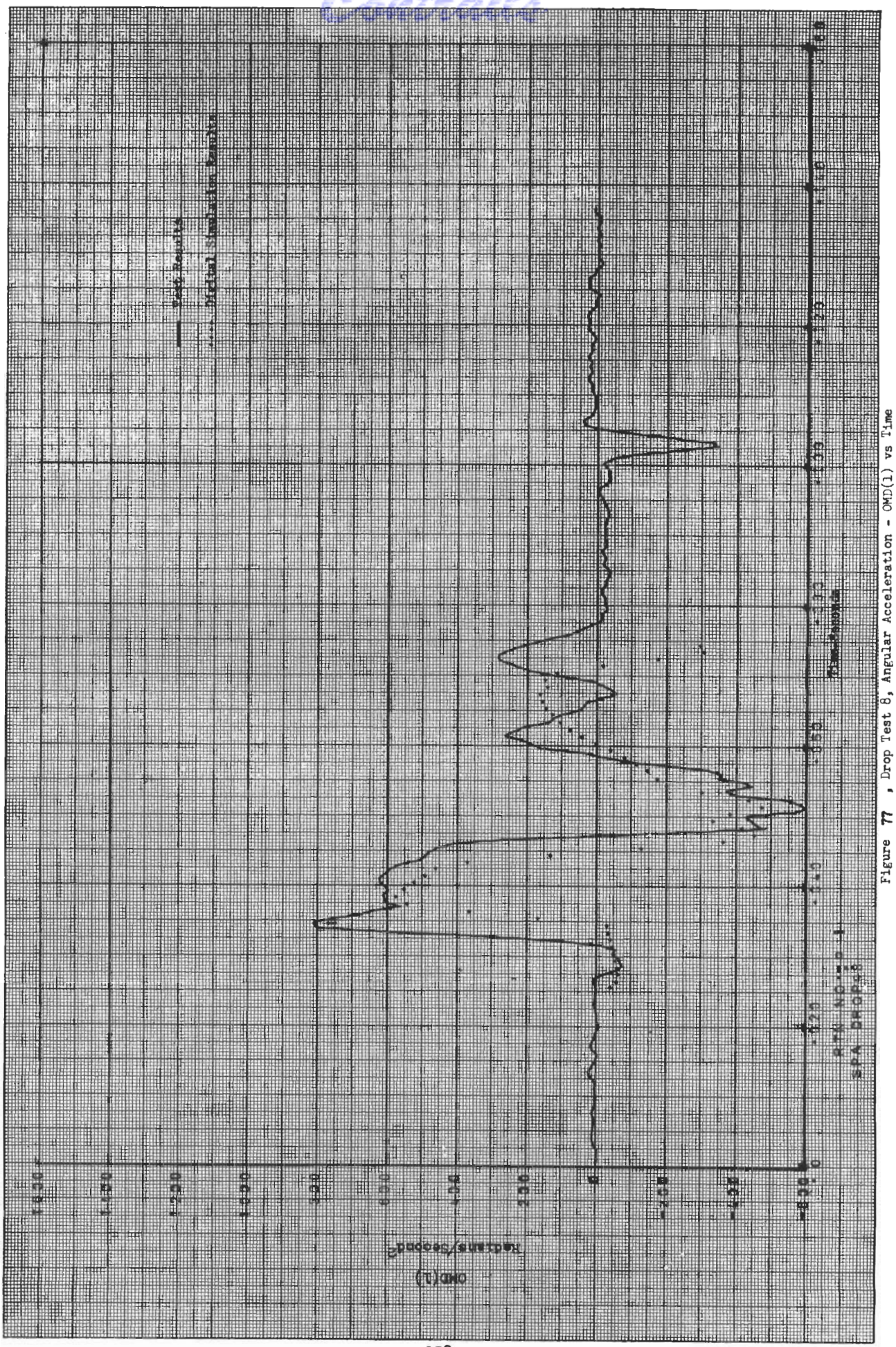

Figure 77 , Drop Test 8, Angular Acceleration - OMD(1) vs Time

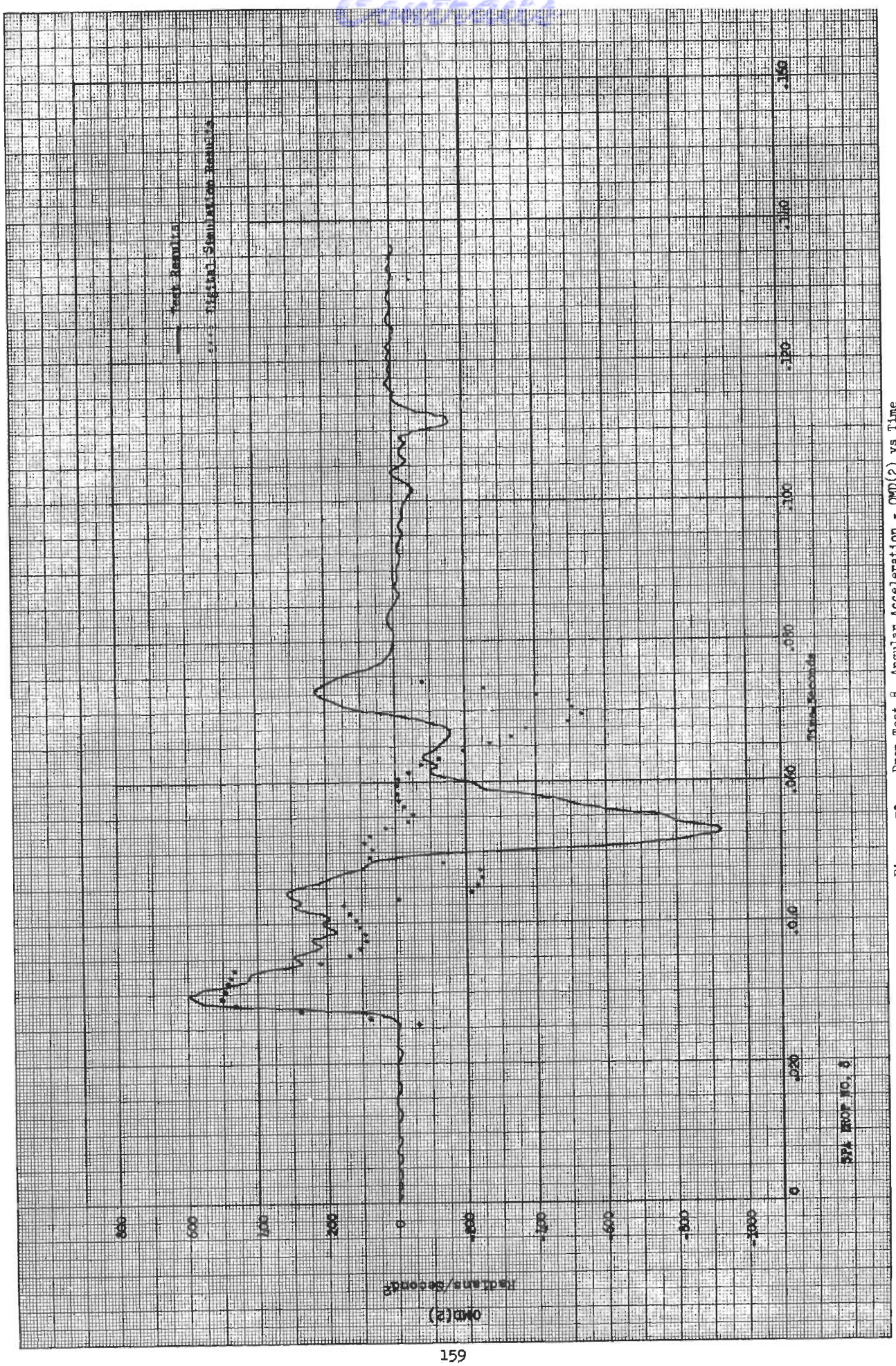

Figure 78 , Drop Test 8, Angular Acceleration - OMD(2) vs Time

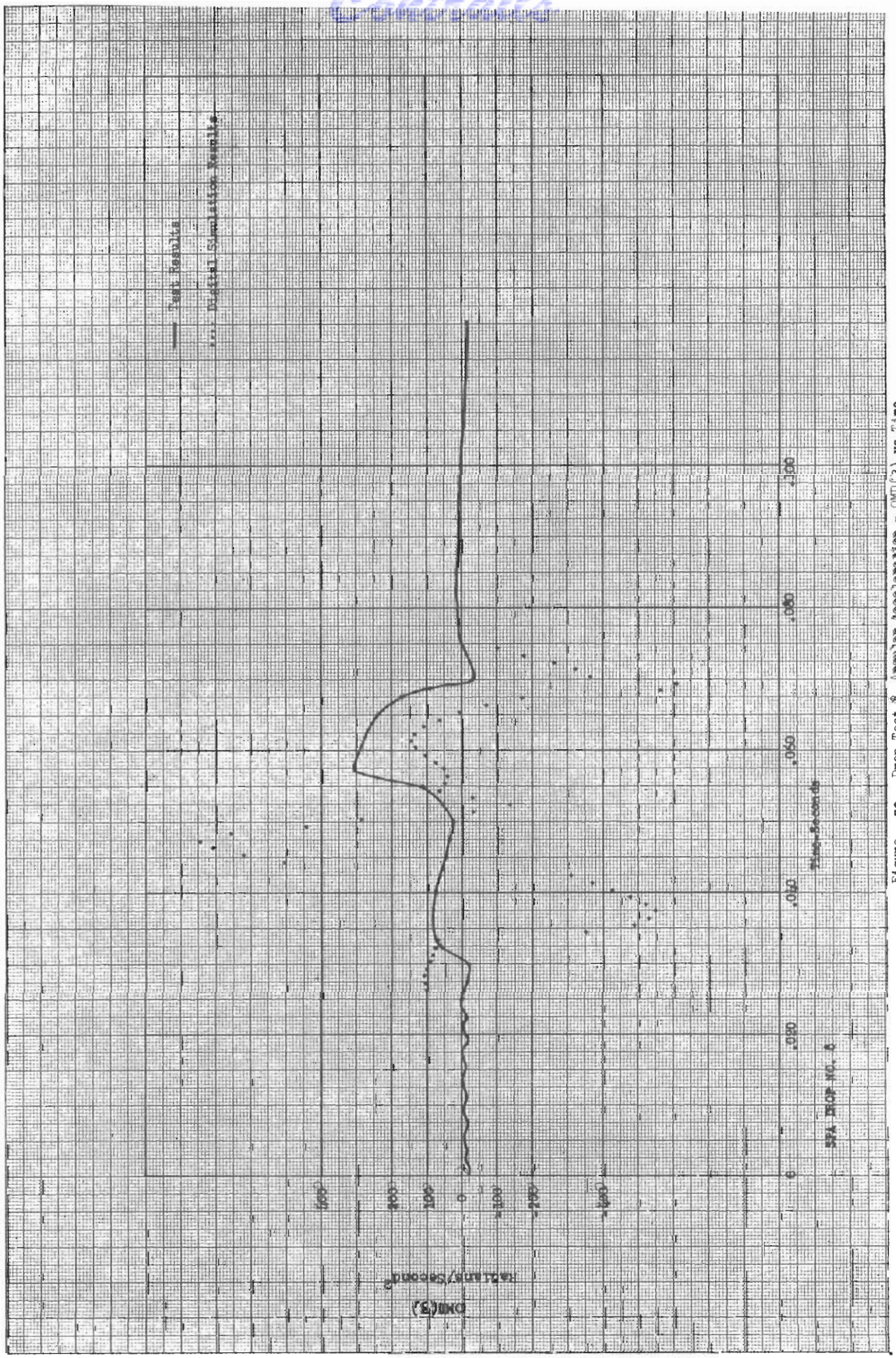

Figure 79 , Drop Test 8, Angular Acceleration - OMD(3) vs Time

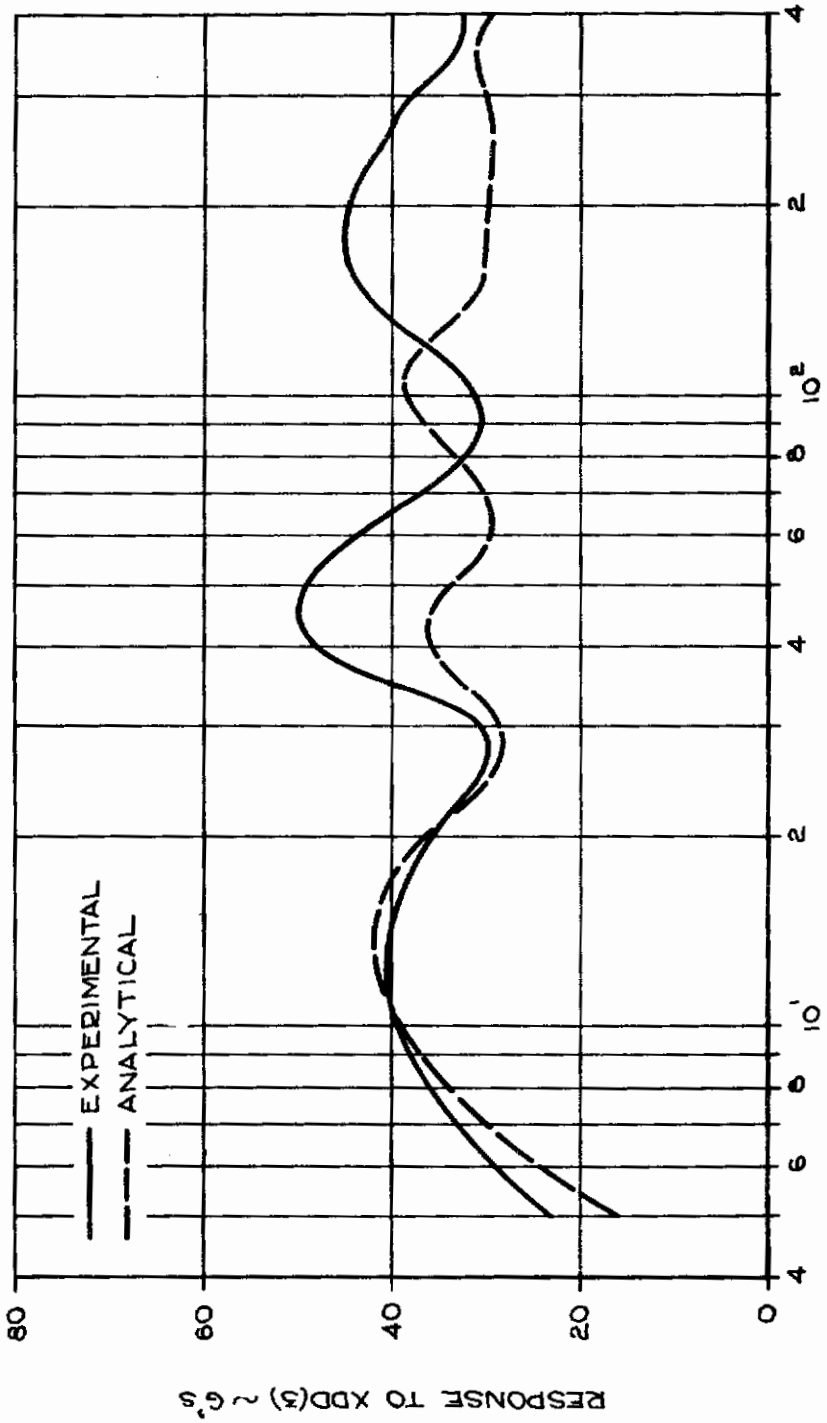

Figure 80, Drop Test 8, Shock Spectra Comparison

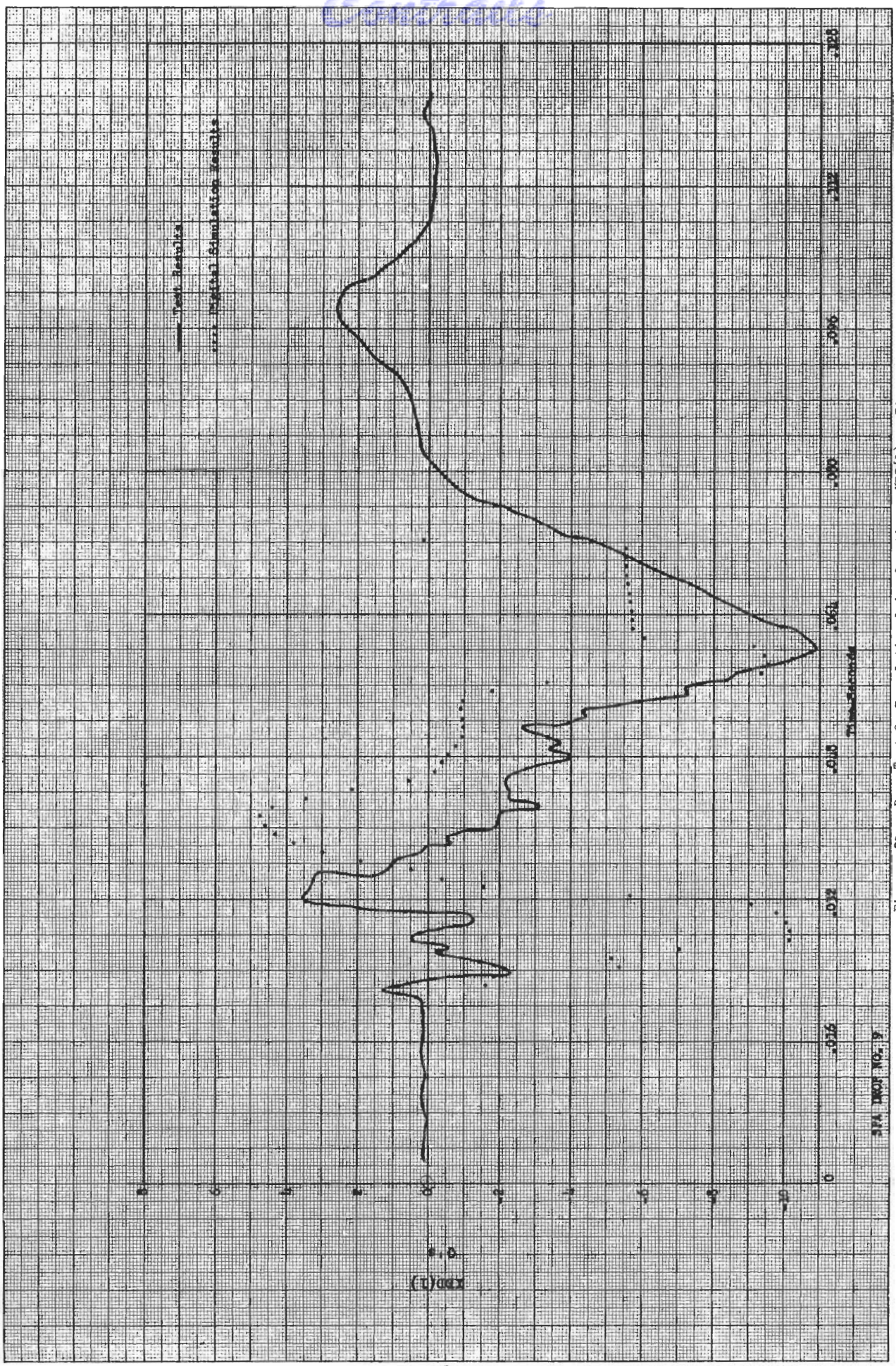

Figure 81 , Drop Test 9, Translational Acceleration - XDD(1) vs Time

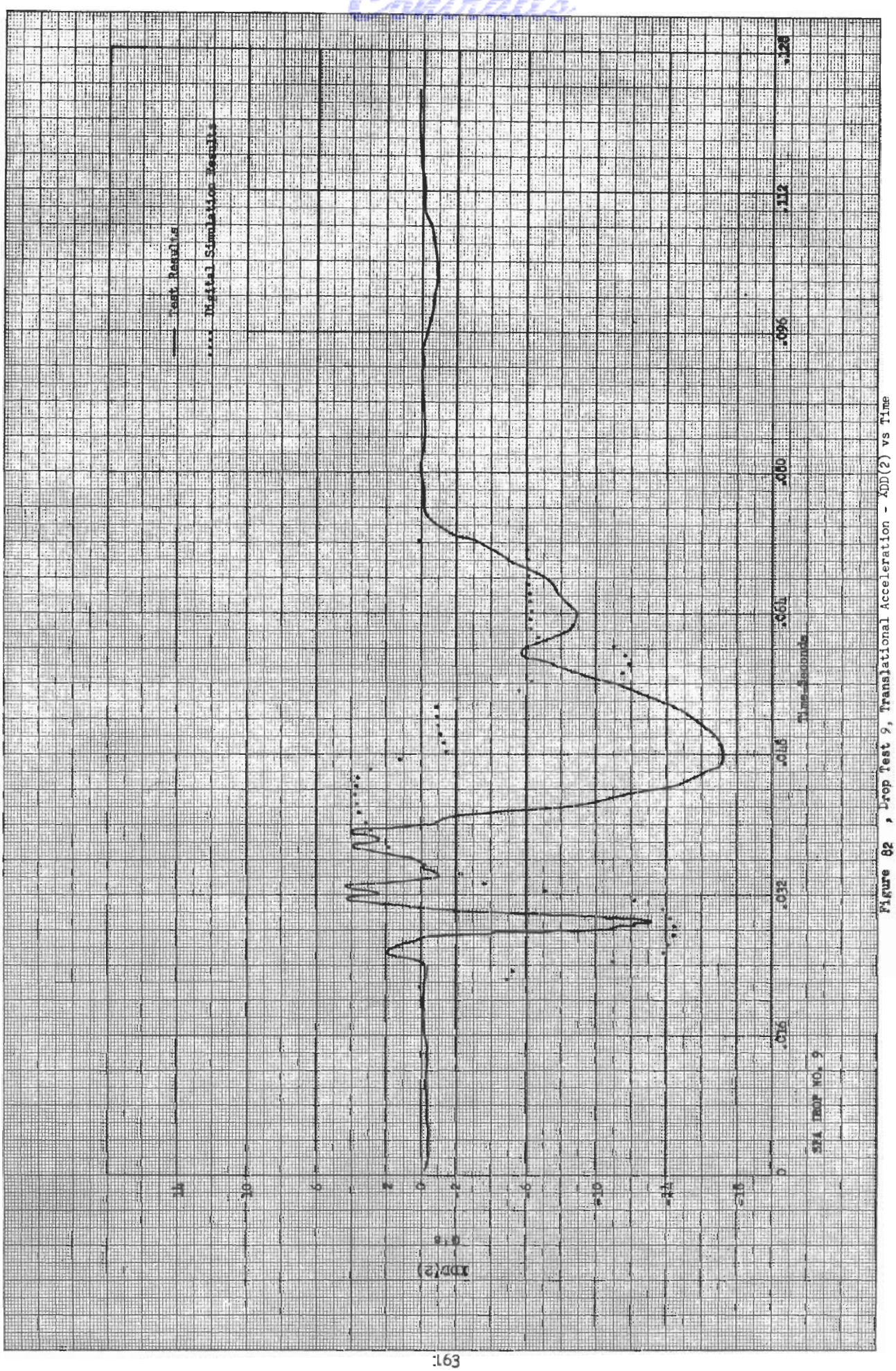

Figure 82 , Drop Test 9, Translational Acceleration - $\ddot{X}_{DD}(2)$ vs Time

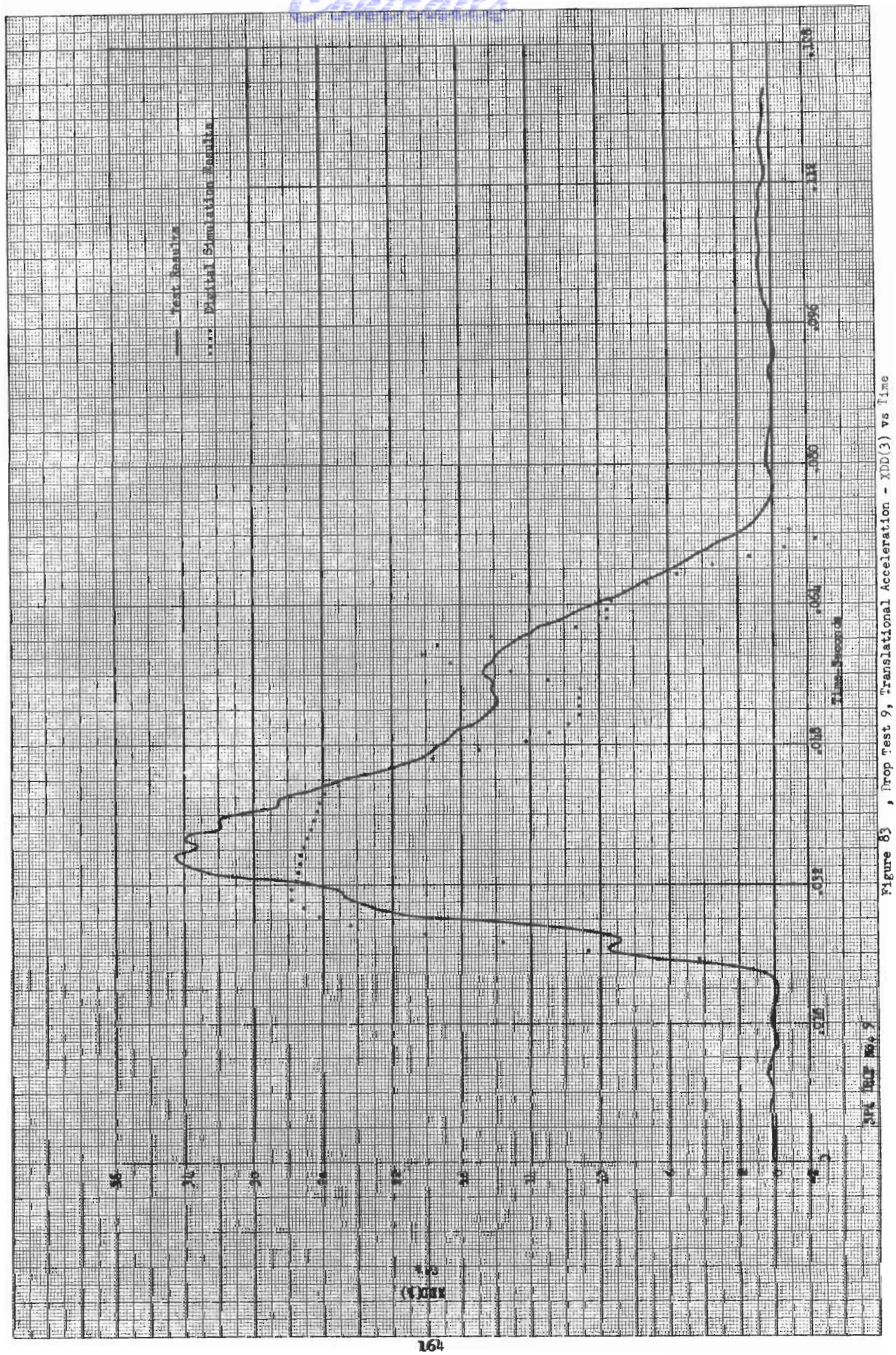

Figure 83 , Drop Test 9, Translational Acceleration - $\ddot{X}_{DD}(3)$ vs Time

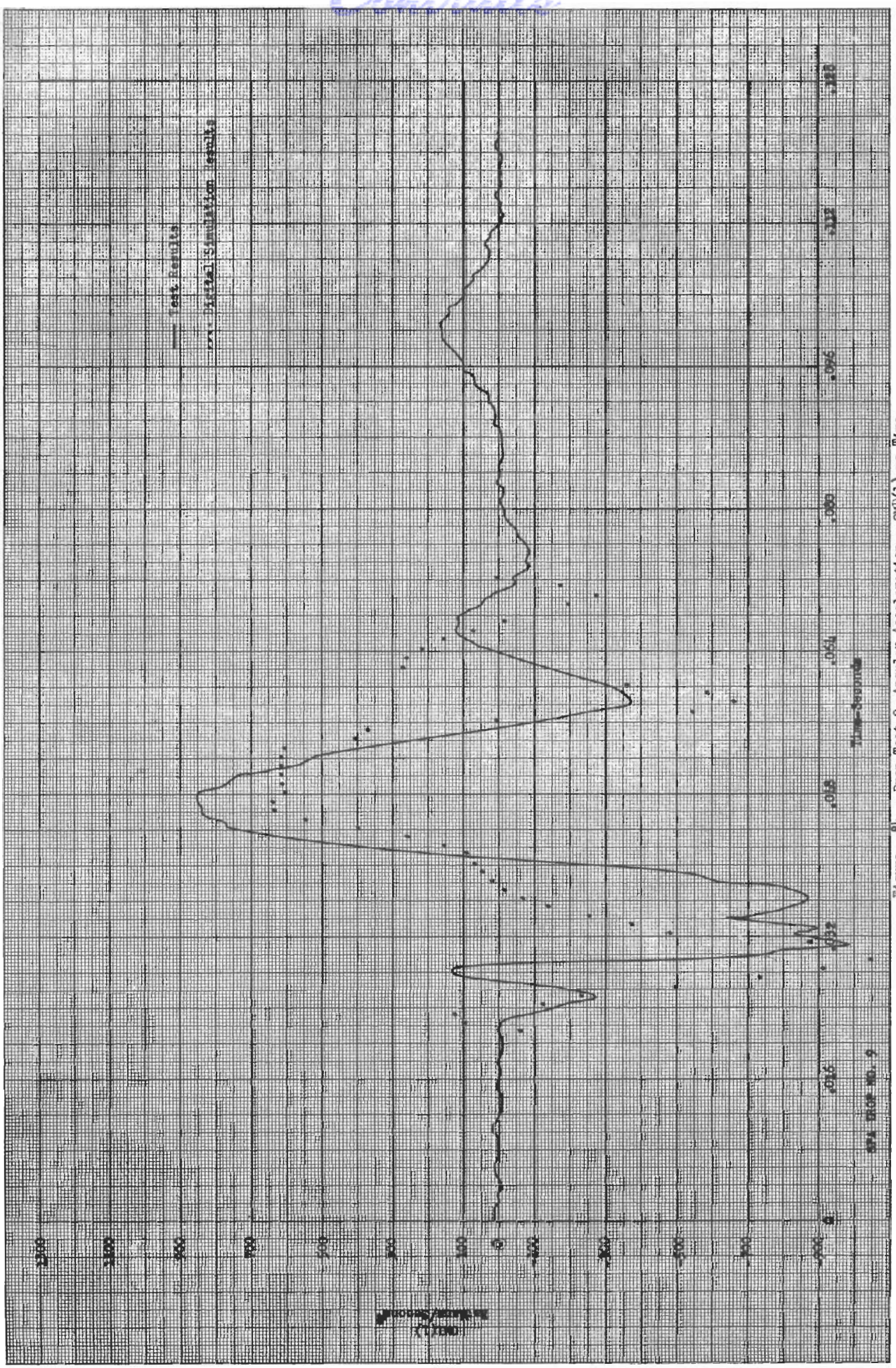

Figure 84 , Drop Test 9, Angular Acceleration - OMD(1) vs Time

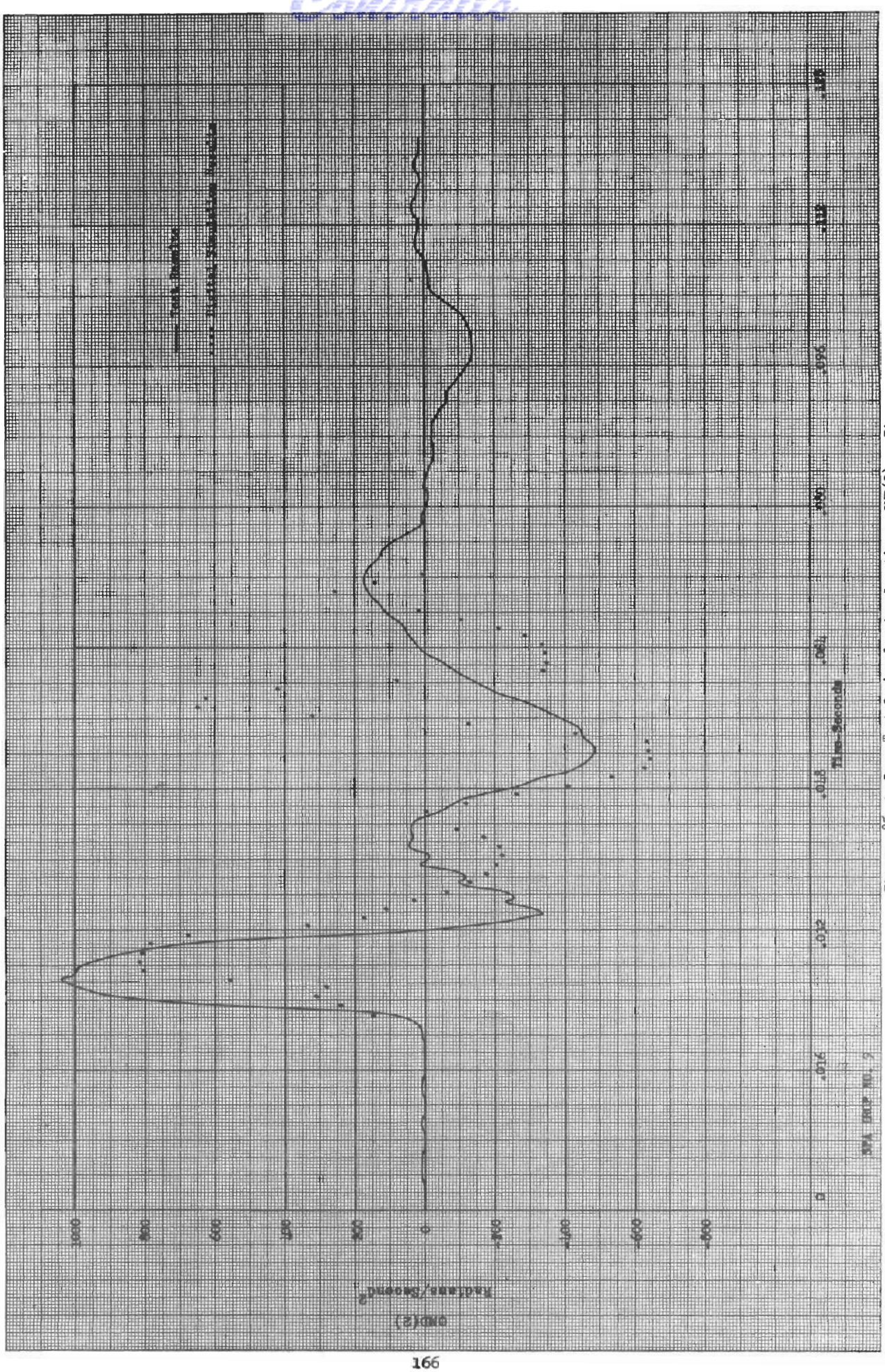

Figure 85 , Drop Test 9, Angular Acceleration - OMD(2) vs Time

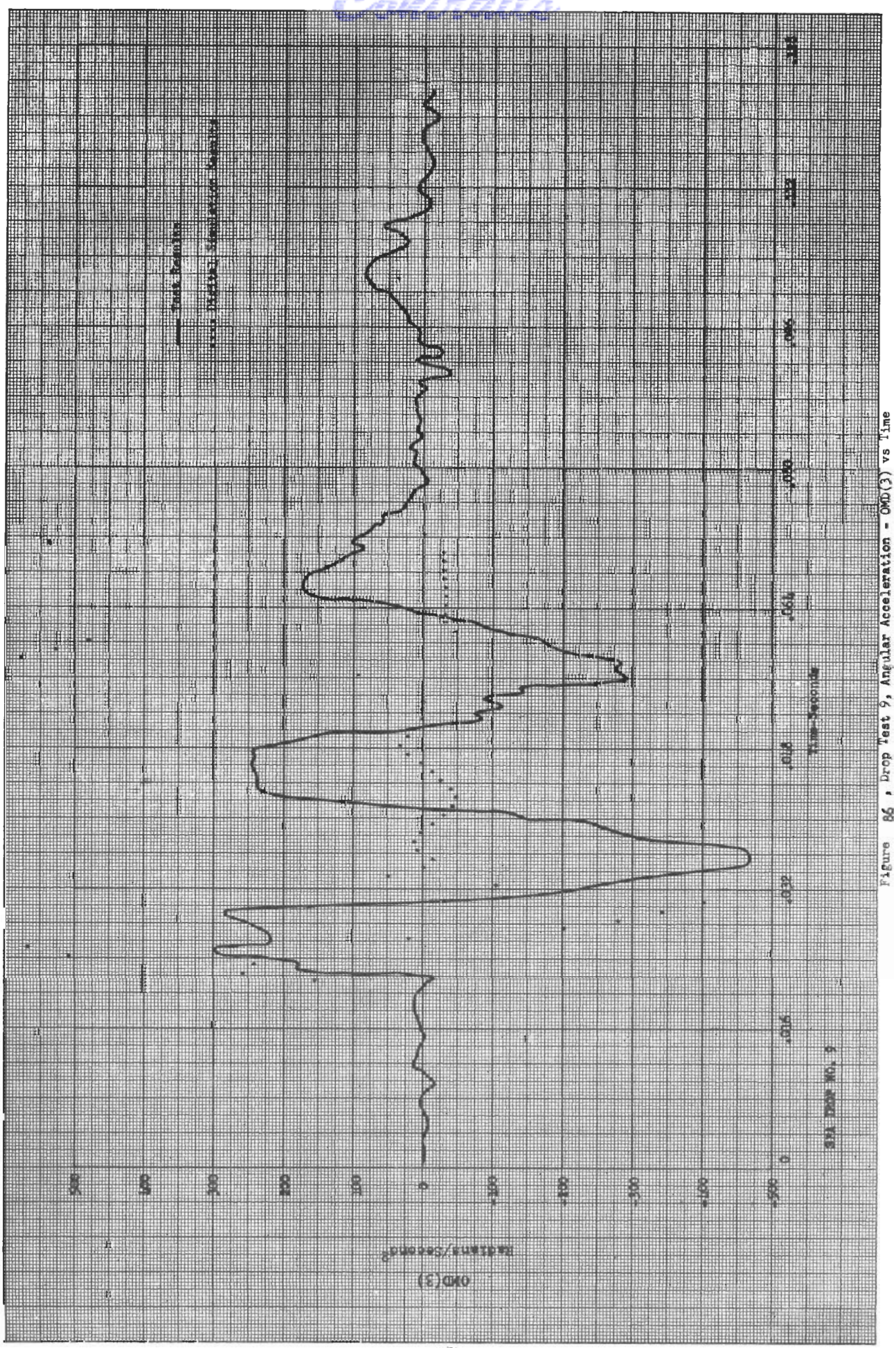

Figure 86 , Drop Test 9, Angular Acceleration - OMD(3) vs Time

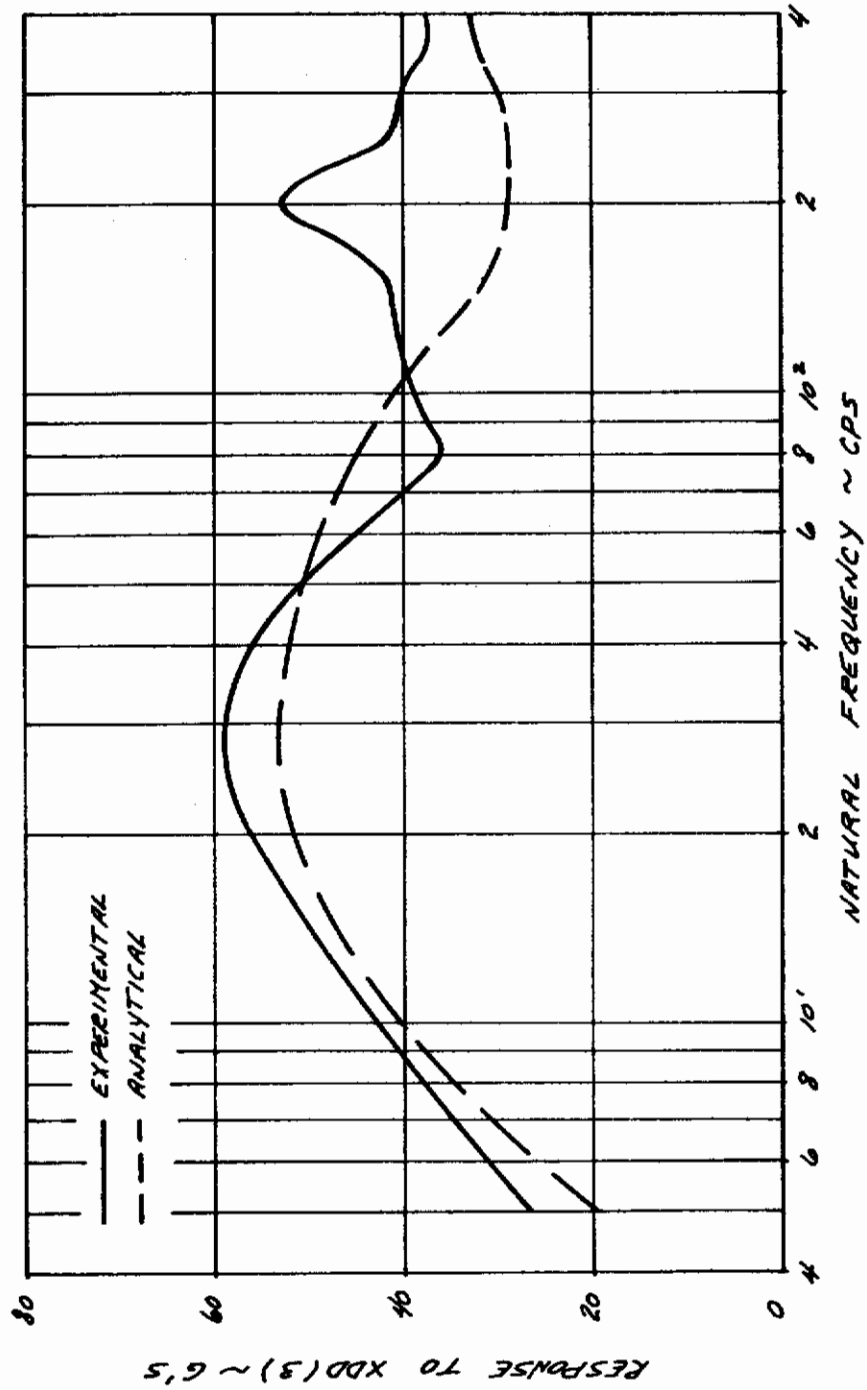

Figure 87, Drop Test 9, Shock Spectra Comparison

excellent correlation for this drop. Figures 88, 90, 91, 92 and 93 correlate excellently while Figure 89 shows poor correlation. Shock spectra for this drop are compared in Figure 94.

Drop 11

This drop test was performed on a 22 degree slope. For the initial conditions chosen, the digital simulation predicted a satisfactory alightment. Unfortunately, these conditions were not met for the drop and the capsule tumbled backward down the slope. Capsule release was not programmed correctly and resulted in a horizontal velocity that was low, a vertical velocity that was high, and the capsule was pitched into the slope at 8.5 degrees. In predicting the instability with the digital simulation, the energy cell forces were increased to allow for the dynamic forcing characteristics of the energy cells. The resulting predicted acceleration time histories are shown in Figures 95 to 100. Generally, excellent correlation is shown for each of the acceleration coordinates.

A cursory examination of tumbling sensitivity to capsule inclination for this drop was made using the digital simulation. It was found that by holding all other parameters constant and decreasing capsule inclination to 7.8 degrees, the test model was able to make a stable alightment on a 22 degree slope. The early release of the test capsule, therefore, resulted in a critical combination of horizontal velocity, vertical velocity and capsule inclination and resulted in the capsule tumbling backward down the hill.

The telepak operated satisfactorily throughout the tumbling and the test model received superficial damage in the form of bent energy cell rods and paint scratches. The bent rods were straightened and no irreparable damage to the test model occurred.

A shock spectra comparing the vertical accelerations is shown in Figure 101.

C. ADEQUACY OF DIGITAL SIMULATIONS

The general adequacy of the articulated leg digital simulation has been shown in the preceding sub-section. The adequacy of the telescoping leg digital simulation is assumed since it was developed with a similar approach and the same attention to detail as in the articulating leg.

The excellent correlation shown for vertical acceleration on all of the drops indicates an adequate mathematical model of the articulation of the leg was developed. The discrepancies noted in peak acceleration levels are a result of inadequate definition of test model physical characteristics and not a discrepancy in the digital simulation. This conclusion is based on the general excellence of the time correlation of the accelerations. For those drops where the initial conditions used in the simulation did not produce the exact leg touchdown timing,

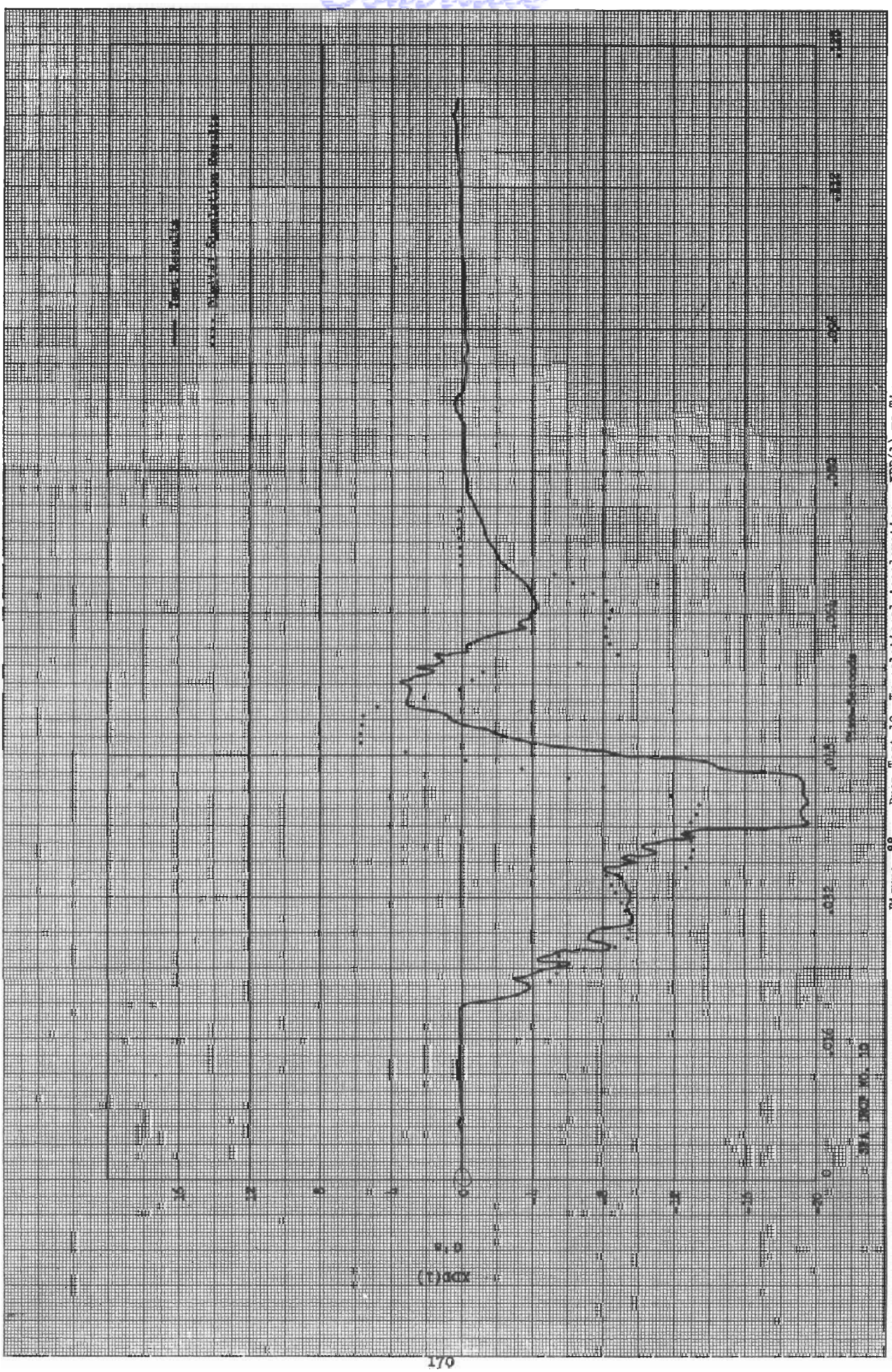

Figure 88 , Drop Test 10, Translational Acceleration - XDD(1) vs Time

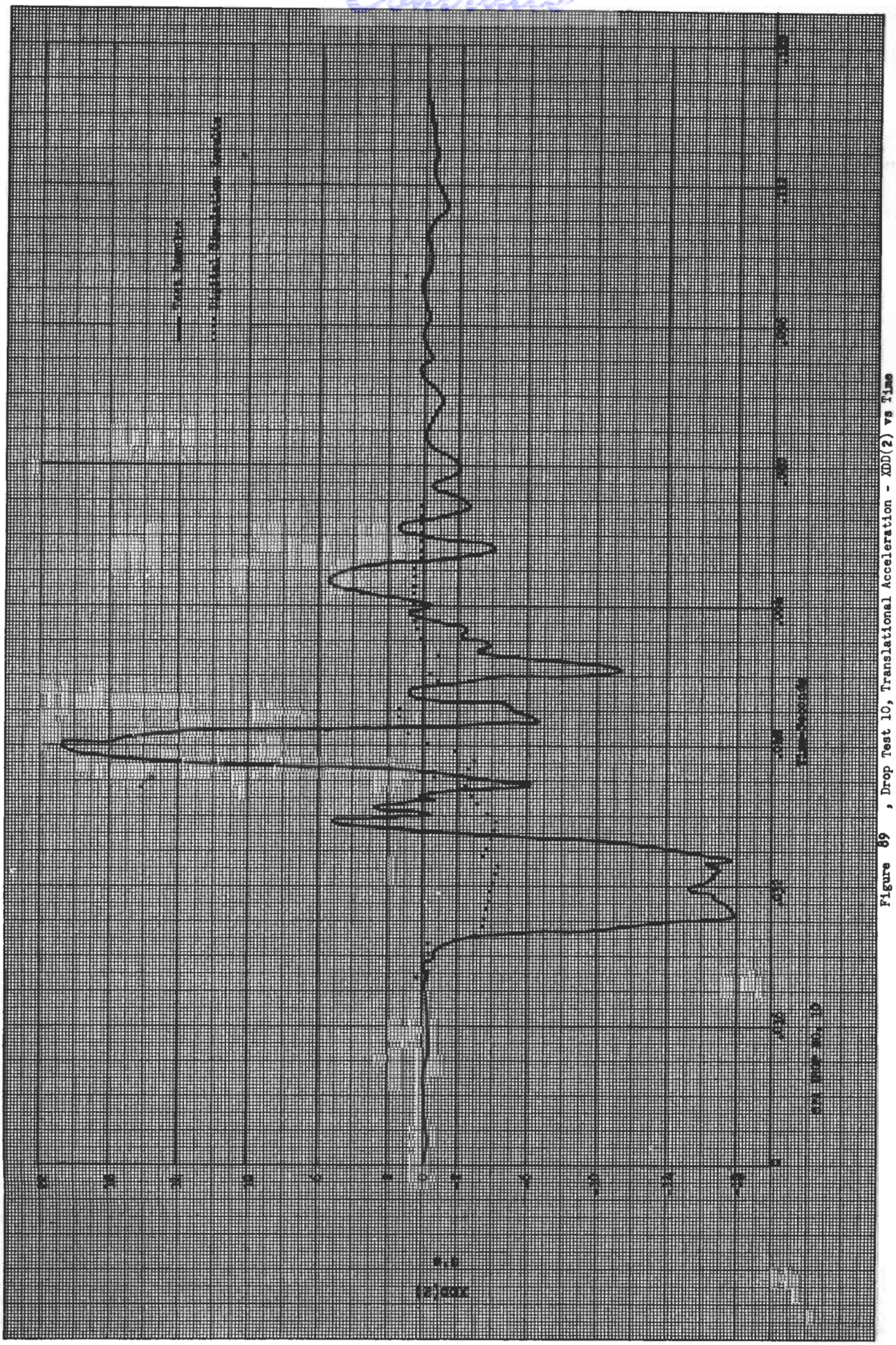

Figure 89 , Drop Test 10, Translational Acceleration - $\ddot{X}D(2)$ vs Time

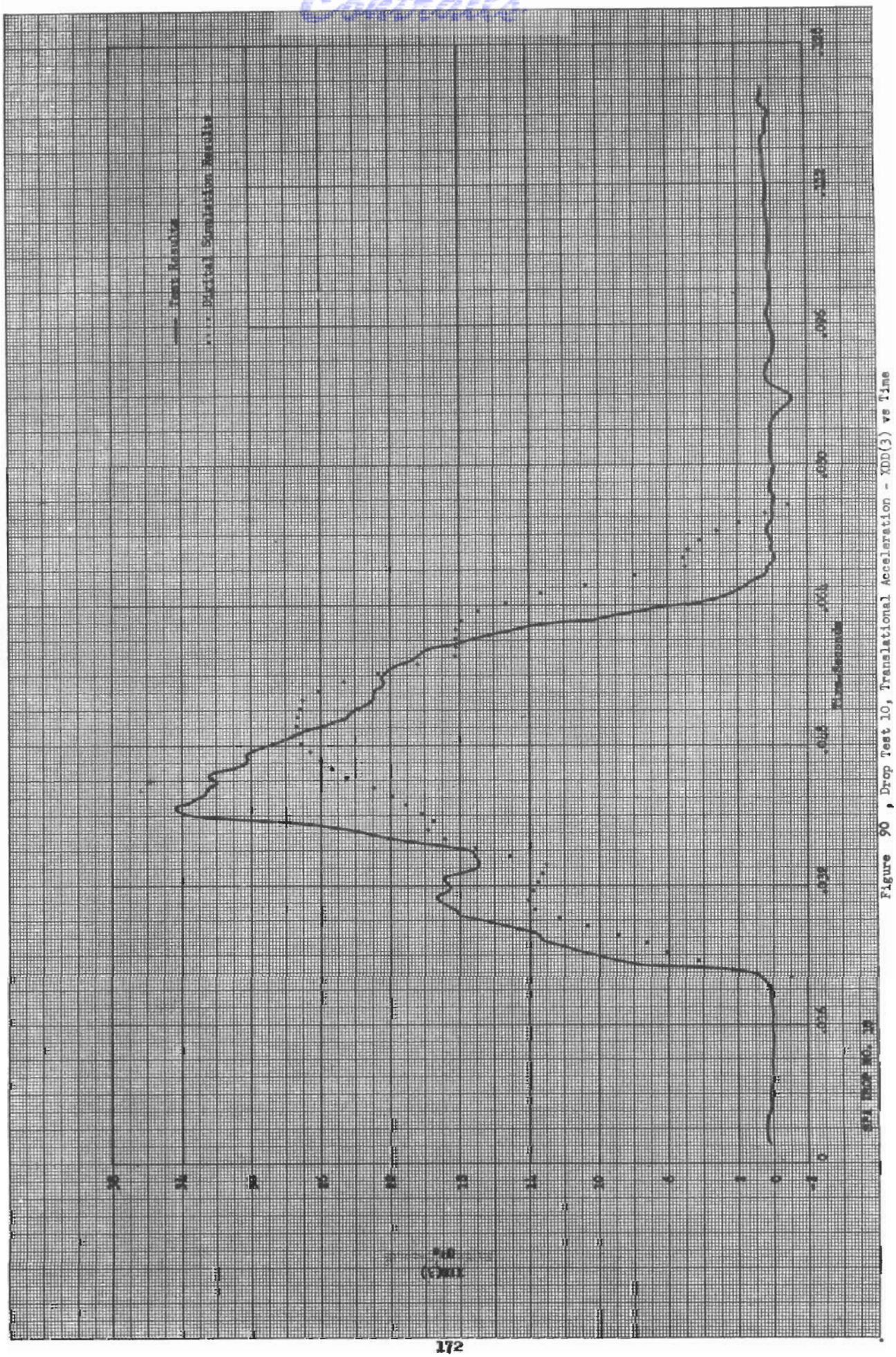

Figure 90 , Drop Test 10, Translational Acceleration - XDD(3) vs Time

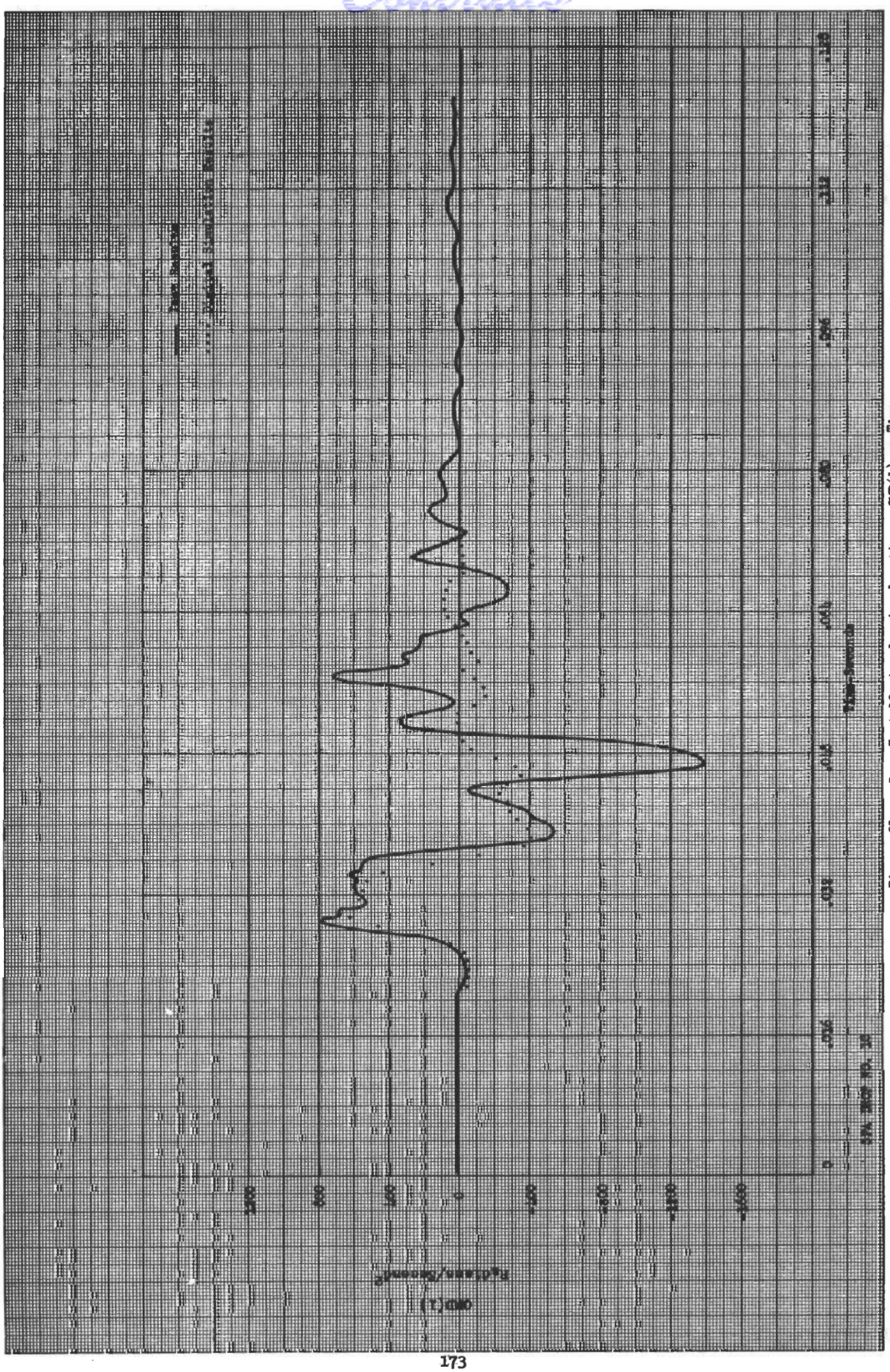

Figure 91 , Drop Test 10, Angular Acceleration - OMD(1) vs Time

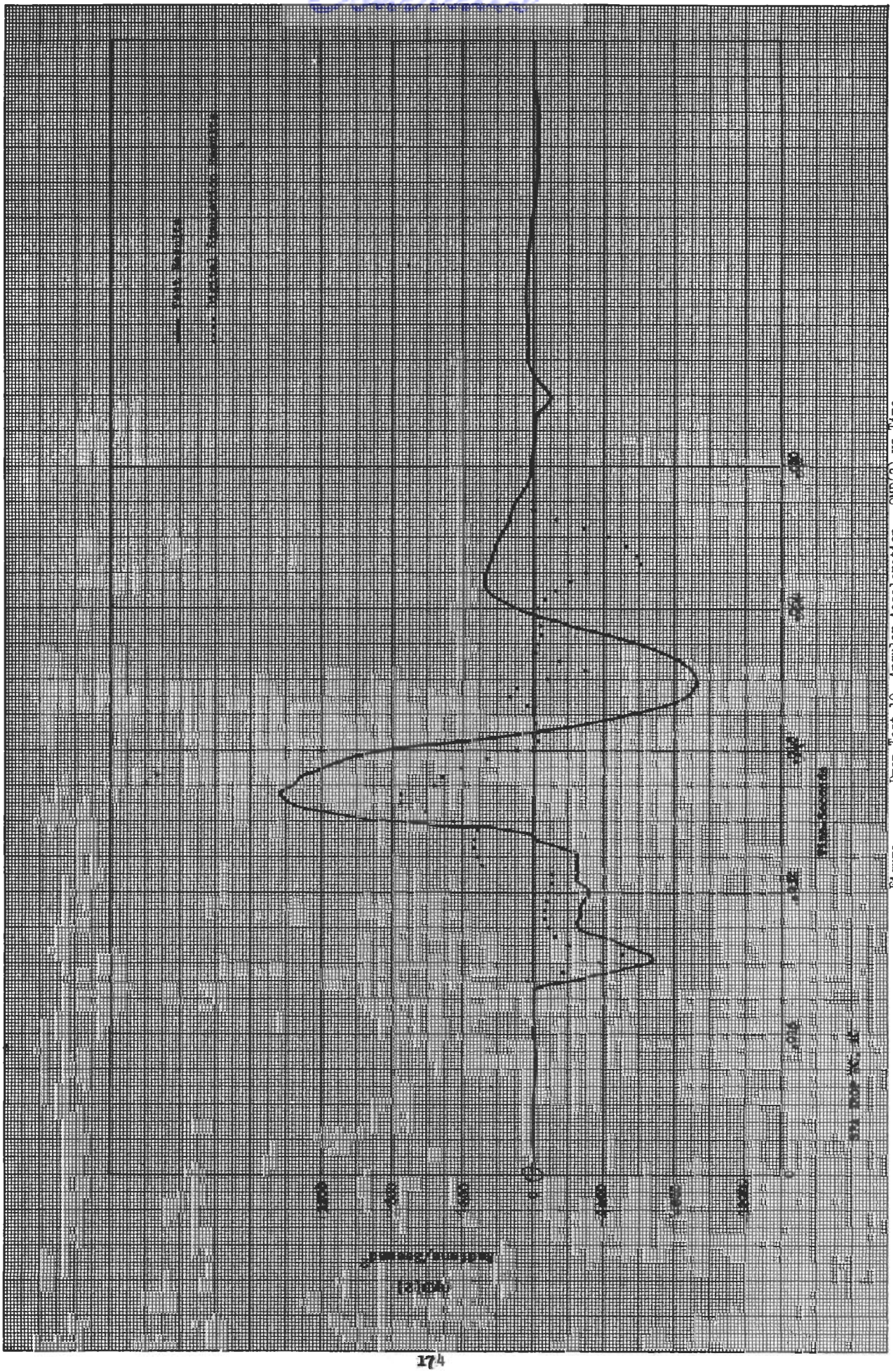

Figure 92 , Drop Test 10, Angular Acceleration - OMD(2) vs Time

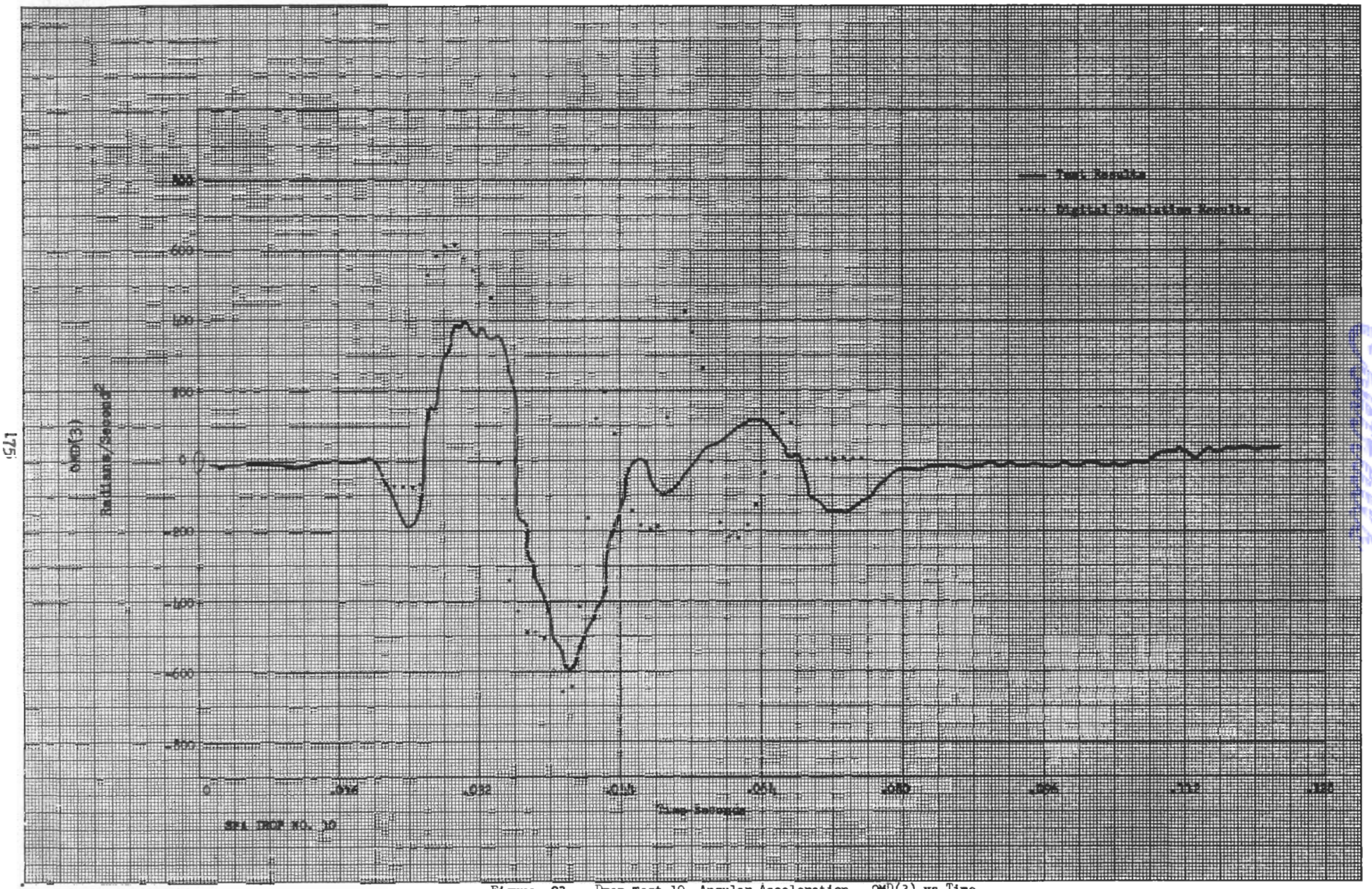

Figure 93 , Drop Test 10, Angular Acceleration - OMD(3) vs Time

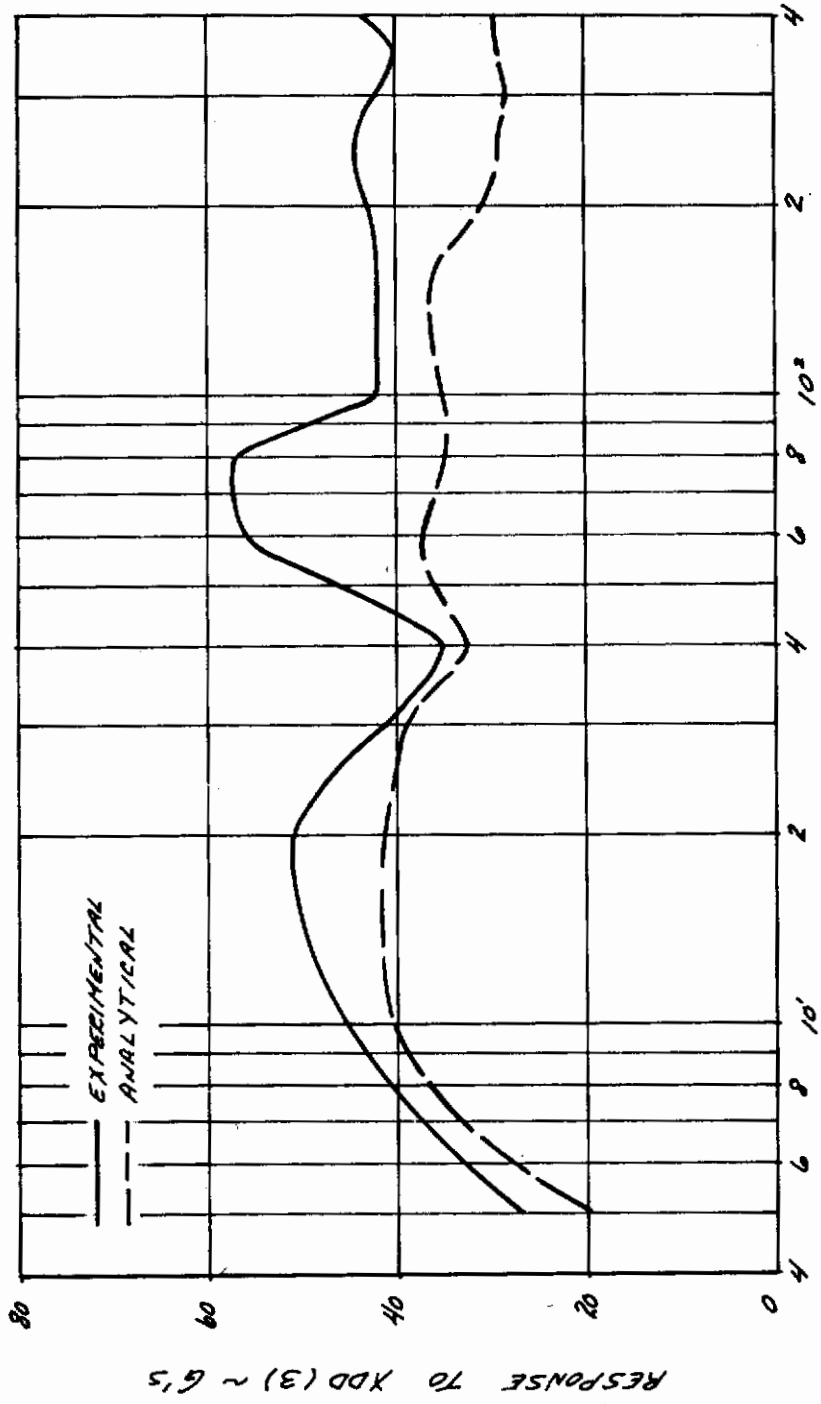

Figure 94, Drop Test 10, Shock Spectra Comparison

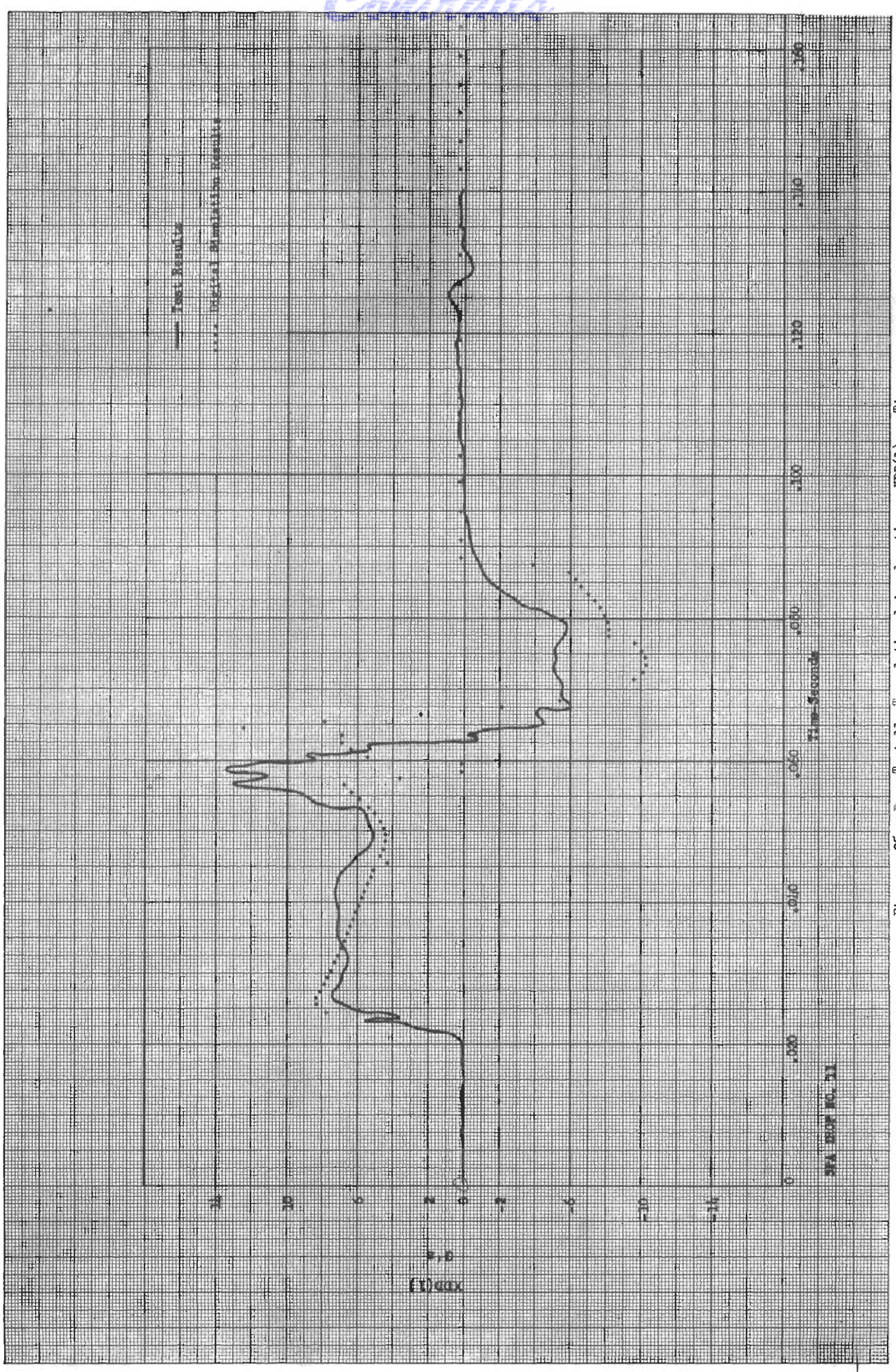

Figure 95 , Drop Test 11, Translational Acceleration - XDD(1) vs Time

Figure 96 , Drop Test 11, Translational Acceleration - XDD(2) vs Time

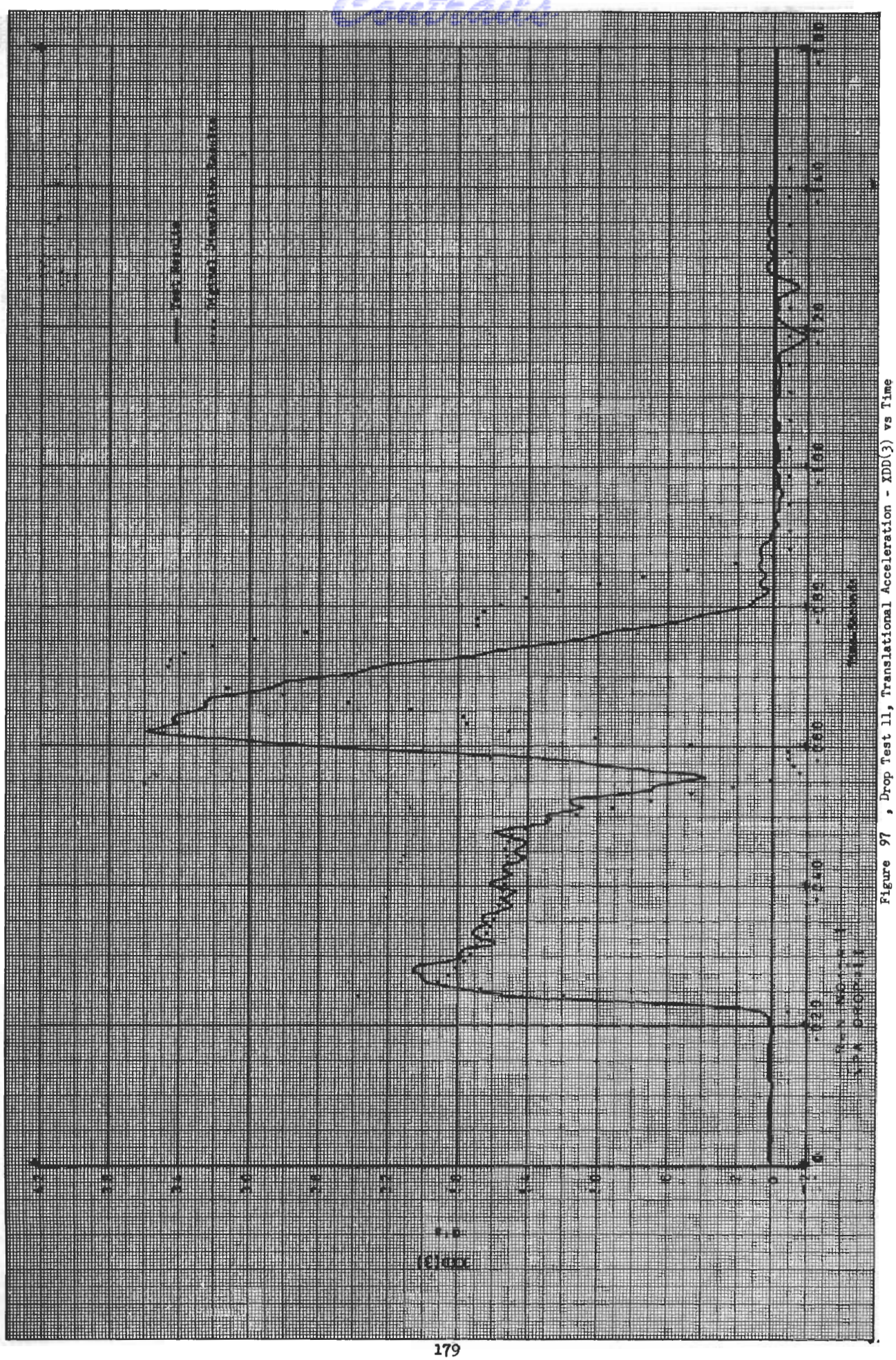

Figure 97 , Drop Test 11, Translational Acceleration - XDD(3) vs Time

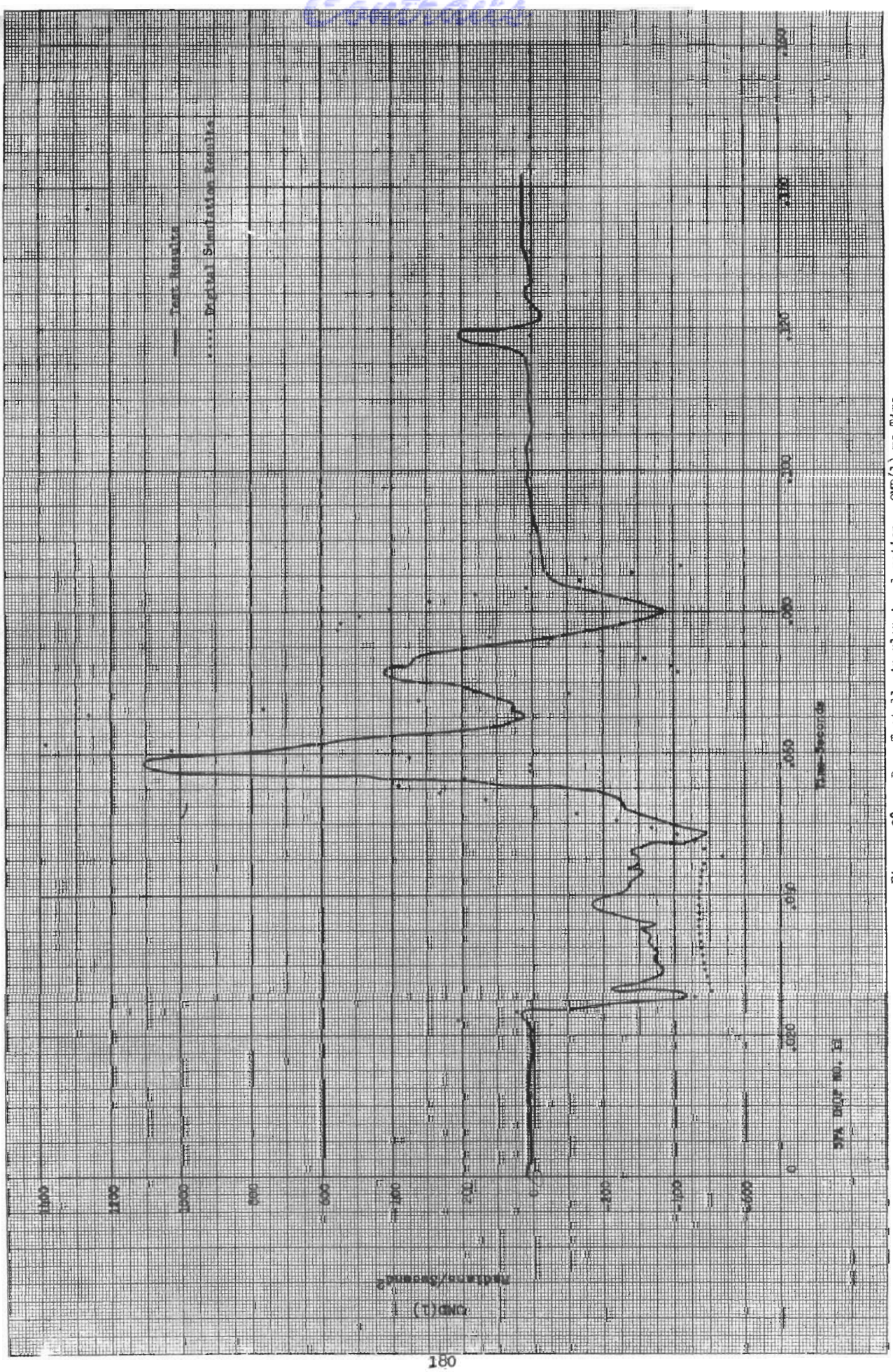

Figure 98 , Drop Test 11, Angular Acceleration - OMD(1) vs Time

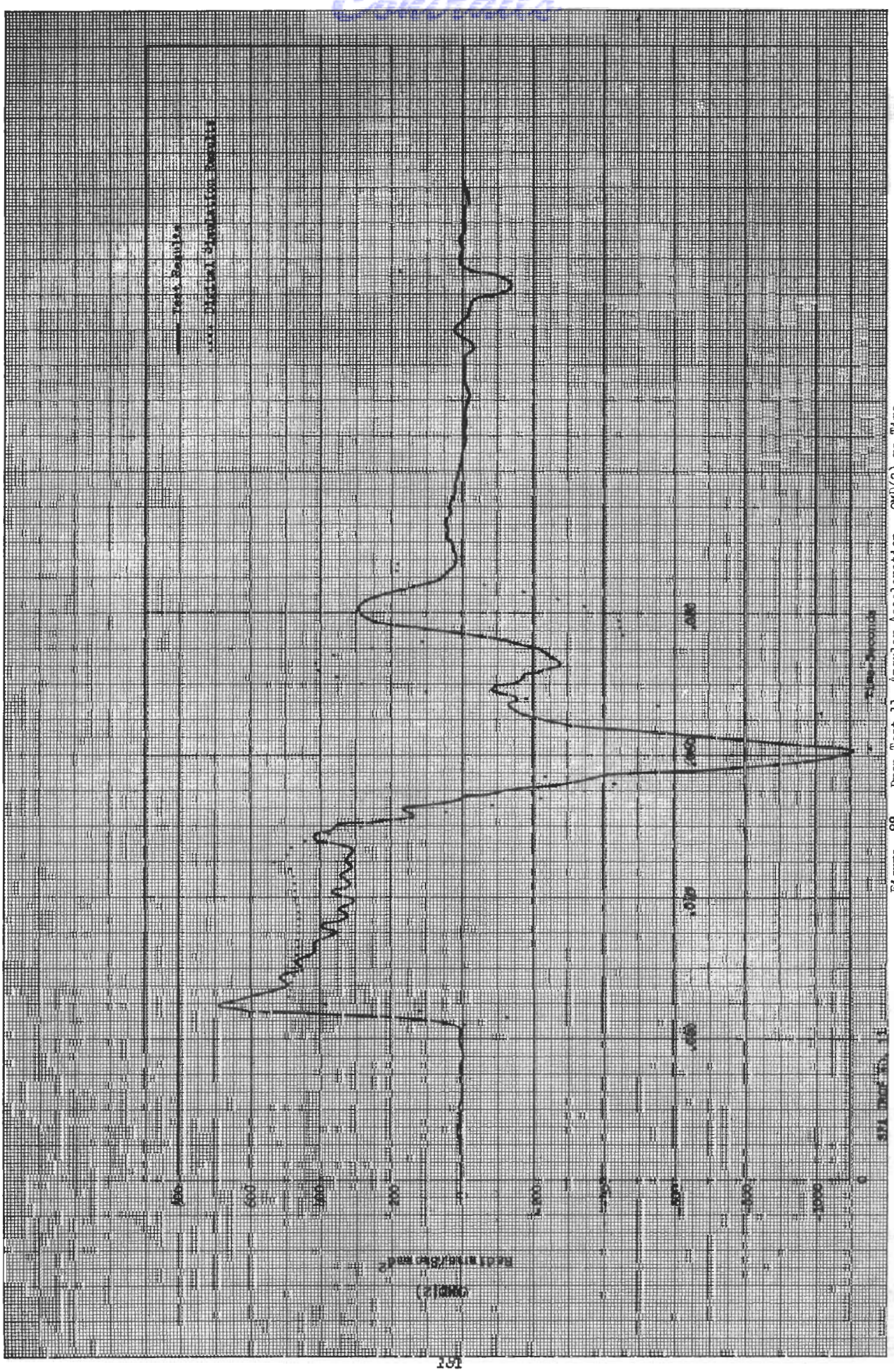

Figure 99 , Drop Test 11, Angular Acceleration - OMD(2) vs Time

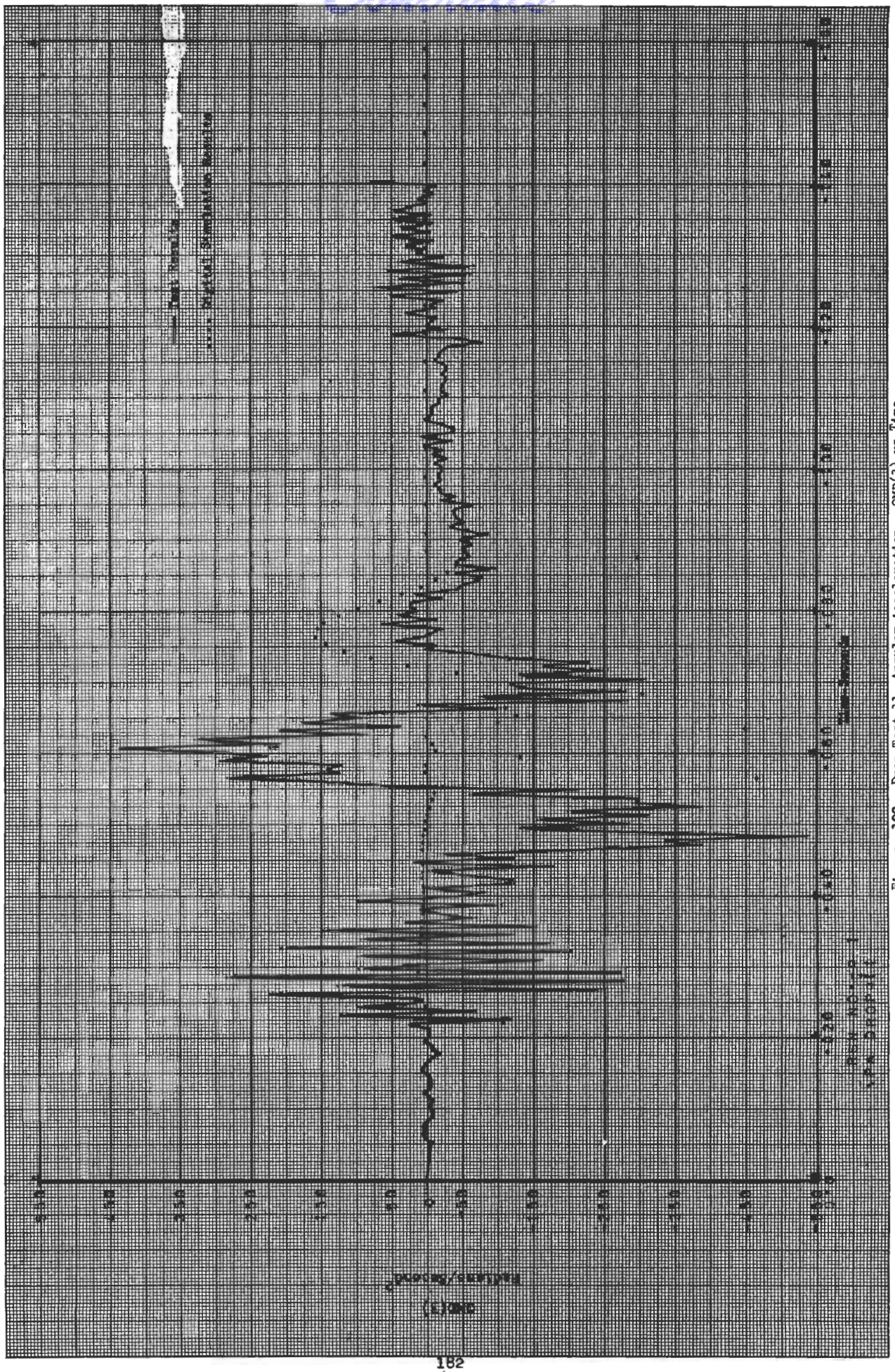

Figure 100 , Drop Test 11, Angular Acceleration - OMD(3) vs Time

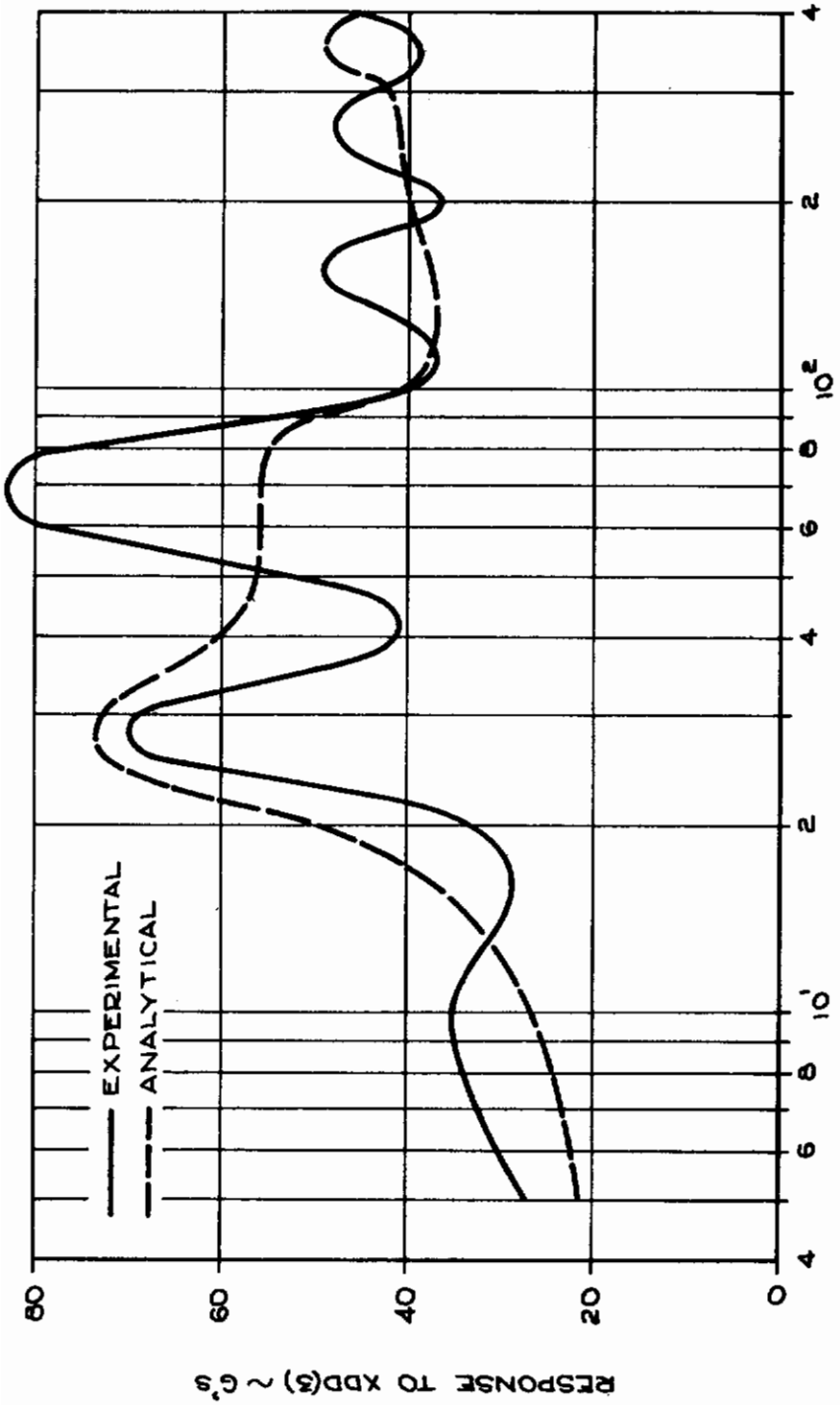

Figure 101, Drop Test 11, Shock Spectra Comparison

relatively small inclination errors (1 or 2 degrees) would produce the desired timing. The inclination errors resulted from the reading of the high speed movies and are caused by the dark background at the test site.

The usefulness of the digital simulations would be enhanced if different force deflection characteristics could be used for each absorber. As discussed in Section VI.B, small variations in energy cell forces produce large angular accelerations which may be of significance for alightment under marginal stability conditions. For a hardware fabrication program, a set of tolerances must be established and a digital simulation offers an economical and accurate means of arriving at acceptable limits. The existing simulations should therefore be modified to accept different force deflection characteristics for each energy cell.

The use of a frictional model of the peg leg/surface interaction is adequate for comparing non-slipping versus slipping type alightments on man-made surfaces. The adequacy of a frictional model for soils is open to question. With an adequate foot pad design, a frictional model is probably adequate. If the soil is penetrated significantly or a "plowing" action takes place, the soil may become a significant energy sink and a frictional model would not be adequate. Certainly this is one facet of the alightment problem in which further detailed study must be made.

It is concluded that the digital simulations are adequate to examine the parameters required under this program. Significant improvements could and should be made prior to attempting the optimization of a given design.

D. COMPARISON OF ABSORBER STROKES AND ENERGY ABSORPTION

The lengths of the honeycomb pads of the energy absorbers were measured before and after each drop. These absorber strokings can be compared against the energy absorber strokings from the digital simulation runs of drops which terminated normally. Drop 5 should not be compared against the simulation results because the simulation stopped when the capsule bottom interfered with the ground, while the test model may have experienced significant absorber strokings after this point in time. Drop 7 cannot be simulated due to the binding of an energy absorber on leg 4. The analytical and experimental absorber strokings should not be compared on Drop 11 because the simulation terminated the run when the model pitched 60 degrees beyond the vertical, while the test model tumbled over and stroked the energy absorbers some additional amount.

The energy absorbed by each pad during a drop may be computed by assuming that the mean static crushing force acted through a distance equal to the permanent deflection. Since there is little difference between the loading and unloading slopes on the honeycomb pads, the accuracy of this method is almost solely dependent upon the validity of the assumption that the dynamic reaction force across the energy absorber is equal to the mean static crushing load. The energy absorbed by each pad in the digital simulation may be computed by converting the permanent alightment system coordinate positions to energy absorber

deflections. Since the loading slopes of the dynamic force deflection characteristics used in the digital simulations account for effects such as terrain compliance and penetration as well as structural compliance, the loading and unloading slopes in the simulation are different. The energy absorbed due to crushing of the pads in the simulation must be corrected for the difference in loading and unloading slopes.

The energy absorbed during each drop may be determined by summing the kinetic and potential energies of the test capsule at the instant of release. The kinetic energy is that associated with the horizontal velocity. The potential energy is computed by determining the difference in the vertical height of the center of gravity between the release point and the final position of the space package after the drop. The nominal drop heights were measured from the contact point of the lowest leg to the point on the ground directly underneath. Thus, two additional terms must be added to the nominal drop height. The change in height of the center of gravity of the test model due to the nutation angle must be added to the nominal drop height. The change in the height of the center of gravity due to the deflection of the alightment system must also be added to the nominal drop height. The energy absorbed for each drop height may be computed in this manner and compared with the summation of the individual absorber energies computed from the experimental and analytical absorber strokings.

The experimental and analytical energy absorber strokings and energy absorption for each comparable drop test are presented in Tables 6 through 13. The total energies from both the experimental and analytical energy absorber strokings are compared with the energy absorbed for each drop test in Figure 102. Examination of Figure 102 indicates that the summation of the individual absorber energies obtained from the absorber strokings in the digital simulations are in excellent agreement with the actual energies absorbed in each drop test. The average difference is less than 0.5 percent and the largest difference is 4.1 percent which is well within the confidence limits on the initial conditions and the computations involved. A comparison between the actual energies absorbed and the summation of the individual absorber energies computed from the experimental strokings indicates that the energies computed from the experimental absorber strokings are consistently low. The average difference is 22.9 percent while the largest and smallest differences are 30.0 percent and 13.3 percent, respectively.

The difference between the actual energy in each drop and the summation of the individual absorber energies obtained from the experimental strokings can be due to three possible causes. The first possible source of energy dissipation is due to energy losses experienced when the spiked end of the test model peg legs penetrated the asphalt. The greatest penetrations experienced during the drop tests were no greater than one quarter of an inch average for the four legs. Assuming a square force pulse at the asphalt which produces 40 g's acceleration on the model to act through the distance of one quarter of an inch yields work which is less than one foot of potential energy. The one foot of potential

TABLE 6

DROP NO. 1, ENERGY ABSORPTION

ENERGY 1,206 FT-LB

Experimental

Upper

Leg No.	1	2	3	4
Stroke (FT)	0.1000	0.0910	0.0975	0.0910
Energy (FT-LB)	235	214	229	214

Lower

Stroke (FT)	0.0067	0	0.0025	0.0017
Energy (FT-LB)	13	0	5	3

Total Energy 913

Percent Error -24.3

Analytical

Upper

Leg No.	1	2	3	4
Stroke (FT)	0.1356	0.1356	0.1356	0.1356
Energy (FT-LB)	275	275	275	275

Lower

Stroke (FT)	0.0086	0.0086	0.0086	0.0086
Energy (FT-LB)	14	14	14	14

Total Energy 1,156

Percent Error -4.1

TABLE 7

DROP NO. 2, ENERGY ABSORPTION

ENERGY 1,232 FT-LB

Experimental

Upper

Leg No.	1	2	3	4
Stroke (FT)	0.0975	0.0850	0.0625	0.0590
Energy (FT-LB)	239	208	153	145

Lower

Stroke (FT)	0.0470	0.0280	0.0540	0.007
Energy (FT-LB)	92	55	127	13

Total Energy 1,032 FT-LB

Percent Error -16.2

Analytical

Upper

Leg No.	1	2	3	4
Stroke (FT)	0.1673	0.1480	0.0924	0.1097
Energy (FT-LB)	367	319	184	225

Lower

Stroke (FT)	0.0421	0.0248	0.0101	0.0119
Energy (FT-LB)	79	45	17	20

Total Energy 1,256 FT-LB

Percent Error +1.9

TABLE 8

DROP NO. 3, ENERGY ABSORPTION

ENERGY 1,428 FT-LB

Experimental

Upper

Leg No.	1	2	3	4
Stroke (FT)	0.0730	0.2560	0.1390	0.0167
Energy (FT-LB)	168	590	320	38

Lower

Stroke (FT)	0.0092	0.0283	0.0208	0
Energy (FT-LB)	19	59	44	0

Total Energy 1,238 FT-LB

Percent Error -13.3

Analytical

Upper

Leg No.	1	2	3	4
Stroke (FT)	0.0366	0.1471	0.2793	0.1471
Energy (FT-LB)	46	296	600	296

Lower

Stroke (FT)	0.0049	0.0209	0.0363	0.0209
Energy (FT-LB)	7	41	73	41

Total Energy 1,400

Percent Error -2.0

TABLE 9

DROP NO. 4, ENERGY ABSORPTION

ENERGY 1,480 FT-LB

Experimental

Upper

Leg No.	1	2	3	4
Stroke (FT)	0.1240	0.0625	0.0120	0.0710
Energy (FT-LB)	292	147	28	167

Lower

Stroke (FT)	0.1260	0.0470	0.0017	0.0360
Energy (FT-LB)	240	90	3	68

Total Energy 1,035 FT-LB

Percent Error -30.0

Analytical

Upper

Leg No.	1	2	3	4
Stroke (FT)	0.2057	0.1137	0.0244	0.1427
Energy (FT-LB)	447	225	42	293

Lower

Stroke (FT)	0.1216	0.0508	0.0049	0.0631
Energy (FT-LB)	228	93	9	117

Total Energy 1,454 FT-LB

Percent Error -1.8

TABLE 10

DROP NO. 6, ENERGY ABSORPTION

ENERGY 2,345 FT-LB

Experimental

Upper

Leg No.	1	2	3	4
Stroke (FT)	0.0975	0.0990	0.0980	0.0950
Energy (FT-LB)	420	426	422	409

Lower

Stroke (FT)	0.0025	0.0017	0.0050	0.0008
Energy (FT-LB)	9	6	17	3

Total Energy 1,712

Percent Error -27.0

Analytical

Upper

Leg No.	1	2	3	4
Stroke (FT)	0.1523	0.1523	0.1523	0.1523
Energy (FT-LB)	578	578	578	578

Lower

Stroke (FT)	0.0086	0.0086	0.0086	0.0086
Energy (FT-LB)	26	26	26	26

Total Energy 2,416

Percent Error +3.0

TABLE 11

DROP NO. 8, ENERGY ABSORPTION

ENERGY 2,375 FT-LB

Experimental

Upper

Leg No.	1	2	3	4
Stroke (FT)	0.0367	0.1020	0.1080	0.0920
Energy (FT-LB)	161	449	475	405

Lower

Stroke (FT)	0.0042	0.0025	0.0440	0.0033
Energy (FT-LB)	15	9	153	11

Total Energy 1,678

Percent Error -29.4

Analytical

Upper

Leg. No.	1	2	3	4
Stroke (FT)	0.1000	0.1621	0.1873	0.1248
Energy (FT-LB)	362	635	747	467

Lower

Stroke (FT)	0.0079	0.0204	0.0393	0.0110
Energy (FT-LB)	25	68	133	35

Total Energy 2,472

Percent Error +4.1

TABLE 12

DROP NO. 9, ENERGY ABSORPTION

ENERGY 2,626 FT-LB

Experimental

Upper

Leg No.	1	2	3	4
Stroke (FT)	0.1460	0.1730	0.0750	0.0340
Energy (FT-LB)	635	754	326	148

Lower

Stroke (FT)	0.0050	0.0080	0.0020	0.0010
Energy (FT-LB)	18	29	7	4

Total Energy 1,921

Percent Error -26.8

Analytical

Upper

Leg No.	1	2	3	4
Stroke (FT)	0.2242	0.2380	0.0823	0.0625
Energy (FT-LB)	147	128	38	34

Lower

Stroke (FT)	0.0417	0.0364	0.0114	0.0103
Energy (FT-LB)	899	958	281	195

Total Energy 2,680

Percent Error +2.1

TABLE 13

DROP NO. 10, ENERGY ABSORPTION

ENERGY 2,572 FT-LB

Experimental

Upper

Leg No.	1	2	3	4
Stroke (FT)	0.1380	0.1040	0.0150	0.0675
Energy (FT-LB)	607	458	66	297

Lower

Stroke (FT)	0.0670	0.0410	0.0010	0.0920
Energy (FT-LB)	241	148	4	332

Total Energy 2,153

Percent Error -16.3

Analytical

Upper

Leg No.	1	2	3	4
Stroke (FT)	0.2425	0.1513	0.0425	0.1342
Energy (FT-LB)	982	588	109	511

Lower

Stroke (FT)	0.0620	0.0291	0.0032	0.0267
Energy (FT-LB)	220	105	9	93

Total Energy 2,617

Percent Error +1.8

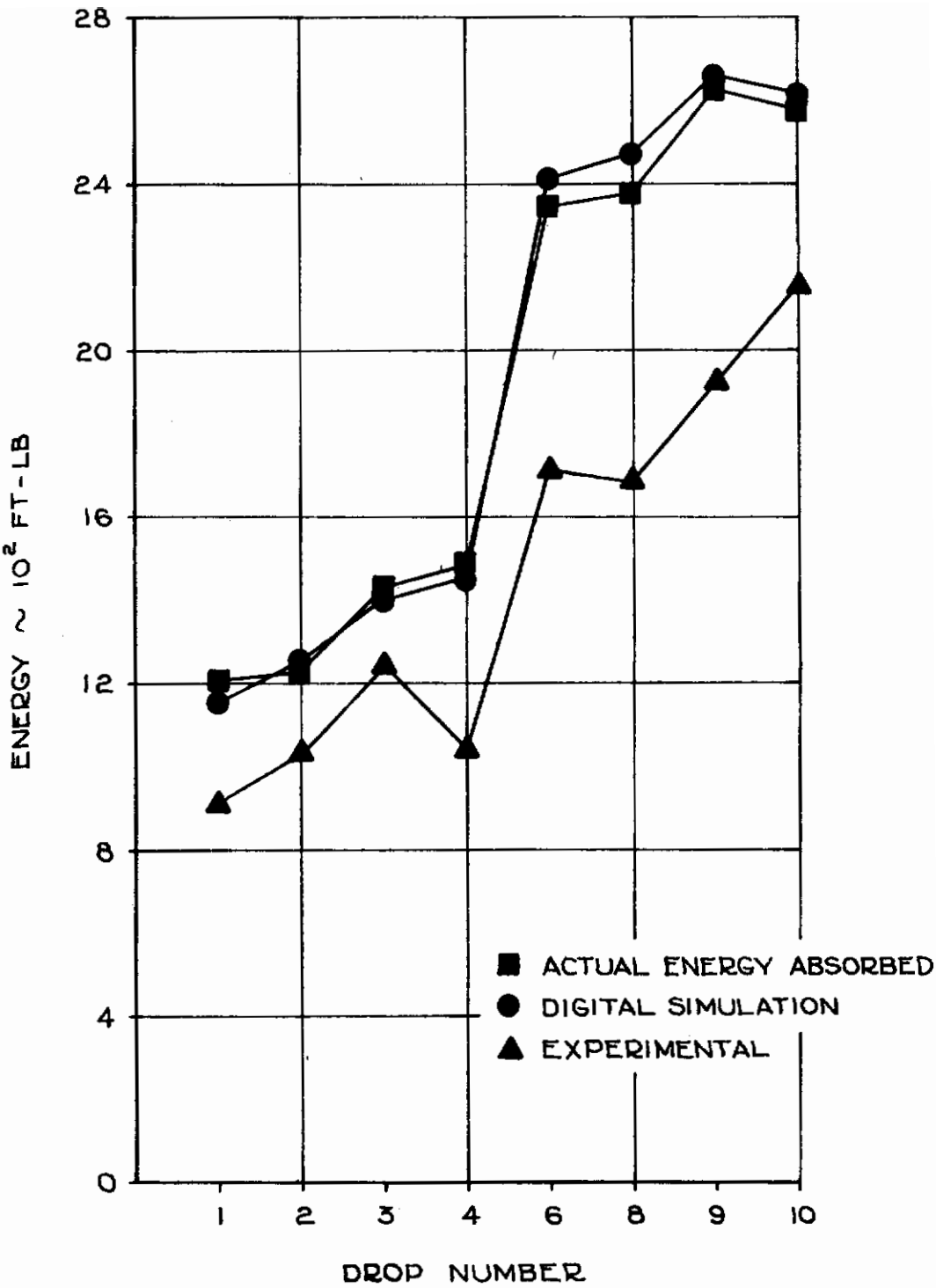

Figure 102, Comparison of Energy Absorption

energy is less than 10 percent of the actual total energy for the 10 foot drops. The 5 foot drops had correspondingly less penetration.

The second possible source of energy dissipation is due to friction between the moving parts such as the pinned joints and the energy cells. The contribution of friction to the energy dissipation is difficult to assess. The friction of the pinned joints when the alightment system is not loaded is insufficient to explain a significant portion of the 22.9 percent energy difference. The friction characteristics of the pinned connections of the alightment system are unknown for the loaded conditions. Since significant loads are carried by the alightment system during stroking, it is not impossible that the loaded frictional characteristics of the pinned joints are responsible for a substantial portion of the 22.9 percent energy difference. The friction between the energy cell rods and end plates is a more likely contributor to the energy difference. At least one instance of binding of the energy cells was noted during the drop tests. Some degree of skewing of the energy cell end plates was noted on almost every drop test. Thus, the friction between the energy cell rods and end plates is definitely a source of some of the energy difference.

The third possible source of the energy difference is due to the honeycomb pads. An increase in the honeycomb crushing load due to dynamic effects, such as air cushioning, strain rate hardening, and dynamic buckling, would explain the energy difference. However, these dynamic effects are generally thought to be insufficient in magnitude in this velocity domain to be responsible for a 20 percent increase in the crushing load.

A comparison between the accelerometer signals and the digital simulation accelerations indicate that the accelerations were consistently higher during the drop test than the simulation predicts. They are, in fact, some 20 percent higher on the average. Therefore, 20 percent larger forces existed during the drop test than were predicted from the static force deflection characteristics of the honeycomb. It is therefore concluded that either frictional effects in the pinned joints and/or energy cells or the dynamic crushing effects of the honeycomb are responsible for most of the 22.9 percent average energy difference between the actual drop test energies and the summation of the individual absorber energies obtained from the drop test strokings.

It is felt that the best explanation for the energy and force characteristic differences are due to a combination of frictional and dynamic effects. It is difficult to assign relative values to each possible source. It is possible to measure the energy cell reaction loads during drop testing by the use of strain gages on the rods. The dynamic effects can be separated from the friction effects of the cell by dynamic testing of the cell and the honeycomb. The potential frictional effects can also be significantly reduced by redesign of the energy cell to better restrain the end plates from skewing.

SECTION VII

GENERAL CONCLUSIONS

The program has shown that a three-dimensional analysis of alightment will adequately predict capsule response. Also, it is feasible to design an alightment system with a 6 percent weight limit which will meet the following impact conditions:

Impact Velocity	35 feet per second vertically
	15 feet per second horizontally
Terrain Slopes	35 degrees
Capsule Inclination	12 degrees

The following specific conclusions were obtained from the program.

A. DESIRABILITY OF THREE-DIMENSIONAL SIMULATION

A three-dimensional simulation is necessary to accurately predict capsule response. Efficient alightment systems must use landing leg systems. This, in turn, means near symmetrical alightment with potential energy being transferred between all six coordinates of the system. A two-dimensional analysis will provide only a crude approximation to the actual alightment dynamics. On the other hand, the three-dimensional analysis will provide sufficient accuracy to finalize a design based on the computer results.

A digital simulation is a powerful design tool for an alightment system development. The articulated leg simulation requires an average of 0.05 computer hours per run on a CDC 3400 unit. Therefore, it is economically feasible to make several hundred runs to develop an alightment system. Landing system loadings in addition to capsule response can be output data from the runs. Complete design optimization can be derived prior to hardware fabrication and test. The use of a three-dimensional simulation should greatly reduce development cost and time for any alightment system. Furthermore, since it is feasible to investigate all alightment parameters, the final design should be superior to a design developed empirically.

B. SIGNIFICANT PARAMETERS

The critical alightment parameter is horizontal velocity. The system design is strongly influenced by the magnitude of the horizontal velocity. Capsule inclination and terrain slope are comparable parameters placing similar requirements on the system. The study has shown the following additional parameters that should be included in future work:

(1) Non-uniformity of load cells resulting in different force deflection characteristics of the individual legs. This causes capsule pitching and can be very significant in a stability analysis.

(2) Interaction between the legs and terrain. Pressure pads plowing the earth or penetration of the earth may be significant energy sinks. Proper utilization of these effects would reduce system requirements. Note that this requires a more refined model than the slip or non-slip simulation used in the program.

(3) Non-flat terrain should be a parameter. For example, it could be assumed that a 2 foot discontinuity or local anomaly could be encountered at any position within the leg span. This increases the severity of the system design requirements.

C. SIGNIFICANCE OF PRESENT STUDY

The present study demonstrates the potential of a three-dimensional simulation. The correlation with test results shows that the simulation is accurate. A cursory definition of alightment system design parameters was obtained demonstrating the feasibility of an alightment system for the program parameters without excessive weight penalties.

D. SHORTCOMINGS OF PRESENT STUDY

The intent of the present study was to perform a parametric analysis of alightment systems for a given set of impact conditions. This was to be accomplished in 200 computer runs. The study has indicated that approximately 400 runs would be required to finalize the design for a single alightment system. The present study is merely a cursory examination of the parameters. One or two alightment systems should be fully analyzed to specifically define the interdependence of all significant parameters. This would define weight as a function of design limitations which could be used in a system trade-off study. The current study shows system feasibility instead of the parametric definition desired.

The simulation should be improved to include the additional parameters of Section VII. B. Also, higher horizontal velocities should be investigated. The 15 foot per second (9 knots) horizontal velocity limit appears low for earth landing. Ground winds in the range of 20 to 30 knots can be encountered a significant percentage of the time. Since horizontal velocity is the critical parameter, the effect of ground speeds in the range of 10 to 30 knots should be investigated. The alightment system design parameters will be almost completely defined by the limits placed on horizontal velocity.

SECTION VIII

RECOMMENDATION FOR FUTURE WORK

A three-phase program is recommended. The parametric analysis using existing programs should be extended to fully define the design parameters necessary for various alightment conditions. Secondly, a specific design should be developed using an improved simulation. Finally, hardware should be fabricated and tested.

A. PARAMETRIC DEFINITION

The existing digital program, though not exactly representative of a final design, is capable of defining the general parameters of a final design. The program should be used to optimize system geometry for the desired set of impact conditions. Foot pad spread, leg forces and stroking, etc., can be defined. Approximately 400 computer runs would be required. The end product would be a general design criteria for a landing system which will function under a given set of impact conditions.

B. SPECIFIC DESIGN CONCEPT

The information obtained in the parametric study should be utilized to develop a specific design. This design concept should include stowage as well as functional characteristics. A digital program should be developed for the concept including refinements concerning terrain foot pad interaction, variable force for each leg, a refined treatment of bottoming and system loading printouts. A final design will develop from this program.

C. ACTUAL DESIGN

A full size system should be fabricated and tested to verify the stress analysis and terrain-foot pad interaction. This would be a final design adapted to a specific capsule.

APPENDIX I

LITERATURE SEARCH

This appendix contains abstracts and principal conclusions derived from the indicated references.

A. P. Cappelli, "Dynamic Analysis for Lunar Alightment", American Institute of Aeronautics and Astronautics Journal, May 1963.

This article presents a simplified three-dimensional alightment dynamic analysis scheme. The mathematical model is a rigid body with the motions described by "Eulerian equations of motion". The forcing functions are described by inelastic crushing of the vertical and lateral energy absorbers. The results presented are for a three legged configuration.

Conclusions: Four criteria for successful lunar alightment are presented. The vehicle must remain stable during alightment. The impact forces and accelerations must be reduced to tolerable limits. The vehicle rebound must be kept to a minimum. The final position of spacecraft must allow operation of the payload components. A complete analytical description of the vehicle motion during alightment will allow the prediction of the success of the alightment.

R. J. Black, "Quadrupedal Landing Gear for Spacecraft", Journal of Spacecraft, March-April 1964.

Stability analyses and experimental model test results are compared and discussed for spacecraft landing impact energy systems using quadrupedal landing gear. Each of the legs is an inverted tripod, with the three struts of each leg having a uniaxial energy absorber. Model scaling methods are discussed and test methods and results presented. A two-dimensional analytical technique for prediction of the motion after first contact of a spacecraft, using such a landing gear, is also presented. The analytical and experimental results are compared to give stability boundaries for combinations of initial horizontal and vertical velocity, terrain slopes, and upper and lower strut stroke loads.

Conclusions: The complete articulation and stroke capabilities of the landing gear system must be duplicated in analytical computations to yield a true picture of vehicle stability. Ground slope stability capability can be increased by increasing the landing gear radius or spread. The rate of change of landing gear radius with terrain slope is nearly constant for slopes between 5 and 20 degrees. The four leg configuration was chosen over others on the basis of a weight versus stability increase criterion. The lower struts enhance the stability of the vehicle, generally when their line of action is below the vehicle center of gravity. An increase in upper strut stroke load, with the lower strut stroke load constant, is stabilizing. The critical (two-dimensional) landing, from a stability standpoint, is a downhill, back-pitched impact with minimum radius on the front legs (a 2-2 impact). Because of the high forward pitch rate after impact, the critical energy-absorption landing condition is an uphill, one-leg forward impact with forward pitch velocity on an infinite coefficient of friction surface. This is particularly critical for systems having low ratios of gear radius to center of gravity height. For large ratios of gear radius to center of gravity height, the critical stability condition becomes the critical

stroke condition for the lower legs because of the resultant reduction in effective forward gear radius.

J. B. Esgar, W. C. Morgan, "Analytical Study of Soft Landing on Gas-Filled Bags", NASA TR R-75, 1960.

Analytical techniques are developed and presented for predicting the deceleration characteristics of vehicles landing on gas-filled bags of various shapes. Bags considered included cylindrical, spherical, and hemispherical shapes. The design concepts called for the use of bags as impact energy absorbers (no rebound) for landings of a space vehicle. This could involve the use of parachutes and parachute drag was considered in the first part of the analysis. Bags with constant area orifices, no orifices, and with variable area orifices were considered for each of the basic bag shapes. The derivations assume an adiabatic process. The sinking velocities are considered to be small compared to the sonic velocity of the gas. The orifices are assumed to be flow type nozzles. The effects of bag height, initial pressure, vehicle mass to bag volume ratio, parachute drag, bag shape, pressure bleed characteristics, and initial velocity on the deceleration characteristics were considered. Maximum decelerations as a function of stroke were determined for various combinations of the bag parameters.

Conclusions: This analysis can be applied to landings on planetary or lunar surfaces as long as the sinking speeds are small compared to the sonic velocity of the gas filling the bag. For high sinking speeds, a light gas such as helium or hydrogen would probably be required. It should be possible to absorb landing shocks with deceleration and onset rates which are within acceptable tolerances for well supported human beings. Acceptable onset rates were exceeded only when acceptable decelerations were exceeded except for special cases. A vertical cylindrical bag was found to be the best shape from the standpoints of maximum deceleration and required stroke. A simple, reliable method for controlled gas bleed is required to give desired onset rates and a constant deceleration after onset. However, bags without orifices could be used if a good means of rapidly deflating them, at the end of the stroke, could be found so as to prevent rebound.

R. K. McFarland, Jr., "A Limit Analysis of Hexagonal Cell Structures Under Axial Load", Technical Report No. 32-186, Jet Propulsion Laboratory, December 1961.

A theoretical analysis is presented for the mean crushing stress in bending and shear of hexagonal honeycomb structures. The resulting formula is as follows:

$$F = \underbrace{\sigma_{yp}\,\frac{t^2}{S^2}\left[\frac{4.75}{K} + 28.628\right]}_{\text{bending deformation}} + \underbrace{1.155\,q_{yp}\,\frac{t}{S}}_{\text{shear deformation}}$$

q_{yp} = shear yield stress

σ_{yp} = tensile yield stress

t = cell wall thickness

S = cell minor diameter

K = represents ratio of one quarter of buckling wavelength to the cell wall width

The equation is fairly insensitive to the value of K. The theoretical value of K was 0.5 and the experimental value 0.4. Experimental values of F were determined for a wide range of t/S ratios and they indicate that the theoretical values are good upper bounds out to a t/S ratio of 0.016. At a t/S of a 0.040 a different mode of failure occurs which is essentially shear deformation. Below this ratio the mode of failure is a collapse in the cell axial direction with the cell walls progressively folding to form alternate symmetric and antisymmetric plates, with like plates stacked on each other. Load-deflection data for a sample with square cross section shows an initial peak load for commencement of collapse followed by a period of relatively constant load for progressive collapse of the specimen.

Conclusions: The mean axial crushing strength of hexagonal honeycomb materials can be predicted with good accuracy up to a cell wall thickness to cell minor diameter ratio of 0.04. The use of high yield stress materials with suitable ductility can result in an appreciable increase in energy absorption properties over presently used aluminum alloy cell structures. After initial collapse has occurred, the force versus deflection curve for axially compressed hexagonal honeycomb structures has essentially a zero slope. The specimen could be shaped to give a desired initial force versus deflection curve.

J. R. McGehee, "A Preliminary Experimental Investigation of an Energy-Absorption Process Employing Frangible Metal Tubing", NASA TN D-1477, October 1962.

Frangible metal tubing as an energy absorber was evaluated in an experimental program involving both static and dynamic loading. Model capsule drop tests were also used to evaluate multiple leg configurations using this energy absorption technique. One end of the tubing was fragmented, under axial load,

against a die. This process is oscillatory but after initial load onset the load-deflection curve oscillates about some essentially constant load level. The onset load can be controlled by either pre-fragmenting the tube end or tapering it. This process gives energy absorption capabilities per pound of absorption material weight which are higher than those of any other material considered in other studies (about 1.3 times greater than balsa wood).

Conclusions: Use of frangible metal tubing as an energy absorber holds promise for use in inelastic capsule alightment systems if the oscillation of the load deflection curve about some central value can be tolerated. This process has very high energy absorption capability. However, the fragments striking the capsule could cause damage.

D. L. Daigle, J. O. Lonborg, "Evaluation of Certain Crushable Materials", Technical Report No. 32-120, Jet Propulsion Laboratory, January 1961.

The results are presented from an experimental evaluation of several crushable materials under dynamic impact loads. These results are in the form of energy absorption capability per unit volume and unit weight; along with measures of crushing strength, maximum proportion of crushing of the material without bottoming, and spring back in percent of the original thickness. Several foam plastics, aluminum honeycomb, and balsa wood were the materials tested. Of these, balsa wood exhibited the greatest volumetric and weight efficiency as an absorption material, with the aluminum honeycomb second and the plastic foams well down on the scale. However, balsa wood has the disadvantage of splintering under dynamic loading unless the area to be crushed is constrained. The angle of the grain of the wood with respect to the crushing direction also effects the energy absorption capability with maximum capability for an angle of zero of the grain with respect to crushing direction. An increase in this angle also has the effect of increasing the spring back. No noticeable effects due to vacuum, on the capabilities of balsa wood, could be found.

Conclusions: No specific conclusions can be drawn about the preponderant advantage of the use of one material over others since the specific application must be considered. However, balsa wood appears to have advantages over the other materials evaluated (aluminum honeycomb and plastic foams) in regards to unit weight and volumetric energy absorption efficiency. Balsa has the disadvantages of splintering and having its absorption capability dependent on grain direction. Vacuum conditions do not appear to effect the absorption characteristics of balsa wood. The spring back of both balsa wood and aluminum honeycomb were found to be "negligible".

"Launching and Alightment Systems for Aero-Space Vehicles", WADD Technical Report 60-857, Cleveland Pneumatic Industries, Inc., AD 263 472, May 1961.

Report on study of shock absorption, stabilization, and launching apparatus for the lunar alightment and launching of manned aero-space vehicles. The third part of a WADD sponsored study which also deals with earth alightment and departure, and orbital rendezvous. Four apparatus concepts were modeled and tested: (1) Imbedment anchors for stabilization of vehicle during and after alightment; (2) Oleo pogo for alightment and departure; (3) Triple vertical collapsing strut using frangible rings for shock mitigation; and (4) Triple oleo outrigger for alightment. Space vehicle dimensions were modeled on a 10 to 1 scale and the various concepts were tested to impact velocities of 33.4 feet per second. Results from tests of oleo pogo and triple oleo struts indicated reliable performance with the benefit of predictable, repetitive energy absorption. Disadvantages are large weight and susceptibility of seals and fluids to deterioration from space environments. The imbedment anchors were spring released inertially on impact and contained an explosive charge which fired the anchor tip into the surface on contact. Simultaneously, the cable from the anchor to the vehicle was braked and tensioned. The triple vertical collapsing strut was of light weight and efficient as an energy absorber, although it was good for only one impact. Aluminum rings ruptured by forcing them over a cone in a telescoping strut were used as the energy absorber. The main problem arose from the ruptured rings jamming the strut.

Conclusions: The type of shock mitigation equipment must be considered early in the vehicle design since there appears to be optimum shock mitigation systems for each type vehicle. Optimum shock mitigation depends on vehicle configuration (center of gravity, mass distribution), allowable mass for mitigation equipment, and landing dynamics and surface characteristics.

R. E. Lavender, "Lunar Logistic System Volume XI, Lunar Touchdown", MTP-M-63-1. Aeroballistics Division, NASA, March 1963.

Results are presented of analytical studies of lunar vehicle touchdown dynamics. Three, four, and five leg configurations were studied with and without the use of stabilization rockets. Parameters considered in the analysis were: coefficient of friction, location of the vehicle center of gravity, foot pad spread, the terrain slope, the vehicle vertical and horizontal landing velocities, and the load factor or design acceleration.

Conclusions: The three leg configuration appears to be worthy of more consideration from this two-dimensional analysis while the five leg system appears less competitive with the four leg system studied in most of the analyses. Reduction in terrain slope and coefficient of friction reduces the landing gear spread requirement as does having the center of gravity low and on

the longitudinal axis of the vehicle. Reduction in the radius of gyration also reduces this requirement. Rather marked changes in the required spread result from the change in slope; a reduction by a factor of 0.4 for a slope decrease from 30 degrees to 10 degrees. A comparable reduction results from a change in the coefficient of friction of from 1.0 to 0.6. Reductions of either the initial horizontal or vertical velocity of 1 meter per second can reduce the required spread by up to 1.5 meters for the configuration studied. The use of a stabilization rocket motor mounted on top of the payload and directed downward through the vehicles center of gravity is very effective in obtaining touchdown stability under extreme conditions of slope and coefficient of friction.

L. F. Fisher, Jr., "Landing-Impact-Dissipation Systems", NASA TN D-975, December 1961.

Results of analytical and experimental investigations of landing energy dissipation systems are reported. The type of system or combination of systems used is seen to depend on design impact velocity requirements, both horizontal and vertical. For large vertical and small horizontal velocities, parachutes and rockets are most feasible. For moderate horizontal and vertical velocities, deformation energy absorbers are most useful. For moderate vertical and high horizontal velocities, skidding is the most useful technique.

Conclusions: Evaluation of landing techniques can be evaluated using computational methods or model testing. A class of energy absorption techniques can be chosen on the basis of the design vertical and horizontal landing velocity requirements.

J. R. McGehee, V. L. Vaughn, Jr., "Model Investigation of the Landing Characteristics of a Re-entry Spacecraft With a Vertical-Cylinder Air Bag for Load Alleviation", NASA TN D-1027, March 1962.

Analytical investigations of the landing characteristics of re-entry vehicles equipped with vertical-cylinder air bag absorbers have been correlated with experimental model test results. These comparisons show that, for flight paths nearly normal to the landing surface, the analytical and experimental studies correlate well. The computational model assumes isothermal compression and expansion through constant area orifices. A scaling technique was developed for model bag volume to permit the use of normal weight, inertia, and dimensional scaling techniques.

Conclusions: For flight paths which nearly coincide with the bags principal axis, the impact acceleration time history of a vehicle using air bag absorbers can be accurately computed. This information can also be obtained using model testing providing that suitable bag volume scaling techniques are used.

V. L. Vaughn, Jr., "Water Landing Impact Accelerations for Three Models of Re-entry Capsules", NASA TN D-145, October 1959.

Experimental results are reported for water impact accelerations of three capsule models, one each with a conical, a spherical, and a convex-concave bottom. Flight paths of 90 degrees and 65 degrees to the horizontal were used with capsule attitudes ranging over zero degree to ±30 degrees. The conical bottomed capsule had the lowest deceleration loads, reaching maximums of 10 g along the capsules primary axes. The spherical bottomed model had the highest loads, approaching 55 g, while the convex-concave model had maximums of about 28 g. All the maximums occurred along the vertical axes of the capsules. Maximum transverse accelerations approached 12 g.

Conclusions: Maximum accelerations along the vertical axis of the capsule for a given vertical contact velocity are higher for inclined flight paths. Acceleration varies as the square of the contact velocity. Increase in contact attitude resulted in reduction in maximum acceleration for the spherical bottom, but had little effect for the other types of surfaces.

J. B. Esgar, "Survey of Energy-Absorption Devices for Soft Landing of Space Vehicles", NASA TN D-1308, June 1962.

Inelastic energy absorption devices, useful for soft landings of space vehicles, are surveyed and their relative merits compared. It is concluded that the device to be used will depend on the mission, but material deformation and friction processes are cited as having the highest energy absorption weight efficiencies. Areas of research recommended include the above processes and combinations of them as well as methods of handling side loads, light weight stabilizing systems, and other combinations of absorption systems.

Conclusions: Combined friction-material deformation processes are seen as the most promising and efficient energy absorption process. The friction process is capable of larger dissipations of energy per pound of material than any other means. However, for specific applications the other processes surveyed are seen to be valuable.

U. J. Blanchard, "Characteristics of a Lunar Landing Configuration Having Various Multiple-Leg Landing-Gear Arrangements", NASA TN D-2027, January 1964.

Model test results are presented for multiple leg lunar module landing arrangements. Four and five symmetrical leg patterns and an asymmetrical four leg pattern were used. Each leg was an inverted tripod, the upper strut of telescoping tubes providing the absorption by stretching of a ductile metal strap. Various flight paths and model attitudes were tested with angular and

linear accelerations recorded for all. Unstable conditions are noted. The five leg system adds stability but not a large amount. The asymmetrical four leg configuration adds considerable stability, primarily because of its leg spread. Tests were conducted by dropping the model from a pendulum onto a hard surface and onto a pumice layer over a hard surface.

Conclusions: Maximum accelerations parallel to the landing surface increase for a soft surface over a hard one. Landings on a soft surface gave rise to more instabilities than for landings on the hard surface. Surface topography, pumice depth, configuration, flight path and attitude, and coefficients of friction were important in this effect (0.4 for the hard surface, 0.7 to 1.0 for the soft). Attenuation in the horizontal direction is desirable to absorb loads which would ordinarily result in excessive bending loads on the lower struts.

S. M. Stubbs, J. R. McGehee, "Investigation of the Landing Characteristics of a Re-entry Vehicle Having Canted Multiple-Air-Bag-Load-Alleviation System", NASA TN D-1934, August 1963.

Experimental model test results and analytical results are presented for the landing acceleration time histories of capsules using canted air bag energy absorbers. The bags were attached between the deployable heat shield and the capsule bottom, and were canted to help in eliminating shear buckling which reduces the bags' energy absorption capabilities. A shear strap prevented the capsule front from overriding the front of the heat shield thus further preventing buckling of the bags. Results were favorable, especially for contact angles which aligned the bag axes with the vertical.

Conclusions: Canting of impact energy absorbing air bags with respect to the capsule vertical axis tends to minimize inefficient shear collapse of the bags on impact.

U. J. Blanchard, "Landing-Impact Characteristics of Load-Alleviating Struts on a Model of a Winged Space Vehicle", NASA TN D-541, October 1960.

The report contains scale model test results of impact loads on a winged space vehicle using deformable struts. A forward, wheeled strut was allowed to deform as were the attachments for the aft skids. The range of vehicle landing parameters included were 13 degrees to 20 degrees alighting attitudes and sinking speeds of 5.5 to 12 feet per second. Maximum full scale accelerations were less than 8 g compared to 40 g for rigid struts.

Conclusions: Deformable struts can be used to significantly reduce impact loading on gliding winged vehicles. The use of wheeled struts or skids has little effect on the landing accelerations.

L. J. Fisher, Jr., "Landing Energy Dissipation for Manned Re-entry Vehicles", NASA TN D-453, September 1960.

A review of analytical and experimental investigations of landing-energy absorption techniques as applied to Manned Re-entry vehicles. The vehicles are divided into two categories: those having essentially vertical descent and those having essentially horizontal paths. Air bags, crushable materials, deformable struts, braking rockets, and shaped surfaces for water landings are considered.

Conclusions: It appears feasible to evaluate landing gear systems for manned re-entry vehicles on the basis of model tests and by computation. Landing gear of the types considered could be designed and analyzed to fit specified stroke requirements and human tolerances.

J. C. Houbolt, S. A. Batterson, "Some Landing Studies Pertinent to Glider-Re-entry Vehicles", NASA TN D-448, August 1960.

Results are presented of analytical studies of the effect of initial conditions on impact loads for glider-re-entry vehicles. The parameters considered are the angular attitude of the glider, its pitch angular velocity, its vertical velocity, the rear landing gear location with respect to the center of gravity, and the effective masses at the landing gears. An experimental study of coefficients of friction of metal skids on concrete, asphalt and lakebed surfaces is reviewed.

Conclusions: Increasing the distance from the center of gravity to the aft landing gear increases the importance of the pitch velocity and acceleration. It may therefore become necessary to design to pitch rate and acceleration as well as vertical rate and acceleration, since it is necessary for this type vehicle to have the rear gear nearer the rear of the vehicle (because of high angle of attack, low lift-drag-ratio landing approaches). Brush type skids or skids of soft metals hold promise for use on landing gear for this type vehicle.

E. L. Hoffman, S. M. Stubbs, J. R. McGehee, "Effect of Load-Alleviating Structure on the Landing Behavior of a Re-entry-Capsule Model", NASA TN D-811, May 1961.

Deformable aluminum legs for impact energy absorption have been evaluated by scale model test and analysis. The acceleration time histories, for a capsule impacting with various flight paths and attitudes, are presented. Good correlation was obtained between test and analytical results once the strain rate sensitive yield stress for the legs had been adjusted. An apparent yield stress increase of 50 percent was necessary to achieve this correlation.

Conclusions: Compliant metal structures can be used to reduce impact loads by plastic deformation and these loads can be predicted analytically

with proper representation of the metal properties. The structural shape can be tailored to give desired acceleration onset rates. For landings on a hard surface at a flight path angle of 55 degrees and an attitude of ± 30 degrees tumbling occurred.

R. C. Dreher, S. A. Batterson, "Coefficients of Friction and Wear Characteristics for Skids Made of Various Metals on Concrete, Asphalt, and Lakebed Surfaces", NASA TN D-999, January 1962.

Results are presented for experimental determinations of coefficients of friction and wear for various metals used as skids on asphalt, concrete, and lakebed surfaces. The tests were conducted for a horizontal velocity range of 20 to 180 feet per second and for a broad range of metals. Some tests involved use of brush skids, the remainder using solid plates attached to the skid fixture. The friction process was concluded to be a combination of shearing and plowing of the softer contact surface. Correlating with this is the fact that the softer metals had the highest coefficients of friction and exhibited the highest wear.

Conclusions: Use of brush type skids and skids of softer metals can give coefficients of friction as high as those for rubber tire brake systems. The coefficient of friction for a solid metal skid on a lakebed is independent of the skid material. For low velocities (20 feet per second) the coefficients of friction for all skids tested were in the .2 to .5 range. Increasing the forward velocity lowered the coefficient of friction for nearly all materials, but the changes were small for most materials. Elevating the temperature of the skid in general decreased the coefficient of friction and decreased its dependence on forward velocity.

R. D. Rowe, E. T. Selig, "Penetration of Simulated Lunar Dust", AD 287-836, Armour Research Foundation.

A study of simulated lunar dust under static and dynamic loads was conducted to study the effects of vacuum conditions on penetration distances for spacecraft lunar landings. The simulated surface material chosen was ground silica sand with grain size predominantly in the 2 to 40 micron range (this is based on the hypothesis that the lunar surface is dust covered with particles in the 1 to 100 micron range). A bulk density range of 50 to 85 pounds per cubic foot was covered for pressure ranges from atmospheric to 10^{-7} torr. Penetration resistances (psi) were determined for these ranges and are presented graphically.

Conclusions: Both bulk density and absolute pressure effect penetration resistance for finely ground silica powders. Thus, material of this type would be more resistant to penetration on the moon. Cratering under rapid loading would not occur under vacuum conditions, rather the material would compress and shear adjacent material.

"Study of Design Criteria for Landing Shock Absorption Devices for Recoverable Flight Vehicles", Radioplane, Division of Northrop Corporation, ASD-TR-61-583, AD 273 096, January 1962.

A report of a theoretical and experimental design study of absorption devices for landing shock for flight vehicles. Type of deployable devices considered were spike decelerators, precontact retardation, mechanical legs or struts, crushable pads, and pressurized air bags. Penetration devices were eliminated because of the variety of terrain on which the device must function. Precontact retardation was eliminated on the grounds of complexity, difficulty in programming descent, and reliability considerations. Inability to reliably control foaming action during deployment operation precluded consideration of foam plastics. Paper honeycomb was considered against inflatable bags. Bags were chosen on a trade-off basis of energy absorption capability and versatility (multi-directional) over weight and cost. Theoretical study of bag design is presented. Experimental model data is used to modify theory. Full scale tests are reported. It was concluded that inflatable bags can be designed to give desired attenuations, preferably using variable orifices. Also contains bibliography.

Conclusions: High weight penalty of leg type absorbers makes them unattractive. However, they can be designed to give predictable results. The choice of bags over honeycomb structures did not take into account more efficient metallic honeycombs which could be tailored to give desired attenuation characteristics.

A. P. Coppa, W. A. Nash, "Dynamic Buckling of Shell Structures Subjected to Longitudinal Impact", ASD-TR-62-744, December 1962.

This document contains a discussion of an experimental and analytical study of the dynamic buckling characteristics of thin walled shell structures under dynamic axial loads. The analysis is based on finite deflection theory. Dimensionless axial stress is plotted versus time for various loading rates and numbers of circumferential half waves. The experimental study involved dynamic loading of pressurized and non-pressurized shells, both rigid impact and impact into a yielding medium. The qualitative results of the analytical and experimental studies agree well.

Conclusions: With increasing loading rates, the buckling load occurs sooner and is increased. Another phenomena for increasing loading rate is that the number of half waves that form around the circumference increases. The analytical and experimental results both bear this out.

F. K. Teichmann, Chi-Teh Wang, G. Gerard, "Buckling of Sandwich Cylinders Under Axial Compression", Journal of Aeronautical Sciences, Vol. 18, No. 6, June 1951, pp. 398-406.

A theory for the buckling of circular sandwich panel walled cylinders under axial compression is formulated. The resultant differential equations are solved for the critical buckling stress for both symmetrical and general circumferential buckling. The buckling stress is presented in a non-dimensional form in terms of parameters characteristic of the sandwich cylinders. The theory is verified experimentally.

"Aircraft Alighting Dynamics", ATC Report No. ARTC-37, Aerospace Industries Association, June 1964.

The report of an Ad Hoc Committee on aircraft alighting dynamics. It contains general discussions of the various aspects of the aircraft alighting problem followed by an indexed bibliography covering these aspects. Considered are landing gear and aircraft dynamics, aerodynamics, surface roughness and material, energy dissipation in landing gear, etc.

C. S. Ades, "Bending Strength of Tubing in the Plastic Range", Journal of Aeronautical Sciences, August 1957, pp. 605-610.

A method is presented for determining the total work to bend and deform a tube into the plastic range. The cross sectional shape of the deformed tube is found as a function of the longitudinal curvature using the principle of least work. The bending moment carried by the tube can be found from this deformed shape by numerical techniques. These analytical results were compared with available experimental data and show good correlation.

Conclusions: The assumptions and numerical methods used in this analysis give good results in comparison to experimental data. These methods appear to give good results even for somewhat anisotropic materials.

M. Feigen, D. Fitzgibbon, E. Burchman, "Characteristics of Energy Absorbing Materials for a Lunar Soft Landing Vehicle", Report 9753-0001-MU-000, Space Technology Laboratory, August 1961.

Investigation of the characteristics of crushable energy absorption materials for use in struts and foot pads for soft landing of Surveyor space craft on the moon. Styrofoam plastic; aluminum multiwave, truss grid, hexcell, and balsa wood were the materials considered. Styrofoam was rejected because of excessive energy storage. Balsa wood was chosen for the absorber material in the struts and aluminum truss grid for absorber units in the foot pads. The

balsa wood demonstrated wide dispersion in its crushing strength and failure mode but was chosen on the basis of its high energy absorption capability per unit weight. The mode of failure can be controlled by constraining the specimens with wrappings or cylindrical containers, but a high degree of quality control is still required in selection of material. Aluminum truss grid in sections orthogonal to each other were bonded together with a foil wrapper to give isotropic crushing load capabilities. Both these materials displayed nearly flat force-deflection curves. The truss grid exhibited strain rate sensitivity while the rest of the materials were relatively insensitive to strain rate.

Conclusions: Balsa wood has a very favorable energy absorption capability but its mode of crushing failure is variable as is its crushing strength. The mode of failure can be largely controlled but careful material selection is required to obtain predictable crushing strength. Aluminum truss grid, because of its geometrical pattern, is adaptable to designs requiring loading in two directions and can be used for three directional loading by orientation of segments of the absorber. For uniaxial loading, other geometries of metallic honeycomb can be used (multiwave, hex). All these can be tailored by shaping or chem-milling to give controllable and predictable force-deflection curves.

S. Lipson, "Cellular Aluminum for Use in Energy Dissipation Systems", NASA CR-93, Frankford Arsenal.

The effects of cellular structure size and interconnection, type of alloy used, heat treating, and specimen dimensions were investigated. The cellular structure is formed by filling the voids of a cylinder of compacted salt grains (of various sizes) with molten metal. The salt is leached from the solidified metal leaving cellular voids. Uniform cell size tended to yield uniform loading during compression of the specimen. Mixtures of two cell size distributions with widely different means tended to lower the compressive yield strength of the resultant specimen. The larger cells tend to collapse first followed by the smaller cells. High strength, heat treated alloys have the most nearly constant loading characteristics of any materials considered. Length to diameter ratios for this type structure greater than 1.5 result is columnar shear failure of the specimen. In addition, this material tends to bulge in the direction normal to the load.

Conclusions: Cellular materials, formed by filling the voids of a compacted granular matrix with molten metal and leaching the matrix out of the solidified mass, can be tailored to give desirable load-deflection characteristics during crushing. The energy dissipation capability for aluminum alloys approaches 15,000 foot-pounds per pound. Disadvantages are that the structure bulges greatly under uniaxial load and is subject to columnar shear failure for length over diameter ratios greater than 1.5. Such materials would also be expensive to produce, requiring a multistage forming process requiring long time periods for some of the stages (leaching and heat treating).

J. R. McGehee, M. E. Hathaway, "Landing Characteristics of a Re-entry Capsule With a Torus-Shaped Air Bag for Load Alleviation", NASA TN D-628, November 1960.

This document contains descriptions of a scale model test program and an analytical study to define the impact acceleration time histories for the landing of a re-entry capsule on a torus-shaped air bag energy absorber. These landings were made on a hard surface (concrete) and water for flight paths at 60 degrees and 90 degrees to the horizontal and capsule attitudes in the range of ± 30 degrees to the vertical. The model scaling required special factors for time, stroke, and velocity during impact because the atmospheric pressure was the same for the model and for full scale. Analytical acceleration time histories were computed using previously developed analytical techniques defining the load-stroke characteristics of air bags with pressure blowout, constant-area orifices. Model test data and analytical results correlated well except for some time shifts induced by the atmospheric pressure not being scaled. Maximum accelerations were 30 g along the capsule vertical axis and 15 g along its horizontal axis for landing on the hard surface. Ninety degree flight path and zero degree attitude gave the 30 g with no horizontal acceleration. A 60 degree path and 30 degree attitude gave 22 g vertical and 15 g horizontal. Landing on water gave accelerations one-third those for a hard surface landing.

Conclusions: A torus-shaped air bag can be used to attenuate landing loads of a re-entry capsule and the full scale loads can be predicted using analytical techniques or scale model testing. The model testing requires careful scaling and some special factors must be introduced to account for atmospheric pressure being the same for full scale and model scale. A vertical landing and attitude on a hard surface gave the highest peak acceleration vector while a flight path of 60 degrees and an attitude of ± 30 degrees gave lateral acceleration of 27 g.

Robert E. Lavender, "Touchdown Dynamics Analysis of Spacecraft for Soft Lunar Landing", NASA TN D-2001, January 1964.

Results are presented on a two-dimensional analytical investigation of spacecraft alightment based on inelastic one-dimensional crushing of the energy absorbers in each leg and a non-penetrable frictional terrain surface model. Parameters which were investigated include local terrain slope, terrain coefficient of friction, initial vertical and horizontal velocities, vehicle radius of gyration, height to the center of gravity, displacement of the center of gravity from the vehicle's longitudinal axis, thrust of stabilization rocket motors, load factor (design acceleration level), and the number of legs. The analysis indicates that the terrain slopes, the terrain coefficient of friction, and the initial vertical and horizontal velocities are all first-order considerations with respect to alightment stability.

Conclusions: The effect of the various parameters upon the alightment system is represented by the landing gear spread or diameter (defined as twice

the radial distance from the center of gravity to a foot pad) which is required for stability for a given set of parameters. An increase in any of the following: the terrain slope, the terrain coefficient of friction, the height to the center of gravity, and the radius of gyration, require an increase in the landing gear diameter to maintain alightment stability. The weight of the vehicle, if the radius of gyration is constant, has no effect upon the landing gear diameter. However, it is impossible to have large variations in the vehicle weight without accompanying variations in the radius of gyration. Therefore, moderate increases in the weight of the vehicle will require an increase in the landing gear diameter required for stability. An increase in the design load factor results in a decrease in the required landing gear diameter. A five legged vehicle requires the smallest landing gear diameter for the two-dimensional case. However, a five legged vehicle is not necessarily optimum due to weight considerations.

"Lunar Landing System Studies for Lunar Landing Vehicles", Report SPP-63-101. Bendix Corporation Aerospace Division, February 28, 1963.

A proposal and results of a proposal are contained in this report dealing with lunar landing alighting gear. The operational design limits for the alightment were: (1) vertical velocity change of 2-20 feet per second, (2) lateral velocity of 0 ± 5 feet per second, (3) vehicle attitude $\pm$ 50 degrees from local vertical, (4) $\pm$ 0.1 radians per second angular velocity, (5) 6 g decelerations longitudinal and 1.5 g transverse, and (6) roll deceleration negligible. Digital and analog stability studies were run as well as an experimental model study. Results of the analyses were generally in agreement with the experimental results.

Conclusions: The four leg inverted tripod alightment gear configuration was chosen as the best trade-off of stability versus weight. Crushable capsule absorbers in each leg strut appear to be the most feasible and simplest over oleo struts, frangible rings or diaphragms, as well as being among the lightest in weight. Oleo struts were considered to be too heavy, and frangible rings or diaphragms had the disadvantage of requiring close dimensional tolerances in the telescoping members to prevent jamming by the fractured elements. Crushed honeycomb pads were recommended as structural bulkheads and the upper part of the top struts could be used as the cylinder to erect the legs by gas pressure. Proposed areas of investigation were (1) shaping of the absorber capsule and choice of material and grid work configuration, (2) experimental investigation of thin tube dynamic buckling and bending characteristics. Crushable absorbers were chosen over other configurations because of simplicity, expected reliability under space environments, and light weight. The major disadvantage was seen to be one stroke absorption capability.

W. C. Walton, H. W. Herr, and H. W. Leonard, "Studies of Touchdown Stability for Lunar Landing Vehicles", Journal of Spacecraft and Rockets, Volume 1, pp. 552-556, September-October 1964.

This article documents a simplified analytical and experimental investigation of three-dimensional stability boundaries of a four legged spacecraft. This document is the only presentation of results of a three-dimensional alightment dynamic analysis which has appeared in the literature to date. The simplified theory is based primarily on the following assumptions: (1) The vehicle including the alightment system are considered to be one rigid body. (2) When a foot of the vehicle impinges upon the landing surface, impulsive forces are produced which immediately stop the foot. (3) The vehicle thereafter rotates as though the foot were pinned until another foot strikes, in which case the pin is released at the moment of the second impact. The ramifications of these assumptions would include the following points: The changes in vehicle geometry due to the alightment system strokes are neglected. The load stroke characteristics of the alightment system including residual compliance are ignored. It is suspected that the residual compliance in the alightment system, which permits the storage of potential enegry in the system, may have a significant influence upon stability characteristics. The assumption that the foot of the vehicle remains fixed during contact with the landing surface may be unduly restrictive. It is suspected that it is undesirable to prohibit sliding of the foot across the landing surface, because the sliding of the foot pad may aid in the stability of the spacecraft.

Conclusions: The most important conclusion presented in the article is that the asymmetrical initial alightment orientation may be more critical than the symmetrical alightment orientation. The two symmetrical alightment orientations (2-2 and 1-2-1) are two-dimensional cases. The asymmetrical alightment orientation is a three-dimensional case. Hence, it is concluded that three-dimensional analyses are required to adequately define the stability boundaries for spacecraft alightment.

APPENDIX II

COMPANY VISITATIONS

Four companies or agencies were visited during the period 27 September 1964 to 14 October 1964. These were:

1. Bendix - South Bend
2. NASA - Langley
3. NASA - Marshall
4. Grumman Aircraft - Bethpage, Long Island, New York

Little disagreement exists between the various companies and agencies as to what constitutes an acceptable space package alightment system. Aluminum honeycomb is accepted as being efficient in terms of weight and volume, reliable, repeatable, and generally insensitive to expected space temperature extremes and vacuums.

Friction as an energy absorber is generally looked on with disfavor, due primarily to the lack of experimental data for application times of less than 0.1 seconds and the abundance of data available from braking systems. After many years of work, braking systems are still subject to slip and stick, static to dynamic coefficient of friction ratios as high as 1.6 and temperature sensitivity. Although very large specific energies are obtained in braking systems (about 150,000 foot-pounds per pound) the consensus of opinion ruled out frictional energy absorbers on the basis of reliability, predictability, adaptability to alighting systems. Bendix especially was opposed to friction although paradoxically, as discussed later.

The inverted tripod is the popular choice for the landing gear. Very little, if any, effort is being expended in examining alternate approaches to legged landing gear. Present lunar alighting system weights do not exceed 2 to 3 percent of the vehicle landing weight and are adequate to meet existing requirements.

Each of the companies visited has or is constructing a three-dimensional mathematical model of an alighting space craft. All but NASA-Marshall have conducted scale model drop tests for comparison with analytical results.

Mathematical models varied widely in complexity. Soil compliance, leg compliance and energy absorber were represented differently at each company. Grumman was the only company examining local surface irregularities analytically.

BENDIX AEROSPACE PRODUCTS DIVISION, South Bend, Indiana

Bendix/South Bend was visited on 28 September 1964 to discuss alightment dynamic analysis and testing and energy absorbers with emphasis upon friction as a means of energy absorption. Messrs. M. O. Lemdley, Robert Schmidt, Raymond Black, Roy Palmer, Bud Chambers, Frank Allbright, Jerry Woo and Don Fletcher were contacted at Bendix Aerospace Products Division.

Bendix's experience in alightment dynamics includes the design and manufacture of aircraft alightment systems, participation in the Apollo Lunar Landing Module and Lunar Excursion Module Alightment system proposals, and current execution of a Bellcom/NASA contract for analysis and experimentation pertinent to lunar alightment.

The energy absorbers which were discussed were honeycomb, balsa wood, friction, pneumatic and hydraulic devices. Honeycomb is favored as the best overall energy absorber for spacecraft alightment systems. Aluminum honeycomb and balsa wood were the energy absorber material candidates in the Apollo proposals. The aircraft alightment systems with which Bendix has had experience were hydraulic. The spacecraft hardware for the Bellcom study is thought to be honeycomb while a frictional device is employed on the drop test model.

Honeycomb is currently favored by Bendix for spacecraft alightment systems due to its reliability, predictability, ability to withstand space environment, near constant load stroke characteristic and its high energy absorbing capability per unit weight and unit volume. Testing of honeycomb at Bendix has indicated that its dynamic properties are very nearly velocity and vacuum insensitive. The initial loading behavior is greatly dependent on the cell orientation. A cross grid cell orientation is presently favored to minimize the load peaking prior to initiation of crushing. Evacuating the intercellular air causes a 5 percent decrease in peak loading. Balsa wood has a high energy absorption per pound; however, its usability without protection in a space environment is doubtful.

Model tests performed in conjunction with analysis use a frictional energy absorber to permit quick refurbishment of the model for additional tests. Arguments advanced in favor of friction for model tests were reliability, repeatability, and reusability. Based on movies of test drops and the actual design of the absorber, it is doubtful that frictional energy absorbers performed as well as desired. High speed movies showed evidence of insufficient stroking of the absorber during impact. Since stability boundaries were being derived experimentally, erroneous conclusions could be reached concerning dynamic stability of a particular configuration.

The use of friction as an energy absorber was discussed in some detail. No data was available concerning friction characteristics for short term

applications (less than 0.1 second). Representative characteristics of aircraft brakes were obtained. Application times for these usually runs 30 to 40 seconds. Typical braking systems during a rejected take-off (RTO) absorb 7 to 9 horsepower per inch^2. At the completion of RTO the braking system is destroyed and often welded together.

Arresting gear on aircraft carriers have application times of 3 to 6 seconds and absorb as much as 10 horsepower per inch^2. For this type of application, the braking system has circulating water to permit re-use of the system within a short time.

Bendix has cerametallic linings that are normally used on aircraft brakes that are capable of operating at 200 degrees C. Bendix personnel were somewhat divided as to what energy absorption levels could be obtained for an application time of less than 0.1 second. Fifteen horsepower per inch^2 was felt to be obtainable and possibly higher. No heat sink requirement would exist for our application provided the frictional interface temperature does not exceed the material capabilities. For ceramic linings, operating pressures of 300 psi are easily attainable. Coefficients of friction of 0.3 to 0.4 normally occur on aircraft brakes using cerametallic and steel as the contact surfaces. Some temperature fading is present on brakes--varying between 10 percent and 20 percent of the nominal braking force. The ratio between static and dynamic coefficients of friction is typically 1.6. After the initial peak a variation of ± 10 percent about the mean is typical in an aircraft disc brake.

NASA - George C. Marshall Space Flight Center, Huntsville, Alabama

NASA-Marshall was visited on 29 and 30 September 1964 to discuss alightment dynamic techniques and analysis.

Robert E. Lavender, Aero-Astrodynamics Laboratory Technical Staff, was contacted on the first day of the visit. Mr. Lavender has been responsible for the alightment dynamic analysis pertinent to a 30,000 pound Lunar Logistics Vehicle, which has completed the preliminary design stage at NASA Huntsville. Mr. Lavender authored three articles on alightment dynamic analysis, which are presented in the literature search.

Mr. Ron Crawford, Propulsion and Vehicle Engineering Laboratory Structures Design, was contacted on the second day of the visit. Mr. Crawford has been responsible for the structural design of the alightment system for the Lunar Logistics Vehicle.

The following is a summary of the discussions concerning alightment criteria, alightment system design criteria, analytical techniques, energy absorbers, and other subjects pertinent to establishing the state-of-the-art for spacecraft alightment.

The initial alightment system configuration considered consisted of a set of vertical telescoping legs with one-dimensional energy absorption capability. The energy absorbers were assumed to exhibit constant load stroke characteristics. This alightment system configuration was disqualified due to weight considerations. The large landing gear diameter of spread required for alightment on a 30 degree slope resulted in high moments acting on the alightment system structure. This alightment system configuration would have constituted 10 to 15 percent of the vehicle weight.

An inverted tripod configuration was selected in preference to the telescoping leg configuration. The members of the inverted tripod contain honeycomb cylinders for energy absorption. The main leg (upper) of each tripod consists of a thin wall tube with hat section stringers. The inverted tripod configuration constitutes 8 to 9 percent of the vehicle weight.

The elasticity of the alightment system increases as the landing gear spread or diameter is increased. The elasticity of the alightment system is suspected to have an important effect on alightment stability due to rebound. Therefore, alightment system optimization may be substantially influenced by the elasticity of the legs.

The selection of an energy absorber on an energy absorbed per unit weight of the absorber material or device is not a valid criterion for the selection of an optimum energy absorber. A more realistic criterion is the energy absorbed per unit weight of the total alightment system. This is a measure of the total system effectiveness including the structure required to utilize a particular material or device as an energy absorber. Other criteria, which should be considered in the selection of an energy absorber material or device, are the repeatability, reliability, predictability, environmental limitations, and adaptability of the load stroke characteristics.

Honeycomb was selected as the energy absorber for the alightment system of the Lunar Logistics Vehicle. The honeycomb accounted for approximately 5 percent of the alightment system weight. Therefore, the energy absorption per unit weight of the honeycomb was not a significant criterion. Honeycomb was selected on the basis of its predictability (constant load stroke characteristic), reliability, and resistance to degradation in the temperature and vacuum environments.

Frangible materials (tubes, shells) were disqualified because of the packaging problems involved and the oscillatory load stroke characteristics.

Frictional devices were not evaluated due to the lack of available data on the application of friction as a means of energy absorption during impact.

Certain design criteria pertinent to the alightment system foot pads were also discussed. The moment exerted on the alightment system by the foot pad

should be minimized. This may be accomplished by using a swivel joint (ball and socket) between the foot pad and the alightment system. The pivot point of the swivel joint should be kept low to minimize the rotation of the foot pad digging into the terrain. The contact surface of the foot pad should be curved to minimize the overturning effect.

The analytical efforts to study spacecraft alightment dynamics at NASA-Huntsville have been restricted to two-dimensional cases. A three-dimensional analysis is presently being formulated to more adequately study spacecraft alightment dynamics. The three-dimensional case is judged to be of possible concern by NASA-Huntsville.

No experimental verification of the analytical results or the concepts have been undertaken to date at NASA-Huntsville.

NASA - Langley

Three branches of the Dynamic Loads Division of NASA-Langley were visited on 29 and 30 September 1964. These branches and persons contacted were:

1. Vibration and Shock - Dr. George W. Brooks, W. Connor, W. C. Walton

2. Structures - Lloyd J. Fisher, Jr., U. J. Blanchard

3. Landing Gear - Sidney A. Batterson

The Vibration and Shock section is engaged in both analysis and test of inverted tripod alighting systems. Each of the three legs of the tripod contain an energy absorbing aluminum honeycomb compression cell. The model alighting gear is similar in concept to that presently contemplated for LEM.

Analysis has progressed to a three-dimensional mathematical model representing the honeycomb as a force versus velocity curve. Soil compliance is treated as a viscous damper for unloading and coefficient of restitution for loading. Leg compliance is included in the force versus velocity curve.

The primary goal of this sections' alighting analysis is dynamic stability boundaries. The three-dimensional model had not been in existence long enough for any noteworthy correlation with experimental results. Little enthusiasm existed for new energy absorbing concepts as opposed to aluminum honeycomb or alighting gear geometry. Inverted tripods and aluminum honeycomb are felt to meet existing needs and make up only 2 to 3 percent of the total spacecraft weight.

Mr. Fishers' section is primarily concerned with model testing, apparently essentially independent of the Vibration and Shock Section, and the development and evaluation of novel energy absorbers. A model test program for a LEM type alighting gear is planned. The model is identical to that used by Grumman for their test program. Considerable work had been done with frangible tubes and although efficient in terms of energy absorbed per unit weight of the tube, potential problems are felt to exist in actually applying this concept to an alighting system. The frangible tube must be subjected to a uniaxial force to ensure occurrence of the frangible action and the shrapnel resulting from energy absorption presents a potential source of damage. Yielding of low nickel steel straps had also been used as an energy absorber located between a simulated heat shield and capsule.

Interest in applications of friction for alighting systems was evidenced by Mr. Fisher although no work is presently being done. Very low (0.1 to 0.2 psi) ground pressure alighting systems may be required in the future.

GRUMMAN AIRCRAFT - Bethpage, Long Island, New York

Grumman Aircraft Company was visited on 30 September 1964. Persons contacted were Eugene Baird, Richard Hildeman and William Mueller. The discussions concerned design concepts and alightment analysis for the Lunar Excursion Module (LEM).

The basic alighting gear is a modified inverted tripod. Three elements comprise the leg with two of them attached to a main strut above the foot pad attachment. Aluminum honeycomb is used as the energy absorber. The allowable acceleration loadings are determined by the spacecraft structural design and not the payload. The alighting system, as presently conceived, represents 4 percent of the total lunar landing weight. A two-stage aluminum honeycomb core is used to absorb the landing velocities. For the first or "soft" step, 2.5 g vertical is obtained for an impact velocity of 10 feet per second. On the second or "hard" step, 5 g vertical are permissible.

The 37 inch diameter foot pads are designed for a landing surface with a bearing strength of 12 psi. The pads are pivoted on the legs through a 35 to 40 degree angle and assuming constant pressure distribution, the foot pad reaction passes through the pivot. The lower limit of the coefficient of friction is 0.1 with 0.4 and 0.5 also checked.

The landing surface is assumed to have 2 foot discontinuities. Angular rates of 5 degrees per second about the spacecraft vertical occur and angular displacements of 5 degrees about inertial vertical and then 5 degrees about a body fixed axis. Large angular accelerations occur to LEM during landing due to a small radius of gyration compared to footprint area. Some displacement of the center of gravity from the geometric center occurs due to landing engine

gimbaling. No significant influence on landing stability had been observed due to this effect.

Surface compliance has not had a significant effect on stability based on analytical results. Surface compliance is represented as a linear spring for loading and a coefficient of restitution for unloading. Unloading damping is a combination of viscous and Coulomb to simulate both structural and bearing friction losses.

APPENDIX III

ALIGHTMENT SYSTEM LOAD ANALYSES

The alightment system reaction loads such as the absorber reaction forces and ground reaction forces dictate the structural loads which the alightment systems must be designed to carry.

LOAD ANALYSIS OF TELESCOPING LEG CONFIGURATIONS

The telescoping leg absorber reaction forces and absorber dimensions are the same for all three configurations in this study. Therefore, only one load, stress, and weight analysis is required for the telescoping leg configurations. The free body diagram of the telescoping leg for the worst loading situation appears as follows.

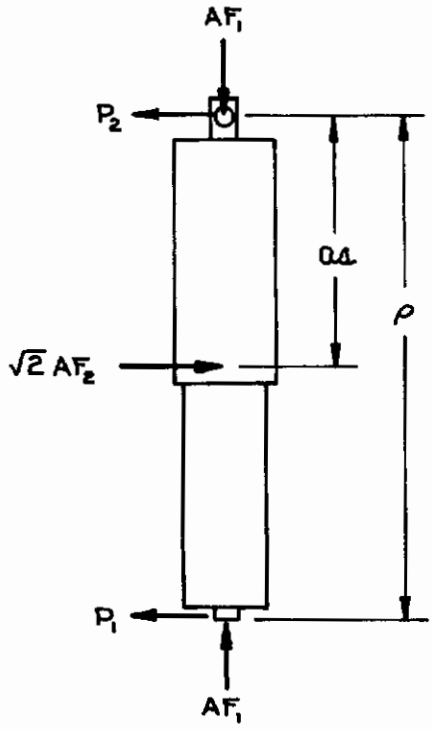

Where:

AF_1 = Axial crushing load = 3,750 pounds

AF_2 = Rotational crushing load = 1,500 pounds

a = Distance from pivot point to the rotational pads = 15.0 inches

ρ = Undeflected length of leg = 30.5 inches

From the equations of static equilibrium, P_1 and P_2 are found to be.

$$P_1 = \frac{\sqrt{2}\, AF_2\, as}{\rho} = 1045 \text{ LB}$$

$$P_2 = \sqrt{2}\, AF_2 \left(1 - \frac{as}{\rho}\right) = 1075 \text{ LB}$$

The free body of the lower portion of the leg illustrates the load distribution at the sliding surfaces. The moment created by P_1 is reacted out by two triangular distributions (ω_2) over a four inch length of bearing area. The shear load due to P_1 is reacted out by a uniform distribution (ω_1). The sliding frictional force is denoted as P_4. The axial energy absorber crushing load is denoted as P_3.

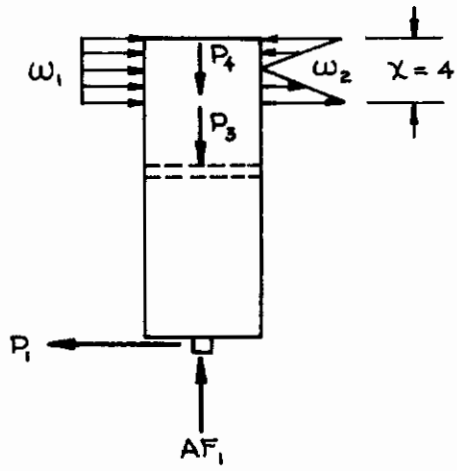

The peak value of the triangular distribution is $6M/\chi^2$. Since the moment is equal to $P_1 (\rho - as)$, the peak value for the distribution is:

$$\omega_2 = \frac{6P_1 (\rho - as)}{\chi^2} = 6070 \text{ LB/IN}$$

The magnitude of the distribution due to the shear load reaction is

$$\omega_1 = \frac{P_1}{\chi} = 261 \text{ LB/IN}$$

The sliding frictional force P_4 is the product of the coefficient of friction μ and the normal forces $\omega_1 \chi$ and $0.5\,\omega_2 \chi$.

$$P_4 = \mu(\omega_1 \chi + 0.5\,\omega_2 \chi)$$

The coefficient of sliding friction between two lubricated (dry film) metals is about 0.05. Using 0.05 for the coefficient of friction gives the following value for P_4.

$$P_4 = 0.05\left[261(4) + 0.5(6070)(4)\right] = 660 \text{ LB}$$

The crushing load on the honeycomb is denoted as P_3.

$$P_3 = AF_1 - P_4 = 3750 - 660 = 3090 \text{ LB}$$

LOAD ANALYSES OF ARTICULATED LEG CONFIGURATIONS

The load analyses for the articulated leg configurations were performed on a digital computer. It was advantageous to use a digital computer due to the complexity of the situation. The absorber reaction forces and member reaction forces are functions of the position ($\alpha^{(2)}$, $\beta^{(2)}$, and $\psi^{(2)}$) of the alightment system. The use of the digital computer permitted the determination of the member loads for a large number of positions of the alightment system. Thus, it is practical to adequately define the loads by determining the member loads throughout the entire spectrum of possible alightment system positions.

The analysis is performed by determination of the member loads which occur during stroking of the upper and lower absorbers at their crushing load. The maximum and minimum loads in each member and the position at which they occurred are sought out as the position of the alightment system is varied for all combinations of the three coordinates $\alpha^{(2)}$, $\beta^{(2)}$, and $\psi^{(2)}$.

The analysis is separable into two portions. First, the absorber reaction forces and geometry are used to determine the reaction loads throughout the alightment system. Second, the distribution of the reaction loads in the members is determined.

One of the basic assumptions in the alightment dynamics simulation is that the inertial effects of the alightment system are negligible in the overall scheme. When this assumption is made, the reaction loads are obtainable from force equilibrium considerations of each member. The geometry and reaction forces for the alightment system are defined in Figures 22, 26, 27 and 103.

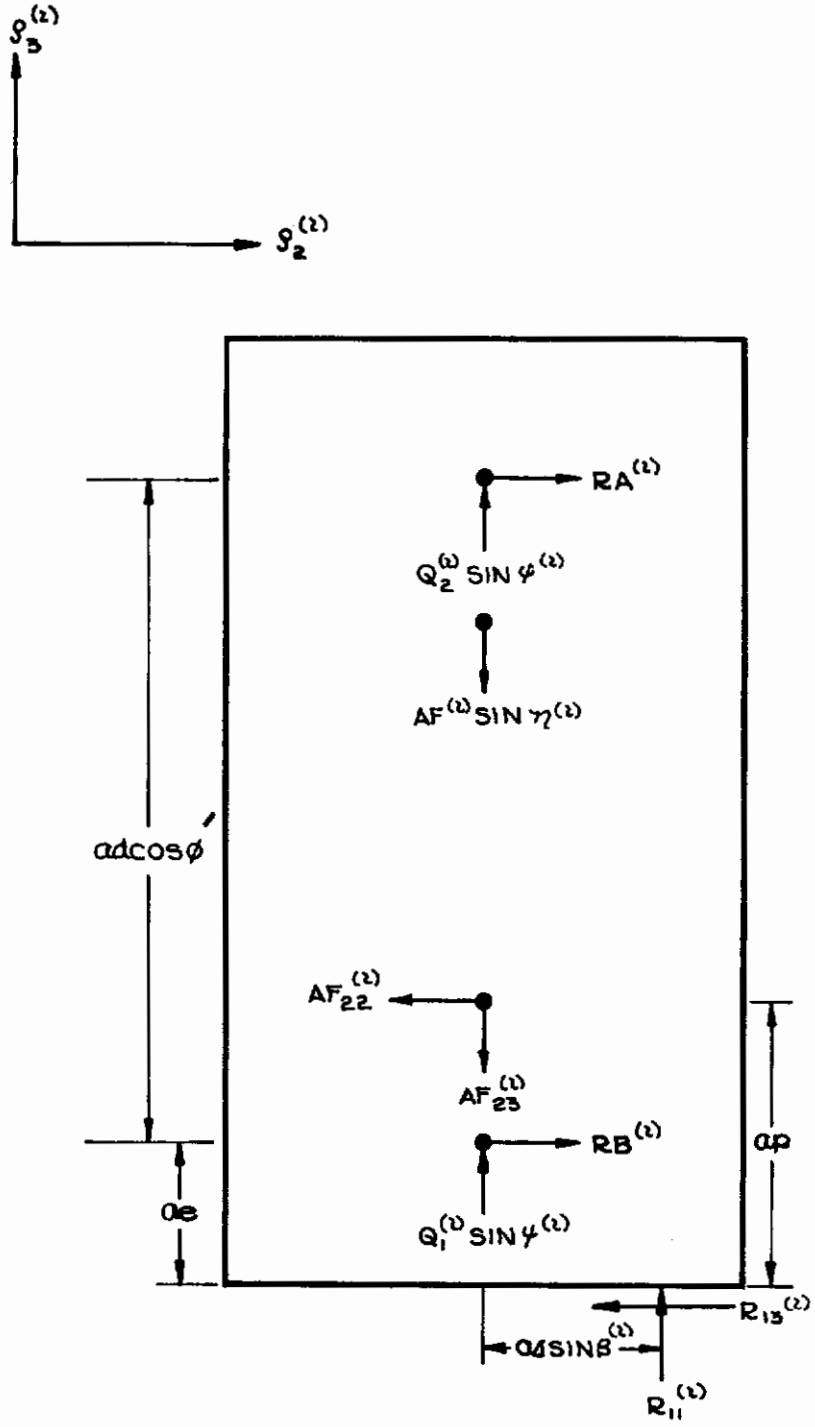

Figure 103: $\rho_2 - \rho_3$ Plane Projection of the Intermediate Member

The free body diagram of the intermediate member in the $S_1 - S_3$ plane is shown in Figure 27. The sum of the forces and moments in this plane are found to be the following (equations 56 through 58).

$$Q_2^{(2)} \sin\psi^{(2)} + Q_1^{(2)} \sin\psi^{(2)} + R_{11}^{(2)} = AF_1^{(2)} \sin\eta^{(2)} + AF_{23}^{(2)} \tag{56}$$

$$Q_2^{(2)} \cos\psi^{(2)} + Q_1^{(2)} \cos\psi^{(2)} - R_{12}^{(2)} = AF_1^{(2)} \cos\eta^{(2)} + AF_{21}^{(2)} \tag{57}$$

$$\begin{aligned} &Q_2^{(2)}(-\cos\psi^{(2)}\, ad \cos\phi' - \sin\psi^{(2)}\, ad \sin\phi') - R_{12}^{(2)}\, ae \\ &+ R_{11}^{(2)}(aa \cos\beta^{(2)} + a\sigma) = (ae - ap)\, AF_{21}^{(2)} + (a\sigma)\, AF_{23}^{(2)} \\ &- \cos\eta^{(2)}(ad \cos\phi' - ag) + \sin\eta^{(2)}(ad \sin\phi' + ah)\, AF_1^{(2)} \end{aligned} \tag{58}$$

where it can be seen from the geometry in Figure 26 that the lower absorber reaction force components are given by equations 50 through 52.

$$AF_{21}^{(2)} = \frac{-(ag \sin\alpha^{(2)} + aa - aa\cos\alpha^{(2)})\cos\beta^{(2)}\, AF_1^{(2)}}{\left[(aa - aa\cos\alpha^{(2)} + ag\sin\alpha^{(2)})^2 + (-ap - aa\sin\alpha^{(2)} - ag\cos\alpha^{(2)})^2\right]^{1/2}} \tag{50}$$

$$AF_{22}^{(2)} = \frac{-(ag \sin\alpha^{(2)} + aa - aa\cos\alpha^{(2)})\sin\beta^{(2)}\, AF_2^{(2)}}{\left[(aa - aa\cos\alpha^{(2)} + ag\sin\alpha^{(2)})^2 + (-ap - aa\sin\alpha^{(2)} - ag\cos\alpha^{(2)})^2\right]^{1/2}} \tag{51}$$

$$AF_{23}^{(2)} = \frac{(ap + aa\sin\alpha^{(2)} + ag\cos\alpha^{(2)})\, AF_2^{(2)}}{\left[(aa - aa\cos\alpha^{(2)} + ag\sin\alpha^{(2)})^2 + (-ap - aa\sin\alpha^{(2)} - ag\cos\alpha^{(2)})^2\right]^{1/2}} \tag{52}$$

The free body diagram of the lower leg is illustrated in Figure 26. The force and moment equilibrium equations in the $\rho_1 - \rho_3$ plane are found to be as follows.

$$\mathcal{F}_1^{(2)} + R_{12}^{(2)} = -AF_{21}^{(2)} \tag{53}$$

$$\mathcal{F}_3^{(2)} - R_{11}^{(2)} = -AF_{23}^{(2)} \tag{54}$$

$$\begin{aligned}&(a_s \sin\alpha^{(2)} + a_l \cos\alpha^{(2)})\mathcal{F}_1^{(2)} + (-a_s \cos\alpha^{(2)} + a_l \sin\alpha^{(2)})\cos\beta^{(2)}\mathcal{F}_3^{(2)} \\ &= -(-a_s \cos\alpha^{(2)} + a_g \sin\alpha^{(2)})\cos\beta^{(2)} AF_{23}^{(2)} \\ &\quad -(a_s \sin\alpha^{(2)} + a_g \cos\alpha^{(2)})AF_{21}^{(2)}\end{aligned} \tag{55}$$

Defining the various terms as follows and placing the six equations in matrix notation yields the following.

$$\begin{bmatrix} 0 & 0 & K_1 & K_1 & 1 & 0 \\ 0 & 0 & K_2 & K_2 & 0 & -1 \\ 0 & 0 & K_3 & 0 & K_4 & K_7 \\ 1 & 0 & 0 & 0 & 0 & 1 \\ 0 & 1 & 0 & 0 & -1 & 0 \\ K_5 & K_6 & 0 & 0 & 0 & 0 \end{bmatrix} \begin{Bmatrix} \mathcal{F}_1^{(2)} \\ \mathcal{F}_3^{(2)} \\ Q_2^{(2)} \\ Q_1^{(2)} \\ R_{11}^{(2)} \\ R_{12}^{(2)} \end{Bmatrix} = \begin{Bmatrix} K_8 \\ K_9 \\ K_{10} \\ K_{11} \\ K_{12} \\ K_{13} \end{Bmatrix} \tag{96}$$

where

$$K_1 = \sin(\psi^{(2)})$$

$$K_2 = \cos(\psi^{(2)})$$

$$K_3 = -ad\left[\cos(\psi^{(2)})\cos\phi' + \sin(\psi^{(2)})\sin\phi'\right]$$

$$K_4 = aa\cos(\beta^{(2)}) + ao$$

$$K_5 = aa\sin(\alpha^{(2)}) + al\cos(\alpha^{(1)})$$

$$K_6 = \left[-aa\sin(\alpha^{(2)}) + al\cos(\alpha^{(2)})\right]\cos(\beta^{(2)})$$

$$K_7 = -al$$

$$K_8 = \sin(\eta^{(2)})\,AF_1^{(1)} + AF_{23}^{(2)}$$

$$K_9 = \cos(\eta^{(2)})\,AF_1^{(1)} + AF_{21}^{(2)}$$

$$K_{10} = \left[ae - ap\right]AF_{21}^{(2)} + ao\,AF_{23}^{(2)}$$

$$-\left[(ad\cos\phi' - ag)\cos(\eta^{(2)}) + (ad\sin\phi' + ah)\sin(\eta^{(2)})\right]AF_1^{(2)}$$

$$K_{11} = -AF_{21}^{(1)}$$

$$K_{12} = -AF_{23}^{(2)}$$

$$K_{13} = -\left[aa\sin(\alpha^{(2)}) + ag\cos(\alpha^{(2)})\right]AF_{21}^{(2)} - \left[-aa\cos(\alpha^{(2)}) + ag\sin(\alpha^{(2)})\right]\cos(\beta^{(2)})\,AF_{23}^{(2)}$$

The six unknowns are solved for by postmultiplying the inverse of the square matrix of equation 96 by the column vector of knowns.

$$\begin{Bmatrix} \mathcal{F}_1^{(2)} \\ \mathcal{F}_3^{(2)} \\ Q_2^{(2)} \\ Q_1^{(2)} \\ R_{11}^{(2)} \\ R_{12}^{(2)} \end{Bmatrix} = \begin{bmatrix} 0 & 0 & K_1 & K_1 & 1 & 0 \\ 0 & 0 & K_2 & K_2 & 0 & -1 \\ 0 & 0 & K_3 & 0 & K_4 & K_7 \\ 1 & 0 & 0 & 0 & 0 & 1 \\ 0 & 1 & 0 & 0 & -1 & 0 \\ K_5 & K_6 & 0 & 0 & 0 & 0 \end{bmatrix}^{-1} \begin{Bmatrix} K_8 \\ K_9 \\ K_{10} \\ K_{11} \\ K_{12} \\ K_{13} \end{Bmatrix} \tag{97}$$

The remaining reaction forces on the lower leg are found by summing the moments about an axis parallel to the ρ_1 axis and the forces in the ρ_2 direction (Figure 26).

$$\mathcal{F}_2^{(2)} = \Big\{ \sin(\beta^{(2)}) \left[a_w \cos(\alpha^{(1)}) - a_g \sin(\alpha^{(2)}) \right] AF_{23}^{(2)}$$

$$+ \sin(\beta^{(2)}) \left[a_w \cos(\alpha^{(2)}) - a_l \sin(\alpha^{(2)}) \right] \mathcal{F}_3^{(2)}$$

$$- \left[a_w \sin(\alpha^{(2)}) + a_g \cos(\alpha^{(2)}) \right] AF_{22}^{(2)} \Big\}$$

$$/ \left\{ a_w \sin(\alpha^{(2)}) + a_l \cos(\alpha^{(2)}) \right\} \tag{61}$$

$$R_{13}^{(2)} = - \mathcal{F}_2^{(2)} - AF_{22}^{(2)} \tag{98}$$

The lateral reactions RA and RB are found by examining the $P_2 - P_3$ plane projection (Figure 103) of the intermediate member. Summing the moments about the application point of RB yields.

$$RA^{(2)} = \frac{\left[ap - ae\right] AF_{22}^{(1)} + \left[ae \sin(\beta^{(2)})\right] R_{11}^{(1)} - \left[ae\right] R_{13}^{(2)}}{ad \cos\phi'} \tag{99}$$

Summing the forces in the P_2 direction yields.

$$RB^{(1)} = -RA^{(2)} + AF_{22}^{(2)} + R_{13}^{(2)} \tag{100}$$

Thus, the loads applied to the upper and lower assemblies of the parallelogram linkage have been determined.

The loads $RA^{(2)}$ and $Q_2^{(2)}$ are applied to the upper assembly as illustrated in Figure 104. The triangular member is assumed to behave as a pinned structure. The loads in the $PU_1^{(2)}$ and $PU_2^{(2)}$ members are determined by summing the forces at their joint.

$$PU_1^{(2)} = \frac{-Q_2^{(2)} \sin(\theta) + RA^{(2)} \cos(\theta)}{2 \sin(\theta) \cos(\theta)} \tag{101}$$

$$PU_2^{(2)} = \frac{-Q_2^{(2)} \sin(\theta) - RA^{(2)} \cos(\theta)}{2 \sin(\theta) \cos(\theta)} \tag{102}$$

The loads $Q_1^{(2)}$ and $RB^{(2)}$ are applied to the lower assembly as illustrated in Figure 105. Due to the symmetry of the structure, the applied load $Q_1^{(2)}$ and $RB^{(2)}$ may be considered to be divided equally between the two joints. The joints are considered to be pinned. The loads in the members are determined by summing the forces at the joints.

$$PL_1^{(2)} = \frac{-Q_1^{(2)} \sin(\gamma) + RB^{(2)} \cos(\gamma)}{2\left(\sin(\gamma)\cos(\rho) + \sin(\rho)\cos(\gamma)\right)} \tag{103}$$

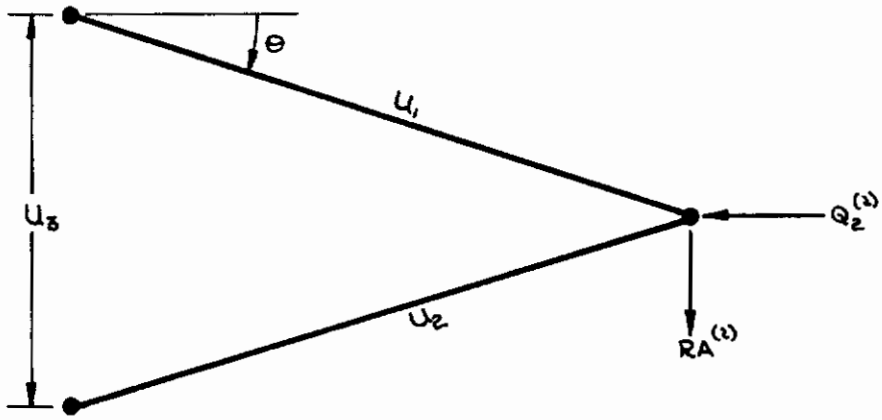

Joint $U_1 - U_2$

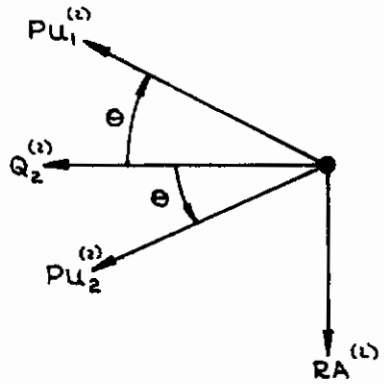

Figure 104: Upper Assembly

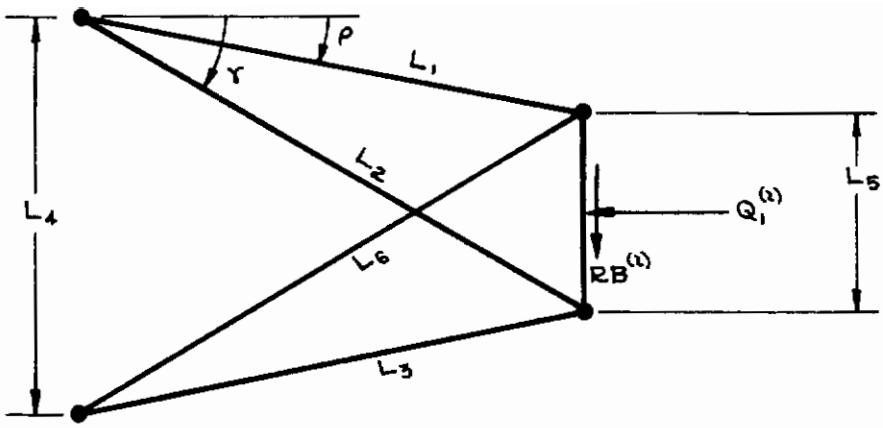

Joint $L_1 - L_6$

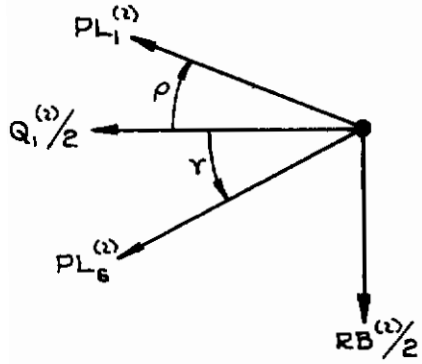

Joint $L_2 - L_3$

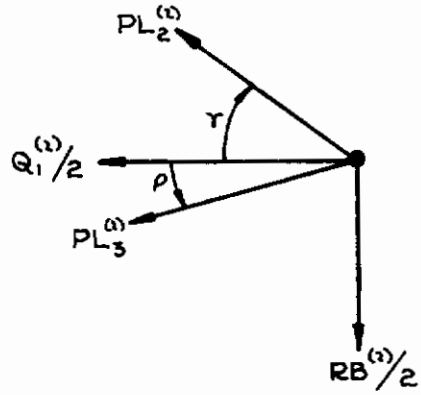

Figure 105: Lower Assembly

$$PL_6^{(2)} = \frac{-Q_1^{(2)} SIN(\rho) - RB^{(2)} COS(\rho)}{2\left(SIN(\gamma) COS(\rho) + SIN(\rho) COS(\gamma)\right)} \tag{104}$$

$$PL_2^{(2)} = \frac{-Q_1^{(2)} SIN(\rho) + RB^{(2)} COS(\rho)}{2\left(SIN(\rho) COS(\gamma) + SIN(\gamma) COS(\rho)\right)} \tag{105}$$

$$PL_3^{(2)} = \frac{-Q_2^{(2)} SIN(\gamma) - RB^{(2)} COS(\rho)}{2\left(SIN(\rho) COS(\gamma) + SIN(\gamma) COS(\rho)\right)} \tag{106}$$

The maximum tension and compression (where applicable) loads and the alightment system position of occurrence are presented in Tables 14 through 20 for the seven articulated leg configurations. The loads for configurations 3, 4, 5, and 7 are nearly the same. The largest loads for these configurations are summarized in Table 21. The loads for configurations 6 and 8 are summarized in Table 22.

TABLE 14

MAXIMUM LOADS CONFIGURATION 3

Member	Load (lbs)	α (deg)	β (deg)	ψ (deg)
PL_1 , (PL_3)	+15,790	2.	-40.	+30.
	-18,462	2.	+130.	-5.
PL_2 , (PL_4)	+15,285	2.	-60.	+30.
	-17,422	2.	+110.	-5.
PU_1 , (PU_2)	+12,790	20.	+120.	-15.
	-32,566	15.	-60.	-5.
RA	+14,345	15.	+90.	-5.
	-14,345	15.	-90.	-5.
RB	+25,808	2.	-90.	-5.
	-25,808	2.	+90.	-5.
Q_1	+33,606	2.	+180.	-5.
	-28,871	2.	0	+30.
Q_2	+42,978	2.	0	+30.
	-10,895	2.	+180	+15.
$R_{12/3}$	+12,972	2.	0	+30.
R_{11}	+48,759	2.	0	+30.
R_{123}	+50,455	2.	0	+30.

TABLE 15

MAXIMUM LOADS CONFIGURATION 4

Member	Load (lbs)	α (deg)	β (deg)	ψ (deg)
PL_1, (PL_3)	+15,790	2.0	-40.	+30.
	-19,291	2.0	+130.	-13.
PL_2, (PL_4)	+15,285	2.0	-60.	+30.
	-17,976	2.0	+110.	-13.
PU_1, (PU_2)	+12,790	2.0	+120.	-15.
	-33,508	15.0	-60.	-13.
RA	+14,576	10.0	+90.	-13.
	-14,576	10.0	-90.	-13.
RB	+26,232	2.0	-90.	-13.
	-26,232	2.0	+90.	-13.
Q_1	+35,677	2.0	+180.	-13.
	-28,871	2.0	0	+30.
Q_2	+42,978	2.0	0	+30.
	-10,895	20.0	+180.	-15.
R_{123}	+12,972	2.0	0	+30.
R_{11}	+48,759	2.0	0	+30.
R_{123}	+50,455	2.0	0	+30.

TABLE 16

MAXIMUM LOADS CONFIGURATION 5

Member	Load (lbs)	α (deg)	β (deg)	ψ (deg)
PL_1, (PL_3)	+16,022	1.0	-40.	+30.
	-19,459	1.0	+130.	-13.
PL_2, (PL_4)	+15,455	1.0	-60.	+30.
	-18,126	1.0	+110.	-13.
PU_1, (PU_2)	+12,790	2.0	+120.	-15.
	-33,508	15.0	-60.	-13.
RA	+14,576	1.0	-90.	-13.
	-14,576	1.0	-90.	-13.
RB	+26,448	1.0	-90.	-13.
	-26,448	1.0	+90.	-13.
Q_1	+35,988	1.0	+180.	-13.
	-29,420	1.0	0	+30.
Q_2	+43,076	1.0	0	+30.
	-10,895	2.0	+180.	-15.
R_{123}	+13,317	1.0	0	+30.
R_{11}	+48,984	1.0	0	+30.
R_{123}	+50,762	1.0	0	+30.

TABLE 17

MAXIMUM LOADS CONFIGURATION 6

Member	Load (lbs)	α (deg)	β (deg)	ψ (deg)
$PL_1, (PL_3)$	+18,338	2.0	-40.	+30.
	-24,163	2.0	+120.	+8.
$PL_2, (PL_4)$	+18,315	2.0	-60.	+30.
	-22,392	2.0	+110.	+8.
$PU_1, (PU_2)$	+12,790	20.0	+120.	-15.
	-50,715	2.0	-60.	+8.
RA	+17,912	6.0	+90.	+8.
	-17,912	6.0	-90.	+8.
RB	+32,289	2.0	-90.	+8.
	-32,289	2.0	+90.	+8.
Q_1	+45,391	2.0	+180.	+8.
	-31,935	2.0	0	+30.
Q_2	+71,366	2.0	0	+30.
	-10,895	20.0	+180.	-15.
R_{123}	+16,135	2.0	0	+30.
R_{11}	+61,909	2.0	0	+30.
R_{123}	+63,977	2.0	0	+30.

TABLE 18

MAXIMUM LOADS CONFIGURATION 7

Member	Load (lbs)	α (deg)	β (deg)	ψ (deg)
PL_1, (PL_3)	+15,790	2.0	-40.	+30.
	-19,532	2.0	+130.	-15.
PL_2, (PL_4)	+15,285	2.0	-60.	+30.
	-18,130	2.0	+110.	-15.
PU_1, (PU_2)	+12,974	20.0	+120.	-20.
	-33,784	15.0	-60.	-15.
R_A	+14,639	10.0	+90.	-15.
	-14,639	10.0	-90.	-15.
R_B	+26,348	2.0	-90.	-15.
	-26,348	2.0	+90.	-15.
Q_1	+36,322	2.0	+180.	-15.
	-28,871	2.0	0	+30.
Q_2	+43,254	25.0	0	-15.
	-11,298	15.0	+180.	-20.
R_{123}	+12,972	2.0	0	+30.
R_{11}	+48,759	2.0	0	+30.
R_{123}	+50,455	2.0	0	+30.

TABLE 19

MAXIMUM LOADS CONFIGURATION 8

Member	Load (lbs)	α (deg)	β (deg)	ψ (deg)
$PL_1, (PL_3)$	+18,338	2.0	-40.	+30.
	-24,163	2.0	+120.	+8.
$PL_2, (PL_4)$	+18,315	2.0	-60.	+30.
	-22,392	2.0	+110.	+8.
$PU_1, (PU_2)$	+12,637	20.0	+120.	-10.
	-50,715	2.0	-60.	+8.
RA	+17,912	6.0	+90.	+8.
	-17,912	6.0	-90.	+8.
RB	+32,290	2.0	-90.	+8.
	-32,290	2.0	+90.	+8.
Q_1	+45,391	2.0	+180.	+8.
	-31,935	2.0	0	+30.
Q_2	+71,366	2.0	0	+30.
	-10,601	20.0	+180.	-10.
R_{123}	+16,135	2.0	0	+30.
R_{11}	+61,909	2.0	0	+30.
R_{123}	+63,977	2.0	0	+30.

TABLE 20

MAXIMUM LOADS CONFIGURATION 9

Member	Load (lbs)	α (deg)	β (deg)	ψ (deg)
$P_{L_1}, (P_{L_3})$	+3,100	1.0	-40.	+30.
	-3,715	1.0	+130.	-13.
$P_{L_2}, (P_{L_4})$	+2,983	1.0	-60.	+30.
	-3,467	1.0	+110.	-13.
$P_{U_1}, (P_{U_2})$	+2,491	20.0	+120.	-15.
	-6,340	15.0	-60.	-13.
R_A	+2,805	15.0	+90.	-13.
R_B	+5,086	1.0	+90.	-13.
Q_1	+6,861	1.0	+180.	-13.
	-5,720	1.0	0	+30.
Q_2	+8,147	1.0	0	+30.
	-2,126	20.0	+180.	-15.
$R_{1,2,3}$	+2,568	1.0	0	+30.
R_{11}	+9,436	1.0	0	+30.
R_{123}	+9,779	1.0	0	+30.

TABLE 21

MAXIMUM LOADS COMBINED CONFIGURATIONS 3, 4, 5 AND 7

Member	Load (lbs)	α (deg)	β (deg)	ψ (deg)
$P_{L_1}, (P_{L_3})$	+16,022	2.0	-40.	+30.
	-19,532	2.0	+130.	-15.
$P_{L_2}, (P_{L_4})$	+15,455	1.0	-60.	+30.
	-18,130	2.0	+110.	-15.
$P_{U_1}, (P_{U_2})$	+12,974	2.0	+120.	-20.
	-33,784	15.0	-60.	-15.
R_A	+14,639	10.0	+90.	-15.
R_B	+26,448	1.0	+90.	-13.
Q_1	+36,322	2.0	+180.	-13.
	-29,420	2.0	0	+30.
Q_2	+43,254	25.0	0	-15.
	-11,298	15.0	+180.	-20.
R_{123}	+16,135	2.0	0	+30.
R_{11}	+48,984	1.0	0	+30.
R_{123}	+63,977	2.0	0	+30.

TABLE 22

MAXIMUM LOADS COMBINED CONFIGURATIONS 6 AND 8

Member	Load (lbs)	α (deg)	β (deg)	ψ (deg)
$P_{L_1}, (P_{L_3})$	+18,338	2.0	-40.	+30.
	-24,163	2.0	+120.	+8.
$P_{L_2}, (P_{L_4})$	+18,315	2.0	-60.	+30.
	-22,392	2.0	+110.	+8.
$P_{U_1}, (P_{U_2})$	+12,790	20.0	+120.	-15.
	-50,715	2.0	-60.	+8.
R_A	+17,912	6.0	+90.	+8.
R_B	+32,290	2.0	+90.	+8.
Q_1	+45,391	2.0	+180.	+8.
	-31,935	2.0	0	+30.
Q_2	+71,366	2.0	0	+30.
	-10,601	20.0	+180.	-10.
R_{123}	+16,135	2.0	0	+30.
R_{11}	+61,909	2.0	0	+30.
R_{123}	+63,977	2.0	0	+30.

APPENDIX IV

ALIGHTMENT SYSTEM STRESS ANALYSES

The alightment system structural members may now be sized out from stress considerations. The maximum shear stress theory of failure (Reference 6, Page 79) is used when appreciable multidirectional loading is experienced. The materials selected are a beryllium aluminum alloy for extrudable members, 7178-T6 aluminum for most of the machined members, and 4130 steel for certain bearing areas. The beryllium aluminum alloy is 31 percent beryllium with a compressive yield strength of 74,000 pound per square inch (Reference 7), a density of 0.074 pounds per cubic inch, and a modulus of elasticity of 34,000,000 pounds per square inch. 7178-T6 aluminum has a yield strength of 69,000 pounds per square inch, a density of 0.100 pounds per cubic inch, and a modulus of elasticity of 10,000,000 pounds per square inch. 4130 steel has a yield strengh of 180,000 pounds per square inch, a density of 0.283 pounds per cubic inch, and a modulus of elasticity of 30,000,000 pounds per square inch. A design factor or safety factor of 1.2 is used due to the reasonably well defined loads and the design goals of minimum weight and one shot functioning.

TELESCOPING LEG STRESS ANALYSIS

The lower portion of the telescoping leg is a thin walled tube with a cap on the bottom end and a polished bearing area along the exterior of the top. The upper portion of the leg is a thin walled tube with a polished bearing area along the inside of the bottom and a cap with pivot lugs on the top end. The axial energy absorber is supported at each end by circular plates which sit on ledges in the upper and lower portions of the telescoping leg. The rotational energy absorbers bear directly against the outside of the upper half of the telescoping leg and are assumed to be supported by the space package structure. The pivot at the top of the leg consists of a double pivot joint which attaches to the space package structure.

Lower Leg Tube

Size: 3.00 inch O.D., 17.5 inch length, 0.050 inch wall thickness.

Material: Be(31)A1.

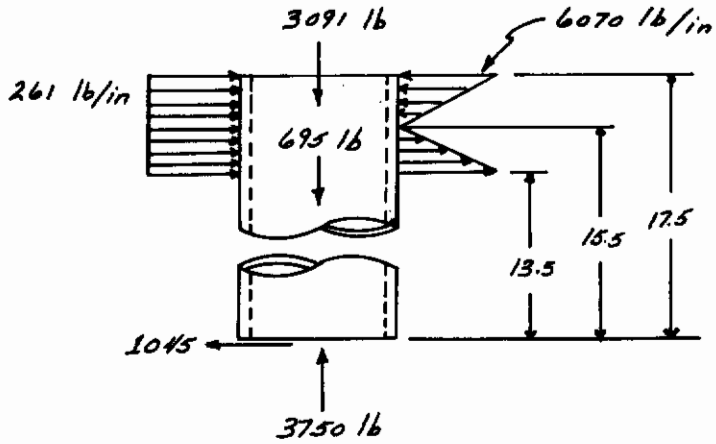

$$A = \pi dt = \pi(2.950)(0.050) = 0.463 \text{ in}^2$$

$$I = \pi r^3 t = \pi (1.450)^3(0.050) = 0.478 \text{ in}^4$$

$$M = P\ell = 1045(15.5) = 16,150 \text{ lb-in}$$

Bending Stress:

$$\sigma_B = \frac{Mc}{I} = \frac{16,150(1.50)}{0.478} = 50,500 \text{ lb/in}^2$$

Compressive Stress:

$$\sigma_c = \frac{P}{A} = \frac{3750}{0.463} = 8,100 \text{ lb/in}^2$$

Column Buckling for Entire Leg:

$$P_{CB} = \frac{\pi^2 EI}{L^2} = \frac{\pi^2(34)(10)^6(0.478)}{(30.5)^2} = 167,000 \text{ lb}$$

The critical column load is 45 times the column loading in this situation. Thus, no further consideration need be given to column bucking.

Local Buckling:

$$\sigma_{LB} = \frac{0.4\,Et}{D}$$

$$\sigma_{LB} = \frac{0.4(34)(10)^6(0.0436)}{3.0} = 198,000 \text{ lb/in}^2$$

The critical local buckling stress is over three times the stress resulting from this loading. Thus, no further consideration need be given to local buckling.

Bearing Stress:

$$\sigma_{BR} = \frac{w_1 + w_2}{d} = \frac{261 + 6070}{3.00} = 2,110 \text{ lb/in}^2$$

Thus, the contact stresses are no problem in the slip joint between the upper and lower portions of telescoping leg.

Combined Stresses:

$$\sigma_{MAX} = \sigma_B + \sigma_C = 50,500 + 8,100 = 58,600 \text{ lb/in}^2$$

Design Factor:

$$f = 74,000/58,600 = 1.26$$

Lower Leg Cap

Size: 3.08 inch diameter circular flat plate, 0.39 inch thick, fixed on the edges with a 0.5 inch diameter pressure area on the under side.

Material: 7178-T6 aluminum

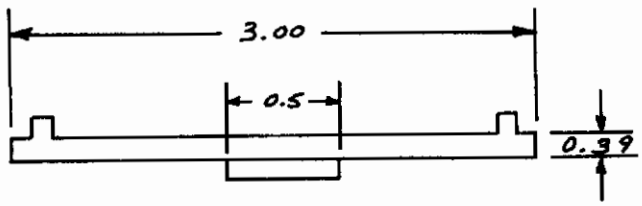

The lower leg cap may be approximated by a flat plate with a distributed load in the center and the outside edge fixed. From Reference 9, Page 196, it is found that the radial and tangential stresses are equal and maximum at the center of the plate. All logarithms in the plate formulae are base e.

Tangential and Radial Stresses:

$$\sigma_t = \sigma_r = \frac{3w(m+1)}{2\pi m t^2}\left[\log\left(\frac{a}{r_o}\right) + \frac{r_o^2}{4a^2}\right]$$

$$= \frac{3(3750)(4.33)}{2\pi(3.33)(0.39)^2}\left[\log\frac{1.5}{0.25} + \frac{(0.25)^2}{4(1.5)^2}\right]$$

$$= 27,500 \text{ lb/in}^2$$

Combined Stresses:

$$\tau_{MAX} = \sigma_r = \sigma_t = 27,500 \text{ lb/in}^2$$

Design Factor:

$$f = \frac{(69,000/2)}{27,500} = 1.25$$

Upper and Lower Plates

Size: 3.00 inch diameter, 0.35 inch thick flat circular plate, with a uniform load applied over a 1.074 diameter at the center, and the edges supported.

Material: 7178-T6 aluminum

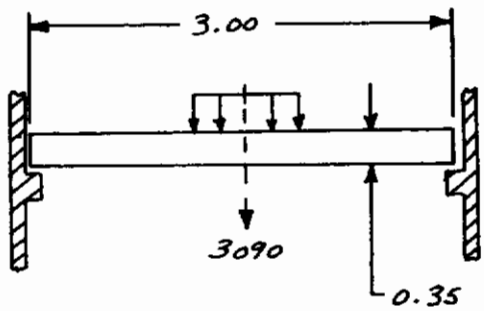

Tangential and Radial Stresses:

$$\sigma_t = \sigma_r = \frac{3w}{2\pi m t^2}\left[m + (m+1)\log\left(\frac{a}{r_o}\right) - (m-1)\frac{r_o^2}{4a^2}\right]$$

$$\sigma_t = \sigma_r = \frac{3(3091)}{2\pi(3.33)(0.35)^2}\left[3.33+4.33\log\left(\frac{1.51}{0.537}\right)-\frac{2.33(.537)^2}{4\ (1.51)^2}\right]$$

$$= 28,100 \text{ lb/in}^2$$

Combined Stresses:

$$\tau_{MAX} = \sigma_r = \sigma_t = 28,100 \text{ lb/in}^2$$

Design Factor:

$$f = \frac{(69,000/2)}{28,100} = 1.24$$

Upper Leg Tube

Size: 3.00 inch I.D., 16.5 inch length, .050 inch wall thickness.

Material: Be(31)AL

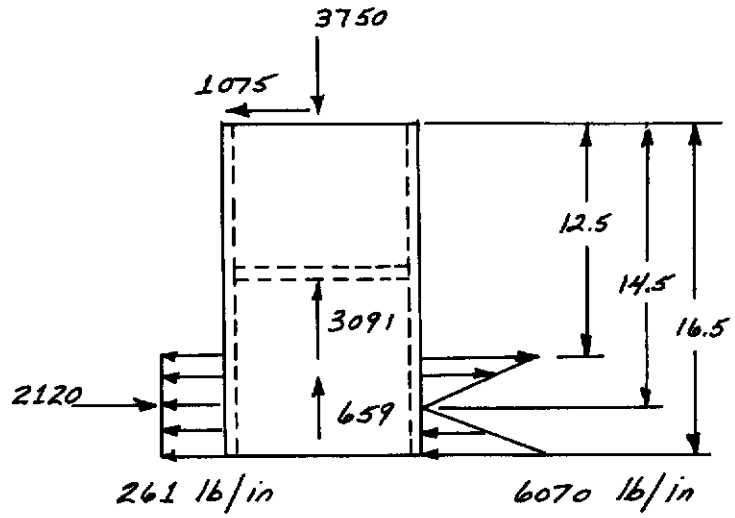

$$A = \pi dt = \pi(3.05)(0.050) = 0.479 \text{ in}^2$$

$$I = \pi r^3 t = \pi(1.525)^3(0.050) = 0.556 \text{ in}^4$$

$$M = \frac{w_2 x^2}{6} = \frac{6070(4)^2}{6} = 16,150 \text{ lb-in}$$

Bending Stress:

$$\sigma_B = \frac{Mc}{I} = \frac{16,150(1.525)}{0.556} = 44,200 \text{ lb/in}^2$$

Compressive Stress:

$$\sigma_c = \frac{P}{A} = \frac{3750}{0.479} = 7,820 \text{ lb/in}^2$$

Combined Stress:

$$\sigma_{MAX} = \sigma_B + \sigma_c = 44,200 + 7,820 = 52,020 \text{ lb/in}^2$$

Design Factor:

$$f = \frac{74,000}{52,020} = 1.42$$

Double Pin Swivel

Size: 0.35 inch square by 1.20 inch length.

Material: 4130 steel.

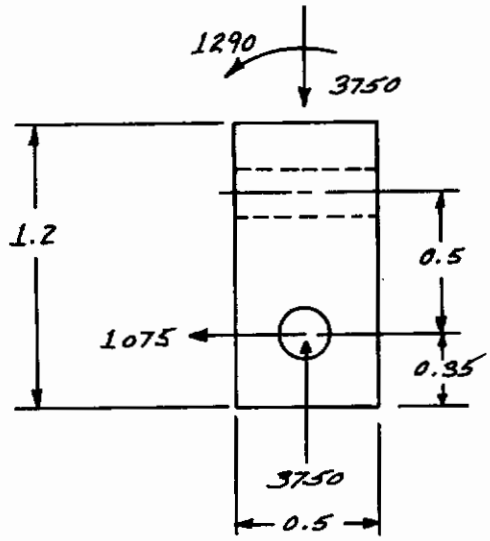

Pins:

$$P = \sqrt{(3750)^2 + (1075)^2} = 3930 \text{ lb}$$

From Reference 10, it is seen that 0.25 inch internal wrenching bolts have a double shear load capability of 9,300 pounds.

Design Factor:

$$f = \frac{9,300}{3,930} = 2.37$$

Bending Stress:

The largest bending stress will occur in the vicinity of the upper pivot.

$$M = P\ell = 1075(0.5) = 538 \text{ lb-in}$$

$$I = \frac{bh^3}{12} = \frac{0.25(0.50)^3}{12} = 0.0026 \text{ in}^4$$

$$\sigma_B = \frac{Mc}{I} = \frac{538(0.25)}{0.0026} = 51,600 \text{ lb/in}^2$$

Compressive Stress:

$$A = 0.5\ (0.25) = 0.125 \text{ in}^2$$

$$\sigma_c = \frac{P}{A} = \frac{3750}{0.125} = 30,000 \text{ lb/in}^2$$

Combined Stresses:

$$\sigma_{MAX} = \sigma_B + \sigma_c = 51,600 + 30,000 = 81,600 \text{ lb/in}^2$$

Design Factor:

$$f = \frac{180,000}{81,600} = 2.20$$

Upper Leg Cap

Size: 3.00 inch diameter circular flat plate, 0.45 inch thickness, fixed on the edges with two pivot lugs on the top side.

Material: 7178-T6 aluminum.

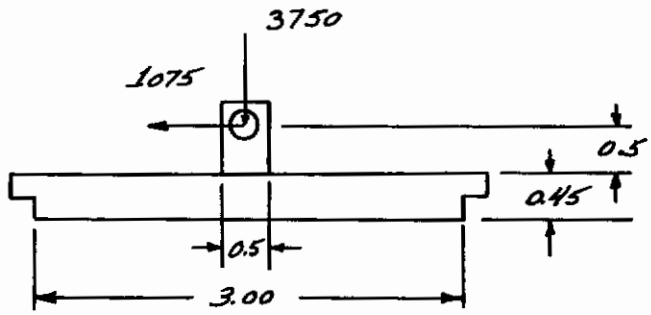

The tangential and radial stresses due to the moment and the axial load are superimposed.

Stresses Due to Moment:

$$M = P\ell = 1075(0.5) = 538 \text{ lb-in}$$

$$\sigma_r = \sigma_t = \frac{3M}{4\pi t^2 r_o}\left[1+\left(\frac{m+1}{m}\right)\log\left(\frac{2(0.45\,a - r_o)}{0.45\,k\,a}\right)\right]$$

$$k = \frac{0.1\,a^2}{(r_o + 0.28a)^2} = \frac{0.1(1.5)^2}{[0.25 + 0.28(1.5)]^2} = 0.500$$

Reference 9, Page 197

$$\sigma_r = \sigma_t = \frac{3(538)}{4\pi^2(0.45)^2(0.25)}\left[1 + \frac{4.33}{3.33}\log\left[\frac{2(0.45(1.5)-0.25)}{0.45(0.50)(1.5)}\right]\right]$$

$$= 1790 \text{ lb/in}^2$$

Stresses Due to Axial Load:

$$\sigma_r = \sigma_t = \frac{3w(m+1)}{2\pi m t^2}\left[\log\left(\frac{a}{r_o}\right) + \frac{r_o^2}{4a^2}\right]$$

$$= \frac{3(3750)(4.33)}{2\pi(3.33)(0.45)^2}\left[\log\left(\frac{1.50}{0.25}\right) + \frac{(0.25)^2}{4(1.5)^2}\right]$$

$$= 20,700 \text{ lb/in}^2$$

Combined Stresses:

$$\sigma_{MAX} = 1790 + 20,700 = 22,490 \text{ lb/in}^2$$

$$\tau_{MAX} = \sigma_{MAX} = 22,490 \text{ lb/in}^2$$

Design Factor:

$$f = \frac{(69,000/2)}{22,490} = 1.53$$

Upper Cap Lugs

Size: 0.75 inch high, 0.5 inch wide, and 0.20 inch thick plates.

Material: 7178-T6 aluminum

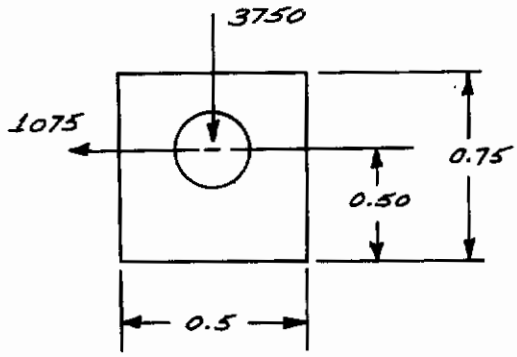

Bearing Stress:

$$\sigma_{BR} = \frac{P}{dt} = \frac{3930}{(0.25)(0.40)} = 39,400 \text{ lb/in}^2$$

Design Factor:

$$f = \frac{69,000}{39,400} = 1.75$$

Bending Stress:

$$M = P\ell = 1075\ (0.5) = 538 \text{ lb-in}$$

$$I = \frac{bh^3}{12} = \frac{0.4(0.5)^3}{12} = 0.00417 \text{ in}^4$$

$$\sigma_B = \frac{Mc}{I} = \frac{538(0.25)}{0.00417} = 30,000 \text{ lb/in}^2$$

Compressive Stress:

$$A = 0.5(0.4) = 0.20 \text{ in}^2$$

$$\sigma_c = \frac{P}{A} = \frac{3750}{0.2} = 18,800 \text{ lb/in}^2$$

Combined Stresses:

$$\sigma_{MAX} = \sigma_B + \sigma_c = 30,000 + 18,800 = 48,800 \text{ lb/in}^2$$

Design Factor:

$$f = \frac{69,000}{48,800} = 1.42$$

ARTICULATED LEG STRESS ANALYSES

The seven articulated leg configurations are handled with three stress analyses. The first stress analysis is applicable to configuration numbers 3, 4, 5 and 7. The second stress analysis covers configuration numbers 6 and 8. The third stress analysis is for configuration number 9. The parallelogram and peg leg assembly is shown in Figure 106.

Configuration Numbers 3, 4, 5 and 7

Upper Truss

Size: 2.75 in O.D., 0.0675 in wall tubing.

Material: Be(31) AL

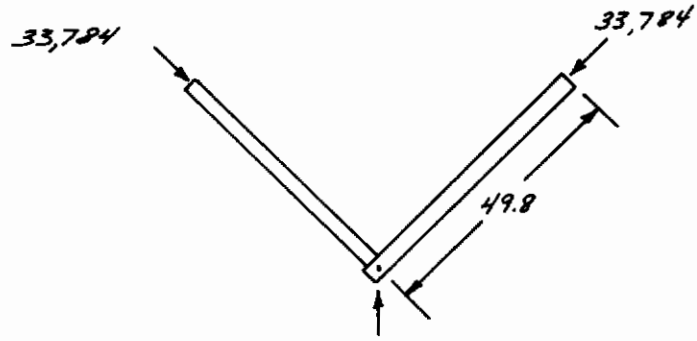

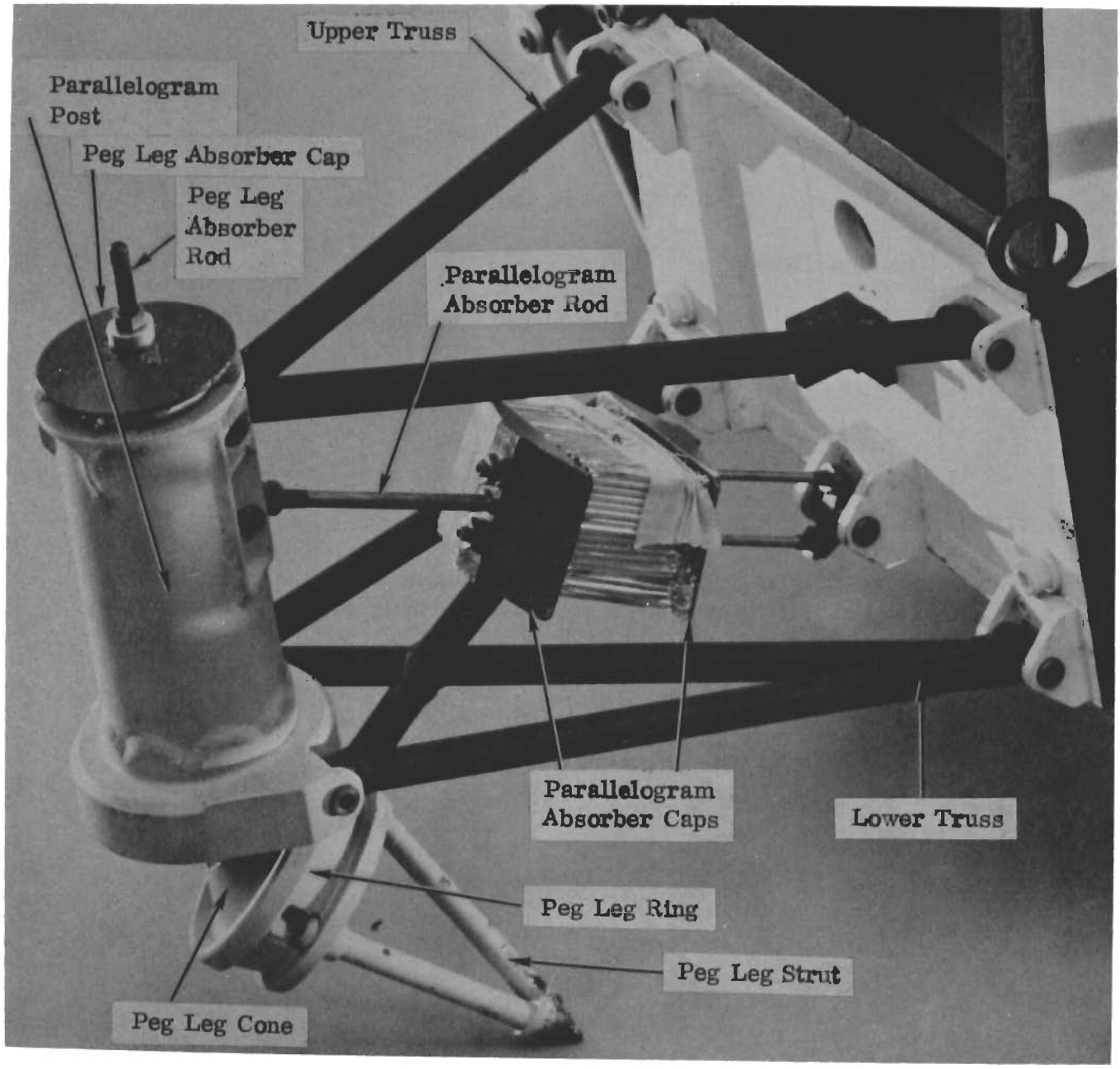

Figure 106, Parallelogram and Peg Leg Assembly

Compressive Stress:

$$A = \pi dt = \pi (2.67)(0.0675) = 0.566 \text{ in}^2$$

$$\sigma_c = \frac{P}{A} = \frac{33,784}{0.566} = 59,700 \text{ lb/in}^2$$

Critical Column Buckling Stress:

$$k(\text{radius of gyration}) = \frac{d}{2\sqrt{2}} = \frac{2.67}{2\sqrt{2}} = 0.944 \text{ in}$$

$$\sigma_{cB} = \frac{\pi^2 E}{(\ell/k)^2} = \frac{\pi^2 (34)(10)^6}{(4.98/0.944)^2} = 12,000,000 \text{ lb/in}^2$$

The critical column buckling stress is two hundred times the column stress for this member. Thus, column buckling is not a concern for this member.

Design Factor:

$$f = \frac{74,000}{59,700} = 1.24$$

Lower Truss

Size: 2.50 in O.D., 0.0426 in-wall tubing.

Material: Be(31)AL

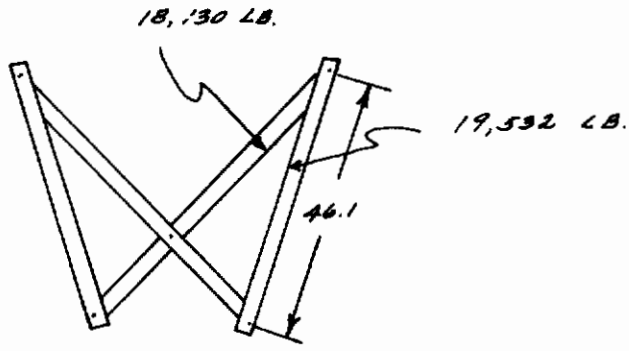

Only the outer member need be analyzed since the inner member is shorter and is loaded slightly less.

Compressive Stress:

$$A = \pi dt = \pi (2.46)(0.0426) = 0.329 \text{ in}^2$$

$$\sigma_c = \frac{P}{A} = \frac{19532}{0.329} = 59,400 \text{ lb/in}^2$$

Critical Buckling Stress:

$$k = \frac{d}{2\sqrt{2}} = \frac{2.46}{2\sqrt{2}} = 0.870 \text{ in}$$

$$\sigma_{cB} = \frac{\pi^2 E}{(\ell/k)^2} = \frac{\pi^2 (34)(10)^6}{(46.1/0.87)^2} = 119,500 \text{ lb/in}^2$$

The critical column buckling load is twice the column stress for this member. Thus, column buckling is not a problem for this member.

Design Factor:

$$f = \frac{74,000}{59,400} = 1.25$$

Peg Leg Strut

Size: 2.0 inch O.D., 0.144 in wall tubing.

Material: Be(31)AL.

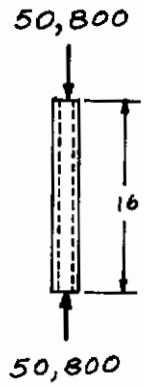

The worst loading condition for the peg leg struts is when the entire reaction load R_{123} is carried on a single strut.

Compressive Stress:

$$A = \pi\, dt = \pi\,(1.856)(0.144) = 0.841 \text{ in}^2$$

$$\sigma_c = \frac{P}{A} = \frac{50,800}{0.841} = 60,400 \text{ lb/in}^2$$

Critical Buckling Stress:

$$k = \frac{d}{2\sqrt{2}} = \frac{1.856}{2\sqrt{2}} = 0.658 \text{ in}$$

$$\sigma_{cB} = \frac{\pi^2 E}{(\ell/k)^2} = \frac{\pi^2 (34)(10)^6}{(16/0.658)^2} = 585,000 \text{ lb/in}^2$$

The critical buckling load is over nine times the column load for this member. Thus, column buckling is not a problem.

Peg Leg Ring

Size: 14.4 inch O.D., ring of irregular cross section.

Material: 7178 - T6 aluminum

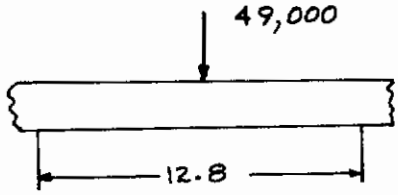

The ring is scaled up geometrically a factor of four from the test model except the thickness in the radial direction which is scaled by 1.14. By scaling the test model values, the following characteristics are obtained.

$I \simeq 8.55 \text{ in}^4$

$c \simeq 2.80 \text{ in}$

Bending Stress:

$$M = \frac{P\ell}{4} = \frac{49,000(12.8)}{4} = 157,000 \text{ lb-in}$$

$$\sigma = \frac{Mc}{I} = \frac{157,000(2.8)}{8.55} = 51,400 \text{ lb/in}^2$$

Design Factor:

$$f = \frac{69,000}{51,400} = 1.34$$

Peg Leg Cone

Size: 0.25 inch thick cone with the peg leg absorber force acting at the apex. A shell analysis, due to the mathematical complexity is not warranted in this application. Therefore, as a conservative estimate assume that a section of width ten times the thickness of the shell acts in direct tension. The thickness is scaled up by 2 and the other dimensions by 4 from the test model.

Material: 7178 - T6 aluminum

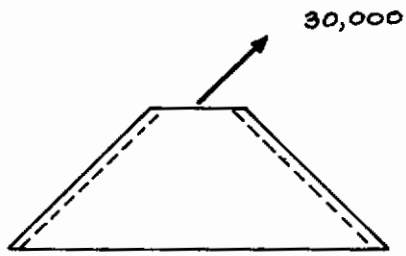

Tensile Stress:

$$\sigma_T = \frac{P}{A} = \frac{30,000}{10(0.25)^2} = 48,000 \text{ lb/in}^2$$

Design Factor:

$$f = \frac{69,000}{48,000} = 1.43$$

Parallelogram Post

Size: 12 inch O.D., 0.083 inch wall tubing. The load application points are reinforced to prevent local buckling.

Material: 7178 - T6 aluminum

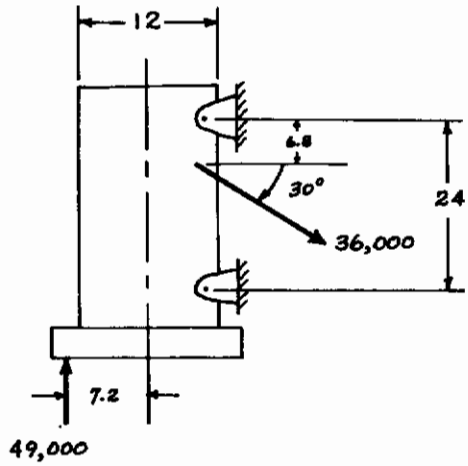

The moment and compressive load due to the peg leg reaction force predominate the loading of the post.

Compressive Stress:

$$A = \pi dt = \pi (11.917)(0.083) = 3.11 \text{ in}^2$$

$$\sigma_c = \frac{P}{A} = \frac{49,000}{3.11} = 15,800 \text{ lb/in}^2$$

Bending Stress:

$$I = \pi r^3 t = \pi (5.958)^3 (0.083) = 55.0 \text{ in}^4$$

$$M = P \ell = 49,000 \ (7.2) = 353,000 \text{ lb-in}$$

$$\sigma_B = \frac{Mc}{I} = \frac{353,000(6.0)}{55.0} = 38,600 \text{ lb/in}^2$$

Combined Stress:

$$\sigma_{MAX} = \sigma_c + \sigma_b = 15,800 + 38,600 = 54,400 \text{ lb/in}^2$$

Design Factor:

$$f = \frac{69,000}{54,400} = 1.26$$

Peg Leg Energy Absorber Rod

Material: 7178 - T6 aluminum

Size: 0.818 inch diameter rod

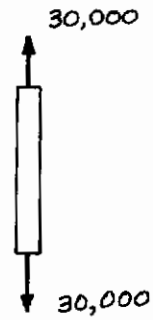

Tensile Stress:

$$A = \frac{\pi}{4} d^2 = 0.785 \ (0.818)^2 = 0.525 \text{ in}^2$$

$$\sigma_T = \frac{P}{A} = \frac{30,000}{0.525} = 57,000 \text{ lb/in}^2$$

Design Factor:

$$f = \frac{69,000}{57,000} = 1.21$$

Peg Leg Absorber Cap

Size: 3.14 inch O.D., 0.818 inch I.D., 0.33 inch thick circular plate.

Material: 7178 - T6 aluminum.

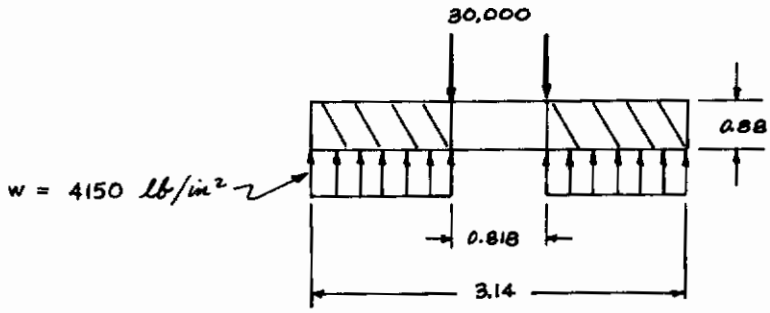

$$\sigma_{MAX} = \sigma_t = \frac{3w}{4\,m\,t^2(a^2 - b2)}\left[4a^4(m+1)\log\left(\frac{a}{b}\right) + 4a^2b^2 + b^4(m-1) - a^4(m+3)\right]$$

Reference 10, Page 199

$$\sigma_{MAX} = \frac{3(4150)}{4(3.33)(0.88)^2\left[(1.57)^2 - (0.409)^2\right]}$$

$$\begin{bmatrix} 4(1.57)^4(4.33)\log\left(\frac{1.57}{.409}\right) \\ +4(1.57)^2(.409)^2 \\ +(.409)^4(2.33) \\ -(1.57)^4(6.33) \end{bmatrix}$$

$$\sigma_{MAX} = 55,200 \text{ lb/in}^2$$

Design Factor:

$$f = \frac{69,000}{55,000} = 1.25$$

Parallelogram Absorber Rods

Size: 0.518 inch diameter rod.

Material: 7178 - T6 aluminum

Tensile Stress:

$$A = \frac{\pi}{4} d^2 = 0.785(0.518)^2 = 0.210 \text{ in}^2$$

$$\sigma_T = \frac{P}{A} = \frac{12,000}{0.210} = 57,000 \text{ lb/in}^2$$

Design Factor:

$$f = \frac{69,000}{57,000} = 1.21$$

Parallelogram Absorber Caps

Size: 3.45 inch diameter, 0.62 inch thick plate, with six 0.52 in holes. The absorber rod loads are distributed by using 0.75 inch diameter washers.

Material: 7178 - T6 aluminum.

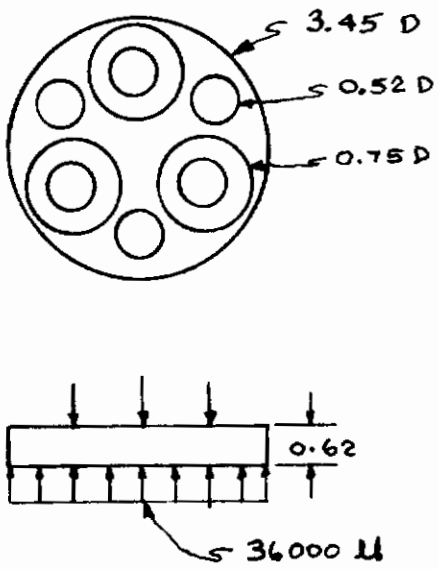

The plate is analyzed by superimposing the stress for, firstly, three uniform loads over small eccentric areas and, secondly, a uniformly distributed load over the entire area. The maximum stresses occur at the point of eccentric loading. The stress at the point of one eccentric loading is not drastically effected by the loading at the other points. Thus, accounting only for the distributed load and one eccentric loading yields the following:

$$\nabla_r = \frac{-3w}{2\pi m t^2}\left[m+(m+1)\log\left(\frac{a-P}{r_o}\right)-(m-1)\left(\frac{r_o^2}{4(a-P)^2}\right)\right]$$

$$+\frac{3w'}{8\pi m t^2}\left[(3m+1)\left(1-\frac{P^2}{a^2}\right)\right]$$

Reference 9, Pages 194 and 195

$$\sigma_r = \frac{-3(12,000)}{2\pi\ 3.33(0.62)^2}\left[3.33+4.33\log\left(\frac{1.725-1.35}{0.375}\right)\frac{-2.33(0.375)^2}{4(1.725-1.35)^2}\right]$$

$$+\frac{3(36,000)}{8\pi(3.33)(0.62)^2}\left[\left(3(3.33)+1\right)\left(1-\left(\frac{1.35}{1.725}\right)^2\right)\right]$$

$$= -12,298 + 14,296 = 1,998 \text{ lb}/\text{in}^2$$

$$\sigma_t = \frac{-3W}{2\pi\ mt^2}\left[m + (m+1)\log\left(\frac{a-P}{r_o}\right) - (m-1)\left(\frac{r_o^2}{4(a-P)^2}\right)\right]$$

$$+\frac{3W'}{8\pi\ mt^2}\left[(3m+1) - (m+3)\frac{P^2}{a^2}\right]$$

$$\sigma_t = \frac{-3(12,000)}{2\pi\ 3.33(0.62)^2}\left[3.33+4.33\log\left(\frac{1.725-1.35}{0.375}\right) - \left(\frac{2.33(.375)^2}{4(1.725-1.35)^2}\right)\right]$$

$$+\frac{3(36,000)}{8\pi(3.33)(0.62)^2}\left[(3(3.33)+1) - 6.33\left(\frac{1.35}{1.75}\right)^2\right]$$

$$= -12,298 + 24,250 = 11,952 \text{ lb/in}^2$$

Combined Stress:

$$\tau_{max} = \frac{\sigma_r + \sigma_t}{2} = \frac{1,998 + 11,952}{2} = 6,975 \text{ lb/in}^2$$

Design Factor:

$$f = \frac{69,000/2}{6,975} = 4.94$$

CONFIGURATION NUMBERS 6 AND 8

Upper Truss

Size: 2.75 in. O.D., 0.101 in. wall tubing.

Material: Be (31) al.

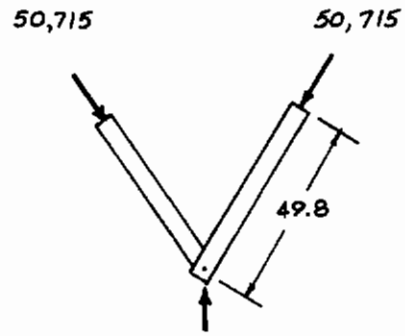

Compressive Stress:

$$A = \pi\, d\, t = \pi\, (2.65)\, (0.101) = 0.840 \text{ in}^2$$

$$\sigma_c = \frac{P}{A} = \frac{50,715}{0.840} = 60,400 \text{ lb/in}^2$$

Design Factor:

$$f = \frac{74,000}{60,400} = 1.23$$

Lower Truss:

Size: 2.50 in. O.D., 0.0528 in. wall tubing.

Material: Be (31) al.

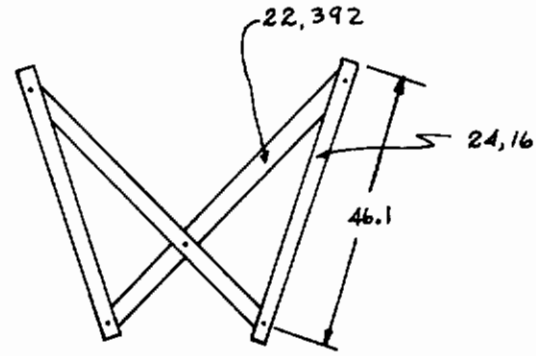

Compressive Stress:

$$A = \pi\, dt = \pi\, (2.45)\, (0.0528) = 0.406 \text{ in}^2$$

$$\sigma_c = \frac{P}{A} = \frac{24,160}{0.406} = 59,500 \text{ lb/in}^2$$

Design Factor:

$$f = \frac{74,000}{59,500} = 1.24$$

Peg Leg Strut

Size: 2.0 in. O.D., 0.181 in. wall tubing.

Material: Be (31) al.

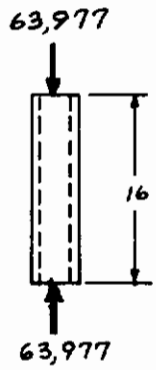

Compressive Stress:

$$A = \pi\, dt = \pi\, (1.82)\, (0.181) = 1.04 \text{ in}^2$$

$$\sigma_c = \frac{P}{A} = \frac{63,977}{1.04} = 61,600 \text{ lb/in}^2$$

Design Factor:

$$f = \frac{74,000}{61,600} = 1.20$$

Peg Leg Ring

Size: 14.4 in. O.D., the ring thickness is now scaled up 1.44 over the test model.

Material: 7178-T6 aluminum

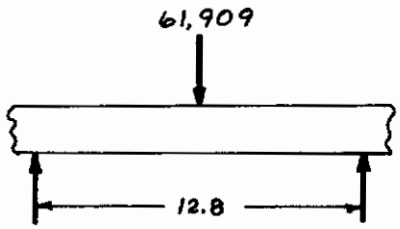

Bending Stress:

$$I \simeq 8.55\left(\frac{1.44}{1.14}\right) = 10.8 \text{ in}^4$$

$$C \simeq 2.8 \text{ in.}$$

$$M = \frac{P\ell}{4} = \frac{61,909(12.8)}{4} = 198,000 \text{ lb-in}$$

$$\sigma_b = \frac{MC}{I} = \frac{198,000(2.8)}{10.8} = 51,300 \text{ lb/in}^2$$

Design Factor:

$$f = \frac{69,000}{51,300} = 1.34$$

Peg Leg Cone

Same as configurations 3, 4, 5 and 7.

Parallelogram Post

Size: 12 in. O.D., 0.100 in. wall tubing with local reinforcements.

Material: 7178-T6 aluminum

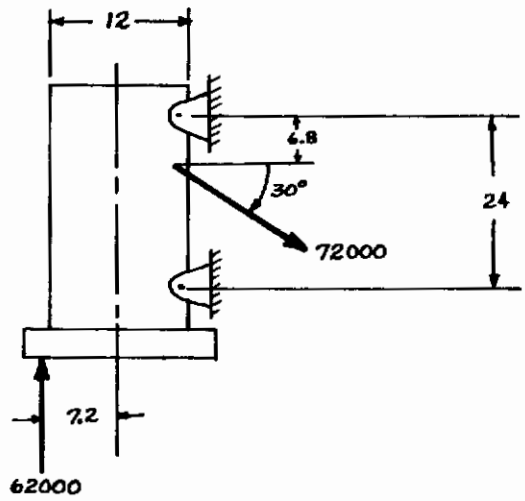

Compressive Stress:

$$A = \pi\, dt = \pi\,(11.9)(0.1) = 3.74 \text{ in}^2$$

$$\sigma_c = \frac{P}{A} = \frac{62,000}{3.74} = 16,600 \text{ lb/in}^2$$

Bending Stress:

$$I = \pi\, r^3 t = \pi\,(5.95)^3\,(0.1) = 66.1 \text{ in}^4$$

$$M = P\ell = 62,000\,(7.2) = 446,000 \text{ lb-in}$$

$$\sigma_B = \frac{Mc}{I} = \frac{446,000(6.0)}{66.1} = 40,500 \text{ lb/in}^2$$

Combined Stress:

$$\sigma_{max} = \sigma_C + \sigma_B = 16,600 + 40,500 = 57,100 \text{ lb/in}^2$$

Design Factor:

$$f = \frac{69,000}{57,100} = 1.21$$

Peg Leg Absorber Rods

Same as configurations 3, 4, 5 and 7.

Peg Leg Absorber Cap

Same as configurations 3, 4, 5 and 7.

Parallelogram Absorber Rods

Size: 0.732 in. diameter rods.

Material: 7178-T6 aluminum

Tensile Stress:

$$A = \frac{\pi}{4} d^2 = 0.785 (.732)^2 = 0.420 \text{ in}^2$$

$$\sigma_T = \frac{P}{A} = \frac{24,000}{0.420} = 57,000 \text{ lb/in}^2$$

Design Factor:

$$f = \frac{69,000}{57,000} = 1.21$$

Parallelogram Absorber Caps

Size: 4.89 in. diameter, 0.92 in. thick plate, with six holes 0.74 in. diameter holes. The absorber rod loads are distributed using 1.25 in. diameter washers.

Material: 7178-T6 aluminum

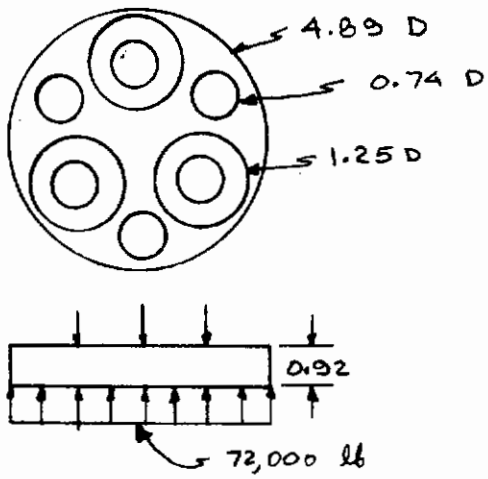

$$\nabla_r = \frac{-3W}{2\pi m t^2}\left[m + (m+1)\log\left(\frac{a-P}{r_o}\right) - (m-1)\left(\frac{r_o^2}{4(a-P)^2}\right)\right]$$

$$+ \frac{3W'}{8\pi m t^2}\left[(3m+1)\left(1 - \frac{P^2}{a^2}\right)\right]$$

$$\nabla_r = -\frac{3(24,000)}{2\pi\, 3.33(0.92)^2}\left[3.33+4.33\left(\frac{2.45-1.825}{0.625}\right) - \frac{2.33(0.625)^2}{4(2.45-1.825)^2}\right]$$

$$+ \frac{3(72,000)}{8\pi(3.33)(0.92)^2}\left[\left(3(3.33)+1\right)\left(1 - \frac{(1.825)^2}{(2.45)^2}\right)\right]$$

$$= -11,171 + 15,955 = 4,784 \text{ lb/in}^2$$

$$\nabla_t = \frac{-3W}{2\pi m t^2}\left[m + (m+1)\log\left(\frac{a-P}{r_o}\right) - (m-1)\left(\frac{r_o^2}{4(a-P)^2}\right)\right]$$

$$+ \frac{3W'}{8\pi m t^2}\left[(3m+1) - (m+3)\frac{P^2}{a^2}\right]$$

$$\nabla_t = \frac{-3\,(24,000)}{2\,\pi\,3.33(0.92)^2}\left[3.33 + 4.33\log\left(\frac{2.45-1.825}{0.625}\right) - \frac{2.33\,(0.625)^2}{4(2.45-1.825)^2}\right]$$

$$+ \frac{3\,(72,000)}{8\,\pi\,(3.33)(0.92)^2}\left[\left(3(3.33)+1\right) - \frac{6.33(1.825)^2}{(2.45)^2}\right]$$

$$= -11,171 + 24,385 = 13,214 \text{ lb/in}^2$$

Combined Stress:

$$\tau_{max} = \frac{\nabla t + \nabla r}{2} = \frac{13,214 + 4,784}{2} = 8,999 \text{ lb/in}^2$$

Design Factor:

$$f = \frac{69,000/2}{8,999} = 3.84$$

CONFIGURATION NUMBER 9

Upper Truss

Size: 1.255 in. O.D., 0.0268 in. wall tubing

Material: Be (31) al.

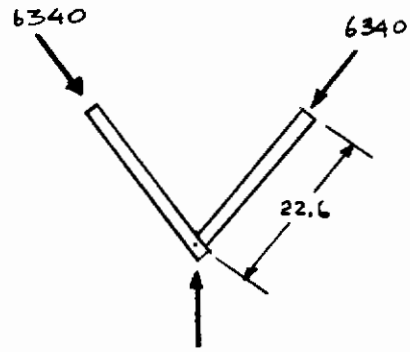

Compressive Stress:

$$A = \pi\, dt = \pi\,(1.228)(0.0268) = 0.1035 \text{ in}^2$$

$$\sigma_c = \frac{P}{A} = \frac{6340}{0.1035} = 61{,}200 \text{ lb/in}^2$$

Critical Column Buckling Stress:

$$k = \frac{d}{2\sqrt{2}} = \frac{1.228}{2\sqrt{2}} = 0.433 \text{ in.}$$

$$\sigma_{CB} = \frac{\pi^2 E}{(\ell/k)^2} = \frac{\pi^2 (34)(10)^6}{(22.6/0.433)^2} = 126{,}000 \text{ lb/in}^2$$

Thus, column buckling is not a concern for this member.

Design Factor:

$$f = \frac{74{,}000}{61{,}200} = 1.21$$

Lower Truss

Size: 1.14 in. O.D., 0.0178 in. wall tubing.

Material: Be (31) al.

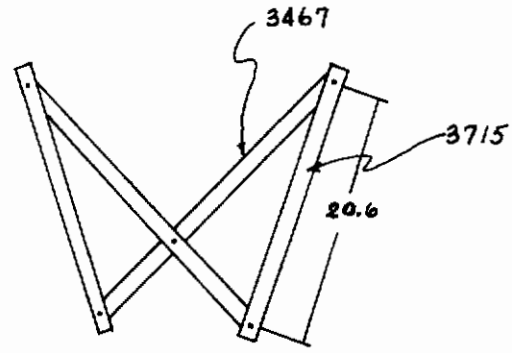

Compressive Stress:

$$A = \pi d t = \pi (1.122)(0.0178) = 0.0627 \text{ in}^2$$

$$\sigma_C = \frac{P}{A} = \frac{3715}{0.0627} = 59,300 \text{ lb/in}^2$$

Design Factor:

$$f = \frac{74,000}{59,300} = 1.25$$

Peg Leg Strut

Size: 0.785 in. O.D., 0.070 in. wall tubing.

Material: Be (31) al.

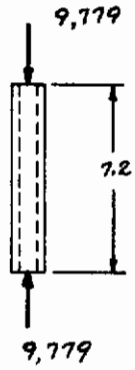

Compressive Stress:

$$A = \pi d t = \pi (0.715)(0.070) = 0.157 \text{ in}^2$$

$$\sigma_C = \frac{P}{A} = \frac{9779}{0.157} = 62,000 \text{ lb/in}^2$$

Design Factor:

$$f = \frac{74,000}{62,000} = 1.20$$

Peg Leg Ring

Size: 6.58 in. O.D. ring of irregular cross section.

Material: 7178-T6 aluminum.

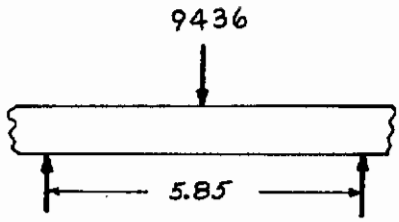

The ring is scaled up geometrically, a factor of 1.825 from the test model except the thickness which is scaled by 0.432.

Bending Stress:

$$I \simeq 0.117(1.825)^3(0.432) = 0.304 \text{ in}^4$$

$$C \simeq 0.70(1.825) = 1.28 \text{ in}$$

$$M = \frac{P\ell}{4} = \frac{9436(5.85)}{4} = 13,800 \text{ lb-in}$$

$$\sigma_B = \frac{MC}{I} = \frac{13,800(1.28)}{0.307} = 57,500 \text{ lb/in}^2$$

Design Factor:

$$f = \frac{69,000}{57,500} = 1.20$$

Peg Leg Cone

Size: 0.101 in. thick cone.

Material: 7178-T6 aluminum.

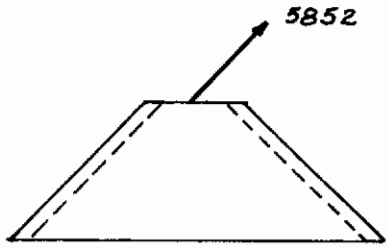

Tensile Stress:

$$\sigma_T = \frac{P}{A} = \frac{5852}{10(0.101)^2} = 57,500 \text{ lb/in}^2$$

Design Factor:

$$f = \frac{69,000}{57,500} = 1.20$$

Parallelogram Post

Size: 5.47 in. O.D., 0.0344 in. wall tubing with local reinforcements.

Material: Be (31) al.

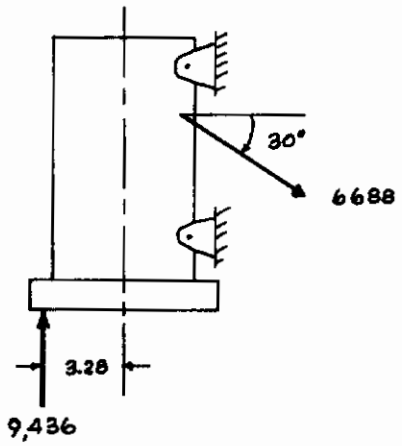

Compressive Stress:

$$A = \pi\, d\, t = \pi\,(5.336)(0.0344) = 0.590 \text{ in}^2$$

$$\sigma_C = \frac{P}{A} = \frac{9436}{0.590} = 16,000 \text{ lb/in}^2$$

Bending Stress:

$$M = P\ell = 9436(3.28) = 31,000 \text{ lb-in}$$

$$I = \pi\, r^3 t = \pi\,(2.668)^3(0.0344) = 2.07 \text{ in}^4$$

$$\sigma_B = \frac{MC}{I} = \frac{31,000\ (2.73)}{2.07} = 40,900 \text{ lb/in}^2$$

Combined Stress:

$$\sigma_{max} = \sigma_C + \sigma_B = 16,000 + 40,900 = 56,900 \text{ lb/in}^2$$

Design Factor:

$$f = \frac{69,000}{56,900} = 1.21$$

Peg Leg Energy Absorber Rod

Size: 0.361 in. diameter rod.

Material: 7178-T6 aluminum.

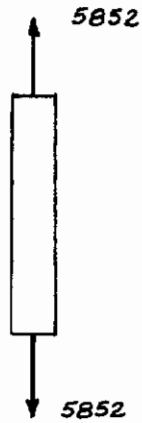

Tensile Stress:

$$A = \frac{\pi}{4} d^2 = 0.785\ (0.361)^2 = 0.102\ in^2$$

$$\sigma_T = \frac{P}{A} = \frac{5852}{0.102} = 57,300\ lb/in^2$$

Design Factor:

$$f = \frac{69,000}{57,300} = 1.20$$

Peg Leg Absorber Cap

Size: 1.76 in. O.D., 1.138 in. I.D., 0.250 in. thick circular plate.

Material: 7178-T6 aluminum.

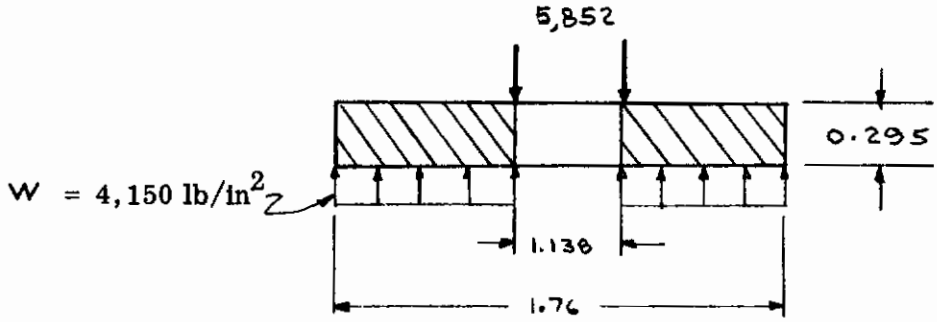

$$\sigma_{max} = \sigma_t = \frac{3\,W}{4m\,t^2\,(a^2-b^2)}\left[4a^4(m+1)\log\left(\frac{a}{b}\right) + 4a^2b^2 + b^4(m-1) - a^4(m+3)\right]$$

$$= \frac{3(4150)}{4(3.33)(0.295)^2\left[(0.88)^2-(0.569)^2\right]}\left[\begin{array}{l} 4(0.88)^4(4.33)\log\left(\frac{0.88}{0.569}\right) \\ + 4(0.88)^2(0.569)^2 \\ + (0.569)^4(2.33) \\ - (0.88)^4(6.33) \end{array}\right]$$

$$\sigma_{max} = 47,203 \text{ lb/in}^2$$

Design Factor:

$$f = \frac{69,000}{47,203} = 1.46$$

Parallelogram Absorber Rods

Size: 0.223 in. diameter rod

Material: 7178-T6 aluminum

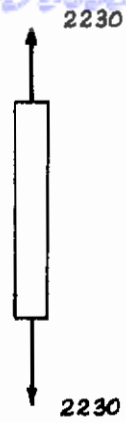

Tensile Stress:

$$A = \frac{\pi}{4} d^2 = 0.785\ (0.223)^2 = 0.039\ in^2$$

$$\sigma_T = \frac{P}{A} = \frac{2230}{0.039} = 57,200\ lb/in^2$$

Design Factor:

$$f = \frac{69,000}{57,200} = 1.20$$

Parallelogram Absorber Caps

Size: 1.48 in. diameter, 0.43 in. thick plate, with six holes 0.23 in. diameter holes. The absorber rod loads are distributed using 0.375 in. diameter washers.

Material: 7178-T6 aluminum.

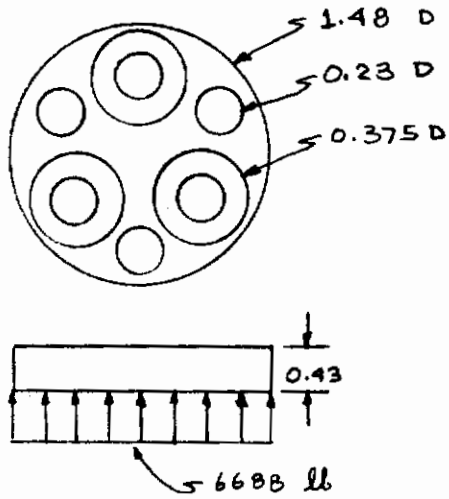

$$\nabla_r = \frac{-3W}{2\pi m t^2}\left[m + (m+1)\log\left(\frac{a-P}{r_o}\right) - (m-1)\left(\frac{r_o^2}{4(a-P)^2}\right)\right]$$

$$+ \frac{3W'}{8\pi m t^2}\left[(3m+1)\left(1 - \frac{P^2}{a^2}\right)\right]$$

$$\nabla_r = \frac{-3(2230)}{2\pi(3.33)(0.43)^2}\left[3.33 + 4.33\log\left(\frac{0.72-0.532}{0.188}\right) - \frac{2.33(.188)^2}{4(.188)^2}\right]$$

$$+ \frac{3(6688)}{8\pi(3.33)(0.43)^2}\left[\left(3(3.33)+1\right)\left(1 - \left(\frac{0.532}{0.72}\right)^2\right)\right]$$

$$= -4,751 + 6,474 = 1,723 \text{ lb/in}^2$$

$$\nabla_t = \frac{-3W}{2\pi m t^2}\left[m + (m+1)\log\left(\frac{a-P}{r_o}\right) - (m-1)\frac{r_o^2}{4(a-P)^2}\right]$$

$$+ \frac{3W'}{8\pi m t^2}\left[(3m+1) - (m+3)\frac{P^2}{a^2}\right]$$

$$\nabla_t = \frac{-3\,(2230)}{2\,\pi\,(3.33)(0.43)^2}\left[3.33+4.33\log\left(\frac{.72-.532}{.188}\right) - \frac{2.33(.188)^2}{4(.72-.532)^2}\right]$$

$$+\frac{3\,(6688)}{8\,\pi\,(3.33)(.43)^2}\left[\left(3(3.33)+1\right) - 6.33\left(\frac{0.532}{0.72}\right)^2\right]$$

$$\nabla_t = -4,751 + 9,773 = 5,022\ \text{lb/in}^2$$

Combined Stress:

$$\tau_{max} = \frac{\nabla_t + \nabla_r}{2} = \frac{5,022 + 1,723}{2} = 3,372\ \text{lb/in}^2$$

Design Factor:

$$f = \frac{69,000/2}{3,372} = 10.23$$

APPENDIX V

ALIGHTMENT SYSTEM WEIGHT ANALYSES

TELESCOPING LEG WEIGHT ANALYSIS

Lower Leg

$W = \rho \pi d t \ell$ = 0.074 (π) (2.95) (0.05) (17.5) = 0.600 lb

Upper Leg

$W = \rho \pi d t \ell$ = 0.074 (π) (3.05) (0.05) (16.5) = 0.586 lb

Lower Plate

$W = \rho \frac{\pi}{4} d^2 t$ = 0.10 (0.785) $(2.90)^2$ (0.35) = 0.231 lb

Upper Plate

$W = \rho \frac{\pi}{4} d^2 t$ = 0.10 (0.785) $(3.00)^2$ (0.35) = 0.247 lb

Lower Cap

$W = \rho \frac{\pi}{4} d^2 t$ = 0.10 (0.785) $(3.00)^2$ (0.39) = 0.275 lb

Allow 20 percent additional for pressure pad and lip.	=	0.055 lb
Total		0.330 lb

Upper Cap

$W = \rho \frac{\pi}{4} d^2 t$ = 0.10 (0.785) $(3.10)^2$ (0.45) = 0.339 lb

Allow 20 percent additional for lug	=	0.068 lb
Total		0.407 lb

Axial Honeycomb

$W = \rho \frac{\pi}{4} d^2 \ell$ = 0.0133 (0.785) $(1.074)^2$ (10.25) = 0.123 lb

Rotational Absorber

$W = \rho A \ell$ = 0.0133 $(0.602)^2$ (5.0) = 0.0241 lb

Swivel

$W = \rho A \ell$ = 0.283 (1.20) (0.5) (0.5) = 0.085 lb

Allow 0.03 lb each for bolts = 0.060 lb

Total 0.145 lb

ARTICULATED LEG WEIGHT ANALYSES

The weight analysis for the articulated leg configurations is a combination of calculated and scaled actual weights from the test model. The use of scaled actual weights gives an accurate weight estimate of assemblies which automatically include fittings, reinforcements, etc. The calculated weights are used for the more straightforward items. The length scale factor from the test model to configuration numbers 3, 4, 5 and 7 is 4.0. The length scale factor from the test model to configuration number 9 is 1.825. A typical scaled weight is of the following form.

$$W = K \frac{\rho}{\rho_{TM}} \frac{\ell}{\ell_{TM}} \frac{A}{A_{TM}} W_{TM} \qquad (107)$$

Where:

W = scaled weight of item

K = estimate of the weight of the item to its assembly weight

ρ/ρ_{TM} = ratio of new material density to the test model material density

A/A_{TM} = ratio of new reference area to the test model area

ℓ/ℓ_{TM} = ratio of new thickness or length to the test model thickness or length

TABLE 23

TELESCOPING LEG WEIGHT BREAKDOWN

Item	Weight (lb)
Lower Leg	0.600
Upper Leg	0.586
Lower Plate	0.231
Upper Plate	0.247
Lower Cap	0.330
Upper Cap	0.407
Swivel	0.145
Axial Honeycomb	0.123
Rotational Honeycomb (4)	0.097
Total Each =	2.766 lbs
Total 4 =	11.064 lbs

System Weight = (11.064) (100) / 300 = 3.69 percent

W_{TM} = actual weight of test model item

The assembly weights of the test model for each leg are given below.

Lower Truss	=	1.27
Upper Truss	=	.82
Parallelogram Absorber	=	1.22
Parallelogram Post	=	2.30
Peg Leg	=	1.10
Total		6.71 lbs

CONFIGURATION NUMBERS 3, 4, 5 AND 7

Upper Truss

$$W = \frac{\rho}{\rho_{TM}} \quad \frac{\ell}{\ell_{TM}} \quad \frac{A}{A_{TM}} \quad W_{TM}$$

$$= \frac{0.074}{0.283}(4)\left(\frac{0.566}{0.0984}\right)(0.82) = 4.80 \text{ lbs}$$

Lower Truss

$$W = \frac{\rho}{\rho_{TM}} \quad \frac{\ell}{\ell_{TM}} \quad \frac{A}{A_{TM}} \quad W_{TM}$$

$$= \frac{0.074}{0.283}(4)\left(\frac{0.329}{0.065}\right)(1.27) = 6.55 \text{ lbs}$$

Peg Leg Strut

$$W = K \quad \frac{\rho}{\rho_{TM}} \quad \frac{\ell}{\ell_{TM}} \quad \frac{A}{A_{TM}} \quad W_{TM}$$

$$= 0.4\left(\frac{0.074}{0.283}\right)(4)\left(\frac{0.841}{0.078}\right)(1.10) = 4.83 \text{ lbs}$$

Peg Leg Ring

$$W = K \frac{\rho}{\rho_{TM}} \frac{\ell}{\ell_{TM}} \frac{A}{A_{TM}} W_{TM}$$

$$= 0.4\ (1)\ (1.14)\ (16)\ (1.10) = 8.02 \text{ lbs}$$

Remainder of Peg Leg

$$W = K \frac{\rho}{\rho_{TM}} \frac{\ell}{\ell_{TM}} \frac{A}{A_{TM}} W_{TM}$$

$$= 0.1\ (1)\ (4)\ (16)\ (1.10) = 7.04 \text{ lbs}$$

Parallelogram Post

$$W = K \frac{\rho}{\rho_{TM}} \frac{\ell}{\ell_{TM}} \frac{A}{A_{TM}} W_{TM}$$

$$= 0.75\ (1)\ (1)\ (16)\ (2.07) = 24.8 \text{ lbs}$$

Remainder of Post

$$W = K \frac{\rho}{\rho_{TM}} \frac{\ell}{\ell_{TM}} \frac{A}{A_{TM}} W_{TM}$$

$$= 0.10\ (1)\ (4)\ (16)\ (2.07) = 13.5 \text{ lbs}$$

Peg Leg Energy Absorber Rod and Link

$$W = K \frac{\rho}{\rho_{TM}} \frac{\ell}{\ell_{TM}} \frac{A}{A_{TM}} W_{TM}$$

$$= 0.15\ \frac{0.10}{0.283}\ (4)\ \frac{0.525}{0.045}\ (2.07) = 5.11 \text{ lbs}$$

Peg Leg Absorber Cap

$$W = \rho A t = 0.10\ (0.785)\left[(3.14)^2 - (0.818)^2\right]\ (0.88) = 0.634 \text{ lb}$$

Parallelogram Absorber Rods

$$W = \rho A \ell = 0.10\ (0.21)\ (24) = 0.503 \text{ lb}$$

Parallelogram Absorber Caps

$$W = \rho A t$$

$$= 0.10\ (0.785)\left[(3.45)^2 - 6(0.52)^2\right]\ (0.62) = 0.500 \text{ lb}$$

Parallelogram Absorber Honeycomb

$$W = \rho A \ell = \frac{23}{1728}\ (8.7)\ (14.5) = 1.68 \text{ lbs}$$

Peg Leg Absorber Honeycomb

$$W = \rho A \ell = \frac{23}{1728}\ (7.2)\ (6) = 0.58 \text{ lb}$$

Peg Leg Cone

$$W = K \frac{\rho}{\rho_{TM}} \frac{\ell}{\ell_{TM}} \frac{A}{A_{TM}} W_{TM}$$

$$= 0.1\ (1)\ (2)\ (16)\ (1.1) = 3.52 \text{ lbs}$$

TABLE 24

ARTICULATED LEG WEIGHT BREAKDOWN
CONFIGURATION NUMBERS 3, 4, 5 AND 7

Item	Weight (lb)
Upper Truss	4.80
Lower Truss	6.55
Peg Leg Strut	4.83
Peg Leg Ring	8.02
Peg Leg Cone	3.52
Remainder of Peg Leg	7.04
Parallelogram Post	24.80
Remainder of Post	13.50
Peg Leg Energy Absorber Rod and Link	5.11
Peg Leg Absorber Cap	0.63
Parallelogram Absorber Rods	3.02
Parallelogram Absorber Caps	1.00
Parallelogram Absorber Honeycomb	1.68
Peg Leg Absorber Honeycomb	0.58
Total Each =	85.08
Total 4 =	340.03

System Weight = (340.03)(100)/3000 = 11.3 percent

Upper Truss

$$W = \frac{\rho}{\rho_{TM}} \quad \frac{\ell}{\ell_{TM}} \quad \frac{A}{A_{TM}} \quad W_{TM}$$

$$= \frac{0.074}{0.283}(4)\left(\frac{0.840}{0.0984}\right) \quad (0.82) = 7.20 \text{ lbs}$$

Lower Truss

$$W = \frac{\rho}{\rho_{TH}} \quad \frac{\ell}{\ell_{TM}} \quad \frac{A}{A_{TM}} \quad W_{TM}$$

$$= \frac{0.074}{0.283}(4)\left(\frac{0.406}{0.065}\right) \quad (1.27) = 8.10 \text{ lbs}$$

Peg Leg Strut

$$W = K \frac{\rho}{\rho_{TM}} \quad \frac{\ell}{\ell_{TM}} \quad \frac{A}{A_{TM}} \quad W_{TM}$$

$$= (0.4)\left(\frac{0.074}{0.283}\right)(4)\left(\frac{1.04}{0.078}\right) \quad (1.10) = 6.09 \text{ lbs}$$

Peg Leg Ring

$$W = K \frac{\rho}{\rho_{TM}} \quad \frac{\ell}{\ell_{TM}} \quad \frac{A}{A_{TM}} \quad W_{TM}$$

$$= 0.4\ (1)\ (1.44)\ (16)\ (1.10) = 10.10 \text{ lbs}$$

Peg Leg Cone

Same as configurations 3, 4, 5 and 7.

$$W = 3.52 \text{ lbs}$$

Remainder of Peg Leg

$$W = K \frac{\rho}{\rho_{TM}} \frac{\ell}{\ell_{TM}} \frac{A}{A_{TM}} W_{TM}$$

$$= 0.10\ (1)\ (5.05)\ (16)\ (1.10) = 8.87 \text{ lbs}$$

Parallelogram Post

$$W = K \frac{\rho}{\rho_{TM}} \frac{\ell}{\ell_{TM}} \frac{A}{A_{TM}} W_{TM}$$

$$= 0.75\ (1) \left(\frac{0.100}{0.083}\right) (16)\ (2.07) = 31.20 \text{ lbs}$$

Remainder of Post

$$W = K \frac{\rho}{\rho_{TM}} \frac{\ell}{\ell_{TM}} \frac{A}{A_{TM}} W_{TM}$$

$$= 0.10\ (1) \left(\frac{0.100}{0.083}\right) (4)\ (16)\ (2.07) = 16.00 \text{ lbs}$$

Peg Leg Energy Absorber Rod and Link

Same as configurations 3, 4, 5 and 7.

W = 5.11 lbs

Peg Leg Absorber Cap

Same as configurations 3, 4, 5 and 7.

W = 0.634 lbs

Parallelogram Absorber Rods

$$W = \rho A \ell = 0.10\ (0.42)\ (24) = 1.01 \text{ lbs}$$

Parallelogram Absorber Caps

$$W = \rho A t = 0.10\ (0.785)\left[(4.89)^2 - 6(0.74)^2\right]\ (0.92) = 1.49 \text{ lbs}$$

Parallelogram Absorber Honeycomb

$$W = \rho A \ell = \frac{23}{1728}\ (17.4)\ (14.5) = 3.36 \text{ lbs}$$

Peg Leg Absorber Honeycomb

Same as configurations 3, 4, 5 and 7.

$$W = 0.634 \text{ lb}$$

CONFIGURATION NUMBER 9

Upper Truss

$$W = \frac{\rho}{\rho_{TM}} \quad \frac{\ell}{\ell_{TM}} \quad \frac{A}{A_{TM}} \quad W_{TM}$$

$$= \frac{0.074}{0.283}\ (1.825)\left(\frac{0.1035}{0.0984}\right)(0.82) = 0.399 \text{ lb}$$

Lower Truss

$$W = \frac{\rho}{\rho_{TM}} \quad \frac{\ell}{\ell_{TM}} \quad \frac{A}{A_{TM}} \quad W_{TM}$$

$$= \frac{0.074}{0.283}\ (1.825)\left(\frac{0.0627}{0.065}\right)(1.27) = 0.568 \text{ lb}$$

TABLE 25

ARTICULATED LEG WEIGHT BREAKDOWN

CONFIGURATION NUMBERS 6 AND 8

Item	Weight (lb)
Upper Truss	7.20
Lower Truss	8.10
Peg Leg Strut	6.09
Peg Leg Ring	10.10
Peg Leg Cone	3.52
Remainder of Peg Leg	8.87
Parallelogram Post	31.20
Remainder of Post	16.00
Peg Leg Energy Absorber Rod and Link	5.11
Peg Leg Absorber Cap	0.63
Parallelogram Absorber Rods	6.06
Parallelogram Absorber Caps	2.98
Parallelogram Absorber Honeycomb	3.36
Peg Leg Absorber Honeycomb	0.63
Total Each =	109.85
Total 4 =	439.4

System Weight = (439.4) (100) / 3000 = 14.8 percent

Peg Leg Strut

$$W = K \frac{\rho}{\rho_{TM}} \frac{\ell}{\ell_{TM}} \frac{A}{A_{TM}} W_{TM}$$

$$= 0.4\left(\frac{0.074}{0.283}\right)(1.825)\left(\frac{0.157}{0.078}\right)(1.1) = 0.413 \text{ lb}$$

Peg Leg Ring

$$W = K \frac{\rho}{\rho_{TM}} \frac{\ell}{\ell_{TM}} \frac{A}{A_{TM}} W_{TM}$$

$$= 0.4\ (1)\ (0.432)\ (1.825)^2\ (1.10) = 0.634 \text{ lb}$$

Peg Leg Cone

$$W = K \frac{\rho}{\rho_{TM}} \frac{\ell}{\ell_{TM}} \frac{A}{A_{TM}} W_{TM}$$

$$= 0.1\ (1)\ (0.81)\ (1.825)^2\ (1.1) = 0.30 \text{ lb}$$

Remainder of Peg Leg

$$W = K \frac{\rho}{\rho_{TM}} \frac{\ell}{\ell_{TM}} \frac{A}{A_{TM}} W_{TM}$$

$$= 0.1\ (1)\ (1.825)\ (1.825)^2\ (1.10) = 0.669 \text{ lb}$$

Parallelogram Post

$$W = K \frac{\rho}{\rho_{TM}} \frac{\ell}{\ell_{TM}} \frac{A}{A_{TM}} W_{TM}$$

$$= 0.75\ (1)\left(\frac{0.0344}{0.083}\right)(1.825)^2\ (2.07) = 2.14 \text{ lbs}$$

Remainder of Post

$$W = K \frac{\rho}{\rho_{TM}} \frac{\ell}{\ell_{TM}} \frac{A}{A_{TM}} W_{TM}$$

$$= 0.10\ (1)\ (1.825)\ (1.825)^2\ (2.07) = 1.27 \text{ lbs}$$

Peg Leg Energy Absorber Rod and Link

$$W = K \frac{\rho}{\rho_{TM}} \frac{\ell}{\ell_{TM}} \frac{A}{A_{TM}} W_{TM}$$

$$= 0.15 \left(\frac{0.10}{0.283}\right) (1.825) \left(\frac{0.102}{0.045}\right) (2.07) = 0.455 \text{ lb}$$

Peg Leg Absorber Cap

$$W = \rho A t = 0.10\ (0.785) \left[(1.76)^2 - (1.138)^2\right] (0.25) = 0.035 \text{ lb}$$

Parallelogram Absorber Rods

$$W = \rho A \ell = 0.10\ (0.039)\ (11.0) = 0.043 \text{ lb}$$

Parallelogram Absorber Caps

$$W = \rho A t = 0.1\ (0.785) \left[(1.48)^2 - 6(0.23)^2\right] (0.43) = 0.072 \text{ lb}$$

Parallelogram Absorber Honeycomb

$$W = \rho A \ell = \frac{23}{1728} (1.61)\ (6.65) = 0.14 \text{ lb}$$

Peg Leg Absorber Honeycomb

$$W = \rho A \ell = \frac{23}{1728} (1.41)\ (2.74) = 0.05 \text{ lb}$$

TABLE 26

ARTICULATED LEG WEIGHT BREAKDOWN

CONFIGURATION NUMBER 9

Item	Weight (lb)
Upper Truss	0.399
Lower Truss	0.568
Peg Leg Strut	0.413
Peg Leg Ring	0.634
Peg Leg Cone	0.300
Remainder of Peg Leg	0.669
Parallelogram Post	2.140
Remainder of Post	1.270
Peg Leg Energy Absorber Rod and Link	0.455
Peg Leg Absorber Cap	0.035
Parallelogram Absorber Rods	0.258
Parallelogram Absorber Caps	0.144
Parallelogram Absorber Honeycomb	0.140
Peg Leg Absorber Honeycomb	0.050
Total Each =	7.475
Total 4 =	29.90

System Weight = (29.90) (100) / 300 = 10.0 percent

APPENDIX VI

EXPERIMENTAL PHASE

The experimental phase was conducted to provide data for correlation with predicted acceleration time-histories obtained from the digital simulation. A series of eleven drops was performed for two scaled configurations of the articulated leg alightment system. Impact conditions were varied to permit two and three-dimensional motion of the space capsule model. The six rigid body accelerations of the capsule were monitored with accelerometers and a telemetry system.

Test Model

The test model was designed to be both a scale model of a 3000 pound and a 300 pound capsule. This permitted using it as both a "soft" and "hard" lander by merely changing the aluminum honeycomb energy cells' crushing force. Figure 107 shows the test capsule in a pre-drop configuration.

The test model as used in the test program has the following weight and inertia characteristics:

Total Weight	228.7 lb (including legs)
Leg Weight	31.2 lb
Pitch and Yaw Inertia	3.326 slug-ft^2
Roll Inertia	2.77 slug-ft^2
Center of Gravity	0.33 feet above lower parallelogram pivots and on the vertical axis

Scaling of the test capsule to the 3000 pound and 300 pound capsule was accomplished by applying the following scale factors to the test model parameters. The scaling technique is described in Reference 11.

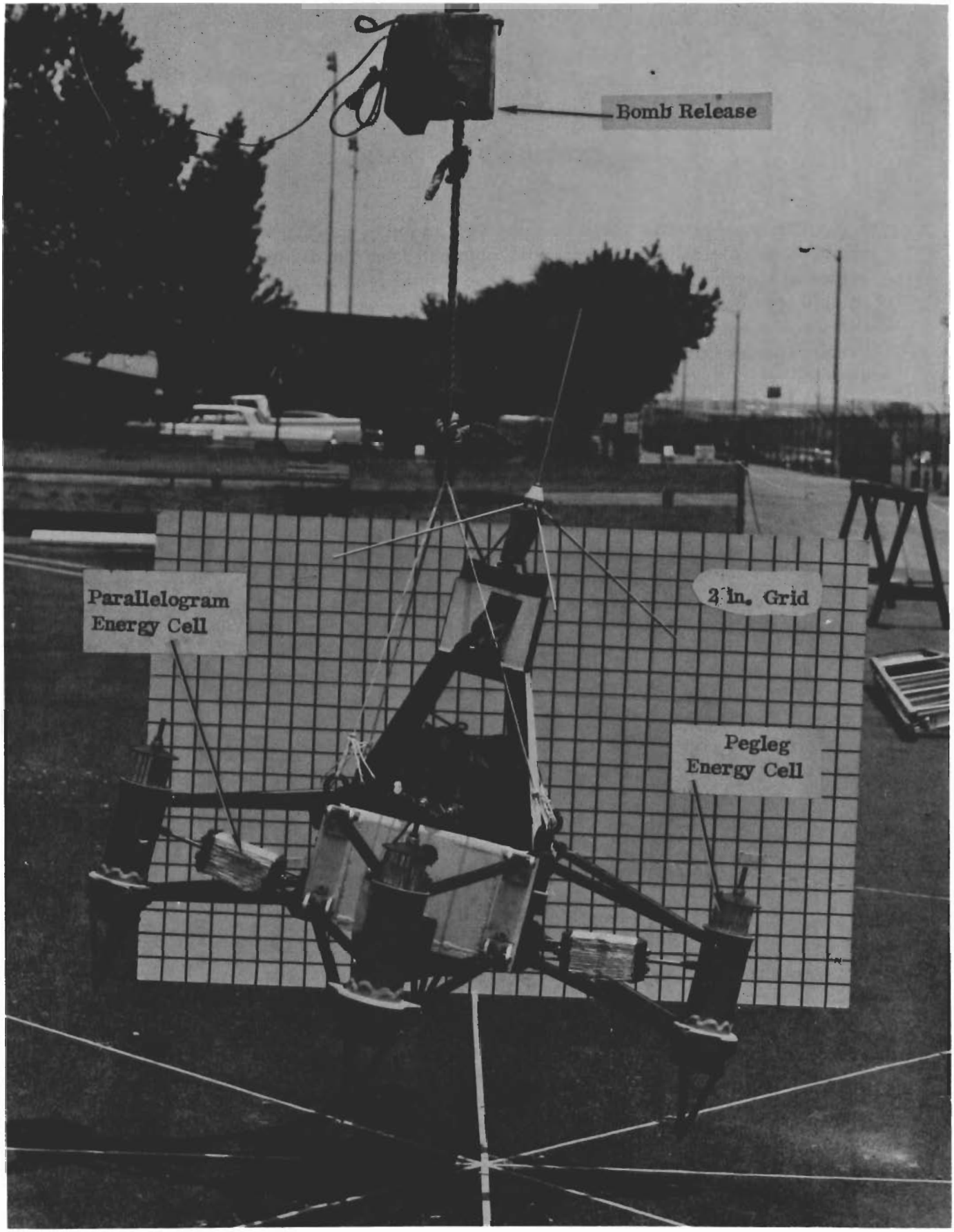

Figure 107 Pre-test view of Test Model

TABLE 27

SCALING FACTORS

Parameter	3000 Pound Capsule	300 Pound Capsule
Acceleration	1.	1.
Length	4.	1.825
Mass	15.2	1.52
Angular Velocity	.5	.739
Energy	60.8	2.78
Force	15.2	1.52
Mass Density	.238	2.5
Mass Moment of Inertia	243.	5.08
Pressure, Stress	.95	.455
Spring Rate	3.8	.833
Time	2.	1.35
Velocity	2.	1.35

The only difficulty encountered during the test program was binding of the parallelogram energy absorber loading pads. Figure 107 shows the locations of parallelogram energy cells. The end pads were provided with guide rods located in the center of the loading area. During the crushing of the aluminum honeycomb the loading pads would not remain normal to the honeycomb cells and binding occurred between the center guide rod and loading pad. This effect is illustrated in the following sketch.

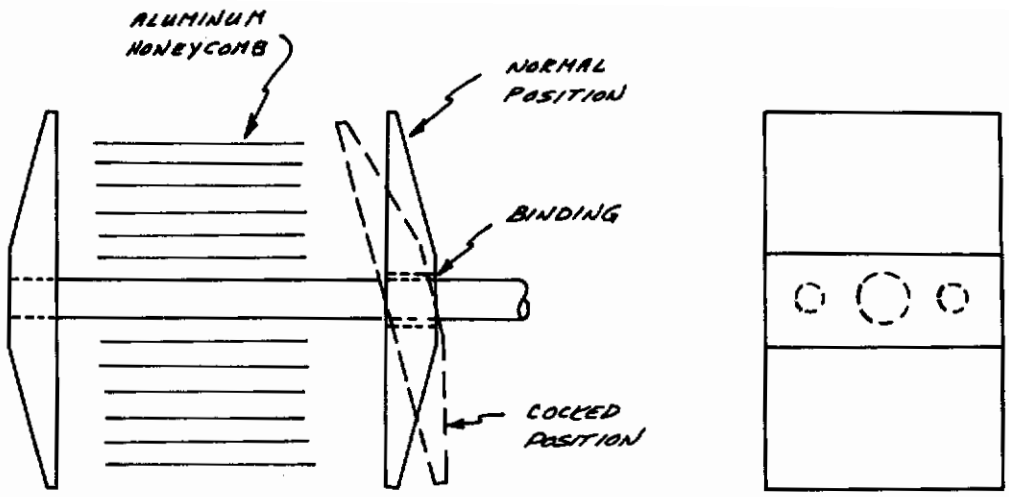

Two effects on capsule response were noted. Deceleration levels were higher than predicted due to the additional force generated by binding and excessive rebound of the capsule occurred due to an increase in the energy stored in elastic deformation of the guide rods.

Future testing should include measuring the forces in the individual energy cells during the drops.

Test Technique

The basic test technique consisted of measuring the static crushing force of each energy cell, establishing the desired capsule angular position relative to the velocity vectors and dropping the capsule from the height required to achieve the desired vertical velocity. Horizontal velocity was generated using a traveling crane with a radius of 40 feet. The crane boom was rotated at an angular velocity commensurate with the desired horizontal velocity.

Post drop measurements consisted of measuring the permanent deflection of each honeycomb cell.

A typical drop test was performed as follows:

1. Measure and record individual honeycomb height and crushing force and the energy cell in which used.

2. Adjust capsule angular position to desired attitude relative to the velocity vectors.

3. Perform pre-test telepak calibration.

4. Raise capsule to required height to generate vertical velocity.

5. If a horizontal velocity is required, rotate the crane at least two complete revolutions to check horizontal velocity.

6. Drop capsule.

7. Perform post-test telepak calibration.

8. Measure permanent deflection in each aluminum honeycomb energy cell.

Two orthogonally oriented high speed cameras were used to record the actual impact. Post-test analysis of the films was used to establish capsule attitude and velocities immediately prior to impact.

Test Instrumentation

Six accelerometer channels comprised the primary instrumentation for the test program. The accelerometers were mounted in pairs to permit both angular and translation accelerations for the six rigid body coordinates to be measured. A telepak was assembled using a REDEYE missile transmitter, mixer and sub-carrier oscillator assembly. Standard dry cells and mercury batteries were used as a power source and chosen to permit the total sequence of drops to be performed without a battery change. A block diagram of the system is shown in Figure 108. The telepak mounted on the test model is shown in Figure 109.

The accelerometers were calibrated individually against a secondary standard. Each test accelerometer's output was compared to a standard accelerometer while both were being subjected to sinusoidal vibration from 20-2000 cps at two different acceleration levels. The following block diagram illustrates the method.

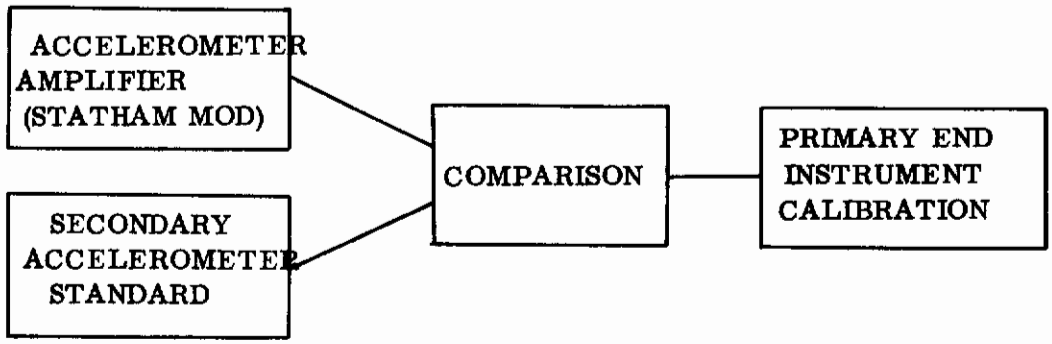

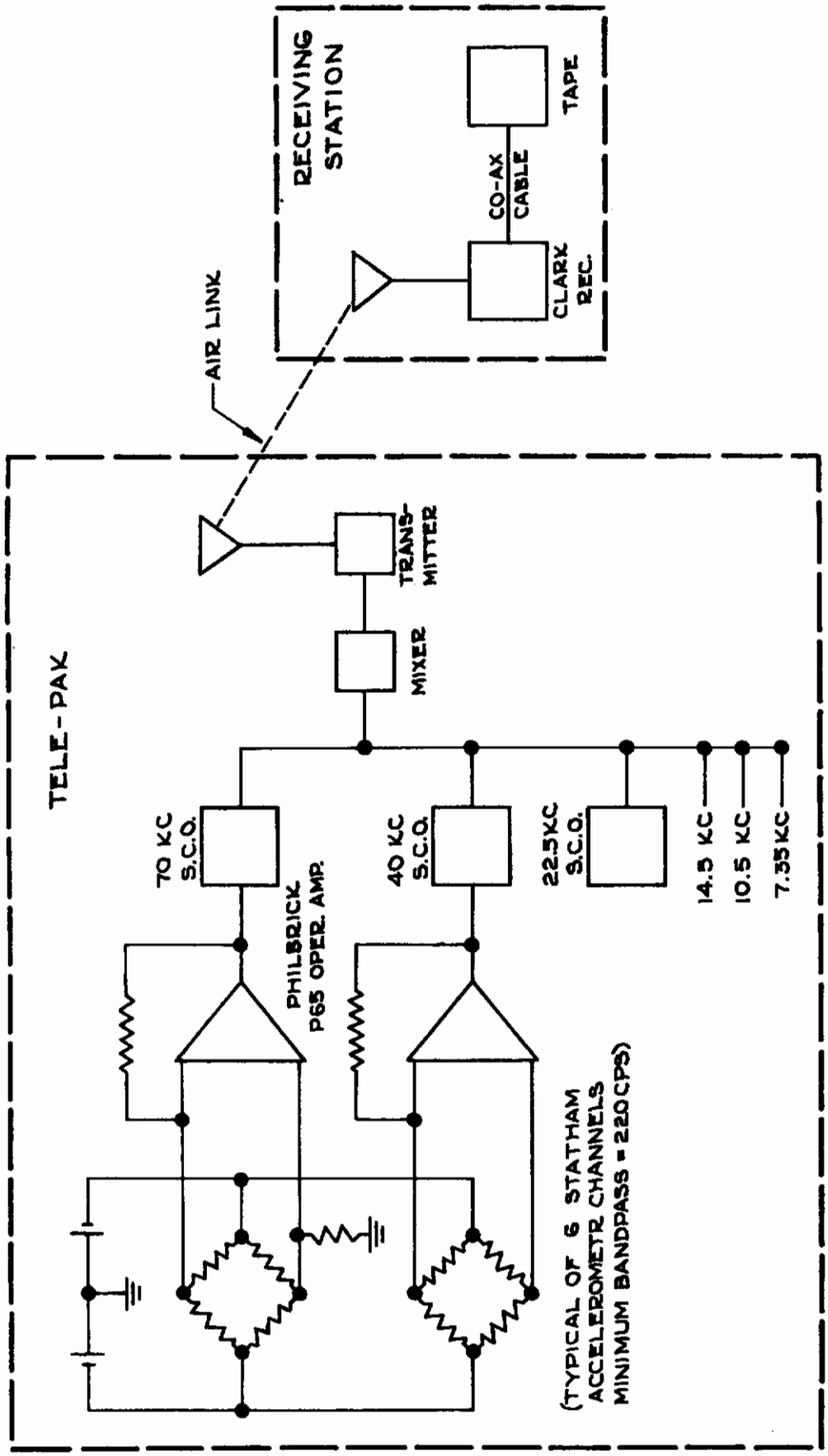

Figure 108: Block Diagram of Telemetry System

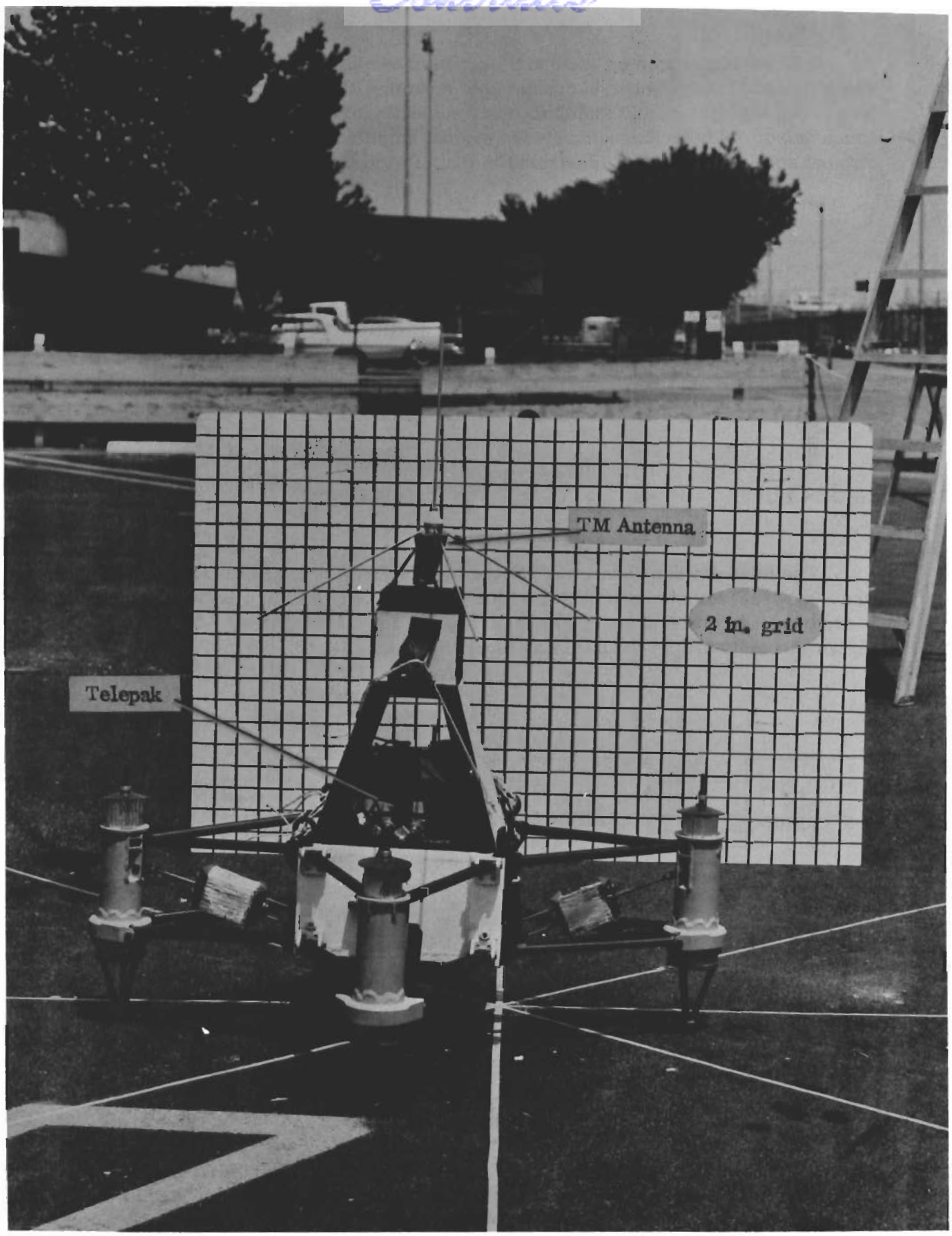

Figure 109 Post Test View of Test Model

The telemetry system (with airlink) was then calibrated using a known shock pulse. This calibration consisted of mounting all six of the accelerometers on a shock test fixture and simultaneously subjecting them to a 50 g trapezoidal shock pulse. This technique combined system amplitude calibration with a channel sense check and is illustrated in the following block diagram.

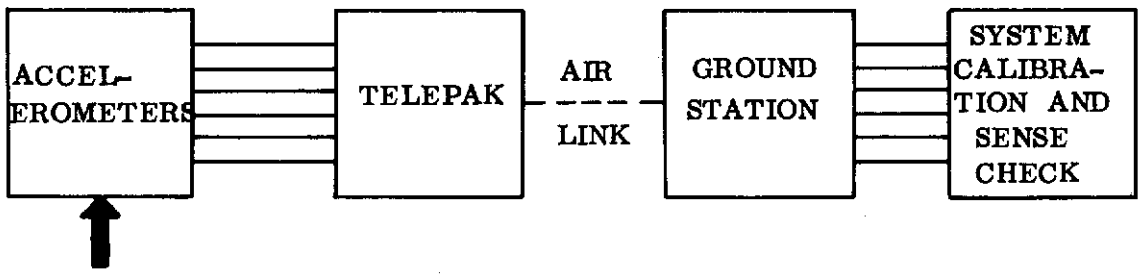

The telepak when connected into the telemetry system was also subjected to a 50 g, trapezoidal shock pulse, with a 0.001 second rise time and a 0.015 second dwell to evaluate its functional capability for the drop tests. This is shown schematically in the following block diagram.

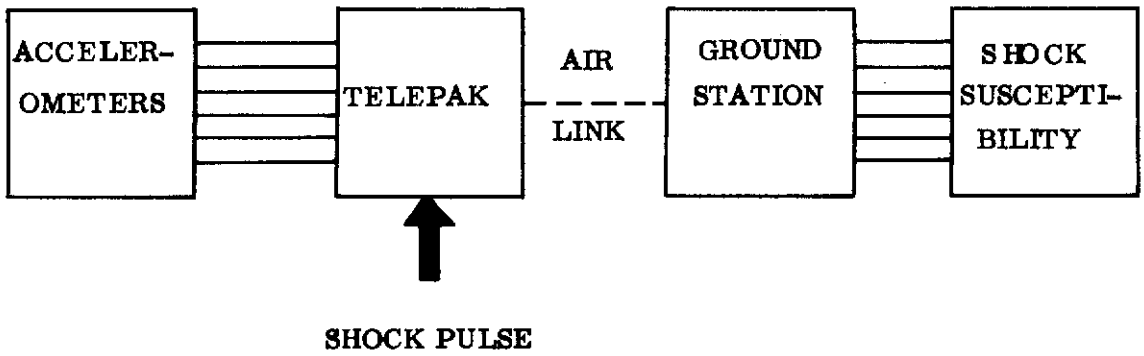

No output occurred on any of the accelerometer channels for this test. On the basis of this test, all of the accelerations obtained during the test program are bona fide capsule acceleration time-histories.

A calibration was also performed immediately prior to and after each drop. This consisted of unbalancing each accelerometer bridge to two known acceleration levels in both a positive and negative direction.

Test Data Reduction

All test data was reduced using digital techniques. The overall method is shown in a block diagram in Figure 110. Each drop test was digitized simultaneously with an oscillographic playback. A single pass was made through the digitizer writing a multiplexed, raw data tape. The oscillographic record was used to determine the adequacy of the analog tape and to determine the required length of the digital file.

The multiplexed, raw data tape was then placed on an IBM 1401 computer and each accelerometer channel stripped out and placed in a single file. This operation also added a correction for the time lag resulting from the multiplexing during digitization. The files corresponding to each accelerometer pair were then added or subtracted point by point and the appropriate calibration factor applied. The resulting tape was in a format suitable for use on an IBM 7044 and represented each of the six capsule rigid body accelerations.

A shock spectra for the vertical translational acceleration (XDD(3)) was then computed and a plotting tape written for the six accelerations for each drop. The accelerations were then plotted using a Benson-Lehner plotter and were in a format such that the plotting tape written by the digital simulation could be plotted directly on the test data plot.

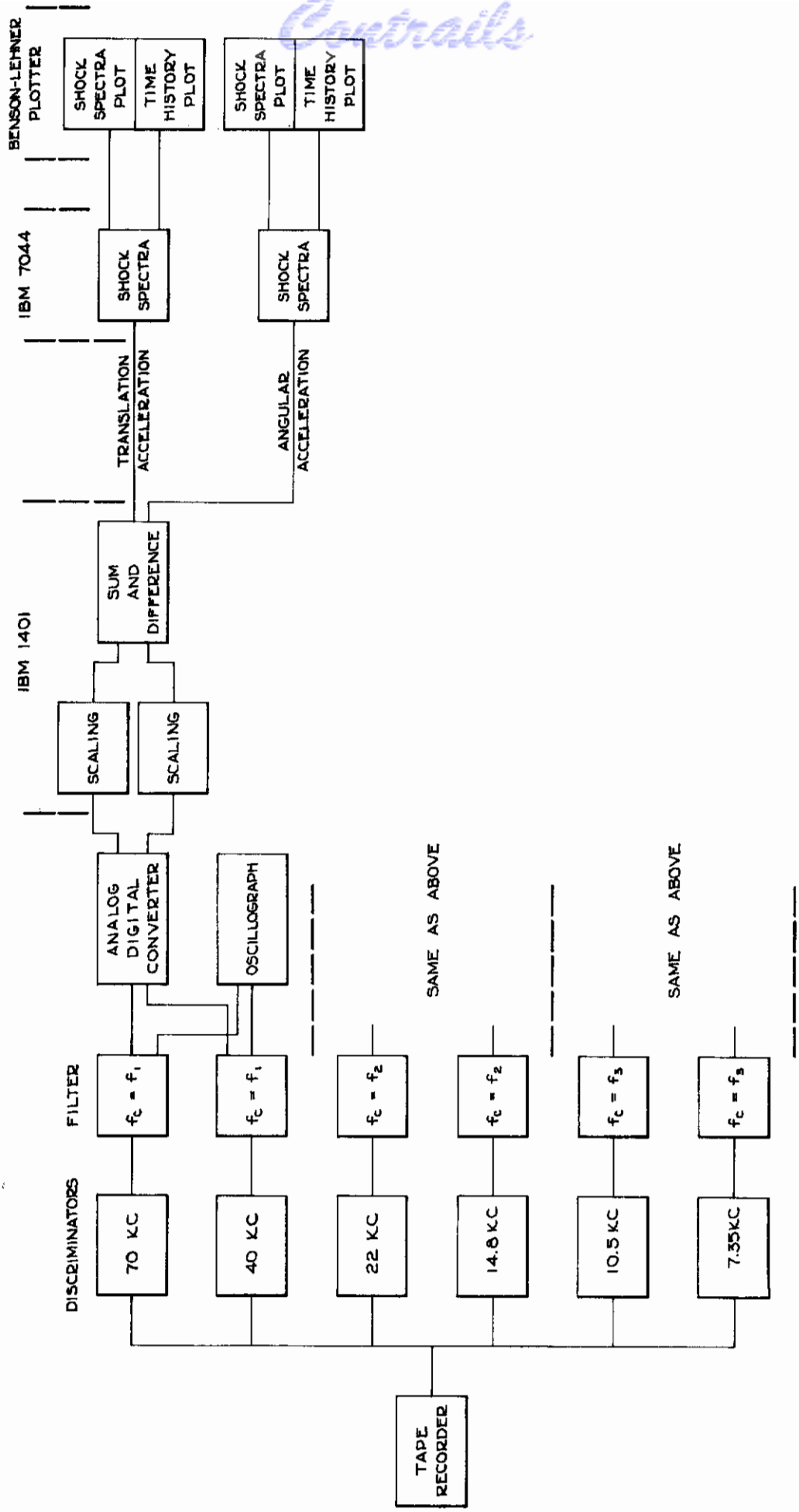

Figure 110, Data Reduction Technique

APPENDIX VII

SOURCE LISTINGS OF DIGITAL SIMULATIONS

Two different digital computer programs are used for the alightment dynamics simulation. The same basic approach is used in both the telescoping leg and articulated leg simulations. However, the simulations were programmed and debugged intermittently, which resulted in little interchangeability between the two programs. Both simulations use the same Differential Equation Monitor for the numerical integration of the equations of motion.

The Differential Equation Monitor consists of the following routines: MAIN, SETUP, ENDFOR, PANIC, PRINT, ADD, CONTRT, HEADNG , INTEG, INTG, PRINTP, SIX, and ARCTAN. The Differential Equation Monitor routines are all written in IBM FORTRAN IV except subroutine SIX. Subroutine SIX sets up the indirect addressing for FORTRAN and must be written in an assembly language. The routine SIX in the listings of this report is written in the IBM MAP language for use on IBM 7044, 7094, and 7044/7094 coupled digital computers.

There are two subroutines as well as the entire Differential Equation Monitor which are common to both the telescoping leg and articulated leg configurations. These are subroutines TIMPIC and SUBLHX.

The telescoping leg configurations simulation is composed of the following subroutines in addition to the Differential Equation Monitor and the two common subroutines above: FUNEV, FORCE, CURVE, SLIP, QUIMOT, and BOUNCE.

The articulated leg configurations simulation is composed of the following subroutines in addition to the Differential Equation Monitor and the two common subroutines above: FUNEV, FORCE, CURVE, SINALP, BRUTE, QUIMOT, and BOUNCE.

The following subroutine names appear in both simulations and have similar functions but are different: FUNEV, FORCE, CURVE, QUIMOT, and BOUNCE.

```
$IBFTC SETUP   LIST,DECK
      SUBROUTINE SETUP
      DIMENSION FTEXIT(20),XNOISE(8),DERTIV(100),ENTRAL(100),NCOLUM(10),     0020
     1FPTH(14),FPTT(200),FPTV(200),ADSSPT(90),CONVER(90),TIMERC(22),EXAC     0030
     2TC(21),DELTC(21),INDC(21),DELPTC(21),NDEGPC(21),IEXPPC(21),IDEGPC(     0040
     321),NOISEC(21),INTILC(21),CHGSUB(21),TIMEIC(61),VRCHAD(60),VRVLAD(     0050
     460),Q(200)                                                             0060
      COMMON  TIME   , DELT   , NSTART , NFIRST , NEXIT  , IPASS
      COMMON  TIME1  , XNOISE , RMT    , DELMTN , DELMTE , DELMTD
      COMMON  ADSSPT , CONVER , CHGSUB , DELMAX , DELMIN , DELTPT
      COMMON  DELPTC , DELTC  , EMAX   , EMIN   , EXACTC , FPTH               0130
      COMMON  FPTT   , FPTV   , FTEXIT , IC     , ICH    , ICHANG            0140
      COMMON  IDEGPC , IDEGPT , IEXPPC , IEXPPT , IND    , INDC              0150
      COMMON  INTILC , JCH    , M      , MCH    , NCHANG , NCOLUM            0160
      COMMON  ND     , NDEGPC , NDEGPT , NOISE  , NOISEC , NPAGES            0170
      COMMON  NPVAR  , NWORDS , RANDOM , TCKERR , TIMAX  , TIMEAD            0180
      COMMON  TIMECH , TIMEIC , TIMEND , TIMEPT , TIMERC , VRCHAD            0190
      COMMON  VRVLAD , DERTIV , ENTRAL , Q                                   0200
      DATA BLANK,RANDOX/0606060606060,0343277244615/
C
C     SETUP FOR RUNGE-KUTTA-MERSON INTEGRATION
C
    5 READ(5,151)(FPTH(I),I=1,14)
      READ(5,160)TIME,DELT,TIMEND,DELTPT,NDEGPT
      READ(5,170)IND
      IF(DELT)10,10,13
   10 WRITE(6,180)DELT
      CALL EXIT
   13 IF(IND.EQ.1)GO TO 90
      MIND=1
      WRITE (6,43)IND,MIND                                                   0490
   43 FORMAT(1H1////,30X,8HDEAR SIR//35X,50HSOMEBODY GOOFED. THE TYPE OF     0500
     1 INTEGRATION SPECIFIED/30X,23HON THE CONTROL CARD IS I4,22H. THIS      0510
     2WAS CHANGED TO I2/30X,42HAND EXECUTED. PLEASE PROOF-READ YOUR DATA     0520
     3.//55X12H THE MONITOR)
      IND=MIND                                                               0540
   90 M=0                                                                    0950
      DO 96 I=1,10                                                           1030
   96 NCOLUM(I)=0                                                            1040
   98 NPVAR=0                                                                1120
      NEXIT=0                                                                1130
      NWORDS=0                                                               1160
      NCHANG=0
      NOISE=0
      TIME1=0.0
      NSTART=1                                                               1140
      NPAGES=1                                                               1150
      NFIRST=1                                                               1200
      IPASS=-1
      DO 100 I=1,20
  100 FTEXIT(I)=BLANK
      RANDOM=RANDOX                                                 SETUP
      CALL PRINT(NWORDS,NCOLUM,NPAGES,NPVAR,NSTART)                          1180
      TIMEPT=TIME                                                            1190
      CALL FUNEV                                                             1250
      NSTART=0                                                               1270
      CALL ENDFOR                                                            1280
      IF(NCOLUM(NPAGES))150,130,150                                          1290
  130 NPAGES=NPAGES-1                                                        1300
      IF(NPAGES.EQ.0)CALL PANIC(45HO NO VARIABLES HAVE BEEN SET UP FOR P
```

```
     1RINTING 1
  150 CALL HEADNG
      CALL FUNEV
      IPASS=0
      NFIRST=0                                                          1460
      CALL CONTRT                                                       1490
      ASSIGN 5 TO N                                                     1500
      GO TO N,(5,1000)                                                  1510
  151 FORMAT(14A6)
  160 FORMAT(4F10.2,I10)
  170 FORMAT(I10)
  180 FORMAT(45H1 THE MONITOR CANNOT OPERATE WITH A DELT OF  F10.4)
 1000 RETURN                                                            1530
      END                                                               1690
$IBFTC ENDFOR  LIST,DECK
      SUBROUTINE ENDFOR
      DIMENSION FTEXIT(20),XNOISE(8),DERTIV(100),ENTRAL(100),NCOLUM(10),     0030
     1FPTH(14),FPTT(200),FPTV(200),ADSSPT(90),CONVER(90),TIMERC(22),EXAC     0040
     2TC(21),DELTC(21),INDC(21),DELPTC(21),NDEGPC(21),IEXPPC(21),IDEGPC(     0050
     321),NOISEC(21),INTILC(21),CHGSUB(21),TIMEIC(61),VRCHAD(60),VRVLAD(     0060
     460),Q(200)                                                             0070
      COMMON  TIME   , DELT   , NSTART , NFIRST , NEXIT  , NSUBRT           0100
      COMMON  NTARGT , XNOISE , RMT    , DELMTN , DELMTE , DELMTD           0110
      COMMON  ADSSPT , CONVER , CHGSUB , DELMAX , DELMIN , DELPT            0120
      COMMON  DELPTC , DELTC  , EMAX   , EMIN   , EXACTC , FPTH            0130
      COMMON  FPTT   , FPTV   , FTEXIT , IC     , ICH    , ICHANG           0140
      COMMON  IDEGPC , IDEGPT , IEXPPC , IEXPPT , IND    , INDC             0150
      COMMON  INTILC , JCH    , M      , MCH    , NCHANG , NCOLUM           0160
      COMMON  ND     , NDEGPC , NDEGPT , NOISE  , NOISEC , NPAGES           0170
      COMMON  NPVAR  , NWORDS , RANDOM , TCKERR , TIMAX  , TIMEAD           0180
      COMMON  TIMECH , TIMEIC , TIMEND , TIMEPT , TIMERC , VRCHAD           0190
      COMMON  VRVLAD , DERTIV , ENTRAL , Q                                  0200
      DATA RPAREN,SAVEW/0000000000034,0777777777700/                  ENDFOR
      FPTV(NWORDS)=OR(AND(FPTV(NWORDS),SAVEW),RPAREN)
      RETURN
      END
$IBFTC PANIC   LIST,DECK
      SUBROUTINE PANIC(FEAR)                                            0010
      COMMON/PAIN/ NPLOT
      DIMENSION FTEXIT(20),XNOISE(8),DERTIV(100),ENTRAL(100),NCOLUM(10),     0020
     1FPTH(14),FPTT(200),FPTV(200),ADSSPT(90),CONVER(90),TIMERC(22),EXAC     0030
     2TC(21),DELTC(21),INDC(21),DELPTC(21),NDEGPC(21),IEXPPC(21),IDEGPC(     0040
     321),NOISEC(21),INTILC(21),CHGSUB(21),TIMEIC(61),VRCHAD(60),VRVLAD(     0050
     460),Q(200),FEAR(20)
      COMMON  TIME   , DELT   , NSTART , NFIRST , NEXIT  , NSUBRT           0100
      COMMON  NTARGT , XNOISE , RMT    , DELMTN , DELMTE , DELMTD           0110
      COMMON  ADSSPT , CONVER , CHGSUB , DELMAX , DELMIN , DELTPT           0120
      COMMON  DELPTC , DELTC  , EMAX   , EMIN   , EXACTC , FPTH            0130
      COMMON  FPTT   , FPTV   , FTEXIT , IC     , ICH    , ICHANG           0140
      COMMON  IDEGPC , IDEGPT , IEXPPC , IEXPPT , IND    , INDC             0150
      COMMON  INTILC , JCH    , M      , MCH    , NCHANG , NCOLUM           0160
      COMMON  ND     , NDEGPC , NDEGPT , NOISE  , NOISEC , NPAGES           0170
      COMMON  NPVAR  , NWORDS , RANDOM , TCKERR , TIMAX  , TIMEAD           0180
      COMMON  TIMECH , TIMEIC , TIMEND , TIMEPT , TIMERC , VRCHAD           0190
      COMMON  VRVLAD , DERTIV , ENTRAL , Q                                  0200
      DATA Q000CT,Q001CT/0777777777777,0606060606060/
      FEND=Q000CT                                                       0350
      DO 20 I=1,20                                                      0360
      IF(FEAR(I)-FEND) 20,30,20
   20 FTEXIT(I)=FEAR(I)
```

```
   30 IF(NSTART.NE.0)GO TO 70
      IF(NEXIT) 40,43,43
   43 GO TO (48,58),NPLOT
   48 WRITE(7,49)
   49 FORMAT(6H 1     )
      END FILE 7
   58 IF(NEXIT)40,60,50
   40 NEXIT=1                                                          0410
      CALL PRINTP                                                      0420
      NEXIT=0                                                          0430
      TIMEPT=TIME+DELTPT                                               0440
      WRITE (6,45)(FTEXIT(I),I=1,20)                                   0450
   45 FORMAT(1HO//20A6)                                                0460
      DO 46 I=1,20                                                     0470
   46 FTEXIT(I)=Q001CT                                                 0490
      GO TO 100                                                        0500
   50 CALL PRINTP                                                      0510
      WRITE (6,45)(FTEXIT(I),I=1,20)                                   0520
      CALL DUMP                                                        0530
   60 NEXIT=1
      CALL PRINTP
   70 NEXIT=0
      WRITE (6,45)(FTEXIT(I),I=1,20)                                   0550
      CALL SETUP                                                       0560
  100 RETURN                                                           0570
      END                                                              0580
$I8FTC PRINT   LIST,DECK
      SUBROUTINE PRINT(HEAD,FORM,VAR,IDP,CON)                          0010
      DIMENSION HEAD(2),FORM(2),PTITLE(2),PFORM(2)                     0020
      DIMENSION FTEXIT(20),XNOISE(8),DERTIV(100),ENTRAL(100),NCOLUM(10),  0030
     1FPTH(14),FPTT(200),FPTV(200),ADSSPT(90),CONVER(90),TIMERC(22),EXAC  0040
     2TC(21),DELTC(21),INDC(21),DELPTC(21),NDEGPC(21),IEXPPC(21),IDEGPC(  0050
     321),NOISEC(21),INTILC(21),CHGSUB(21),TIMEIC(61),VRCHAD(60),VRVLAD(  0060
     460),Q(200)                                                       0070
      COMMON  TIME   , DELT   , NSTART , NFIRST , NEXIT  , NSUBRT      0100
      COMMON  NTARGT , XNOISE , RMT    , DELMTN , DELMTE , DELMTD      0110
      COMMON  ADSSPT , CONVER , CHGSUB , DELMAX , DELMIN , DELTPT      0120
      COMMON  DELPTC , DELTC  , EMAX   , EMIN   , EXACTC , FPTH        0130
      COMMON  FPTT   , FPTV   , FTEXIT , IC     , ICH    , ICHANG      0140
      COMMON  IDEGPC , IDEGPT , IEXPPC , IEXPPT , IND    , INDC        0150
      COMMON  INTILC , JCH    , M      , MCH    , NCHANG , NCOLUM      0160
      COMMON  ND     , NDEGPC , NDEGPT , NOISE  , NOISEC , NPAGES      0170
      COMMON  NPVAR  , NWORDS , RANDOM , TCKERR , TIMAX  , TIMEAD      0180
      COMMON  TIMECH , TIMEIC , TIMEND , TIMEPT , TIMERC , VRCHAD      0190
      COMMON  VRVLAD , DERTIV , ENTRAL , Q                             0200
      IF(NWORDS)5,2,5                                                  0340
      DATA Q000CT,Q001CT,Q002CT,Q003CT/0006060606063,0314425606060,07401
     130602601,0013304606060/
    2 PTITLE(1)=Q000CT                                                PRINT
      PTITLE(2)=Q001CT                                                 0380
      PFORM(1)=Q002CT                                                  0400
      PFORM(2)=Q003CT                                                  0420
      GO TO 50                                                         0430
    5 IF(NDEGPT-IDP)100,20,20
   20 NCOLUM(NPAGES)=NCOLUM(NPAGES)+1                                  0470
      DO 30 I=1,2                                                      0480
      NWORDS=NWORDS+1                                                  0490
      FPTT(NWORDS)=HEAD(I)
   30 FPTV(NWORDS)=FORM(I)
      NPVAR=NPVAR+1                                                    0530
```

```
      CONVER(NPVAR)=CON                                                  0540
      ADSSPT(NPVAR)=ADRS(VAR)                                            0550
      IF( 9-NCOLUM(NPAGES))40,40,100                                     0560
   40 IF(10-NPAGES)100,100,45
   45 CALL ENDFOR
      NPAGES=NPAGES+1                                                    0600
      NCOLUM(NPAGES)=0
   50 DO 60 I=1,2                                                        0620
      NWORDS=NWORDS+1                                                    0630
      FPTT(NWORDS)=PTITLE(I)                                             0640
   60 FPTV(NWORDS)=PFORM(I)                                              0650
  100 IF(90-NPVAR)110,120,120                                            0660
  110 WRITE(6,115)
  115 FORMAT(50HOMORE THAN 90 VARIABLES HAVE BEEN SET UP FOR PRINT)
      CALL EXIT
  120 RETURN                                                             0680
      END                                                                0690
$IBFTC ADD      LIST,DECK
      SUBROUTINE ADD(X,X1,A,B,C)
      DOUBLE PRECISION DA, DB, DX, DX1
      DA=A
      DX=X
      DX1=X1
      DB=DA + DX + DX1
      B=DB
      C=DB - B
      RETURN
      END
$IBFTC CONTRT  LIST,DECK
      SUBROUTINE CONTRT                                                  0010
      DIMENSION FTEXIT(20),XNOISE(8),DERTIV(100),ENTRAL(100),NCOLUM(10),  0020
     1FPTH(14),FPTT(200),FPTV(200),ADSSPT(90),CONVER(90),TIMERC(22),EXAC  0030
     2TC(21),DELTC(21),INDC(21),DELPTC(21),NDEGPC(21),IEXPPC(21),IDEGPC(  0040
     321),NOISEC(21),INTILC(21),CHGSUB(21),TIMEIC(61),VRCHAD(60),VRVLAD(  0050
     460),Q(200)                                                         0060
      COMMON  TIME   , DELT   , NSTART , NFIRST , NEXIT  , NSUBRT        0100
      COMMON  NTARGT , XNOISE , RMT    , DELMTN , DELMTF , DELMTD        0110
      COMMON  ADSSPT , CONVER , CHGSUB , DELMAX , DELMIN , DELTPT
      COMMON  DELPTC , DELTC  , EMAX   , EMIN   , EXACTC , FPTH         0130
      COMMON  FPTT   , FPTV   , FTEXIT , IC     , ICH    , ICHANG       0140
      COMMON  IDEGPC , IDEGPT , IEXPPC , IEXPPT , IND    , INDC         0150
      COMMON  INTILC , JCH    , M      , MCH    , NCHANG , NCOLUM       0160
      COMMON  ND     , NDEGPC , NDEGPT , NOISE  , NOISEC , NPAGES       0170
      COMMON  NPVAR  , NWORDS , RANDOM , TCKERR , TIMAX  , TIMEAD       0180
      COMMON  TIMECH , TIMEIC , TIMEND , TIMEPT , TIMERC , VRCHAD       0190
      COMMON  VRVLAD , DERTIV , ENTRAL , Q                              0200
C
C     CONTRT FOR RUNGE-KUTTA-MERSON INTEGRATION
C
   20 IF(TIMEPT-(TIME+DELT/5.0))25,25,60
   25 CALL PRINTP                                                       0390
      TIMEPT=TIME+DELTPT                                                0400
   60 CALL INTEG                                                        0530
      IF(TIMEND-(TIME+DELT/5.0))170,170,20
  170 NEXIT=1                                                           0850
      CALL PRINTP                                                       0860
      WRITE (6,180)                                                     0870
  180 FORMAT(24HOFLIGHT TIME HAS RUN OUT )                              0920
      CALL HEADNG
      NFIRST=1
```

```
      CALL FUNFV                                                          0890
      RETURN
      END                                                                 0930
$IBFTC HEADNG  LIST,DECK
      SUBROUTINE HEADNG
C
C     PRINT HEADING AND INITIAL CONDITIONS
C
      DIMENSION FTEXIT(20),XNOISE(8),DERTIV(100),ENTRAL(100),NCOLUM(10),  0020
     1FPTH(14),FPTT(200),FPTV(200),ADSSPT(90),CONVER(90),TIMERC(22),EXAC  0030
     2TC(21),DELTC(21),INDC(21),DELPTC(21),NDEGPC(21),IEXPPC(21),IDEGPC(  0040
     321),NOISEC(21),INTILC(21),CHGSUB(21),TIMEIC(61),VRCHAD(60),VRVLAD(  0050
     460),Q(200)                                                          0060
      COMMON  TIME   , DELT   , NSTART , NFIRST , NEXIT  , NSUBRT         0100
      COMMON  NTARGT , XNOISE , RMT    , DELMTN , DELMTE , DELMTD         0110
      COMMON  ADSSPT , CONVER , CHGSUB , DELMAX , DELMIN , DELTPT
      COMMON  DELPTC , DELTC  , EMAX   , EMIN   , EXACTC , FPTH          0130
      COMMON  FPTT   , FPTV   , FTEXIT , IC     , ICH    , ICHANG         0140
      COMMON  IDEGPC , IDEGPT , IEXPPC , IEXPPT , IND    , INDC           0150
      COMMON  INTILC , JCH    , M      , MCH    , NCHANG , NCOLUM         0160
      COMMON  ND     , NDEGPC , NDEGPT , NOISE  , NOISEC , NPAGES         0170
      COMMON  NPVAR  , NWORDS , RANDOM , TCKERR , TIMAX  , TIMEAD         0180
      COMMON  TIMECH , TIMEIC , TIMEND , TIMEPT , TIMERC , VRCHAD         0190
      COMMON  VRVLAD , DERTIV , ENTRAL , Q                                0200
      WRITE(6,210)(FPTH(I),I=1,14)
      WRITE (6,200)TIME                                                   1340
      WRITE (6,220)                                                       1350
      WRITE (6,230)DELT,TIMEND,DELTPT,NDEGPT                              1360
      WRITE(6,240)NCHANG,NOISE,IND,RANDOM
      RETURN
  200 FORMAT(1H046X20HCONDITIONS AT TIME =F12.7)                          1580
  210 FORMAT(1H1,17X,14A6)
  220 FORMAT(8HOCONTROL//)                                                1600
  230 FORMAT(13H INTEG DELTA=F10.7,7X13HTIME TO END =F9.4,5X18HINTERVAL
     1OF PRINT=F10.7,4X,14HDEGREE PRINT =I4)
  240 FORMAT(13H CHANGE NO. =I5,10X15HNO. OF NOISES =I4,8X20HTYPE OF INT
     1EGRATION=I4,10X14HSTART RANDOM =O13)
      END
$IBFTC INTEG   LIST,DECK
      SUBROUTINE INTEG
      DIMENSION  XK1(100),  XK2(100),  XK3(100),  XK4(100)
      DIMENSION FTEXIT(20),XNOISE(8),DERTIV(100),ENTRAL(100),NCOLUM(10),  0020
     1FPTH(14),FPTT(200),FPTV(200),ADSSPT(90),CONVER(90),TIMERC(22),EXAC  0030
     2TC(21),DELTC(21),INDC(21),DELPTC(21),NDEGPC(21),IEXPPC(21),IDEGPC(  0040
     321),NOISEC(21),INTILC(21),CHGSUB(21),TIMEIC(61),VRCHAD(60),VRVLAD(  0050
     460),Y(100),ENDR(100)
      COMMON  TIME   , DELT   , NSTART , NFIRST , NEXIT  , IPASS
      COMMON  TIME1  , XNOISE , RMT    , DELMTN , DELMTE , DELMTD
      COMMON  ADSSPT , CONVER , CHGSUB , DELMAX , DELMIN , DELPT          0110
      COMMON  DELPTC , DELTC  , EMAX   , EMIN   , EXACTC , FPTH           0120
      COMMON  FPTT   , FPTV   , FTEXIT , IC     , ICH    , ICHANG         0130
      COMMON  IDEGPC , IDEGPT , IEXPPC , IEXPPT , IND    , INDC           0140
      COMMON  INTILC , JCH    , M      , MCH    , NCHANG , NCOLUM         0150
      COMMON  ND     , NDEGPC , NDEGPT , NOISE  , NOISEC , NPAGES         0160
      COMMON  NPVAR  , NWORDS , RANDOM , TCKERR , TIMAX  , TIMEAD         0170
      COMMON  TIMECH , TIMEIC , TIMEND , TIMEPT , TIMERC , VRCHAD         0180
      COMMON  VRVLAD , DERTIV , ENTRAL , Y      , ENDR
C
C     RUNGE-KUTTA-MERSON INTEGRATION ROUTINE
C     FOR DIFFERENTIAL EQUATION MONITOR
```

```
C      PROBLEM NO. 849
C
       DO 30 I=ND,100
   30  Y(I)=CLAIND(ENTRAL(I))
   35  DELTA=DELT/3.0
       CALL ADD(TIME,TIME1,DELTA,TIME,TIME1)
       DO 40 I=ND,100
       XK1(I)=CLAIND(DERTIV(I))*DELT
   40  ENTRAL(I)=STOIND(Y(I)+XK1(I)/3.0,ENTRAL(I))
       CALL FUNEV
       DO 50 I=ND,100
       XK2(I)=CLAIND(DERTIV(I))*DELT
   50  ENTRAL(I)=STOIND(Y(I)+(XK2(I)+XK1(I))/6.0,ENTRAL(I))
       CALL FUNEV
       DELTA=DELT/6.0
       CALL ADD(TIME,TIME1,DELTA,TIME,TIME1)
       DO 60 I=ND,100
       XK3(I)=CLAIND(DERTIV(I))*DELT
   60  ENTRAL(I)=STOIND(Y(I)+0.375*XK3(I)+0.125*XK1(I),ENTRAL(I))
       CALL FUNEV
       DELTA=0.5*DELT
       CALL ADD(TIME,TIME1,DELTA,TIME,TIME1)
       DO 70 I=ND,100
       XK4(I)=CLAIND(DERTIV(I))*DELT
   70  ENTRAL(I)=STOIND(Y(I)+2.0*XK4(I)+0.5*XK1(I)-1.5*XK3(I),ENTRAL(I))
       IPASS=1
       CALL FUNEV
       IPASS=0
       RETURN
       END
$IBFTC INTG    LIST,DECK
       SUBROUTINE INTG(XD,X)                                                0010
       DIMENSION FTEXIT(20),XNOISE(8),DERTIV(100),ENTRAL(100),NCOLUM(10),   0020
      1FPTH(14),FPTT(200),FPTV(200),ADSSPT(90),CONVER(90),TIMERC(22),EXAC   0030
      2TC(21),DELTC(21),INDC(21),DELPTC(21),NDEGPC(21),IEXPPC(21),IDEGPC(   0040
      3210),NOISEC(21),INTILC(21),CHGSUB(21),TIMEIC(61),VRCHAD(60),VRVLAD(  0050
      460),Q(200)                                                           0060
       COMMON  TIME   , DELT   , NSTART , NFIRST , NEXIT  , NSUBRT          0100
       COMMON  NTARGT , XNOISE , RMT    , DELMTN , DELMTE , DELMTD          0110
       COMMON  ADSSPT , CONVER , CHGSUB , DELMAX , DELMIN , DELPT           0120
       COMMON  DELPTC , DELTC  , EMAX   , EMIN   , EXACTC , FPTH            0130
       COMMON  FPTT   , FPTV   , FTEXIT , IC     , ICH    , ICHANG          0140
       COMMON  IDEGPC , IDEGPT , IEXPPC , IEXPPT , IND    , INDC            0150
       COMMON  INTILC , JCH    , M      , MCH    , NCHANG , NCOLUM          0160
       COMMON  ND     , NDEGPC , NDEGPT , NOISE  , NOISEC , NPAGES          0170
       COMMON  NPVAR  , NWORDS , RANDOM , TCKERR , TIMAX  , TIMEAD          0180
       COMMON  TIMECH , TIMEIC , TIMEND , TIMEPT , TIMERC , VRCHAD          0190
       COMMON  VRVLAD , DERTIV , ENTRAL , Q                                 02
       NSTART=NSTART+1                                                      0320
       ND=102-NSTART
       ENTRAL(ND)=ADRS(X)
       DERTIV(ND)=ADRS(XD)
       RETURN                                                               0350
       END                                                                  0360
$IBFTC MAIX    LIST,DECK
C
C      MAIN PROGRAM
C      DIFFERENTIAL EQUATION MONITOR, SIMPLIFIED VERSION (11-11-65)
C      RUNGE-KUTTA-MERSON INTEGRATION
C
```

```
      CALL DVCHK(IDV)
      GO TO (10,20),IDV
   10 WRITE(6,15)
   15 FORMAT(35HOSYSTEM LEFT DIVIDE CHECK LIGHT ON    )
   20 CALL SETUP
      END                                                              MAIN0040
$IBFTC PRINTP  LIST,DECK
      SUBROUTINE PRINTP                                                  0010
      DIMENSION FTEXIT(20),XNOISE(8),DERTIV(100),ENTRAL(100),NCOLUM(10),  0020
     1FPTH(14),                    ADSSPT(90),CONVER(90),TIMERC(22),EXAC  0030
     2TC(21),DELTC(21),INDC(21),DELPTC(21),NDEGPC(21),IEXPPC(21),IDEGPC(  0040
     321),NOISEC(21),INTILC(21),CHGSUB(21),TIMEIC(61),VRCHAD(60),VRVLAD(  0050
     460),Q(200)                                                         0060
      DIMENSION FPTT1(20),FPTT2(20),FPTT3(20),FPTT4(20),FPTT5(20),FPTT6(  0070
     120),FPTT7(20),FPTT8(20),FPTT9(20),FPTT10(20),FPTV1(20),FPTV2(20),F  0080
     2PTV3(20),FPTV4(20),FPTV5(20),FPTV6(20),FPTV7(20),FPTV8(20),FPTV9(2  0090
     30),FPTV10(20),PT(9,50,10),PTTIME(50)                               0100
      COMMON  TIME   , DELT   , NSTART , NFIRST , NEXIT  , NSUBRT        0130
      COMMON  NTARGT , XNOISE , RMT    , DELMTN , DELMTE , DELMTD        0140
      COMMON  ADSSPT , CONVER , CHGSUB , DELMAX , DELMIN , DELTPT       0150
      COMMON  DELPTC , DELTC  , EMAX   , EMIN   , EXACTC , FPTH         0160
      COMMON  FPTT1  , FPTT2  , FPTT3  , FPTT4  , FPTT5  , FPTT6        0170
      COMMON  FPTT7  , FPTT8  , FPTT9  , FPTT10 , FPTV1  , FPTV2        0180
      COMMON  FPTV3  , FPTV4  , FPTV5  , FPTV6  , FPTV7  , FPTV8        0190
      COMMON  FPTV9  , FPTV10 , FTEXIT , IC     , ICH    , ICHANG       0200
      COMMON  IDEGPC , IDEGPT , IEXPPC , IEXPPT , IND    , INDC         0210
      COMMON  INTILC , JCH    , M      , MCH    , NCHANG , NCOLUM       0220
      COMMON  ND     , NDEGPC , NDEGPT , NOISE  , NOISEC , NPAGES       0230
      COMMON  NPVAR  , NWORDS , RANDOM , TCKERR , TIMAX  , TIMEAD       0240
      COMMON  TIMECH , TIMEIC , TIMEND , TIMEPT , TIMERC , VRCHAD       0250
      COMMON  VRVLAD , DERTIV , ENTRAL , Q                              0260
      M=M+1                                                             0480
      I=0                                                               0490
      PTTIME(M)=TIME                                                    0500
      DO 100 N=1,NPAGES                                                 0510
      LSTOP=NCOLUM(N)                                                   0520
      DO 100 L=1,LSTOP                                                  0530
      I=I+1                                                             0540
      IF(CONVER(I))80,90,80                                             0550
   80 PT(L,M,N)=CLAIND(ADSSPT(I))*CONVER(I)                             0560
      GO TO 100                                                         0570
   90 PT(L,M,N)=CLAIND(ADSSPT(I))                                       0580
  100 CONTINUE                                                          0590
      IF(50-M)120,120,110                                               0600
  110 IF(NEXIT)120,230,120                                              0610
  120 WRITE (6,240)(FPTH(I),I=1,14)                                     0620
      NSTOP=NCOLUM(1)                                                   0630
      NSTOPT=2*NSTOP+2                                                  0640
      WRITE (6,250)(FPTT1(I),I=1,NSTOPT)                                0650
      WRITE (6,FPTV1)(PTTIME(L),(PT(N,L,1),N=1,NSTOP),L=1,M)            0660
      IF(NPAGES-1)200,200,130                                           0670
  130 WRITE (6,240)(FPTH(I),I=1,14)                                     0680
      NSTOP=NCOLUM(2)                                                   0690
      NSTOPT=2*NSTOP+2                                                  0700
      WRITE (6,250)(FPTT2(I),I=1,NSTOPT)                                0710
      WRITE (6,FPTV2)(PTTIME(L),(PT(N,L,2),N=1,NSTOP),L=1,M)            0720
      IF(NPAGES-2)200,200,140                                           0730
  140 WRITE (6,240)(FPTH(I),I=1,14)                                     0740
      NSTOP=NCOLUM(3)                                                   0750
      NSTOPT=2*NSTOP+2                                                  0760
```

```
      WRITE (6,250)(FPTT3(I),I=1,NSTOPT)                                    0770
      WRITE (6,FPTV3)(PTTIME(L),(PT(N,L,3),N=1,NSTOP),L=1,M)                0780
      IF(NPAGES-3)200,200,150                                               0790
  150 WRITE (6,240)(FPTH(I),I=1,14)                                         0800
      NSTOP=NCOLUM(4)                                                       0810
      NSTOPT=2*NSTOP+2                                                      0820
      WRITE (6,250)(FPTT4(I),I=1,NSTOPT)                                    0830
      WRITE (6,FPTV4)(PTTIME(L),(PT(N,L,4),N=1,NSTOP),L=1,M)                0840
      IF(NPAGES-4)200,200,160                                               0850
  160 WRITE (6,240)(FPTH(I),I=1,14)                                         0860
      NSTOP=NCOLUM(5)                                                       0870
      NSTOPT=2*NSTOP+2                                                      0880
      WRITE (6,250)(FPTT5(I),I=1,NSTOPT)                                    0890
      WRITE (6,FPTV5)(PTTIME(L),(PT(N,L,5),N=1,NSTOP),L=1,M)                0900
      IF(NPAGES-5)200,200,170                                               0910
  170 WRITE (6,240)(FPTH(I),I=1,14)                                         0920
      NSTOP=NCOLUM(6)                                                       0930
      NSTOPT=2*NSTOP+2                                                      0940
      WRITE (6,250)(FPTT6(I),I=1,NSTOPT)                                    0950
      WRITE (6,FPTV6)(PTTIME(L),(PT(N,L,6),N=1,NSTOP),L=1,M)                0960
      IF(NPAGES-6)200,200,180                                               0970
  180 WRITE (6,240)(FPTH(I),I=1,14)                                         0980
      NSTOP=NCOLUM(7)                                                       0990
      NSTOPT=2*NSTOP+2                                                      1000
      WRITE (6,250)(FPTT7(I),I=1,NSTOPT)                                    1010
      WRITE (6,FPTV7)(PTTIME(L),(PT(N,L,7),N=1,NSTOP),L=1,M)                1020
      IF(NPAGES-7)200,200,190                                               1030
  190 WRITE (6,240)(FPTH(I),I=1,14)                                         1040
      NSTOP=NCOLUM(8)                                                       1050
      NSTOPT=2*NSTOP+2                                                      1060
      WRITE (6,250)(FPTT8(I),I=1,NSTOPT)                                    1070
      WRITE (6,FPTV8)(PTTIME(L),(PT(N,L,8),N=1,NSTOP),L=1,M)                1080
      IF(NPAGES-8)200,200,191                                               1090
  191 WRITE (6,240)(FPTH(I),I=1,14)                                         1100
      NSTOP=NCOLUM(9)                                                       1110
      NSTOPT=2*NSTOP+2                                                      1120
      WRITE (6,250)(FPTT9(I),I=1,NSTOPT)                                    1130
      WRITE (6,FPTV9)(PTTIME(L),(PT(N,L,9),N=1,NSTOP),L=1,M)                1140
      IF(NPAGES-9)200,200,192                                               1150
  192 WRITE (6,240)(FPTH(I),I=1,14)                                         1160
      NSTOP=NCOLUM(10)                                                      1170
      NSTOPT=2*NSTOP+2                                                      1180
      WRITE (6,250)(FPTT10(I),I=1,NSTOPT)                                   1190
      WRITE (6,FPTV10)(PTTIME(L),(PT(N,L,10),N=1,NSTOP),L=1,M)              1200
  200 M=0                                                                   1210
  230 RETURN                                                                1220
  240 FORMAT(1H117X14A6)                                                    1230
  250 FORMAT(20A6)                                                          1240
      END                                                                   1250
$IBMAP SIX     DECK
*
*      ROUTINES TO ALLOW INDIRECT ADDRESSING IN FORTRAN
*
       ENTRY   ADRS                                                 DEMD1170
       ENTRY   CLAIND                                               DEMD1150
       ENTRY   STOIND                                               DEMD1160
ADRS   SAVE    1,2
       CLA     3,4
       STA     TEMP
       CLA     TEMP
```

```
        RETURN  ADRS
CLAIND  SAVE    1,2
        CLA*    3,4
        STA     *+1
        CLA     **
        RETURN  CLAIND
STOIND  SAVE    1,2
        CLA*    4,4
        STA     *+2
        CLA*    3,4
        STO     **
        CLA*    4,4
        RETURN  STOIND
 TEMP   PZE
        END
$IBFTC ARCTAN  LIST,DECK
    1 FUNCTION ARCTAN(Y,X)                                          0010
   10 IF(X)20,90,110                                                0020
   20 IF(Y)30,50,70                                                 0030
   30 ARCTAN=ATAN(Y/X)-3.1415927                                    0040
   40 GO TO 120                                                     0050
   50 ARCTAN=3.1415927                                              0060
   60 GO TO 120                                                     0070
   70 ARCTAN=3.1415927+ATAN(Y/X)                                    0080
   80 GO TO 120                                                     0090
   90 IF(Y)92,91,92                                                 0100
   91 ARCTAN=0.0                                                    0110
      GO TO 120                                                     0120
   92 ARCTAN=SIGN(1.5707964,Y)                                      0130
  100 GO TO 120                                                     0140
  110 ARCTAN=ATAN(Y/X)                                              0150
  120 RETURN                                                        0160
      END                                                           0170
```

```
$IBFTC TIMPIK  DECK,LIST
      SUBROUTINE TIMPIC
C     THIS SUBROUTINE IS USED FOR BOTH THE TELESCOPING AND ARTICULATED
C     LEG SIMULATIONS
      DIMENSION ZH(3)
      COMMON/ANGL/PHP,PSP,TH,KFIRST,KRETRN
      COMMON/BOUND/OMEG1,LKX,A1,B1,C1,U,G,SGAM,CGAM,CRTR,W,WD,LEH
      DIMENSION LKX(3,3),W(3),WD(3),LEH(3,3)
      COMMON/FREE/T,LHX(3,3),TMIN,KONVER,DPH,DPS,CT,ST,ZX(3,4),C2,DT,LKH
     1(3,3)
      COMMON/FUN/LEPX(3,3),LETAX(3,3),Q(3,4),MOM(3,4),B(3,4),R(3),RD(3),
     1RDD(3),XD(3),XDD(3),OMEG(3),TAU,M,ROLLD,ROLL,YAWD,YAW,PITCHD,PITCH
     2,OMEGD(3),IPASS,CDR,CRD,Z3F(4),ZET3P(3,4),RHO
      REAL LEH,LHX,LKX
      NCUT=0
      PH=DPH*T+PHP
      PS=DPS*T+PSP
      SPH=SIN(PH )
      CPH=COS(PH )
      SPS=SIN(PS )
      CPS=COS(PS )
      CALL SUBLHX(SPH,CPH,SPS,CPS,CT,ST,LHX)
      SAVE=T
      DO 1 N=1,4
      T=SAVE
      KONVRX=0
    2 DO 9 I=1,3
      ZH(I)=0.
      DO 9 J=1,3
    9 ZH(I)=ZH(I)+LHX(I,J)*ZX(J,N)
      Z=0.
      DO 10 I=1,3
   10 Z=Z+ZH(I)*LEH(3,I)
      F    =R(3)+RD(3)*T+Z-C2*T**2
      IF((KFIRST.EQ.0).AND.(F.LE.1.E-4))GO TO 30
      IF(ABS(F    ).LE.1.E-4)GO TO 4
      IF(KONVRX.EQ.1)GO TO 3
      IF(F.GE.1.E-4)GO TO 1
      TN=T
      TP=T-DT
      KONVRX=1
    7 T=.5*(TP+TN)
      PH=DPH*T+PHP
      PS=DPS*T+PSP
      SPH=SIN(PH )
      CPH=COS(PH )
      SPS=SIN(PS )
      CPS=COS(PS )
      CALL SUBLHX(SPH,CPH,SPS,CPS,CT,ST,LHX)
      GO TO 2
    3 NCUT=NCUT+1
      IF(NCUT.GT.25) GOTO8
      IF(F)5,4,6
    5 TN=T
      GOTO7
    6 TP=T
      GOTO7
   30 KRETRN=1
      GO TO 31
    8 T=TP
```

```
  4 TMIN=AMIN1(T,TMIN)
    KONVER=1
  1 CONTINUE
 31 RETURN
    END
```

```
$I8FTC LHXSUB  DECK,LIST
      SUBROUTINE SUBLHX(SPH,CPH,SPS,CPS,CT,ST,LHX)
C     THIS SUBROUTINE IS USED FOR BOTH THE TELESCOPING AND ARTICULATED
C     LEG SIMULATIONS
      DIMENSION LHX(3,3)
      REAL LHX
      LHX(1,1)=CPH*CPS-SPH*CT*SPS
      LHX(1,2)=-SPH*CPS-SPS*CT*CPH
      LHX(1,3)=ST*SPS
      LHX(2,1)=CPH*SPS+SPH*CT*CPS
      LHX(2,2)=-SPH*SPS+CPH*CT*CPS
      LHX(2,3)=-ST*CPS
      LHX(3,1)=ST*SPH
      LHX(3,2)=ST*CPH
      LHX(3,3)=CT
      RETURN
      END
```

```
$IBFTC FUNEV
      SUBROUTINE FUNEV
C
C     SPACE PACKAGE ALIGHTMENT
C     PROBLEM NO. 970
C
C     THIS SUBROUTINE IS USED FOR THE TELESCOPING LEG SIMULATION
      COMMON TIME,DELT,NSTART,NFIRST,NEXIT ,IPASS,NTARGT,XNOISE(8),
     1RMT,DELMTN,DELMTE,DELMTD,ROMCOM(1482)
      COMMON/JOHN/THETA
      COMMON/BOUND/OMEG1,LKX,A1,B1,C1,U,G,SGAM,CGAM,CRTR,W,WD,LEH
      COMMON/TRANS/AL(4),ALP(4),BET(4),SENR,RZERO
      COMMON/FUN/LEPX(3,3),LETAX(3,3),F(3,4),MOM(3,4),B(3,4),R(3),RD(3),
     1RDD(3),XD(3),XDD(3),OMEG(3),TAU,M,ROLLD,ROLL,YAWD,YAW,PITCHD,PITCH
     2,OMEGD(3),IPASS,CDR,CRD,Z3F(4),ZET3P(3,4),RHO
      DIMENSION DDX(7,3)
      DIMENSION LEH(3,3)
      DIMENSION NP(19),W(3),WD(3),FF(3)
      DIMENSION LKX(3,3),YL(19),     XL(3),XM(3),YU(19),              V(3
     1),LEPK(3,3),ID(24)
      DIMENSION IDL(20),IOR(20),DSC(20)
      COMMON/PAIN/ NPLOT
      REAL LEPX,LETAX,      LEPK,LKX,MOM,M
      IF(NSTART)100,200,10
   10 CONTINUE
    2 FORMAT(2E10.8,I10)
    1 FORMAT(6E10.8)
   11 FORMAT (3E10.4)
   12 FORMAT(4I10,2E10.8)
C
C     INITIAL INPUT CONDITIONS ARE READ INTO THE PROGRAM
C
      N=4
      READ(5,12)NDLT,NPLOT,NSTOP,NSHOCK,TAUS,TIMSHK
      IF(NSHOCK.EQ.2)NSHOCK=0
      NSHOCK=NSHOCK+1
      READ (5,11) R
      READ (5,11) V
      READ (5,11)ROLL, YAW, PITCH
      READ (5,11) OMEG
      READ (5,11) A1, B1, C1
      READ (5,11) GM, CRTHA, CRTR
      READ (5,11) G, GAMA
      READ(5,11)((LETAX(I,J),J=1,3),I=1,3)
      READ (5,11) ((B(I,J),I=1,3),J=1,N)
      IF(V(3).GT.0.)V(3)=-V(3)
      IPASS=4
      NOPRNT=0
      NCOUNT=0
      NSET=1
      U=1./G
      M=GM/32.17
      NVALUE=0
      NCARD=0
      VB=SQRT(B(1,1)**2+B(2,1)**2+(B(3,1)-RHO)**2)
      CDR=0.01745329
      CRD=1.0/CDR
      THETA=0.0
      CRTAGL=COS(CRTHA*CDR)
      ROLL=ROLL*CDR
```

```
      YAW=YAW*CDR
      PITCH=PITCH*CDR
      GAMA=GAMA*CDR
      SGAM=SIN(GAMA)
      CGAM=COS(GAMA)
      PERIOD=0.0
      CALL FORCE
      GO TO (13,14),NPLOT
   13 READ(5,15)IDP
   15 FORMAT(I3)
      READ(5,16)(IOR(J),DSC(J),J=1,20)
   16 FORMAT(4(I10,E10.0))
      WRITE(7,17)
   17 FORMAT(126H3      -8005 -8005 -8005 -8005 -8005 -8005 -8005 -8005 -
     18005 -8005 -8005 -8005 -8005 -8005 -8005 -8005 -8005 -8005 -8005 -
     28005 )
      IDC=0
C
C     INTERNAL CONVERSION AND SET UP.
C
C
C     BOUNDARY CONDITION FOR QUIESENCE OF MOTION CRITERIA.
C
   14 DLT=DELT
      VNDLT=FLOAT(NDLT)
      VVDELT=VNDLT*DELT
C
C     INITIALIZE THE TRANSFORMATION MATRIX BETWEEN THE EPSILON AND KAPPA
C     COORDINATE SYSTEMS.
C
      LEPK(1,1)=1.0
      LEPK(1,2)=0.0
      LEPK(1,3)=0.0
      LEPK(2,1)=0.0
      LEPK(2,2)=CGAM
      LEPK(2,3)=-SGAM
      LEPK(3,1)=0.0
      LEPK(3,2)=SGAM
      LEPK(3,3)=CGAM
C
C     TRANSFORM THE INITIAL TRANSLATIONAL AND ROTATIONAL VELOCITIES.
C
      DO 20 I=1,3
      W(I)=0.
      RD(I)=0.0
      DO 20 J=1,3
      W(I)=W(I)+LETAX(I,J)*OMEG(J)
   20 RD(I)=RD(I)+LEPK(I,J)*V(J)
      QUIVEL=.025*(ABS(M*RD(3))+SQRT((A1*OMEG(1))**2+(B1*OMEG(2))**2))
      QUIVEX=.025*(M*SQRT(RD(1)**2+RD(2)**2)+ABS(C1*OMEG(3)))
C
C     SET UP INDIRECT ADDRESSING FOR THE INTEGRATION ROUTINE
C     IN THE D.E. MONITOR.
C
      CALL INTG(RDD(1),RD(1))
      CALL INTG(RDD(2),RD(2))
      CALL INTG(RDD(3),RD(3))
      CALL INTG(WD(1),W(1))
      CALL INTG(WD(2),W(2))
      CALL INTG(WD(3),W(3))
```

```
      CALL INTG(ROLLD,ROLL)
      CALL INTG(YAWD,YAW)
      CALL INTG(PITCHD,PITCH)
      CALL INTG(RD(1),R(1))
      CALL INTG(RD(2),R(2))
      CALL INTG(RD(3),R(3))
  100 NSUBRT=1000
C
C     FORMAT SETUP FOR THE PRINT ROUTINE.
C
      CALL PRINT(12H  R(1) (FT) ,12H,E12.4      ,R(1),ID(1),0)
      CALL PRINT(12H  RD(1) FPS ,12H,E12.4      ,RD(1),ID(1),0)
      CALL PRINT(12H XDD(1) (G) ,12H,E12.4      ,XDD(1),ID(1),U)
      CALL PRINT(12H  R(2) (FT) ,12H,E12.4      ,R(2),ID(2),0)
      CALL PRINT(12H  RD(2) FPS ,12H,E12.4      ,RD(2),ID(2),0)
      CALL PRINT(12H XDD(2) (G) ,12H,E12.4      ,XDD(2),ID(1),U)
      CALL PRINT(12H  R(3) (FT) ,12H,E12.4      ,R(3),ID(3),0)
      CALL PRINT(12H  RD(3) FPS ,12H,E12.4      ,RD(3),ID(3),0)
      CALL PRINT(12H XDD(3) (G) ,12H,E12.4      ,XDD(3),ID(1),U)
      CALL PRINT(12HOMEGA(1)R/S ,12H,E12.4      ,OMEG(1),ID(4),0)
      CALL PRINT(12HOMD(1) R/S2 ,12H,E12.4      ,OMEGD(1),ID(4),0)
      CALL PRINT(12HOMEGA(2)R/S ,12H,E12.4      ,OMEG(2),ID(5),0)
      CALL PRINT(12HOMD(2) R/S2 ,12H,E12.4      ,OMEGD(2),ID(5),0)
      CALL PRINT(12HOMEGA(3)R/S ,12H,E12.4      ,OMEG(3),ID(6),0)
      CALL PRINT(12HOMD(3) R/S2 ,12H,E12.4      ,OMEGD(3),ID(6),0)
      CALL PRINT(12H ROLL (DEG) ,12H,E12.4      ,ROLL,ID(7),CRD)
      CALL PRINT(12H  YAW (DEG) ,12H,E12.4      ,YAW,ID(8),CRD)
      CALL PRINT(12HPITCH (DEG) ,12H,E12.4      ,PITCH,ID(9),CRD)
      CALL PRINT(12H FORCE(1,1) ,12H,E12.4      ,F(1,1),ID(13),0)
      CALL PRINT(12H FORCE(2,1) ,12H,E12.4      ,F(2,1),ID(15),0)
      CALL PRINT(12H FORCE(3,1) ,12H,E12.4      ,F(3,1),ID(17),0)
      CALL PRINT(12HMOMENT(1,1) ,12H,E12.4      ,MOM(1,1),ID(19),0)
      CALL PRINT(12HMOMENT(2,1) ,12H,E12.4      ,MOM(2,1),ID(21),0)
      CALL PRINT(12HMOMENT(3,1) ,12H,E12.4      ,MOM(3,1),ID(23),0)
      CALL  PRINT(12HAX LENGTH 1 ,12H,E12.4      ,AL(1),0,0)
      CALL  PRINT(12HALPHA 1(DEG),12H,E12.4      ,ALP(1),0,57.295779)
      CALL  PRINT(12HBETA 1 (DEG),12H,E12.4      ,BET(1),0,57.295779)
      CALL PRINT(12H FORCE(1,2) ,12H,E12.4      ,F(1,2),ID(13),0)
      CALL PRINT(12H FORCE(2,2) ,12H,E12.4      ,F(2,2),ID(15),0)
      CALL PRINT(12H FORCE(3,2) ,12H,E12.4      ,F(3,2),ID(17),0)
      CALL PRINT(12HMOMENT(1,2) ,12H,E12.4      ,MOM(1,2),ID(19),0)
      CALL PRINT(12HMOMENT(2,2) ,12H,E12.4      ,MOM(2,2),ID(21),0)
      CALL PRINT(12HMOMENT(3,2) ,12H,E12.4      ,MOM(3,2),ID(23),0)
      CALL  PRINT(12HAX LENGTH 2 ,12H,E12.4      ,AL(2),0,0)
      CALL  PRINT(12HALPHA 2(DEG),12H,E12.4      ,ALP(2),0,57.295779)
      CALL  PRINT(12HBETA 2 (DEG),12H,E12.4      ,BET(2),0,57.295779)
      CALL PRINT(12H FORCE(1,3) ,12H,E12.4      ,F(1,3),ID(13),0)
      CALL PRINT(12H FORCE(2,3) ,12H,E12.4      ,F(2,3),ID(15),0)
      CALL PRINT(12H FORCE(3,3) ,12H,E12.4      ,F(3,3),ID(17),0)
      CALL PRINT(12HMOMENT(1,3) ,12H,E12.4      ,MOM(1,3),ID(19),0)
      CALL PRINT(12HMOMENT(2,3) ,12H,E12.4      ,MOM(2,3),ID(21),0)
      CALL PRINT(12HMOMENT(3,3) ,12H,E12.4      ,MOM(3,3),ID(23),0)
      CALL  PRINT(12HAX LENGTH 3 ,12H,E12.4      ,AL(3),0,0)
      CALL  PRINT(12HALPHA 3(DEG),12H,E12.4      ,ALP(3),0,57.295779)
      CALL  PRINT(12HBETA 3 (DEG),12H,E12.4      ,BET(3),0,57.295779)
      CALL PRINT(12H FORCE(1,4) ,12H,E12.4      ,F(1,4),ID(13),0)
      CALL PRINT(12H FORCE(2,4) ,12H,E12.4      ,F(2,4),ID(15),0)
      CALL PRINT(12H FORCE(3,4) ,12H,E12.4      ,F(3,4),ID(17),0)
      CALL PRINT(12HMOMENT(1,4) ,12H,E12.4      ,MOM(1,4),ID(19),0)
      CALL PRINT(12HMOMENT(2,4) ,12H,E12.4      ,MOM(2,4),ID(21),0)
```

```
      CALL PRINT(12HMOMENT(3,4) ,12H,E12.4       ,MOM(3,4),ID(23),0)
      CALL  PRINT(12HAX LENGTH 4 ,12H,E12.4       ,AL(4),0,0)
      CALL  PRINT(12HALPHA 4(DEG),12H,E12.4       ,ALP(4),0,57.295779)
      CALL  PRINT(12HBETA 4 (DEG),12H,E12.4       ,BET(4),0,57.295779)
      CALL PRINT(12H  TRANS (G) ,12H,E12.4       ,XXOD,ID(11),0)
      CALL PRINT(12H THETA (DEG),12H,E12.4       ,THETA,ID(10),CRD)
      GO TO 500
C
C     POST INITIALIZATION PHASE OF THE PROGRAM.
C
  200 SROLL=SIN(ROLL)
      CROLL=COS(ROLL)
      SYAW= SIN(YAW)
      CYAW= COS(YAW)
      SPITCH=SIN(PITCH)
      CPITCH=COS(PITCH)
C
C     COMPUTATION OF THE TRANSFORMATION MATRIX BETWEEN THE KAPPA
C     AND CHI COORDINATE SYSTEMS.
C
      LKX(1,1)=CROLL*CYAW
      LKX(1,2)=-SROLL*CPITCH+CROLL*SYAW*SPITCH
      LKX(1,3)=SROLL*SPITCH+CROLL*SYAW*CPITCH
      LKX(2,1)=SROLL*CYAW
      LKX(2,2)=CROLL*CPITCH+SROLL*SYAW*SPITCH
      LKX(2,3)=-CROLL*SPITCH+SROLL*SYAW*CPITCH
      LKX(3,1)=-SYAW
      LKX(3,2)=CYAW*SPITCH
      LKX(3,3)=CYAW*CPITCH
      IF(NFIRST)227,228,227
  227 IF(NOPRNT.EQ.1)GOTO228
      NOPRNT=1
      RL=ROLL*CRD
      YW=YAW*CRD
      PH=PITCH*CRD
      GA=GAMA*CRD
C
C     WRITE OUT INITIAL INPUT PARAMETERS.
C
      WRITE(6,420)GA,RL,YW,PH
      WRITE(6,439)(OMEG(I),I=1,3)
      WRITE(6,436)(V(I),I=1,3)
      WRITE(6,442)GM
      WRITE(6,430)A1,B1,C1
      WRITE(6,441)((B(I,J),J=1,4),I=1,3)
      WRITE(6,443)((LETAX(I,J),J=1,3),I=1,3)
      WRITE(6,445)NDLT,G,CRTHA
      WRITE(6,3)CRTR
      GO TO(446,447),NPLOT
  446 WRITE(6,448)
      WRITE(6,1449)AID,IDP
 1449 FORMAT(//49X8HTITLE = 3A6///51X17HDEGREE OF PLOT = I3)
      GO TO 449
  447 WRITE(6,450)
  449 GO TO(451,452),NSTOP
  451 WRITE(6,453)
      GOTO458
  452 WRITE(6,454)
  458 GOTO(455,456),NSHOCK
  455 WRITE(6,457)
```

```
      GOTO 228
  456 WRITE(6,459)TIMSHK
C
C     COMPUTE THE TRANSFORMATION MATRIX BETWEEN THE EPSILON AND
C     CHI COORDINATE SYSTEMS.
C
  228 DO 32 I=1,3
      DO 32 J=1,3
      LEPX(I,J)=0.0
      DO 32 K=1,3
   32 LEPX(I,J)=LEPX(I,J)+LEPK(I,K)*LKX(K,J)
C
C     EVALUATE THE FORCING FUNCTIONS.
C
   33 CALL FORCE
      IF(R(3).LT.CRTR)CALL PANIC(60HOTHE SPACE PACKAGE HAS EXCEEDED THE
     1CRITICAL DISPLACEMENT.      )
      DO 40 I=1,3
      FF(I)=0.
      DO 40 J=1,N
   40 FF(I)=FF(I)+F(I,J)
C
C     COMPUTATION OF THE MOMENTS IN THE CHI COORDINATE SYSTEM
C     DUE TO THE FORCES.
C
      XL(1)=0.0
      XL(2)=0.0
      XL(3)=0.0
      DO 230 J=1,N
      XL(1)=XL(1)+B(2,J)*F(3,J)-B(3,J)*F(2,J)+MOM(1,J)
      XL(2)=XL(2)+B(3,J)*F(1,J)-B(1,J)*F(3,J)+MOM(2,J)
  230 XL(3)=XL(3)+B(1,J)*F(2,J)-B(2,J)*F(1,J)+MOM(3,J)
C
C     SUMMATION OF THE XL AND ZM MOMENTS AND THE TRANSFORMATION FROM THE
C     CHI TO THE ETA COORDINATE SYSTEM.
C
      DO 250 I=1,3
      XM(I)=0.
      DO 250 J=1,3
  250 XM(I)=XM(I)+LETAX(I,J)*XL(J)
C
C     TRANSFORMATION OF THE FORCES FROM THE CHI TO THE EPSILON
C     COORDINATE SYSTEMS AND THE EVALUATION OF THE BASIC TRANSLATIONAL
C     EQUATIONS OF MOTION.
C
  260 DO 280 I=1,3
      RDD(I)=0.0
      DO 270 J=1,3
  270 RDD(I)=RDD(I)+LEPX(I,J)*FF(J)
  280 RDD(I)=RDD(I)/M+LEPK(I,3)*(-G)
C
C     THE EVALUATION OF EULER DYNAMICAL EQUATIONS.
C
      WD(1)=(XM(1)-W(2)*W(3)*(C1-B1))/A1
      WD(2)=(XM(2)-W(1)*W(3)*(A1-C1))/B1
      WD(3)=(XM(3)-W(1)*W(2)*(B1-A1))/C1
C
C     TRANSFORMATION OF THE INSTANTANEOUS ANGULAR ACCELERATION FROM THE
C     ETA TO THE CHI COORDINATE SYSTEM.
C
```

```
      DO 350 I=1,3
      OMEGD(I)=0.
      OMEG(I)=0.
      DO 350 J=1,3
      OMEGD(I)=OMEGD(I)+LETAX(J,I)*WD(J)
  350 OMEG(I)=OMEG(I)+LETAX(J,I)*W(J)
C
C     EVALUATION OF THE INSTANTANEOUS ROLL,YAW,AND PITCH RATES.
C
      ROLLD=(OMEG(2)*SPITCH+OMEG(3)*CPITCH)/CYAW
      YAWD=OMEG(2)*CPITCH-OMEG(3)*SPITCH
      PITCHD=OMEG(1)+SYAW/CYAW*(OMEG(2)*SPITCH+OMEG(3)*CPITCH)
C
C     TRANSFORMATION OF THE INSTANTANEOUS TRANSLATIONAL VELOCITIES
C     FROM THE CHI TO THE EPSILON COORDINATE SYSTEMS.
C
      DO 360 I=1,3
      XD(I)=0.
      DO 360 J=1,3
  360 XD(I)=XD(I)+LEPX(J,I)*RD(J)
      IF(IPASS.EQ.4)GO TO 366
      IPASS=IPASS+1
      GO TO 500
  366 IPASS=1
C
C     SET UP VARIABLES FOR PLOTTING
C
      GO TO (1000,1200),NPLOT
 1000 IF(TIME.EQ.0.0) GO TO 1002
      IDC=IDC+1
      IF(IDC.LT.IDP) GO TO 1200
      IDC=0
 1002 IDL(1 )=IOR(1 )+INT(TIME*DSC(1))
      IDL(2 )=IOR(2 )+INT(DSC(2 )*R(1))
      IDL(3 )=IOR(3 )+INT(DSC(3 )*R(2))
      IDL(4 )=IOR(4 )+INT(DSC(4 )*R(3))
      IDL(5 )=IOR(5 )+INT(DSC(5 )*RD(1))
      IDL(6 )=IOR(6 )+INT(DSC(6 )*RD(2))
      IDL(7 )=IOR(7 )+INT(DSC(7 )*RD(3))
      IDL(8 )=IOR(8 )+INT(DSC(8 )*XDD(1)*U)
      IDL(9 )=IOR(9 )+INT(DSC(9 )*XDD(2)*U)
      IDL(10)=IOR(10)+INT(DSC(10)*XDD(3)*U)
      IDL(11)=IOR(11)+INT(DSC(11)*OMEGD(1))
      IDL(12)=IOR(12)+INT(DSC(12)*OMEGD(2))
      IDL(13)=IOR(13)+INT(DSC(13)*OMEGD(3))
      IDL(14)=IOR(14)+INT(DSC(14)*ROLL*CDR)
      IDL(15)=IOR(15)+INT(DSC(15)*YAW *CDR)
      IDL(16)=IOR(16)+INT(DSC(16)*PITCH*CDR)
      IDL(17)=IOR(17)+INT(DSC(17)*XXDD)
      IDL(18)=IOR(18)+INT(DSC(18)*OMEG(1))
      IDL(19)=IOR(19)+INT(DSC(19)*OMEG(2))
      IDL(20)=IOR(20)+INT(DSC(20)*OMEG(3))
      WRITE(7,1010)IDL
 1010 FORMAT(6X,20(I5,1X))
      IF(NFIRST.EQ.0) GO TO 980
      IF(NPOO.NE.0) GO TO 950
      NPOO=1
      NPOW=0
  950 NPOW=NPOW+1
      GO TO (980,960),NPOW
```

```
  960 NPOW=0
      WRITE(7,965)
  965 FORMAT(6H 1
      END FILE 7
  980 CONTINUE
 1200 CONTINUE
C
C     THE RUN IS ABORTED IF THE TEST AGAINST THE CRITICAL NUTATION
C     ANGLE HAS BEEN SATISFIED.
C
      IF((CPITCH*CYAW).GT.CRTAGL)GO TO 367
      CALL PANIC(59HOTHE SPACE PACKAGE HAS EXCEEDED THE CRITICAL NUTATIO
     1N ANGLE)
      GO TO 500
C
C     EVALUATION OF THE EULER NUTATION ANGLE THETA.
C
  367 THETA=ARSIN(SQRT(SYAW**2+CYAW**2*SPITCH**2))
      ENR=0.5*(M*(RD(1)**2+RD(2)**2+RD(3)**2)+A1*OMEG(1)**2+
     1B1*OMEG(2)**2+C1*OMEG(3)**2)+GM*((R(3)-RZERO)*CGAM-R(2)*SGAM)+SENR
C
C     TRANSFORMATION OF THE INSTANTANEOUS TRANSLATIONAL ACCELERATIONS
C     FROM THE CHI TO THE EPSILON COORDINATE SYSTEMS, AND
C     THE COMPUTATION OF THE ABSOLUTE MAGNITUDE OF THE RESULTANT
C     TRANSLATIONAL AND ROTATIONAL ACCELERATIONS.
C
      IF(NSTOP.EQ.2) GO TO 711
      IF(TIME.LT.0.05) GO TO 711
      NCOUNT=NCOUNT+1
      IF(NCOUNT.NE.50) GO TO 711
      CALL QUIMOT
      NCOUNT=0
  711 CONTINUE
      XXDD=0.
      OMEG1=0.
      OMEGD1=0.
      DO 369 I=1,3
      XDD(I)=0.
      DO 368 J=1,3
  368 XDD(I)=XDD(I)+LEPX(J,I)*RDD(J)
      XXDD=XXDD+XDD(I)**2
      OMEG1=OMEG1+OMEG(I)**2
  369 OMEGD1=OMEGD1+OMEGD(I)**2
      XXDD=(SQRT(XXDD))/G
      OMEGD1=SQRT(OMEGD1)
      OMEG1=SQRT(OMEG1)
      IF(NSHOCK.EQ.1)GOTO460
      NVALUE=NVALUE+1
      IF(TIME.LE.TIMSHK)GOTO473
      NSHOCK=1
      GOTO464
  473 DO461 I=1,3
  461 DDX(NVALUE,I)=XDD(I)*U
      IF(NVALUE.NE.7)GOTO460
  464 NCARD=NCARD+1
      DO462 I=1,3
  462 PUNCH 463,(DDX(J,I),J=1,7      ),I,NCARD
  463 FORMAT(7F10.5,I2,I8)
      NVALUE=0
C
```

```
C     EVALUATION OF THE CRITERIA FOR THE INTEGRATION INTERVAL.
C
  460 IF(ABS(XXDD-1.0)-1.0E-5)372,372,376
  372 IF(NSET.LT.3)GO TO 375
  374 IF(NSHOCK.EQ.1)GOTO467
      NSHOCK=1
      IF(NVALUE.EQ.0)GOTO467
      NCARD=NCARD+1
      DO466 I=1,3
  466 PUNCH 463,(DDX(J,I),J=1,7      ),I,NCARD
  467 IF(NDLT.GT.0) GOTO700
      CALL BOUNCE
      NSET=1
      GO TO 500
  700 DO 410 K=1,4
      IF(ZET3P(3,K)+(RD(3)*CGAM-RD(2)*SGAM-VB*OMEG1)*VNDLT*DLT      -.5*(
     1G+OMEGD1*VB)*(VNDLT*DLT )**2)701,701,410
  410 CONTINUE
      DELT=VVDELT
      GOTO500
  701 DELT=DLT
      NSET=1
      GOTO500
  375 NSET=NSET+1
      GO TO 500
  376 NSET=1
      GO TO (378,500),NSTOP
C
C     COMPUTE THE VELOCITY OF THE C.G. OF THE SPACE PACKAGE
C     FOR THE QUIESENCE OF MOTION TEST.
C
  378 RRD=ABS(M*RD(3))+SQRT((A1*OMEG(1))**2+(B1*OMEG(2))**2)
      IF(QUIVEL-RRD)385,380,380
  380 IF(PERIOD-TAUS*TAU)390,400,400
  385 PERIOD=DLT
      GO TO 500
  390 PERIOD=PERIOD+DLT
      GO TO 500
  400 RRDX=M*SQRT(RD(1)**2+RD(2)**2)+ABS(C1*OMEG(3))
      IF(RRDX.GT.QUIVEX)GO TO 401
      CALL PANIC(33HOQUIESENCE OF MOTION HAS OCCURED.)
  401 CALL PANIC(120HOTHE CAPSULE IS IN A STABLE POSITION.  CHECK RD(1),
     1 RD(2) AND OMEG(3) TO DETERMINE IF QUIESENCE OF MOTION WILL OCCUR.
     2     )
  420 FORMAT(///49X19HTERRAIN SLOPE (DEG)//53X8HGAMMA = F7.3///45X30HROT
     1ATIONAL DISPLACEMENTS (DEG)//29X4HROLL23X3HYAW23X5HPITCH/ 7X3F27.3
     2)
  430 FORMAT(//43X 37HMASS MOMENTS OF INERTIA (SLUGS-FT**2)//53X3HA =F8.
     12/53X 3HB =F8.2/53X 3HC =F8.2)
  436 FORMAT(//45X 33HTRANSLATIONAL VELOCITIES (FT/SEC)//29X4HV(1) 22X
     14HV(2) 24X 4HV(3)/7X 3F27.3)
  439 FORMAT(//45X 31HROTATIONAL VELOCITIES (RAD/SEC)//29X9HOMEGA (1)
     116X 9HOMEGA (2) 16X 9HOMEGA (3)/14X   3E25.5)
  441 FORMAT(///46X29HABSORBER ATTACHMENT LOCATIONS//43X6HB(I,1)4X6HB(I,
     12)4X6HB(I,3)4X6HB(I,4)//(39X4F10.2))
  442 FORMAT(//50X 26HSPACE PACKAGE WEIGHT (LBS)/56X F7.2)
  443 FORMAT(1H139X45HINERTIA CHARACTERISTICS TRANSFORMATION MATRIX//(40
     1X 3F12.2))
  445 FORMAT(///40X41HFREE FLIGHT INTEGRATION STEP-UP INTEGER =,I3///50X
     121HGRAVITY (FT/SEC**2) = F5.2///45X25HCRITICAL NUTATION ANGLE =
```

```
   2F5.2,6H DEGS.)
448 FORMAT(///42X39HTHE PLOTTING OPTION HAS BEEN ACTIVATED.)
450 FORMAT(///40X43HTHE PLOTTING OPTION HAS NOT BEEN ACTIVATED.)
453 FORMAT(///35X53HTHE QUIESENCE OF MOTION CRITERIA HAVE BEEN ACTIVAT
   1ED.    )
454 FORMAT(///33X57HTHE QUIESENCE OF MOTION CRITERIA HAVE NOT BEEN ACT
   1IVATED.    )
457 FORMAT(///33X57HTHE CARD OUTPUT FOR SHOCK SPECTRA HAS NOT BEEN ACT
   1IVATED.   )
459 FORMAT(///35X53HTHE CARD OUTPUT FOR SHOCK SPECTRA HAS BEEN ACTIVAT
   1ED.  ///39X37HMAXIMUM TIME FOR SHOCK SPECTRA DATA =  F8.5)
  3 FORMAT(///38X37HCRITICAL TRANSLATIONAL DISPLACEMENT = F6.3,4H FT.)
500 RETURN
    END
```

```
$IBFTC FORCE
      SUBROUTINE FORCE
C     THIS SUBROUTINE IS USED FOR THE TELESCOPING LEG SIMULATION
      COMMON TIME,DELT,NSTART,NFIRST,NEXIT ,IPASS,NTARGT,XNOISE(8),
     1RMT,DELMTN,DELMTE,DELMTD,ROMCOM(1482)
      COMMON/TRANS/AL(4),ALP(4),BET(4),SENR,RZERO
      COMMON/FUN/LEPX(3,3),LETAX(3,3),F(3,4),MOM(3,4),B(3,4),R(3),RD(3),
     1RDD(3),XD(3),XDD(3),OMEG(3),TAU,M,ROLLD,ROLL,YAWD,YAW,PITCHD,PITCH
     2,OMEGD(3),IPASS,CDR,CRD,Z3F(4),ZET3P(3,4),RHO
      DIMENSION SLOPE(2),DAMP(2),ZET2P(3,4),Z3PSD(3,4),ZETA(3,4)
     1    ,FIN(10  ),DELIN(10  ),KLAST(9,4),DELMAX(9,4),Z3P(3,4)
      DIMENSION DELPST(9,4),FMAX(9,4),AF(9),ILOAD(9,4),DELZ(9,4)
      DIMENSION IGRUND(4),ZETP(3,4),TEMP(3),GAM(9),ISSLIP(4),AP(3),AR(3
     1),GXM(9),KCONT(9),FE(3),FINX(10),DELINX(10),PDLPST(9,4),
     2                   FD(9),CGB(9),SGB(9)
      DIMENSION PDPSTX(9),DELPSX( 9),FMAXX( 9),DELMXX( 9),DELZX( 9)
      DIMENSION PRF(3,4),PRMOM(3,4),PRALP(4),PRAL(4)
      COMMON/ST/ALM(4),ALMIN(4)
      REAL MOM,LEPX,LETAX,KCONT,M
      IF(NSTART)1,4,1
    1 READ(5,600)NPAD,NCUP
      READ (5,3) FIN
      READ (5,3) DELIN
      READ (5,3) FINX
      READ (5,3) DELINX
      READ(5,3)RHO,SLOPE,DAMP
      READ(5,3)(GXM(J),J=2,9)
      READ(5,3)DMU,SMU,AS,SPRGAL
      IF(NCUP.EQ.1.AND.NPAD.NE.4)CALL PANIC(35HOSINCE NCUP=1, NPAD MUST
     1EQUAL 4.                    )
      DO 39 I=2,9
   39 GAM(I)=CDR*GXM(I)
      PI=3.14159265
    3 FORMAT(5E10.8)
  600 FORMAT(5I10)
      TAU=PI*SQRT(M/SLOPE(1))
      NOPRNT=0
      DUMMY=0.0
      DO 5 N=1,4
      ISSLIP(N)=1
      AL(N)=RHO
      ALP(N)=0.
      BET(N)=0.
      ALM(N)=0.0
      ALMIN(N)=1.0E+6
      IGRUND(N)=0
      DO  43 I=1,3
   43 ZET3P(I,N)=0.
      NPADP1=NPAD+1
      DO 8 I=1,NPADP1
      KLAST(I,N)=1
      ILOAD(I,N)=1
      DELMAX(I,N)=0.
      PDLPST(I,N)=0.0
      DELPST(I,N)=0.0
      FMAX(I,N)=0.
    8 DELZ(I,N)=0.
      DO 9 I=1,2
    9 ZETA(I,N)=0.
      ZETA(3,N)=-RHO
```

```
  5 Z3PSD(3,N)=0.
    GOTO 10
  4 IF(IPASS.NE.1)GOTO 2
    DO 42 N=1,4
 42 Z3F(N)=ZET3P(3,N)
  2 DO 6 I=1,4
    DO 6 J=1,3
    Z3P(J,I)=ZET3P(J,I)
    ZET2P(J,I)=0.
    ZET3P(J,I)=0.
    DO 6 K=1,3
    ZET3P(J,I)=ZET3P(J,I)+LEPX(J,K)*ZETA(K,I)
  6 ZET2P(J,I)=ZET2P(J,I)+LEPX(J,K)*B(K,I)
    IF(IPASS-3)100,101,102
100 C=3.
    GO TO 103
101 C=2.
    GO TO 103
102 C=1.
103 C4=1./(2.*DELT)
104 DO 7 J=1,3
    DO 7 I=1,4
    ZET2P(J,I)=ZET2P(J,I)+R(J)
  7 ZET3P(J,I)=ZET3P(J,I)+ZET2P(J,I)
    IF(NOPRNT.EQ.1)GOTO14
    NOPRNT=1
    XMIN=ZET3P(3,1)
    DO 11  I=2,4
 11 XMIN=AMIN1(XMIN,ZET3P(3,I))
    R(3)=R(3)-XMIN
    DO 12 I=1,4
    ZET2P(3,I)=ZET2P(3,I)-XMIN
 12 ZET3P(3,I)=ZET3P(3,I)-XMIN
    WRITE(6,301)(FIN(I),DELIN(I),FINX(I),DELINX(I),I=1,10)
    WRITE(6,302)SLOPE
    WRITE(6,305)DAMP,RHO
    WRITE(6,601)NPAD
    NPAD=NPAD+1
    IF (NCUP.EQ.1)WRITE(6,609)
    WRITE(6,303)(GXM(J),J=2,NPAD)
    WRITE(6,304)DMU,SMU,AS
    WRITE(6,425)(R(I),I=1,3)
    RZERO=R(3)
 14 DET=LEPX(1,1)*LEPX(2,2)-LEPX(1,2)*LEPX(2,1)
    DO 56 N=1,4
    IF(ZET3P(3,N).GE.0.)GOTO17
    IF(IGRUND(N).NE.0)GO TO 18
    IGRUND(N)=1
    DO 41 K=1,2
 41 Z3PSD(K,N)=ZET3P(K,N)
 18 DO 13 K=1,3
 13 TEMP(K)=Z3PSD(K,N)-ZET2P(K,N)
    DO 19 I=1,3
    ZETP(I,N)=0.0
    DO 19 K=1,3
 19 ZETP(I,N)=ZETP(I,N)+LEPX(K,I)*TEMP(K)
    ITERAT=0
    NIT=0
    DO 708 J=1,NPAD
    DELZX(J)=DELZ(J,N)
```

```
      PDPSTX(J)=PDLPST(J,N)
      DELPSX(J)=DELPST(J,N)
      FMAXX(J)=FMAX(J,N)
  708 DELMXX(J)=DELMAX(J,N)
   35 AL(N)=SQRT(ZETP(1,N)**2+ZETP(2,N)**2+ZETP(3,N)**2)
      DEFN=RHO-AL(N)
      J=1
      IF(DEFN.GE.DELZ(1,N)) GO TO 704
      IF(ITERAT.EQ.0) GO TO 17
      AF(1)=0.0
      GO TO 107
  704 CALL CURVE(FIN     ,DELIN     ,KLAST(1,N),IPASS,DELMAX(1,N),DEFN,S
     1LOPE(1),DAMP(1),DELPST(1,N),DELT,FMAX(1,N),AF(1),ILOAD(1,N),DELZ(1
     2,N),ITERAT,PDLPST(1,N),FD(1),J,N)
      IF(ITERAT.EQ.4) GO TO 40
  107 SA=SQRT(ZETP(1,N)**2+ZETP(2,N)**2)/AL(N)
      ALP(N)=ARSIN(SA)
      IF(ITERAT.NE.0) GO TO 706
      IF((ABS(ZETP(2,N)).LT.1.E-5).AND.(ABS(ZETP(1,N)).LT.1.E-5))
     1GO TO 120
      GO TO 20
  120 BET(N)=0.0
      GO TO 22
   20 BET(N)=ATAN2(ZETP(2,N),ZETP(1,N))
   22 CB=COS(BET(N))
      SB=SIN(BET(N))
  706 CA=COS(ALP(N))
  701 ALPM=0.0
      BETM=0.0
      DO 21 J=2,NPAD
      IF(ITERAT.NE.0) GO TO 702
      CGB(J)=AS*COS(GAM(J)-BET(N))
  702 DEFN=   ALP(N)*CGB(J)
      IF(DEFN.LE.DELZ(J,N)) GO TO 21
      CALL CURVE(FINX    ,DELINX    ,KLAST(J,N),IPASS,DELMAX(J,N),DEFN,S
     1LOPE(2),DAMP(2),DELPST(J,N),DELT,FMAX(J,N),AF(J),ILOAD(J,N),DELZ(J
     2,N),ITERAT,PDLPST(J,N),FD(J),J,N)
      IF(ITERAT.EQ.4) GO TO 40
      IF(NCUP.NE.1)GOTO606
      GOTO(1500,607,602,603,604),J
  607 NCUPX=4
      GOTO605
  602 NCUPX=5
      GOTO605
  603 NCUPX=2
      GOTO605
  604 NCUPX=3
  605 DELZ(NCUPX,N)=DELZ(J,N)
      DELMAX(NCUPX,N)=DELMAX(J,N)
  606 IF(ITERAT.NE.0) GO TO 703
      SGB(J)=SIN(GAM(J)-BET(N))*AS
  703 ALPM=ALPM+AF(J)*   CGB(J)
      BETM=BETM+AF(J)*SGB(J)
   21 CONTINUE
   34 FALP=ALPM/AL(N)
      FBET=BETM/AL(N)
      F(3,N)=SA*FALP+CA*AF(1)
      F(2,N)=CA*SB*FALP+CB*FBET-SA*SB*AF(1)
      F(1,N)=CA*CB*FALP-SB*FBET-SA*CB*AF(1)
      DO 23 I=1,3
```

```
      FE(I)=0.
      DO 23 J=1,3
   23 FE(I)=FE(I)+LEPX(I,J)*F(J,N)
      IF(FE(3).GT.0.)GO TO 25
      IF(ITERAT.EQ.0) GO TO 50
      FE(3)=0.0
   25 FE12=SQRT(FE(1)**2+FE(2)**2)
      IF(ITERAT.EQ.1)GO TO 705
      IF(ISSLIP(N).EQ.1)GO TO 27
      COEF=SMU
      GO TO 28
   27 COEF =DMU
   28 FF=COEF*FE(3)
      IF(FE12.GT.FF)GO TO 705
      ISSLIP(N)=0
      GO TO 44
  705 FF=DMU*FE(3)
      ISSLIP(N)=1
   40 CALL SLIP (FF,FE12,ALP(N),ITERAT,NIT,SLOPE(2),ALPM,AS,
     1F(1,N),F(2,N),F(3,N),ZETP(1,N),ZETP(2,N),ZETP(3,N),AL(N))
      IF(ITERAT.EQ.1) GO TO 48
      IF(ITERAT.EQ.2) GO TO 57
      IF(ITERAT.EQ.3) GO TO 49
      DO 55 I=1,3
      F(I,N)=PRF(I,N)
   55 MOM(I,N)=PRMOM(I,N)
      ALP(N)=PRALP(N)
      AL(N)=PRAL(N)
      GO TO 57
   48 CA=COS(ALP(N))
      SA=SIN(ALP(N))
      IF(NIT.GT.1) GO TO 45
      DO 33 I=1,3
      AP(I)=0.
      DO 33 J=1,3
   33 AP(I)=AP(I)+LEPX(J,I)*ZET2P(J,N)
   45 ZETP(1,N)=AL(N)*SA*CB
      ZETP(2,N)=AL(N)*SA*SB
      DO 32 I=1,2
   32 AR(I)=-ZETP(I,N)-AP(I)
      ZETP(3,N)=-AP(3)+(AR(1)*(LEPX(1,2)*LEPX(2,3)-LEPX(1,3)*LEPX(2,2))-
     1AR(2)*(LEPX(1,1)*LEPX(2,3)-LEPX(1,3)*LEPX(2,1)))/DET
   57 DO 707 J=1,NPAD
      PDLPST(J,N)=PDPSTX(J)
      DELZ(J,N)=DELZX(J)
      DELPST(J,N)=DELPSX(J)
      FMAX(J,N)=FMAXX(J)
  707 DELMAX(J,N)=DELMXX(J)
      IF(ITERAT.EQ.2) GO TO 44
      IF(ITERAT.EQ.4) GO TO 56
      GOTO35
   49 IF(IPASS.EQ.1) GO TO 44
      Z3PSD(1,N)=(ZET2P(1,N)+LEPX(1,1)*ZETP(1,N)+LEPX(1,2)*ZETP(2,N)+
     1LEPX(1,3)*ZETP(3,N)+Z3PSD(1,N))*0.5
      Z3PSD(2,N)=(ZET2P(2,N)+LEPX(2,1)*ZETP(1,N)+LEPX(2,2)*ZETP(2,N)+
     1LEPX(2,3)*ZETP(3,N)+Z3PSD(2,N))*0.5
      ITERAT=0
   44 MOM(1,N)=-F(2,N)*ZETP(3,N)+F(3,N)*ZETP(2,N)
      MOM(2,N)=-F(3,N)*ZETP(1,N)+F(1,N)*ZETP(3,N)
      MOM(3,N)=-F(1,N)*ZETP(2,N)+F(2,N)*ZETP(1,N)
```

```
      ALU=-DELZX(1)+RHO
      SA=SIN(ALP(N))
      CA=COS(ALP(N))
      ZETA(1,N)=ALU*SA*CB
      ZETA(2,N)=ALU*SA*SB
      ZETA(3,N)=-ALU*CA
      ALM(N)=AMAX1(ALM(N),ALP(N))
      ALMIN(N)=AMIN1(ALMIN(N),AL(N))
      GO TO 15
   17 IF(IGRUND(N).EQ. 0)GOTO50
      AL(N)=RHO-DELZ(1,N)
      ITERAT=0
      IGRUND(N)=0
      ISSLIP(N)=1
   50 DO 36 I=1,3
      F(I,N)=0.
   36 MOM(I,N)=0.
   15 DO 58 I=1,3
      PRF(I,N)=F(I,N)
   58 PRMOM(I,N)=MOM(I,N)
      PRALP(N)=ALP(N)
      PRAL(N)=AL(N)
   56 CONTINUE
   10 RETURN
 1500 CALL PANIC(24H MAX ITERATIONS EXCEEDED)
  301 FORMAT(///40X40HDYNAMIC FORCE DEFLECTION CHARACTERISTICS //47X5HAX
     1IAL 12X10HROTATIONAL//42X16HFORCE   DEFLECT.4X16HFORCE   DEFLECT./
     242X5H(LBS)5X4H(FT)6X5H(LBS)5X4H(FT)/(37XF10.2,F10.5,F10.2,F10.5))
  302 FORMAT(///49X24HUNLOADING SLOPES (LB/FT)//47X5HAXIAL 12X10HROTATIO
     1NAL//33X2E20.5)
  305 FORMAT(///49X20HDAMPING COEFFICIENTS//47X5HAXIAL12X10HROTATIONAL//
     133X2E20.5///44X22HABSORBER LENGTH (FT) =F7.3)
  425 FORMAT(//45X 32HTRANSLATIONAL DISPLACEMENTS (FT)//29X4HR(1) 22X
     14HR(2) 24X 4HR(3)/7X 3F27.3)
  303 FORMAT(///35X48HANGULAR LOCATIONS OF ROTATIONAL ABSORBERS (DEG.)//
     123X6HGAM(1)4X6HGAM(2)4X6HGAM(3)4X6HGAM(4)4X6HGAM(5)4X6HGAM(6)4X
     26HGAM(7)4X6HGAM(8)/19X8F10.2)
  304 FORMAT(///45X32HTERRAIN COEFFICIENTS OF FRICTION//50X7HDYNAMIC 10X
     16HSTATIC/49XF10.2,7XF10.2///40X40HLEVER ARM TO ROTATIONAL ABSORBER
     2S (FT) =F6.2)
  306 FORMAT(/5X78HSUBROUTINE FORCE HAS TEMPORARILY REDUCED THE SLIPPING
     1 TOLERANCE ON LEG NUMBER I1,9H AT TIME=E16.8)
  601 FORMAT(///40X23HTHIS CONFIGURATION HAS I1,17H PADS AT EACH LEG)
  609 FORMAT(///39X41HOPPOSITE ROTATIONAL ABSORBERS ARE COUPLED        )
      END
```

```
$IBFTC QUIMOT
      SUBROUTINE QUIMOT
C     THIS SUBROUTINE IS USED FOR THE TELESCOPING LEG SIMULATION
      COMMON/JOHN/THETA
      COMMON/BOUND/OMEG1,LKX,A1,B1,C1,U,G,SGAM,CGAM,CRTR,W,WD,LEH
      COMMON/FUN/LEPX(3,3),LETAX(3,3),F(3,4),MOM(3,4),B(3,4),R(3),RD(3),
     1RDD(3),XD(3),XDD(3),OMEG(3),TAX,M,ROLLD,ROLL,YAWD,YAW,PITCHD,PITCH
     2,OMEGD(3),IPASS,CDR,CRD,Z3F(4),ZET3P(3,4),RHO
      COMMON/ST/ALP(4),AL(4)
      REAL M
      DIMENSION XI(3,4),XH(4),D(4),ETA(4),TAU(4),GAMDCR(4),GAMDOT(4),XIM
     1(4),DXI(4)
      DIMENSION BETWRT(4)
      DIMENSION LKX(3,3),W(3),WD(3),LEH(3,3)
      GM=G*M
      ISET=0
      BETWRT(1)=-135.0*CDR
      BETWRT(2)=- 45.0*CDR
      BETWRT(3)=+45.0*CDR
      BETWRT(4)=+135.0*CDR
      DO 1 I=1,4
    1 TAU(I)=1.7
      DO 5 I=1,4
      J=I+1
      IF(J.GT.4)J=1
      XI(1,I)=AL(I)*SIN(ALP(I))*COS(BETWRT(I))+B(1,I)
      XI(1,J)=AL(J)*SIN(ALP(J))*COS(BETWRT(I))+B(1,J)
      XI(2,I)=AL(I)*SIN(ALP(I))*SIN(BETWRT(I))+B(2,I)
      XI(2,J)=AL(J)*SIN(ALP(J))*SIN(BETWRT(I))+B(2,J)
      XI(3,I)=-AL(I)*COS(ALP(I))+B(3,I)
      XI(3,J)=-AL(J)*COS(ALP(J))+B(3,J)
      XIM(I)=      XI(1,I)**2+XI(2,I)**2+XI(3,I)**2
      XIM(J)=      XI(1,J)**2+XI(2,J)**2+XI(3,J)**2
    2 DXI(I)=(XI(1,J)-XI(1,I))**2+(XI(2,J)-XI(2,I))**2+(XI(3,J)-XI(3,I))
     1**2
      XH(I)=XIM(I)+(XIM(I)+DXI(I)-XIM(J))**2/(-4.0*DXI(I))
      D(I)=SQRT(XIM(I)-XH(I))
      XH(I)=SQRT(XH(I))
      DXI(I)=SQRT(DXI(I))
      ETA(I)=XI(3,I)+ D(I)*(XI(3,J)-XI(3,I))/DXI(I)
    3 TAU(I)=ARSIN(-ETA(I)/XH(I))
      IF(ABS(TAU(I)+THETA)*CRD.GE.90.0) GO TO 5
      GAMDOT(I)=OMEG1+ SQRT(RD(1)**2+RD(2)**2+RD(3)**2)/XH(I)
      GAMDCR(I)=SQRT(2.0*GM*XH(I)*(1.0-SIN(TAU(I)+THETA))/(M*XH(I)**2+A1
     1))
    4 IF(GAMDOT(I).LT.GAMDCR(I))ISET=ISET+1
    5 CONTINUE
      IF(ISET.LT.4)GO TO 10
      WRITE(6,101) GAMDCR
      WRITE(6,100) GAMDOT
      CALL PANIC(41HTHE SPACE PACKAGE IS IN A STABLE POSITION)
  100 FORMAT(///4X10HGAMDOT(1)=E16.8,4X10HGAMDOT(2)=E16.8,4X10HGAMDOT(3)
     1=E16.8,4X10HGAMDOT(4)=E16.8///)
  101 FORMAT(///4X10HGAMDCR(1)=E16.8,4X10HGAMDCR(2)=E16.8,4X10HGAMDCR(3)
     1=E16.8,4X10HGAMDCR(4)=E16.8///)
   10 RETURN
      END
```

```
$IBFTC SLIP
      SUBROUTINE SLIP (FF,FE12,ALP,ITERAT,NIT,SLOPE,ALPM,AS,
     1F1,F2,F3,Z1,Z2,Z3,AL)
C     THIS SUBROUTINE IS USED FOR THE TELESCOPING LEG SIMULATION
      COMMON TIME,DELT,NSTART,NFIRST,NEXIT ,IPASS,NTARGT,XNOISE(8),
     1RMT,DELMTN,DELMTE,DELMTD,ROMCOM(1482)
      REAL LITALP,LFF,LFE12
      IF(ITERAT.EQ.4) GO TO 31
      IF(FF+FE12.LE.50.0) ITERAT=3
      DEN=FF+FE12
      IF(DEN.LT.100.0) DEN=100.
      IF(ITERAT.EQ.1) GO TO 29
      IF(ITERAT.EQ.3) GO TO 413
  405 A=1000.
      FALP=ALP
      FFF=FF
      FFE12=FE12
      FF1=F1
      FF2=F2
      FF3=F3
      FZ1=Z1
      FZ2=Z2
      FZ3=Z3
      FAL=AL
      NDA=0
      TOL=0.001
      VNIT=0.0
      ITERAT=1
      KONVER=0
      DA=0.10*ALPM/(SLOPE*AS**2)
      IF(DA.LT.0.00005) DA=0.00005
      IF(DA.GT.ALP*.1)DA=.10*ALP
      NTROUB=0
   29 ASAVE=A
      PDA=DA
      A=ABS( (FE12-FF)/DEN)
      IF(KONVER.EQ.1) GO TO 30
      DA=DA*SQRT(1.0+VNIT)
      IF(DA.LE.0.0) NDA=1
      IF(ABS(DA).GT.ALP*.1) DA=(DA/ABS(DA))*0.1*ALP
   30 IF(ABS(ASAVE-A).LT.1.E-7.AND.A.LT.1.0) GO TO 45
      IF(A.GT.TOL  )GO TO 48
      IF(KONVER.EQ.0) GO TO 48
      IF(FF+FE12.GT.5.00*(FFF+FFE12)
     1.OR.ABS((FALP-ALP)/FALP).GT.0.1) GO TO 31
      ITERAT=3
      GO TO 413
   45 ITERAT=2
      GO TO 413
   48 NIT=NIT+1
      VNIT=FLOAT(NIT)
      IF(NIT.LT.20)GO TO 47
      TOL=0.1
      IF(NIT.LT.30) GO TO 47
      IF((FF+FE12).GT.200.) GO TO 46
      ITERAT=2
      GO TO 413
   46 ITERAT=4
      GO TO 413
   47 IF(KONVER.EQ.1)GOTO406
```

```
      IF(FE12.GT.FF)GOTO407
      KONVER=1
      LITALP=ALP
      BIGALP=PALP
      NIT=2
      VNIT=0.0
      IF(DA.GT.0.0) GO TO 49
      BFF=FF
      BFE12=FE12
      LFF=PFF
      LFE12=PFE12
      GO TO 408
   49 LFF=FF
      LFE12=FE12
      BFF=PFF
      BFE12=PFE12
      GOTO408
  407 PALP=ALP
      IF(A.LE.ASAVE) GO TO 412
  404 ALP=ALP+DA
      DA=-DA
  412 ALP    =ALP    -DA
      PFF=FF
      PFE12=FE12
      IF(DA.GT.0.0) GO TO 50
      LFF=FF
      LFE12=FE12
      GO TO 410
   50 BFF=FF
      BFE12=FE12
      GOTO410
  406 IF(FE12.GT.FF)GOTO409
      LITALP=ALP
      LFF=FF
      LFE12=FE12
      GO TO 411
  409 BIGALP=ALP
      BFF=FF
      BFE12=FE12
  411 IF(NDA.EQ.1) GO TO 414
      IF(NIT.GT.9) GO TO 414
      GO TO 408
  414 ALP=(BIGALP+LITALP)*0.5
      GO TO 410
  408 ALP=LITALP+(BIGALP-LITALP)/(1.0+(BFF-BFE12)/(LFE12-LFF))
  410 IF(ALP    .GT.0.)GO TO 413
      IF(NTROUB.EQ.1)GO TO 17
      NTROUB=1
      ALP    =0.
  413 RETURN
   17 ITERAT=2
      GO TO 413
   31 ITERAT=2
      FF=FFF
      FE12=FFE12
      ALP=FALP
      F1=FF1
      F2=FF2
      F3=FF3
      Z1=FZ1
```

```
Z2=FZ2
Z3=FZ3
AL=FAL
GO TO 413
END
```

```
$IBFTC XCURVE
      SUBROUTINE CURVE(FIN,DELIN,KLAST,IPASS,DELMAX,DEFN,SLOPE,DAMP,
     1DELPST,DELT,FMAX,AF,ILOAD,DELZ,ITERAT,PDLPST,FD,J,N)
C     THIS SUBROUTINE IS USED FOR THE TELESCOPING LEG SIMULATION
      DIMENSION FIN(10),DELIN(10)
      NSET=0
  200 IF(DEFN-DELMAX)300,240,240
  240 AA=DEFN
      DO 250 K=KLAST,9
      BB=DELIN(K)
      CC=DELIN(K+1)
      IF(AA.GE.BB.AND.AA.LE.CC)GO TO 260
  250 CONTINUE
      IF(NSET.EQ.1) GO TO 253
      KLAST=1
      NSET=1
      GO TO 240
  253 IF(ITERAT.NE.0) GO TO 251
      WRITE(6,252)DEFN,J,N
  252 FORMAT(1H1,19HOVER DEFLECTION OF E16.8,9H  AT PAD I2,9H  OF LEG I2
     1)
      CALL PANIC (29HO DEFLECTION NOT WITHIN TABLE)
  260 D=(AA-BB)/(CC-BB)
      AF=FIN(K)+D*(FIN(K+1)-FIN(K))
      KLAST=K
      IF (IPASS.EQ.1)GOTO500
      IF(DEFN.LE.DELMAX)GOTO500
      FMAX=AF
      DELMAX=DEFN
      DELZ=DELMAX-FMAX/SLOPE
      GO TO 500
  300 IF(IPASS-3)310,320,330
  310 C13=3.0
      C12=2.0
      C11=1.0
      GO TO 400
  320 C13=4.0
      C12=3.0
      C11=1.0
      GO TO 400
  330 C13=1.0
      C12=1.0
      C11=0.0
  400 FS=FMAX-SLOPE*(DELMAX-DEFN)
      IF(FS.LT.0.0) FS=0.0
      IF(DAMP.LT.1.E-5) GO TO 390
      FD=DAMP*(C13*(DEFN-DELPST)+C11*(DELPST-PDLPST))/(DELT*C12)
  402 IF (ABS(FD).LE.1.E-5) GO TO 401
      IF((FS/ABS(FD)).GT.1.1111111)GOTO401
      FD=SIGN(FS,FD)*.9
      GO TO 401
  390 FD=0.0
  401 AF=FS+FD
      IF(AF.GT.FMAX) AF=FMAX
      IF(AF.LT.0.) AF=0.0
  500 IF(IPASS.NE.4) GO TO 510
      PDLPST=DELPST
      DELPST=DEFN
  510 RETURN
  251 ITERAT=4
```

```
GO TO 510
END
```

```
$IBFTC BOUNCX
      SUBROUTINE BOUNCE
C     THIS SUBROUTINE IS USED FOR THE TELESCOPING LEG SIMULATION
      COMMON TIME,DELT,NSTART,NFIRST,NEXIT ,IPASS,NTARGT,XNOISE(8),
     1RMT,DELMTN,DELMTE,DELMTD,ROMCOM(1482)
      COMMON/JOHN/THETA
      COMMON/ANGL/PH ,PS ,TH,KFIRST,KRETRN
      COMMON/BOUND/OMEG1,LKX,A1,B1,C1,U,G,SGAM,CGAM,CRTR,W,WD,LEH
      COMMON/TRANS/AL(4),ALP(4),BET(4),SENR,RZERO
      COMMON/FUN/LEPX(3,3),LETAX(3,3),F(3,4),MOM(3,4),B(3,4),R(3),RD(3),
     1ROD(3),XD(3),XDD(3),OMEG(3),TAU,M,ROLLD,ROLL,YAWD,YAW,PITCHD,PITCH
     2,OMEGD(3),IPASS,CDR,CRD,Z3F(4),ZET3P(3,4),RHO
      COMMON/FREE/T,LHX(3,3),TMIN,KONVER,DPH,DPS,CT,ST,ZX(3,4),C2,DT,LKH
     1(3,3)
      DIMENSION LKX(3,3),W(3),WD(3),LEH(3,3)
      DIMENSION Z1(4)
      REAL LEH,LHX,LKX ,LKH,LETAX ,LEPX
      FTIM(SV,SQ,S)=(SV+S*SQRT(SQ))*U/CGAM
      FSQ(SV,SDEL)=SV**2-2.*G*SDEL*CGAM
      KONVER=0
      KFIRST=0
      KRETRN=0
      C2=.5*G*CGAM
      PH=ATAN2 (OMEG(1),OMEG(2))
      SPH=SIN(PH)
      CPH=COS(PH)
      PS=0.
      SPS=0.
      CPS=1.
      OMEG12=SQRT(OMEG(1)**2+OMEG(2)**2)
      IF((ABS(OMEG12).GT.1.E-5).OR.(ABS(OMEG(3)).GT.1.E-5))GOTO1
      ST=0.
      IF(OMEG(3).GE.0.)GO TO 2
      TH=3.1415927
      CT=-1.
      GO TO 4
    2 CT=1.
      TH=0.
      GO TO 4
    1 TH=ATAN2(A1*OMEG12,C1*OMEG(3))
      CT=COS(TH)
      ST=SIN(TH)
    4 CALL SUBLHX(SPH,CPH,SPS,CPS,CT,ST,LHX)
      DO 6 I=1,3
      DO 6 J=1,3
      LEH(I,J)=0.
      LKH(I,J)=0.
      DO 6 K=1,3
      LKH(I,J)=LKH(I,J)+LKX(I,K)*LHX(J,K)
    6 LEH(I,J)=LEH(I,J)+LEPX (I,K)*LHX(J,K)
      C=C1/(A1-C1)
      DPH=OMEG(3)/(1.+C)
      DPS=C*DPH/CT
      ZMAX=0.
      DO 7 N=1,4
      SA=SIN(ALP(N))
      ZX(1,N)=B(1,N)+AL(N)*SA*COS(BET(N))
      ZX(2,N)=B(2,N)+AL(N)*SA*SIN(BET(N))
      ZX(3,N)=B(3,N)-AL(N)*COS(ALP(N))
      Z1(N)=SQRT (ZX(1,N)**2+ZX(2,N)**2+ZX(3,N)**2)
```

```
  7 ZMAX=AMAX1(ZMAX,Z1(N0))
    SV=RD(3)
    SDEL=CRTR-R(3)
    SQ=FSQ(SV,SDEL)
    IF(SQ.LE.0.)GOTO31
    T3=FTIM(SV,SQ,1.)
    TMIN=T3
    SDEL=ZMAX-R(3)
    SQ=FSQ(SV,SDEL)
    IF(SQ.LE.0.)GOTO30
    T1=FTIM(SV,SQ,-1.)
    T2=FTIM(SV,SQ,1.)
    T=0.
    IF(T.GT.T1)GO TO 8
    DT=T1/25.
    IF(DT.GT.DELT)GOTO10
    DT=DELT
 10 DO 12 I=1,25
    CALL TIMPIC
    IF(KONVER.EQ.1)GO TO 100
    IF(KRETRN.EQ.1)GO TO 31
    KFIRST=1
    T=T+DT
 12 CONTINUE
    GOTO8
 30 T2=0.
  8 T=T2
    SDEL=T3-T2
    DT=SDEL/25.
    IF(DT.GT.DELT)GOTO14
    DT=DELT
 14 DO 16 I=1,25
    CALL TIMPIC
    IF(KONVER.EQ.1)GO TO 100
    IF(KRETRN.EQ.1)GO TO 31
    KFIRST=1
    T=T+DT
 16 CONTINUE
    CALL PANIC(115HTHE FREE FLIGHT EQUATIONS INDICATE THAT CAPSULE WIL
   1L EXCEED THE CRITICAL THETA BEFORE RECONTACTING THE GROUND.
   2 )
100 T=TMIN-2.*DELT
    PH=DPH*T+PH
    PS=DPS*T+PS
    SPH=SIN(PH )
    CPH=COS(PH )
    SPS=SIN(PS )
    CPS=COS(PS )
    CALL SUBLHX(SPH,CPH,SPS,CPS,CT,ST,LHX)
    R(2)=R(2)+RD(2)*T+5.*SGAM*G*T**2
    R(1)=R(1)+RD(1)*T
    R(3)=R(3)+RD(3)*T-C2*T**2
    RD(3)=RD(3)-2.*C2*T
    RD(2)=RD(2)+G*SGAM*T
    DO 32 I=1,3
    DO 32 J=1,3
    LEPX(I,J)=0.0
    LKX(I,J)=0.0
    DO 32 K=1,3
    LKX(I,J)=LKX(I,J)+LKH(I,K)*LHX(K,J)
```

```
 32 LEPX(I,J)=LEPX(I,J)+LEH(I,K)*LHX(K,J)
    OMEG(1)=DPS*ST*SPH
    OMEG(2)=DPS*ST*CPH
    OMEGD(1)=DPH*DPS*ST*CPH
    OMEGD(2)=-DPH*DPS*ST*SPH
    DO 17 I=1,3
    XDD(I)=0.0
    WD(I)=0.
    W(I)=0.
    DO 17 J=1,3
    XDD(I)=XDD(I)+LEPX(J,I)*RDD(J)
    W(I)=W(I)+LETAX(I,J)*OMEG(J)
 17 WD(I)=WD(I)+LETAX(I,J)*OMEGD(J)
    IF(ABS(LKX(3,1)).GT..99985) CALL PANIC(110H COS(YAW) AT RECONTACT
   1IS NEARLY EQUAL TO ZERO.  THIS CONDITION CAN NOT BE HANDLED BY THE
   2 D.E.MONITOR.
    PITCH=ATAN2(LKX(3,2),LKX(3,3))
    ROLL=ATAN2(LKX(2,1),LKX(1,1))
    SP=SIN(PITCH)
    CP=COS(PITCH)
    SR=SIN(ROLL)
    CR=COS(ROLL)
    IF(ABS(SP)-.707)20,21,21
 20 YAW=ATAN2(-LKX(3,1),LKX(3,3)/CP)
    GOTO22
 21 YAW=ATAN2(-LKX(3,1),LKX(3,2)/SP)
 22 SY=SIN(YAW)
    CY=COS(YAW)
    ROLLD=(OMEG(2)*SP+OMEG(3)*CP)/CY
    YAWD=OMEG(2)*CP-OMEG(3)*SP
    PITCHD=OMEG(1)+SY/CY*(OMEG(2)*SP+OMEG(3)*CP)
    THETA=ARSIN(SQRT(SY**2+CY**2*SP**2))
    N=T/DELT
    XN=N
    XT=XN*DELT
    WRITE(6,200)TIME
    TIME=TIME+XT
    IF(T-XT.GT..5*DELT) TIME=TIME+DELT
    WRITE(6,201)TIME
    CALL QUIMOT
 31 RETURN
200 FORMAT(////////10X67HSUBROUTINE BOUNCE HAS TAKEN CONTROL FROM THE D
   1.E. MONITOR AT TIME = F8.4)
201 FORMAT(10X50HCONTROL WAS RETURNED TO THE D.E. MONITOR AT TIME = F8
   1.4)
    END
```

```
$IBFTC FUNEX   LIST,DECK
C
      SUBROUTINE FUNEV
C
C     SPACE PACKAGE ALIGHTMENT
C     PROBLEM NO. 970
C
C     THIS SUBROUTINE IS USED FOR THE ARTICULATED LEG SIMULATION
      COMMON TIME,DELT,NSTART,NFIRST,NEXIT ,IPASS,NTARGT,XNOISE(8),
     1RMT,DELMTN,DELMTE,DELMTD,ROMCOM(1482)
      COMMON/JOHN/THETA
      COMMON/BOUND/OMEG1,LKX,A1,B1,C1,U,G,SGAM,CGAM,CRTR,W,WD,LEH
      COMMON/TRANS/PS(4),ALP(4),BET(4),KONFIG,SENR,RZERO
      COMMON/FUN/LEPX(3,3),LETAX(3,3),F(3,4),MOM(3,4),B(3,4),R(3),RD(3),
     1RDD(3),XD(3),XDD(3),OMEG(3),TAU,M,ROLLD,ROLL,YAWD,YAW,PITCHD,PITCH
     2,OMEGD(3),IPASS,CDR,CRD,Z3F(4),ZET3P(3,4),RHO
      DIMENSION DDX(7,3)
      DIMENSION LEH(3,3)
      DIMENSION NP(19),W(3),WD(3),FF(3)
      DIMENSION LKX(3,3),YL(19),     XL(3),XM(3),YU(19),              V(3
     1),LEPK(3,3),ID(24)
      COMMON/PAIN/ NPLOT
      DIMENSION IDL(20),IDR(20),DSC(20)
      REAL LEPX,LETAX,      LEPK,LKX,MOM,M
      IF(NSTART)100,200,10
   10 CONTINUE
    2 FORMAT(2E10.8,I10)
    1 FORMAT(6E10.8)
   11 FORMAT (3E10.4)
   12 FORMAT(5I10)
C
C     INITIAL INPUT CONDITIONS ARE READ INTO THE PROGRAM
C
      N=4
      NPOW=0
      NPOO=0
      READ(5,12)NDLT,NPLOT,NSTOP,NSHOCK,KONFIG
      READ(5,11)TAUS,TIMSHK
      IF(NSHOCK.EQ.2)NSHOCK=0
      NSHOCK=NSHOCK+1
      READ (5,11) R
      READ (5,11) V
      READ (5,11)ROLL, YAW, PITCH
      READ (5,11) OMEG,
      READ (5,11) A1, B1, C1
      READ (5,11) GM, CRTHA, CRTR
      READ (5,11) G, GAMA
      READ(5,11)((LETAX(I,J),J=1,3),I=1,3)
      READ (5,11) ((B(I,J),I=1,3),J=1,N)
      IF(V(3).GT.0.)V(3)=-V(3)
      IPASS=4
      NOPRNT=0
      NCOUNT=0
      NSET=1
      U=1./G
      M=GM/32.17
      NVALUE=0
      NCARD=0
      VB=SQRT(B(1,1)**2+B(2,1)**2+(B(3,1)-RHO)**2)
      CDR=0.01745329
```

```
      CRD=1.0/CDR
      THETA=0.0
      CRTAGL=COS(CRTHA*CDR)
      ROLL=ROLL*CDR
      YAW=YAW*CDR
      PITCH=PITCH*CDR
      GAMA=GAMA*CDR
      SGAM=SIN(GAMA)
      CGAM=COS(GAMA)
      PERIOD=0.0
      CALL FORCE
      GO TO (13,14),NPLOT
   13 READ(5,15)IDP
   15 FORMAT(I3)
      READ(5,16)(IOR(J),DSC(J),J=1,20)
   16 FORMAT(4(I10,E10.0))
      WRITE(7,17)
   17 FORMAT(126H3     -8005 -8005 -8005 -8005 -8005 -8005 -8005 -8005 -
     18005 -8005 -8005 -8005 -8005 -8005 -8005 -8005 -8005 -8005 -
     28005 )
      IDC=0
C
C     INTERNAL CONVERSION AND SET UP.
C
C
C     BOUNDARY CONDITION FOR QUIESENCE OF MOTION CRITERIA.
C
   14 DLT=DELT
      VNDLT=FLOAT(NOLT)
      VVDELT=VNDLT*DELT
C
C     INITIALIZE THE TRANSFORMATION MATRIX BETWEEN THE EPSILON AND KAPPA
C     COORDINATE SYSTEMS.
C
      LEPK(1,1)=1.0
      LEPK(1,2)=0.0
      LEPK(1,3)=0.0
      LEPK(2,1)=0.0
      LEPK(2,2)=CGAM
      LEPK(2,3)=-SGAM
      LEPK(3,1)=0.0
      LEPK(3,2)=SGAM
      LEPK(3,3)=CGAM
C
C     TRANSFORM THE INITIAL TRANSLATIONAL AND ROTATIONAL VELOCITIES.
C
      DO 20 I=1,3
      W(I)=0.
      RD(I)=0.0
      DO 20 J=1,3
      W(I)=W(I)+LETAX(I,J)*OMEG(J)
   20 RD(I)=RD(I)+LEPK(I,J)*V(J)
      QUIVEX=.025*(M*SQRT(RD(1)**2+RD(2)**2)+ABS(C1*OMEG(3)))
      QUIVEL=.025*(ABS(M*RD(3))+SQRT((A1*OMEG(1))**2+(B1*OMEG(2))**2))
C
C     SET UP INDIRECT ADDRESSING FOR THE INTEGRATION ROUTINE
C     IN THE D.E. MONITOR.
C
      CALL INTG(RDD(1),RD(1))
      CALL INTG(RDD(2),RD(2))
```

```
      CALL INTG(RDD(3),RD(3))
      CALL INTG(WD(1),W(1))
      CALL INTG(WD(2),W(2))
      CALL INTG(WD(3),W(3))
      CALL INTG(ROLLD,ROLL)
      CALL INTG(YAWD,YAW)
      CALL INTG(PITCHD,PITCH)
      CALL INTG(RD(1),R(1))
      CALL INTG(RD(2),R(2))
      CALL INTG(RD(3),R(3))
  100 NSUBRT=1000
C
C     FORMAT SETUP FOR THE PRINT ROUTINE.
C
      CALL PRINT(12H  R(1) (FT) ,12H,E12.4       ,R(1),ID(1),0)
      CALL PRINT(12H  RD(1) FPS ,12H,E12.4       ,RD(1),ID(1),0)
      CALL PRINT(12H XDD(1) (G) ,12H,E12.4       ,XDD(1),ID(1),U)
      CALL PRINT(12H  R(2) (FT) ,12H,E12.4       ,R(2),ID(2),0)
      CALL PRINT(12H  RD(2) FPS ,12H,E12.4       ,RD(2),ID(2),0)
      CALL PRINT(12H XDD(2) (G) ,12H,E12.4       ,XDD(2),ID(1),U)
      CALL PRINT(12H  R(3) (FT) ,12H,E12.4       ,R(3),ID(3),0)
      CALL PRINT(12H  RD(3) FPS ,12H,E12.4       ,RD(3),ID(3),0)
      CALL PRINT(12H XDD(3) (G) ,12H,E12.4       ,XDD(3),ID(1),U)
      CALL PRINT(12HOMEGA(1)R/S ,12H,E12.4       ,OMEG(1),ID(4),0)
      CALL PRINT(12HOMD(1) R/S2 ,12H,E12.4       ,OMEGD(1),ID(4),0)
      CALL PRINT(12HOMEGA(2)R/S ,12H,E12.4       ,OMEG(2),ID(5),0)
      CALL PRINT(12HOMD(2) R/S2 ,12H,E12.4       ,OMEGD(2),ID(5),0)
      CALL PRINT(12HOMEGA(3)R/S ,12H,E12.4       ,OMEG(3),ID(6),0)
      CALL PRINT(12HOMD(3) R/S2 ,12H,E12.4       ,OMEGD(3),ID(6),0)
      CALL PRINT(12H ROLL (DEG) ,12H,E12.4       ,ROLL,ID(7),CRD)
      CALL PRINT(12H  YAW (DEG) ,12H,E12.4       ,YAW,ID(8),CRD)
      CALL PRINT(12HPITCH (DEG) ,12H,E12.4       ,PITCH,ID(9),CRD)
      CALL PRINT(12H FORCE(1,1) ,12H,E12.4       ,F(1,1),ID(13),0)
      CALL PRINT(12H FORCE(2,1) ,12H,E12.4       ,F(2,1),ID(15),0)
      CALL PRINT(12H FORCE(3,1) ,12H,E12.4       ,F(3,1),ID(17),0)
      CALL PRINT(12HMOMENT(1,1) ,12H,E12.4       ,MOM(1,1),ID(19),0)
      CALL PRINT(12HMOMENT(2,1) ,12H,E12.4       ,MOM(2,1),ID(21),0)
      CALL PRINT(12HMOMENT(3,1) ,12H,E12.4       ,MOM(3,1),ID(23),0)
      CALL  PRINT(12H PSI(1) DEG ,12H,E12.5       ,PS(1),0,57.295779)
      CALL  PRINT(12HALPHA 1(DEG),12H,E12.5       ,ALP(1),0,57.295779)
      CALL  PRINT(12HBETA 1 (DEG),12H,E12.5       ,BET(1),0,57.295779)
      CALL PRINT(12H FORCE(1,2) ,12H,E12.4       ,F(1,2),ID(13),0)
      CALL PRINT(12H FORCE(2,2) ,12H,E12.4       ,F(2,2),ID(15),0)
      CALL PRINT(12H FORCE(3,2) ,12H,E12.4       ,F(3,2),ID(17),0)
      CALL PRINT(12HMOMENT(1,2) ,12H,E12.4       ,MOM(1,2),ID(19),0)
      CALL PRINT(12HMOMENT(2,2) ,12H,E12.4       ,MOM(2,2),ID(21),0)
      CALL PRINT(12HMOMENT(3,2) ,12H,E12.4       ,MOM(3,2),ID(23),0)
      CALL  PRINT(12H PSI(2) DEG ,12H,E12.5       ,PS(2),0,57.295779)
      CALL  PRINT(12HALPHA 2(DEG),12H,E12.5       ,ALP(2),0,57.295779)
      CALL  PRINT(12HBETA 2 (DEG),12H,E12.5       ,BET(2),0,57.295779)
      CALL PRINT(12H FORCE(1,3) ,12H,E12.4       ,F(1,3),ID(13),0)
      CALL PRINT(12H FORCE(2,3) ,12H,E12.4       ,F(2,3),ID(15),0)
      CALL PRINT(12H FORCE(3,3) ,12H,E12.4       ,F(3,3),ID(17),0)
      CALL PRINT(12HMOMENT(1,3) ,12H,E12.4       ,MOM(1,3),ID(19),0)
      CALL PRINT(12HMOMENT(2,3) ,12H,E12.4       ,MOM(2,3),ID(21),0)
      CALL PRINT(12HMOMENT(3,3) ,12H,E12.4       ,MOM(3,3),ID(23),0)
      CALL  PRINT(12H PSI(3) DEG ,12H,E12.5       ,PS(3),0,57.295779)
      CALL  PRINT(12HALPHA 3(DEG),12H,E12.5       ,ALP(3),0,57.295779)
      CALL  PRINT(12HBETA 3 (DEG),12H,E12.5       ,BET(3),0,57.295779)
      CALL PRINT(12H FORCE(1,4) ,12H,E12.4       ,F(1,4),ID(13),0)
```

```
      CALL PRINT(12H FORCE(2,4) ,12H,E12.4       ,F(2,4),ID(15),0)
      CALL PRINT(12H FORCE(3,4) ,12H,E12.4       ,F(3,4),ID(17),0)
      CALL PRINT(12HMOMENT(1,4) ,12H,E12.4       ,MOM(1,4),ID(19),0)
      CALL PRINT(12HMOMENT(2,4) ,12H,E12.4       ,MOM(2,4),ID(21),0)
      CALL PRINT(12HMOMENT(3,4) ,12H,E12.4       ,MOM(3,4),ID(23),0)
      CALL  PRINT(12H PSI(4) DEG ,12H,E12.5       ,PS(4),0,57.295779)
      CALL  PRINT(12HALPHA 4(DEG),12H,E12.5       ,ALP(4),0,57.295779)
      CALL  PRINT(12HBETA 4 (DEG),12H,E12.5       ,BET(4),0,57.295779)
      CALL PRINT(12H  TRANS (G) ,12H,E12.4       ,XXDD,ID(11),0)
      CALL PRINT(12H THETA (DEG),12H,E12.4       ,THETA,ID(10),CRD)
      GO TO 500
C
C     POST INITIALIZATION PHASE OF THE PROGRAM.
C
  200 SROLL=SIN(ROLL)
      CROLL=COS(ROLL)
      SYAW= SIN(YAW)
      CYAW= COS(YAW)
      SPITCH=SIN(PITCH)
      CPITCH=COS(PITCH)
C
C     COMPUTATION OF THE TRANSFORMATION MATRIX BETWEEN THE KAPPA
C     AND CHI COORDINATE SYSTEMS.
C
      LKX(1,1)=CROLL*CYAW
      LKX(1,2)=-SROLL*CPITCH+CROLL*SYAW*SPITCH
      LKX(1,3)=SROLL*SPITCH+CROLL*SYAW*CPITCH
      LKX(2,1)=SROLL*CYAW
      LKX(2,2)=CROLL*CPITCH+SROLL*SYAW*SPITCH
      LKX(2,3)=-CROLL*SPITCH+SROLL*SYAW*CPITCH
      LKX(3,1)=-SYAW
      LKX(3,2)=CYAW*SPITCH
      LKX(3,3)=CYAW*CPITCH
      IF(NFIRST)227,228,227
  227 IF(NOPRNT.EQ.1)GOTO228
      NOPRNT=1
      RL=ROLL*CRD
      YW=YAW*CRD
      PH=PITCH*CRD
      GA=GAMA*CRD
C
C     WRITE OUT INITIAL INPUT PARAMETERS.
C
      WRITE(6,420)GA,RL,YW,PH
      WRITE(6,439)(OMEG(I),I=1,3)
      WRITE(6,436)(V(I),I=1,3)
      WRITE(6,442)GM
      WRITE(6,430)A1,B1,C1
      WRITE(6,441)((B(I,J),J=1,4),I=1,3)
      WRITE(6,443)((LETAX(I,J),J=1,3),I=1,3)
      WRITE(6,445)NDLT,G,CRTHA
      WRITE(6,3)CRTR
      GO TO(446,447),NPLOT
  446 WRITE(6,448)
      WRITE(6,1449)AID,IDP
 1449 FORMAT(//49X8HTITLE = 3A6///51X17HDEGREE OF PLOT = I3)
      GO TO 449
  447 WRITE(6,450)
  449 GO TO(451,452),NSTOP
  451 WRITE(6,453)
```

```
      GOTO458
  452 WRITE(6,454)
  458 GOTO(455,456),NSHOCK
  455 WRITE(6,457)
      GOTO501
  456 WRITE(6,459)TIMSHK
  501 GOTO(502,503),KONFIG
  502 WRITE(6,504)
      GOTO 228
  503 WRITE(6,505)
C
C     COMPUTE THE TRANSFORMATION MATRIX BETWEEN THE EPSILON AND
C     CHI COORDINATE SYSTEMS.
C
  228 DO 32 I=1,3
      DO 32 J=1,3
      LEPX(I,J)=0.0
      DO 32 K=1,3
   32 LEPX(I,J)=LEPX(I,J)+LEPK(I,K)*LKX(K,J)
C
C     EVALUATE THE FORCING FUNCTIONS.
C
   33 CALL FORCE
      IF(R(3).LT.CRTR)CALL PANIC(60HOTHE SPACE PACKAGE HAS EXCEEDED THE
     1CRITICAL DISPLACEMENT.
      DO 40 I=1,3
      FF(I)=0.
      DO 40 J=1,N
   40 FF(I)=FF(I)+F(I,J)
C
C     COMPUTATION OF THE MOMENTS IN THE CHI COORDINATE SYSTEM
C     DUE TO THE FORCES.
C
      XL(1)=0.0
      XL(2)=0.0
      XL(3)=0.0
      DO 230 J=1,N
      XL(1)=XL(1)+B(2,J)*F(3,J)-B(3,J)*F(2,J)+MOM(1,J)
      XL(2)=XL(2)+B(3,J)*F(1,J)-B(1,J)*F(3,J)+MOM(2,J)
  230 XL(3)=XL(3)+B(1,J)*F(2,J)-B(2,J)*F(1,J)+MOM(3,J)
C
C     SUMMATION OF THE XL AND ZM MOMENTS AND THE TRANSFORMATION FROM THE
C     CHI TO THE ETA COORDINATE SYSTEM.
C
      DO 250 I=1,3
      XM(I)=0.
      DO 250 J=1,3
  250 XM(I)=XM(I)+LETAX(I,J)*XL(J)
C
C     TRANSFORMATION OF THE FORCES FROM THE CHI TO THE EPSILON
C     COORDINATE SYSTEMS AND THE EVALUATION OF THE BASIC TRANSLATIONAL
C     EQUATIONS OF MOTION.
C
  260 DO 280 I=1,3
      RDD(I)=0.0
      DO 270 J=1,3
  270 RDD(I)=RDD(I)+LEPX(I,J)*FF(J)
  280 RDD(I)=RDD(I)/M+LEPK(I,3)*(-G)
C
C     THE EVALUATION OF EULER DYNAMICAL EQUATIONS.
```

```
C
      WD(1)=(XM(1)-W(2)*W(3)*(C1-B1))/A1
      WD(2)=(XM(2)-W(1)*W(3)*(A1-C1))/B1
      WD(3)=(XM(3)-W(1)*W(2)*(B1-A1))/C1
C
C     TRANSFORMATION OF THE INSTANTANEOUS ANGULAR ACCELERATION FROM THE
C     ETA TO THE CHI COORDINATE SYSTEM.
C
      DO 350 I=1,3
      OMEGD(I)=0.
      OMEG(I)=0.
      DO 350 J=1,3
      OMEGD(I)=OMEGD(I)+LETAX(J,I)*WD(J)
  350 OMEG(I)=OMEG(I)+LETAX(J,I)*W(J)
C
C     EVALUATION OF THE INSTANTANEOUS ROLL,YAW,AND PITCH RATES.
C
      ROLLD=(OMEG(2)*SPITCH+OMEG(3)*CPITCH)/CYAW
      YAWD=OMEG(2)*CPITCH-OMEG(3)*SPITCH
      PITCHD=OMEG(1)+SYAW/CYAW*(OMEG(2)*SPITCH+OMEG(3)*CPITCH)
C
C     TRANSFORMATION OF THE INSTANTANEOUS TRANSLATIONAL VELOCITIES
C     FROM THE CHI TO THE EPSILON COORDINATE SYSTEMS.
C
      DO 360 I=1,3
      XD(I)=0.
      DO 360 J=1,3
  360 XD(I)=XD(I)+LEPX(J,I)*RD(J)
      IF(IPASS.EQ.4)GO TO 366
      IPASS=IPASS+1
      GO TO 500
  366 IPASS=1
C
C     SET UP VARIABLES FOR PLOTTING
C
      GO TO (1000,1200),NPLOT
 1000 IF(TIME.EQ.0.0) GO TO 1002
      IDC=IDC+1
      IF(IDC.LT.IDP) GO TO 1200
      IDC=0
 1002 IDL(1 )=IOR(1 )+INT(TIME*DSC(1))
      IDL(2 )=IOR(2 )+INT(DSC(2 )*R(1))
      IDL(3 )=IOR(3 )+INT(DSC(3 )*R(2))
      IDL(4 )=IOR(4 )+INT(DSC(4 )*R(3))
      IDL(5 )=IOR(5 )+INT(DSC(5 )*RD(1))
      IDL(6 )=IOR(6 )+INT(DSC(6 )*RD(2))
      IDL(7 )=IOR(7 )+INT(DSC(7 )*RD(3))
      IDL(8 )=IOR(8 )+INT(DSC(8 )*XDD(1)*U)
      IDL(9 )=IOR(9 )+INT(DSC(9 )*XDD(2)*U)
      IDL(10)=IOR(10)+INT(DSC(10)*XDD(3)*U)
      IDL(11)=IOR(11)+INT(DSC(11)*OMEGD(1))
      IDL(12)=IOR(12)+INT(DSC(12)*OMEGD(2))
      IDL(13)=IOR(13)+INT(DSC(13)*OMEGD(3))
      IDL(14)=IOR(14)+INT(DSC(14)*ROLL*CDR)
      IDL(15)=IOR(15)+INT(DSC(15)*YAW *CDR)
      IDL(16)=IOR(16)+INT(DSC(16)*PITCH*COR)
      IDL(17)=IOR(17)+INT(DSC(17)*XXDD)
      IDL(18)=IOR(18)+INT(DSC(18)*OMEG(1))
      IDL(19)=IOR(19)+INT(DSC(19)*OMEG(2))
      IDL(20)=IOR(20)+INT(DSC(20)*OMEG(3))
```

```
      WRITE(7,1010)IDL
 1010 FORMAT(6X,20(I5,1X))
      IF(NFIRST.EQ.0) GO TO 980
      IF(NPOO.NE.0) GO TO 950
      NPOO=1
      NPOW=0
  950 NPOW=NPOW+1
      GO TO (980,960),NPOW
  960 NPOW=0
      WRITE(7,965)
  965 FORMAT(6H 1
      END FILE 7
  980 CONTINUE
 1200 CONTINUE
C
C     THE RUN IS ABORTED IF THE TEST AGAINST THE CRITICAL NUTATION
C     ANGLE HAS BEEN SATISFIED.
C
      IF((CPITCH*CYAW).GT.CRTAGL)GO TO 367
      CALL PANIC(59HOTHE SPACE PACKAGE HAS EXCEEDED THE CRITICAL NUTATIO
     1N ANGLE)
      GO TO 500
C
C     EVALUATION OF THE EULER NUTATION ANGLE THETA.
C
  367 THETA=ARSIN(SQRT(SYAW**2+CYAW**2*SPITCH**2))
      ENR=0.5*(M*(RD(1)**2+RD(2)**2+RD(3)**2)+A1*OMEG(1)**2+
     1B1*OMEG(2)**2+C1*OMEG(3)**2)+GM*((R(3)-RZERO)*CGAM-R(2)*SGAM)+SENR
C
C     TRANSFORMATION OF THE INSTANTANEOUS TRANSLATIONAL ACCELERATIONS
C     FROM THE CHI TO THE EPSILON COORDINATE SYSTEMS, AND
C     THE COMPUTATION OF THE ABSOLUTE MAGNITUDE OF THE RESULTANT
C     TRANSLATIONAL AND ROTATIONAL ACCELERATIONS.
C
      IF(NSTOP.EQ.2) GO TO 711
      IF(TIME.LT.0.05) GO TO 711
      NCOUNT=NCOUNT+1
      IF(NCOUNT.NE.50) GO TO 711
      CALL QUIMOT
      NCOUNT=0
  711 CONTINUE
      XXDD=0.
      OMEG1=0.
      OMEGD1=0.
      DO 369 I=1,3
      XDD(I)=0.
      DO 368 J=1,3
  368 XDD(I)=XDD(I)+LEPX(J,I)*RDD(J)
      XXDD=XXDD+XDD(I)**2
      OMEG1=OMEG1+OMEG(I)**2
  369 OMEGD1=OMEGD1+OMEGD(I)**2
      XXDD=(SQRT(XXDD))/G
      OMEGD1=SQRT(OMEGD1)
      OMEG1=SQRT(OMEG1)
      IF(NSHOCK.EQ.1)GOTO460
      NVALUE=NVALUE+1
      IF(TIME.LE.TIMSHK)GOTO473
      NSHOCK=1
      GOTO464
  473 DO461 I=1,3
```

```
  461 DDX(NVALUE,I)=XDD(I)*U
      IF(NVALUE.NE.7)GOTO460
  464 NCARD=NCARD+1
      DO462 I=1,3
  462 PUNCH 463,(DDX(J,I),J=1,7      ),I,NCARD
  463 FORMAT(7F10.5,I2,I8)
      NVALUE=0
C
C     EVALUATION OF THE CRITERIA FOR THE INTEGRATION INTERVAL.
C
  460 IF(ABS(XXDD-1.0)-1.0E-5)372,372,376
  372 IF(NSET.LT.3)GO TO 375
  374 IF(NSHOCK.EQ.1)GOTO467
      NSHOCK=1
      IF(NVALUE.EQ.0)GOTO467
      NCARD=NCARD+1
      DO466 I=1,3
  466 PUNCH 463,(DDX(J,I),J=1,7      ),I,NCARD
  467 IF(NDLT.GT.0) GOTO700
      CALL BOUNCE
      NSET=1
      GO TO 500
  700 DO 410 K=1,4
      IF(ZET3P(3,K)+(RD(3)*CGAM-RD(2)*SGAM-VB*OMEG1)*VNDLT*DLT      -.5*(
     1G+OMEGD1*VB)*(VNDLT*DLT )**2)701,701,410
  410 CONTINUE
      DELT=VVDELT
      GOTO500
  701 DELT=DLT
      NSET=1
      GOTO500
  375 NSET=NSET+1
      GO TO 500
  376 NSET=1
      GO TO (378,500),NSTOP
C
C     COMPUTE THE VELOCITY OF THE C.G. OF THE SPACE PACKAGE
C     FOR THE QUIESENCE OF MOTION TEST.
C
  378 RRD=ABS(M*RD(3))+SQRT((A1*OMEG(1))**2+(B1*OMEG(2))**2)
      IF(QUIVEL-RRD)385,380,380
  380 IF(PERIOD-TAUS*TAU)390,400,400
  385 PERIOD=DLT
      GO TO 500
  390 PERIOD=PERIOD+DLT
      GO TO 500
  400 RRDX=M*SQRT(RD(1)**2+RD(2)**2)+ABS(C1*OMEG(3))
      IF(RRDX.GT.QUIVEX)GO TO 401
      CALL PANIC(33HOQUIESENCE OF MOTION HAS OCCURED.)
  401 CALL PANIC(120HOTHE CAPSULE IS IN A STABLE POSITION.  CHECK RD(1),
     1 RD(2) AND OMEG(3) TO DETERMINE IF QUIESENCE OF MOTION WILL OCCUR.
     2      )
  420 FORMAT(///49X19HTERRAIN SLOPE (DEG)//53X8HGAMMA = F7.3///45X30HROT
     1ATIONAL DISPLACEMENTS (DEG)//29X4HROLL23X3HYAW23X5HPITCH/ 7X3F27.3
     2)
  430 FORMAT(//43X 37HMASS MOMENTS OF INERTIA (SLUGS-FT**2)//53X3HA =F8.
     12/53X 3HB =F8.2/53X 3HC =F8.2)
  436 FORMAT(//45X 33HTRANSLATIONAL VELOCITIES (FT/SEC)//29X4HV(1) 22X
     14HV(2) 24X 4HV(3)/7X 3F27.3)
  439 FORMAT(//45X 31HROTATIONAL VELOCITIES (RAD/SEC)//29X9HOMEGA (1)
```

```
   116X 9HOMEGA (2) 16X 9HOMEGA (3)/14X   3E25.5)
441 FORMAT(///46X29HABSORBER ATTACHMENT LOCATIONS//43X6HB(I,1)4X6HB(I,
   12)4X6HB(I,3)4X6HB(I,4)//(39X4F10.2))
442 FORMAT(//50X 26HSPACE PACKAGE WEIGHT (LBS)/56X F7.2)
443 FORMAT(1H1139X45HINERTIA CHARACTERISTICS TRANSFORMATION MATRIX//(40
   1X 3F12.2))
445 FORMAT(///40X41HFREE FLIGHT INTEGRATION STEP-UP INTEGER =,I3///50X
   121HGRAVITY (FT/SEC**2) = F5.2///45X25HCRITICAL NUTATION ANGLE =
   2F5.2,6H DEGS.)
448 FORMAT(///42X39HTHE PLOTTING OPTION HAS BEEN ACTIVATED.)
450 FORMAT(///40X43HTHE PLOTTING OPTION HAS NOT BEEN ACTIVATED.)
453 FORMAT(///35X53HTHE QUIESENCE OF MOTION CRITERIA HAVE BEEN ACTIVAT
   1ED.    )
454 FORMAT(///33X57HTHE QUIESENCE OF MOTION CRITERIA HAVE NOT BEEN ACT
   1IVATED.    )
457 FORMAT(///33X57HTHE CARD OUTPUT FOR SHOCK SPECTRA HAS NOT BEEN ACT
   1IVATED.   )
459 FORMAT(///35X53HTHE CARD OUTPUT FOR SHOCK SPECTRA HAS BEEN ACTIVAT
   1ED.  ///39X37HMAXIMUM TIME FOR SHOCK SPECTRA DATA =  F8.5)
  3 FORMAT(///38X37HCRITICAL TRANSLATIONAL DISPLACEMENT = F6.3,4H FT.)
505 FORMAT(///49X25HCOMPRESSION CONFIGURATION   )
504 FORMAT(///51X21HTENSION CONFIGURATION   )
500 RETURN
    END
```

```
$IBFTC FORCEX  DECK,LIST
      SUBROUTINE FORCE
C     THIS SUBROUTINE IS USED FOR THE ARTICULATED LEG SIMULATION
      COMMON/SNAP/TMS,TMQ
      COMMON/STCR/PSM(4),ALM(4),AU,AO,AE,AS,AL
      COMMON/FIXUP/C70,C71,C72,C73,C74
      COMMON TIME,DELT,NSTART,NFIRST,NEXIT ,IPASS,NTARGT,XNOISE(8),
     1RMT,DELMTN,DELMTE,DELMTD,ROMCOM(1482)
      COMMON/TRANS/PS(4),ALP(4),BET(4),KONFIG,SENR,RZERO
      COMMON/BNCTEN/ZETP(12),LXZET(3,3,4)
      COMMON/FUN/LEPX(3,3),LETAX(3,3),FX(3,4),MOMX(3,4),B(3,4),R(3),RD(3
     1),RDD(3),XD(3),XDD(3),OMEG(3),TAU,M,ROLLD,ROLL,YAWD,YAW,PITCHD,PIT
     2CH,OMEGD(3),IPASS,CDR,CRD,Z3F(4),ZET3P(3,4),DDDD
      DIMENSION SLOPE(2),DAMP(2),ZET2P(3,4),Z3PSD(3,4),ZETA(3,4)
      DIMENSION IGRUND(4),ZETP(3,4),TEMP(3),ISSLIP(4),FE(3),FINX(10),DEL
     1INX(10),LEPZET(3,3,4),LXZET(3,3,4),F(3,4),MOM(3,4)
      DIMENSION DELPST(2,4),FMAX(2,4),AF(2),ILOAD(2,4),DELZ(2,4),FIN(10)
     1,DELIN(10),KLAST(2,4),DELMAX(2,4),Z3P(3,4),FD(2)
      DIMENSION DELPSX(2),FMAXX(2),DELMXX(2),PDLPST(2,4),PDLPSX(2)
      DIMENSION DELZX(2)
      DIMENSION NSNAP(4)
      REAL LITALP
      REAL MOM,M,LEPX,LETAX,LEPZET,LXZET,MOMX
      IF(NSTART)1,4,1
    1 READ (5,3) FIN
      READ (5,3) DELIN
      READ (5,3) FINX
      READ (5,3) DELINX
      READ(5,3)SLOPE,DAMP
      READ(5,3)DMU,SMU,PSI
      SMUX=SMU
      DMUX=DMU
      READ(5,201)(((LXZET(I,J,N),J=1,3),I=1,3),N=1,4)
      READ(5,3)TMS,TMQ,PIT
  201 FORMAT(3E10.8)
      READ(5,3)AA,AB,AU,AD,AS
      READ(5,3)AL,AE,AO,AQ,AP
      READ(5,3)AZ,AC,PHX
      READ(5,3)AG,AH,SPRG,PLD
      PHI=PHX*CDR
      AS2=AS**2
      AGAB=AG+AB
      AOAS=AO+AS
      AHAA=AH+AA
      AEAL=AE+AL
      APAQ=AP+AQ
      AU2=AU**2
      XA=0.
      UA=1./AU
      AL2=AL**2
      ASAL=AS*AL
      C8=2.*AS2+AL2-AU2
      PI=3.14159265
    3 FORMAT(5E10.8)
      TAU=PI*SQRT(M/SLOPE(1))
      NOPRNT=0
      PSI=PSI*CDR
      CP=COS(PSI)
      SP=SIN(PSI)
      ZET3      =AU*SP-AEAL
```

```
      ZET1      =AU*CP+AO
      SA=0.
      SPH=SIN(PHI)
      CPH=COS(PHI)
      C80=-AHAA-AD*SPH
      C81=-AGAB+AD*CPH
      C82=AD*SPH-AA
      C83=C81+AG
      RHO=SQRT((AU*SP+C81)**2+(AU*CP+C80)**2)
      DO 5 N=1,4
      ISSLIP(N)=1
      ALP(N)=0.
      PS(N)=PSI
      BET(N)=0.
      NSNAP(N)=0
      ALM(N)=0.0
      PSM(N)=-1.5
      IGROUND(N)=0
      DO  43 I=1,3
   43 ZET3P(I,N)=0.
      DO 9 I=1,2
      KLAST(I,N)=1
      ILOAD(I,N)=1
      DELMAX(I,N)=0.
      FMAX(I,N)=0.
      DELZ(I,N)=0.
      DELPST(I,N)=0.
    9 PDLPST(I,N)=0.
      ZETA(1,N)=ZET1
      ZETA(2,N)=0.
      ZETA(3,N)=ZET3
    5 Z3PSD(3,N)=0.
      GOTO 10
    4 IF(IPASS.NE.1)GOTO 2
      DO 42 N=1,4
   42 Z3F(N)=ZET3P(3,N)
    2 DO 202 N=1,4
      DO 202 J=1,3
      DO 202 I=1,3
      LEPZET(I,J,N)=0.
      DO 202 K=1,3
  202 LEPZET(I,J,N)=LEPZET(I,J,N)+LEPX(I,K)*LXZET(K,J,N)
      IF(TIME.GT.TMS.AND.TIME.LT.TMQ)WRITE(6,1001)(((LEPZET(I,J,N),J=1,3
     1),I=1,3),N=1,4)
      DO 7 J=1,3
      DO 7 I=1,4
      Z3P(J,I)=ZET3P(J,I)
      ZET2P(J,I)=0.
      ZET3P(J,I)=0.
      DO 6 K=1,3
      ZET3P(J,I)=ZET3P(J,I)+LEPZET(J,K,I)*ZETA(K,I)
    6 ZET2P(J,I)=ZET2P(J,I)+LEPX(J,K)*B(K,I)
      ZET2P(J,I)=ZET2P(J,I)+R(J)
    7 ZET3P(J,I)=ZET3P(J,I)+ZET2P(J,I)
      IF(TIME.GT.TMS.AND.TIME.LT.TMQ)WRITE(6,1002)((ZET3P(J,I),I=1,4),J=
     11,3),((ZET2P(J,I),I=1,4),J=1,3)
      SENR=0.
      IF(NFIRST)13,14,13
   13 IF(NOPRNT.EQ.1)GOTO14
      NOPRNT=1
```

```
      XMIN=ZET3P(3,1)
      DO 11  I=2,4
   11 XMIN=AMIN1(XMIN,ZET3P(3,I))
      R(3)=R(3)-XMIN
      DO 12 I=1,4
      ZET2P(3,I)=ZET2P(3,I)-XMIN
   12 ZET3P(3,I)=ZET3P(3,I)-XMIN
      WRITE(6,301)(FIN(I),DELIN(I),FINX(I),DELINX(I),I=1,10)
      WRITE(6,425)(R(I),I=1,3)
      WRITE(6,305)PHX,AD,AU,AE,AO,AS,AL,AP,AQ,RHO,AB,AA,AZ,AC
      WRITE(6,613)AG,AH,SPRG,PLD
      WRITE(6,302)SLOPE
      WRITE(6,303)DAMP
      WRITE(6,304) OMU,SMU
      WRITE(6,630)
      DO 376 K=1,4
      WRITE(6,632)K
  376 WRITE(6,634)((LXZET(I,J,K),J=1,3),I=1,3)
      RZERO=R(3)
   14 DO 15 N=1,4
      NFAIL=0
      SAVEA=ALP(N)
      SAVEB=BET(N)
      SAVEP=PS(N)
      IF(ZET3P(3,N).GE.0.)GOTO17
      IF(TIME.GT.TMS.AND.TIME.LT.TMQ)WRITE(6,1701)
     1SAVEA,SAVEB,SAVEP
      IF(TIME.GT.TMS.AND.TIME.LT.TMQ)WRITE(6,1701)
     1(ZETA(I,N),I=1,3)
      IF(IGRUND(N).NE.0)GO TO 18
      IGRUND(N)=1
  913 Z3PSD(1,N)=ZET3P(1,N)
      Z3PSD(2,N)=ZET3P(2,N)
   18 DO 19  I=1,3
      ZETP(I,N)=0.0
      DO 19 K=1,3
      TEMP(K)=Z3PSD(K,N)-ZET2P(K,N)
   19 ZETP(I,N)=ZETP(I,N)+LEPZET(K,I,N)*TEMP(K)
      IF(TIME.GT.TMS.AND.TIME.LT.TMQ)WRITE(6,1007)(ZETP(I,N),I=1,3)
      ITERAT=0
      NTWICE=0
      NOMORE=0
      NIT=0
      DO 39 I=1,2
      DELPSX(I)=DELPST(I,N)
      PDLPSX(I)=PDLPST(I,N)
      DELZX(I)=DELZ(I,N)
      FMAXX(I)=FMAX(I,N)
   39 DELMXX(I)=DELMAX(I,N)
      C21=ZETP(1,N)-AO
      C31=ZETP(3,N)+AE
      C16=2.*AS*(AL+C31)
      C17=-2.*(AS2-AL*C31)
      C20SQ=C21**2
      C19SQ=ZETP(2,N)**2
      C18=C8+C31**2-C19SQ+C20SQ
      C25=C17**2-4.*AS2*C20SQ
      C26=C16**2-4.*AL2*C20SQ
      C27=2.*C16*C17+8.*ASAL*C20SQ
      C28=2.*C16*C18-8.*ASAL*C20SQ
```

```
      C29=2.*C17*C18+8.*AS2*C20SQ
      C35=4.*(AS2-C19SQ)*C20SQ-C18**2
      C27SQ=C27**2
      C29SQ=C29**2
      C2625=C26-C25
      C2535=C25-C35
      C70=C2625**2+C27SQ
      C71=2.*(C28*C2625+C27*C29)
      C72=2.*C2625*C2535+C28**2+C29SQ-C27SQ
      C73=2.*(C28*C2535-C27*C29)
      C74=C29SQ-C2535**2
      IF(TIME.GT.TMS.AND.TIME.LT.TMQ)WRITE(6,1004)N,TIME,IPASS
  921 CALL SINALP(                          SA,ALP(N),IQUIT)
      IF(IQUIT.EQ.1)GOTO17
      CA=COS(ALP(N))
      C20=AL*SA-AS*CA
      C26=AS+C20
      C18=AS*SA+AL*CA
      SP=UA*(C18+C31)
      PS(N)=ARSIN(SP)
      CP=COS(PS(N))
      Z4=ZET2P(3,N)+LEPZET(3,1,N)*(AU*CP+AOAS)+LEPZET(3,3,N)*(AU*SP-AE)
      IF(Z4.LT.0.)GOTO 115
      IF(ALP(N).LE..00001)GO TO 82
      BET(N)=ATAN2(ZETP(2,N),C21-AU*CP)
      SB=SIN(BET(N))
      CB=COS(BET(N))
      ZCH=C26*SB
      IF(TIME.GT.TMS.AND.TIME.LT.TMQ)
     1WRITE(6,916)ZCH,ZETP(2,N)
  916 FORMAT(5X3HZCHE20.8,5X3HZETE20.8)
      IF(ABS(ZCH-ZETP(2,N)).LT..005)GOTO35
      NFAIL=NFAIL+1
      IF(NFAIL.GT.4)GOTO920
      BX=C70*SA+C71
      CX=BX*SA+C72
      DX=-(CX*SA+C73)
      CHX=C74-DX*SA
      IF(TIME.GT.TMS.AND.TIME.LT.TMQ)
     1WRITE(6,922)CHX
  922 FORMAT(5X3HCHXE20.8)
      C74=DX
      C73=CX
      C72=BX
      C71=C70
      C70=0.
      GOTO921
  920 CALL PANIC(13HERROR IN ZETP
  115 WRITE(6,116)N
  116 FORMAT(1H1///5X38HTHE INTERMEDIATE MEMBER OF LEG NUMBER I1,23HHAS
     1STRUCK THE TERRAIN.//)
      CALL PANIC(55HAN INTERMEDIATE MEMBER OF A LEG HAS STRUCK THE TERRA
     1IN.)
   82 SB=0
      CB=0
      BET(N)=0.
   35 GO TO(84,85),KONFIG
   84 DEFN=SQRT((AU*CP+C80)**2+(AU*SP+C81)**2)-RHO
      ETA=ATAN2(AU*SP+C81,AU*CP+C80)
      GO TO 86
```

```
700 IF(ITERAT.EQ.0)GOTO17
    IF((NIT.GT.25).OR.(NTWICE.EQ.1)) GO TO 17
    IF(PIT.GT.0.)WRITE(6,612)N,TIME,XA,ALP(N)
    GOTO705
799 NOMORE=1
    ALP(N)=SAVEA
    GOTO413
 85 DEFN=RHO-SQRT((AC*CP-AZ*SP+C82)**2+(AC*SP+AZ*CP-C83)**2)
    ETA=ATAN2(-AC*SP-AZ*CP+C83,AC*CP-AZ*SP+C82)
 86 IF(TIME.GT.TMS.AND.TIME.LT.TMQ)WRITE(6,1005)SA,CA,SP,CP,SB,CB,SE,C
   1E
    IF(DEFN.LE.DELZ(1,N))GOTO700
    J=1
    IF(TIME.GT.TMS.AND.TIME.LT.TMQ)WRITE(6,1006)N,J,KLAST(J,N),DELMAX(
   1J,N),DELPST(J,N),FMAX(J,N),DELZ(J,N),PDLPST(J,N),DEFN,AF(J),FD(J)
    CALL CURVE(FIN     ,DELIN     ,KLAST(1,N),IPASS,DELMAX(1,N),DEFN,S
   1LOPE(1),DAMP(1),DELPST(1,N),DELT,FMAX(1,N),AF(1),ILOAD(1,N),DELZ(1
   2,N),ITERAT,PDLPST(1,N),FD(1))
    IF(TIME.GT.TMS.AND.TIME.LT.TMQ)WRITE(6,1006)N,J,KLAST(J,N),DELMAX(
   1J,N),DELPST(J,N),FMAX(J,N),DELZ(J,N),PDLPST(J,N),DEFN,AF(J),FD(J)
402 IF(AF(1).LE..0)GOTO700
    IF(ITERAT.EQ.0)SENR=.5*SLOPE(1)*(DEFN-DELZ(1,N))**2+SENR
    C30=AS*SA+AQ*CA
    C16=AS*CA-AQ*SA
    C17=1./(SP*CB*C20+CP*C18)
    ZP=SQRT((-C16+AS)**2+(-AP-C30)**2)
    DEFN=-APAQ+ZP
    J=2
    IF(TIME.GT.TMS.AND.TIME.LT.TMQ)WRITE(6,1006)N,J,KLAST(J,N),DELMAX(
   1J,N),DELPST(J,N),FMAX(J,N),DELZ(J,N),PDLPST(J,N),DEFN,AF(J),FD(J)
    IF(DEFN.LE.DELZ(J,N))GOTO103
    CALL CURVE(FINX    ,DELINX    ,KLAST(2,N),IPASS,DELMAX(2,N),DEFN,S
   1LOPE(2),DAMP(2),DELPST(2,N),DELT,FMAX(2,N),AF(2),ILOAD(2,N),DELZ(2
   2,N),ITERAT,PDLPST(2,N),FD(2))
    IF(TIME.GT.TMS.AND.TIME.LT.TMQ)WRITE(6,1006)N,J,KLAST(J,N),DELMAX(
   1J,N),DELPST(J,N),FMAX(J,N),DELZ(J,N),PDLPST(J,N),DEFN,AF(J),FD(J)
    IF(ITERAT.EQ.0)SENR=SENR+.5*SLOPE(2)*(DEFN-DELZ(2,N))**2+.5*SPRG*D
   1EFN**2
    AF(2)=AF(2)+SPRG*DEFN+PLD
104 FP4=(C16*AP+C30*AS)*AF(2)/ZP
    GOTO(87,88),KONFIG
103 AF(2)=SPRG*DEFN+PLD
    GOTO 104
 87 SE=SIN(ETA-PS(N))
    C25=SE*AF(1)
    GO TO 89
 88 CE=COS(ETA+PS(N))
    SE=SIN(ETA+PS(N))
    C25=(AC*SE+AZ*CE)*AF(1)*UA
 89 F(1,N)=(CP*FP4-C20*C25)*CB*C17
    F(3,N)=(SP*FP4*CB+C18*C25)*C17
    F(2,N)=(FP4-C20*F(3,N))*SB/C18
    IF(NOMORE.EQ.1)GOTO96
    DO 23 I=1,3
    FE(I)=0.
    DO 23 J=1,3
 23 FE(I)=FE(I)+LEPZET(I,J,N)*F(J,N)
    IF(TIME.GT.TMS.AND.TIME.LT.TMQ)WRITE(6,1009)(F(I,N),I=1,3),FE
    IF(FE(3).LE.0.)GO TO 700
 25 FE12=SQRT(FE(1)**2+FE(2)**2)
```

```
917 IF(ITERAT.EQ.1)GO TO 40
    IF(ISSLIP(N).EQ.1)GO TO 27
    COEF=SMU
    GO TO 28
 27 COEF =DMU
 28 FF=COEF*FE(3)
    IF(FE12.GT.FF)GOTO405
    ISSLIP(N)=0
    GOTO44
405 A=1000.
    ISSLIP(N)=1
    SAVEP=PS(N)
    ITERAT=1
    DO 91 I=1,3
    TEMP(I)=0.
    DO91 J=1,3
 91 TEMP(I)=TEMP(I)+LEPZET(J,I,N)*ZET2P(J,N)
    KONVER=0
    DA=.005
    IF(DA.GT.ALP(N))DA=.49*ALP(N)
    NTROUB=0
 40 FF=DMU*FE(3)
 29 ASAVE=A
    A=ABS( (FE12-FF)/FF)
    C29D=1./(LEPZET(1,2,N)*LEPZET(2,1,N)-LEPZET(1,1,N)*LEPZET(2,2,N))
    IF(PIT.GT.0.)WRITE(6,612)N,TIME, A,ALP(N),PS(N)
    IF(PIT.GT.0.)WRITE(6,411)FF,FE12
    IF(A.GT..001 )GO TO 48
    IF(ITERAT.EQ.0)GO TO 44
 96 ZETP(1,N)=AU*CP+AO+C26*CB
    ZETP(2,N)=C26*SB
    ZETP(3,N)=AU*SP-AE-C18
    IF(IPASS.NE.1)GOTO49
    GOTO44
702 WRITE(6,706)TIME
706 FORMAT(//8H*** TIME  F10.4)
    GOTO96
 48 IF(KONVER.EQ.1)GOTO406
    IF(FE12.GT.FF)GOTO407
    NAT=0
    KONVER=1
    BIGALP=ALP(N)
    LITALP=ALP(N)-DA
    GOTO408
407 IF(A.LE.ASAVE)GOTO412
705 ALP(N)=ALP(N)-DA
703 DA=-DA
    IF(NTWICE.EQ.1)GOTO799
    NTWICE=1
412 ALP(N)=ALP(N)+DA
    NIT=NIT+1
    IF(NIT.GT.25)GOTO799
    GOTO410
406 IF(FE12.GT.FF)GOTO409
    BIGALP=ALP(N)
    GOTO408
409 LITALP=ALP(N)
408 ALP(N)=.5*(BIGALP+LITALP)
    NAT=NAT+1
    IF(NAT.GT.14)GOTO702
```

```
410 IF(ALP(N).GT.0.)GO TO 413
    IF(NTROUB.EQ.1)GO TO 17
    NTROUB=1
    ALP(N)=0.
413 SA=SIN(ALP(N))
    CA=COS(ALP(N))
    C20=AL*SA-AS*CA
    C26=AS+C20
    C18=AS*SA+AL*CA
    C25=C26*CB+AO+TEMP(1)
    C27=C26*SB+TEMP(2)
    C28=-C18+TEMP(3) -AE
    C29=(LEPZET(1,3,N)*LEPZET(2,2,N)-LEPZET(2,3,N)*LEPZET(1,2,N))*C29D
    DO 8 I=1,2
    PDLPST(I,N)=PDLPSX(I)
    DELZ(I,N)=DELZX(I)
    DELPST(I,N)=DELPSX(I)
    FMAX(I,N)=FMAXX(I)
  8 DELMAX(I,N)=DELMXX(I)
    IF(ABS(LEPZET(2,2,N)).GT.ABS(LEPZET(1,2,N)))GO TO 92
    I=1
    GO TO 93
 92 I=2
 93 C35=UA*(-C28-C25*C29+(LEPZET(I,3,N)+C29*LEPZET(I,1,N))*C27/LEPZET(
   1I,2,N))
    AT=ATAN2(C29,1.0)
    ASX=ARSIN(C35/SQRT(1.+C29**2))
    PS1=ASX-AT
    PS2=SIGN(3.1415927-ABS(ASX),ASX)-AT
    DPS1=ABS(SAVEP-PS1)
    DPS2=ABS(SAVEP-PS2)
    IF(DPS1.GT.3.1415927)DPS1=ABS(DPS1-6.2831853)
    IF(DPS2.GT.3.1415927)DPS2=ABS(DPS2-6.2831853)
    IF(DPS1.LT.DPS2)GOTO94
    PS(N)=PS2
    GOTO 83
 94 PS(N)=PS1
 83 CP=COS(PS(N))
    SP=SIN(PS(N))
    GOTO35
 49 DO 701 I=1,2
    Z3PSD(I,N)=ZET2P(I,N)
    DO 701 K=1,3
701 Z3PSD(I,N)=Z3PSD(I,N)+LEPZET(I,K,N)*ZETP(K,N)
 44 MOM(1,N)=-F(2,N)*ZETP(3,N)+F(3,N)*ZETP(2,N)
    MOM(2,N)=-F(3,N)*ZETP(1,N)+F(1,N)*ZETP(3,N)
    MOM(3,N)=-F(1,N)*ZETP(2,N)+F(2,N)*ZETP(1,N)
    NSNAP(N)=1
    DO 203 I=1,3
    FX(I,N)=0.
    MOMX(I,N)=0.
    DO 203 K=1,3
    FX(I,N)=FX(I,N)+LXZET(I,K,N)*F(K,N)
203 MOMX(I,N)=MOMX(I,N)+LXZET(I,K,N)*MOM(K,N)
    ALM(N)=AMAX1(ALM(N),ALP(N))
    PSM(N)=AMAX1(PSM(N),PS(N))
    GO TO 15
 17 IGRUND(N)=0
    ISSLIP(N)=1
    C18=AS*SA+AL*CA
```

```
      C20=AL*SA-AS*CA
      C26=AS+C20
      ZETP(1,N)=AU*CP+AO+C26*CB
      ZETP(2,N)=C26*SB
      ZETP(3,N)=AU*SP-AE-C18
      IF(TIME.GT.TMS.AND.TIME.LT.TMQ)WRITE(6,1007)(ZETP(I,N),I=1,3)
      IF(NSNAP(N).EQ.0)GO TO 117
      TZ1=AU*COS(SAVEP)+AO
      TZ3=AU*SIN(SAVEP)-AEAL
      TEST=ZET2P(3,N)+LEPZET(3,1,N)*TZ1+LEPZET(3,3,N)*TZ3
      IF(TEST.LT.0.)GO TO 112
      NSNAP(N)=0
      ZETA(1,N)=TZ1
      ZETA(2,N)=0.
      ZETA(3,N)=TZ3
  117 BET(N)=0.
      ALP(N)=0.
      GO TO 114
  112 SA=SIN(SAVEA)
      CA=COS(SAVEA)
      C26=AS+AL*SA-AS*CA
      C18=AS*SA+AL*CA
      ZETA(1,N)=AU*COS(SAVEP)+AO+C26*COS(SAVEB)
      ZETA(2,N)=C26*SIN(SAVEB)
      ZETA(3,N)=AU*SIN(SAVEP)-AE-C18
      IF(TIME.GT.TMS.AND.TIME.LT.TMQ)WRITE(6,1701)
     1SAVEA,SAVEB,SAVEP
      IF(TIME.GT.TMS.AND.TIME.LT.TMQ)WRITE(6,1701)
     1(ZETA(I,N),I=1,3)
 1701 FORMAT(3E20.8)
      ALP(N)=SAVEA
      BET(N)=SAVEB
  114 PS(N)=SAVEP
   50 DO 36 I=1,3
      FX(I,N)=0.
   36 MOMX(I,N)=0.
   15 CONTINUE
   10 RETURN
  305 FORMAT(///42X36HTENSION AND COMPRESSION LEG GEOMETRY//
     149X13HPHI (DEG.) = F10.4//56X5HAD = F10.4//56X5HAU = F10.4//
     256X5HAE = F10.4//56X5HAO = F10.4//56X5HAS = F10.4//56X5HAL =
     3F10.4//56X5HAP = F10.4//56X5HAQ = F10.4//55X6HRHO = F10.4//56X5  H
     4AB = F10.4//56X5HAA = F10.4//56X5HAZ =   F10.4//56X5HAC = F10.4)
  301 FORMAT(///40X40HDYNAMIC FORCE DEFLECTION CHARACTERISTICS //46X5HUP
     1PER 15X5HLOWER//42X16HFORCE   DEFLECT.4X16HFORCE   DEFLECT./
     242X5H(LBS)5X4H(FT)6X5H(LBS)5X4H(FT)/(37XF10.2,F10.5,F10.2,F10.5))
  302 FORMAT(1H149X24HUNLOADING SLOPES (LB/FT)//46X5HUPPER 15X5HLOWER//
     133X2F20.3)
  303 FORMAT(///49X20HDAMPING COEFFICIENTS//46X5HUPPER15X5HLOWER//
     133X2F20.3)
  425 FORMAT(1H145X32HTRANSLATIONAL DISPLACEMENTS (FT)//29X4HR(1) 22X
     14HR(2) 24X 4HR(3)/7X 3F27.3)
  304 FORMAT(///45X32HTERRAIN COEFFICIENTS OF FRICTION//50X7HDYNAMIC 10X
     16HSTATIC/50XF5.2,11XF5.2)
  630 FORMAT(///37X44HABSORBER ORIENTATION TRANSFORMATION MATRICES)
  632 FORMAT(//54X 3HLEG I2)
  634 FORMAT(12X 3F24.3)
 1001 FORMAT(30X6HLEPZET/(3E20.8/3E20.8/3E20.8/))
 1002 FORMAT(20X5HZET3P/(4E20.8/4E20.8/4E20.8)/20X5HZET2P/(4E20.8))
 1003 FORMAT(5X1HYE17.8,5X2HSAE17.8,5X1HGE17.8,5X2HGPE17.8)
```

```
1004 FORMAT(2X1HNI2,6H  TIMEF7.4,5X5HIPASSI2)
1005 FORMAT(5X2HSAF11.8,3H CAF11.8,3H SPF11.8,3H CPF11.8,3H SBF11.8,3H
    1CBF11.8,3H SEF11.8,3H CEF11.8)
1006 FORMAT(5X2HN I2,3X2HJ I2,5X5HKLASTI3,3X6HDELMAXE16.8,3X6HDELPSTE16
    1.8,5X4HFMAXE16.8/5X4HDELZE16.8,3X5HPDPSTE16.8,3X4HDEFNE16.8,3X2HAF
    2E16.8,5X2HFDE16.8)
1007 FORMAT( 5X4HZETP, 3E20.8)
1008 FORMAT(5X3HTMS3E18.8,5X3HTMQ3E18.8)
1009 FORMAT(5X1HF3E17.8,5X2HFE3E17.8)
 411 FORMAT(5X2HFFE20.8,5X4HFE12E20.8)
 612 FORMAT(2X1HNI2,2X4HTIME,E16.8,2X1HAE16.8,2X3HALPE16.8,2X2HPSE16.8)
 404 FORMAT(5X3HBETE16.8,2X2HBFE16.8,2X2HDBE16.8,2X2HDAE16.8)
 613 FORMAT(/56X5HAG = F10.4//56X5HAH = F10.4///30X15HSPRING CONSTANT F
    110.1,5X7HPRELOAD F10.1)
     END
```

```
$IBFTC SINALX  DECK,LIST
      SUBROUTINE SINALP(                          SA,ALP,IQUIT)
C     THIS SUBROUTINE IS USED FOR THE ARTICULATED LEG SIMULATION
      COMMON/FIXUP/C70,C71,C72,C73,C74
      COMMON/SNAP/TMS,TMQ
      COMMON TIME,DELT,NSTART,NFIRST,NEXIT ,IPASS,NTARGT,XNOISE(8),
     1RMT,DELMTN,DELMTE,DELMTD,ROMCOM(1482)
      DIMENSION SP(4),SN(4),ALPX(4),SALP(4)
      SAVEA=ALP
      IQUIT=0
      SA=SIN(ALP)
      NOLOOP=0
      DO 80 I=1,25
  102 SAVE=SA
      SA2=SA*SA
      SA3=SA2*SA
      G=C70*SA3*SA+C71*SA3+C72*SA2+C73*SA-C74
      GP=4.*C70*SA3+3.*C71*SA2+2.*C72*SA+C73
      SA=SA-G/GP
      IF(SA.LT.0.)GOTO100
      Y=ABS (SAVE-SA)
      IF(TIME.GT.TMS.AND.TIME.LT.TMQ)WRITE(6,1003)Y,SA,G,GP
      IF(Y.LE.5.E-7)GO TO 81
   80 CONTINUE
  100 SA=0.
      IF(ABS(C74).LT..5E-5)GOTO 81
  110 GSIGN=SIGN(1.,-C74)
      G=-C74
      IF(TIME.GT.TMS.AND.TIME.LT.TMQ)WRITE(6,1003)Y,SA,G
      DO 101 I=1,10
  105 SA=SA+.1
      SA2=SA*SA
      SA3=SA2*SA
      G=C70*SA3*SA+C71*SA3+C72*SA2+C73*SA-C74
      IF(TIME.GT.TMS.AND.TIME.LT.TMQ)WRITE(6,1003)Y,SA,G
      IF(ABS(G).LT..5E-5)GO TO 81
      IF(GSIGN.NE.SIGN(1.,G))GO TO 106
  101 CONTINUE
      IQUIT=1
      GOTO10
  106 IF(G.GT.0.)GO TO 107
      SAN=SA
      SAP=SA-.1
      GO TO 108
  107 SAP=SA
      SAN=SA-.1
  108 CALL BRUTE(SAN,SAP,SA)
   81 IF(SA.LT.0..OR.SA.GT.1.)GOTO100
      ALP=ARSIN(SA)
      IF(ABS(SAVEA-ALP).LT..05)GO TO 10
      NCHNG=0
      GSIGN=SIGN(1.,-C74)
      SA=0
      NOLOOP=1
      DO 1 I=1,10
      SA=SA+.1
      SA2=SA*SA
      SA3=SA2*SA
      G=C70*SA3*SA+C71*SA3+C72*SA2+C73*SA-C74
      IF(GSIGN.EQ.SIGN(1.,G))GO TO 1
```

```
      NCHNG=NCHNG+1
      GSIGN=-GSIGN
      IF(G.GT.0.)GO TO 200
      SN(NCHNG)=SA
      SP(NCHNG)=SA-.1
      GO TO 1
  200 SP(NCHNG)=SA
      SN(NCHNG)=SA-.1
    1 CONTINUE
      IF(NCHNG.LT.2)GO TO 2
      DO 5 I=1,NCHNG
      CALL BRUTE(SN(I),SP(I),SALP(I))
    5 ALPX(I)=ARSIN(SALP(I))
      SA=SALP(1)
      AMIN=ABS(ALPX(1)-SAVEA)
      ALP=ALPX(1)
      DO 6 I=2,NCHNG
      AMINX=ABS(ALPX(I)-SAVEA)
      IF(AMIN.LT.AMINX)GO TO 6
      AMIN=AMINX
      ALP=ALPX(I)
      SA=SALP(I)
    6 CONTINUE
      GO TO 10
    2 SA=SIN(ALP)
   10 RETURN
 1003 FORMAT(5X1HYE17.8,5X2HSAE17.8,5X1HGE17.8,5X2HGPE17.8)
      END
```

```
$IBFTC QUIMOT  DECK,LIST
      SUBROUTINE QUIMOT
C     THIS SUBROUTINE IS USED FOR THE ARTICULATED LEG SIMULATION
      COMMON/JOHN/THETA
      COMMON/BOUND/OMEG1,LKX,A1,B1,C1,U,G,SGAM,CGAM,CRTR,W,WD,LEH
      COMMON/FUN/LEPX(3,3),LETAX(3,3),F(3,4),MOM(3,4),B(3,4),R(3),RD(3),
     1RDD(3),XD(3),XDD(3),OMEG(3),TAX,M,ROLLD,ROLL,YAWD,YAW,PITCHD,PITCH
     2,OMEGD(3),IPASS,CDR,CRD,Z3F(4),ZET3P(3,4),RHO
      COMMON/FREE/T,LHX(3,3),TMIN,KONVER,DPH,DPS,CT,ST,ZX(3,4),C2,DT,LKH
     1(3,3)
      COMMON/STCR/PSM(4),ALM(4),AU,AO,AE,AS,AL
      COMMON/BNCTEN/ZETA(12),LXZET(3,3,4)
      REAL M,LXZET
      DIMENSION XI(3,4),XH(4),D(4),ETA(4),TAU(4),GAMDCR(4),GAMDOT(4),XIM
     1(4),DXI(4)
      DIMENSION TEMP(3,2)
      DIMENSION LKX(3,3),W(3),WD(3),LEH(3,3)
      GM=G*M
      ISET=0
      BETWR1=-135.0*CDR
      BETWR2=+135.0*CDR
      CB1=COS(BETWR1)
      CB2=COS(BETWR2)
      SB1=SIN(BETWR1)
      SB2=SIN(BETWR2)
      DO 5 I=1,4
      J=I+1
      IF(J.GT.4)J=1
      CPI=COS(PSM(I))
      CPJ=COS(PSM(J))
      SPI=SIN(PSM(I))
      SPJ=SIN(PSM(J))
      SAI=SIN(ALM(I))
      SAJ=SIN(ALM(J))
      CAI=COS(ALM(I))
      CAJ=COS(ALM(J))
      XI(1,I)=AU*CPI+AO+(AS-AS*CAI+AL*SAI)*CB1
      XI(1,J)=AU*CPJ+AO+(AS-AS*CAJ+AL*SAJ)*CB2
      XI(2,I)=(AS-AS*CAI+AL*SAI)*SB1
      XI(2,J)=(AS-AS*CAJ+AL*SAJ)*SB2
      XI(3,I)=AU*SPI-AE-AS*SAI-AL*CAI
      XI(3,J)=AU*SPJ-AE-AS*SAJ-AL*CAJ
      DO 6 K=1,3
      TEMP(K,1)=0.0
      TEMP(K,2)=0.0
      DO 6 L=1,3
      TEMP(K,2)=TEMP(K,2)+LXZET(K,L,J)*XI(L,J)
    6 TEMP(K,1)=TEMP(K,1)+LXZET(K,L,I)*XI(L,I)
      DO 7 K=1,3
      XI(K,I)=TEMP(K,1)+B(K,I)
    7 XI(K,J)=TEMP(K,2)+B(K,J)
      XIM(I)=      XI(1,I)**2+XI(2,I)**2+XI(3,I)**2
      XIM(J)=      XI(1,J)**2+XI(2,J)**2+XI(3,J)**2
    2 DXI(I)=(XI(1,J)-XI(1,I))**2+(XI(2,J)-XI(2,I))**2+(XI(3,J)-XI(3,I))
     1**2
      XH(I)=XIM(I)+(XIM(I)+DXI(I)-XIM(J))**2/(-4.0*DXI(I))
      D(I)=SQRT(XIM(I)-XH(I))
      XH(I)=SQRT(XH(I))
      DXI(I)=SQRT(DXI(I))
      ETA(I)=XI(3,I)+ D(I)*(XI(3,J)-XI(3,I))/DXI(I)
```

```
  3 TAU(I)=ARSIN(-ETA(I)/XH(I))
    IF(ABS(TAU(I)+THETA)*CRD.GE.90.0) GO TO 5
    GAMDOT(I)=OMEG1+ SQRT(RD(1)**2+RD(2)**2+RD(3)**2)/XH(I)
    GAMDCR(I)=SQRT(2.0*GM*XH(I)*(1.0-SIN(TAU(I)+THETA))/(M*XH(I)**2+A1
   1))
  4 IF(GAMDOT(I).LT.GAMDCR(I))ISET=ISET+1
  5 CONTINUE
    IF(ISET.LT.4)GO TO 10
    WRITE(6,101) GAMDCR
    WRITE(6,100) GAMDOT
    CALL PANIC(41HTHE SPACE PACKAGE IS IN A STABLE POSITION)
100 FORMAT(///4X10HGAMDOT(1)=E16.8,4X10HGAMDOT(2)=E16.8,4X10HGAMDOT(3)
   1=E16.8,4X10HGAMDOT(4)=E16.8///)
101 FORMAT(///4X10HGAMDCR(1)=E16.8,4X10HGAMDCR(2)=E16.8,4X10HGAMDCR(3)
   1=E16.8,4X10HGAMDCR(4)=E16.8///)
 10 RETURN
    END
```

```
$IBFTC XCURVE  LIST,DECK
      SUBROUTINE CURVE(FIN,DELIN,KLAST,IPASS,DELMAX,DEFN,SLOPE,DAMP,
     1DELPST,DELT,FMAX,AF,ILOAD,DELZ,ITERAT,PDLPST,FD)
C     THIS SUBROUTINE IS USED FOR THE ARTICULATED LEG SIMULATION
      DIMENSION FIN(10),DELIN(10)
  200 IF(DEFN-DELMAX)300,240,240
  240 AA=DEFN
      IF(AA.LT.DELIN(KLAST)) KLAST=1
      DO 250 K=KLAST,9
      BB=DELIN(K)
      CC=DELIN(K+1)
      IF(AA.GE.BB.AND.AA.LE.CC)GO TO 260
  250 CONTINUE
      CALL PANIC (29HO DEFLECTION NOT WITHIN TABLE)
  260 D=(AA-BB)/(CC-BB)
      AF=FIN(K)+D*(FIN(K+1)-FIN(K))
      KLAST=K
      IF (IPASS.EQ.1)GOTO500
      IF(DEFN.LE.DELMAX)GOTO500
      FMAX=AF
      DELMAX=DEFN
      DELZ=DELMAX-FMAX/SLOPE
      GO TO 500
  300 IF(IPASS-3)310,320,330
  310 C13=3.0
      C12=2.0
      C11=1.0
      GO TO 400
  320 C13=4.0
      C12=3.0
      C11=1.0
      GO TO 400
  330 C13=1.0
      C12=1.0
      C11=0.0
  400 FS=FMAX-SLOPE*(DELMAX-DEFN)
      IF(FS.LT.0.0) FS=0.0
      IF(DAMP.LT.1.E-5) GO TO 390
      FD=DAMP*(C13*(DEFN-DELPST)+C11*(DELPST-PDLPST))/(DELT*C12)
  402 IF (ABS(FD).LE.1.E-5) GO TO 401
      IF((FS/ABS(FD)).GT.1.1111111)GOTO401
      FD=SIGN(FS,FD)*.9
      GO TO 401
  390 FD=0.0
  401 AF=FS+FD
      IF(AF.GT.FMAX) AF=FMAX
      IF(AF.LT.0.) AF=0.0
  500 IF(IPASS.NE.4) GO TO 510
      PDLPST=DELPST
      DELPST=DEFN
  510 RETURN
      END
```

```
$IBFTC BOUNCX  DECK,LIST
      SUBROUTINE BOUNCE
C     THIS SUBROUTINE IS USED FOR THE ARTICULATED LEG SIMULATION
      COMMON TIME,DELT,NSTART,NFIRST,NEXIT ,IPASS,NTARGT,XNOISE(8),
     1RMT,DELMTN,DELMTE,DELMTD,ROMCOM(1482)
      COMMON/JOHN/THETA
      COMMON/BNCTEN/ZETP(12),LXZET(3,3,4)
      COMMON/ANGL/PH ,PS ,TH,KFIRST,KRETRN
      COMMON/BOUND/OMEG1,LKX,A1,B1,C1,U,G,SGAM,CGAM,CRTR,W,WD,LEH
      COMMON/FUN/LEPX(3,3),LETAX(3,3),F(3,4),MOM(3,4),B(3,4),R(3),RD(3),
     1RDD(3),XD(3),XDD(3),OMEG(3),TAU,M,ROLLD,ROLL,YAWD,YAW,PITCHD,PITCH
     2,OMEGD(3),IPASS,CDR,CRD,Z3F(4),ZET3P(3,4),RHO
      COMMON/FREE/T,LHX(3,3),TMIN,KONVER,DPH,DPS,CT,ST,ZX(3,4),C2,DT,LKH
     1(3,3)
      DIMENSION LKX(3,3),W(3),WD(3),LEH(3,3)
      DIMENSION Z1(4),LXZET(3,3,4),ZETP(3,4)
      REAL LXZET
      REAL LEH,LHX,LKX ,LKH,LETAX ,LEPX
      FTIM(SV,SQ,S)=(SV+S*SQRT(SQ))*U/CGAM
      FSQ(SV,SDEL)=SV**2-2.*G*SDEL*CGAM
      KONVER=0
      KFIRST=0
      KRETRN=0
      C2=.5*G*CGAM
      PH=ATAN2 (OMEG(1),OMEG(2))
      SPH=SIN(PH)
      CPH=COS(PH)
      PS=0.
      SPS=0.
      CPS=1.
      OMEG12=SQRT(OMEG(1)**2+OMEG(2)**2)
      IF((ABS(OMEG12).GT.1.E-5).OR.(ABS(OMEG(3)).GT.1.E-5))GOTO1
      ST=0.
      IF(OMEG(3).GE.0.)GO TO 2
      TH=3.1415927
      CT=-1.
      GO TO 4
    2 CT=1.
      TH=0.
      GO TO 4
    1 TH=ATAN2(A1*OMEG12,C1*OMEG(3))
      CT=COS(TH)
      ST=SIN(TH)
    4 CALL SUBLHX(SPH,CPH,SPS,CPS,CT,ST,LHX)
      DO 6 I=1,3
      DO 6 J=1,3
      LEH(I,J)=0.
      LKH(I,J)=0.
      DO 6 K=1,3
      LKH(I,J)=LKH(I,J)+LKX(I,K)*LHX(J,K)
    6 LEH(I,J)=LEH(I,J)+LEPX (I,K)*LHX(J,K)
      C=C1/(A1-C1)
      DPH=OMEG(3)/(1.+C)
      DPS=C*DPH/CT
      ZMAX=0.
      DO 7 N=1,4
      DO 9 I=1,3
      Z=0
      DO 11 J=1,3
   11 Z=Z+LXZET(I,J,N)*ZETP(J,N)
```

```
  9 ZX(I,N)=Z+B(I,N)
    Z1(N)=SQRT (ZX(1,N)**2+ZX(2,N)**2+ZX(3,N)**2)
  7 ZMAX=AMAX1(ZMAX,Z1(N))
    SV=RD(3)
    SDEL=CRTR-R(3)
    SQ=FSQ(SV,SDEL)
    IF(SQ.LE.0.)GOTO31
    T3=FTIM(SV,SQ,1.)
    TMIN=T3
    SDEL=ZMAX-R(3)
    SQ=FSQ(SV,SDEL)
    IF(SQ.LE.0.)GOTO30
    NSQ=1
    T1=FTIM(SV,SQ,-1.)
    T2=FTIM(SV,SQ,1.)
    T=0.
    IF(T.GT.T1)GO TO 8
    DT=T1/25.
    GO TO 12
 30 T2=0.
 10 NSQ=2
  8 T=T2
    SDEL=T3-T2
    DT=SDEL/25.
 12 IF(DT.GT.DELT) GO TO 14
    DT=DELT
 14 DO 16 I=1,25
    CALL TIMPIC
    IF(KONVER.EQ.1)GO TO 100
    IF(KRETRN.EQ.1)GO TO 31
    KFIRST=1
    T=T+DT
 16 CONTINUE
    IF(NSQ.EQ.1) GO TO 10
    CALL PANIC(115HTHE FREE FLIGHT EQUATIONS INDICATE THAT CAPSULE WIL
   1L EXCEED THE CRITICAL THETA BEFORE RECONTACTING THE GROUND.
   2 )
100 T=TMIN-2.*DELT
    PH=DPH*T+PH
    PS=DPS*T+PS
    SPH=SIN(PH )
    CPH=COS(PH )
    SPS=SIN(PS )
    CPS=COS(PS )
    CALL SUBLHX(SPH,CPH,SPS,CPS,CT,ST,LHX)
    R(2)=R(2)+RD(2)*T+5.*SGAM*G*T**2
    R(1)=R(1)+RD(1)*T
    R(3)=R(3)+RD(3)*T-C2*T**2
    RD(3)=RD(3)-2.*C2*T
    RD(2)=RD(2)+G*SGAM*T
    DO 32 I=1,3
    DO 32 J=1,3
    LEPX(I,J)=0.0
    LKX(I,J)=0.0
    DO 32 K=1,3
    LKX(I,J)=LKX(I,J)+LKH(I,K)*LHX(K,J)
 32 LEPX(I,J)=LEPX(I,J)+LEH(I,K)*LHX(K,J)
    OMEG(1)=DPS*ST*SPH
    OMEG(2)=DPS*ST*CPH
    OMEGD(1)=DPH*OMEG(2)
```

```
      OMEGD(2)=-DPH*OMEG(1)
      DO 17 I=1,3
      XDD(I)=0.0
      WD(I)=0.
      W(I)=0.
      DO 17 J=1,3
      XDD(I)=XDD(I)+LEPX(J,I)*RDD(J)
      W(I)=W(I)+LETAX(I,J)*OMEG(J)
   17 WD(I)=WD(I)+LETAX(I,J)*OMEGD(J)
      IF(ABS(LKX(3,1)).GT..99985) CALL PANIC(110H COS(YAW) AT RECONTACT
     1IS NEARLY EQUAL TO ZERO.  THIS CONDITION CAN NOT BE HANDLED BY THE
     2 D.E.MONITOR.                          )
      PITCH=ATAN2(LKX(3,2),LKX(3,3))
      ROLL=ATAN2(LKX(2,1),LKX(1,1))
      SP=SIN(PITCH)
      CP=COS(PITCH)
      SR=SIN(ROLL)
      CR=COS(ROLL)
      IF(ABS(SP)-.707)20,21,21
   20 YAW=ATAN2(-LKX(3,1),LKX(3,3)/CP)
      GOTO22
   21 YAW=ATAN2(-LKX(3,1),LKX(3,2)/SP)
   22 SY=SIN(YAW)
      CY=COS(YAW)
      ROLLD=(OMEG(2)*SP+OMEG(3)*CP)/CY
      YAWD=OMEG(2)*CP-OMEG(3)*SP
      PITCHD=OMEG(1)+SY*ROLLD
      THETA=ARSIN(SQRT(SY**2+(CY*SP)**2))
      N=T/DELT
      XN=N
      XT=XN*DELT
      WRITE(6,200)TIME
      TIME=TIME+XT
      IF(T-XT.GT..5*DELT) TIME=TIME+DELT
      WRITE(6,201)TIME
      CALL QUIMOT
   31 RETURN
  200 FORMAT(////////10X67HSUBROUTINE BOUNCE HAS TAKEN CONTROL FROM THE D
     1.E. MONITOR AT TIME = F8.4)
  201 FORMAT(10X50HCONTROL WAS RETURNED TO THE D.E. MONITOR AT TIME = F8
     1.4)
      END
```

```
$IBFTC BRUTEX  DECK,LIST
      SUBROUTINE BRUTE(SAN,SAP,SA)
C     THIS SUBROUTINE IS USED FOR THE ARTICULATED LEG SIMULATION
      COMMON TIME,DELT,NSTART,NFIRST,NEXIT ,IPASS,NTARGT,XNOISE(8),
     1RMT,DELMTN,DELMTE,DELMTD,ROMCOM(1482)
      COMMON/FIXUP/C70,C71,C72,C73,C74
      COMMON/SNAP/TMS,TMQ
      NIT=0
  108 SA=.5*(SAN+SAP)
      NIT=NIT+1
      IF(NIT.GT.15)RETURN
      SA2=SA*SA
      SA3=SA2*SA
      G=C70*SA3*SA+C71*SA3+C72*SA2+C73*SA-C74
      IF(ABS(G).LT..5E-5)RETURN
      IF(TIME.GT.TMS.AND.TIME.LT.TMQ)WRITE(6,1003)Y,SA,G
 1003 FORMAT(5X1HYE17.8,5X2HSAE17.8,5X1HGE17.8,5X2HGPE17.8)
      IF(G.GT.0.)GO TO 109
      SAN=SA
      GO TO 108
  109 SAP=SA
      GO TO 108
      END
```

APPENDIX VIII

INSTRUCTIONS FOR USE OF THE DIGITAL SIMULATIONS

The data cards for the digital simulations are prepared in the format described in Figures 111 through 114. A complete set of data cards are used for each run. The first three cards are read by the Differential Equation Monitor and the remainder of the cards by subroutines FUNEV and FORCE.

The following variables are common to both the telescoping leg and articulated leg simulation.

TITLE Any combination of alphanumeric characters in Columns 1 through 80. It will be printed out at the top of each page of the motion time histories.

t_o Arbitrary reference time in seconds for instant of impact.

Δt Integration increment in seconds.

t_f Time in seconds at which the simulation will stop if none of the termination criteria are satisfied.

$\rho \Delta t$ Time interval in seconds for printing the motion time histories.

NDLT Free flight integration interval step-up factor. If this is zero, the free flight equations of motion will be used instead of numerical integration and the stability criteria will also be applied.

NPLOT A value of 1 will write a plotting tape of the motion time histories. A value of 2 suppresses it.

NSTOP A value of 1 will activate the quiescence of motion criteria. A value of 2 will suppress the quiescence of motion criteria.

NSHOCK A value of 1 activates the punched card output of the translational accelerations for use in shock spectra analysis. A value of 2 suppresses this option.

TAUS The number of periods of oscillation of the space package on the alightment system compliance through which the quiescence of motion criteria must be satisfied before the run is terminated.

TIMSHK The time in seconds at which the card output of the translational accelerations will stop.

R_1, R_2, and R_3 The components in feet of the translational position vector of the center of gravity of the space package at impact. The third component is determined by the program. Typically the input values for these three quantities are all zero. This locates the initial terrain reference system directly under the capsule center of gravity.

V_1, V_2, and V_3 The components, in feet/second, of the translational velocity vector of the center of gravity of the space package, V_3 is the vertical component and should be a negative quantity. V_2 is the horizontal velocity component away from the terrain for positive terrain slopes. V_1 is the velocity component out of the plane of the page.

ROLL, YAW, and PITCH The angular orientation of the space package in degrees at the instant of impact.

Ω_1, Ω_2, and Ω_3 The angular rates about the geometric body fixed axes in radians/second at the instant of impact.

A, B, and C The mass moments of inertia in slug/feet^2 about the principal axes of the space package. If A $\neq$ B subroutine BOUNCE can not be used (NDLT $\neq$ 0).

WEIGHT The weight of the space package in pounds.

Θ CRITICAL The angle in degrees between the inertial vertical and the roll axis of the space package beyond which the space package will unquestionably tumble over.

R_3 CRITICAL The distance in feet from the center of gravity to the bottom of the body of the space package.

G The magnitude of the acceleration of gravity in feet/second^2.

γ The terrain slope in degrees.

ℓ_{ij} The ij element of the transformation matrix to the principal axes from the geometric body fixed axes.

b_{ij} The ith component in feet of the attachment position reference in the geometric body fixed axes of the jth alightment system.

FIN_i The ith force value in pounds of the dynamic force deflection characteristics of the vertical energy absorbers.

$FINX_i$ The ith force value in pounds of the dynamic force deflection characteristics of the horizontal energy absorbers.

$DELIN_i$ The ith deflection value in feet of the dynamic force deflection characteristics of the vertical energy absorbers.

$DELINX_i$ The ith deflection value in feet of the dynamic force deflection characteristics of the horizontal energy absorbers.

$SLOPE_1$ and $SLOPE_2$ The spring rates in pounds/foot of the vertical and horizontal energy absorbers, respectively.

$DAMP_1$ and $DAMP_2$ The viscous damping coefficients in pounds-seconds/foot of the vertical and horizontal energy absorbers, respectively.

μ_D The dynamic or sliding coefficient of friction between the terrain and the alightment system footpads.

μ_S The static coefficient of friction between the terrain and the alightment system footpads.

IDP The data thinning factor for the plotting tape. If IDP = 1, the values for each Δt will be written. If IDP = 5, every fifth Δt will be written.

IOR_i and DSC_i These are the origin location and the scale factors for the ith word of the plotting tape. The plotting tape contains a series of twenty integer word records. The twenty words in order are: time, the 1, 2 and 3 components of the translational displacement, the 1, 2 and 3 components of the translational velocity, the 1, 2 and 3 components of the translational acceleration, the 1, 2 and 3 components of the angular acceleration, the roll, yaw, and pitch angles, the absolute magnitude of the translational acceleration, and the 1, 2 and 3 components of the angular velocities. The origin and scale factor convert the variables into a grid network for a mechanical plotter.

The following variables appear only in the telescoping leg simulation.

NPAD The number of rotational energy absorbers on each leg. The maximum is eight.

RHO The undeflected length in feet of the telescoping leg from the pivot point to the footpad.

γ_i The angular position in degrees of the ith rotational energy absorber referenced from the one direction of the geometric body fixed axis.

AS The lever arm in feet from the pivot point of the telescoping leg to the rotational energy absorbers.

The following variables appear only in the articulated leg simulation.

ℓXZ_{ijk} - The ij element of the transformation matrix from the kth alightment system coordinate system to the geometric body fixed axes.

PSIZ The initial magnitude in degrees of the alightment system position coordinate $\psi^{(i)}$.

AA, AB, AU, AD, AS, AL, AE, AO, AQ, AP, AZ, AC, AG, and AH The geometry dimensions in feet of the articulated leg configuration as illustrated in Figure 22.

PHI The angular offset in degrees of the parallelogram of the articulated leg alightment system.

SPRG The spring rate in pounds/foot of the light return spring on the peg leg of the articulated leg configuration.

PLD The preload in pounds on the return spring at the returned position.

GENERAL DYNAMICS | POMONA

FORM 6-374

FORTRAN CODING AND DATA FORM

PAGE 1 OF 2

PROBLEM: SPACE PACKAGE ALIGHTMENT TELESCOPING LEG SIMULATION

PROGRAMMER: STRUCTURAL DYNAMICS

AWO | EWO | WAP | PHONE EXT. | DATE

Line	Cols 1–10	Cols 11–20	Cols 21–30	Cols 31–40	Cols 41–50	Cols 51–60
1	← TITLE →					
2	t_o	Δt	t_f	$P\Delta t$		
3	1	,				
4	NDLT	NPLOT	NSTOP	NSHOCK	TAUS	TIMSHK
5	R_1	R_2	R_3			
6	V_1	V_2	V_3			
7	ROLL	YAW	PITCH			
8	Ω_1	Ω_2	Ω_3			
9	A	B	C			
10	WEIGHT	$\theta_{CRITICAL}$	$R_{3\ CRITICAL}$			
11	G	γ				
12	ℓ_{11}	ℓ_{12}	ℓ_{13}			
13	ℓ_{21}	ℓ_{22}	ℓ_{23}			
14	ℓ_{31}	ℓ_{32}	ℓ_{33}			
15	b_{11}	b_{12}	b_{13}			
16	b_{21}	b_{22}	b_{23}			
17	b_{31}	b_{32}	b_{33}			
18	b_{41}	b_{42}	b_{43}			
19	NPAD					
20	FIN_1	→	→	→	FIN_5	
21	FIN_6	→	→	→	FIN_{10}	
22	$DELIN_1$	→	→	→	$DELIN_5$	
23	$DELIN_6$	→	→	→	$DELIN_{10}$	
24	$FINX_1$	→	→	→	$FINX_5$	
25	$FINX_6$	→	→	→	$FINX_{10}$	
26	$DELINX_1$	→	→	→	$DELINX_5$	
27	$DELINX_6$	→	→	→	$DELINX_{10}$	
28	RHO	$SLOPE_1$	$SLOPE_2$	$DAMP_1$	$DAMP_2$	
29	γ_1	→	→	→	γ_5	
30	γ_6	γ_7	γ_8			

Figure 111, Telescoping Leg Simulation Input Format, 1 of 2

GENERAL DYNAMICS | POMONA

FORM 6-374

FORTRAN CODING AND DATA FORM

PAGE 2 OF 2

PROBLEM | AWO | EWO | WAP

PROGRAMMER | PHONE EXT. | DATE

```
      uD          uS          AS
IDP
      IOR1        DSC1        IOR2        DSC2
                                                                  IOR20       DSC20
```

Figure 112, Telescoping Leg Simulation Input Format, 2 of 2

FORTRAN CODING AND DATA FORM

PAGE 1 OF 2

PROBLEM: SPACE PACKAGE ALIGHTMENT ARTICULATED LEG SIMULATION

AWO | EWO | WAP

PROGRAMMER: STRUCTURAL DYNAMICS

PHONE EXT. | DATE

Cols 1–10	Cols 11–20	Cols 21–30	Cols 31–40	Cols 41–50
← TITLE →				
t_o	Δt	t_f	$P\Delta t$	
1	•			
NDLT	NPLOT	NSTOP	NSHOCK	1
TAUS	TIMSHK			
R_1	R_2	R_3		
V_1	V_2	V_3		
ROLL	YAW	PITCH		
Ω_1	Ω_2	Ω_3		
A	B	C		
WEIGHT	$\theta_{CRITICAL}$	$R_{3\ CRITICAL}$		
G	Υ			
ℓ_{11}	ℓ_{12}	ℓ_{13}		
ℓ_{21}	ℓ_{22}	ℓ_{23}		
ℓ_{31}	ℓ_{32}	ℓ_{33}		
b_{11}	b_{12}	b_{13}		
b_{21}	b_{22}	b_{23}		
b_{31}	b_{32}	b_{33}		
b_{41}	b_{42}	b_{43}		
FIN_1	→	→	→	FIN_5
FIN_6	→	→	→	FIN_{10}
$DELIN_1$	→	→	→	$DELIN_5$
$DELIN_6$	→	→	→	$DELIN_{10}$
$FINX_1$	→	→	→	$FINX_5$
$FINX_6$	→	→	→	$FINX_{10}$
$DELINX_1$	→	→	→	$DELINX_5$
$DELINX_6$	→	→	→	$DELINX_{10}$
$SLOPE_1$	$SLOPE_2$	$DAMP_1$	$DAMP_2$	
μD	μS	PSIZ		

Figure 113, Articulated Leg Simulation Input Format, 1 of 2

FORTRAN CODING AND DATA FORM

PAGE 2 OF 2

PROBLEM | AWD | EWD | WAP

PROGRAMMER | PHONE EXT. | DATE

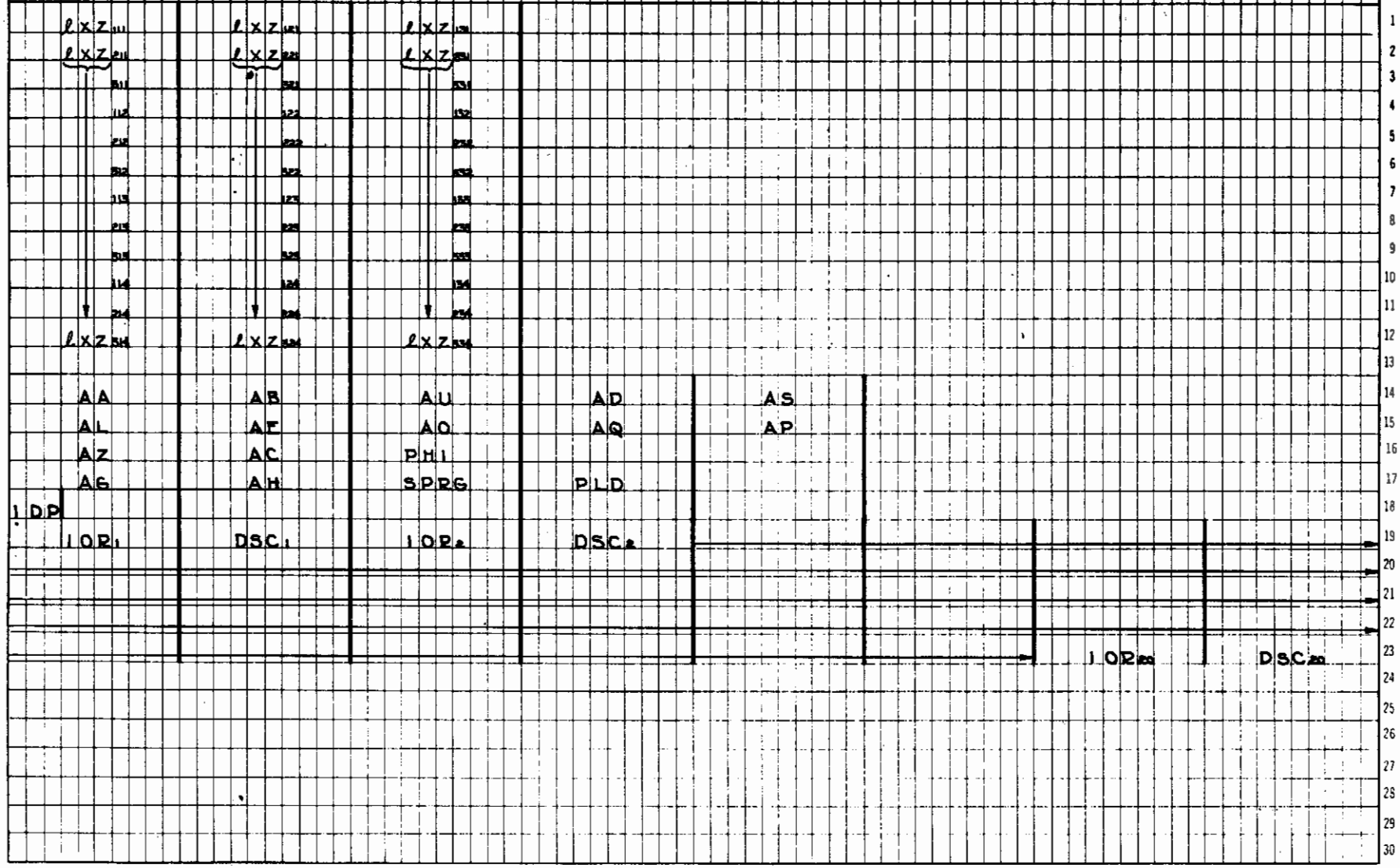

Figure 114, Articulated Leg Simulation Input Format, 2 of 2

REFERENCES

(1) Slowik, J. and Weir, W., "Investigation of Crew Escape System Surface Impact Techniques for Advanced Aerospace Vehicles," Technical Documentary Report No. ASD-TDR-63-173, AD 411-946, 15 May 1963, Unclassified.

(2) Frazer, Duncan, and Collar, "Elementary Matrices," Cambridge Press, 1957, Page 251.

(3) Etkin, Bernard, "Dynamics of Flight," John Wiley and Sons, 1959.

(4) Thomson, W. T., "Space Dynamics," John Wiley and Sons, 1961.

(5) Walton, W. C., Herr, H. W., and Leonard, H. W., "Studies of Touchdown Stability for Lunar Landing Vehicles," Journal of Spacecraft and Rockets, Volume 1, Pages 552-556, September-October 1964.

(6) Seely, M. S., Smith J. O., "Advanced Mechanics of Materials," John Wiley and Sons, 1952.

(7) Feen, R. W., Glass, R. A., Needham, R. A., and Steinberg, M. A., "Beryllium-Aluminum Alloys," Journal of Spacecraft, Volume 2, No. 1, January-February 1965, Pages 87-93.

(8) Shanley, F. R., "Strength of Materials," McGraw-Hill, 1957, Page 602.

(9) Roark, R. J., "Formulas for Stress and Strain," McGraw-Hill, 1954.

(10) "Strength of Metal Aircraft Elements," MIL-HDBK-5, March 1955, Page 213.

(11) Black, R. J., "Quadrupedal Landing Gear Systems for Spacecraft," Journal of Spacecraft, March-April 1964.

UNCLASSIFIED
Security Classification

DOCUMENT CONTROL DATA - R&D
(Security classification of title, body of abstract and indexing annotation must be entered when the overall report is classified)

1. ORIGINATING ACTIVITY *(Corporate author)*
General Dynamics Corporation
Pomona Division
Pomona, California

2a. REPORT SECURITY CLASSIFICATION
UNCLASSIFIED

2b. GROUP

3. REPORT TITLE
Investigation of Space Package Alightment Dynamic Load Design Criteria

4. DESCRIPTIVE NOTES *(Type of report and inclusive dates)*
Final Report July 1964 - March 1966

5. AUTHOR(S) *(Last name, first name, initial)*
York, Kenneth C.
Ingels, Clyde R.
Maloney, John G.

6. REPORT DATE
October 1966

7a. TOTAL NO. OF PAGES
376

7b. NO. OF REFS
11

8a. CONTRACT OR GRANT NO.
AF33(615)-1832

b. PROJECT NO. 1370

c. Task No. 137008

d.

9a. ORIGINATOR'S REPORT NUMBER(S)
AFFDL-TR-66-33

9b. OTHER REPORT NO(S) *(Any other numbers that may be assigned this report)*

10. AVAILABILITY/LIMITATION NOTICES
This document is subject to special export controls and each transmittal to foreign governments or foreign nationals may be made only with prior approval of AFFDL (FDD).

11. SUPPLEMENTARY NOTES
None

12. SPONSORING MILITARY ACTIVITY
Air Force Flight Dynamics Laboratory (FDDS)
Wright-Patterson AFB, Ohio 45433

13. ABSTRACT

This report presents the results of a limited parametric study of ten space package alightment systems. A state-of-the-art review in alightment dynamics was conducted prior to beginning the parametric study.

Two three-dimensional digital simulations were developed for use in the parametric study. Each of these simulates a basic design concept of an alightment system. Two types of alightment systems were examined. One for a 300 pound capsule with electronic cargo and one for a 3000 pound capsule with human cargo. An experimental program was performed to permit a comparison of predicted and measured acceleration time histories during alightment. Generally excellent correlation was shown.

Energy absorbing material or techniques are shown to be a secondary consideration in determining the efficiency of an alightment system. A three-dimensional digital simulation of alightment dynamics is concluded to be mandatory in the development of an alightment system.

The feasibility of an alightment system, weighing six percent of the capsule, to alight successfully on a 35 degree slope with a 12 degree capsule inclination is shown. Such a system is capable of handling a vertical velocity of 35 feet per second and a horizontal velocity of 15 feet per second.

DD FORM 1 JAN 64 1473

UNCLASSIFIED
Security Classification

UNCLASSIFIED

Security Classification

14. KEY WORDS	LINK A		LINK B		LINK C	
	ROLE	WT	ROLE	WT	ROLE	WT
Energy Absorption Space Package Alightment System Dynamics						

INSTRUCTIONS

1. ORIGINATING ACTIVITY: Enter the name and address of the contractor, subcontractor, grantee, Department of Defense activity or other organization *(corporate author)* issuing the report.

2a. REPORT SECURITY CLASSIFICATION: Enter the overall security classification of the report. Indicate whether "Restricted Data" is included. Marking is to be in accordance with appropriate security regulations.

2b. GROUP: Automatic downgrading is specified in DoD Directive 5200.10 and Armed Forces Industrial Manual. Enter the group number. Also, when applicable, show that optional markings have been used for Group 3 and Group 4 as authorized.

3. REPORT TITLE: Enter the complete report title in all capital letters. Titles in all cases should be unclassified. If a meaningful title cannot be selected without classification, show title classification in all capitals in parenthesis immediately following the title.

4. DESCRIPTIVE NOTES: If appropriate, enter the type of report, e.g., interim, progress, summary, annual, or final. Give the inclusive dates when a specific reporting period is covered.

5. AUTHOR(S): Enter the name(s) of author(s) as shown on or in the report. Enter last name, first name, middle initial. If military, show rank and branch of service. The name of the principal author is an absolute minimum requirement.

6. REPORT DATE: Enter the date of the report as day, month, year; or month, year. If more than one date appears on the report, use date of publication.

7a. TOTAL NUMBER OF PAGES: The total page count should follow normal pagination procedures, i.e., enter the number of pages containing information.

7b. NUMBER OF REFERENCES: Enter the total number of references cited in the report.

8a. CONTRACT OR GRANT NUMBER: If appropriate, enter the applicable number of the contract or grant under which the report was written.

8b, 8c, & 8d. PROJECT NUMBER: Enter the appropriate military department identification, such as project number, subproject number, system numbers, task number, etc.

9a. ORIGINATOR'S REPORT NUMBER(S): Enter the official report number by which the document will be identified and controlled by the originating activity. This number must be unique to this report.

9b. OTHER REPORT NUMBER(S): If the report has been assigned any other report numbers *(either by the originator or by the sponsor)*, also enter this number(s).

10. AVAILABILITY/LIMITATION NOTICES: Enter any limitations on further dissemination of the report, other than those imposed by security classification, using standard statements such as:

(1) "Qualified requesters may obtain copies of this report from DDC."

(2) "Foreign announcement and dissemination of this report by DDC is not authorized."

(3) "U. S. Government agencies may obtain copies of this report directly from DDC. Other qualified DDC users shall request through _____."

(4) "U. S. military agencies may obtain copies of this report directly from DDC. Other qualified users shall request through _____."

(5) "All distribution of this report is controlled. Qualified DDC users shall request through _____."

If the report has been furnished to the Office of Technical Services, Department of Commerce, for sale to the public, indicate this fact and enter the price, if known.

11. SUPPLEMENTARY NOTES: Use for additional explanatory notes.

12. SPONSORING MILITARY ACTIVITY: Enter the name of the departmental project office or laboratory sponsoring *(paying for)* the research and development. Include address.

13. ABSTRACT: Enter an abstract giving a brief and factual summary of the document indicative of the report, even though it may also appear elsewhere in the body of the technical report. If additional space is required, a continuation sheet shall be attached.

It is highly desirable that the abstract of classified reports be unclassified. Each paragraph of the abstract shall end with an indication of the military security classification of the information in the paragraph, represented as *(TS), (S), (C), or (U)*.

There is no limitation on the length of the abstract. However, the suggested length is from 150 to 225 words.

14. KEY WORDS: Key words are technically meaningful terms or short phrases that characterize a report and may be used as index entries for cataloging the report. Key words must be selected so that no security classification is required. Identifiers, such as equipment model designation, trade name, military project code name, geographic location, may be used as key words but will be followed by an indication of technical context. The assignment of links, rules, and weights is optional.

UNCLASSIFIED

Security Classification